Technical Report Documentation Page

| 1. Report No. | 2. Government Accession No. | 3. Recipient's Catalog No. |
|---|---|---|
| FHWA/TX-02/1388-1 | | |

| 4. Title and Subtitle | 5. Report Date |
|---|---|
| Development Length of 0.6-Inch Prestressing Strand in Standard I-Shaped Pretensioned Concrete Beams | December 1999 |
| | 6. Performing Organization Code |

| 7. Author(s) | 8. Performing Organization Report No. |
|---|---|
| R. W. Barnes, N. H. Burns, and M. E. Kreger | Research Report 1388-1 |

| 9. Performing Organization Name and Address | 10. Work Unit No. (TRAIS) |
|---|---|
| Center for Transportation Research<br>The University of Texas at Austin<br>3208 Red River, Suite 200<br>Austin, TX 78705-2650 | 11. Contract or Grant No.<br>Research Study 0-1388 |

| 12. Sponsoring Agency Name and Address | 13. Type of Report and Period Covered |
|---|---|
| Texas Department of Transportation<br>Research and Technology Transfer Office<br>P.O. Box 5080<br>Austin, TX 78763-5080 | Research Report (9/95-8/98) |
| | 14. Sponsoring Agency Code |

15. Supplementary Notes

Project conducted in cooperation with the U.S. Department of Transportation, Federal Highway Administration, and the Texas Department of Transportation.

16. Abstract

The use of 0.6 in prestressing strand at a center-to-center spacing of 2 in allows for the optimal implementation of High Strength Concrete (HSC) in precast, prestressed concrete bridge superstructures. For this strand configuration, partial debonding of strands is a desirable alternative to the traditional method of draping to alleviate extreme concrete stresses after prestress release. Experimental evidence suggests that existing code provisions addressing the anchorage of pretensioned strands do not adequately describe their behavior. In addition, the anchorage behavior of partially debonded strands is not fully understood.

Results are reported from a research study conducted to determine the anchorage behavior of 0.6 in strands at 2 in spacing in full-size, plant-cast AASHTO Type I I-beams. Concrete strengths ranged up to 15,000 psi. Strand featured either a bright mill finish or a rusted surface condition. A variety of strand debonding configurations were investigated. The use of pull-out capacities and strand draw-in measurements to predict the anchorage behavior of prestressing strands was also examined.

Along with recommended design procedures for anchorage of prestressing strand, a review of the evolution and shortcomings of existing code provisions is presented. The use of this strand configuration is concluded to be safe, and partial debonding of prestressing strands is shown to be an effective means of reducing stresses in the end regions of pretensioned beams.

| 17. Key Words | 18. Distribution Statement |
|---|---|
| prestressed concrete, anchorage, debonding, transfer length high strength concrete (HSC), development length | No restrictions. This document is available to the public through the National Technical Information Service, Springfield, Virginia 22161. |

| 19. Security Classif. (of report) | 20. Security Classif. (of this page) | 21. No. of pages | 22. Price |
|---|---|---|---|
| Unclassified | Unclassified | 338 | |

Form DOT F 1700.7 (8-72) Reproduction of completed page authorized

# DEVELOPMENT LENGTH OF 0.6-INCH PRESTRESSING STRAND IN STANDARD I-SHAPED PRETENSIONED CONCRETE BEAMS

**by**

**R. W. Barnes, N. H. Burns, and M. E. Kreger**

Research Report 1388-1

*Research Project 0-1388*

*DEVELOPMENT LENGTH OF 15-MM (0.6-IN.) DIAMETER PRESTRESSING STRAND AT 50-MM (2-INCH) GRID SPACING IN STANDARD I-SHAPED PRETENSIONED CONCRETE BEAMS*

conducted for the
Texas Department of Transportation

In cooperation with the
U.S. Department of Transportation
Federal Highway Administration

by the
CENTER FOR TRANSPORTATION RESEARCH
BUREAU OF ENGINEERING RESEARCH
THE UNIVERSITY OF TEXAS AT AUSTIN

December 1999

*Research performed in cooperation with the Texas Department of Transportation and the U.S. Department of Transportation, Federal Highway Administration.*

# ACKNOWLEDGMENTS

We greatly appreciate the financial support from the Texas Department of Transportation that made this project possible. The support of the project directors, Mary Lou Ralls (BRG) and Arnold Cohen (DES), and program coordinator, Richard Wilkison (DES), is also very much appreciated. We thank Project Monitoring Committee members David Hohmann (DES), Gerald Lankes (CST), and John Vogel (HOU). We would also like to thank Don Harley (FHWA) and Sue Lane (FHWA) for their assistance on this project.

The authors would also like to thank the employees of the Texas Concrete Company—particularly Bruce Williams and Burson Patton—for their cooperation during the specimen fabrication phase of this study. Graduate Research Assistants Heather Jobson and John Grove contributed directly to the research, as did Jon Kilgore (SAT). We gratefully acknowledge the hard work of Usnik Tuladhar, Justin Billodeau, Kevin Skyrmes, Guclu Sumen, Shane Hadeed, Sherman White, Cem Topkaya, Jenny Mejia, Nicole Garcia, Disney Burns, and a host of other student researchers who volunteered their time and efforts at the Phil M. Ferguson Structural Engineering Laboratory.

# DISCLAIMER



N. H. Burns, P.E. #20801

M.E. Kreger, P.E. #65541

*Research Supervisors*

# TABLE OF CONTENTS

# LIST OF TABLES

# LIST OF FIGURES

# SUMMARY

The use of 0.6 in prestressing strand at a center-to-center spacing of 2 in allows for the optimal implementation of High Strength Concrete (HSC) in precast, prestressed concrete bridge superstructures. For this strand configuration, partial debonding of strands is a desirable alternative to the more traditional method of draping strands to alleviate extreme concrete stresses after prestress release. Recent experimental evidence suggests that existing code provisions addressing the anchorage of pretensioned strands do not adequately describe the behavior of these strands. In addition, the anchorage behavior of partially debonded strands is not fully understood. These uncertainties have combined to hinder the full exploitation of HSC in pretensioned concrete construction.

A research study was conducted to determine the anchorage behavior of 0.6 in strands at 2 in spacing in full-size bridge members. The experimental program consisted of assessing transfer and development lengths in plant-cast AASHTO Type I I-beams. The influence of concrete compressive strengths ranging from 5700 to 14,700 psi was examined. In order to consider the full range of strand surface conditions found in practice, the prestressing strand featured either a bright mill finish or a rusted surface condition. The anchorage behavior of partially debonded strands was investigated by using a variety of strand debonding configurations—including debonded strand percentages as high as 75 percent. A limited investigation of the effect of horizontal web reinforcement on anchorage behavior was performed. Pull-out tests were performed in an attempt to correlate results with the bond quality of the strands used in the study. The correlation between strand draw-in and the anchorage behavior of prestressing strands was also examined.

A review of the evolution and shortcomings of existing code provisions for the anchorage of prestressing strands is presented. Results of the experimental program are reported, along with recommended design procedures based on these results and those from other studies. The use of 0.6 in strand at 2 in spacing is concluded to be safe, and partial debonding of prestressing strands is shown to be an effective means of reducing stresses in the end regions of pretensioned girders.

# CHAPTER 1: INTRODUCTION

## 1.1 BACKGROUND

The vast majority of short- to moderate-span highway bridges constructed in Texas feature precast, pretensioned girder superstructure systems. The ubiquity of this superstructure type, depicted in Figure 1.1, results from the efficiency associated with the fabrication and erection of precast, pretensioned bridge members. The relatively recent advent of High Performance Concrete (HPC), which features increased strength and/or durability, promises continued advances in the structural and economic efficiencies exhibited by this type of superstructure.

**Figure 1.1: Highway Bridge Featuring Precast, Pretensioned I-Beam Superstructure**

High Strength Concrete (HSC)—featuring a compressive strength in excess of 9000 psi (62 MPa)—represents a subset of HPC. The prestressing force required to fully precompress the tensile zone in standard AASHTO I-beams constructed of HSC cannot be provided using the most prevalent tendon configuration—0.5 in (12.7 mm) diameter strands with a 2 in (50 mm) grid spacing (Castrodale, Kreger, and Burns 1988b). The use of 0.6 in (15.2 mm) strands, commonly used in post-tensioning applications, at the same grid spacing represents a potential solution to this problem. This larger strand size allows the introduction of forty percent more prestressing force than the 0.5 in (12.7 mm) strand.

Full precompression of the bottom fiber of the beam allows the largest possible service load moment to be resisted without exceeding the allowable tension stress in the concrete. In addition, a forty-percent increase in reinforcement area can result in a comparable increase in ultimate capacity. Thus, HSC beams reinforced with 0.6 in (15.2 mm) strand offer significantly improved performance when considering either service or strength limit states. Exploitation of this symbiotic relationship between higher concrete strength and larger amounts of prestressed reinforcement promises bridges that benefit from having longer span lengths or fewer girders per span. Researchers at Lund University in Sweden recently concluded that the combination of HSC and 0.6 in strands in prefabricated I-shaped girders results in a 15 percent reduction in the direct girder costs (Persson, Johansson, and Johansson 1999). Economic benefits can also result from the combination of 0.6 in strands (15.2 mm) with normal strength concrete. Thirty percent fewer strands may be used (compared to 0.5 in strands) to achieve the same prestress force, reducing the labor costs associated with installing strands. The reduction in number of strands increases the eccentricity of the resultant prestress force. This, in turn, may allow the deletion of a few more strands.

Although maximizing the prestress force applied to the bottom flange is ideal for resisting in-service load effects, it may pose difficulties during the construction process. The stresses that occur in a precast beam immediately after transfer of prestress usually dictate the configuration of prestressing reinforcement that may be used. Prior to the application of external loads, a large amount of prestressing in the bottom flange can result in excessive tensile

stresses in the top fibers in the end regions of the beam. These stresses are usually controlled by one of two methods: strand draping or debonding.

Draped strands, also known as “depressed” or “harped” strands, have long been used to control induced stresses at prestress transfer, or “release.” The prestress force remains constant in magnitude, but the resulting concrete stresses are controlled by varying the eccentricity of this prestress force. The draped strands lie within the bottom flange along the central portion of the span, where the maximum moments are expected. However, the draped strands rise as they approach the ends of the beam. In this manner, the concrete stresses remain within allowable limits in the end regions, where the moment due to gravity loads is relatively small.

Although draping of strands has been used successfully for decades, it has some disadvantages. Depressing the strands is done while the strands are stressed and can be dangerous. Flawed strands have been known to fracture during this process. Hold-down assemblages have also failed resulting in worker fatalities. Applying draping techniques to 0.6 in (15.2 mm) strand intensifies this danger due to the significantly higher force involved. For this reason, precasters are reluctant to drape this larger-diameter strand. In addition, draped strands are located higher in the prestressing bed anchorages, and therefore exert a large overturning moment on these anchorages. Because most current prestressing beds were designed for draping of 0.5 in (12.7 mm) strand, draping of 0.6 in (15.2 mm) strands might force the strengthening of existing anchorages.

Partial debonding of strands, also known as “blanketing” or “jacketing,” is a simpler and safer alternative to draping. Rather than varying the eccentricity of the strands, the prestress force applied to the end regions of the beam is decreased by preventing bond between some of the tendons and the concrete. This is most commonly achieved by wrapping the area to be debonded in flexible plastic tubing and sealing the ends. This method may be used to tailor the induced concrete stresses to remain within allowable limits. Strand debonding offers an added benefit in that it can be easily applied to precast members with inclined webs, such as the Texas Department of Transportation (TxDOT) U-beam shown in Figure 1.2.

**Figure 1.2: TxDOT U-Beam**

The potential benefits of HSC can be realized fully through the use of 0.6 in (15.2 mm) strands at a spacing of 2 in (50 mm). In turn, use of partial strand debonding can result in the safer, simpler, and more flexible implementation of this strand configuration. These three elements—HSC, large-diameter strand, and debonding—represent an efficient combination of materials and methods for use in precast, pretensioned bridge substructures.

The integrity of all reinforced and prestressed concrete structures depends upon adequate anchorage of the reinforcement. The existing ACI and AASHTO code provisions concerning the anchorage of pretensioned strands are based on research results obtained from specimens constructed of outdated materials. In addition, the code expressions do not adequately reflect the dispersion evident in the experimental results on which they are based (Tabatabai and Dickson 1993).

Experimental research has revealed that the anchorage behavior of debonded tendons can differ significantly from that of fully bonded tendons. As a result of these studies, ACI and AASHTO codes include a modification to be applied to some debonded strands. However, it can be argued that this modification is specific to the particular specimens tested, and may not adequately reflect the anchorage behavior of debonded strands over the full range of possible loads, geometries, and member reinforcement schemes. A more rational approach to predicting the anchorage behavior of debonded strands might result in an improvement of existing code provisions.

In 1988, after researchers at North Carolina State University reported much larger than expected values of transfer and development length for uncoated strands of varying sizes (Cousins, Johnston, and Zia 1990), the Federal Highway Administration (FHWA) revised the criteria for strand development length (FHWA 1988). These revisions included a moratorium on the use of 0.6 in (15.2 mm) strand in pretensioned applications, and a sixty percent increase in the calculated value of development length for fully bonded strands. Minimum center-to-center strand spacing was set as four times the nominal strand diameter. By prohibiting the use of 0.6 in (15.2 mm) strand and forcing 0.5 in (12.7 mm) strand to a grid spacing of at least 2 in (50 mm), these revisions effectively impeded the full exploitation of HSC in pretensioned applications.

Some research in recent years has focused on factors that do not currently play a role in code expressions pertaining to anchorage behavior of pretensioned strands. Test programs (Mitchell et al. 1993; Gross and Burns 1995) have indicated that strands embedded in HSC exhibit improved anchorage behavior when compared to those cast in normal strength concrete. After a review of development length test results obtained from various research studies, Buckner (1995) concluded that development length is a function of the tendon strain, or elongation, at ultimate. He proposed that the code development length expression be modified to reflect the influence of this elongation.

In order to further investigate the anchorage behavior of large-diameter prestressing strands, the Center for Transportation Research of The University of Texas at Austin along with Texas Tech University initiated a joint research study in 1995 entitled *Development Length of 15-mm (0.6-inch) Diameter Prestressing Strand at 50-mm (2-inch) Grid Spacing in Standard I-shaped Pretensioned Concrete Beams*. The details of this study, funded by the Texas Department of Transportation (TxDOT) as Research Project No. 0-1388 and by FHWA as Program No. SPR 0511, are described in this report.

After reviewing the results of several research programs spawned in the wake of its 1988 revisions, FHWA modified these revisions in 1996 to allow the use of 0.6 in (15.2 mm) strand at a grid spacing of 2 in (50 mm) and the use of 0.5 in (12.7 mm) strand at a grid spacing of 1.75 in (44 mm)(FHWA 1996). Although this decision again allows the effective use of HSC in pretensioned beams, uncertainty remains regarding the anchorage performance of both fully bonded and debonded strands.

## 1.2 OBJECTIVES

The stated objective of the research was to measure the transfer and development lengths for 0.6 in (15.2 mm) diameter prestressing strand at 2 in (50 mm) grid spacing in tests of several standard AASHTO Type I pretensioned beams. The more general objective of the study was a better understanding of the anchorage behavior of pretensioned concrete flexural members. In order to achieve this general objective, several specific objectives were identified:

1. Assess the effect of concrete strength on anchorage behavior,
2. Examine the anchorage behavior of strands exhibiting the range of surface conditions found in practice, and
3. Develop rational means of predicting the anchorage behavior of debonded strands.

In addition, research effort was focused on assessing the usefulness of pull-out tests and strand draw-in measurements as indicators of anchorage behavior. Rather than investigate the effect of strand elongation on flexural bond behavior, specimens were designed to have ultimate strand elongation values of at least 3.5 percent. Thus, the results obtained should represent worst-case behavior with regard to strand elongation.

## 1.3 SCOPE

The research study encompassed transfer and development length testing of thirty-six plant-cast, AASHTO Type I (Texas Type A), pretensioned concrete I-beams. Transfer length testing was performed at the plant; both immediate and long-term transfer lengths were measured. Corresponding values of strand draw-in were also measured. Pull-out tests were performed in an effort to quantify strand bond quality. Development length tests were performed on thirty beams at the Phil M. Ferguson Structural Engineering Laboratory at The University of Texas at Austin. Development length testing of the remaining six beams was carried out at Texas Tech University. In an effort to achieve ultimate tendon elongation values exceeding 3.5 percent, a cast-in-place, composite deck was added to each beam prior to development length testing.

Three different levels of beam concrete strength were investigated. Compressive strengths at prestress release varied from 4000 to 11,000 psi (27 to 76 MPa). Strengths at time of development length testing ranged from 5700 to 14,700 psi (39 to 102 MPa). Specimens were reinforced with strands having either a "bright" or a "rusted" surface condition. A variety of strand debonding schemes were tested. Some specimens contained strands that were all fully bonded, while other specimens featured percentages of debonded strands ranging up to 75 percent. The study included a limited investigation of the effect of horizontal web reinforcement on anchorage behavior.

## 1.4 ORGANIZATION OF REPORT

Chapter 2 includes a discussion of the anchorage behavior of pretensioning strands, as well as a brief history of the development of current code provisions regarding this topic. The details of the specimens tested in the experimental program are described in Chapter 3. Chapter 4 contains a discussion of the issue of strand bond quality. Results of companion pull-out tests performed as a part of the experimental program are also presented and discussed in this chapter. The transfer length test program is described in Chapter 5. Results of transfer length testing are discussed and compared with existing code expressions as well as those suggested by other researchers. Based on the results of this test program and others, a conservative design expression for transfer length is proposed Chapter 6 focuses on the use of measured strand draw-in values to predict anchorage behavior. Test results are discussed and compared to the results of corresponding transfer length tests. The results of the development length test program are reported and discussed in Chapter 7. Behavior of the test specimens is compared with that indicated by the relevant code provisions. A conservative design expression for development length is proposed based on the results of this and other relevant studies. The influence of cracking on the necessary development length is discussed. Chapter 8 is a collection of recommendations for anchorage design of prestressing strands and for further research. A brief summary of the research study and the resulting conclusions are presented in Chapter 9.

## 1.5 NOTATION

There is no standard system of notation for the various properties described and referred to in this report. Notation systems vary among different codes and research documents. The notation adopted in the AASHTO LRFD Code (1998) is used for terms and properties in this report. The author has selected appropriate notation for any property noted in this report that is not defined in the AASHTO LRFD Code. Each symbol is defined or described in the text upon its first appearance (and often at other instances). A table of symbols used may be found under the heading "Notation" immediately prior to the reference list at the end of the report. Where possible, the notational equivalents found in the ACI (1999) and AASHTO Standard Codes (1996) are reported as well.

# CHAPTER 2: ANCHORAGE BEHAVIOR IN PRETENSIONED MEMBERS

## 2.1 INTRODUCTION

Adequate anchorage of reinforcement is vital to the integrity of structural concrete. Reinforcement for concrete members and connections is usually proportioned based on the assumption that the reinforcement is adequately anchored. Once the reinforcement amount and pattern are selected, the adequacy of the reinforcement anchorage is checked. If the resulting anchorage capacity is deficient, the size, amount, or configuration of the reinforcement is then altered in such a way as to ensure that potential anchorage demands are met or exceeded. If less than adequate anchorage is provided, the structure will be unable to resist the flexural, shear or torsional forces for which it was designed, and if actual loads approach those assumed in design, a premature failure is likely to occur.

Anchorage of reinforcement is generally provided by bond between the reinforcement and the concrete along a length of bar or tendon; by bearing of the reinforcement or a mechanical attachment against the concrete; or a combination of bond and bearing. In the case of precast, pretensioned construction, anchorage of prestressing tendons is usually accomplished by means of bond along a straight length of each tendon.

This chapter includes a description of the current philosophy regarding anchorage of prestressing strands in pretensioned members. The historical development of existing code provisions and relevant research studies are summarized. In addition, the feasibility and potential ramifications of alternate design philosophies and methods are discussed.

## 2.2 DEFINITIONS

This section provides definitions and descriptions of several terms key to the discussion of anchorage behavior.

### 2.2.1 Development Length

Development length, $l_d$, is the shortest bonded length of bar or tendon along which the bar or tendon stress can increase from zero to the stress required for achievement of the full nominal strength at the section under consideration. For nonprestressed reinforcement, $l_d$ usually represents the bonded length necessary to develop a stress of $f_y$, the yield stress of the reinforcement. Because the stress in prestressing reinforcement, $f_p$, continues to increase with increasing strain, $l_d$ for prestressing strand represents the bonded tendon length necessary to fully develop $f_{ps}$, the stress in the prestressing steel required for the nominal resistance of the member. Thus, if the length of tendon bonded on either side of the section under consideration is less than the development length, $l_d$, the member will be unable to attain the calculated nominal resistance because the tendon cannot achieve the required stress, $f_{ps}$.

Development length as defined here is known as "anchorage length" in European practice. When used in European practice, the term "development length" refers to the extent of the anchorage zone, i.e. the distance over which the influence of the prestressing force is distributed throughout the cross section. This subject is discussed further in the subsequent section and in Section 5.3.4.

For nonprestressed reinforcement, the development length is calculated according to the assumption of an average bond stress, $\overline{u}$ , that can be resisted prior to bond failure. On the other hand, the development length of pretensioned reinforcement has historically been subdivided into two distinct portions—the transfer length and the flexural bond length—each characterized by a unique average bond capacity.

### 2.2.2 Transfer Length

Transfer length, $l_t$, is defined as the bonded tendon length required to develop the full effective prestress force in a prestressing tendon. The term has no meaning for nonprestressed reinforcement. Due to losses, the prestress level varies with time. Thus, the prestress force of interest with regard to anchorage behavior is that corresponding to the prestress in the tendon after losses, $f_{pe}$.

Transfer length has also been defined as the distance required to transfer the prestress from the tendon to the concrete (Buckner 1994). This definition can be misleading because it could conceivably be construed as indicating that the transfer length defines the extent of the pretensioned anchorage zone. In reality, the anchorage zone of pretensioned members extends beyond the transfer length of the tendons. At the end of the transfer length, equilibrium ensures that the full prestress force has been applied to the concrete. However, Base (1958b) has demonstrated that this prestress force is not yet fully distributed over the cross section at this point. An additional distance is required to achieve the distribution of stresses calculated based on the "plane sections remain plane" assumption of engineering beam theory. Thus, the transfer length plus this additional distance defines the full extent of the anchorage zone, which corresponds to the European definition of "development length" mentioned in the preceding section. The extent of the pretensioned anchorage zone is not explicitly addressed in North American practice. The portion of the anchorage zone corresponding to the North American "transfer length" is known as the "transmission length" in European practice.

Aside from constituting an integral portion of the development length, the transfer length is important because of its association with the extent of the pretensioned anchorage zone. The accuracy of any attempt to predict the actual material stresses at a specific location within the anchorage zone depends upon the accuracy of the estimation of the transfer length. For example, knowledge of the transfer zone boundaries is necessary for the accurate calculation of concrete stresses for comparison with Service Limit State allowable stress limits at transfer and under service loading. In this step of the design exercise, *overestimation* of the transfer length can produce a significant error with actual stress magnitudes being larger than calculated.

Accurate transfer length estimation is also crucial to shear design, especially because shear demand is usually greatest in the transfer regions of pretensioned members. Sectional shear resistance calculations require knowledge of the level of precompression in the concrete, which in turn depends upon the location of the section under investigation relative to the anchorage zone boundaries. In this type of design exercise, *underestimation* of the transfer length is unconservative.

Realistic estimation of the extent of the anchorage zone is also critical to the design of anchorage zone reinforcement. Strut-and-tie models are of great value to designers attempting to improve anchorage zone reinforcement details. Safe and efficient use of these models depends upon accurate estimates for the range of possible transfer lengths. Shorter transfer lengths result in larger values of transverse tensile stresses in the anchorage zone.

Upon release of the pretensioning force, the decrease in tendon tension along the transfer length results in a proportional increase in tendon diameter. So long as the strength of the surrounding concrete remains intact, this radial expansion results in an increased frictional bond capacity between the reinforcement and the concrete. Thus, the transfer bond stresses, $u_t$, are higher than those possible in regions where this expansion does not occur. This enhanced bond capacity due to the expansion of the pretensioned reinforcement was explained by Hoyer and Friedrich (1939), and is commonly known as the "Hoyer Effect."

Further discussion of transfer bond theory is included in Section 2.4.

### 2.2.3 Flexural Bond Length

Flexural bond length, $l_{fb}$, is defined as the distance, in addition to the transfer length, over which the tendon must be bonded to the concrete in order that a stress $f_{ps}$ may develop in the tendon at nominal strength of the member. Aside from a change in notation, the replacement of "strand" with "tendon," and the replacement of "ultimate" with "nominal," this is the definition of flexural bond length included in the Commentary to the ACI 318-63 Code, in which the current expression for development length was first included (Tabatabai and Dickson 1993). The buildup of tendon stress along the flexural bond length results from flexural bond stress, $u_{fb}$, between the tendon and the surrounding concrete. As opposed to transfer bond stresses, which result from the application of prestress to the member, flexural bond stresses result from the application of external loads and deformations (Janney 1954). Thus, flexural bond stress is analogous to the bond stress that occurs along the straight development length of nonprestressed reinforcement. Although flexural bond stresses must also occur along the transfer length under the imposition of external loads, they are generally disregarded due to their small magnitude if the concrete remains uncracked in this region.

Theory involving flexural bond and the influence of cracking is presented in Section 2.5.

## 2.3 CODE PROVISIONS FOR ANCHORAGE OF FULLY BONDED STRANDS

The present expression for the development length of fully bonded strands was first incorporated in the 1963 version of ACI's *Standard Building Code Requirements for Reinforced Concrete* (ACI 318-63; Tabatabai and Dickson 1993). It was subsequently incorporated into AASHTO's *Standard Specifications for Highway Bridges* (in 1973) and *LRFD Bridge Design Specifications*. This section includes a brief history of the evolution of the relevant provisions along with a discussion of some of their shortcomings.

### 2.3.1 Relevant ACI and AASHTO Code Clauses and Commentary

The relevant provisions for the development of prestressing strand are found in Section 12.9 of the ACI Code (ACI 318-99), Article 5.11.4 of the AASHTO LRFD Specification (AASHTO 1998), and Section 9.28 of the AASHTO Standard Specification. Other than minor discrepancies in wording and notation, the AASHTO Standard Specification provisions for development length are identical to those in the ACI Code. As the AASHTO LRFD specifications are largely similar, the ACI provisions will be reported herein and significant discrepancies with the AASHTO LRFD specification will be noted.

The provisions of ACI 318-99, Section 12.9 — *Development of prestressing strand* that are relevant to fully bonded strands are worded as follows:

> **12.9.1** — Three- or seven-wire pretensioning strand shall be bonded beyond the critical section for a development length, in inches, not less than[1]
>
> $$\left( f_{ps} - \frac{2}{3} f_{pe} \right) d_b$$
>
> where $d_b$ is strand diameter in inches, and $f_{ps}$ and $f_{pe}$ are expressed in kips/in$^2$.
>
> **12.9.2** — Limiting the investigation to cross sections nearest each end of the member that are required to develop full design strength under specified factored loads shall be permitted.

Though the value calculated in 12.9.1 is defined as "development length," ACI 318-99 and the AASHTO Standard Specification refrain from using the notation, $l_d$, which is reserved for the development length of nonprestressed reinforcement. The AASHTO LRFD Specification uses $l_d$ to represent the development length of prestressed and nonprestressed reinforcement.

The ACI 318R-99 Commentary Section R12.9 states that "the development length requirements for prestressing strand are intended to provide bond integrity for the strength of the member." The Commentary goes on to state that the expression for $l_d$ given is equivalent to the expression:

$$l_d = \frac{f_{pe}}{3} d_b + \left( f_{ps} - f_{pe} \right) d_b$$

where the first term represents the transfer length (as defined in Section 2.2.2 above) and the second term represents the flexural bond length (as defined in Section 2.2.3 above). To illustrate this concept, the Commentary includes the figure reproduced here as Figure 2.1. In this figure, the steel stress is shown to increase linearly along the transfer length. Along the flexural bond length, the slope of the depicted steel stress curve decreases steadily. The Commentary goes on to state that the expressions for transfer length and flexural bond length are based on tests of members prestressed with clean strands featuring diameters of ¼, ⅜, and ½ in (6.4, 9.5, and 12.7 mm). The maximum value of $f_{ps}$ for these tests is reported as 275 ksi (1895 MPa). The Commentary cites papers by Hanson and Kaar (1959); Kaar, LaFraugh, and Mass (1963), and Kaar and Magura (1965)[2].

---

[1] Notation has been modified to reflect the system of notation used throughout this report. Also, the parenthetical expression is used as a constant without units.

[2] The citation of Kaar and Magura (1965) in this portion of the Commentary appears to be a mistake. This reference is vital to the evolution of provisions regarding the development length of *debonded* strands, but has little relevance to the expression for development length of fully bonded strand. The fully bonded strands in this study featured

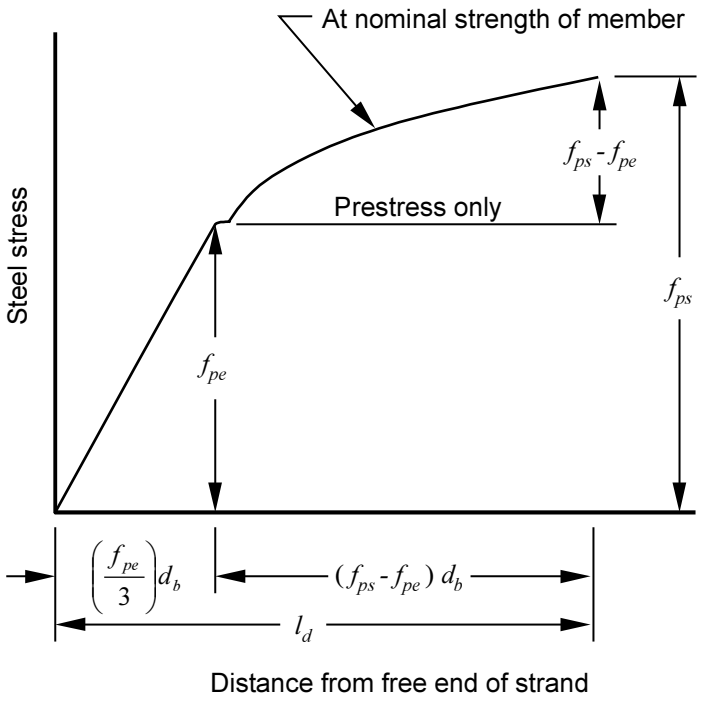


**Figure 2.1: Variation of Steel Stress with Distance from Free End of Strand (from ACI 318R-99, Fig. R12.9)**

The development length provisions of the AASHTO LRFD Specification differ from the original ACI in a few details. Article 5.11.4.1 of this specification states that the prestress force may be assumed to increase linearly along the transfer length and "in a parabolic manner" along the flexural bond length. These statements verbally mimic the relationship illustrated in Figure 2.1. The particular shape of the parabolic profile along the flexural bond length is apparently left to the discretion of the practitioner. The article goes on to state that the transfer length may be taken as 60 strand diameters, and that the development length may be calculated as $\left(f_{ps} - \frac{2}{3} f_{pe}\right) d_b$ just as in ACI 318-99 Section 12.9. If combined with the $\frac{f_{pe}}{3} d_b$ expression for transfer length stated in the ACI 318 Commentary, the assumed transfer length of $60 d_b$ would indicate an assumed value of $f_{pe}$ equivalent to 180 ksi (1240 MPa). The AASHTO LRFD Specification lacks any statement resembling that of ACI 318-99 Section 12.9.2, which limits the number of cross sections at which development length is checked.

In addition to these provisions regarding the development length of prestressing strand, the shear provisions of the ACI Code and AASHTO specifications include statements concerning the transfer length of prestressing strand. According to ACI 318-99, the nominal shear capacity of pretensioned members when subjected to web-shear cracking is calculated as the sum of $V_{cw}$, the nominal shear strength provided by concrete when diagonal cracking results from excessive principal tensile stress in the web, and $V_s$, the nominal shear strength provided by shear reinforcement. The value of $V_{cw}$ at a section under consideration depends upon the compressive stress in the concrete at the centroid (or web/flange junction) at that section. Section 11.4.3 of the Code states that when the critical section for shear lies within the transfer length of the prestressing tendons, "the reduced prestress shall be considered when computing $V_{cw}$.…The prestress force shall be assumed to vary linearly from zero at end of tendon to a maximum at a distance from end of tendon equal to the transfer length, assumed to be 50 diameters for strand…." Thus, in this portion of the Code the transfer length is assumed equal to $50 d_b$, which corresponds to the

---

bonded lengths considerably longer than those predicted by the Code expression and therefore provide no verification of the adequacy of the expression. In addition, these results were published two years after the expression first appeared in ACI 318-63.

expression $\frac{f_{pe}}{3} d_b$ given in Commentary Section R12.9 when $f_{pe}$ is 150 ksi (1035 MPa). No reference is cited in the Commentary for Section 11.4.3. Similar language is included in the shear provisions of the AASHTO Standard Specification.

The shear provisions of the AASHTO LRFD Specification differ from those given above. Among the *General Requirements* for shear and torsion resistance, Article 5.8.2.3 *Transfer and Development Lengths* simply states that "[t]he provisions of Article 5.11.4 shall be considered." Article 5.11.4 includes the anchorage provisions described above. The commentary accompanying Article 5.8.2.3 elaborates: "The reduced prestress in the transfer length reduces $V_p$, $f_{pc}$, and $f_{pe}$. The transfer length influences the tensile force that can be resisted by the tendons at the inside edge of the bearing area." In short, this article reminds the practitioner that a proper estimate of the actual effective prestress value at the section under consideration should be used when calculating the shear and torsional resistance according to the provisions of the AASHTO LRFD specification. The final sentence of the article commentary indicates that the appropriate value of developed prestress should be used in calculating the required amount of longitudinal (bottom chord) reinforcement required at the inside edge of the bearing area at simple end supports (Article 5.8.3.5). No comparable provision exists for prestressing reinforcement in the ACI Code or the AASHTO Standard Specification.

### 2.3.2 Background Research

The existing code provisions for the development length of fully bonded pretensioned strands are based on the results of two studies conducted in the Research and Development Laboratories of the Portland Cement Association (PCA) in the late 1950s and early 1960s. The results of these studies are reported in papers by Hanson and Kaar (1959) and by Kaar, LaFraugh, and Mass (1963). These research studies are summarized in this section. Because Hanson and Kaar rely heavily upon the bond theory espoused by Janney (1954), his study is also presented here.

#### *2.3.2.1 Janney (1954)*

Janney reports the results of a study investigating the transfer bond and flexural bond behavior of specimens pretensioned with wires or strands. Although only a few of the test specimens contained seven-wire strand, some of the theoretical hypotheses are quite relevant. First, Janney uses an elastic, thick-walled cylinder analysis to predict the concrete stresses surrounding the tendon transfer length. Assuming elastic properties characteristic of materials in use at the time, Janney calculates that, if the concrete behaves elastically, maximum radial compressive stresses and circumferential (hoop) tensile stresses on the order of 3300 psi (23 MPa) would result from a prestress of 120 ksi (825 MPa). Because these circumferential tensile stresses far exceed the tensile capacity of the concrete, it can be assumed that the concrete behaves inelastically along almost the entire transfer length. Repeating this analysis with an initial prestress level and material properties characteristic of those found in modern pretensioned structures, the elastic thick-walled cylinder analysis predicts circumferential stress levels ranging from 6000 psi (41 MPa) for NSC ( $E_c \approx 4000$ ksi [28 GPa]) to 10,000 psi (69 MPa) for HSC ( $E_c \approx 7000$ ksi [48 GPa]). Hence, inelastic behavior along most of the transfer length is to be expected.

Janney also contributes the theory that general bond slip, defined as slip along the entire bonded length of strand, occurs when the "wave" of maximum flexural bond stress overlaps the region of prestress transfer bond, i.e. the transfer length. Because flexural bond stresses are largest on either side of flexural cracks, this wave of maximum flexural bond stress progresses ahead of flexural cracking. As the load is increased, the wave travels from the point of maximum moment toward the support regions for simply supported beams. The high levels of steel stress induced by cracking cause the strand diameter to contract. When the wave overlaps the transfer bond region, this contraction counteracts the prestress transfer bond that results from the Hoyer Effect, resulting in general bond slip. This theory is further discussed in Section 2.5 below.

Janney's experimental results indicate that both transfer and flexural bond behavior improve with surface roughness. In addition, transfer lengths appear to have decreased slightly with increasing concrete strength.

#### *2.3.2.2 Hanson and Kaar (1959)*

This study consisted of an investigation of flexural bond in beams pretensioned with seven-wire strand of ¼, ⅜, and ½ in (6.4, 9.5, and 12.7 mm) diameter. In all, 47 simply-supported, pretensioned beam specimens were tested to

failure. The general procedure consisted of evaluating the moments that resulted in initial strand end slip and in ultimate strength of each specimen. The embedment length of strand (the bonded length of strand beyond the critical section) and the strand diameter were the principal variables studied. Other variables included strand surface condition, reinforcement percentage, and concrete strength.

The beam specimens had rectangular cross sections featuring widths ranging from 4 to 8 in (102 to 203 mm) and reinforcement depths of 5.5 to 11.5 in (140 to 292 mm). The span-to-depth ratios, cross section dimensions, and prestress amounts were such that diagonal shear cracking should not have occurred. None was reported. Several types of prestressing steel were used. Although the ultimate strength of each type of strand appeared to be in excess of 250 ksi (1725 MPa), a variety of stress-strain curves were exhibited. The Grade 270, low-relaxation steel prevalent in current practice was not used.

Hanson and Kaar calculated the average bond stress over the *entire* embedment length (including the transfer length) at both general bond slip and ultimate load. General bond slip was evidenced by slip of the strand end relative to the beam end. Using these average bond stress values, they concluded that the average bond stress occurring just prior to general bond slip decreases with increasing embedment length. Using the experimentally determined values of average bond stress at general bond slip, a chart was developed to predict the strand embedment length required to prevent general bond slip at a particular steel stress for the three strand sizes tested. The chart is applicable only to strand initially tensioned to 150 ksi (1035 MPa) and embedded in concrete with a compressive strength of approximately 5500 psi (38 MPa). For an ultimate steel stress of 250 ksi (1725 MPa), the chart predicts that embedment lengths of $200d_b$ for ¼ in strand and $250d_b$ for ⅜ and ½ in strand are required to prevent general bond slip. Due to a lack of research regarding the influence of repeated loads, prevention of general bond slip is the recommended criterion for adequate anchorage. Thus, using the design procedure recommended by Hanson and Kaar, these values represent the development length required for strands under the given conditions.

In addition, Hanson and Kaar conclude that rusting of strand increases the moment at general bond slip on average, although one specimen showed no significant improvement when compared to a companion specimen with clean strand. They also conclude that, due to mechanical bond resistance, seven-wire strand develops additional beam strength even after general bond slip.

Hanson and Kaar assert that the results of the 47 beam tests support Janney's (1954) flexural bond wave theory, confirming that general bond slip occurs when the peak of the flexural bond stress wave reaches the transfer zone.

#### *2.3.2.3 Kaar, LaFraugh, and Mass (1963)*

This study focused on transfer lengths and the influence of concrete strength. Thirty-six rectangular prisms were tested, resulting in a total of 72 transfer lengths. The 36 transfer lengths reported represent averages of two companion transfer lengths. Concrete compressive strengths varied from 1660 to 5000 psi (11 to 34 MPa) at the time of prestress transfer. One mix design was used for all specimens; the strengths at transfer were varied from specimen to specimen by releasing the prestress at ages varying from one to thirty days. Strands of ¼, ⅜, ½, and 0.6-in (6.4, 9.5, 12.7, and 15.2 mm) diameter were employed. Prestress levels immediately after transfer, $f_{pi}$, ranged from 146 to 180 ksi (1010 to 1240 MPa). Transfer lengths were evaluated by means of concrete surface strain measurements performed with a Whittemore mechanical strain gauge. In an effort to evaluate the effect of time on transfer length, measurements were performed at ten ages ranging from immediately after transfer to one year.

No systematic variation of transfer length with concrete strength was found for strand diameters up to ½ in. Transfer lengths appeared to decrease with increasing concrete strength for the 0.6 in strands. Transfer lengths increased an average of six percent over the course of a year; all increases were less than twenty percent. The transfer lengths measured at the end of the specimen where the strands were cut averaged about twenty to thirty percent higher than those at the dead end of the specimen. The transfer length was found to be roughly proportional to the strand diameter for all strands except the 0.6 in strands. The 0.6 in strands exhibited transfer lengths shorter than would be expected if the transfer length were proportional to the diameter. This disparity was attributed to slight surface weathering of the 0.6 in strands in transit.

### 2.3.3 Evolution of Development Length Expression

Although the experimental results of these PCA studies were used to create the code development length expression, nothing resembling this expression is included in the reports from either study. Tabatabai and Dickson (1995) describe how the ACI Prestressed Concrete Committee transformed the research results into the development length

expression given in Section 2.3.1 above. Preliminary relationships for the transfer length, the flexural bond length, and the development length were prepared by Alan H. Mattock. The full committee then modified Mattock's recommended development length expression to arrive at the $\left( f_{ps} - \frac{2}{3} f_{pe} \right) d_b$ expression first published in the 1963 ACI 318 Building Code.

Mattock's proposed expression for transfer length is exactly that still found in Commentary Section R12.9: $\frac{f_{pe}}{3} d_b$. Mattock derived this expression from the results of the PCA tests summarized above and data from tests performed on eight specimens for the American Association of Railroads. These data, included in the Tabatabai and Dickson (1995) paper, do not differ significantly from the Kaar, LaFraugh, and Mass (1964) data, except that transfer lengths were only measured immediately after transfer. Hanson and Kaar (1959) did not publish transfer length measurements, but stated that the average transfer bond stress, $\overline{u}_t$, was assumed to be 400 psi (2.76 MPa) based on tests performed previously at PCA. In deriving his expression, Mattock adopted this value of average transfer bond stress.

Mattock used the following equilibrium relationship to derive the transfer length expression:

**Equation 2.1** $$\overline{u}_t l_t \Sigma o = A_{ps} f_{pe}$$

where

$\overline{u}_t$ = average transfer bond stress = 400 psi (2.76 MPa)

$l_t$ = transfer length

$\Sigma o$ = strand perimeter = $\frac{4}{3} \pi d_b$

$A_{ps}$ = strand cross-sectional area = $0.725 \frac{\pi d_b^2}{4}$

$d_b$ = nominal strand diameter

$f_{se}$ = effective strand prestress

The left-hand side of the equation represents the total force between the concrete and the steel along the surface of the strand in the transfer length. The right-hand side represents the total force in the strand at the end of the transfer length. Static equilibrium of the free body consisting of the transfer length of strand requires that the two sides of the expression be equal. Solving the equation for the transfer length yields the expression found in the ACI Commentary Section R12.9:

**Equation 2.2** $$l_t = 0.34 \text{ ksi}^{-1} f_{pe} d_b \approx \frac{f_{pe} d_b}{3 \text{ ksi}}$$

Tabatabai and Dickson (1995) also report that the following statement was included in a draft of the proposed code revisions regarding anchorage for ACI 318-63:

> For steel with a clean surface, released gently to a stress of 150 ksi, the prestress at the centroid of the member cross section may be assumed to vary linearly from zero at the face of the member to a maximum at a distance from the end face equal to 50 diameters for strand and 100 diameters for single wire.

They theorize that this is likely the source of the transfer length value of 50 strand diameters found in Section 11.4.3 of the Code shear provisions. However, this section allows the use of $50 d_b$ regardless of the amount of prestress, the strand surface condition, or the method of prestress release. Current practice involves prestress values considerably higher than 150 ksi (1035 MPa) after release.

The method Mattock employed to arrive at an expression for flexural bond length was somewhat more complex. In reporting the results of their study on flexural bond, Hanson and Kaar (1959) do not conclude that a limiting value of average flexural bond stress results in either general bond slip or maximum moment resistance. Rather, they agree

with Janney (1954) that general bond slip is caused when the peak of the high bond stress wave reaches the prestress transfer zone. The resulting decrease in strand diameter reduces the frictional resistance due to the Hoyer Effect, and general bond slip occurs.

Apparently, Mattock and/or the members of the Prestressed Concrete Committee found this concept difficult to codify, so an average flexural bond stress approach was formulated based on a reappraisal of the Hanson and Kaar data. Using data obtained from some of Hanson and Kaar's beam tests, Mattock constructed a straight-line relationship between the flexural bond length available in each specimen (normalized in terms of strand diameter) and the increase in strand stress due to flexure at the critical section 1) when general bond slip occurred and 2) at ultimate. The available flexural bond length was calculated by subtracting the estimated transfer length from the embedment length of strand. The increase in strand stress due to flexure at general bond slip was calculated by subtracting the effective prestress value from the value of strand stress occurring at the load causing slip. The increase in strand stress due to flexure at ultimate was calculated in a similar manner. Mattock stated that the straight-line relationship developed "appears to be a reasonable mean line for the points representing general bond slip…." Mattock's relationship to avoid bond slip is represented by Equation 2.3:

**Equation 2.3**
$$f_{ps} - f_{pe} \le 0.9\left(\frac{l_e - l_t}{d_b}\right) \text{ksi}$$

where

$f_{ps}$ = strand stress at ultimate strength

$l_e$ = embedment length of strand beyond critical section

Or, if the flexural bond length necessary to prevent bond slip is desired, Equation 2.3 may be solved for $l_{fb}$:

**Equation 2.4**
$$l_{fb} = \frac{(f_{ps} - f_{pe})d_b}{0.9 \text{ ksi}}$$

Assuming Mattock's estimate of the transfer length is correct, these relationships are conservative with respect to general bond slip for eleven of the twenty specimens considered. They are unconservative for nine of the specimens. Thus, as inferred by Mattock, Equation 2.4 represents the *average* flexural bond length required to prevent general bond slip, rather than a conservative value.

Prior to finalization of the 1963 Code, the expression for flexural bond length was altered, resulting in the expression shown as Equation 2.5:

**Equation 2.5**
$$l_{fb} = (f_{ps} - f_{pe})d_b \text{ ksi}^{-1}$$

Thus, the resulting expression, which underestimates the flexural bond length at general bond slip for ten of the twenty specimens considered, is even less conservative than that proposed by Mattock.

The final expression for development length was obtained by adding the expressions for transfer length (Equation 2.2) and flexural bond length (Equation 2.5). The relationship still found in the present code results:

$$l_d = l_t + l_{fb} = \frac{f_{pe}}{3} d_b + (f_{ps} - f_{pe})d_b = (f_{ps} - \frac{2}{3} f_{pe})d_b$$

### 2.3.4 Inadequacy of Existing Code Expression for Development Length

This section consists of a discussion of the problems inherent in the existing code expression for the development length of prestressing strand. The discussion is subdivided into two parts. The first part addresses the discrepancies between the adopted expression and the research results from which it evolved. Potential deficiencies arising from changes in materials and design practice over the past four decades are taken up in the second part.

#### *2.3.4.1 Discrepancies with Results of Background Research*

Consider the current development length expression in comparison with the design recommendations made by Hanson and Kaar (1959). Both design approaches were developed with the goal of preventing general bond slip

prior to reaching the nominal flexural strength of the member. A comparison can be made between the development lengths predicted by the two methods for a beam typical of the practice at the time. For this example, a steel stress at nominal strength, $f_{ps}$, of 230 ksi (1585 MPa) is assumed. The strands are initially tensioned to a stress of 150 ksi (1035 MPa). A value of effective prestress after losses, $f_{pe}$, of 132 ksi (910 MPa) is assumed. For ½ in (12.7 mm) diameter strands embedded in 5500 psi (38 MPa) concrete, Hanson and Kaar recommend a development length, $l_d$, of 104 in (2.64 m). Application of the code expression results in $(f_{ps} - \frac{2}{3} f_{pe})d_b = 142 d_b$ = 71 in (1.8 m). Examination of Hanson and Kaar's experimental results indicates that the actual embedment length required to prevent general bond slip in a specimen with these properties lay somewhere between 77 and 90 in (1.96 and 2.29 m). Thus, the development length resulting from the code expression appears to be ten to twenty percent shorter than that actually required to prevent general bond slip. Hanson and Kaar's more conservative method results in a development length fifteen to thirty-five percent longer than required. Why do the two methods, ostensibly derived from the same body of experimental results, arrive at markedly different development length values with opposite implications with regard to safety?

One fault with the code expression is that it does not reflect the significant dispersion evident in the data from the PCA studies. At every step in the evolution of the expression, attention was focused on the average, rather than extreme, behavior (Tabatabai and Dickson 1995). While the average initial transfer bond stress value of 400 psi (2.76 MPa) selected by Mattock is not unreasonable when compared with the PCA results, more detailed analysis shows that the average bond stresses obtained from these tests featured a coefficient of variation of approximately 27 percent. Approximately thirty percent of Kaar, LaFraugh, and Mass's (1964) reported results yield initial transfer bond stresses less than 300 psi![3] With dispersion such as this, the common occurrence of transfer lengths significantly longer than those predicted by Mattock's transfer length expression should be expected.

Dependence on average performance without due consideration of extreme behavior results in poor design practice with regard to safety. Contrast the philosophy used to formulate the strand development equation with that employed in the evolution of the development length provisions for deformed reinforcing steel. Although the bond stress relationship used to formulate the relevant expressions for reinforcing steel is based on average behavior, the final expressions incorporate the influence of a 0.8 reduction factor to reflect the dispersion in the background data. The use of this "hidden" resistance factor results in provisions that safely bound the test data (Orangun, Jirsa, and Breen 1977).

The average transfer bond stress value of 400 psi used by Mattock is representative of the average performance of the PCA tests when the equilibrium relationship given in Equation 2.1 above is solved using the prestress immediately after transfer ($f_{pi}$). However, when incorporated into the code expression, the effective prestress value after all losses ($f_{pe}$) is used. The use of $f_{pe}$ implies that the transfer length decreases as the steel stress decreases due to time-dependent losses. The results reported by Kaar, LaFraugh, and Mass (1964) show that the opposite is true. Transfer length tends to *increase* slightly with time. Thus, the inaccuracy of the $\frac{f_{pe}}{3} d_b$ expression for the transfer length increases as time-dependent losses accumulate.

The inability of the $\frac{f_{pe}}{3} d_b$ expression to safely bound the long-term transfer lengths reported by Kaar, LaFraugh, and Mass is demonstrated in Figure 2.2 and Figure 2.3. Figure 2.2 is a histogram representing the ratios obtained when dividing each of the long-term transfer lengths obtained in the PCA study ($l_{t,test}$) by the transfer length calculated by means of the $\frac{f_{pe}}{3} d_b$ expression ($l_{t,calc}$). In order to estimate the value of $f_{pe}$ corresponding to the test results taken at 365 days, a reduction of twenty percent was taken from the reported values of prestress immediately after transfer ($f_{pi}$). This estimation seems reasonable in light of the concrete strains reported at 56 days for one of the specimens. The histogram shows that the measured long-term transfer lengths were, on average, more than 50 percent longer than those predicted by the $\frac{f_{pe}}{3} d_b$ expression. This expression underestimates the long-term transfer length for more than 90 percent of the reported values!

[3] Each of these reported results represents the average of two transfer lengths taken from companion specimens. Thus, the actual coefficient of variation of all the measured transfer lengths is likely larger than that reported here.

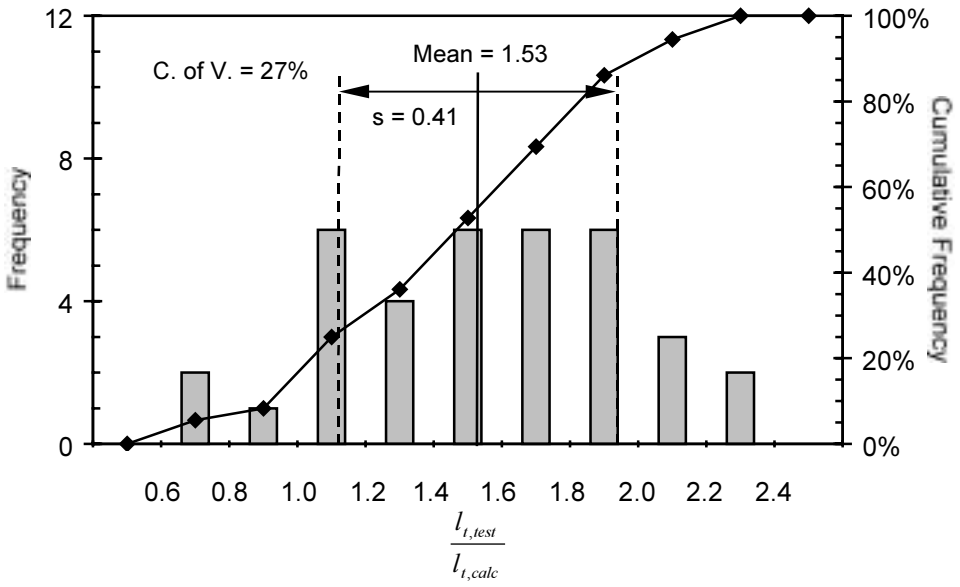


**Figure 2.2: Histogram—Ratios of Long-Term $l_t$ Values Obtained by Kaar, LaFraugh, and Mass to $l_{t,calc}$ from ACI 318 Commentary ($\frac{f_{pe}}{3} d_b$)**

Similar results are obtained from the $50d_b$ expression for transfer length found in the shear provisions of the ACI Code and AASHTO Standard Specification. Figure 2.3 displays these results. For the specimens tested, the $50d_b$ expression gives slightly more conservative results than the $\frac{f_{pe}}{3} d_b$ expression because the $f_{pe}$ values were less than 150 ksi (1035 MPa). Still, transfer lengths were underestimated for 80 percent of the reported results.

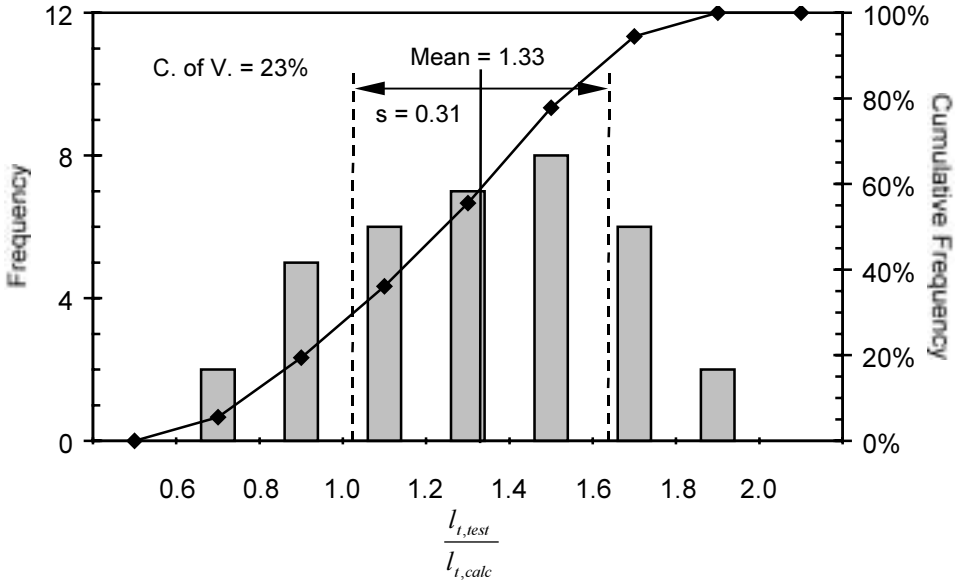


**Figure 2.3: Histogram—Ratios of Long-Term $l_t$ Values Obtained by Kaar, LaFraugh, and Mass to $l_{t,calc}$ from ACI 318 Shear Provisions ($50d_b$)**

Figure 2.4 represents a comparison of the reported long-term transfer lengths to the expression $l_{t,calc} = 0.55 f_{pt} d_b$. Rather than including the prestress value after losses, this expression depends on the prestress immediately after transfer. Thus, the magnitude of the predicted transfer length does not decrease with the age of the specimen. The coefficient of 0.55 is used to obtain an expression that only underestimates the transfer length for about five percent of the reported results. The average value of $\frac{l_{t,test}}{f_{pt} d_b}$ is 0.41 for the PCA data.

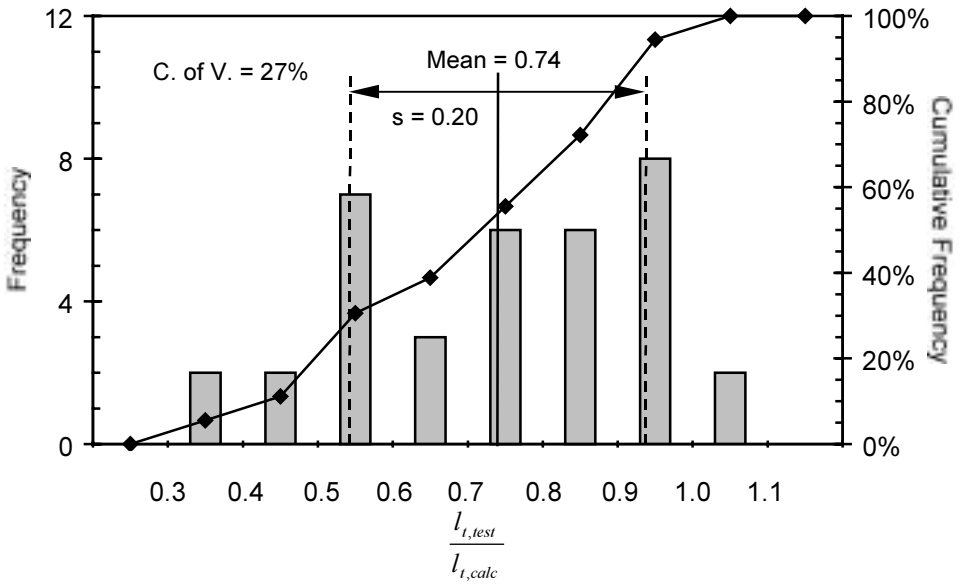


**Figure 2.4: Histogram—Ratios of Long-Term $l_t$ Values Obtained by Kaar, LaFraugh, and Mass to $l_{t,calc} = 0.55 f_{pt} d_b$**

As discussed in Section 2.3.3, the chosen expression for flexural bond length also represents average behavior without consideration of the dispersion of the test data. The $l_{fb} = (f_{ps} - f_{pe}) d_b$ expression is only conservative with regard to general bond slip for ten of the twenty specimens considered. The expression $l_{fb} = 1.7(f_{ps} - f_{pe}) d_b$ is conservative with regard to general bond slip for about ninety percent of the tests considered. On the other hand, the expression $l_{fb} = 1.25(f_{ps} - f_{pe}) d_b$ is conservative with respect to general bond slip for about two-thirds of the specimens, and is conservative with respect to development of nominal flexural strength for 95 percent of the specimens.

Thus, the relationships for both transfer length and flexural bond length that are incorporated in the code development length expression are unconservative for a large portion of the test results from which they were derived. In addition, the technique of using a limiting uniform flexural bond stress to predict the flexural bond length necessary to prevent general bond slip does not completely agree with the findings of the PCA researchers (Janney 1954; Hanson and Kaar 1959). The researchers theorized that general bond slip was initiated by large magnitudes of bond stress (and the accompanying large gradients of steel stress) occurring near or in the prestress transfer region. Mattock's approach, on the other hand, depends upon a relatively uniform average bond stress along the entire flexural bond length. This assumption is adequate for assessing the bond capacity of deformed reinforcing bars because a small amount of slip tends to distribute bond resistance somewhat evenly among the deformations within the development length. However, when general bond slip is the specified failure criterion, as has been the case historically with prestressing strand, the assumption of a uniform distribution of bond stress at failure may be unrealistic.

#### *2.3.4.2 Inadequacies Due to Evolving Materials and Design Practice*

In the years since the development length equation was first codified, changing material properties and design practice have brought other potential shortcomings to light. The tendons originally investigated consisted of stress-relieved strand with a guaranteed ultimate strength of 250 ksi (1725 MPa). Present practice dictates the almost exclusive use of low relaxation strand featuring ultimate strengths of at least 270 ksi (1860 MPa). In addition to the higher levels of effective prestress and ultimate stress that result, the newer strands feature a ratio of cross-sectional area to perimeter about six to seven percent larger than that of the strand used in the PCA research. Thus, the bond stress necessary to develop a given strand stress is accordingly larger. As discussed in Chapter 1, the use of 0.6 in (15.2 mm) strand is increasingly desired, and strands of this size were not included in the study reported by Hanson and Kaar (1959).

Likewise, the concrete compressive strengths employed in the PCA tests do not approach the strengths now possible. In 1949, Freyssinet wrote:

> [Transfer] bond stress can only attain a certain maximum value which depends on the friction and on the maximum pressure which the concrete can exert on the wire; this maximum pressure depends on the tensile strength and on the hardness of the concrete surrounding the wire. The performance of a bond anchorage therefore depends upon the quality of the concrete (Guyon 1953).

In tests on concrete specimens with concrete compressive strengths ranging from 2800 to 7000 psi (20 to 50 MPa) at release, Ratz, Holmjanski, and Kolner (1958) found that transfer bond "depends to a high degree upon the strength of the concrete." Rüsch and Rehm (1963) observed that transfer lengths decreased with increasing concrete strength, but with considerable scatter in the data. Tests performed at the Ferguson Structural Engineering Laboratory indicated that transfer lengths in HSC specimens tend to be smaller than in NSC specimens (Castrodale, Kreger, and Burns 1988a). Based on experimental results, Mitchell et al. (1993) proposed expressions for transfer length and development length that include the influence of concrete strength.

Russell and Burns (1993) found that the shear cracking in or near the prestress transfer zone can lead to bond failure. Just as the wave of high bond stresses associated with flexural cracks can lead to the initiation of general bond slip, so can the bond stresses acting on either side of shear cracks. If general bond slip occurs in a transfer bond region that is subject to high shear forces, the shear resistance mechanism can be compromised, resulting in a premature shear failure. This mode of failure is independent of the flexural bond stress approach incorporated in the code expression of development length. Thus, the expression is inadequate with respect to this type of failure.

## 2.4 TRANSFER BOND THEORY

Upon detensioning of the pretensioned tendons at the ends of members, the tendons shorten and slip relative to the surrounding concrete along a finite length at either end. Bond stresses develop between the tendon and the concrete along this transfer length, resulting in a buildup of concrete compressive stress parallel to the axis of the tendon. After release, there is no axial stress in the tendon at the free end. At the other end of the transfer length, sometimes referred to as the "attack" or "front" end, the stress in the tendon reaches a value of prestress that is constant (aside from the influence of weight-induced stresses) over the entire length between transfer lengths. The integrity of the prestressed member depends upon the anchorage of the tendon(s) within the transfer length. This section consists of a discussion of the various mechanisms and influences at work along the transfer length.

### 2.4.1 Transfer Bond Stress

Consider the infinitesimally small length, $dx$, of reinforcement embedded in concrete shown in Figure 2.5. Equilibrium along the axis of the tendon requires:

$$T + dT = T + u dx \Sigma o$$

where

$T$ = tendon force = $A_{ps} f_t$

$u$ = bond stress

$\Sigma o$ = tendon perimeter

Solving for the bond stress results in the following:

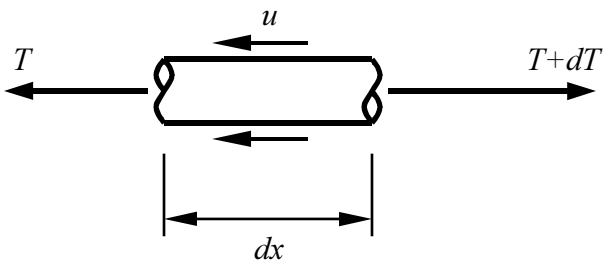


**Figure 2.5: Reinforcement Subject to Tensile Force and Bond Stress**

**Equation 2.6**

$$u = \frac{1}{\Sigma o}\frac{dT}{dx} = \frac{A_{ps}}{\Sigma o}\frac{df_p}{dx}$$

which indicates that the bond stress is proportional to the rate of change of the tendon tension force and the tendon stress. In other words, the bond stress is proportional to the tendon stress gradient.

If the relationship between bond stress and tendon stress is extended over a finite length, $l$, an expression for average bond stress, $\overline{u}$ , results:

**Equation 2.7**

$$\overline{u} = \frac{A_{ps}}{\Sigma o}\frac{\Delta f_p}{l}$$

Over the transfer length, $l_t$, the total change in prestress immediately following transfer is $f_{pt}$. The average transfer bond stress, $\overline{u}_t$ , is given by:

**Equation 2.8**

$$\overline{u}_t = \frac{A_{ps}}{\Sigma o}\frac{f_{pt}}{l_t}$$

Accordingly, the transfer length can be written in terms of the average transfer bond stress:

**Equation 2.9**

$$l_t = \frac{A_{ps}}{\Sigma o}\frac{f_{pt}}{\overline{u}_t}$$

### 2.4.2 Mechanisms

The various mechanisms that potentially contribute to prestress transfer bond have been categorized and described in a variety of ways. Three general groups of mechanisms can be identified: adhesion, friction, and mechanical resistance (Janney 1954; Hanson and Kaar 1959). Adhesion plays a minimal role in the development of transfer bond stresses because the relative slip of the tendon with respect to the surrounding concrete destroys the adhesion between the two materials.

Because of the sliding action of the tendon along the transfer length, friction plays a significant role in the development of transfer bond stresses. In order to develop frictional bond stresses, radial compressive stresses are required. The development of these radial compressive stresses has been attributed to a number of mechanisms. The most well known is the "Hoyer Effect," described in Section 2.2.2 above, where the longitudinal contraction results in a radial expansion of the tendon. This Poisson expansion induces compression perpendicular to the steel-concrete interface. Stocker and Sozen (1970) have also attributed radial compressive stresses to a "lack of fit" mechanism. This theory holds that small changes in the tendon cross-section cause a wedging action upon movement of the tendon relative to the concrete. Evans (1951) cites the frictional influence of small particles that break free from the concrete upon slip and wedge between the tendon and the concrete. Shrinkage of the surrounding concrete can also contribute to the radial compressive stresses that induce frictional resistance.

Mechanical resistance, or "interlock," stems from the axial component of bearing stress existing between the tendon and the surrounding concrete that results from the helical shape of the seven-wire strand. Because the free end of

the strand is unrestrained against twist, the resistance of the strand to "unwinding" is small (Stocker and Sozen 1970). However, Russell and Burns (1993a) theorize that once the strand near the free end is restrained by bond resulting from the other mechanisms, particularly the Hoyer Effect, mechanical interlock can add significantly to the bond stress along the transfer length. The radial component of the bearing stress between the concrete and steel also contributes to the development of frictional bond stresses.

As discussed in Section 2.3.2.1 above, the circumferential concrete tensile stresses resulting from the Hoyer Effect are such that inelastic concrete response, characterized by limited radial cracking of the concrete adjacent to the strand, should be prevalent throughout almost the entire transfer length. Only in a small region adjacent to the attack end of the transfer length are the stresses small enough that elastic behavior is expected. For this reason, Hoyer's model of bond stresses that increase exponentially from the attack end to the free end of the transfer length is invalid. In the portions of the transfer length where the strand expansion is greatest (near the free end), the inelastic deformations of the surrounding concrete will result in concrete response that is less stiff than in the regions where the strand expansion and resulting concrete deformation are more limited.

The relationship between the strand expansion and the resulting radial compressive stresses can be thought of as a spring system in which the spring represents the response of the surrounding concrete. When pushed beyond its elastic limit, the spring exhibits a stiffness that decreases with increasing deformation. Thus, in the inelastic region, the spring force (radial compressive stress) produced by large deformations (tendon expansion) is moderated by an associated decrease in spring stiffness (cracking of concrete). The magnitude of radial compressive stress may remain relatively uniform along the transfer length, despite the difference in radial deformations. Since friction stresses are typically proportional to the corresponding normal stresses on the interface, frictional bond stresses might be expected to remain relatively uniform along most of the transfer length. The predominately linear nature of prestress increase within the transfer zone seen in most experimental transfer length studies supports the contention that the transfer bond stress is relatively uniform.

### 2.4.3 Influence of Concrete Strength

Studies indicating the influence of concrete strength on transfer bond behavior are cited in Section 2.3.4.2 above. This section includes a discussion of the reasons one might expect concrete strength to affect the transfer length.

As discussed above, the concrete surrounding the tendon transfer length may be separated into two behavioral zones: the zone of elastic response, which lies adjacent to the attack end of the transfer length where the stresses generated from the Hoyer Effect are relatively small; and the zone of inelastic response, which exists along the vast majority of the transfer length where the stresses exceed the elastic capacity of the concrete. An elastic, thick-walled cylinder analysis indicates that the zone of inelastic response occupies approximately 90 to 95 percent of the transfer length for common prestressing materials and practice.[4]

In the zone of elastic behavior, the radial compressive stress and resulting frictional bond stress are almost directly proportional to the change in steel stress and the elastic modulus, $E_c$, of the surrounding concrete. In the inelastic zone, the radial compressive stress depends directly upon the response of the concrete to the radial expansion of the tendon. Since the concrete response is softened by the radial cracking in this region, the stiffness of the system depends both the tensile capacity of the concrete and $E_c$.

Hence, along the entire transfer length, the radial compressive stresses and the resulting frictional stresses depend upon either the tensile capacity of the concrete, the elastic modulus of the concrete, or both. Standard North American design practice holds that both the stiffness and tensile capacity of normal-weight concrete are proportional to the square root of the concrete compressive strength. In accordance with this line of reasoning, the average bond stress along the transfer length can be characterized as proportional to the square root of the concrete compressive strength. Combination of this relationship with Equation 2.9 results in the following hypothetical relationship between transfer length and concrete strength:

$$l_t \propto \frac{1}{\sqrt{f'_c}}$$

[4] $n = \frac{E_p}{E_c}$ = 4 to 7; $f_{pt}$ = 180 to 200 ksi (1240 to 1380 MPa); $E_p \approx 57000\sqrt{f'_c}$; $f_{ct} \approx 6.7\sqrt{f'_c}$

If the tensile strength of the concrete is too small in relation to the induced stresses, splitting failure may occur in the concrete between adjacent strands or in the cover between strands and the surface of the member. This mode of anchorage failure becomes more likely with the reduction of strand spacing or cover (thereby reducing the size of the concrete cylinder that resists the circumferential tensile stresses) and the increase of prestress force. Accordingly, it is important to experimentally verify that the cover and clear spacing between strands are adequate to prevent anchorage failure for the range of practical concrete strengths.

### 2.4.4 Time-Dependent Effects

Various research studies have indicated that prestress transfer length increases with time. Evans (1951) reports that the transfer length of 0.08 in (2 mm) diameter wire nearly doubled in 2.5 years. Wire-reinforced specimens tested by Base (1957) exhibited transfer length increases of up to ten percent in four months, with almost all change occurring in the first ten to twenty days. Base also reports transfer length increases for 0.2 in (5 mm) wire that ranged from 0 to 3 in (0 to 76 mm) within the first ten days, with no change occurring thereafter. As discussed in Section 2.3.2.3, Kaar, LaFraugh, and Mass (1964) found increases of up to twenty percent for specimens prestressed with seven-wire strand. The average increase over one year was six percent. Bruce, Russell, Roller, and Martin (1994) report increases of approximately ten percent over the first 28 days for full-size members constructed with HSC. Lane (1992; 1998) reports "no pattern to the values for percentage change in transfer length" up to an age of 365 days for rectangular, concentrically prestressed specimens. However, beam specimens in the same study experienced increases of thirty percent in the first 28 days and seven percent thereafter. Logan (1997) reports growth of measured draw-in values for "poor bond quality" strands of up to 66 percent in 21 days. "High bond quality" strands also displayed significant growth of measured draw-in.[5]

The increase of transfer length with time is most likely attributable to the inelastic behavior of the concrete surrounding the transfer length. Although the tendon stress tends to decrease over time with the accumulation of time-dependent losses due to creep, shrinkage, and relaxation, the inelastic response of the concrete largely prevents the recovery of these stresses. Because the concrete is stressed beyond the elastic limit in tension, some continued softening of the concrete "grip" on the tendon is possible due to stable radial crack growth and stress redistribution over time. This is a likely source of the "bond creep" phenomenon that causes transfer length growth. Shrinkage of the concrete surrounding the strand might provide some additional radial compressive stress and bond resistance over time, but this beneficial effect may be hampered due to the cracked nature of the concrete along much of the transfer length.

### 2.4.5 Other Considerations

Numerous other factors have been cited as affecting transfer bond behavior. Several are discussed in this section.

#### *2.4.5.1 Concrete Quality and Placement*

Most researchers and practitioners would agree that proper concrete placement and consolidation is vital to the effectiveness of prestress transfer bond. Evans (1951) reports that a delay in concrete placement at one end of a test specimen resulted in an excessive value of transfer length. Anderson and Anderson (1976) state that the "primary cause of excessive free end slip and premature flexural bond failure in prestressed members is poor consolidation of concrete around the strands." Unfortunately, the quality of concrete placement and consolidation is difficult to quantify. Particular attention should be paid to the workability of concrete used for pretensioned applications. Diligence with regard to this topic is critical when fabricating members with HSC.

The significant in-study dispersion of transfer length results evident from studies like that of Kaar, LaFraugh, and Mass (1964) is at least partially attributable to the role that the concrete plays in the development of prestress transfer bond. Aside from the inconsistencies that may result from minor differences in concrete consolidation, the dependence upon inelastic concrete behavior results in significant variability.

One phenomenon associated with concrete placement that has received little research effort with respect to pretensioned members is the well-known "top bar effect" exhibited by mild reinforcing steel. Bars located near the top of a member (in the casting position) tend to exhibit decreased bond stress capacity relative to those located near

[5] The issue of strand bond quality is addressed in Chapter 4 of this report. A discussion of the relationship between measured draw-in and transfer length is included in Chapter 6.

the bottom of the member. This has been attributed to the settlement of concrete beneath the top bars during consolidation. The resulting settlement results in a slightly looser fit between the steel and concrete than occurs in the bottom bars.

Base (1958a) reports that transfer lengths of wires at the top of members during casting had significantly longer transfer lengths than wires at the bottom. Stocker and Sozen (1970) propose that anchorage length be increased as much as 40 percent for strands with 12 in (305 mm) or more concrete cast beneath them. Accordingly, the CEB-FIP Model Code 1990 specifies an increase in transfer length of approximately 40 percent for top strands. The ACI and AASHTO provisions include an increase of 30 percent for the development length of deformed reinforcing bars cast more than 12 in (305 mm) above the bottom of the member, but no similar consideration is included for prestressing strand.

#### *2.4.5.2 Tendon Characteristics*

It is generally accepted that the configuration of the tendon affects the bond behavior. Seven-wire strand exhibits significantly larger bond capacity than straight wire. The helical pattern of the strand is thought to offer mechanical resistance that is unavailable to the straight wire. Similarly, deformations of the tendon surface are also known to improve bond.

The surface condition of the reinforcement also effects the bond behavior. Improved bond performance has been attributed to surface weathering of prestressing strand (ACI 318R-99, R12.9) due to the enhanced frictional resistance offered. Research results have varied. Base (1958a) reports no discernible effect due to pre-rusting of wires. Ban, Muguruma, and Morita (1960) note transfer lengths of rusted strand approximately one-half to two-thirds of those of unrusted strands. Janney (1963) found that rusted strand specimens exhibited transfer lengths about two-thirds of those found in "bright" strand specimens. Hanson (1969) reports a 30 percent improvement with rusted strands. Holmberg and Lindgren (1970) note that "rough" strand resulted in a 40 percent reduction in transfer length. Logan (1997) found no evidence of benefit from the use of weathered strand. Martin and Scott (1976) argue that although rusted strand has produced shorter transfer lengths, it is an "impractical production solution" because the optimum degree of rust is difficult to evaluate. In addition, they state that plants generally use up strand at such a rapid rate that assumption of a certain degree of weathering is unreasonable.

Another issue related to strand surface condition is that of surface contamination. When tensioned prior to casting, strands are especially prone to the accidental application of form oil. The contamination of strands with form oil can significantly degrade the friction that normally develops between the tendon and the concrete, resulting in excessive transfer lengths (Russell and Burns 1993).

Logan (1997) has shown that a significant difference in bond performance exists among the strands produced by various manufacturers. This research involving strand bond quality is discussed more fully in Chapter 4. Rose and Russell (1997) cite the theory that the different drawing lubricants used by various manufacturers lead to different frictional properties of the strand-concrete interface. Wire drawn with water-soluble sodium stearates is thought to have better bond characteristics than wire drawn with non-water-soluble calcium stearates. Another theory holds that the induction heating used for stress relief may burn off less of the residual lubricant than was burned off by the older technique of convection heating. The convection heating may also oxidize impurities on the strand surface, which results in a rougher surface.

#### *2.4.5.3 Method of Prestress Release*

Studies investigating the effect of prestress release method on transfer length have shown that sudden prestress release often results in longer transfer lengths than gradual prestress release (Base 1958a; Kaar, LaFraugh, and Mass 1963; Rüsch and Rehm 1963; Holmberg and Lindgren 1970; Rose and Russell 1997). This phenomenon is generally attributed to the dynamic effects associated with the transfer of energy from the strand to the concrete member. Russell and Burns (1993) indicate that this effect may be more prevalent in small transfer length test specimens than in full-scale members. The CEB-FIP Model Code 1990 specifies an increase in transfer length of 25 percent for member subject to sudden release of prestress.

#### *2.4.5.4 Confining Reinforcement*

The influence of confining reinforcement was investigated by Russell and Burns (1993a). The transverse reinforcement consisted of mild steel hoops that enclosed the entire group of strands in each specimen. No significant influence on transfer length was observed.

The minimal effectiveness of reinforcement that confines the entire group of strands is probably due to its inability to resist the circumferential tensile strains and resulting radial cracks that develop in the concrete between strands. To increase transfer bond stresses effectively, transverse reinforcement would have to be positioned to intersect potential splitting planes between adjacent strands. Maximum efficiency would result from positioning reinforcement immediately adjacent to the strand, where tensile stresses are largest. The large number of strands and relatively small strand spacing characteristic of most pretensioned members precludes the cost-effective use of transverse reinforcement to decrease transfer length.

### 2.4.6 Influence of Cracking

The role of the radial compressive stresses generated at the concrete-steel interface is crucial to development of bond in the transfer length. Frictional bond stresses depend directly on the radial compressive stresses that are present. Cracking that occurs transverse to the tendon axis is extremely detrimental to transfer bond. Such cracking, resulting from the influence of flexure, shear, or torsion, results in a sharp increase in the steel tensile stress that must be developed at the cracked section. This increase in tensile stress reverses the beneficial Hoyer Effect along a length of strand on either side of the crack. The resulting radial contraction of the strand decreases the radial compressive stresses present on the concrete-steel interface. The inelastic state of the concrete surrounding the strand contributes to this decrease in radial compressive stress. Accordingly, the transfer bond stress on the interface decreases, reducing the amount of prestress developed in the strand and transferred to the concrete. Due to this loss of tendon and bond stress, the strand will slip until its resulting radial expansion again produces the bond stresses to equilibrate its axial tension (which has decreased slightly during the process). This slip induces a lengthening of the transfer length.

If the applied load is sustained and the accompanying drop in concrete stresses parallel to the strand is such that additional cracking occurs at proximate sections within the transfer length, the entire process can repeat indefinitely until the bond stresses are inadequate to develop the amount of tendon stress required to resist the applied load. This type of rapidly progressing failure can also result if the applied load increases beyond that which initiates the cracking in the transfer length.

The causative crack need not occur within the transfer length to initiate this process. As long as a crack occurs close enough that its influence—in the form of radial strand contraction—extends into the transfer length, the process may begin. This phenomenon is discussed further in the subsequent section.

Limited transverse cracking due to shrinkage or thermal effects has been known to occur prior to the transfer of prestress. These cracks generally close upon application of the prestress force to the concrete. So long as applied loads are such that these cracks do not reopen, the failure progression will not initiate.

## 2.5 FLEXURAL BOND AND CRACKING

The direct relationship between bond stress and the steel stress gradient was derived in the preceding section. Flexural bond stresses are those stresses generated between the concrete and reinforcement that allow the variation in the steel stress along the tendon length. Prior to cracking, the change in steel stress resulting from external loads is relatively small (usually less than 20 ksi [140 MPa]). Accordingly, the flexural bond stresses present in uncracked concrete are very small (typically less than 20 psi [140 kPa]).

Figure 2.6 depicts a portion of a simply supported beam prior to the application of external loads. For simplicity of discussion, the weight of the beam is neglected. Diagrams of the moment due to applied load, the steel stress, and the bond stress are shown beneath the beam. The magnitudes of the cracking moment, $M_{cr}$, and nominal moment strength, $M_n$, are indicated on the moment diagram. The stress in the prestressed reinforcement increases linearly along the transfer length, $l_t$, of the tendon until the effective prestress value, $f_{pe}$, is reached. Because, there is no applied load, the only bond stresses present are the transfer bond stresses, $u_t$, along the transfer length.

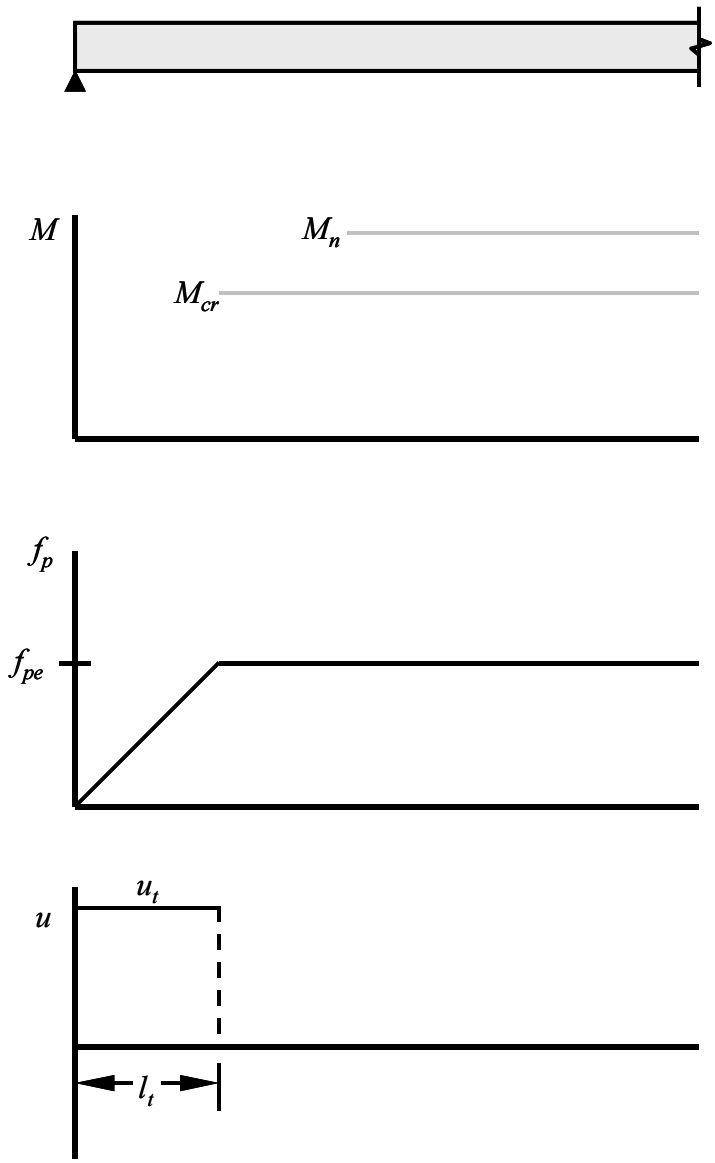


**Figure 2.6: Applied Moment, Steel Stress, and Bond Stress Diagrams for Portion of Simply Supported Beam Prior to Application of Loading**

Figure 2.7 depicts the beam and the associated effects immediately prior to initiation of cracking in the maximum moment region. The beam is loaded symmetrically by two concentrated loads of equal magnitude. Thus, a region of constant moment exists between the loads, and a linear moment gradient occupies the shear span between the support and the nearest applied load.

The cross section is uncracked along the entire span. Because the full cross section resists the applied moment, the steel stress diagram is only slightly altered from its original state. Accordingly, the flexural bond stresses are also quite small. There is no flexural bond stress in the constant moment region because the resulting steel stress is constant.

Once the moment exceeds the cracking moment, cracking occurs in the maximum moment region between the concentrated loads as shown in Figure 2.8. Because the reinforcement must now resist the tension force at the cracks, a pronounced increase in steel stress occurs at these locations. These steel stresses are theoretically equivalent to those calculated by cracked section analysis. Away from the region where the cracking moment is exceeded, the full concrete section is effective in resisting tension, and the stresses in the steel remain small.

Although the average flexural bond stress between cracks in the maximum moment region remains zero, local flexural bond stresses, often referred to as "in and out" bond stresses, are developed between the cracks. The tendon slips relative to the concrete adjacent to the cracks, and these local bond stresses transfer a portion of the tension from the steel into the concrete. Thus, cross sections that lie between cracks are somewhat stiffer than indicated by a cracked section analysis because the concrete shares some of the tensile stress. This effect is commonly known as "tension stiffening." The amount of stress transferred from the steel to the concrete and the resulting magnitude of the tension stiffening effect depend upon the local flexural bond stresses that can be developed.

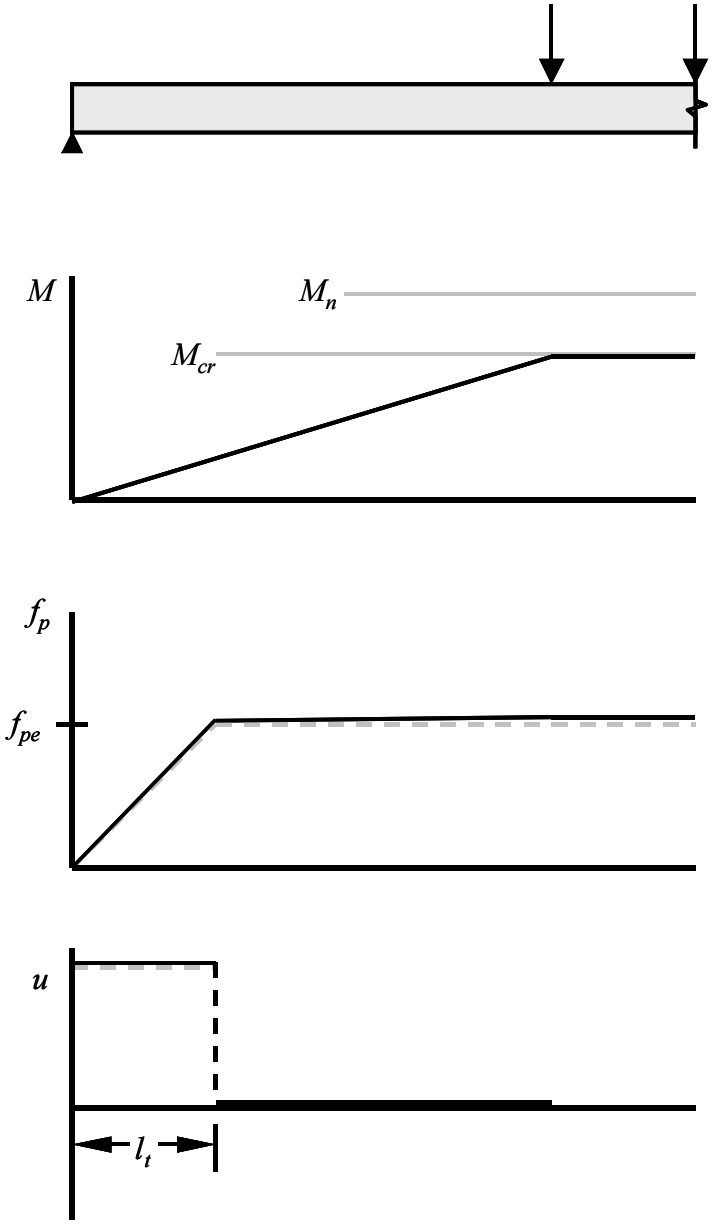


**Figure 2.7: Applied Moment, Steel Stress, and Bond Stress Diagrams for Portion of Simply Supported Beam Immediately Prior to Flexural Cracking**

Similarly, flexural bond stresses are required to develop the significant steel stress increase that occurs at the boundary between cracked and uncracked behavior. The length of strand labeled "Crack Influence Length" in Figure 2.8 lies within the region where the cracking moment is not exceeded. However, significant flexural bond

stresses are required along this length of tendon so that the required steel stress may occur at the cracked section. Thus, this region behaves similarly to the regions between the cracks. On one side, the crack influence length is bounded by the outermost crack. On the other, influence of cracking on the steel stress ceases at the section where relative slip between the tendon and concrete ends and bond stress is equivalent to that required for uncracked section behavior. The total change in tendon stress that occurs over the crack influence length is dictated by the difference between the tendon stress required for the uncracked section to resist the moment at one end and that required for the cracked section to resist the moment at the other. Thus, the length over which the crack influences the steel stress is determined by this difference in tendon stress and the flexural bond stresses that can be developed. Larger flexural bond stress capacities result in smaller crack influence lengths. In the figures that follow, the flexural bond stress capacity is indicated by the peaks of the local bond stress profile. The flexural bond stresses that occur along the crack influence length represent the "flexural bond stress wave" that Janney (1954) and Hanson and Kaar (1959) describe.

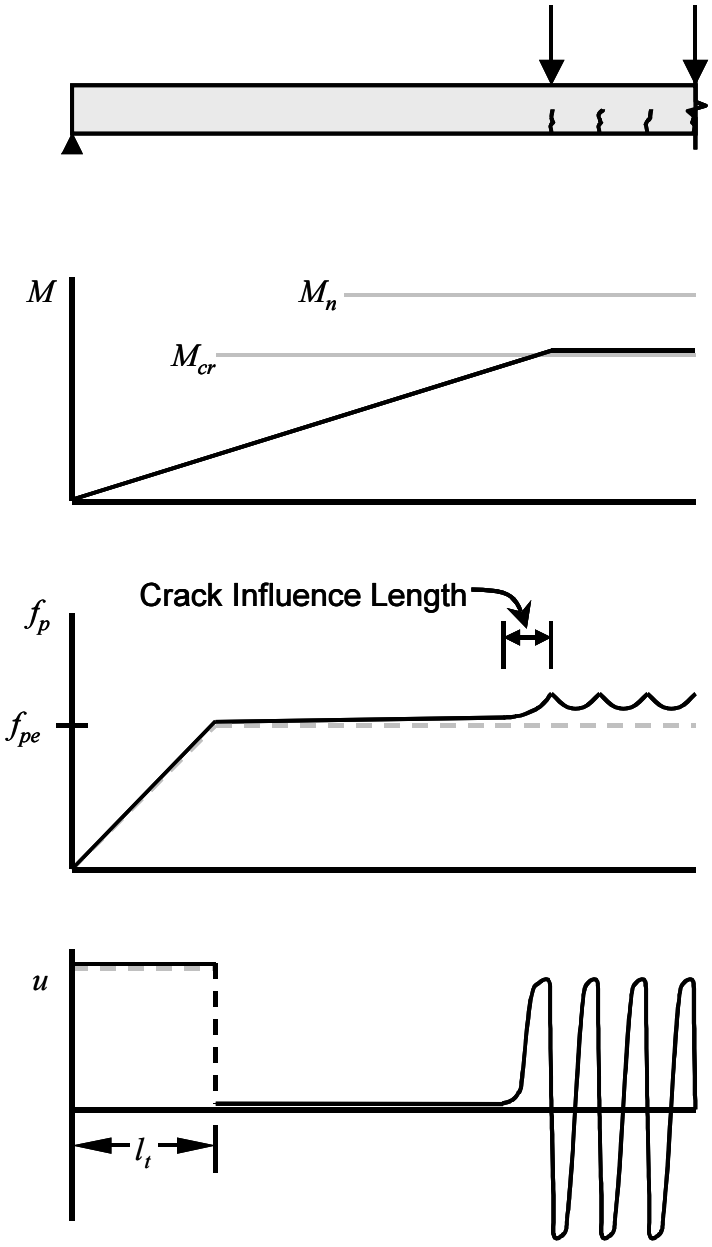


**Figure 2.8: Applied Moment, Steel Stress, and Bond Stress Diagrams for Portion of Simply Supported Beam After Flexural Cracking in Maximum Moment Region**

As can be seen in Figure 2.9 and Figure 2.10, flexural cracking progresses toward the support as the applied load increases. The crack influence length and accompanying flexural bond wave advance ahead of the cracking. Note that as the cracking spreads into the shear span, the steel stress is different at successive crack locations. Therefore, the average flexural bond stress between cracks is nonzero in the region of moment gradient. The local bond stresses are still limited by approximately the same bond stress capacity as in the constant moment region.

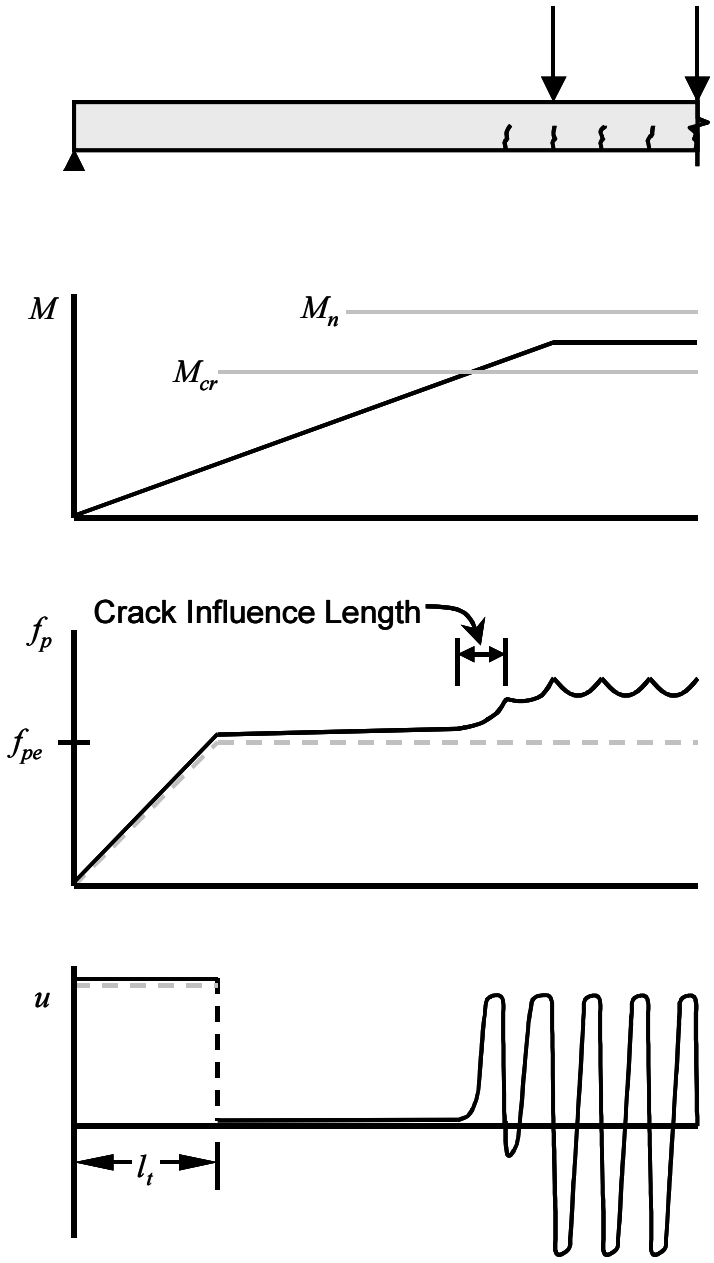


**Figure 2.9: Applied Moment, Steel Stress, and Bond Stress Diagrams for Portion of Simply Supported Beam as Cracking Progresses Toward Support**

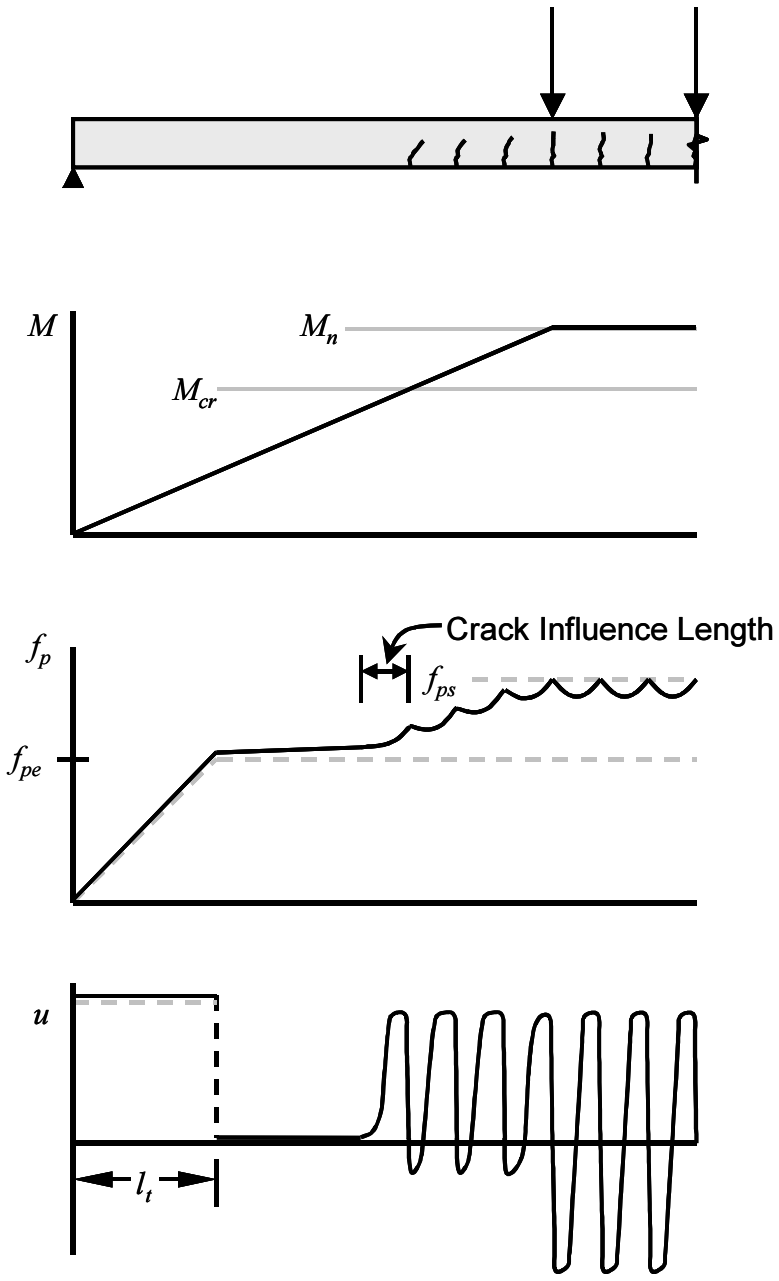


**Figure 2.10: Applied Moment, Steel Stress, and Bond Stress Diagrams for Portion of Simply Supported Beam at Nominal Flexural Strength**

When the moment due to external loads equals the nominal moment capacity of the section, the crack influence length (and flexural bond wave) are still quite removed from the transfer length of the tendon. Only a very small increase in steel stress has occurred within the transfer length. So long as the member is more than a few weeks old, the magnitude of this increase is such that the prestress occurring in the transfer length at nominal strength is less than that experienced immediately after transfer, $f_{pt}$. Therefore, the transfer bond capacity of the strand is not exceeded, and general bond slip (slip along the entire length of strand) cannot occur. Thus, the length of bonded strand between the end of the member and the critical section constitutes more than enough embedment length to develop $f_{ps}$ without general bond slip.

The next set of figures (Figure 2.11 through Figure 2.15) illustrates the same process except that the critical section for maximum moment lies substantially closer to the end of the member. Therefore, less embedded length of strand

is available to develop $f_{ps}$. The sequence is nearly identical to that for the specimen with a longer embedment length until cracking starts to progress toward the transfer length. The average bond stresses are slightly higher because the same change in steel stress must occur over a shorter length of strand. Regardless, in the regions of the beam that are free of the influence of cracking, the bond stresses and steel stresses are still quite small.

Note that this embedment length is short enough so that when the nominal flexural strength of the beam is reached, the crack influence length and flexural bond wave have just extended to the end of transfer length. At this point, the slightest increase in moment would result in the crack influence length (or flexural bond wave) impinging on the transfer length. The resulting steel stress increase in the transfer length and the accompanying decrease in radial compressive stresses would lead to general bond slip as outlined by Janney (1954) and described in Section 2.4.6 above. Thus, prevention of general bond slip depends upon effective separation of the crack influence length and the transfer length. The embedment length featured in this second set of figures represents the necessary flexural development length for the beam when loaded in this fashion.

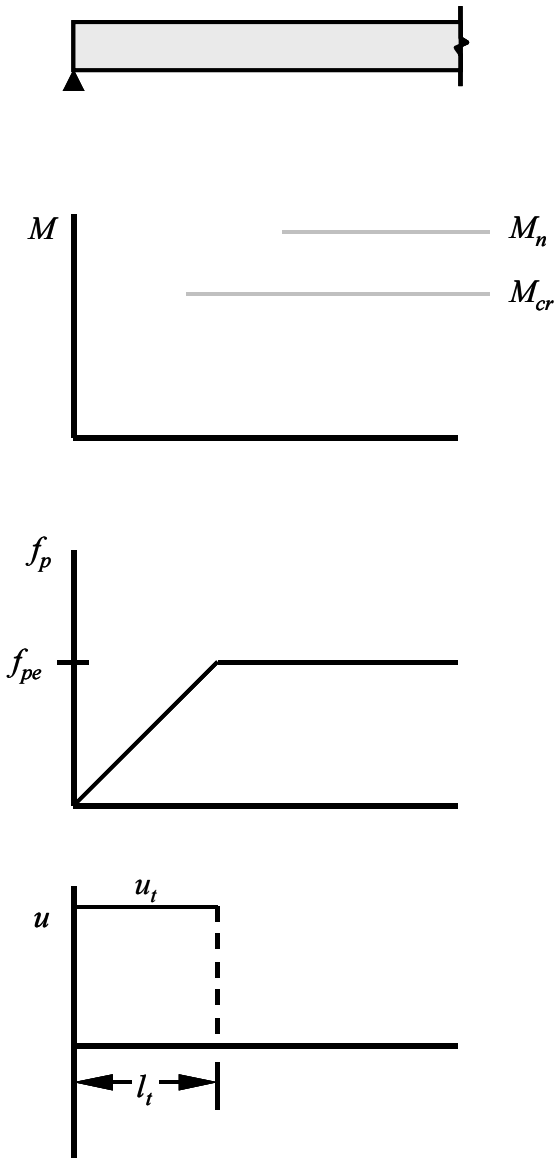


**Figure 2.11: Applied Moment, Steel Stress, and Bond Stress Diagrams for Portion of Simply Supported Beam Prior to Application of Loading—Short Embedment Length**

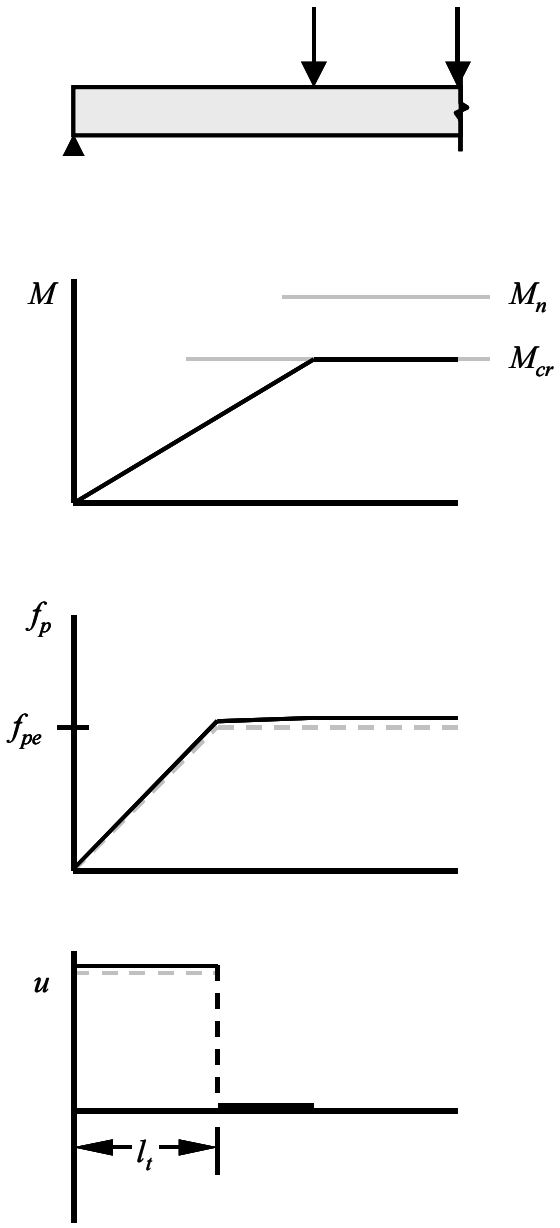


**Figure 2.12: Applied Moment, Steel Stress, and Bond Stress Diagrams for Portion of Simply Supported Beam Immediately Prior to Flexural Cracking—Short Embedment Length**

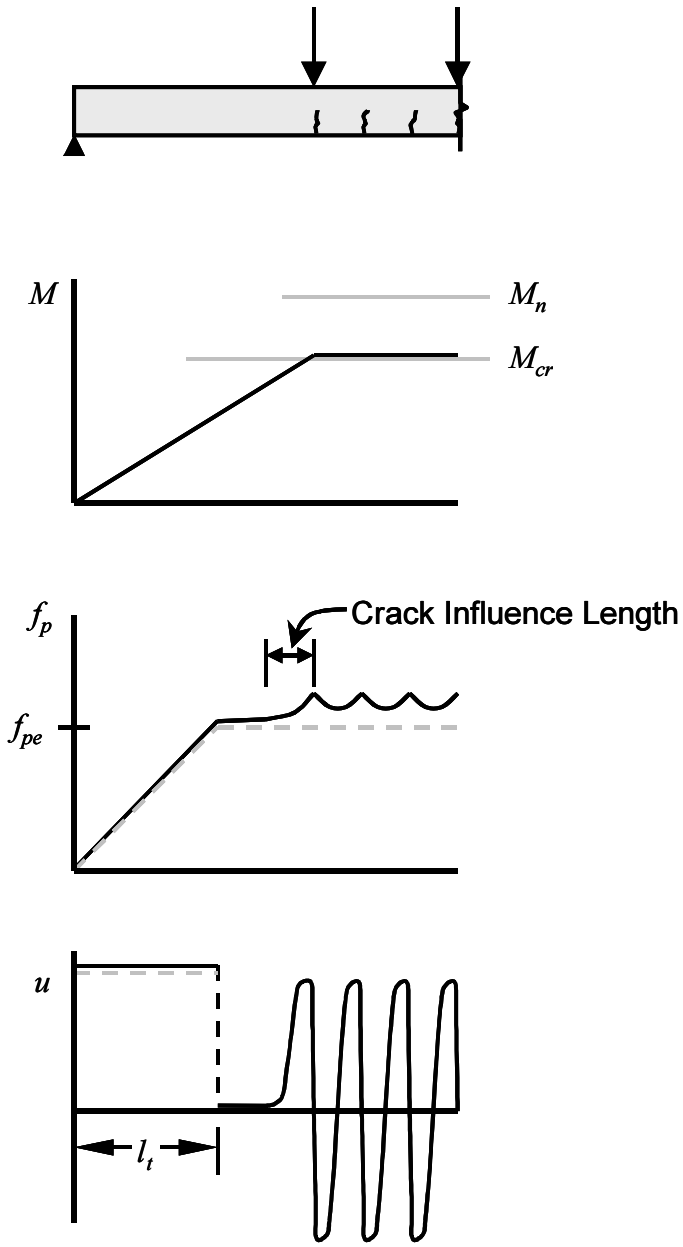


**Figure 2.13: Applied Moment, Steel Stress, and Bond Stress Diagrams for Portion of Simply Supported Beam After Flexural Cracking in Maximum Moment Region—Short Embedment Length**

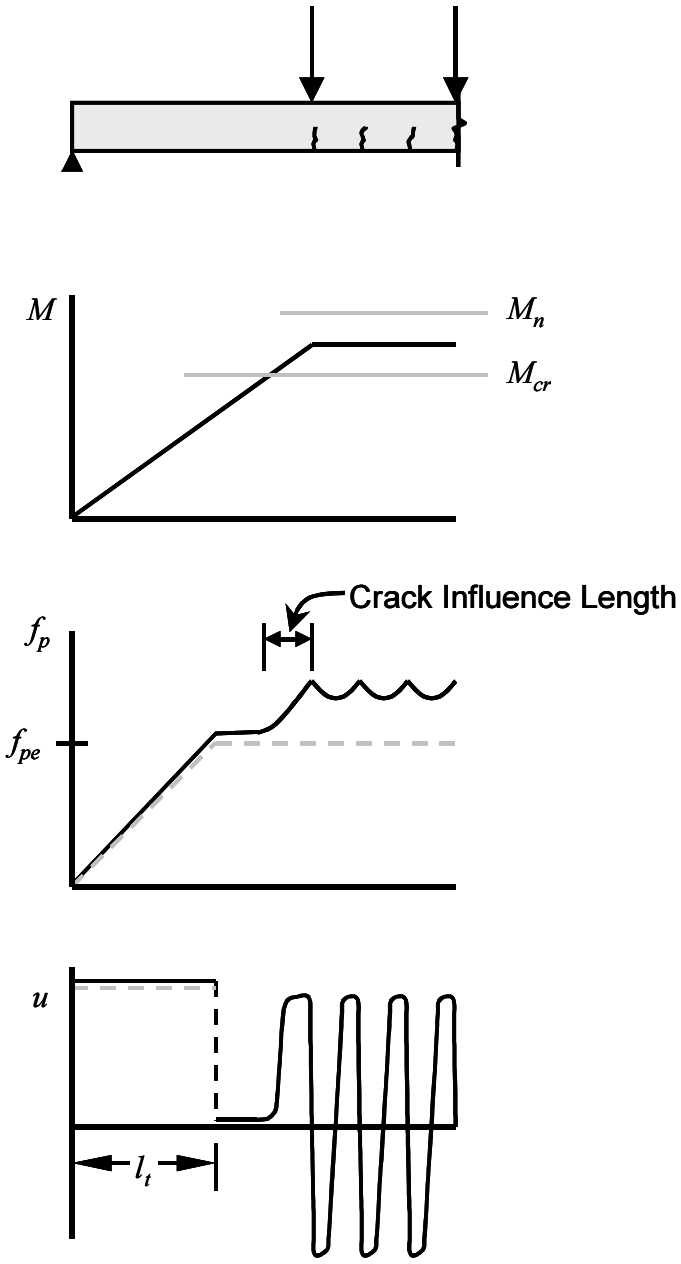


**Figure 2.14: Applied Moment, Steel Stress, and Bond Stress Diagrams for Portion of Simply Supported Beam as Cracking Progresses Toward Support—Short Embedment Length**

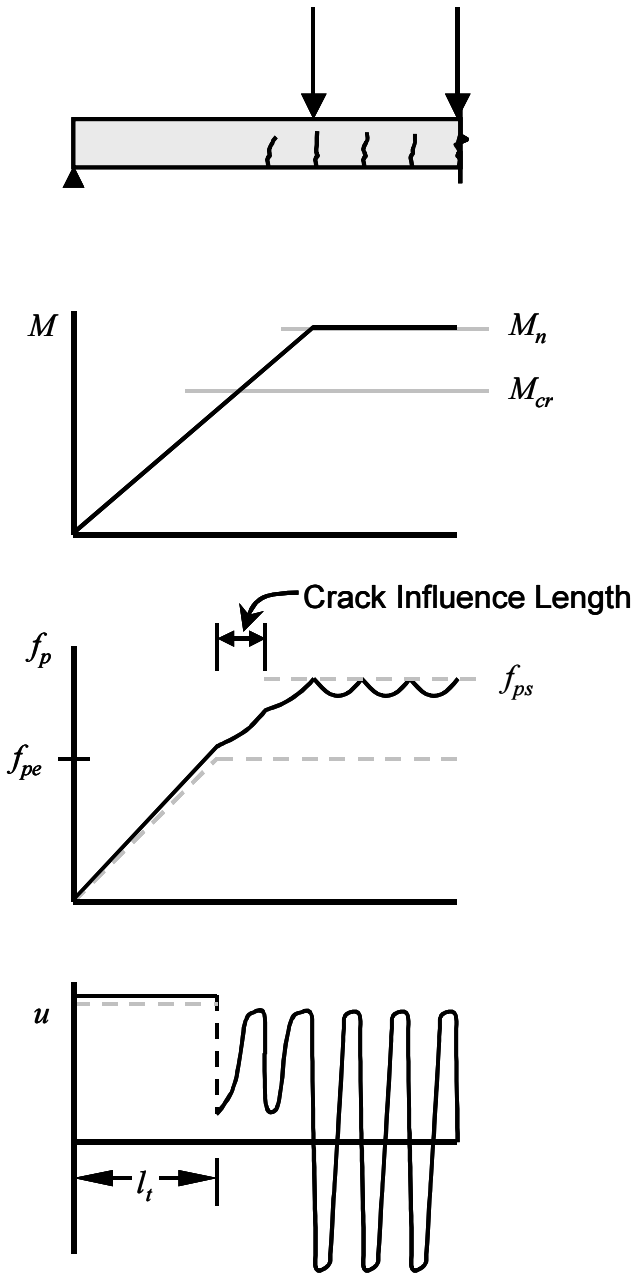


**Figure 2.15: Applied Moment, Steel Stress, and Bond Stress Diagrams for Portion of Simply Supported Beam at Nominal Flexural Strength—Short Embedment Length**

Avoidance of general bond slip requires that the transfer length be free from the influence of cracking. Based on the behavior discussed above, the necessary development length to prevent general bond slip due to flexural cracking encompasses 1) the transfer length, 2) the length of the shear span subjected to a moment that exceeds the cracking moment, and 3) the crack influence length. This is compatible with the prediction model for anchorage failure suggested by Russell and Burns (1993): "If cracks propagate through the anchorage zone of a strand, or immediately next to the transfer zone, then failure of the strand anchorage is imminent." If "immediately next to the transfer length" is defined as within the crack influence length, and failure is defined as general bond slip, this prediction model agrees with that described above.

Later in the same report, Russell and Burns (1994) state that "if cracks do not occur within its transfer zone, a pretensioned strand will develop its prestressing force plus any additional tensioned [sic] required by external

loads." In this instance, the potential for general bond slip resulting from a crack opening just outside the transfer length, i.e. such that the crack influence length extends into the transfer length, is overlooked. Russell and Burns go on to suggest design recommendations for the anchorage of pretensioned strands. These recommendations are based on the condition that cracking within the transfer length be avoided. This practice is logical as long as cracking is avoided not only within the transfer length, but also at any location where the crack influence length might extend into the transfer length.

In order to effectively apply this theory, a conservative assessment of the potential crack influence length must be performed. The change in steel stress, $\Delta f_p$, that must be developed by the bond stresses along the influence length is approximately equal to the increase in steel stress that occurs upon cracking of the concrete. In other words, $\Delta f_p$ may be estimated as $f_{p,cr} - f_{p,un}$, where $f_{p,cr}$ and $f_{p,un}$ are the values of steel stress that resist the cracking moment according to cracked section analysis and uncracked section analysis, respectively. Typical values of $\Delta f_p$ at cracking for pretensioned members range up to 40 ksi (280 MPa). Generally, smaller reinforcement ratios result in larger values of $\Delta f_p$ at cracking. Given $\Delta f_p$ and some knowledge of the bond stresses acting along the strand, the crack influence length may be estimated using the relationship in Equation 2.7 above.

Based on pull-out and push-in type tests with short embedment lengths, den Uijl (1997) proposed the following lower-bound relationship for bond stress as a function of slip and change in prestress:[6]

**Equation 2.10** $$u = 326 + 1100\delta - 1.875\Delta f_p + 1.125\left|\Delta f_p\right|$$

where

$u$ = bond stress (psi)

$\delta$ = slip (in)

$\Delta f_p$ = change in steel stress (ksi, positive in tension)

The first two terms on the right-hand side represent the bond stress resulting from sliding friction and the lack-of-fit effect. The third term represents the Hoyer effect, and the fourth term represents the mechanical interlock that results from the pitch of the strand. Over the range of parameters that might be expected along the crack influence length, the expression yields values of bond stress ranging from approximately 300 to 330 psi (2.1 to 2.3 MPa). Results of pull-out tests on strands with short embedment lengths reported by Stocker and Sozen (1970) indicate that these values represent a conservative lower bound for strand diameters up to ½ in (12.7 mm). Larger diameters were not tested.

Rearranging Equation 2.7 yields:

**Equation 2.11** $$l = \frac{\Delta f_p}{\overline{u}} \frac{A_{ps}}{\Sigma o}$$

Assuming a conservative value of 300 psi (2.1 MPa) for the average bond stress and a maximum value of 40 ksi (280 MPa) for $\Delta f_p$, Equation 2.11 yields a crack influence length of slightly less than $20d_b$ for seven-wire strand. Accordingly, the Russell and Burns criterion for prevention of general bond slip may be refined to state:

> If cracking propagates through the transfer length of strand or through the bonded length of strand within twenty strand diameters of the transfer length, general bond slip is imminent.

The effect of the reinforcement ratio, $\rho$, on the magnitude of $\Delta f_p$ at cracking is important. Because smaller values of $\rho$ result in larger steel stress magnitudes immediately after cracking, the crack influence length should increase with decreasing values of $\rho$. This suggests an alternate, or complementary, reasoning for the increased development length requirement proposed by Buckner (1995) for lightly reinforced members.

---

[6] The equation presented here represents den Uijl's relationship when converted to English units and formulated in terms of the bond stress acting on the actual strand perimeter $\left(\frac{4}{3}\pi d_b\right)$ rather than $\pi d_b$.

Based on test results from studies conducted at Purdue (Abdalla, Ramirez, and Lee 1993) and Florida DOT (Shahawy and Batchelor 1991), Buckner concluded that members characterized by large values of strand elongation at nominal strength exhibited a smaller average flexural bond stress at general bond slip. Because of the large strains that occur after the strand yields, the accompanying Poisson contraction of the strand results in a significant decrease in average bond capacity. This decrease depends on the change in strand strain, $\Delta\varepsilon_p$, rather than strand stress, $\Delta f_p$. Following this line of reasoning, Buckner proposes that the flexural bond length portion—$l_{fb} = \left(f_{ps} - f_{pe}\right)d_b$ —of the code development length expression be magnified for values of steel strain at nominal strength, $\varepsilon_{ps}$, beyond 0.010. The magnification factor varies linearly from 1.0 to 2.0 as the $\varepsilon_{ps}$ varies from 0.010 to 0.035. Den Uijl (1997) modified Equation 2.10 above to reflect the effect of post-yield strains:

$$u = 326 + 1100\delta - 54000\Delta\varepsilon_p + 1.125\left|\Delta f_p\right|$$

If this relationship is valid for large strain magnitudes, it indicates that the bond stress capacity decreases rapidly after strand yield. In flexural members with reinforcement ratios small enough to allow steel strain values approaching 0.035 at nominal strength, more than half of the flexural bond length may experience strains in excess of 0.010. The potentially severe degradation of bond over this length justifies the magnification of flexural bond length proposed by Buckner.

According to the anchorage failure criterion suggested by Russell and Burns (1993), only cracking within (or possibly near) the transfer zone of a pretensioned strand will result in bond failure. They maintain that "if cracking does not occur in the transfer zone of a pretensioned strand, then that strand can be expected to develop its full tension." This criterion is therefore independent of any consideration of the available bond stress capacity along the flexural bond length. Historically, however, bond failure (in the form of general bond slip) has been assumed as dependent upon the bond stress capacity of the strand. This philosophy was evident throughout the evolution of the code provisions discussed above. Is it possible for general bond slip to occur prior to cracking in or near the transfer length?

In the discussion that focused on the preceding series of figures, it was tacitly assumed that adequate strand bond capacity exists to develop the necessary steel stress at the critical section until cracking in or near the transfer length caused general bond slip. This is not necessarily the case. Consider a member in which the local bond stress capacity decreases significantly after yielding as discussed above. Once flexural yielding has occurred along a portion of the flexural bond length, bond stress capacity in this region may decrease rapidly accompanied by increased local strand slip. A significant share of the bond stress demand is then redistributed over a length of strand adequate to develop the steel stress necessary to resist the applied moment. As the bond stresses decrease in the maximum moment region and redistribute by means of slip to the outer regions of the beam, the beam behavior starts to transition towards that characteristic of a beam reinforced with unbonded tendons anchored at the ends of the member. Accordingly, the curvature at the cracked sections in the maximum moment region increases beyond that predicted by cracked section analysis.

Subjected to small increases in applied moment, the region of strand yield extends significantly. The region of the beam subjected to moments exceeding the cracking moment extends only slightly. Thus, the majority of the bond stress demand progresses rapidly to the end of the cracked region and beyond the outermost crack. The crack influence length increases as more of the bond demand is redistributed to this region. Eventually, the crack influence length and associated flexural bond stress wave can extend to the transfer length and cause general bond slip.

In summary, there are two possible modes of bond failure that result in general bond slip, both of which are characterized by the imposition of high flexural bond stresses on the transfer length:

1. Local bond stress capacity is reached and/or reduced over portions of the strand subjected to high flexural demands. The bond stresses necessary for equilibrium are then redistributed towards the transfer length of the strand. Once the resulting wave of high flexural bond stress reaches the transfer length, the resulting steel stress gradient causes radial contraction of the strand thereby degrading the transfer bond stresses. With no remaining length over to which to redistribute the required bond demand, general bond slip occurs. This mode of failure corresponds to that described by Janney (1954). The required development length depends upon the bond capacity along the bonded length of strand when subjected to the critical loading. This bond capacity varies along the length of strand in accordance with the local slip and local change in steel strain.

2. Adequate bond stress capacity exists to develop the required steel stress at nominal strength, but achievement of this strength at the critical section necessitates cracking A) within the transfer length of strand or B) such that the crack influence length extends into the transfer length. Such a crack results in radial strand contraction within the transfer length that overcomes the transfer bond capacity. The resulting general bond slip reduces the prestress along the entire length of strand. As the effective prestress reduces, more cracking ensues and a rapidly progressing bond failure results. So long as the local bond stress capacity is sufficient to preclude the first mode of failure, this second failure mode capacity depends on the cracking resistance of the cross section relative to the applied loads.

General bond slip can also result from a combination of the two modes. The second mode reflects the location of the cracking and the resulting crack influence length. The first mode reflects an extension of the crack influence length due to excessive bond demand. The progression of excessive flexural bond stresses from the peak moment region to the transfer length represents the reasoning espoused by Janney (1954) and Hanson and Kaar (1959). Neither mode of failure is uniquely addressed by the current code provisions. Rather, these provisions are based on the experimental results which may have reflected either failure mode. The average bond stress approach used to formulate the development length expression for fully bonded strands appears to be more in line with the first mode of failure, which depends upon the local bond capacity along the flexural bond length.

Regardless of which of the two failure modes prevailed in the PCA tests, the results reflect predominantly flexural behavior. Due to the specimen and loading geometries, all cracks were of the flexural type. Russell and Burns (1993) maintain that the second mode of failure can also be caused by shear cracking. Diagonal cracks that cross the transfer length (or near enough that they influence the transfer length) will also generate general bond slip and the resulting loss of effective prestress. This loss of prestress force can result in a premature shear failure of the member due to either or both of two causes. First, the capacity of bottom chord of the truss model for shear resistance may become deficient as the available strand stress decreases. Second, the shear resistance attributed to the concrete, $V_c$, may decrease significantly in tandem with the drop in effective prestress. Either of these effects may result in an undesirable, non-ductile mode of failure.

## 2.6 CODE PROVISIONS FOR ANCHORAGE OF PARTIALLY DEBONDED STRANDS

The code provisions for anchorage of fully bonded strands discussed in Section 2.3 above are augmented for application to partially debonded (jacketed) strands. The additional provisions for jacketed strands are discussed in this section.

### 2.6.1 Relevant ACI and AASHTO Code Clauses and Commentary

ACI 318-99, Section 12.9 includes the following provision pertaining to partially debonded strands:

> **12.9.3** — Where bonding of a strand does not extend to the end of member, and design includes tension at service load in precompressed tensile zone as permitted by 18.4.2, development length specified in 12.9.1 shall be doubled.

The corresponding section of the Commentary cites research by Kaar and Magura (1965) and Rabbat et al. (1979) and states:

> Exploratory tests that study the effect of debonded strand … on performance of pretensioned girders, indicated that the performance of these girders with embedment lengths twice those required by 12.9.1 closely matched the flexural performance of similar pretensioned girders with strand fully bonded to ends of girders.… Subsequent tests indicated that in pretensioned members designed for zero tension in the concrete under service load conditions…, the development length for debonded strands need not be doubled.

The corresponding provisions for the AASHTO Standard and LRFD specifications are substantively equivalent. In addition, Article 5.11.4.3 of the AASHTO LRFD specification contains provisions that are not found in the ACI or AASHTO Standard specifications (the statements are numbered here for convenient reference):

1. The number of partially debonded strands should not exceed 25 percent of the total number of strands.

2. The number of debonded strands in any horizontal row shall not exceed 40 percent of the strands in that row.

3. The length of debonding of any strand shall be such that all limit states are satisfied with consideration of the total developed resistance at any section being investigated.

4. Debonded strands shall be symmetrically distributed about the centerline of the member. Debonded lengths of pairs of strands that are symmetrically positioned about the centerline of the member shall be equal.

5. Exterior strands in each horizontal row shall be fully bonded.

The importance of the third statement lies with its apparent contradiction of the ACI (and AASHTO Standard) provision given above (Section 2.3.1) and repeated here:

> **12.9.2** — Limiting the investigation to cross sections nearest each end of the member that are required to develop full design strength under specified factored loads shall be permitted.

Thus, while the ACI and AASHTO Standard specifications allow adequate anchorage to be verified by checking the development length relative to a single section for each end of the member, the AASHTO LRFD provision appears to indicate the importance of verifying the development of adequate sectional resistance throughout members containing debonded strands.

The AASHTO LRFD Commentary indicates that higher debonding percentages might be implemented based on successful past practice as long as shear resistance in the anchorage region is thoroughly investigated. The dependence of shear resistance mechanisms on the anchorage strength of reinforcement is stressed. No specific reasoning is provided for the limitations contained in the second, fourth, and fifth statements.

### 2.6.2 Background Research

The provision included in Section 12.9.3 of ACI 318-99 is the result of the two PCA experimental studies discussed in this section.

#### *2.6.2.1 Kaar and Magura (1965)*

Kaar and Magura conducted experimental tests on five girder specimens to compare the anchorage behavior of partially debonded strands to draped strands. The specimens represented half-scale models of AASHTO Type III I-girders, and were reinforced with twelve ⅜ in (9.5 mm) strand. A 3 in x 39 in (76 mm x 991 mm) cast-in-place composite slab was added to each girder. The ultimate strand strength, $f_{pu}$, was assumed to be 150 ksi (1035 MPa).

Three of the girders were designed to compare the anchorage behavior under the flexural effects of both static and dynamic loadings. One of these three girders featured draped strands. The other two flexural specimens featured debonded strands—one with the code-specified development length, one with twice the code-specified development length. Each of these specimens was subjected to 5 million cycles of design service load and then tested statically to failure. Debonding did not affect behavior during the application of the service load cycles. During static loading to destruction, general bond slip occurred in debonded strands in both of the debonded specimens. Despite the general bond slip, the specimen with twice the code-specified development length showed only a slight deficiency in ultimate load (approximately 2 percent) when compared with the draped strand specimen. However, the specimen

with the code-specified development length displayed a significant drop in prestress level after general bond slip and resisted approximately 84 percent of the expected failure load.

Two other girders were used to compare the shear performance of debonded and draped strands. These two girders—one containing draped strands and one containing debonded strands—were tested statically to destruction. The debonded strands were bonded twice the code-specified development length beyond the critical section. Stirrups were spaced at 1.5 times the spacing required by the 1963 ACI Code to encourage a shear-type failure. Despite general bond slip of all debonded strands, the capacity and load-deflection behavior of the debonded specimen closely matched that of the draped specimen.

Because of these experimental results, the 1971 version of the ACI 318 Code included a provision that development length for debonded strands be twice that required for fully bonded strands.

#### *2.6.2.2 Rabbat et al. (1979)*

Rabbat et al. tested six AASHTO Type II I-girders with 5 in x 58 in (127 mm x 1473 mm) composite concrete slabs to assess the effects of fatigue on the anchorage of debonded strands. The girders were reinforced with 0.44 in (11.1 mm), Grade 250, stress-relieved strands. The specimens were divided into two groups according to the maximum bottom fiber stress during the cyclic load phase: three specimens were cycled to a maximum bottom fiber stress of zero and three were cycled to a maximum bottom fiber tensile stress of $6\sqrt{f'_c}$ (calculated assuming an uncracked section). One specimen in each of these groups contained draped strands; the rest had partially debonded strands. One of the debonded specimens in each group featured the development length specified by the code for fully bonded strands. The remaining specimen in the zero tension group also featured this development length, but additional confining reinforcement was placed around the strands. The remaining specimen in the $6\sqrt{f'_c}$ group was characterized by the development length recommended by the code for debonded strands (twice that for fully bonded strands).

Crack formers (sheet metal) were placed in the bottom flange in the midspan region. All six specimens were loaded statically to the load corresponding to $6\sqrt{f'_c}$ bottom fiber tensile stress in order to assure cracking at the crack formers prior to initiating the cyclic loading program. The intention was to apply 5 million cycles of service load and then test statically to failure. All three specimens subjected to a service load stress of $6\sqrt{f'_c}$ (one draped, one with a single development length, and one with double development length) failed prematurely due to strand fracture after approximately 3 to 4 million cycles. There were indications that the strand fatigue was aggravated by fretting between the strands and the crack formers. No useful information was obtained from these tests regarding the static ultimate load. The maximum strand end slip measured for the specimen with double the development length was 0.006 in (0.15 mm) after 1 million cycles and remained virtually unchanged up to the final reading at 2.5 million cycles. The maximum strand end slip measured for the specimen with a single development length was 0.025 in (0.6 mm) after 2.5 million cycles. Twenty percent of this slip occurred after the first 1 million cycles. Although this continued growth was extremely small, the behavior of this particular specimen was labeled as "bond fatigue."

All of the specimens subjected to zero tension during the cyclic load phase survived all 5 million cycles. The largest strand slip was 0.015 in (0.4 mm). All three specimens exhibited loads at least as large as expected for flexural failure under static loading to destruction. No significant behavioral enhancement due to the additional confining reinforcement was observed. Based on these results, it was recommended that the development length of debonded strands does not need to be doubled if no tension is allowed in the precompressed tensile zone under service loads. Because of the bond fatigue noted for the specimen with a single development length that was subjected to $6\sqrt{f'_c}$ service level tensile stress, doubling the development length for debonded strands was still recommended for members in which the precompressed tensile zone is subject to tension under service loads. Accordingly, the wording of ACI 318-99 Section 12.9.3 quoted above was first included in the 1983 Code. Shear behavior was not investigated in this study.

### 2.6.3 Comments on Background Research

The formulation of the code expression for the development of fully bonded strands is primarily a reflection of the first mode of failure discussed in Section 2.5 above. This mode of failure depends on the local bond stress that can

be developed between the steel and the concrete in the anchorage zone. The local bond interaction between the steel and the concrete does not depend on whether the strand is debonded along some remote portion of its length. Rather, the more likely source of the differing behavior between fully bonded and partially debonded strands is the second mode of anchorage failure—that precipitated by cracking in or near the transfer length.

The behavior of a simply supported beam prestressed with only fully bonded strands is compared to that of a beam prestressed with partially debonded strands in Figure 2.16. In fully bonded specimens (Figure 2.16a), the anchorage zones are located at the ends of the members. Thus, anchorage failures of fully bonded strands in these beams should only occur when the span is less than approximately twice the development length. For members constructed with 0.5 in (12.7 mm) strands, anchorage problems would only be expected for spans of approximately 13 ft (4 m) or less. Even if the necessary development length is 50–60 percent longer than that given by the current expression, anchorage failures would not be expected for bridge spans longer than 20 ft (6 m).

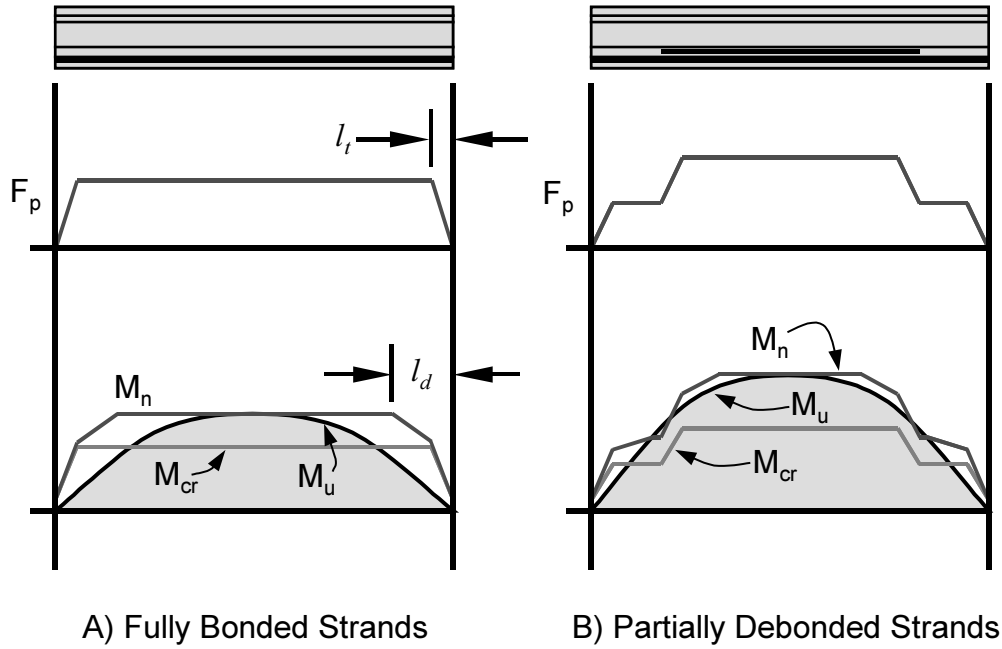


**Figure 2.16: Comparison of Beams with Fully Bonded Strands and Partially Debonded Strands Subjected to Maximum Moment**

In beams that contain partially debonded strands (Figure 2.16b), anchorage zones exist within the interior regions of the member, where they are more likely to be subjected to significant flexural demand. Not only is the reduced moment capacity in these regions more likely to be critical for design, but flexural cracking also occurs at lower load levels than would be expected in comparable beams with all strands fully bonded. In addition, debonding of strands results in a decrease in effective prestress force towards the support regions, where shear demand is most pronounced. These conditions promote the likelihood that anchorage failure will initiate as a result of cracking in or near the transfer length rather than because of a progressive breakdown in the local bond stress capacity along the flexural bond length.

The moment diagram for the beam with partially debonded strands in Figure 2.16b also indicates the similarity between this type of beam and that of a beam that has some tensile reinforcement terminated within the span. It is logical that the design rules applicable to terminating nonprestressed tensile reinforcement also be applied when determining the bonded tendon length required to provide adequate strength under ultimate loads.

Considering both of the studies cited above regarding debonded strands, all of the debonded specimens which featured an anchorage length equal to the code-specified development length for fully bonded strands displayed extensive cracking within strand transfer lengths at ultimate. In the Kaar and Magura study, regardless of development length provided, general bond slip was first reported for each pair of debonded strands at approximately the load that would have produced flexural cracking within the transfer length. The girder that failed prematurely had suffered general bond slip due to transfer length cracking in all of the debonded strands prior to

failure. Thus, 50 percent of the total number of strands had been subjected to some loss of anchorage. At the section where failure actually occurred, 40 percent of the bonded strands had been subjected to anchorage deterioration, and the sectional moment was 76 percent of that calculated based on the assumption of perfect bond. In the girder with twice the code-specified development length, transfer length cracking and the associated general bond slip had only affected one-sixth of the total number of strands. This girder achieved 96 percent of the calculated ultimate load. Apparently, considerable residual stress remained in the strands after general bond slip in both these girders.

The "bond fatigue" occurring in one specimen from the Rabbat et al. study can be explained by the influence of cracking on the transfer length. The aforementioned crack formers were located within the transfer length of two of the strands in this specimen. The specimen was cracked prior to cyclic loading. The magnitude of the cyclic load was selected to achieve a stress of $6\sqrt{f'_c}$ in the extreme concrete fiber based on the uncracked sectional analysis that would typically be used for design. This ensured that with every load cycle, the crack opened, and *within their transfer length* two strands were subjected to stresses well in excess of the effective prestress level. With the resulting radial strand contraction and loss of the Hoyer Effect, it is hard to imagine slip *not* occurring under these circumstances. Even under this cyclical demand, the slip growth appeared to stabilize prior to fatigue failure of the strands, and the maximum value of slip after 2.5 million cycles was quite small. Rather than double the entire development length to prevent bond fatigue due to service level tension in the precompressed tensile zone, it seems that a more direct and universally applicable approach would limit the allowable service level concrete tensile stress within the transfer length to zero.

Two specimens with debonded strands from the Rabbat et al. study survived the cyclic loading program. When these specimens were tested statically to failure, the transfer lengths of the four debonded strands were subjected to loads well in excess of the cracking load. Cracking occurred within these transfer lengths, but no information on strand end slips is provided in the literature. Although these four strands likely lost some anchorage integrity, the predicted ultimate moment of the member was achieved. There were a total of 24 strands, of which two were not prestressed. A partial loss of anchorage of such a relatively small proportion of the total number of strands is likely to have had little effect on the ultimate capacity of the girder, particularly if the member had enough deformation capacity to activate steel stresses larger than expected in the fully bonded strands. The reported final deflections, which were equal to approximately 5 percent of the span length, that occurred without loss of moment resistance indicate that significant deformation capacity was observed.

## 2.7 INFLUENCE OF CRACKING ON THE ANCHORAGE OF PRETENSIONED STRANDS

Published research results indicate the influence of cracking on the anchorage of pretensioned strands. Obdalla, Ramirez, and Lee (1993) report the results of tests conducted on five pairs of simply supported, pretensioned I-beams and box beams at Purdue University. One beam in each pair featured debonded strands, while the other had an identical strand pattern with all strands fully bonded. Premature failures of the debonded specimens were always precipitated by web shear or flexure-shear cracking within or very near the transfer length of the debonded strands. After the resulting strand slip, the girders eventually failed because the strands could not provide the horizontal force required to resist the combined flexural and shear demand.

The web shear cracking loads were adequately predicted by the ACI/AASHTO Standard expression for $V_{cw}$, but flexure-shear cracks generally opened at loads less than those indicated by the ACI/AASHTO Standard expression for $V_{ci}$. A more conservative prediction for the flexure-shear cracking load resulted from disregarding the prestress of any strands that were not completely developed at the section under consideration when calculating $V_{ci}$. While flexure-shear cracks were critical in causing the anchorage failure of the partially debonded strands, web shear cracks that extended through the transfer length resulted in the failure of fully bonded strands near the support.

Based on results obtained from an extensive experimental study, Russell and Burns (1993) proposed that anchorage failures did not occur if cracking was prevented in the prestress transfer zone. The corresponding design procedure entails preventing flexural cracks by limiting the moment in the transfer zone to the calculated cracking moment, and preventing web shear cracks in the transfer length by limiting the shear demand to $V_{cw}$ in this region. Several instances of bond/shear failures occurred in the test program. In these failures, cracking led to bond deterioration along the strand transfer length. In addition to reducing the concrete contribution to shear resistance, the accompanying loss of prestress force rendered the strands unable to sustain the horizontal force necessary to resist the applied shear and moment.

Previous research has revealed two important observations concerning the interaction of cracking and the strand anchorage:

1. Cracks that open within the transfer length, or near enough to influence the strand stress within the transfer length, result in strand slip and a partial loss of strand anchorage. Partially debonded strands are particularly susceptible to this type of bond deterioration because they are anchored away from the ends of members.
2. Accurate prediction of sectional cracking resistance requires careful consideration of the variable nature of the effective prestress force within the anchorage zone, especially in members with partially debonded strands.

In particular, the ACI/AASHTO Standard expression for $V_{ci}$ does not consistently indicate the load that causes flexure-shear cracking. This is likely because the $V_{ci}$ expression is based on the assumption that flexure-shear cracks open first as flexure cracks at the bottom fiber and then progress under the combined influence of flexure and shear. Because the shear cracking resistance can be significantly reduced in debonded regions, cracks may also initiate at the junction of the web and bottom flange due to the simultaneous influence of flexure *and* shear. This type of crack initiation is not addressed in the codes, but may be predicted by means of calculating the principal tensile stress at the web-flange junction. This type of cracking may be visually indistinguishable from classic flexure-shear cracking because the crack rapidly extends to the bottom fiber after initiation. The ability to predict this type of cracking is vital to prevention of strand slip in some debonded strand anchorage zones.

## 2.8 ANCHORAGE FAILURE CRITERIA AND DESIGN PHILOSOPHY

Throughout the evolution of code provisions concerning the anchorage of fully bonded and partially debonded pretensioned strands, no clear definition of anchorage failure has been agreed upon nor adopted. Hanson and Kaar (1959) recommended that avoidance of general bond slip be the criterion for anchorage design. They maintained that although most specimens exhibited additional resistance after initiation of general bond slip, the influence of repeated loads was yet undetermined. Therefore, post-slip resistance should not be relied upon. Mattock echoed this philosophy when proposing the flexural bond length expression to be incorporated in the 1963 ACI 318 Code. The ACI 318R-63 Commentary states that the code provisions are "intended to ensure that failure of a pretensioned prestressed member shall not occur by the strand pulling through the concrete as a result of failure in flexural bond" (Tabatabai and Dickson 1993). It seems clear that general bond slip was the accepted criterion for determining anchorage failure in pretensioned members at that time.

By the time that the modifications for debonded strands appeared in the Code provisions (1971 and 1983) this philosophy appears to have changed. General bond slip of debonded strands was reported for all of Kaar and Magura's (1965) test specimens, yet some of these strands were judged to be adequately anchored, while others were not. Rather, the evaluation of adequate anchorage was based on the load-deflection behavior and ultimate strength of each specimen. Rabbat et al. (1979) report that strand slip occurred under cyclic service loads for specimens regardless of whether or not the anchorage length was determined to be adequate. The adequacy of anchorage under cyclic loading was determined according to whether or not the slip continued to increase with repeated loading. The code modifications resulting from these two studies seem to reflect a shift in emphasis from preventing strand slip to ensuring adequate resistance of the member.

On what criteria should anchorage design be based? Theoretically, sufficient anchorage capacity should be provided so that the performance of the member (and overall structure) is adequate with regard to the limit state under consideration. Under the repetitive loading that characterizes the Service Limit State, general bond slip is unacceptable. Prevention of strand slip under repetitive loads precludes progressive bond failure due to "bond fatigue," and ensures that load-deflection behavior will not suffer from inadequate bond.

For the Strength (or Ultimate) Limit State, adequate anchorage performance is that which allows the member to achieve the required ultimate strength and fail according to the intended (usually flexural) mechanism. Thus, the member resistance should exceed all demands that might result from potential load configurations. Extensive damage is not a concern when designing for the Strength Limit State as long as the critical loads are adequately resisted. Repeated loads are not considered. Prevention of general bond slip is not a strict necessity under these conditions, but it allows simple calculation of member capacities according to the standard assumption of "perfect bond." Unfortunately, previous research has shown that preventing general bond slip, particularly in members with debonded strands, is not as simple as providing a standard strand development length. In addition to providing an

anchorage length adequate to prevent progressive failure of local bond capacity, strand transfer lengths must be protected from the influence of all types of cracking. Current code provisions do not adequately address this issue.

On the other hand, general bond slip might be allowed when designing for the Strength Limit State if adequate strength at all sections can be ensured. This is the general approach used for determining cutoff lengths of straight mild steel reinforcement. A development length is calculated based on a conservative assessment of the anchorage capacity of the bar after slip. So long as this development length is provided (and a bevy of accompanying rules are satisfied), calculation of member strength according to resistance models (flexural, shear, torsion, etc.) is relatively simple.

Adapting this approach to pretensioned strands could simplify one portion of the design process while complicating another. For example, rather than dedicating extensive analytical effort to determining the susceptibility of multiple sections to a variety of cracking mechanisms, the presence of cracking along the development could be presupposed. A more conservative expression for development length would be required because cracking would hinder the rapid buildup of prestress along the transfer length that is reflected in the current expression. In return, the calculation of the required anchorage length would be much simpler. Accurate calculation of resistance to moment, shear, and torsion at sections within the strand development length would depend upon due consideration of the reduced capacity of the strand. Depending upon the experimentally determined relationship between bond capacity and strand slip along the development length, employment of strain compatibility analysis might be necessary for determination of the strand stress available from adjacent strands that are fully developed at these sections, if present.

Calculation of shear resistance must be carefully considered when strand slip is allowed under Strength Limit State design. Once slip of the strand occurs within the transfer length, the development of the effective prestress force over the original transfer length can no longer be safely assumed. Likewise, the effective prestress applied to the concrete is reduced as well. This can significantly affect the concrete contribution to shear strength, $V_c$, regardless of which resistance model is employed for shear design. An increase in shear reinforcement can compensate for this partial loss of concrete shear resistance. The reduction of capacity in the longitudinal reinforcement itself along the development length must also be considered. The ACI/AASHTO Standard provisions do not require evaluation of the adequacy of longitudinal reinforcement to resist the demands of both flexure *and* shear.[7] This must be checked considering the limited strand capacity along the development length. The AASHTO LRFD specification includes this equilibrium check (Article 5.8.3.5).

In summary, the prevention of general bond slip under ultimate load conditions requires considerable computational effort, particularly for debonded strands. However, if slip is precluded, calculation of sectional resistance is relatively simple because perfect bond can safely be assumed. Prevention of slip requires adequate anchorage length *and* prevention of cracking within strand transfer lengths. This might prove difficult for some members, particularly those with partially debonded strands. This obstacle may be overcome if cracking is allowed within the transfer length, which also eliminates the computational effort required to ensure that cracking does not occur. This approach is analogous to that currently used for development of nonprestressed reinforcement. A more conservative development length must then be assumed, and calculation of sectional resistance must be performed judiciously. Unfortunately, the reliability of this approach cannot be assessed until adequate experimental evidence is obtained to determine a conservative estimate of strand development length in the presence of transfer length cracking. The usefulness of this technique for conservatively estimating the strand capacity for use in moment and shear resistance computation must also be experimentally assessed.

The anchorage behavior of partially debonded strands has been likened to that of cutoff mild steel reinforcement. Although they perform similarly under the influence of external loads, economic considerations dictate different philosophies for the two reinforcement types. In the case of cutoff bars, material savings are maximized when the bars are cut as short as possible without compromising safety. For prestressing strand, on the other hand, material and labor savings are maximized when debonding lengths are minimized.

The minimum amount of strand debonding is dictated by the allowable concrete (tensile and compressive) stresses immediately after prestress transfer. Once the minimum amount of debonding has been determined accordingly, the designer must verify that the resulting bonded length of strand provides adequate anchorage under the demands of the Service and Strength Limit States. If the anchorage is judged to be deficient, the bonded length of strand cannot be increased as would be the case with mild steel reinforcement. Such an increase would result in excessive

[7] This inadequacy is addressed for the case of mild steel reinforcement by requiring that bars be extended one effective depth, $d$, beyond the section where they are no longer required to resist flexural loads (MacGregor 1996, 308–311). There is no corresponding provision for prestressing reinforcement.

concrete stresses at transfer, unless the concrete strength were increased accordingly. A simple but highly effective solution to this potential problem is the installation of a few prestressing strands near the top of the member. This practice can reduce the concrete stress magnitudes at transfer while significantly enhancing the web shear cracking resistance (Russell and Burns 1993).

## 2.9 ANCHORAGE DESIGN

The anchorage design of pretensioned members can be subdivided into a series of general procedures discussed in the subsections below. The discussion addresses the design of simply supported members, but the general procedures can be extended to other support configurations as well.

### 2.9.1 Design of Midspan Section for Flexural Resistance

The member size, concrete strength and configuration of prestressing strands are determined according to the flexural demands on the midspan section. The amount of prestressing reinforcement required is typically controlled by 1) the allowable concrete tensile stress at the bottom fiber under Service Limit State loading and 2) ultimate moment resistance under Strength Limit State loading.

### 2.9.2 Determination of Strand Debonding Lengths and Configuration

Once the number, size and pattern of prestressing strands has been determined, the allowable concrete stresses immediately after transfer dictate the possible strand debonding configurations. Conservative assessment of the critical concrete stresses requires a lower-bound estimate of the transfer length. ACI and AASHTO codes provide no guidance for selecting a lower-bound value for transfer length. Considering the large variability of transfer lengths, assumption of a transfer length of zero is safe and simple without being unduly conservative. Strands should not be debonded over lengths longer than necessary to satisfy allowable stress limits. If multiple strands require long debonded lengths, staggered debonding should be employed if possible (Russell and Burns 1993).

### 2.9.3 Service Limit State Anchorage Performance Checks

General bond slip should be precluded under repetitive Service Limit State loads. Because development of large longitudinal steel stresses is not required under service loads, general bond slip due to excessive flexural bond demand (first bond failure mode) need not be checked for the Service Limit State. However, the second mode of failure—general bond slip resulting from cracking in or near the transfer length—should be checked. This type of slip can be precluded by checking that no net concrete tensile stress occurs along the bonded length of strand within 20 strand diameters of the transfer length. In contrast with the approach for checking concrete stresses immediately after transfer, conservative design with respect to anchorage capacity requires that a conservative *upper bound* estimate be made of the transfer length. Theoretically, prevention of cracking requires that the modulus of rupture not be exceeded in tension. However, cracking of the bottom flange may have occurred previously due to a variety of causes, e.g. periodic overloads, drying shrinkage prior to prestress release, etc. The limitation of zero tension prevents opening of existing cracks under repetitive, service load conditions. This check will probably only be critical if strand debonding extends into the midspan region of the girder.

### 2.9.4 Strength Limit State Anchorage Performance Checks

As discussed in Section 2.8 above, two distinct methods might be used to verify adequate anchorage performance for the Strength Limit State. The first, Method A, implements an expression for development length that results from an assumption that no strand slip occurs within the transfer length. The current development length expression for fully bonded strands is tacitly based on this assumption. The development length expression incorporates regions of transfer bond and flexural bond, and is formulated to preclude the first mode of general bond slip failure. In order for this development length to be adequate, the second mode of general bond slip failure—caused by cracking that influences the strand transfer length—must also be prevented. Once cracking has influenced the transfer length, the transfer bond capacity degrades rapidly, and the necessary development length grows longer.

Thus, application of Method A requires that the resistance to cracking be checked at the beginning (initiation of bond) and end (transfer length plus crack influence length) of each susceptible transfer zone. At each such section, several types of cracking must be obviated. Prevention of flexural cracking requires that the concrete stress at the extreme tensile fiber be limited under full Strength Limit State loading. This type of cracking is most likely in

transfer zones that lie closest to midspan. Web shear cracks may be prevented by verifying that the principle tensile stress at the centroid (or at the junction of web and top flange if the centroid lies within the flange) is less than a limiting value. This type of cracking is most prevalent in transfer zones near supports. Cracks resulting from shear-flexure interaction at intermediate transfer zones must also be prevented. This can be achieved by limiting the principal stress at the junction of the web and bottom flange to a critical value. Once all possible types of transfer zone cracking have been precluded, the development length calculated with the assumption of enhanced transfer bond is valid.

The benefit of adopting Method A is the shorter development length that results from taking advantage of enhanced bond capacity along the transfer length portion. The obvious disadvantage of this method is the amount of computational effort that must be expended to verify that the transfer zones are not susceptible to the influence of cracking under full Strength Limit State loading.

The second method, Method B, does not require this effort because the effects of cracking in the transfer zone are factored in to the calculated development length. Accordingly, the development length expression used in Method B will result in a development lengths significantly larger than those calculated from the Method A expression. Because transfer zone cracking is allowed by Method B, the enhanced bond capacity offered by transfer bond is forfeited. A greater factor of safety should also be incorporated into the Method B expression because of the potential lack of ductility that may result from strand slip.

Although this method of calculating anchorage capacity is analogous to that used for nonprestressed reinforcement, no significant research effort has been expended to evaluate its appropriateness for design. The validity of such an approach has yet to be verified experimentally, nor has a lower-bound value for average bond stress been suggested for application over a long embedment length subjected to significant cracking. This method's potential benefits in terms of design simplicity and broad applicability appear to justify further investigation.

### 2.9.5 Calculation of Prestress Forces at Sections Where Strands Are Not Fully Developed

When nominal resistances (such as $M_n$, $V_n$, or $T_n$) are calculated at sections that lie within the tendon development length, careful consideration must be given to the amount of prestress force that may be relied upon.

If Method A is chosen and no cracking is anticipated within the strand transfer length, the available steel stress at a section may be estimated using the bilinear relationship depicted in Figure 2.17. Conservative lower bound estimates of the average transfer bond stress capacity, $\overline{u}_t$, and the average flexural bond capacity, $\overline{u}_{fb}$, are used to predict the steel stress capacity corresponding to the bonded length provided. Calculation of the steel stress within the transfer length should not be critical for nominal resistance calculations because the concrete is not allowed to crack in this region. Otherwise, Method A would not be applicable.

If Method B is employed, the extent of cracking need not be checked, and the available steel stress at any section may be estimated from the simple linear relationship shown in Figure 2.18. For a specific bonded length, a conservative lower bound estimate of the average bond capacity, $\overline{u}$, can be used to calculate the steel stress available for load resistance. Once the available steel stress is obtained, sectional capacities may be computed. Rather than calculate resistance capacities at a multitude of sections, the capacities at the beginning and end of the development length can be calculated, and intermediate values may be interpolated.

Regardless of the method chosen, special care must be taken to estimate the prestress force available from a group of strands that have different bonded lengths at a section. Once the available stress and corresponding strain have been calculated for the strand with the shortest bonded length, stresses in the accompanying strands must be calculated assuming compatibility of strains.

Once the available prestress force has been calculated for a section where strands are not fully developed, the average concrete stress resulting from this prestress force can be calculated for use in shear and torsional resistance computations. It is important that the reduced level of prestress be considered at these sections so that the concrete contribution to the nominal resistance not be overestimated. Failure to consider the reduced concrete prestress and reduced steel stress available after cracking and slip may result in premature failures like the post-slip shear failures reported by Russell and Burns (1993).

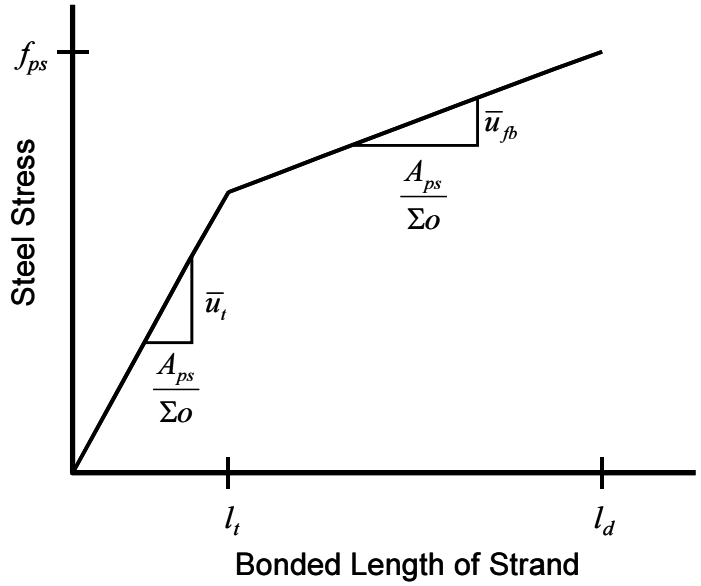


**Figure 2.17: Method A Relationship Between Steel Stress Capacity and Bonded Anchorage Length (No General Bond Slip)**

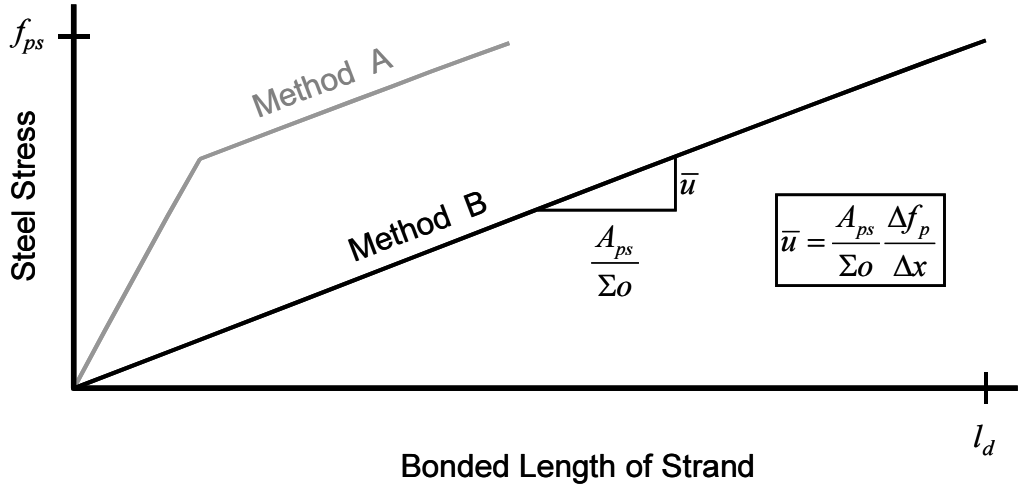


**Figure 2.18: Method B Relationship Between Steel Stress Capacity and Bonded Anchorage Length (General Bond Slip Allowed)**

# CHAPTER 3: TEST SPECIMEN DETAILS

## 3.1 INTRODUCTION

The specimens tested in this study consisted of a total of thirty-six AASHTO Type I (TxDOT Type A) I-beams. Development length testing of six of the I-beams (beam pairs L0R, L4R, and L6R) was performed by researchers at Texas Tech University, and the results are reported by Burkett and Kose (1999). This chapter includes a description of the test specimens and details regarding their design and construction.

## 3.2 SPECIMEN IDENTIFICATION

The specimen identification system used throughout this report is summarized in Figure 3.1 below.

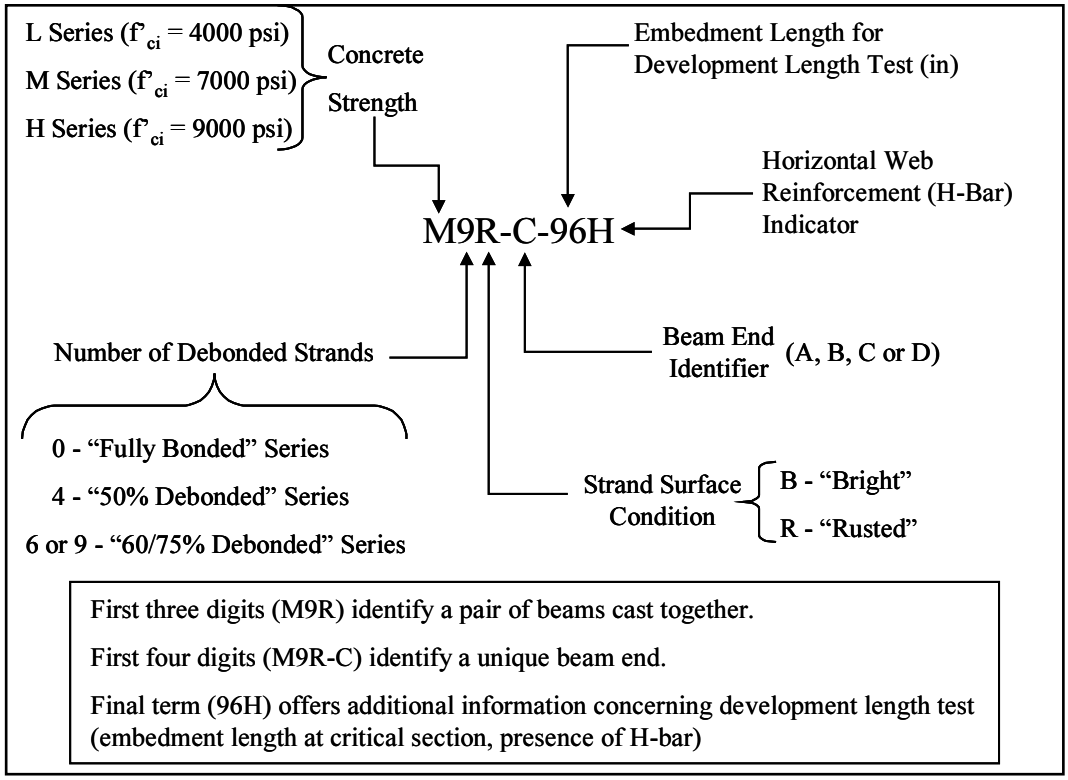


**Figure 3.1: Specimen Identification System**

The thirty-six beams were cast in pairs. Each pair represented a unique combination of concrete strength, debonding configuration, and strand surface condition. These three variables are indicated by the first three digits of the specimen identification. Thus, "M9R" represents the beam pair cast with the M-Series concrete mix and rusted strands; nine (75 percent) of these strands were partially debonded. The fourth digit of the identifier specifies a particular beam end. The beam ends were identified according to casting position as depicted in Figure 3.2. All four beam ends were essentially identical except that horizontal web reinforcement was present in End C. In some cases, the prestress release method varied among beam ends. This is explained further in Section 5.2.2. The use of the first four digits, such as M9R-C, is adequate to specify each of the seventy-two beam ends tested for transfer and development length.

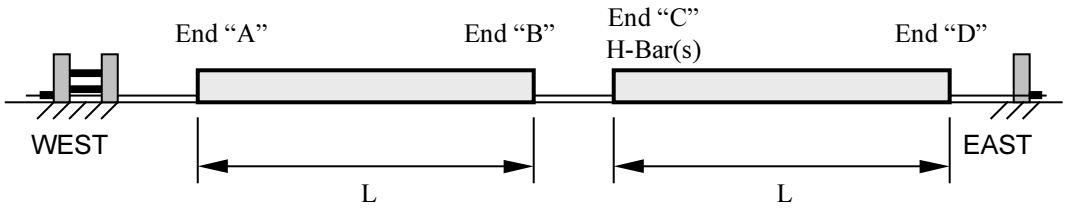


L = 40 ft (12.19 m) for "Fully Bonded" Series (x0x Specimens)

L = 54 ft (16.46 m) for both "Debonded" Series (x4x, x6x and x9x Specimens)

**Figure 3.2: Casting Configuration for Typical Beam Pair**

The final term ("96H" in Figure 3.1) is used to offer additional information concerning the development length test on a particular beam end. Thus, beam end M9R-C-96H was subjected to development length testing with an embedment length of 96 in (2438 mm) and contained horizontal web reinforcement (H).

As a further example of the strand identification system, consider beam end L0B-B-72. This identifies end "B" of the beam pair cast with L Series concrete and bright strands. The strands were fully bonded, and the development length test was performed with an embedment length of 72 in (1829 mm) relative to the critical section. No horizontal web reinforcement was present.

## 3.3 SPECIMEN DESIGN

Full-size AASHTO Type I (TxDOT Type A) beams were used in the study. The dimensions of this cross section type are shown in Figure 3.3. Prior to development length testing, a cast-in-place reinforced concrete slab (or "deck") was added to the beam. The 60 in by 6.5 in (1524 mm x 165 mm) deck was cast to model the composite behavior typical of bridge girders and to ensure that the elongation of bottom row of strands reached the prescribed limit prior to failure.

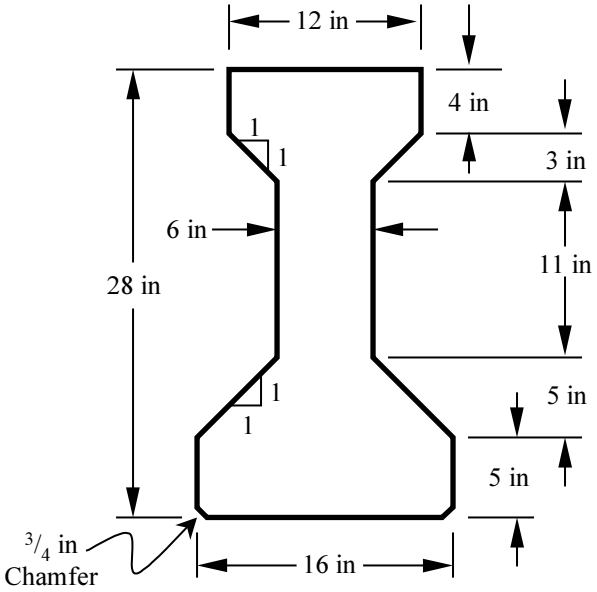


**Figure 3.3: Dimensions of AASHTO Type I Cross Section (1 in = 25.4 mm)**

### 3.3.1 Strand Patterns

Figure 3.4 depicts the scheme used to label specific strands in each specimen. The strands are depicted as viewed from the end of the beam.

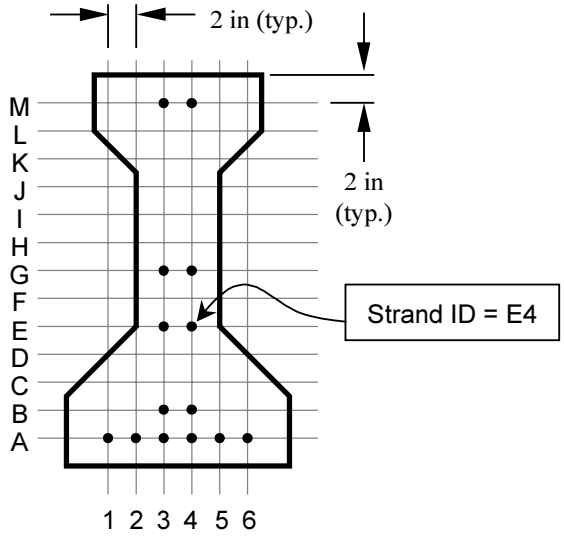


**Figure 3.4: Strand Identification Key (1 in = 25.4 mm)**

Table 3.1 and Table 3.2 provide the details of the various strand layouts and debonding patterns for the test specimens. Selection of strand layouts was subject to a variety of constraints. To satisfy the minimum elongation requirement of 3.5 percent in the bottom row of strands at ultimate flexural strength, the beams had to be considerably underreinforced. In addition, because of the relatively small dimensions of the cross-section compared with more typical bridge girders, placing more than six to eight strands in the bottom flange of the normal-strength beams (L Series) would have resulted in excessive compressive stresses in the bottom flange at release. In direct opposition to these constraints, having a large number of strands was desirable in order to provide a variety of percentages of debonded strand. At various times during specimen design, the sponsor requested that the following percentages of strands be debonded: 0, 25, 37.5, 50, and 75 percent. If limited to a symmetrical strand pattern, at least sixteen total strands would have been required to generate all of these debonding percentages. However, given the elongation requirement and allowable stress limits, this was impossible. Generally, the beams were designed with the maximum number of strands that could be used while satisfying ACI and AASHTO allowable stress requirements and the 3.5 percent elongation constraint.

**Table 3.1: Tendon Location and Debonding Schedule**

| Specimen ID | Strand ID (see Figure 3.4) | | | | | | | | | | | | | |
|---|---|---|---|---|---|---|---|---|---|---|---|---|---|---|
| | A1 | A2 | A3 | A4 | A5 | A6 | B3 | B4 | E3 | E4 | G3 | G4 | M3 | M4 |
| L0x | FB | FB | FB | FB | FB | FB | — | — | — | — | — | — | FB | FB |
| M0B and H0B | FB | FB | FB | FB | FB | FB | FB | FB | — | — | — | — | FB | FB |
| M0R and H0R | FB | 12 | 12 | 12 | 12 | FB | FB | FB | — | — | — | — | FB | FB |
| L4x and M4x | FB | 36 | 72 | 72 | 36 | FB | FB | FB | — | — | — | — | FB | FB |
| H4x | FB | 36 | 72 | 72 | 36 | FB | FB | FB | — | — | — | — | — | — |
| L6x | FB | — | 72 | 72 | — | FB | 108 | 108 | 36 | 36 | FB | FB | — | — |
| M9x and H9x | FB | 108 | 72 | 72 | 108 | FB | 108 | 108 | 36 | 36 | 36 | FB | — | — |

x = wildcard placeholder (e.g. L4x includes L4B and L4R)
FB = fully bonded strand
# = debonded length of strand in inches (1 in = 25.4 mm)
— = strand not present in specimen

**Table 3.2: Specified Jacking Stress, $f_{pj}$, for Top Strands (M3 and M4)**

| Specimen ID | $f_{pj}$ ksi (MPa) |
|---|---|
| x0x | 92 (635) |
| L4x | 202.5 (1395) |
| M4x | 46 (315) |

x = wildcard placeholder

According to standard practice, strands were tensioned to 75 percent of the specified tensile strength, $f_{pu}$. Thus, the jacking stress, $f_{pj}$, was 202.5 ksi (1395 MPa). However, the strands in the top (Strands M3 and M4) of some of the specimens were not fully prestressed. In some of the specimens with lower percentages of debonded strands or lower concrete strengths, these top strands were necessary to control the top fiber tensile stresses at release. To adequately control these stresses, less than full prestress was often required from these top strands. The values of $f_{pj}$ specified for strands M3 and M4 are given in Table 3.2 for the specimens in which they are present.

In order to satisfy allowable stress limits with regard to compression in the bottom fiber, a pair of strands was omitted from the bottom flange in beam pairs L0x and L6x. Thus, these beams had two fewer strands in the bottom flange than their higher strength companions.

With respect to debonding percentages/patterns, the beams are divided into three general groups. The first group, denoted with a "0" as the second digit of the identifier, represent strands with little or no debonding. Beam pairs L0B, M0B, H0B, and L0R contain no debonded strands. The strands in beam pairs M0R and H0R are not "fully bonded" because four of the strands in the bottom flange in each end were partially debonded for a length of 12 in (305 mm). This small amount of debonding was specified in an attempt to minimize the influence of the support reaction on the development length of these strands. This is discussed more fully in Chapter 7. Because the debonding of these strands occurs only over the support, they are included with the "fully bonded" specimen group. As discussed above, because debonding was not used to control top and bottom fiber stresses at release in these fully bonded specimens, top strands were required for all specimens in the group. In addition, two of the bottom flange strands were omitted from the lower strength specimens in the group.

This first group of specimens had a length 40 ft (12.19 m). Because of the extra length provided for debonding of strands, the specimens in the second and third group had a length of 54 ft (16.46 m).

The second group of specimens, represented by a "4" as the second digit of the identifier, featured partial debonding of 50 percent of the bottom flange strands. A staggered debonding pattern was employed. Two of the strands (A2 and A5) were debonded for a length of 36 in (914 mm); two others (A3 and A4) were debonded for a length of 72 in (1829 mm). Because of the use of debonding to lower the stresses in the end regions of the girders, top strands were only required for beam pairs L4x and M4x. The prestress required in these top strands decreased with increasing concrete compressive strength.

The third group of specimens, represented by either a "6" or a "9" as the second digit of the identifier, featured partial debonding of more than 50 percent of the bottom flange strands. Here again, a staggered debonding pattern was employed. Partially debonded strands were debonded over 36, 72, or 108 in (914, 1829, or 2743 mm) lengths. Because of allowable compressive stress limitations, only ten strands could be placed in the L6x specimens. Six of these ten strands were then partially debonded, resulting in a debonded percentage of 60 percent. The higher concrete strengths of the M9x and H9x specimens allowed the use of twelve strands, eight of which were to be partially debonded. However, after the L6x specimens were cast, the sponsor requested that the remainder of the specimens have 75 percent of the strands partially debonded. Because no more than twelve strands could be placed in these specimens (M9x and H9x), this percentage was impossible to obtain symmetrically. Accordingly, one of the strands located in the web of the specimens (Strand G3) was debonded for a length of 36 in (914 mm). Thus, nine of the twelve strands were partially debonded in an unsymmetrical pattern.

In the specimens with more than 50 percent of strands debonded, a pair of strands was placed within the beam web (Strands G3 and G4), and another pair was placed at the junction of the web and the bottom flange (Strands E3 and E4). This was done in an attempt to investigate whether these strands would behave differently than their counterparts within the bottom flange.

The debonding patterns used in these specimens violated the requirements of the AASHTO LRFD Code (1998) Section 5.11.4.3 in several ways. First, in the specimens with partially debonded strands, the number of partially debonded strands significantly exceeded 25 percent of the total number of strands as limited by the LRFD Code. Second, in all rows in which strands were debonded, more than the LRFD Code maximum 40 percent of the strands in the row were debonded. Third, in the M9x and H9x specimens, debonded strands were not symmetrically distributed about the centerline of the member as required. Finally, the exterior strands in several of the horizontal rows (Rows B, E, and G) were partially debonded. The LRFD Code requires that exterior strands in each horizontal row be fully bonded.

### 3.3.2 Deck Design

Design details of the cast-in-place deck are shown in Figure 3.5. The primary purpose of the deck slab is to provide a large compression flange for the beam. The width of the deck allows the neutral axis to be high in the member at flexural failure, resulting in a large curvature and high strains in the tension reinforcement. Using strain compatibility analysis, the deck size was selected to result in a total elongation of at least 3.5 percent in the bottom row of strands at flexural failure. A 28-day concrete compressive strength of 6000 psi (41 MPa) was specified for the deck. Use of a lesser strength would have required a larger deck to achieve the same degree of strand elongation. In addition, specifying a higher 28-day concrete strength allowed for development length testing at an earlier age, thus accelerating the testing schedule.

As depicted in Figure 3.5, deck reinforcement consisted of two mats (top and bottom) of orthogonal #4 reinforcing bars. The bars were spaced to provide a reinforcement ratio that roughly approximated that of a typical bridge deck.

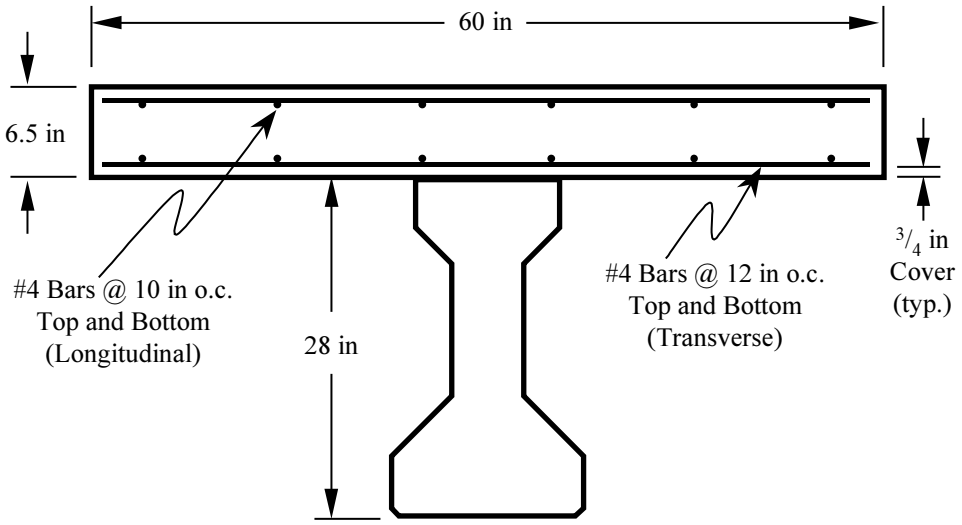


**Figure 3.5: Dimensions and Reinforcement of Cast-in-Place Composite Deck (1 in = 25.4 mm)**

### 3.3.3 Mild Steel Beam Reinforcement

Mild steel reinforcement for the precast beams corresponded to that used in standard TxDOT practice. Reinforcement for the 40 ft (12.19 m) beams is shown in Figure 3.6. Reinforcement for the 54 ft (16.46 m) specimens, which contain debonded strands, is shown in Figure 3.7. Figure 3.8 illustrates the details of each of the bar types shown in Figure 3.6 and Figure 3.7. The bar types (R, S, X, etc.) are labeled according to TxDOT practice.

In the 40 ft beams, the "V" bars, which aid in confining the bottom flange, were placed as shown on TxDOT standard I-beam designs. For the beams with partially debonded strands, the location of the "V" bars was extended to confine the bottom flange throughout the expected transfer lengths of the debonded strands. The horizontal web reinforcement, or H-bar(s), which were placed in End "C" of each beam pair, also served as a deviation from standard TxDOT practice.

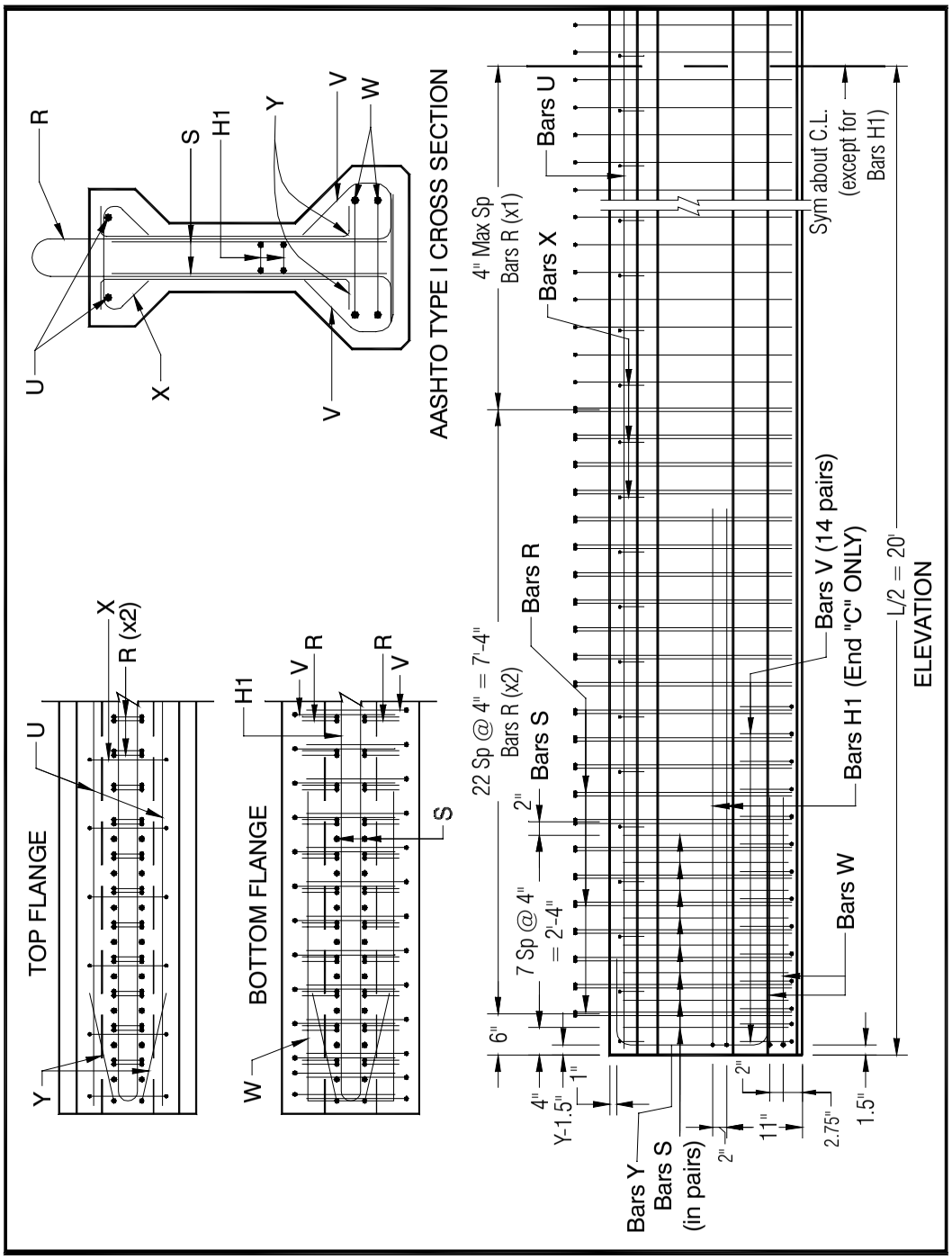


**Figure 3.6: Mild Steel Reinforcement for Specimens L0x, M0x, and H0x (1 in = 25.4 mm)**

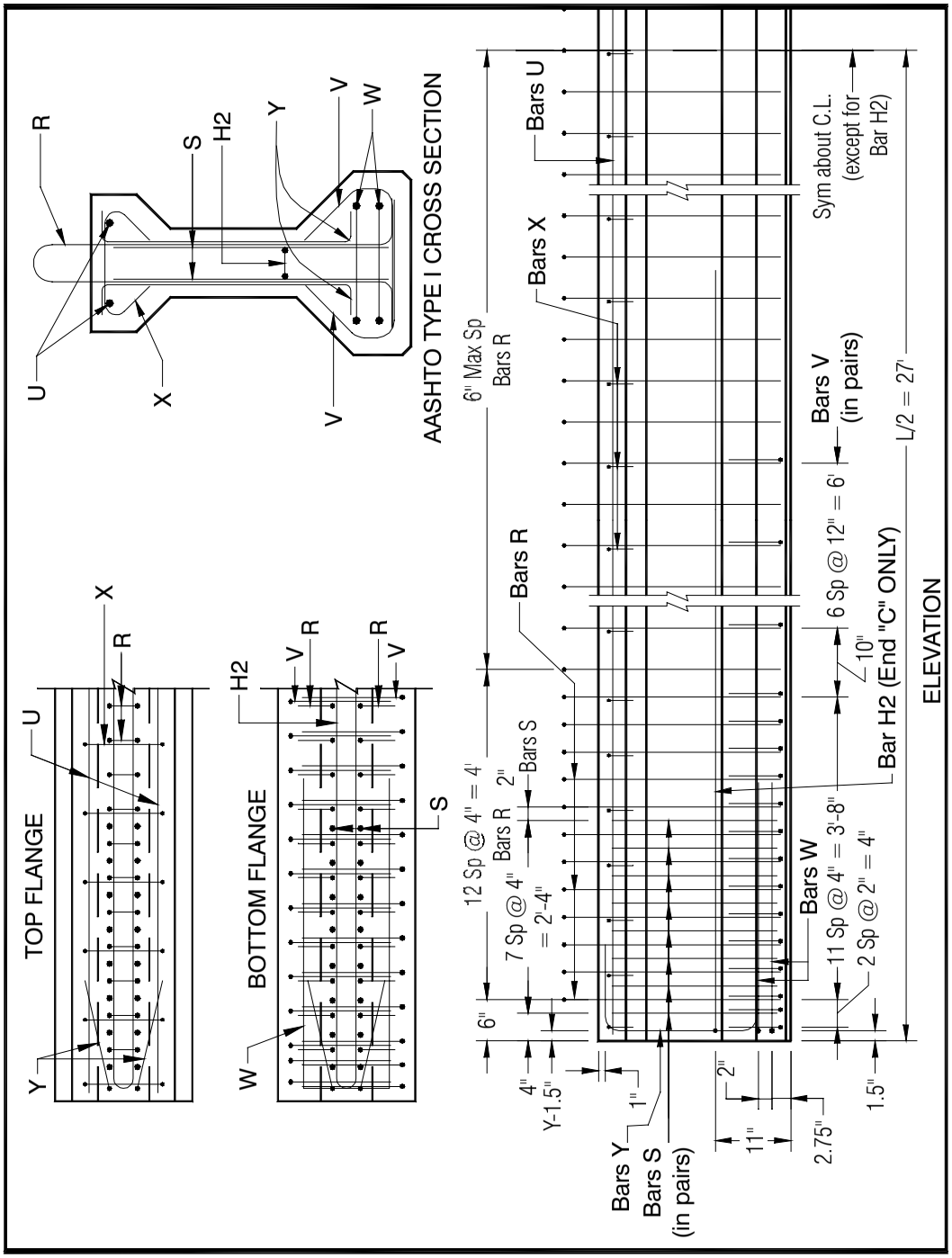


**Figure 3.7: Mild Steel Reinforcement for Specimens L4x, M4x, H4x, L6x, M9x, and H9x (1 in = 25.4 mm)**

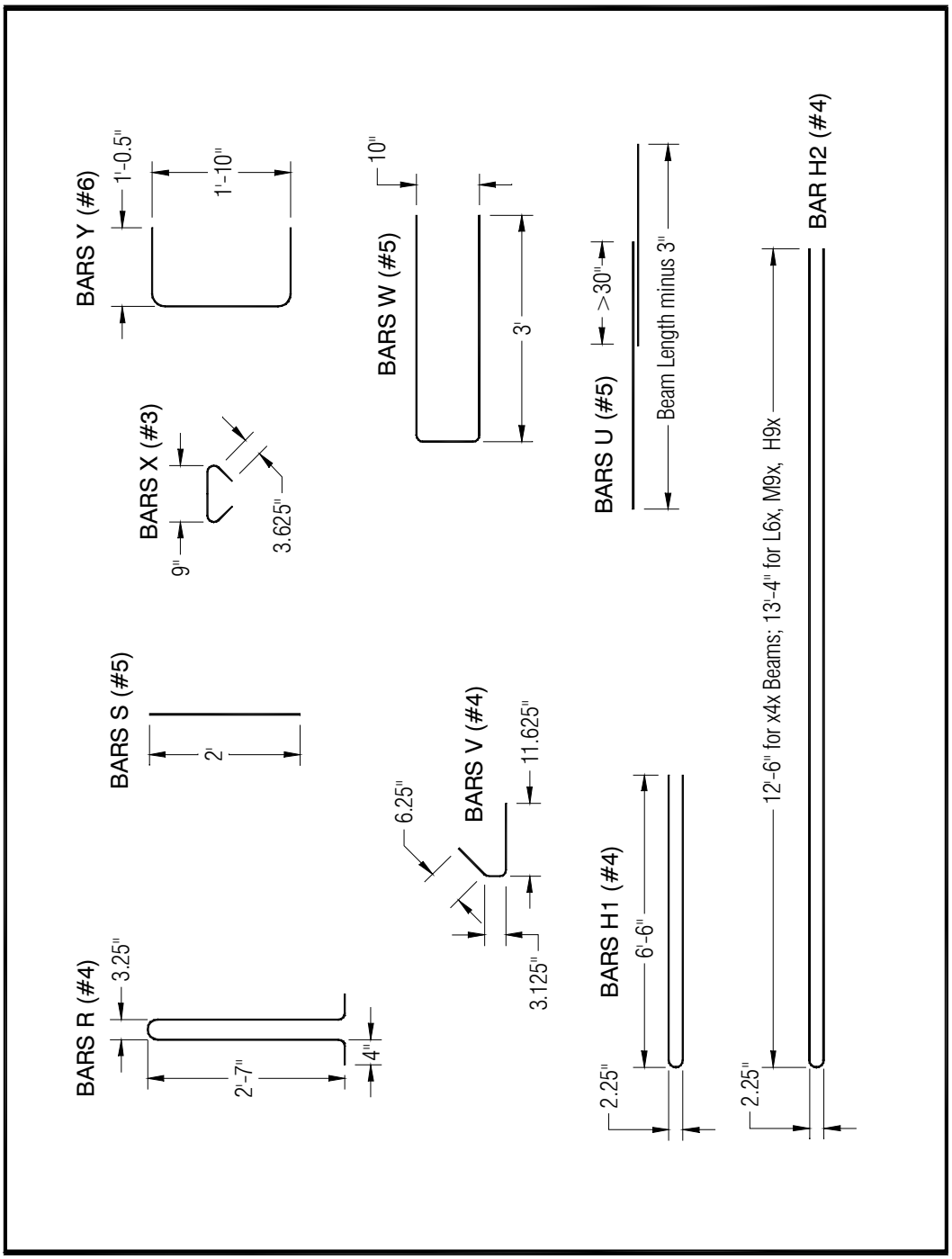


**Figure 3.8: Reinforcement Details (1 in =25.4 mm)**

The most significant deviation in terms of mild steel reinforcement was that of the shear reinforcement, or "R" bars. Because the development length testing process involved the application of large concentrated loads relatively close to the supports, a significant increase in shear reinforcement was required compared to the TxDOT standard design for this size I-beam. The maximum applied load, and hence the shear to be resisted, depended on the geometry of each development length test. The shear span—and the expected shear force—of each test was directly linked to the embedment length to be tested. Unfortunately, it was impossible to precisely determine during the design phase what embedment lengths would be tested.

In general, the shortest probable shear span was estimated for each test series, and a maximum expected shear force was calculated based on the expected flexural capacity of the specimen. Stirrups were then proportioned according to the shear provisions of the ACI 318 and AASHTO Standard Codes to provide this shear capacity (assuming that the concrete would be able to adequately resist the resulting diagonal compression in the beam web). These stirrup layouts have since been checked according to the Sectional Design Model of the AASHTO LRFD Code (Section 5.8.3) and were found to satisfy these requirements also. Because the stirrups ("R" bars) were proportioned based on conservative estimates of the expected shear, the shear capacity provided was often well in excess of the actual applied shear during the development length tests, especially for tests with longer embedment lengths.

Horizontal web reinforcement ("H" bars) was placed in one end (End C) of each beam pair. These H bars were #4 reinforcing bars bent into a hairpin and placed inside the vertical shear reinforcement in the bottom of the web. The number of bars was determined based on recommendations by Russell and Burns (1993, 196–198), who suggested that this type of reinforcement might enhance the post-slip capacity of the member. Here again, proper design of the reinforcement depended on knowledge of the ultimate shear force during development length testing. However, the embedment length—and the resulting shear—for End C would necessarily depend on the experimental behavior of other beam ends (A and B) in the same beam pair. An embedment length was assumed based on the existing ACI/AASHTO Code relationship for development length, and the calculations were carried out using the value of shear force that resulted. Unfortunately, the critical embedment length always proved to be shorter than the value assumed, and the shear applied during the test therefore exceeded that assumed during H-bar design. Consequently, the capacity provided by the H bars—relative to the test shear force—proved to be smaller than that recommended by Russell and Burns.

## 3.4 MATERIAL PROPERTIES

This section includes a description of the various materials used in the construction of the test specimens. These materials include the concrete for the precast, pretensioned I-beams, the cast-in-place concrete for the deck slab, the prestressed reinforcement, and the non-prestressed, mild steel reinforcement. Material properties are discussed.

### 3.4.1 Precast Concrete

Three distinct concrete mixes were used to cast the precast, pretensioned concrete I-beams at the Texas Concrete Company plant in Victoria, Texas. A comparison of the specified properties of the three mixes is shown in Table 3.3. The mix proportions for these three concrete mixes are tabulated in Appendix A. The concrete for all three mixes displayed a slump of approximately 8 in (200 mm) at the onset of casting. The release strength, $f'_{ci}$, was obtained in less than twenty-four hours.

**Table 3.3: Specified Properties of Precast Concrete Mixes**

| Specimen Series | $f'_{ci}$ psi (MPa) | $f'_c$ psi (MPa) |
|---|---|---|
| L | 4000 (28) | 5000–7000 (34–48) |
| M | 7000 (48) | 9500–11500 (66–79) |
| H | 9000 (62) | 13000–15000 (90–103) |

The L-Series concrete represented concrete normally used in the pretensioned prestressed concrete industry for bridge girders. The range of $f'_c$ shown in Table 3.3 reflects the desired compressive strength of the concrete at an age of 28 days. The coarse aggregate for this mix consisted of ¾-in (19-mm) river gravel. A 28 percent fly ash replacement was used; the resulting water-to-cementitious-materials ratio was approximately 0.33.

The M-Series concrete was a high strength concrete also containing ¾-in (19-mm) river gravel. Here again, the range of $f'_c$ shown in Table 3.3 reflects the desired compressive strength of the concrete at an age of 28 days. This mix featured a 25 percent fly ash replacement and a water-to-cementitious-materials ratio of 0.28. Actual concrete compressive strengths for this mix tended toward the high side of the specified strength range.

The H-Series concrete was a high strength concrete containing ½-in (10-mm) crushed limestone coarse aggregate. This mix featured a fly ash replacement of 35 percent and a water-to-cementitious-materials ratio of 0.25. The range of $f'_c$ shown in Table 3.3 for this mix reflects the desired compressive strength of the concrete at an age of 56 days. Actual compressive strengths for this mix tended toward the low side of this specified range. A few specimens in this series never reached the specified concrete strength range.

Concrete compressive strength and modulus of elasticity were monitored at various ages by means of the test methods described in ASTM C39-93 and ASTM C469-94, respectively. Cylinders dimensions were 4 in x 8 in (102 mm x 203 mm). Neoprene pads with steel end caps were used for testing. The measured mechanical properties of the concrete test specimens are tabulated in Appendix B.

Two methods of curing were used for the precast concrete test cylinders. Cylinders cured by the first method, denoted as "member-cured," were used for all precast beam specimens. These cylinders were placed adjacent to (against the forms and beneath the curing blankets) the companion beam specimens immediately after casting. Once the forms were removed from the I-beams, the test cylinders were stored in the same environment as the beams until testing.

The second method of curing, known as "match curing," was also used for test cylinders cast with most of the beam specimens. This method involved using special cylinder molds to match the temperature of the concrete in the companion beam. The beam concrete temperature was evaluated by means of a thermocouple placed in the bottom flange of one beam in each pair. This temperature, along with that of the cylinder molds, was monitored periodically, and a heating element in each cylinder mold was turned on or off accordingly. In this manner, the curing temperature of the cylinders closely followed that of the beam. This curing system, the details of which are more thoroughly described by Myers and Carrasquillo (1998), has the potential to become widely used by precast producers in the future. Thus, these values of cylinder strength were recorded for potential use in calibrating future behavioral relationships based on the experimental data obtained from this study. The average strengths obtained from cylinders cured by both methods at various ages are tabulated in Table B.5 of Appendix B.

### 3.4.2 Cast-in Place Concrete

The concrete for the cast-in-place, composite deck slab was delivered to the Ferguson Laboratory from ready-mix supplier Capitol Aggregates of Austin, Texas. The specified 28-day strength of this concrete was 6000 psi (41 MPa). The mix proportions for this concrete are also tabulated in Appendix A. The water-to-cement ratio for this mix was approximately 0.48. The slump of the concrete during casting operations was typically in the range of 2–4 in (50–100 mm). The cylinder compressive strength of the concrete was assessed at ages of 7, 14, and 28 days. In addition, strengths were recorded and the modulus of elasticity, $E_c$, was evaluated when shores were removed after casting as well as at the time of development length testing. Concrete compressive strength was evaluated according to ASTM C39-93 procedures, except that neoprene pads in combination with steel caps were used at the cylinder ends. Modulus of elasticity was determined according to ASTM C469-94. Standard 6 in x 12 in (152 mm x 305 mm) cylinders were used for the cast-in-place concrete. The measured mechanical properties of the concrete at various ages are tabulated in Appendix B.

### 3.4.3 Prestressing Steel

The prestressing steel used in this study was 0.6 in (15.2 mm) diameter, ASTM A416, Grade 270, low relaxation, seven-wire prestressing strand. The strand was manufactured at the Houston plant of Shinko Wire America (now American Spring Wire) and shipped to the Texas Concrete Company in Victoria. The cross-sectional area of the strand was 0.217 $in^2$ (140 $mm^2$).

#### *3.4.3.1 Stress-Strain Relationship*

Tension tests performed on samples of the strand revealed a modulus of elasticity, $E_p$, of 28,000 ksi (193 GPa). Although the guaranteed ultimate stress, $f_{pu}$, was 270 ksi (1860 MPa), the strand exhibited strengths in excess of 280 ksi (1930 MPa) prior to fracture in tension tests. Because large strains were expected in the strands prior to flexural failure, a stress-strain relationship based on a Menegotto and Pinto power formula (Devalapura and Tadros 1992) was developed from these results. This stress-strain relationship, which is compared with the relationship given by the *PCI Design Handbook* (1999, 11-22) in Figure 3.9, was used in the analysis of development length test results. The PCI relationship was inadequate because it did not reflect stresses higher than 270 ksi.

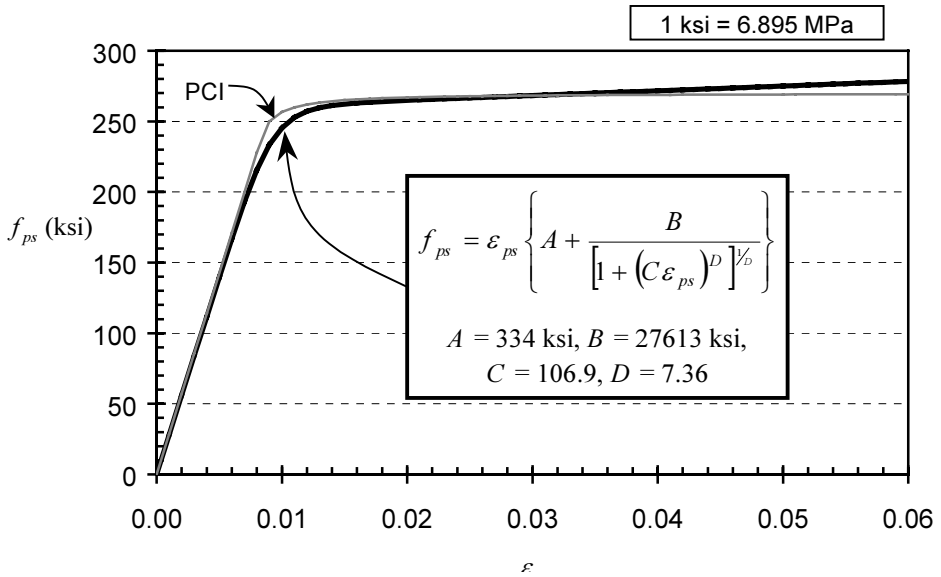


**Figure 3.9: Stress-Strain Curve of Prestressing Strand (Compared with Relationship from *PCI Design Handbook*)**

### *3.4.3.2 Strand Surface Condition*

In an effort to bound the typical strand surface conditions that might be found in practice, half of the specimens were prestressed with strand featuring a "bright" surface condition, while the other half were prestressed with "rusted" strand. For this study, bright strand was defined as strand in the as-received condition. This strand was stored indoors between uses. Typical bright strands are shown in Figure 3.10. The strand had a smooth surface texture that was free from rust aside from an occasional light spotting resulting from atmospheric exposure during fabrication of the beam reinforcement cages. This exposure was generally limited to three days prior to casting. Because a small amount of weathering may have occurred during this period, this strand surface condition may be more akin to strand identified as "slightly weathered" in some laboratory-research projects. No attempt was made to clean the strand.

**Figure 3.10: "Bright" Strand Surface Condition**

"Rusted" strand had been exposed to weather in the precasting yard for several months resulting in a significant coating of rust. Typical rusted strands are shown in Figure 3.11. This corrosion had not advanced to the point of significantly affecting the cross-sectional area of the strand, nor were corrosion products easily removed from the surface of the strand. No attempt was made to clean the rusted strand.

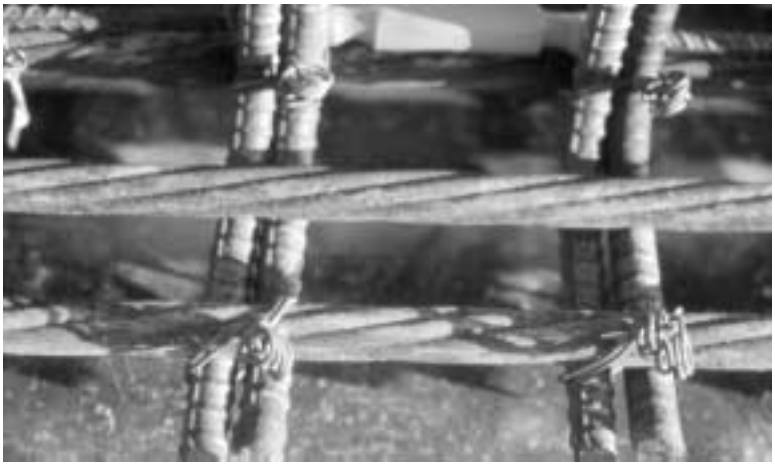

**Figure 3.11: "Rusted" Strand Surface Condition**

### 3.4.4 Mild Reinforcing Steel

The mild steel used to reinforce the beam and slab consisted of ASTM A615 Grade 60 reinforcing bars. The modulus of elasticity of this reinforcement was assumed to be 29,000 ksi (200 GPa) for analysis purposes. All mild steel reinforcement that contributed to the flexural strength of the member consisted of #4 and #5 bars. Tension tests on samples of these bars revealed a yield stress, $f_y$, of 61 ksi (420 MPa). This value was used in the analysis of development length test results. Reinforcement details are given in Figures 3.5 through 3.8. Actual reinforcement is depicted in Figures 3.12 through 3.15.

## 3.5 FABRICATION OF PRECAST I-BEAMS

Strand for the precast beams was generally positioned and tensioned one day prior to casting. The specified jacking stress, $f_{pj}$, was verified by checking both the hydraulic pressure in the jacking system and the elongation of the strands. Once the strands were adequately tensioned, jacketing of any partially debonded strands commenced. Flexible polyethylene tubing was placed around the length of strand to be debonded. A second layer of tubing was placed to cover the slit in the first layer. The entire length of tubing was then taped to close any gaps and to secure the tubing. After strand jacketing was completed, the mild steel reinforcing cage was fabricated. The beam reinforcement is shown in Figure 3.12 and Figure 3.13.

**Figure 3.12: Reinforcement for Pair of I-Beams**

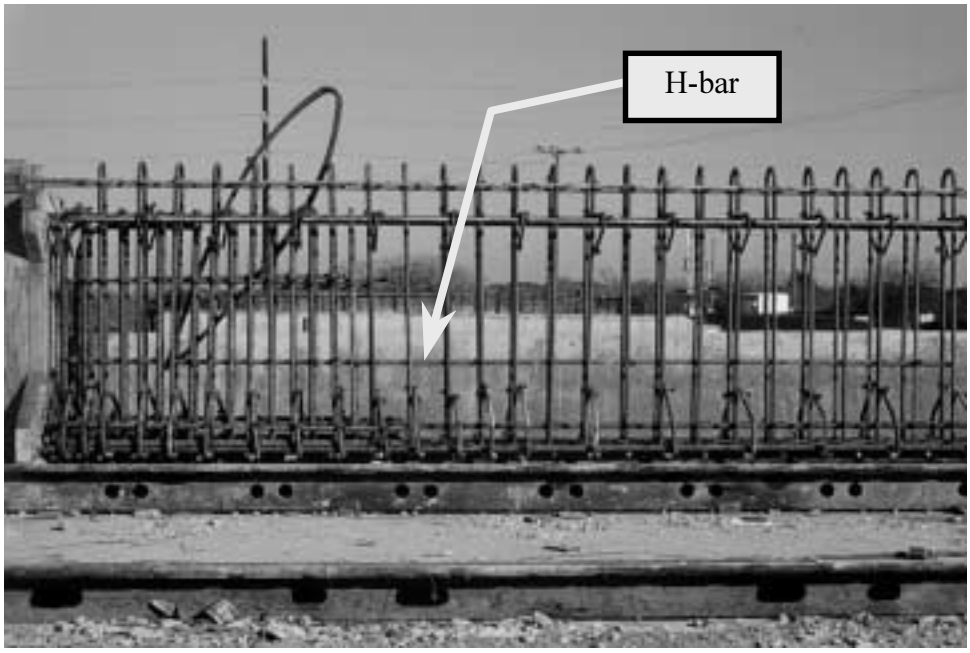


**Figure 3.13: Anchorage Zone Reinforcement for Specimen L4B-C**

On the day that the beams were cast, operations began with cleaning the prestressing bed. Form release agent was then applied to the soffit form in the manner shown in Figure 3.14. The release agent was carefully squirted in a thin stream on the form so that the reinforcement was not contacted. The flexible brush shown in Figure 3.14 was then used to distribute the release agent over the form area so that the bond quality of the strands was not compromised due to contamination.

The side forms were then placed and secured as shown in Figure 3.15. After batching, the concrete was placed and consolidated by means of internal vibration as shown in Figure 3.16. Test cylinders were cast from the concrete batch simultaneous with the beam casting. As discussed in Chapter 4, the block containing strands for pull-out testing was cast immediately after the I-beams. Once the exposed top surface of each I-beam was given a wire-brush finish, curing blankets were placed as shown in Figure 3.17. Finally, the entire bed was covered with tarpaulins. For most of the specimens, no steam curing was applied. However, for the few specimens cast when air temperatures were expected to drop below approximately 50 degrees F (10 degrees C), a limited amount of steam curing was utilized. Enough steam was used to bring ambient curing temperatures up to a level generally experienced during warmer weather.

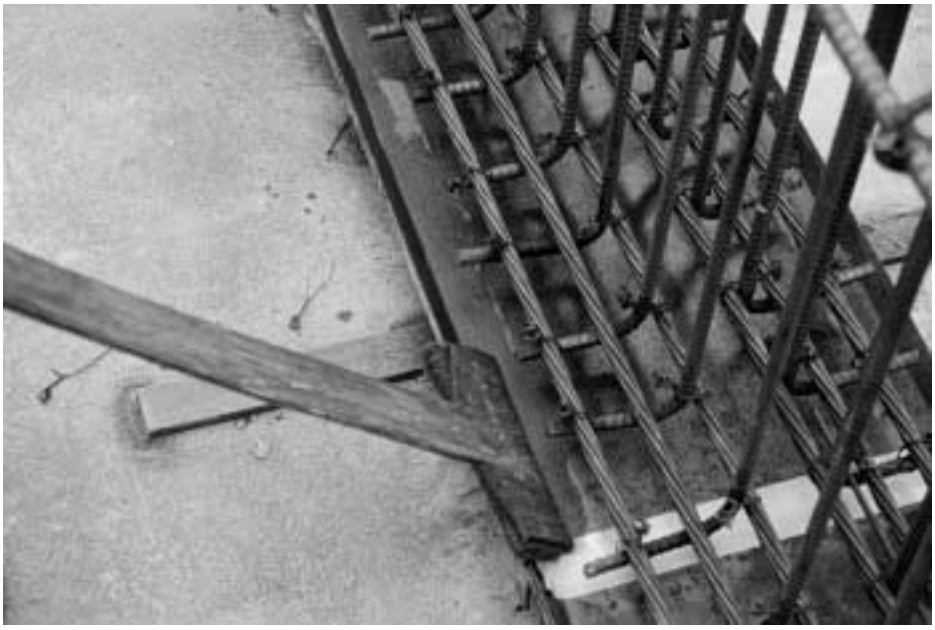

**Figure 3.14: Distributing Form Release Agent over Soffit Form Surface**

**Figure 3.15: Placement of Side Forms**

**Figure 3.16: Casting and Vibrating Precast Beam Concrete**

**Figure 3.17: Covering Precast Beams with Curing Blankets**

On the morning after casting, the side forms were removed. Instrumentation of the beams for transfer length testing then commenced as described in Chapter 5. Cylinders were tested to monitor the strength of the beam specimens prior to release. Once the specified release strength was reached, the prestress force was transferred to the concrete by flame-cutting the tensioned strands as shown in Figure 3.18. After the completion of initial transfer length testing, the beams were transported by lift trucks into storage until long-term transfer length testing was performed.

**Figure 3.18: Transfer of Prestress by Flame-Cutting**

## 3.6 FABRICATION OF COMPOSITE DECK SLAB

Each beam pair was transported by truck to the Ferguson Laboratory. Once the two beams were moved into the laboratory, preparation for deck slab casting began. Reusable plywood forms were used for slab fabrication. One deck slab was cast at a time. Figure 3.19 shows the form system during assembly. Once the forms were installed, leveled and sealed, form release agent was sprayed on the form surfaces. Slab reinforcing bars were then placed and secured as can be seen in Figure 3.20.

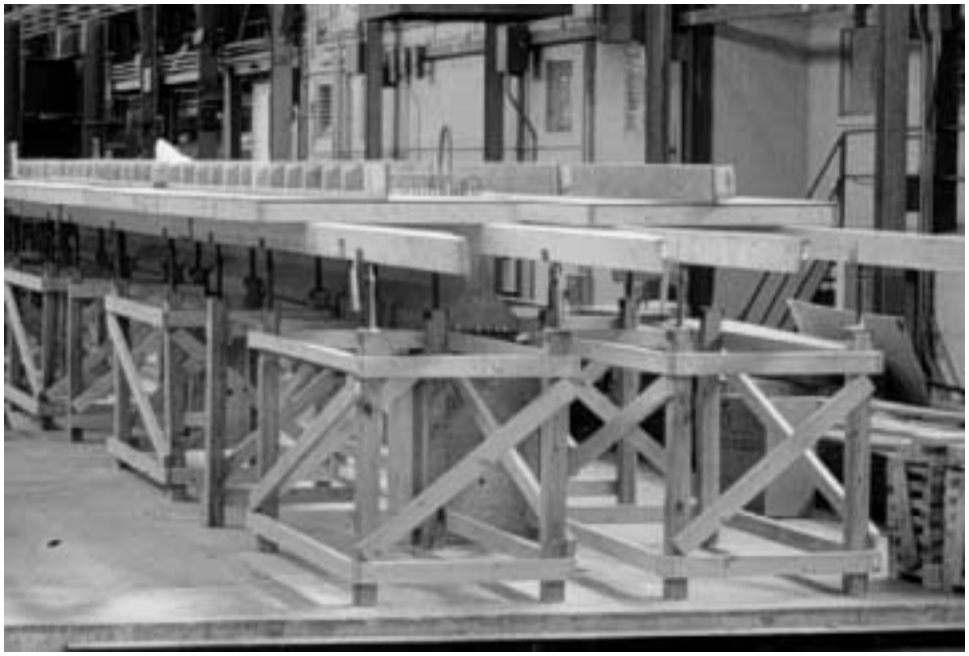

**Figure 3.19: Forms for Cast-in-Place Deck Slab**

**Figure 3.20: Slab Reinforcement Prior to Casting**

Both the slab forms and the precast I-beam were shored during casting of the deck concrete. The ready-mix concrete was placed within the forms by means of a crane-suspended bucket. The deck slab and test cylinders were cast concurrently. Consolidation of the deck concrete was achieved with the aid of internal vibrators. Once the concrete was screeded with a straightedge, the surface was bull-floated as shown in Figure 3.21. The surface was then hand-floated, and a trowel-finish was applied. The concrete cured under polyethylene sheeting for one week.

**Figure 3.21: Bull-Floating Surface of Slab after Casting**

After a few days, shores and forms were removed. After this operation the weight of the slab, which had been transferred directly to the floor via shoring, was transferred to the beam supports through the flexural resistance of the composite beam. The age, concrete strength, modulus of elasticity of both the beam and slab concrete upon removal of shores and forms is reported in Table B.2 of Appendix B. Once the forms and shores were removed, deck slab fabrication steps were repeated for the second beam of the pair.

# CHAPTER 4: STRAND PULL-OUT TESTING

## 4.1 INTRODUCTION

A program of strand pull-out testing was performed to assess the bond quality of the prestressing strand used in this study. This chapter provides historical background on the use of this type of test, a description of the test procedure and the results of the test program.

## 4.2 BACKGROUND

For many years, researchers paid scant attention to the idea that strand bond quality might vary significantly depending on the manufacturer or, more specifically, the strand manufacturing process. Test results obtained in 1986 at North Carolina State University (NCSU) forced practitioners to seriously consider this possibility. Transfer lengths of 0.5 in (12.7 mm), uncoated strand measured in the NCSU study were approximately two to three times the ACI and AASHTO design value of $50d_b$ (Cousins, Johnston and Zia 1990). The results of this study eventually led to the 1988 FHWA restrictions and modifications discussed in Section 1.1. The modifications included the increase of calculated development length by 60% (FHWA 1988).

While evaluating the NCSU results on behalf of the Precast/Prestressed Concrete Institute (PCI), Logan (1997) noticed that the measured strand draw-in values for the NCSU specimens were significantly larger than draw-in values measured for hollow-core slabs at his precast concrete plant. Since the strands used in the hollow-core slabs were produced by a different manufacturer than those in the NCSU study, Logan recommended that a test program be conducted to compare the bond quality of strand from various manufacturers.

### 4.2.1 CTC Pull-out Tests

Because, there was no accepted standard test method for bond quality the PCI Prestressing Steel Committee decided in 1992 to use a simple pull-out test procedure developed by Moustafa in 1974 for testing lifting loops at the Concrete Technology Corporation (CTC) in Tacoma, Washington. The test method consisted of measuring the maximum pull-out force resisted by an untensioned, 0.5 in strand embedded 18 in (457 mm) within a concrete test block (Moustafa 1974). The 1992 test program included strand from seven different manufacturers. These tests were again performed at CTC under the supervision of Moustafa. Strand from three of the manufacturers exceeded the average maximum capacity of 38.2 kips (170 kN) established in the 1974 tests. The average capacity of these strands ranged from 41.2 to 42.8 kips (183 kN to 190 kN). However, strand from the remaining four manufacturers exhibited average capacities significantly less than this benchmark value, ranging from 19.6 to 23.5 kips (87 to 104 kN). Based on their pull-out capacities, the various strands could be classified in two distinct behavioral groups. Logan (1997) notes that the pull-out capacity for strand used at his plant exceeded the 1974 benchmark. He also reports that the 1992 results suggest a reason for the poor performance of the NCSU strand, but abstains from stating whether or not the manufacturer of this strand was among the seven included in the test program.

### 4.2.2 University of Oklahoma Test Program

Some members of the PCI Prestressing Steel Committee objected to the use of the simple pull-out test because it may not accurately represent the bond performance of pretensioned strand. This objection led to a research study undertaken at the University of Oklahoma to evaluate the effectiveness of various test methods for strand bond quality. "As-received" strand from three manufacturers was included in the test program (Rose and Russell 1997). Strand from one of the manufacturers was also tested with three other surface conditions: cleaned (with muriatic acid), silane-treated (emulating a slightly lubricated surface) and weathered. Transfer lengths in pretensioned beams containing the various strand types were measured with a detachable, mechanical (DEMEC) strain gauge. These transfer lengths were compared with results obtained from simple (Moustafa) pull-out tests, pull-out tests of pretensioned strand, and measurements of the strand draw-in at release in the beam specimens.

The Oklahoma researchers found the pull-out tests of pretensioned strand difficult to perform. The results of these tests were inconsistent with the other methods. Thus, they recommended that these tests not be used in evaluating strand bond quality. On the other hand, the simple pull-out tests on untensioned strand yielded results that

correlated well with the measured transfer lengths (excluding the silane-treated specimens). In spite of this correlation, the pull-out test results were overly sensitive to changes in transfer length; i.e. small differences in measured transfer lengths between specimens resulted in relatively large differences in maximum pull-out capacity in the companion tests. As a result, the relationship established between pull-out capacity and transfer length is impractical. For pull-out capacities as low as zero, the relationship predicts transfer lengths shorter than given by ACI and AASHTO code expressions. Thus, the data was judged to be inconclusive regarding the validity and usefulness of the simple pull-out test. The researchers recommended the use of strand draw-in measurements as the best means of assessing bond quality. Draw-in measurements are discussed in detail in Chapter 6 of this report.

The loading rate used in the Oklahoma simple pull-out tests differed significantly from that of the Moustafa procedure. The Oklahoma researchers carefully measured strand displacements under load, and as a result, each of their tests took approximately twenty minutes to complete. The earlier CTC tests using the Moustafa procedure were completed in less than two minutes each. Faster loading rates typically result in higher pull-out capacities. Rose and Russell hypothesize that the different loading rate caused the Oklahoma pull-out specimens to exhibit a larger apparent sensitivity to bond quality than the Moustafa test specimens. They recommend that future testing utilize the loading rate of the Moustafa Test.

### 4.2.3 Stresscon Test Program

Unsatisfied with the results of the Oklahoma study, Logan initiated a test program at Stresscon Corporation in Colorado to correlate the results of Moustafa pull-out tests with the results of development length tests of both simply-supported and cantilever beam specimens (Logan 1997). The study included "as-received" strand supplied by five concrete producers. A sixth set consisted of weathered strand from one of the five producers. The weathered strand was described has having a "light coating of rust." For each of the six groups of strands, results of Moustafa pull-out tests on the strand were compared with measured draw-in lengths and development length test results for ten beam specimens. Four of the strand groups had average pull-out capacities above 36 kips (160 kN). Maximum pull-out resistance of these strands typically occurred immediately prior to abrupt failure at a loaded-end displacement ranging from 0.5 to 2 in (13 to 50 mm). Logan classifies these groups as having "high bond quality." The remaining two strand groups had average pull-out capacities of approximately 11 kips (49 kN). These strands pulled out gradually, and the peak resistance occurred after 6 to 8 in (150 to 200 mm) of loaded-end displacement. Little paste bond appeared between the strand and the concrete for these two groups. This indicates a lack of adhesion between the steel and concrete, which may result from residual lubricant on the surface of the strands. Logan classifies these strands as having "poor bond quality."

Based on the results of the development length tests, Logan concludes that there is a significant difference in bond quality among different manufacturers. The strands classified as having "high bond quality" based on their Moustafa pull-out capacities (>36 kips) all exhibited development lengths less than indicated by the ACI development length equation. The "poor bond quality" strands all experienced a substantial increase in draw-in during the first 21 days (measurements were not made after 21 days) and exhibited development lengths greater than indicated by the ACI equation. Thus, Logan contends that an average Moustafa test capacity of at least 36 kips (160 kN) with a standard deviation of ten percent or less for a six sample group should be required for 0.5-in pretensioning strand. This standard might be lowered based on future test results from strand with pull-out capacities between 12 and 36 kips. Logan recommends that the Moustafa test also be performed with a range of concrete mixes and with 0.6 in (15.2 mm) strand so as to potentially broaden its applicability.

In order to assess the bond quality of the strand used in this study relative to strand used in previous research, companion pull-out tests were performed for each set of beam specimens cast. As recommended by Logan, the test program consists of pull-out tests of 0.6 in strand embedded in concrete of various strengths.

## 4.3 SPECIMEN PREPARATION

A single pull-out test block containing six strand specimens was cast as a companion to each pair of beam specimens. Pull-out test block details are shown in Figure 4.1. The representative strand specimens were cut from the actual strand used in the companion beam specimens. These six strand specimens and the supporting light reinforcement cage were assembled at approximately the same time as the beam reinforcement. The reinforcement cage should have had minimal effect on results because the reinforcement was located at the extreme ends of the embedded length of strand, and no load-induced cracking was observed in the test specimens. The strands were positioned to have an embedment length of 18 in (460 mm). An additional 2 in (50 mm) length of each strand was

jacketed immediately inside the finished surface of the concrete. Strands had a side cover of 6 in (150 mm) and a center-to-center spacing of 12 in (300 mm). The end of each strand was supported 4 in (100 mm) above the bottom of the block. Each block was cast immediately after the placement of the same concrete in the beam pair. The concrete was consolidated with the same internal vibration technique used for the companion beams. Figure 4.2 and Figure 4.3 show the pull-out block being cast, and Figure 4.4 shows the formed and finished block. The pull-out block forms were stripped on the same day as those for the companion beams.

The concrete composition of the test block differed from that proposed by Logan. For a standard bond quality acceptance test, Logan proposes the use of a concrete mix that contains no high-range, water-reducing admixtures. In addition, he limits the concrete strength at the time of testing to between 3500 and 5900 psi (24.7 and 40.7 MPa). In this program, the actual beam specimen concrete was used for the pull-out block. These mixes contained a high-range, water-reducing admixture and achieved strengths at the time of pull-out testing that ranged from 4400 to 11710 psi (30.3 to 80.7 MPa). Concrete mix design quantities are detailed in Appendix A.

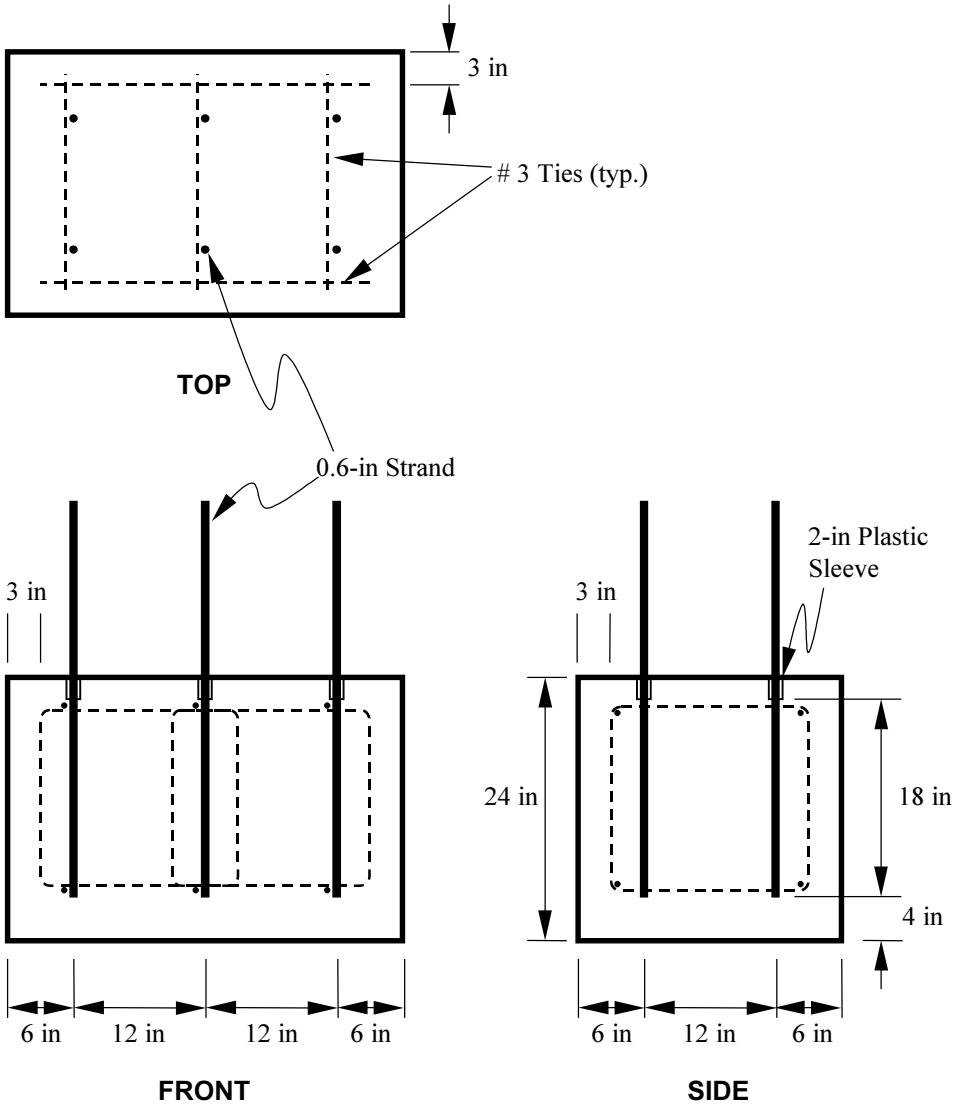


**Figure 4.1: Pull-Out Test Block Details (1 in = 25.4 mm)**

**Figure 4.2: Pull-out Test Block at Onset of Casting**

**Figure 4.3: Casting Pull-out Test Block**

**Figure 4.4: Finished Pull-Out Test Block**

## 4.4 TEST PROCEDURE

Pull-out testing was generally performed at the precast plant two to three days after casting (one to two days after release of prestress in the companion beam specimens). The pull-out test setup is shown in Figure 4.5. First, the bridging device was slipped over the strand to be tested. This was followed by a 100-kip (44 kN), shear-type load cell with a center hole. Next a 50 ton, single-acting, hydraulic cylinder was mounted on the load cell such that the strand extended through the cylinder's center hole. A plate and self-seating chuck were then used to anchor the strand against the piston of the hydraulic cylinder. By means of a manually-controlled, variable-speed, air-powered pump, load was applied at an approximate rate of 20 kips (90 kN) per minute until the maximum load was reached. The approximate displacement of the strand relative to the surface of the block at maximum load was recorded.

The testing procedure closely matched that proposed by Logan (1997, 87–90) with a few modifications. First, the bridging device did not exactly match that proposed by Logan. Nonetheless, the distance from the strand to each load-bearing leg of the device was approximately the same as with Logan's device. Logan specifies the use of a "pull-jack" with a travel of at least 12 in (305 mm). In these tests, a center-hole jack was used to "push" against a chuck which, in turn, "pulled" on the strand. The stroke of this jack was approximately 3 in (75 mm). However, this shorter length of travel proved adequate. The maximum pull-out capacity was always reached at a loaded-end displacement less than 3 in.

**Figure 4.5: Pull-out Test in Progress**

## 4.5 RESULTS AND DISCUSSION

Results of the 0.6 in (15.2 mm) strand pull-out tests are reported in the six tables that follow (Table 4.1 through Table 4.6). A few of the strand specimens were embedded for lengths longer than 18 in (460 mm) in the earliest blocks tested (Series L0B, L4B, L0R, M0B, M4B and H0B). These longer embedment lengths provided little significant information, and the results of these tests are not reported here. Thus, there are fewer than six results for the corresponding test blocks. There are four "failure types" listed. *Fracture* indicates a loss of resistance due to fracture of one or more of the wires composing the strand. *Abrupt Slip* represents an irrecoverable loss of resistance resulting from an abrupt slip. This abrupt portion of the total slip generally measured approximately $^{3}/_{8}$ in (8 to 11 mm) and followed some gradual slip. *Gradual* indicates that the resistance first increased and then began to diminish as the slip gradually increased. *Test Halted* represents a test that was stopped deliberately after reaching a load higher than the nominal breaking strength of the strand (58.6 kips [261 kN]).

**Table 4.1: Pull-Out Test Results—Bright Strand, Low Strength Concrete**

| Test ID | $f'_c$ at Test Age psi (MPa) | Maximum Load kips (kN) | Pull-out Length at Max. Load in (mm) | Failure Type |
|---|---|---|---|---|
| L4B-A | 4970 (34.3) | 46.1 (205) | 1.15 (29) | Abrupt Slip |
| L4B-B | | 51.0 (227) | 1.15 (29) | Abrupt Slip |
| L4B-C | | 54.1 (241) | 1.25 (32) | Abrupt Slip |
| L6B-A | 5500 (37.9) | 58.4 (260) | 1.50 (38) | Fracture |
| L6B-B | | 58.4 (260) | 0.75 (19) | Fracture |
| L6B-C | | 57.9 (258) | 2.00 (51) | Fracture |
| L6B-D | | 59.4 (264) | 2.00 (51) | Fracture |
| L6B-E | | 58.6 (261) | 2.25 (57) | Fracture |
| L6B-F | | 58.1 (258) | 2.00 (51) | Fracture |

**Table 4.2: Pull-Out Test Results—Rusted Strand, Low Strength Concrete**

| Test ID | $f'_c$ at Test Age psi (MPa) | Maximum Load kips (kN) | Pull-out Length at Max. Load in (mm) | Failure Type |
|---|---|---|---|---|
| L0R-A | 5100 (35.2) | 48.1 (214) | 1.00 (25) | Gradual |
| L0R-B | | 47.3 (210) | 0.40 (10) | Gradual |
| L0R-C | | 50.2 (223) | 0.20 (5) | Gradual |
| L4R-A | 4400 (30.3) | 42.5 (189) | 0.25 (6) | Gradual |
| L4R-B | | 47.3 (210) | 2.00 (51) | Gradual |
| L4R-C | | 39.9 (258) | 0.25 (6) | Gradual |
| L4R-D | | 43.0 (177) | 0.25 (6) | Gradual |
| L4R-E | | 45.2 (201) | 1.00 (25) | Gradual |
| L4R-F | | 44.7 (199) | 0.25 (6) | Gradual |
| L6R-A | 5450 (37.6) | 47.8 (213) | 0.25 (6) | Gradual |
| L6R-B | | 47.3 (210) | 0.15 (4) | Gradual |
| L6R-C | | 48.0 (214) | 0.15 (4) | Gradual |
| L6R-D | | 46.8 (208) | 0.15 (4) | Gradual |
| L6R-E | | 46.3 (206) | 0.15 (4) | Gradual |
| L6R-F | | 48.3 (215) | 0.15 (4) | Gradual |

**Table 4.3: Pull-Out Test Results—Bright Strand, Medium Strength Concrete**

| Test ID | $f'_c$ at Test Age psi (MPa) | Maximum Load kips (kN) | Pull-out Length at Max. Load in (mm) | Failure Type |
|---|---|---|---|---|
| M0B-A | 7800 (53.8) | 58.9 (262) | 0.50 (13) | Test Halted |
| M0B-B | | 59.2 (263) | 0.25 (6) | Test Halted |
| M4B-A | 9440 (65.1) | 61.8 (275) | 0.50 (13) | Fracture |
| M4B-B | | 62.1 (276) | 0.55 (14) | Fracture |
| M4B-C | | 62.1 (276) | 0.45 (11) | Fracture |
| M9B-A | 8170 (56.3) | 58.0 (258) | 0.75 (19) | Fracture |
| M9B-B | | 59.3 (264) | 0.70 (18) | Fracture |
| M9B-C | | 58.5 (260) | 0.80 (20) | Fracture |
| M9B-D | | 59.5 (265) | 1.05 (27) | Fracture |
| M9B-E | | 59.0 (262) | 1.50 (38) | Abrupt Slip |
| M9B-F | | 58.0 (258) | 1.10 (28) | Fracture |

**Table 4.4: Pull-Out Test Results—Rusted Strand, Medium Strength Concrete**

| Test ID | $f'_c$ at Test Age psi (MPa) | Maximum Load kips (kN) | Pull-out Length at Max. Load in (mm) | Failure Type |
|---|---|---|---|---|
| M0R-A | 8290 (57.2) | 55.5 (247) | 0.25 (6) | Gradual |
| M0R-B | | 53.8 (239) | 0.15 (4) | Gradual |
| M0R-C | | 42.2 (188) | 0.40 (10) | Gradual |
| M0R-D | | 45.6 (203) | 0.80 (20) | Gradual |
| M0R-E | | 41.7 (185) | 0.65 (17) | Gradual |
| M0R-F | | 52.8 (235) | 0.90 (23) | Gradual |
| M4R-A | 8970 (61.8) | 61.3 (273) | 0.50 (13) | Fracture |
| M4R-B | | 60.6 (270) | 1.00 (25) | Test Halted |
| M4R-C | | 59.1 (263) | 1.15 (29) | Test Halted |
| M4R-D | | 57.5 (256) | 1.50 (38) | Abrupt Slip |
| M4R-E | | 61.1 (272) | 0.75 (19) | Test Halted |
| M4R-F | | 60.6 (270) | 0.50 (13) | Test Halted |
| M9R-A | 9420 (65.0) | 53.5 (238) | 1.15 (29) | Gradual |
| M9R-B | | 46.1 (205) | 0.50 (13) | Gradual |
| M9R-C | | 55.2 (246) | 1.80 (46) | Gradual |
| M9R-D | | 33.0 (147) | 1.80 (46) | Gradual |
| M9R-E | | 48.8 (217) | 1.30 (33) | Gradual |
| M9R-F | | 55.0 (245) | 1.10 (28) | Gradual |

**Table 4.5: Pull-Out Test Results—Bright Strand, High Strength Concrete**

| Test ID | $f'_c$ at Test Age psi (MPa) | Maximum Load kips (kN) | Pull-out Length at Max. Load in (mm) | Failure Type |
|---|---|---|---|---|
| H0B-A | 11070 (76.3) | 54.6 (243) | — | Abrupt Slip |
| H0B-B | | 54.1 (241) | 0.75 (19) | Abrupt Slip |
| H0B-C | | 57.7 (257) | 0.75 (19) | Abrupt Slip |
| H4B-A | 10050 (69.3) | 43.0 (191) | 2.15 (55) | Gradual |
| H4B-B | | 38.2 (170) | 1.75 (44) | Gradual |
| H4B-C | | 30.0 (133) | 1.50 (38) | Gradual |
| H4B-D | | 33.6 (149) | 1.75 (44) | Gradual |
| H4B-E | | 39.9 (177) | 2.00 (51) | Gradual |
| H4B-F | | 49.3 (219) | 1.90 (48) | Gradual |
| H9B-A | 10420 (71.8) | 51.3 (228) | 1.30 (33) | Gradual |
| H9B-B | | 59.0 (262) | 1.70 (43) | Abrupt Slip |
| H9B-C | | 57.5 (256) | 1.10 (28) | Gradual |
| H9B-D | | 55.3 (246) | 0.60 (15) | Gradual |
| H9B-E | | 57.3 (255) | 0.90 (23) | Gradual |
| H9B-F | | 56.8 (253) | 1.15 (29) | Gradual |

**Table 4.6: Pull-Out Test Results—Rusted Strand, High Strength Concrete**

| Test ID | $f'_c$ at Test Age psi (MPa) | Maximum Load kips (kN) | Pull-out Length at Max. Load in (mm) | Failure Type |
|---|---|---|---|---|
| H0R-A | 10480 (72.3) | 47.6 (212) | 0.15 (4) | Gradual |
| H0R-B | | 48.8 (217) | 0.10 (3) | Gradual |
| H0R-C | | 54.8 (244) | 0.20 (5) | Gradual |
| H0R-D | | 55.7 (248) | 0.20 (5) | Gradual |
| H0R-E | | 42.7 (190) | 0.10 (3) | Gradual |
| H0R-F | | 50.1 (223) | 0.15 (4) | Gradual |
| H4R-A | 11710 (80.7) | 47.3 (210) | 1.75 (44) | Gradual |
| H4R-B | | 50.0 (222) | 1.25 (32) | Gradual |
| H4R-C | | 55.7 (248) | 1.65 (42) | Gradual |
| H4R-D | | 57.9 (258) | 2.00 (51) | Gradual |
| H4R-E | | 59.9 (266) | 0.75 (19) | Fracture |
| H4R-F | | 58.6 (261) | 0.75 (19) | Fracture |
| H9R-A | 10690 (73.7) | 52.0 (231) | 1.45 (37) | Gradual |
| H9R-B | | 46.4 (206) | 2.25 (57) | Gradual |
| H9R-C | | 54.3 (242) | 0.15 (4) | Gradual |
| H9R-D | | 44.9 (200) | 0.10 (3) | Gradual |
| H9R-E | | 45.6 (203) | 0.85 (22) | Gradual |
| H9R-F | | 50.6 (225) | 0.20 (5) | Gradual |

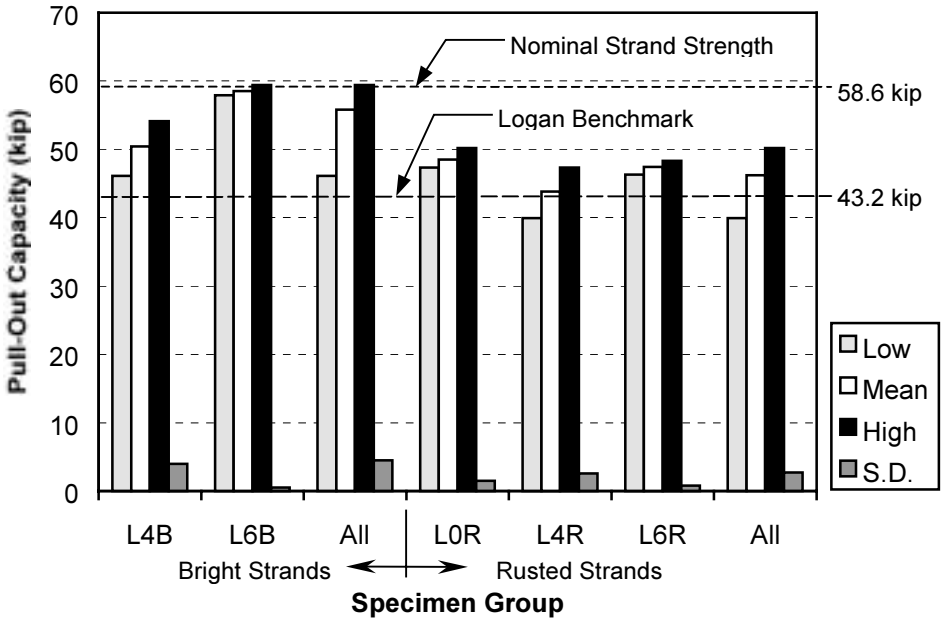


**Figure 4.6: Moustafa Pull-out Test Results for Specimens with Concrete Strengths within the Range Recommended by Logan (1997) (1 kip = 4.45 kN)**

Figure 4.6 summarizes the results of the tests performed on strands embedded within blocks with concrete compressive strengths within the range specified by Logan for strand bond quality assessment (3500 to 5900 psi [24.7 to 40.7 MPa]). The dashed horizontal lines on the figure represent the nominal strand strength and the pull-out load corresponding to Logan's recommendation for "high bond quality." As discussed in Section 4.2.3, Logan recommends a required average pull-out capacity of 36 kips (160 kN) for 0.5 in (12.5 mm) strand. This corresponds to an average bond stress of 955 psi (6.58 MPa) over the 18 in (460 mm) embedment of the strand. To achieve an equivalent average bond stress on a 0.6 in (15.2 mm) strand with an 18 in embedment length, a pull-out force of 43.2 kips (192 kN) is required.[1] Thus, 43.2 kips is indicated as the "Logan Benchmark" in Figure 4.6.

The figure illustrates that the average pull-out capacity for each test group exceeds the benchmark value, and that all coefficients of variation are less than 10 percent. Thus, both the "bright" and "rusted" strands used in this study appear to be capable of high bond quality. Logan's research indicates that the transfer and development length of these strands should be less than or equal to the values given by the relevant ACI expressions. On average, the pull-out capacities for the rusted strand are slightly lower than those of the bright strand. This difference may indicate slightly poorer bond quality for the rusted strands or it may reflect that the concrete strength for the L4R test block was approximately 12 percent less than the lowest concrete strength for the bright strand specimens (L4B).

Figure 4.7 illustrates the pull-out capacities of all bright strand specimens with respect to the concrete strength at the time of testing. Figure 4.8 displays the rusted strand results in a like manner. In general, the average capacities of the bright strand groups approached or equaled the breaking strength of the strand for concrete strengths above approximately 5500 psi (40 MPa). The strands from group H4B are an exception ($f'_c$ = 10050 psi). The results from this group are conspicuously lower than those of the other bright strand groups. This may be due to the rapid loss of workability experienced with the H-Series concrete mix. This mix usually started to stiffen considerably about fifteen to thirty minutes after mixing. Pull-out test blocks were cast from the concrete remaining upon completion of the beam specimens. In the particular case of the H4B specimens, the workers had particular difficulty placing and consolidating the concrete for the test block. Less than ideal consolidation of the concrete around the strands likely resulted in reduced pull-out capacity of these specimens. Transfer and development length tests conducted on the beam specimens (H4B) constructed of this particular batch of concrete indicated no poorer bond quality than other tests involving bright strand specimens.

A comparison of Figure 4.8 with Figure 4.7 shows that the pull-out capacities of the rusted strand specimens were generally less than those of the bright strand specimens over the entire concrete strength range. This is noteworthy because it seems to contradict the widely accepted opinion that surface weathering increases bond capacity (see Section 2.4.5.2). The average capacity of each rusted specimen group exceeds the Logan benchmark, but two of the groups (M0R and M9R) feature coefficients of variation that exceed the 10 percent limit recommended. The M0R strands ($f'_c$ = 8290 psi) and M9R strands ($f'_c$ = 9420 psi) have coefficients of variation of 13 and 17 percent, respectively. The rusted strand data seem to indicate a slight increase in pull-out capacity with increasing concrete strength. However, any increase is relatively small considering the extensive range of concrete strengths tested.

[1] Because the embedment length remains 18 in, the bonded surface area of the strand is proportional to the diameter of the strand. Thus, the corresponding pull-out force for the 0.6-in strand is $36\,\text{kip} \times \frac{0.6\,\text{in}}{0.5\,\text{in}} = 43.2\,\text{kip}$.

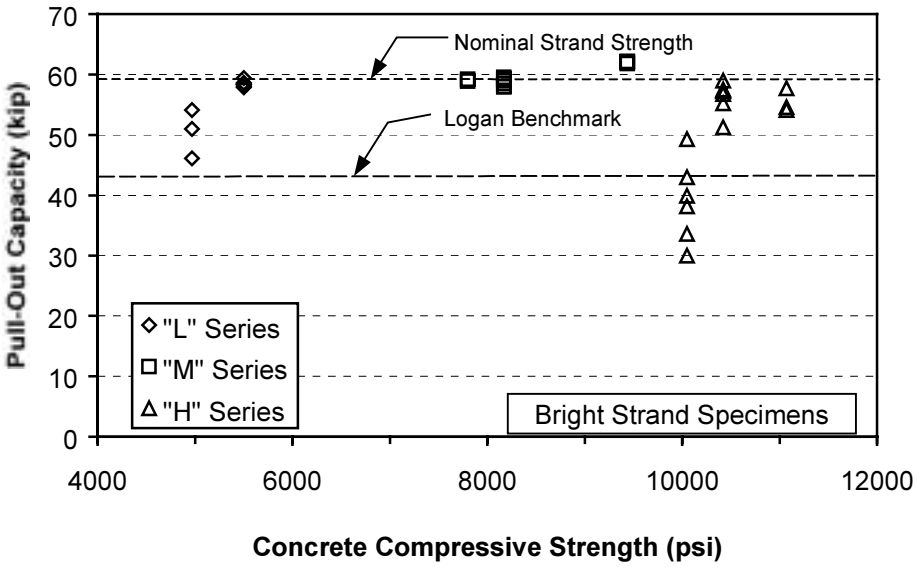


**Figure 4.7: Pull-Out Capacities of All Bright Strand Specimens (1 kip = 4.45 kN, 1000 psi = 6.89 MPa)**

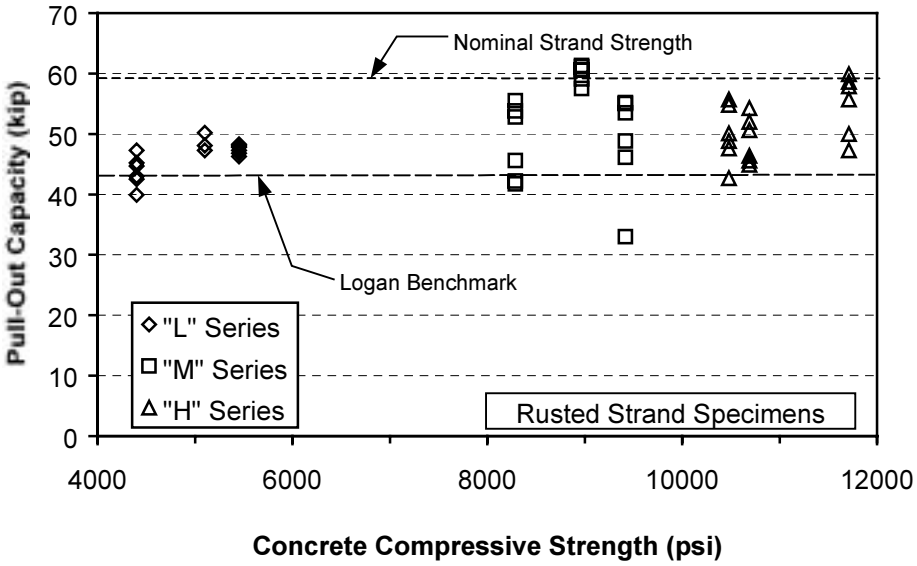


**Figure 4.8: Pull-Out Capacities of All Rusted Strand Specimens (1 kip = 4.45 kN, 1000 psi = 6.89 MPa)**

## 4.6 SUMMARY AND CONCLUSIONS

Recent studies suggest that strand bond behavior may vary significantly depending upon the strand manufacturer. The Moustafa Pull-Out Test has been proposed as a means of identifying strands that are likely to exhibit substandard bond quality. Eighteen sets of Moustafa Pull-Out Tests were performed in this study. Both the "bright" and "rusted" strand types satisfied the conditions proposed for classification as strands with "high bond quality." Therefore, if Logan's theory holds true, the transfer and development lengths of these strands should not exceed design values suggested by the ACI and AASHTO code expressions.

Average pull-out capacities of rusted strand specimens tended to be slightly lower than those of bright strand specimens. This trend appears to discount the ability of surface weathering to increase the bond capacity of seven-wire strands. Pull-out capacity may increase slightly with increasing concrete compressive strength, but this trend is indefinite. Any clear trend with respect to concrete strength is obscured by the relative dispersion of test results for concrete strengths (at time of testing) greater than 8000 psi (55 MPa).

Successful implementation of HSC requires vigilant attention to concrete quality. The poor pull-out performance of one test series utilizing HSC reflects the rapid degradation of workability that may be associated with concrete mixes that are designed to achieve 1-day compressive strengths in excess of 7000 psi (48 MPa). Casting operations involving HSC should be carefully planned and monitored to insure that all concrete is placed and consolidated prior to initial set.

# CHAPTER 5: TRANSFER LENGTH TEST PROGRAM

## 5.1 INTRODUCTION

Transfer length testing was performed on all thirty-six beams in the research study. One-third of the beam specimens (x0x Series) had only one transfer zone at each end. Due to the staggered debonding of strands, a second one-third of the beam specimens (x4x Series) featured three transfer zones at each end, and the remaining one-third of the specimens contained four transfer zones at each end. This resulted in a total of 192 transfer zones for testing. Transfer lengths were determined for 184 of these zones. To the author's knowledge, this represents a larger number of results than the cumulative number of transfer length results for 0.6 in (15.2 mm) strand reported previously.

For almost all the specimens, testing was performed to determine transfer lengths immediately after transfer of prestress force as well as at a later date. The later testing (hereafter referred to as "long-term" testing) occurred at concrete ages ranging from 19 to 148 days. This chapter describes the procedure used to determine the transfer length for each transfer zone tested, the results obtained from the test program, and the inferences drawn from these results. The results are compared to transfer length relationships developed by other researchers.

## 5.2 TEST PROCEDURE

Transfer lengths were determined by applying the 95% Average Maximum Strain (AMS) Method to measured concrete compressive strains resulting from the transfer of prestress force to the concrete. Although other methods have been used in other research studies, the 95% AMS Method is well established and has been recommended in recent FHWA studies for determining transfer lengths and for comparing results from various studies (Buckner 1994; Lane 1998). Russell and Burns (1993) explain and justify the application of this method. Concrete surface compressive strains were measured by means of a detachable mechanical (DEMEC) strain gauge with a 7.87 in (200 mm) gauge length.

**Figure 5.1: Pair of Beam Specimens after Side Form Removal**

### 5.2.1 Specimen Preparation

Specimen preparation commenced with the stripping of side forms early on the morning after each pair of beam specimens was cast. Figure 5.1 shows a pair of beam specimens on the prestressing bed after removal of side forms. At each end of each beam, a line of DEMEC locating discs were epoxied to the bottom flange on each side face. Each stainless steel DEMEC locating disc had a diameter of 0.25 in (6.3 mm) with a central 0.04 in (1 mm) drilled hole for positioning one of the conical measuring points on the DEMEC gauge. A fast-setting, two-part epoxy was used to bond the points to the concrete surface.

A typical line of DEMEC discs was placed at the same level as the centroid of the strands located within 4 in (102 mm) of the beam soffit. The first disc was placed 0.98 in (25 mm) from the end of the beam; subsequent discs were placed at intervals of 1.97 in (50 mm). Placement of the first four locating discs is illustrated in Figure 5.2. Each line of discs extended well beyond the expected transfer length(s) for the beam.

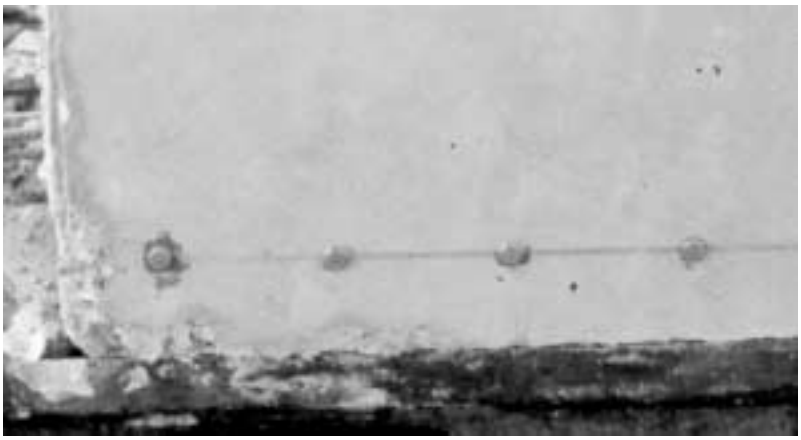

**Figure 5.2: First Four DEMEC Locating Discs in Line (End of Beam at Left)**

Once all eight lines of locating discs had been placed, preliminary readings were performed with the DEMEC gauge and recorded. Overlapping readings were taken for every 7.87 in (200 mm) interval between locating discs. Each reading was taken twice and recorded. Readings were retaken if the recorded pair differed by more than 0.00013 in (0.0032 mm). Figure 5.3 shows the performance of a DEMEC gauge reading.

**Figure 5.3: Performing a Measurement with DEMEC Gauge**

### 5.2.2 Application of Prestress Force

Once all preliminary DEMEC readings were recorded, the prestress force was applied to the beams by detensioning the prestressed strands. All strands were detensioned by means of a flame-cutting process. Gradual release methods have been used in a few previous UT research studies, and outside researchers have cited this as a potential cause for the shorter than expected transfer lengths that resulted. For this study, researchers wanted to ensure that a more sudden release method was used. Two distinct flame-cutting procedures were used, resulting in three possible release conditions for specimen ends.

For approximately two-thirds of the specimen pairs, prestressing strands were detensioned by what will hereafter be termed the "simultaneous release" method. This method entailed the flame-cutting of each strand at locations on both ends of both beams before cutting any other strands. This was accomplished by three welders who together attempted to cut each strand simultaneously at three locations (one at each end of the bed, and one between the two beams). In this manner, *all* the prestress force from each strand was introduced into all four of the beam ends prior to the cutting of subsequent strands.

The second method of prestress release used in this study entailed flame-cutting all the strands at one location between the two beams. Thus, the prestress force in each strand was introduced suddenly into the interior ends of the beam pair. At the exterior ends of the pair, on the other hand, the prestress force transferred to the concrete was gradually stepped up. An incremental concrete stress increase resulted because the decrease in strand tension force due to each single strand cut on the interior ends of the beam was approximately evenly distributed among all the strands at the exterior ends of the beams. This practice was used in an attempt to simulate a more gradual release of prestress at the exterior ends of specimens. The *interior* beam end transfer zones subjected to this release method are referred to as "live release" transfer zones, while the corresponding *exterior* zones are referred to as "dead release" zones. This release method was used for the following beam specimen pairs: M0R, H0R, M9B, H9B, M9R, and H9R.

### 5.2.3 Concrete Surface Strain Measurements

Immediately after the transfer of prestress force to the concrete, the DEMEC gauge readings were repeated on each overlapping 7.87 in (200 mm) interval composing each line of locating discs. The reading and recording procedure was identical to that described above for the preliminary readings. The readings taken immediately after prestress release were later used to calculate concrete compressive strain profiles and determine "initial" transfer lengths through the process described in Section 5.3.

For each pair of beam specimens, DEMEC readings were taken once again at an advanced age. This age ranged from 19 days (18 days after release) to 148 days (147 days after release). These readings were used to construct "long-term" compressive strain profiles and determine the corresponding long-term transfer lengths.

## 5.3 TRANSFER LENGTH DETERMINATION

This section describes the process used to determine the initial and long-term transfer lengths based on the data obtained from DEMEC gauge readings.

### 5.3.1 Construction of Surface Compressive Strain Profile

The first step in the process involves the construction of the surface compressive strain profile for each beam end. The compressive strain for each measured 7.87 in (200 mm) interval was calculated by multiplying the DEMEC gauge factor by the difference between 1) the reading recorded at the time under investigation and 2) the preliminary reading recorded for that interval. Because overlapping readings were taken, each location on the line was included within the gauge length of three separate reading intervals. Thus, the strain value assigned to each disc location was calculated by averaging the strain values for the three 7.87 in (200 mm) intervals that included the location. The procedure for assigning strain values to particular points is illustrated in Figure 5.4.

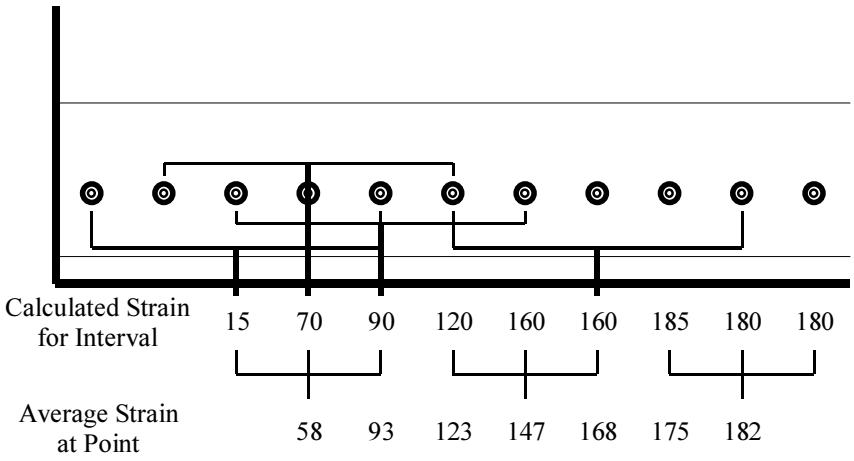


**Figure 5.4: Assignment of Surface Compressive Strain Values**

Once strain values were assigned to each disc location, corresponding values from either side of the beam were averaged to generate one surface strain profile for each end of each beam specimen.

Next, the resulting profiles of measured strain were corrected to account for the effects of specimen weight. In most early research, transfer length specimens were relatively small and/or prestressed concentrically. If prestressed concentrically, the specimens usually remained supported along their entire length and deformations due to weight were minimal. Even if prestressed eccentrically, the specimens were relatively short and light. Accordingly, any strain resulting from member weight was very small compared to the strains due to prestress alone.

For this study, full-scale specimens were eccentrically prestressed. Once the prestress was applied, the beams cambered off the bed, and the member weight was transmitted to the supported ends of the beam through flexural resistance. The tensile component of strain that resulted from weight-induced curvature at each point was large enough to alter the shape of the strain profile. Figure 5.5 shows both measured and corrected strain profiles for beam end H0B-C. The moment due to weight increases with increasing distance from the end of the beam toward midspan, as does the tensile strain component resulting from this moment. Therefore, the "plateau" value of the measured compressive strain curve tends to decrease with increasing distance from the end of the beam.

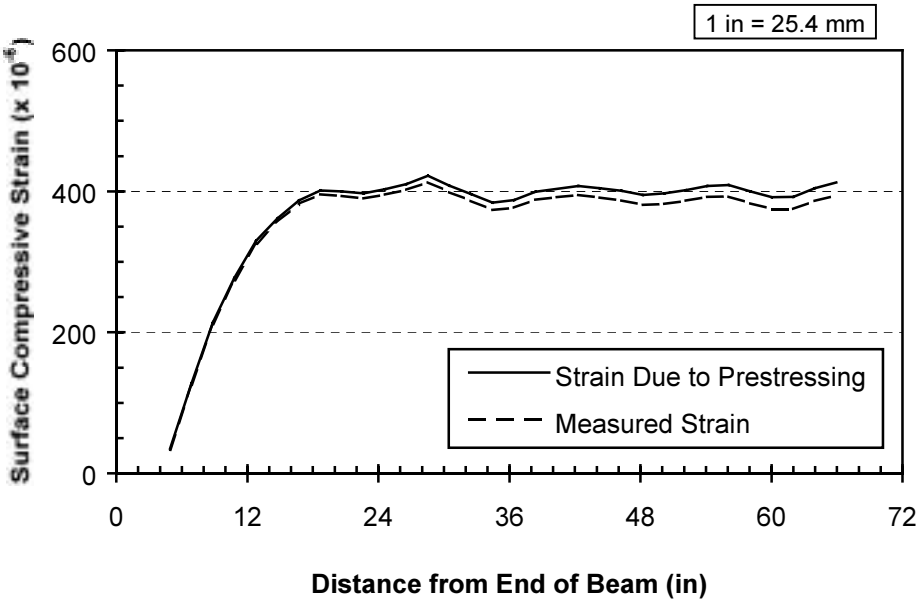


**Figure 5.5: Correction of Strain Profile to Remove Strain Due to Beam Weight**

If the strain profile is not corrected to reflect the strain due to prestress only, an erroneous value of the strain plateau is calculated. This, in turn, may result in an error on the order of 5 percent when determining the apparent transfer length. Therefore, the effect of member weight was discounted by adding the calculated magnitude of the tensile component to the measured compressive strain value at each location. The resulting profile more accurately reflects the influence of the prestress force alone. The magnitude of the tensile strain due to member weight at each location was calculated on the basis of engineering beam theory using the formulation in Equation 5.1.

**Equation 5.1**

$$\varepsilon_{w,DEMEC} = \frac{My_{DEMEC}}{E_c I_{tr}}$$

Where:

$\varepsilon_{w,DEMEC}$ = magnitude of strain component due to member weight

$M$ = moment due to member weight

$y_{DEMEC}$ = vertical distance from centroid of transformed section to line of locating discs

$E_c$ = modulus of elasticity of concrete

$I_{tr}$ = moment of inertia of transformed section

Creep strains were considered when performing this correction for the long-term strain profiles. For the long-term profiles, both the immediate strain component and the creep strain component due to member weight were calculated, and a similar adjustment was made. Creep strains were calculated by the procedure described by Collins and Mitchell (1991, 67–72).

### 5.3.2 Determination of Average Maximum Strain (AMS)

Once the strain profile was constructed for one end of a beam specimen, the next step involved the identification of the average maximum strain (AMS) value for each transfer zone. First, the strain values that lay in the likely plateau domain were identified by visual inspection. The value of the average maximum strain was then calculated as the arithmetic mean of these strain values. Figure 5.6 illustrates both the initial and long-term average maximum strain values for each of the three transfer zones of beam end H4R-A.

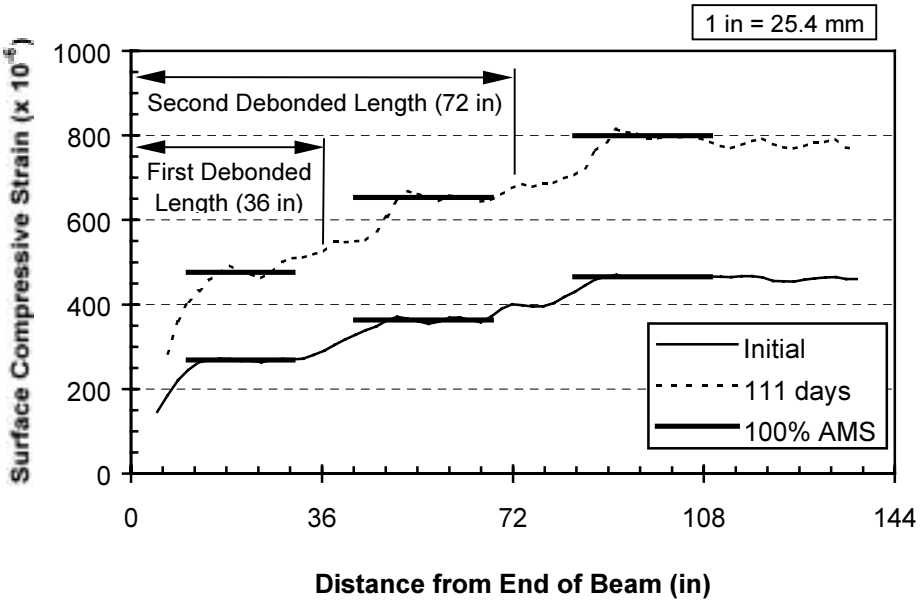


**Figure 5.6: Location of Average Maximum Strain Values for Specimen with Three Transfer Zones (Beam End H4R-A)**

### 5.3.3 Determination of 95% AMS Value

According to the 95% AMS Method, the apparent transfer length is bounded by the point where the compressive strain profile intersects the horizontal line representing 95 percent of the average maximum strain for the transfer zone. This section details the determination of the 95% AMS value for the initial and long-term strain profiles.

#### *5.3.3.1 Initial Transfer Length*

The most straightforward case is that of the initial transfer length for strands that are fully bonded. This case is represented by the "Initial" profile in the first (leftmost) transfer zone in Figure 5.6. For this case, the 95% AMS value was simply determined by multiplying the average maximum strain by 0.95.

For the transfer zones of partially debonded strands, only the compressive strain induced by the strands in question was considered. Thus, the 95% AMS value for this case represents a strain value that lies 95 percent of the way between the average maximum strain value for the previous transfer zone and the average maximum strain value for the transfer zone in question. Equation 5.2 depicts this relationship in mathematical form.

**Equation 5.2** $$95\%AMS_i = AMS_{i-1} + 0.95(AMS_i - AMS_{i-1})$$

In this case, simply multiplying the average maximum strain value by 0.95 would have resulted in an artificially small 95% AMS value. The magnitude of such an error would increase with subsequent transfer zones. Russell and Burns (1996) reported that the average transfer lengths of partially debonded strands were somewhat shorter than those of fully bonded strands. This discrepancy is likely due to the fact that these transfer lengths were obtained by applying the 0.95 factor to the *total* strain for the partially debonded strands, rather than the strain *portion* that resulted from the prestress force in these strands.

#### *5.3.3.2 Long-Term Transfer Length*

Application of the 95% AMS Method to long-term strain profiles must be rationally considered. Due to time-dependent deformations of the specimen, long-term compressive strains are typically on the order of two to three times the initial strains. Because of this large increase in strain, careless application of the 95% AMS Method to long-term strain profiles could result in unreasonably short transfer lengths.

Consider how the different types of time-dependent concrete deformation affect the strain profile. Creep strain is assumed to be proportional to the applied load. Thus, creep strains should result in an *amplification* of the strain profile. For this type of deformation, one expects the slope of the non-plateau portion of the strain profile to increase at the same rate as the value of the average maximum strain. Therefore, using a factor of 0.95 to locate the intersection value of strain remains rational.

Strain due to shrinkage, on the other hand, is usually considered to be independent of applied load. Thus, shrinkage strains should result in a *translation* of the strain profile. For this type of deformation, the slope of the non-plateau portion of the strain profile remains constant as the average maximum strain increases. In this case, applying a five percent reduction to the long-term average maximum strain may result in a significantly larger reduction along the distance axis than occurred for the initial transfer length estimation. Thus, if the actual transfer length remains the same as shrinkage strains increase, using a fixed percentage AMS value to determine the transfer length will result in the erroneous conclusion that the transfer length is decreasing with time.

Selecting an AMS reduction factor that precisely reflects the relative amounts of creep and shrinkage strains would be difficult. Such a factor would differ from specimen to specimen and from age to age. The calculation process would involve the uncertainties inherent in creep and shrinkage estimations. The computational effort would be entirely out of proportion to the minimal increase in accuracy obtained. In order to keep the process as simple as possible while erring on the side of conservatism, the following method was adopted in this study.

Instead of applying the identical procedure to the long-term results as was used in the initial transfer length calculations, the long-term average maximum strains were reduced by the same *value* of strain as were the initial average maximum strains. For example, if the initial AMS value for fully bonded strands was 100 microstrain and the long-term AMS value was 500 microstrain, then the 95% AMS values were calculated as 95 and 495 microstrain, respectively. In effect, this method assumes that all time-dependent strains are of the shrinkage-type. Assuming that all time-dependent strains were caused by creep would result in a long-term 95% AMS value of 0.95(500) = 475 microstrain. The most accurate value should lie somewhere between 475 and 495 microstrain,

but it is safer to accept the latter value. Long-term 95% AMS values for partially debonded strands were determined in a like manner.

### 5.3.4 Determination of Apparent Transfer Length

Once each 95% AMS value was established, the transfer length apparent from the measured concrete surface strain profile was determined by measuring the distance between the start of bond to the point of intersection between the strain profile and the 95% AMS value. The start of bond location was assumed as the end of the member for fully bonded strands and the end of jacketing for partially debonded strands. Figure 5.7 illustrates the apparent transfer lengths determined from the strain profiles shown in Figure 5.6. Surface strain profiles and the corresponding apparent transfer lengths for all specimens are recorded in Appendix C.

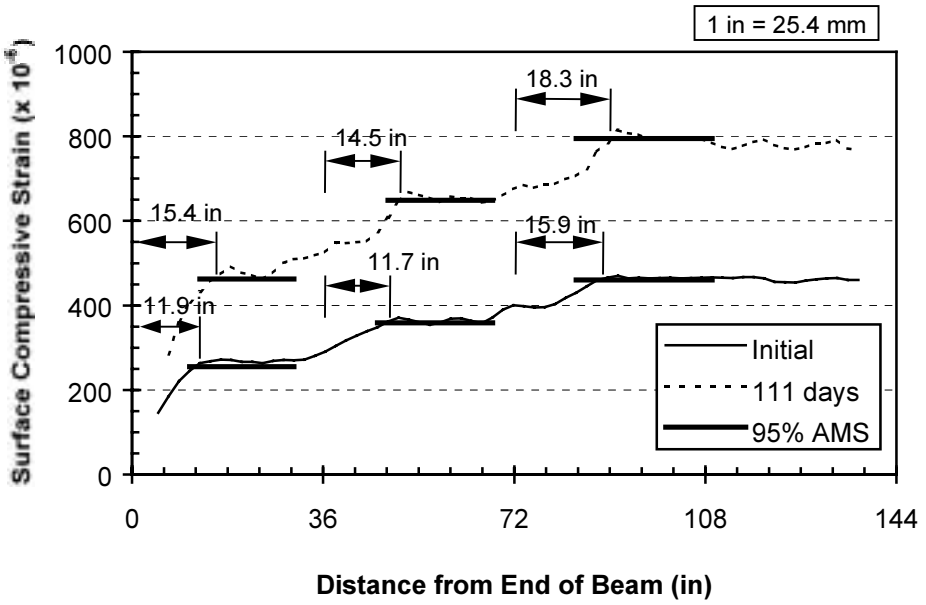


**Figure 5.7: Determination of Apparent Transfer Lengths (Beam End H4R-A)**

In most previous research studies, the value of transfer length apparent from the surface strain profile has been assumed to be equivalent to the actual transfer length of the strand(s) in question. This practice implies that one of the assumptions vital to engineering beam theory—that plane sections remain plane—holds true along the transfer length. If this assumption is true and the cross section is in equilibrium, then the concrete stress indicated by the concrete surface strain is proportional to the reinforcing steel stress at the same depth. Although this assumption is a valuable tool in the analysis and design of regions, often termed "B-regions," that lie some distance away from discontinuities and applied loads, it does not apply to anchorage zones—either pre- or post-tensioned. The non-linear distribution of stress and strain in such discontinuous regions, or "D-regions," is commonly described as "shear lag."

Although considerable research effort has been devoted to the behavior of post-tensioned anchorage zones (Breen et al. 1994), scant attention has been paid to the distribution of concrete stresses in pretensioned anchorage zones. This can be attributed to the fact that anchorage zone research has been focused on the control of high compressive stresses immediately ahead of the anchorage device and the tensile (or "bursting" stresses) that are normal to the tendon axis. Due to the gradual build-up of concrete stresses in pretensioned anchorage zones these compressive and bursting stresses are less critical than in post-tensioned anchorage zones. However, the extent of both types of anchorage zones (i.e. the region for which plane sections do not remain plane) can be significantly larger than the length over which the tendon prestress force is fully developed. By measuring compressive strains at a variety of depths within the same anchorage zone, Base (1958a) has shown this to be true for full-scale pretensioned members.

The difference between the transfer length and the extent of the pretensioned anchorage zone is acknowledged by the CEB-FIP Model Code 1990. The extent of the pretensioned anchorage zone is termed the "development length"

(the property referred to as "development length" in American codes is defined as "anchorage length" in Model Code 1990). Clause *6.9.11.6. Development Length* defines "the distance from the end face of the member to the concrete cross-section beyond which the distribution of the longitudinal stresses is considered linear" as the "development length." For rectangular cross-sections with straight tendons the development length, $l_p$, is calculated as:

**Equation 5.3**

$$l_p = \left[h^2 + \left(0.6 l_{bpt}\right)^2\right]^{1/2} > l_{bpt}$$

Where:

$h$ = the total depth of the cross section

$l_{bpt}$ = "transmission length" of the tendon (equivalent to "transfer length" in American codes).

This expression clearly reflects the influence of the member size on the disparity between the transfer length and the extent of the anchorage zone. For members with total depths less than 80 percent of the transfer length, the transfer length and the length of the anchorage zone are assumed to be equal. As the total depth of the member increases relative to the transfer length, the extent of the anchorage zone becomes more dependent on the member size than on the transfer length. For members with I-shaped cross sections, little specific guidance is given.

Assuming that plane sections remain plane in the anchorage zone has not led to significant errors in many past studies because of the type of specimens used. The majority of historical transfer length specimens were small. Specifically, the member dimensions were small relative to the transfer lengths under investigation. Thus, the stresses and strains due to prestressing were distributed fairly evenly at the end of the actual strand transfer length. Usually, these specimens featured fully bonded strands that were evenly distributed throughout the cross section. Therefore, prestress forces had to distribute over distances that were small, especially in relation to the transfer length.

Buckner (1994) implemented a finite element analysis that indicated that the effect of shear lag on apparent transfer length in these smaller specimens is relatively minor (less than 10 percent increase from actual). The effect did increase with increasing specimen size relative to transfer length. His reported results are for specimens with cross-sectional dimensions up to one-third the actual transfer length. Thus, according to the CEB-FIP expression (Equation 5.3 above), the stress distribution should be quite linear at the end of the transfer length. Buckner also postulates that the 5-percent plateau reduction inherent in the 95% AMS Method compensates for much of the error due to shear lag. This is unlikely, however, because the 5-percent reduction was originally intended to counter the profile-rounding effects that result from the use of long, overlapping gauge lengths like those used in this study (Russell and Burns 1993; Base 1958a).

In studies that featured larger and/or eccentrically prestressed members, researchers usually attempted to minimize the potential error due to shear lag by measuring the surface strains at the depth of the reinforcement centroid. The effectiveness of this technique is dependent upon the cross-sectional size and shape and the distribution of the prestressing reinforcement. In order to illustrate the concept of shear lag and how it affects the relationship between surface strains and tendon strains, typical strain contours of a horizontal section through the anchorage region are shown in Figure 5.8.

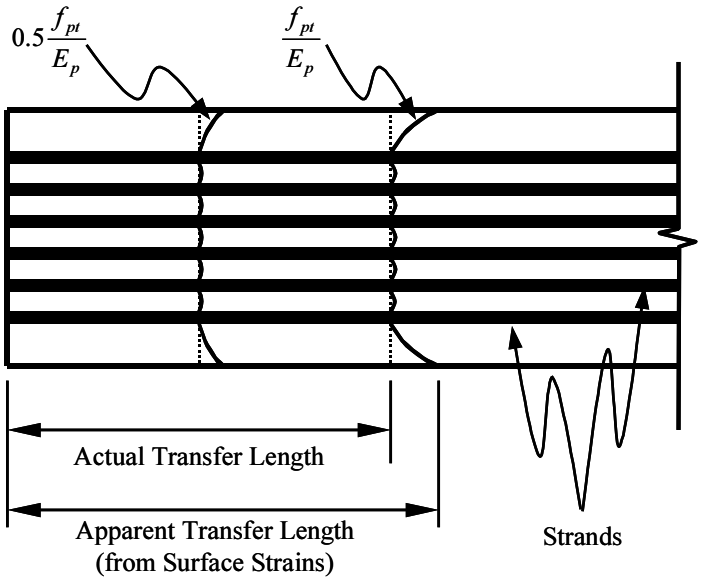


**Figure 5.8: Strain Contours at Horizontal Section through Bottom Flange at Depth of Strands**

The specimens in this study were quite susceptible to the effects of shear lag. First, the specimens were 28 in (710 mm) deep and as wide as 16 in (406 mm). Therefore, the prestress had to distribute over cross-sectional distances that were quite large relative to the expected transfer length. Many of the specimens featured staggered debonding patterns. Thus, the prestress force was often developed in only two to four strands within each transfer length. Because a single line of DEMEC discs was used to evaluate the surface strain profile, distances between developing strands and the DEMEC line differed substantially between different transfer zones within the same specimen. For example, some of the fully bonded strands lay less than 3 in (75 mm) from the DEMEC line, yet some of the groups of debonded strands were as far away as 7 in (180 mm) horizontally and 11 in (280 mm) vertically. Thus, it was necessary to adopt a procedure that would at least allow for the effective comparison of the behavior of the various strand groups, and ideally result in an accurate estimation of the actual strand transfer length.

### 5.3.5 Determination of Actual Transfer Length

A three-dimensional finite element model was developed to assess the relationship between the apparent and actual transfer lengths for the specimens in this study. This section relates details regarding the finite element model and the procedure used to calculate actual transfer lengths based on the apparent transfer lengths obtained from surface strain profiles.

#### *5.3.5.1 Finite Element Model*

##### *5.3.5.1.1 Assumptions*

The stress in the prestressing tendon after release was assumed to vary linearly from zero at the start of bond to $f_{si}$, the level of prestress in the strand immediately after release, at the end of the actual transfer length. The concrete was assumed to be homogeneous and exhibit isotropic and linearly elastic stress-strain behavior. A value of 0.2 was assumed for Poisson's Ratio, and the Elastic Modulus was assumed equal to 4800, 6400 and 7200 ksi (33, 44 and 50 GPa) for the L-, M-, and H-Series specimens, respectively.

##### *5.3.5.1.2 Description*

A finite element mesh was constructed to reflect each unique combination of concrete strength level and debonding pattern used in the test program. Symmetry was utilized to reduce the mesh to a volume defined by one-half of the

I-beam cross section by one-half of the beam length. The mesh consisted of both 20-node (brick) and 15-node (wedge) continuum elements. The 20-node elements used reduced integration. Element dimensions were typically 2 in x 2 in x 2 in (51 mm x 51 mm x 51 mm) or less. For elements that lay adjacent to the transfer length of the strand, the dimension parallel to the axis of the strand was reduced to 1 in (25 mm).

### *5.3.5.2 Procedure*

The procedure consisted of first assuming a transfer length, and then applying the prestress force linearly over the transfer length at each strand location. A linear static perturbation analysis was then performed to determine the resulting stresses and strains in the concrete. The resulting surface strains were evaluated along a line corresponding to the DEMEC locating disc line for the specimen being modeled. These strains were converted to equivalent average strains over a 7.87 in (200 mm) gauge length and then subjected to the same procedure as described in Section 5.3 above to determine the apparent transfer length that would be indicated applying the 95% AMS Method to the surface strain profile.

Figure 5.9 shows the surface compressive strain profile that results from the finite element analysis of beam of the H4x Series with an assumed actual transfer length of 12 in (305 mm). The dashed line represents the surface strain profile predicted from standard beam theory assuming that plane sections remain plain throughout the length of the specimen. Note how this profile differs significantly from the surface strain profile that results from the finite element model, which includes the effects of shear lag. The strands that lay closest to the DEMEC line were fully bonded. Thus, the finite element solution most closely matches beam theory in the transfer zone for these strands. The disparity is larger in the transfer zones of the debonded strands.

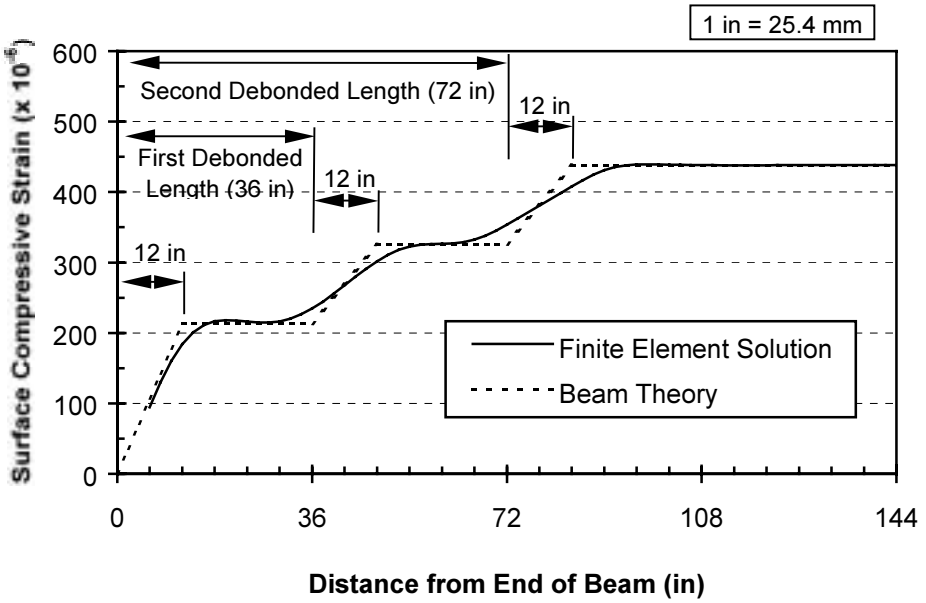


**Figure 5.9: Surface Compressive Strain Profiles Predicted for an Actual Transfer Length of 12 in (305 mm)**

Once the 95% AMS method was applied to the surface strains resulting from the finite element analysis, the process was repeated several times on the same specimen model. Each repetition was characterized by a different assumed value for the actual transfer length. Once the process had been repeated for several transfer lengths, a relationship between actual transfer length (over which the tendons develop the effective prestress) and apparent transfer length (which is measured along the line of DEMEC locating discs on the surface of the member) could be plotted for each transfer zone. The relationships obtained for the three anchorage zones of the H4x Series specimens are plotted in Figure 5.10. Here again it is evident that the behavior of the fully bonded strands most closely matches that of beam theory. The disparity between the actual and apparent transfer lengths decreases with increasing transfer length.

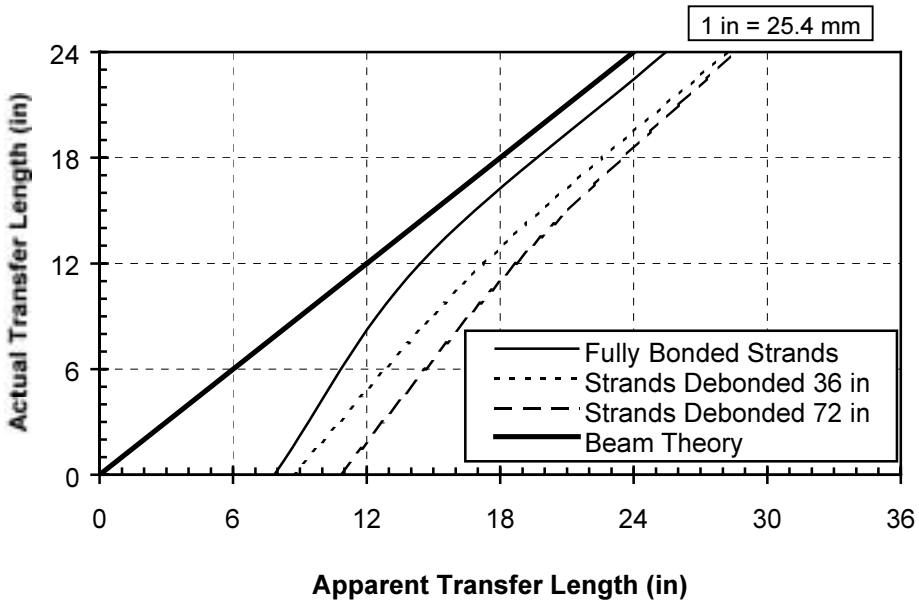


**Figure 5.10: Relationship Between Actual Strand Transfer Length and Apparent Transfer Length for H4x Specimens**

Once this relationship was established for each transfer zone, the apparent transfer length obtained from the experimental test program could be translated into an estimate of the actual tendon transfer length.

As an example, consider the long-term transfer length of the fully bonded strands in Beam End H4R-A. The measured compressive strain profile for this end is depicted in Figure 5.7. Applying the 95% AMS Method yields the apparent transfer length of 15.4 in (390 mm) as indicated in the figure. According to the results of the finite element analysis as plotted in Figure 5.10, an apparent (surface) transfer length of 15.4 in (390 mm) corresponds to an actual (tendon) transfer length of 13 in (330 mm) for fully bonded strands in the H4x specimens. The value of 13 in is therefore reported as the long-term transfer length in Table 5.6 below.

### 5.3.6 Precision of Reported Results

Several factors must be considered when assessing the accuracy of the transfer length results gleaned from this study. First, the distance between adjacent surface strain measurements was 1.97 in (50 mm), thus any attempt to assign a precision smaller than this value to the apparent transfer length relies on interpolated values. Second, strain readings were not taken in the most ideal of conditions. DEMEC readings were performed by researchers who were subjected to awkward positions and sometimes exposed to temperatures lower than 40ºF (4ºC), or as was more often the case, in excess of 100ºF (38ºC), for hours at a time. In light of these circumstances, it would be misleading to report final transfer length values with a precision better than 1 in (25 mm).

## 5.4 RESULTS AND DISCUSSION

Surface strain profiles and the corresponding apparent transfer lengths for all specimens are recorded in Appendix C. Using the procedure described in Section 5.3.5, these apparent transfer lengths were converted to actual transfer lengths. The resulting actual transfer lengths for bright strand specimens are reported in Table 5.1, Table 5.2, and Table 5.3. The results for rusted strand specimens are reported in Table 5.4, Table 5.5, and Table 5.6.

**Table 5.1: Transfer Length Results for L Series, Bright Strand Specimens (1 in = 25.4 mm)**

| Specimen ID | | Debonded Length in | Method of Prestress Release | Initial Transfer Length in | Long-Term | |
|---|---|---|---|---|---|---|
| | | | | | Age days | Transfer Length in |
| L0B | A | 0 | Simultaneous | 23 | 22 | 26 |
| | B | 0 | Simultaneous | 19 | | 25 |
| | C | 0 | Simultaneous | 25 | 23 | 30 |
| | D | 0 | Simultaneous | 21 | | 36 |
| L4B | A | 0 | Simultaneous | 14 | 56 | 19 |
| | | 36 | | 18 | | 18 |
| | | 72 | | 5 | | 10 |
| | B | 0 | Simultaneous | 22 | 56 | 25 |
| | | 36 | | 17 | | 25 |
| | | 72 | | 16 | | 13 |
| | C | 0 | Simultaneous | 15 | 105 | 18 |
| | | 36 | | 9 | | 15 |
| | | 72 | | 12 | | 15 |
| | D | 0 | Simultaneous | 21 | — | — |
| | | 36 | | 10 | | — |
| | | 72 | | 14 | | — |
| L6B | A | 0 | Simultaneous | 21 | 138 | 23 |
| | | 36 | | 17 | | 17 |
| | | 72 | | 10 | | 12 |
| | | 108 | | 21 | | 22 |
| | B | 0 | Simultaneous | 17 | 138 | 13 |
| | | 36 | | 12 | | 10 |
| | | 72 | | 14 | | 12 |
| | | 108 | | 13 | | 13 |
| | C | 0 | Simultaneous | 24 | 138 | 25 |
| | | 36 | | 14 | | 16 |
| | | 72 | | 18 | | 16 |
| | | 108 | | 12 | | 13 |
| | D | 0 | Simultaneous | 19 | 138 | 18 |
| | | 36 | | 7 | | 10 |
| | | 72 | | 16 | | 15 |
| | | 108 | | 9 | | 13 |

**Table 5.2: Transfer Length Results for M Series, Bright Strand Specimens (1 in = 25.4 mm)**

| Specimen ID | | Debonded Length in | Method of Prestress Release | Initial Transfer Length in | Long-Term | |
|---|---|---|---|---|---|---|
| | | | | | Age days | Transfer Length in |
| M0B | A | 0 | Simultaneous | 17 | 60 | 22 |
| | B | 0 | Simultaneous | 18 | | 19 |
| | C | 0 | Simultaneous | 16 | 77 | 18 |
| | D | 0 | Simultaneous | 15 | | 16 |
| M4B | A | 0 | Simultaneous | 10 | 54 | 14 |
| | | 36 | | 10 | | 11 |
| | | 72 | | 11 | | 9 |
| | B | 0 | Simultaneous | 11 | 54 | 13 |
| | | 36 | | 11 | | 15 |
| | | 72 | | 14 | | 19 |
| | C | 0 | Simultaneous | 12 | 63 | 22 |
| | | 36 | | 11 | | 9 |
| | | 72 | | 14 | | 14 |
| | D | 0 | Simultaneous | 11 | 63 | 16 |
| | | 36 | | 12 | | 13 |
| | | 72 | | 9 | | 14 |
| M9B | A | 0 | Dead | 22 | 26 | 20 |
| | | 36 | | 23 | | 22 |
| | | 72 | | 14 | | 18 |
| | | 108 | | 6 | | 5 |
| | B | 0 | Live | 11 | 26 | 12 |
| | | 36 | | 23 | | 18 |
| | | 72 | | 15 | | 13 |
| | | 108 | | 4 | | 4 |
| | C | 0 | Live | 18 | 26 | 14 |
| | | 36 | | 8 | | 6 |
| | | 72 | | 13 | | 8 |
| | | 108 | | 4 | | 7 |
| | D | 0 | Dead | 21 | 26 | 23 |
| | | 36 | | 10 | | 7 |
| | | 72 | | 8 | | 5 |
| | | 108 | | 4 | | 6 |

**Table 5.3: Transfer Length Results for H Series, Bright Strand Specimens (1 in = 25.4 mm)**

| Specimen ID | | Debonded Length in | Method of Prestress Release | Initial Transfer Length in | Long-Term | |
|---|---|---|---|---|---|---|
| | | | | | Age days | Transfer Length in |
| H0B | A | 0 | Simultaneous | 16 | 19 | 15 |
| | B | 0 | Simultaneous | 14 | | 16 |
| | C | 0 | Simultaneous | 13 | 20 | 16 |
| | D | 0 | Simultaneous | 16 | | 17 |
| H4B | A | 0 | Simultaneous | 12 | 84 | 18 |
| | | 36 | | 12 | | 12 |
| | | 72 | | 18 | | 19 |
| | B | 0 | Simultaneous | 10 | 84 | 12 |
| | | 36 | | 12 | | 13 |
| | | 72 | | 15 | | 13 |
| | C | 0 | Simultaneous | 10 | 97 | 14 |
| | | 36 | | 17 | | 20 |
| | | 72 | | 8 | | 10 |
| | D | 0 | Simultaneous | 13 | 97 | 16 |
| | | 36 | | 18 | | 16 |
| | | 72 | | 14 | | 15 |
| H9B | A | 0 | Dead | 14 | 83 | 16 |
| | | 36 | | 16 | | 16 |
| | | 72 | | 18 | | 19 |
| | | 108 | | 5 | | 10 |
| | B | 0 | Live | 13 | 83 | 14 |
| | | 36 | | 12 | | 11 |
| | | 72 | | 15 | | 13 |
| | | 108 | | 10 | | 12 |
| | C | 0 | Live | 15 | 83 | 14 |
| | | 36 | | 24 | | 19 |
| | | 72 | | — | | 11 |
| | | 108 | | 7 | | 10 |
| | D | 0 | Dead | 15 | 83 | 13 |
| | | 36 | | 19 | | 18 |
| | | 72 | | 9 | | 9 |
| | | 108 | | 9 | | 9 |

**Table 5.4: Transfer Length Results for L Series, Rusted Strand Specimens (1 in = 25.4 mm)**

| Specimen ID | | Debonded Length in | Method of Prestress Release | Initial Transfer Length in | Long-Term | |
|---|---|---|---|---|---|---|
| | | | | | Age days | Transfer Length in |
| L0R | A | 0 | Simultaneous | 16 | 38 | 19 |
| | B | 0 | Simultaneous | 15 | | 16 |
| | C | 0 | Simultaneous | 14 | 38 | 18 |
| | D | 0 | Simultaneous | 16 | | 18 |
| L4R | A | 0 | Simultaneous | 14 | 122 | 15 |
| | | 36 | | 11 | | 15 |
| | | 72 | | 12 | | 12 |
| | B | 0 | Simultaneous | 12 | 122 | 11 |
| | | 36 | | 11 | | 15 |
| | | 72 | | 12 | | 13 |
| | C | 0 | Simultaneous | 16 | 122 | 15 |
| | | 36 | | — | | — |
| | | 72 | | — | | — |
| | D | 0 | Simultaneous | 12 | 122 | 13 |
| | | 36 | | 15 | | 15 |
| | | 72 | | 27 | | 24 |
| L6R | A | 0 | Simultaneous | 16 | 148 | 15 |
| | | 36 | | 7 | | 7 |
| | | 72 | | 13 | | 11 |
| | | 108 | | 8 | | 9 |
| | B | 0 | Simultaneous | 13 | 148 | 12 |
| | | 36 | | 7 | | 9 |
| | | 72 | | 15 | | 14 |
| | | 108 | | 12 | | 10 |
| | C | 0 | Simultaneous | 10 | 148 | 11 |
| | | 36 | | 11 | | 16 |
| | | 72 | | 10 | | 12 |
| | | 108 | | 13 | | 14 |
| | D | 0 | Simultaneous | 14 | 148 | 10 |
| | | 36 | | 14 | | 14 |
| | | 72 | | 7 | | 15 |
| | | 108 | | 6 | | 12 |

**Table 5.5: Transfer Length Results for M Series, Rusted Strand Specimens (1 in = 25.4 mm)**

| Specimen ID | | Debonded Length in | Method of Prestress Release | Initial Transfer Length in | Long-Term | |
|---|---|---|---|---|---|---|
| | | | | | Age days | Transfer Length in |
| M0R | A | 12 | Dead | 15 | 89 | 21 |
| | B | 12 | Live | 22 | | 24 |
| | C | 12 | Live | 24 | 89 | 31 |
| | D | 12 | Dead | 19 | | 22 |
| M4R | A | 0 | Simultaneous | 10 | 78 | 13 |
| | | 36 | | 13 | | 10 |
| | | 72 | | 11 | | 17 |
| | B | 0 | Simultaneous | 13 | 78 | 15 |
| | | 36 | | 15 | | 16 |
| | | 72 | | 9 | | 16 |
| | C | 0 | Simultaneous | 17 | 78 | 21 |
| | | 36 | | 10 | | 12 |
| | | 72 | | 10 | | 15 |
| | D | 0 | Simultaneous | 10 | 78 | 12 |
| | | 36 | | 14 | | 11 |
| | | 72 | | 9 | | 11 |
| M9R | A | 0 | Dead | 17 | 98 | 17 |
| | | 36 | | 23 | | 24 |
| | | 72 | | 8 | | 13 |
| | | 108 | | 3 | | 3 |
| | B | 0 | Live | 13 | 98 | 15 |
| | | 36 | | 14 | | — |
| | | 72 | | 22 | | 27 |
| | | 108 | | 10 | | 12 |
| | C | 0 | Live | 9 | 98 | 12 |
| | | 36 | | 14 | | 15 |
| | | 72 | | 9 | | 9 |
| | | 108 | | 6 | | 6 |
| | D | 0 | Dead | 11 | 98 | 8 |
| | | 36 | | 13 | | — |
| | | 72 | | 14 | | 13 |
| | | 108 | | 6 | | 8 |

**Table 5.6: Transfer Length Results for H Series, Rusted Strand Specimens (1 in = 25.4 mm)**

| Specimen ID | | Debonded Length in | Method of Prestress Release | Initial Transfer Length in | Long-Term | |
|---|---|---|---|---|---|---|
| | | | | | Age days | Transfer Length in |
| H0R | A | 12 | Dead | 19 | 94 | 21 |
| | B | 12 | Live | 19 | | 22 |
| | C | 12 | Live | 24 | 94 | 21 |
| | D | 12 | Dead | 15 | | 20 |
| H4R | A | 0 | Simultaneous | 9 | 111 | 13 |
| | | 36 | | 6 | | 9 |
| | | 72 | | 9 | | 12 |
| | B | 0 | Simultaneous | 9 | 111 | 11 |
| | | 36 | | 15 | | 15 |
| | | 72 | | 12 | | 10 |
| | C | 0 | Simultaneous | 8 | 111 | 13 |
| | | 36 | | 10 | | 12 |
| | | 72 | | 7 | | 7 |
| | D | 0 | Simultaneous | 10 | 111 | 14 |
| | | 36 | | 20 | | 17 |
| | | 72 | | 10 | | 8 |
| H9R | A | 0 | Dead | 13 | 98 | 15 |
| | | 36 | | 6 | | — |
| | | 72 | | 6 | | 13 |
| | | 108 | | 14 | | 14 |
| | B | 0 | Live | 14 | 98 | 18 |
| | | 36 | | 14 | | 10 |
| | | 72 | | 15 | | 21 |
| | | 108 | | 13 | | 20 |
| | C | 0 | Live | 13 | 98 | 17 |
| | | 36 | | 15 | | 15 |
| | | 72 | | 6 | | 8 |
| | | 108 | | 6 | | 5 |
| | D | 0 | Dead | 9 | 98 | 11 |
| | | 36 | | 4 | | 6 |
| | | 72 | | 9 | | 11 |
| | | 108 | | 8 | | 8 |

The following sections describe the trends observed from the results of this study. The effects of concrete strength and tendon prestress, time, strand surface condition, and method of prestress release are discussed.

### 5.4.1 Concrete Strength and Tendon Prestress

As discussed in Section 2.4.1, equilibrium of forces along the strand transfer length indicates that the initial transfer length, $l_{t,init}$, should be proportional to both the diameter of the strand, $d_b$, and the equilibrium stress in the tendon immediately following release, $f_{pt}$. The initial transfer length should be inversely proportional to the average transfer bond stress capacity, $\overline{u}_{tb}$, between the tendon and the surrounding concrete. Thus:

**Equation 5.4**

$$l_{t,init} \propto \frac{f_{pt}}{\overline{u}_{tb}} d_b .$$

Because much of the concrete immediately surrounding the tendon is subjected to tensile stress levels well beyond the elastic range (Janney 1954), the assumption that the transfer length decreases with the tendon stress over time is unreasonable. To the contrary, these high stress levels should cause some continued softening of the concrete-to-steel bond with time. This softening may be attributed to growth of microcracking due to circumferential (hoop) tension and possibly creep under radial compression. These time-dependent, inelastic effects suggest that the simplest approach to estimating the long-term transfer length, $l_t$, would be to assume that it too is proportional to $f_{pt}$ and $d_b$, while remaining inversely proportional to the initial value of $\overline{u}_{tb}$.

As discussed in Section 2.4.3, the average transfer bond capacity should depend most heavily on the tensile strength and stiffness of the surrounding concrete. In North American practice for normal-weight concrete, both the stiffness and tensile strength of concrete are assumed proportional to the square root of the concrete compressive strength (ACI 318-99, 8.5.1, 9.5.2.3). Because the initial transfer length is determined at the time of release, it is logical to use the concrete compressive strength at release, $\sqrt{f'_{ci}}$, for formulating $\overline{u}_{tb}$. Therefore, relationships for the initial and long-term transfer lengths may be formulated as in Equation 5.5 and Equation 5.6, respectively, where $\alpha_{init}$ and $\alpha_{long\ term}$ represent constants of proportionality.

**Equation 5.5**

$$l_{t,init} = \alpha_{init} \frac{f_{pt}}{\sqrt{f'_{ci}}} d_b$$

**Equation 5.6**

$$l_t = \alpha_{long\ term} \frac{f_{pt}}{\sqrt{f'_{ci}}} d_b$$

For the bright strand specimens in the test program, Figure 5.11 illustrates the relationship between the measured long-term transfer lengths and $\frac{f_{pt}}{\sqrt{f'_{ci}}} d_b$. As might be expected for a transfer length study (Rose and Russell 1997), especially one where instrumentation and measurements were performed in the field, the dispersion of the data is quite large. This dispersion alone should serve as a caution against the use of an average value in transfer length expressions for design. Based on a linear regression analysis, a central value of $\alpha_{long\ term}$ = 0.342 ksi$^{-0.5}$ (10.8 psi$^{0.5}$/ksi, 0.130 MPa$^{-0.5}$) was determined. The correlation coefficient, R, for this regression has a value of 0.37.

The correlation of long-term and initial transfer lengths with other likely combinations of variables was also evaluated. In general, the value of the original tendon prestress (at time of tendon tensioning), $f_{pj}$, could be substituted for $f_{pt}$ with an insignificant difference in correlation. Likewise, the square root of the 28-day (or 56-day for the H Series specimens) concrete compressive strength, $\sqrt{f'_c}$, could be substituted for $\sqrt{f'_{ci}}$ without a significant loss of correlation. For the specimens in this test program, the relationship between $f_{pj}$ and $f_{pt}$ was fairly uniform, as was the relationship between $\sqrt{f'_c}$ and $\sqrt{f'_{ci}}$. Thus, while interchange of these parameters should result in different values of the proportionality constant, $\alpha$, it should not significantly affect the coefficient of correlation.

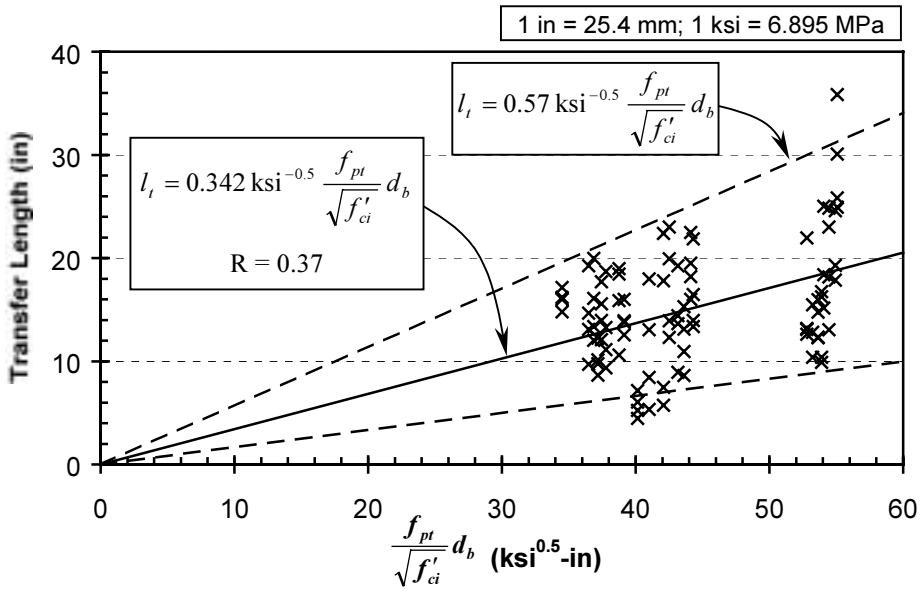


**Figure 5.11: Transfer Length as a Function of Tendon Prestress and Concrete Strength at Release—Bright Strand Specimens**

Very little correlation was evident for relationships that did not include the concrete strength in some form. The maximum coefficient of correlation found for this type of relationship was R = 0.08 for the relationship $l_t \propto f_{pt} d_b$. Likewise, no significant correlation was found between measured transfer lengths and expressions that included concrete compressive strength (without the square root), either $f'_{ci}$ or $f'_c$. This finding is logical because the concrete surrounding the tendon should crack due to circumferential tensile stresses before radial compressive stresses can approach the compressive strength of the concrete.

The dashed lines in Figure 5.11 represent upper and lower bounds for $\alpha_{\text{long term}}$ that bound at least 95 percent of the data. The upper-bound line represents $\alpha_{\text{long term}}$ = 0.57 ksi$^{-0.5}$ (18 psi$^{0.5}$/ksi, 0.22 MPa$^{-0.5}$). Based on the data from this test program alone, this would appear to be a logical value of $\alpha_{\text{long term}}$ for use in an expression to predict the transfer length of bright strand for anchorage purposes.

Figure 5.12 illustrates the relationship between the measured long-term transfer lengths for the rusted strand specimens and $\frac{f_{pt}}{\sqrt{f'_{ci}}}\,d_b$. The bright strand data, best-fit line, and upper and lower bounds (from Figure 5.11) are shown in gray for comparison. Little significant correlation was found for the rusted strand transfer lengths with respect to any of the parameters evaluated. On average, the rusted strand transfer lengths were shorter than those of bright strands, but the dispersion was larger. Despite the shorter average transfer lengths, the dispersion is of such magnitude that the upper and lower bound expressions determined from the bright strand data serve as effective estimates of the upper and lower bounds of the rusted transfer lengths. It appears that the relative disparity between the transfer lengths for bright and rusted strands is concentrated in the area of the chart where larger transfer lengths are expected. This may indicate that the relative improvement in bond capacity resulting from surface weathering may be effectively limited to lower concrete strength levels. These lower strength levels are typical of many of the past studies that have shown a significant shortening of transfer length due to surface weathering/roughness (Ban, Muguruma and Morita 1960, Janney 1963; Hanson 1969; Holmberg and Lindgren 1970; Rose and Russell 1997). Specific comparisons between the behavior of bright and rusted strand specimens are addressed in Section 5.4.3.

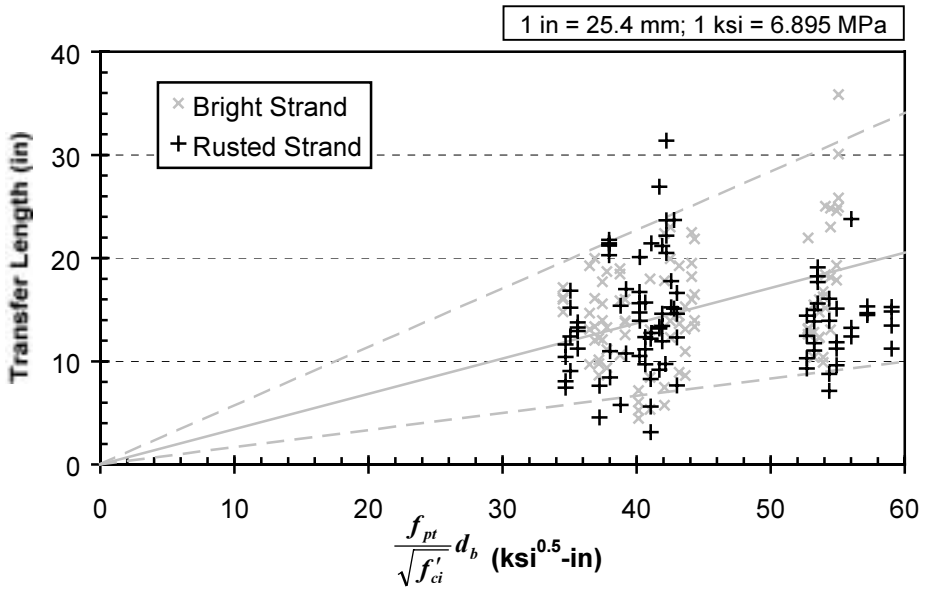


**Figure 5.12: Transfer Length as a Function of Tendon Prestress and Concrete Strength at Release—Rusted and Bright Strand Specimens**

Based on the theoretical considerations and correlation results discussed above, it seems logical to base expressions for estimating transfer length on the relationship $l_t = \alpha \frac{f_{pt}}{\sqrt{f'_{ci}}} d_b$. While the test results indicate that similar reliability might be obtained by substituting $f_{pj}$ or $\sqrt{f'_c}$ for the corresponding parameters, a few practical reasons also favor the use of $l_t = \alpha \frac{f_{pt}}{\sqrt{f'_{ci}}} d_b$. Developing an expression based on $f_{pt}$ allows the practitioner to freely substitute $f_{pj}$ for the sake of simplicity and speed without sacrificing conservatism. In the pretensioning industry, $f'_{ci}$ is often of more practical design and construction importance than $f'_c$. Through allowable stress considerations, the release strength determines how much prestressing reinforcement may be used in a member. Most importantly, the specified release strength usually more *reliably* indicates the actual release strength than the specified 28-day strength indicates the actual long-term strength. The prestress force is not transferred to the concrete until the specified release strength has been achieved. Thus, confidence in the achievement of the specified strength at release is greater than that for strength at 28 or 56 days.

### 5.4.2 Time

While some studies have revealed significant increases in transfer length with time (Evans 1951; Base 1957, 1958b; Kaar, LaFraugh and Mass 1963; Logan 1997; Lane 1998), others have exhibited less than significant increases (Rüsch and Rehm 1963; Lane 1992). Figure 5.13 illustrates the effect of time on transfer length for the bright strand specimens in this study. The ratio of long-term transfer length to initial transfer length is plotted versus the time elapsed after prestress release for each set of readings taken. Each vertical bar represents the average ratio for a set of specimens plus or minus one standard deviation.

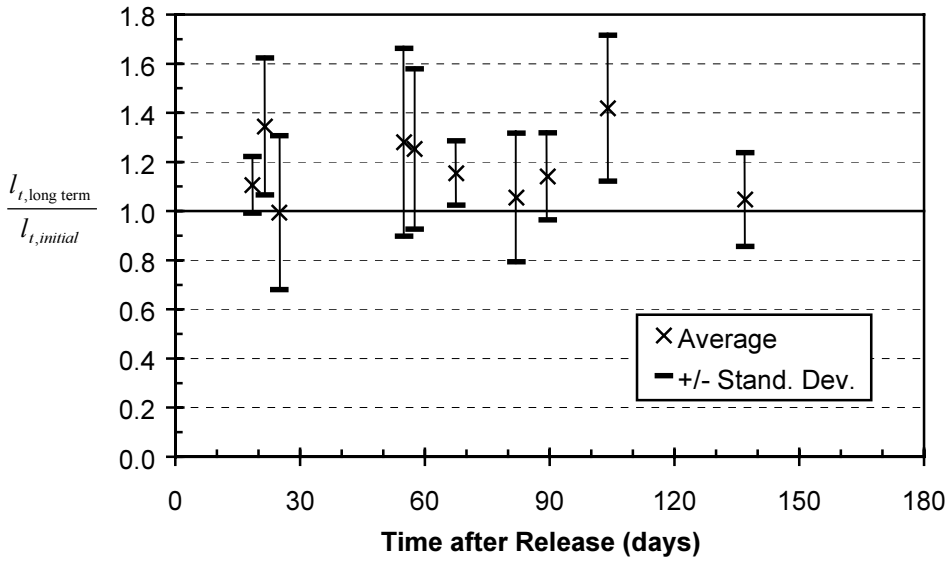


**Figure 5.13: Effect of Time on Transfer Length—Bright Strand Specimens**

The extent of the bars indicates that there was considerable dispersion among the various amounts of increase within a specimen group. For the bright strand specimens, the average ratio of long-term transfer length to initial transfer length was 1.13 with a coefficient of variation of 28 percent. Inspection of Figure 5.13 indicates no definite trend of continued growth beyond an age of twenty days. Thus, it may be inferred that the preponderance of the transfer length increase occurs in the first few weeks after casting. This roughly corresponds with the findings of Base (1957, 1958b), who states that almost all change occurred within the first twenty days, and Lane (1998), who reports an average increase of thirty percent in the first twenty-eight days, and only seven percent thereafter.

For bright strands on the ends of members subjected to the "dead" release method, the average increase with time was approximately 10 percent. On the opposite, "live" release, ends, there was no average increase beyond the initial transfer length.

The bright strand results indicate the possibility that higher concrete strengths might slightly inhibit the growth of transfer length with time. However, this trend is far from conclusive, especially considering that no such trend was indicated in the rusted strand specimens.

The increase of transfer length of rusted strand specimens over time is illustrated similarly in Figure 5.14. Here again, the significant portion of the transfer length growth appears to have taken place in the first few weeks after prestress transfer. For these specimens, the average ratio of long-term transfer length to initial transfer length is 1.17 with a coefficient of variation of 24 percent. There was no significant variation in the time-dependent behavior of the rusted strand with regard to either concrete strength or release method.

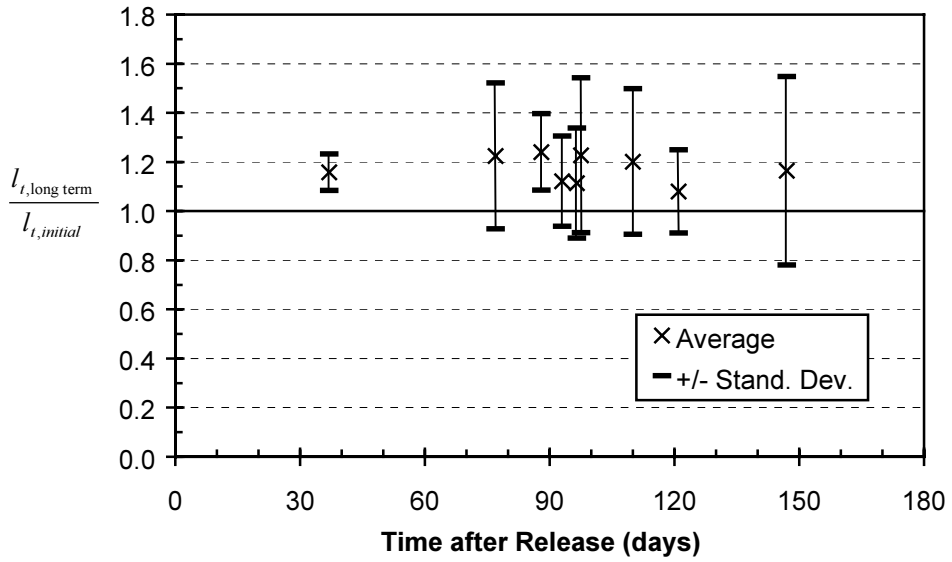


**Figure 5.14: Effect of Time on Transfer Length—Rusted Strand Specimens**

### 5.4.3 Strand Surface Condition

A wide variety of test results have been reported with regard to the effect of strand weathering on transfer length (see Section 2.4.5.2). Some researchers have found transfer lengths for rusted strand as small as one-half of those for bright strand (Ban, Muguruma, and Morita 1960). Others have found no discernible improvement in the transfer length of wire (Base 1958a) or strand (Logan 1997) due to rust.

Table 5.7 indicates the relative performance of rusted strands versus bright strands in this study. In an effort to equitably compare the performance of strands with the two surface conditions, the transfer lengths have been normalized with respect to $\frac{f_{pt}}{\sqrt{f'_{ci}}} d_b$. For each experimentally determined value of transfer length, a value of $\alpha$ was determined based on the relationship $l_t = \alpha \frac{f_{pt}}{\sqrt{f'_{ci}}} d_b$. The boldface values in Table 5.7 represent the average ratio of $\alpha_{rusted}$ to $\alpha_{bright}$ among the companion specimens in a set. These values therefore indicate the average ratio of the normalized transfer length for rusted strand specimens to the normalized transfer length of bright strand specimens. The row and column labels describe the concrete strength series and method of prestress release that define each companion set. The number of comparisons and coefficient of variation characteristic of each set are also included.

**Table 5.7: Effect of Rusted Surface Condition on Normalized Transfer Length Relative to Bright Surface Condition**

| | | Simultaneous Release | | Dead Release | | Live Release | | All Release Methods | |
|---|---|---|---|---|---|---|---|---|---|
| | | Initial | Long Term | Initial | Long Term | Initial | Long Term | Initial | Long Term |
| L Series | $n$ | 30 | 27 | 0 | 0 | 0 | 0 | 30 | 27 |
| | $\overline{X}$ | **0.87** | **0.78** | — | — | — | — | **0.87** | **0.78** |
| | $C.V.$ | 0.53 | 0.32 | — | — | — | — | 0.53 | 0.32 |
| M Series | $n$ | 12 | 12 | 7 | 7 | 7 | 7 | 26 | 26 |
| | $\overline{X}$ | **1.12** | **1.11** | **0.96** | **1.04** | **1.31** | **1.59** | **1.13** | **1.22** |
| | $C.V.$ | 0.24 | 0.32 | 0.52 | 0.67 | 0.49 | 0.51 | 0.40 | 0.51 |
| H Series | $n$ | 12 | 12 | 7 | 7 | 7 | 8 | 26 | 27 |
| | $\overline{X}$ | **0.84** | **0.86** | **0.87** | **0.85** | **0.91** | **1.03** | **0.87** | **0.91** |
| | $C.V.$ | 0.30 | 0.22 | 0.82 | 0.37 | 0.19 | 0.36 | 0.46 | 0.32 |
| All Strength Series | $n$ | 54 | 51 | 14 | 14 | 14 | 15 | 82 | 80 |
| | $\overline{X}$ | **0.92** | **0.88** | **0.92** | **0.95** | **1.11** | **1.30** | **0.95** | **0.97** |
| | $C.V.$ | 0.43 | 0.33 | 0.65 | 0.56 | 0.45 | 0.51 | 0.47 | 0.47 |

$n$ = Number of direct comparison ratios $(\frac{\alpha_{rusted}}{\alpha_{bright}})$ in set; $l_t = \alpha \frac{f_{pt}}{\sqrt{f'_{ci}}} d_b$

$\overline{X}$ = Arithmetic mean of ratios

$C.V.$ = Coefficient of variation of ratios

On average, it appears that the rusted strand specimens had slightly shorter transfer lengths than the bright strand specimens. This was particularly evident for the lower-strength L-Series specimens. For these specimens, the rusted strand transfer lengths averaged about 13 percent shorter than bright strand transfer lengths at release. The long-term disparity was even more pronounced, increasing to approximately 22 percent. These calculations reinforce the observation made in Section 5.4.1 that the disparity between rusted and bright strand transfer lengths appeared to be concentrated among the specimens with lower concrete strengths. These strength levels are characteristic of those used in past studies for which significant disparities have been found between the behavior of bright and rusted strand (Ban, Muguruma and Morita 1960, Janney 1963; Hanson 1969; Holmberg and Lindgren 1970; Rose and Russell 1997).

The unpredictability of rusted strand behavior becomes apparent upon inspection of the results for the M-Series specimens. On average, use of rusted strand in these specimens resulted in *longer* transfer lengths than obtained with bright strand. The behavior is most pronounced in the specimen ends that were subjected to the "live" release condition. In these specimens, the average rusted strand transfer lengths were initially approximately 30 percent longer than those for bright strand. Over time, the relative disparity increased to almost 60 percent. The behavior of these specimens indicates that the combination of sudden release and rusted strand may have detrimental effects on transfer bond behavior. The shock resulting from the dynamic release of prestress may cause portions of the rust product to break free of the strand surface. Because the concrete hardened against this rust product rather than the underlying surface of the strand, the separation of the rust product from the strand may result in less friction between the strand and the concrete than would be case for concrete cast against bright strand.

This detrimental interaction of rust and sudden release was less evident in the H-Series specimens, but the relative behavior of the rusted strands in the specimen ends subjected to "live" release was the worst in this series as well. Unfortunately, none of the L-Series specimens were subjected to the "live" release method.

### 5.4.4 Method of Prestress Release

Studies that have investigated the effect of prestress release method on transfer length have shown that sudden prestress release usually results in longer transfer lengths than gradual prestress release (Base 1958a; Kaar, LaFraugh, and Mass 1963; Rüsch and Rehm 1963; Holmberg and Lindgren 1970; Rose and Russell 1997). In a manner similar to that used for comparing the relative performance of bright and rusted strands in Table 5.7 above, Table 5.8 compares the performance of transfer lengths subjected to the "live" method of prestress release to those subjected to the "dead" release method. The L-Series specimens were only subjected to the "simultaneous" release method. These three methods of prestress release are described in Section 5.2.2 above.

**Table 5.8: Effect of Live Prestress Release on Normalized Transfer Length Relative to Dead Prestress Release**

| | | Bright Strands | | Rusted Strands | | All Surface Conditions | |
|---|---|---|---|---|---|---|---|
| | | Initial | Long Term | Initial | Long Term | Initial | Long Term |
| L Series | $n$ | 0 | 0 | 0 | 0 | 0 | 0 |
| | $\overline{X}$ | — | — | — | — | — | — |
| | $C.V.$ | — | — | — | — | — | — |
| M Series | $n$ | 8 | 8 | 8 | 8 | 16 | 16 |
| | $\overline{X}$ | **0.97** | **0.89** | **1.44** | **1.54** | **1.21** | **1.22** |
| | $C.V.$ | 0.37 | 0.37 | 0.63 | 0.69 | 0.59 | 0.68 |
| H Series | $n$ | 7 | 8 | 9 | 9 | 16 | 17 |
| | $\overline{X}$ | **1.07** | **0.99** | **1.48** | **1.33** | **1.30** | **1.17** |
| | $C.V.$ | 0.38 | 0.22 | 0.60 | 0.46 | 0.56 | 0.42 |
| All Strength Series | $n$ | 15 | 16 | 17 | 17 | 32 | 33 |
| | $\overline{X}$ | **1.02** | **0.94** | **1.46** | **1.43** | **1.25** | **1.19** |
| | $C.V.$ | 0.36 | 0.29 | 0.60 | 0.58 | 0.57 | 0.56 |

$n$ = Number of direct comparison ratios $(\frac{\alpha_{live}}{\alpha_{dead}})$ in set; $l_t = \alpha \frac{f_{pt}}{\sqrt{f'_{ci}}} d_b$

$\overline{X}$ = Arithmetic mean of ratios

$C.V.$ = Coefficient of variation of ratios

Among bright strand specimens, the average performance of the live release specimens was neither consistently better nor consistently worse than that of the dead release specimens. Although these results might seem to contradict those of earlier studies regarding prestress release, this may not be the case. Although Rüsch and Rehm (1963) report transfer length increases of up to 20 percent due to sudden prestress release, the disparity between release methods decreased with increasing concrete compressive strength at release, $f'_{ci}$, in specimens containing seven-wire bright strand. The largest value of $f'_{ci}$ for these specimens corresponds roughly with that of the L-Series specimens in the present study. Based on their results, the lack of disparity between the results of the live and dead release methods for the M- and H-Series specimens appears rational. Since the method of prestress release was not varied for the L-strength specimens, it is impossible to determine whether a larger disparity would have resulted at lower concrete strength levels.

For the rusted strand specimens, on the other hand, considerable disparity exists between the live release results and the dead release results. On average, the live release method results in transfer lengths 30 to 50 percent longer than the dead release method. The apparently detrimental combination of rusted surface condition and sudden prestress release was discussed in the previous section.

It is more difficult to assess the effects of the simultaneous release method to either the live or dead method because there are no true "companion" specimens. Although direct comparisons are impossible to construct, broad inferences may be drawn from the average $\alpha$ values for all specimens subjected to each release method. Application of this type of comparison indicates that the simultaneous release method yielded normalized transfer lengths comparable to those of the dead release method for both bright and rusted strand. This indicates that the detrimental effects of flame cutting may be at least partially mitigated by cutting each strand at every member end on a pretensioning bed prior to cutting subsequent strands.

## 5.5 COMPARISON OF TEST DATA WITH RECOMMENDED EXPRESSIONS

The purpose of this section is to compare the transfer length data obtained in this study with other published expressions for transfer length calculation. The expressions are divided into two categories depending on whether or not they reflect the influence of concrete strength. As an introduction, Figure 5.15 and Figure 5.16 compare the data to the upper-bound expression $l_t = 0.57\,\text{ksi}^{-0.5}\dfrac{f_{pt}}{\sqrt{f'_{ci}}}d_b$ developed in Section 5.4.1 and serve as examples of the figures to follow. In Figure 5.15, the actual transfer lengths determined from this test program are plotted versus the transfer length calculated from the expression $l_t = 0.57\,\text{ksi}^{-0.5}\dfrac{f_{pt}}{\sqrt{f'_{ci}}}d_b$ using the measured concrete strength at release $f'_{ci}$ and the value of prestress immediately following release, $f_{pt}$, obtained from elastic analysis. A line through the origin with a slope of unity represents the case where the measured transfer length equals that predicted by the expression. In order for the expression to serve as an adequate formula for design, this line should approximate the general trend of the data yet serve as an upper bound to at least 95 percent of the points. In the case of Figure 5.15, because the expression in question was developed from the test data, it satisfies these criteria with respect to the bright strand data. On the other hand, the expression does not model the trend of the rusted data well, but it still serves as an adequate upper bound.

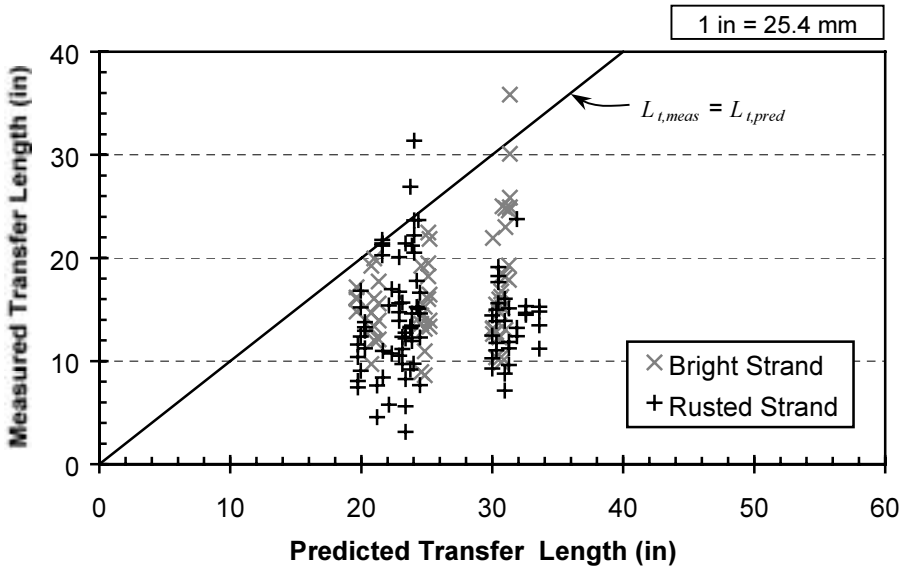


**Figure 5.15: Comparison of Measured Transfer Lengths to $l_t = 0.57\,\text{ksi}^{-0.5}\dfrac{f_{pt}}{\sqrt{f'_{ci}}}d_b$**

Figure 5.16 plots the ratio of calculated transfer length (based on the expression in question) to the measured transfer length versus the 28-day (or 56-day) concrete compressive strength, $f'_c$. In this type of chart, a horizontal line representing an ordinate of unity indicates perfect agreement between predicted and measured values of transfer

length. If the expression in question serves as an adequate design formula, the horizontal line will serve as an upper bound to at least 95 percent of the data, and the overall trend of the data should exhibit minimal slope. Here again, the expression $l_t = 0.57\,\text{ksi}^{-0.5}\dfrac{f_{pt}}{\sqrt{f'_{ci}}}d_b$ appears to satisfy these conditions with respect to the bright strand data. For the bright strand data, the expression seems slightly overconservative at lower concrete strength levels, but it remains an adequate upper bound over the full range of concrete strengths.

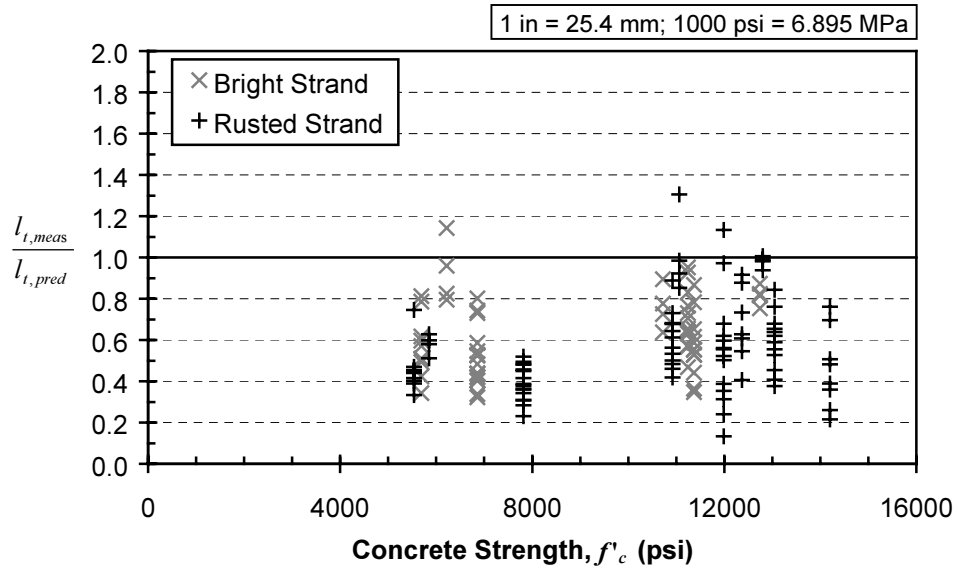


**Figure 5.16: Comparison to $l_t = 0.57\,\text{ksi}^{-0.5}\dfrac{f_{pt}}{\sqrt{f'_{ci}}}d_b$ over Concrete Strength Range**

### *5.5.1.1 Expressions That Exclude Concrete Strength*

Figure 5.17 and Figure 5.18 compare the data from the test program to the expression for transfer length included in ACI Building Code Commentary, $l_t = \dfrac{f_{pe}}{3\,\text{ksi}}d_b$ (ACI 318-99, R12.9). The history of this expression is presented in Section 2.3. It was originally formulated as an expression for *average* transfer length, and its usefulness as an expression for safe design is dubious. Nonetheless, Figure 5.17 indicates that it serves as an adequate upper bound for the data from this test program. Close inspection of Figure 5.18 reveals that it does not follow the general trend of the data with respect to concrete strength. It grows increasingly conservative as concrete strength increases.

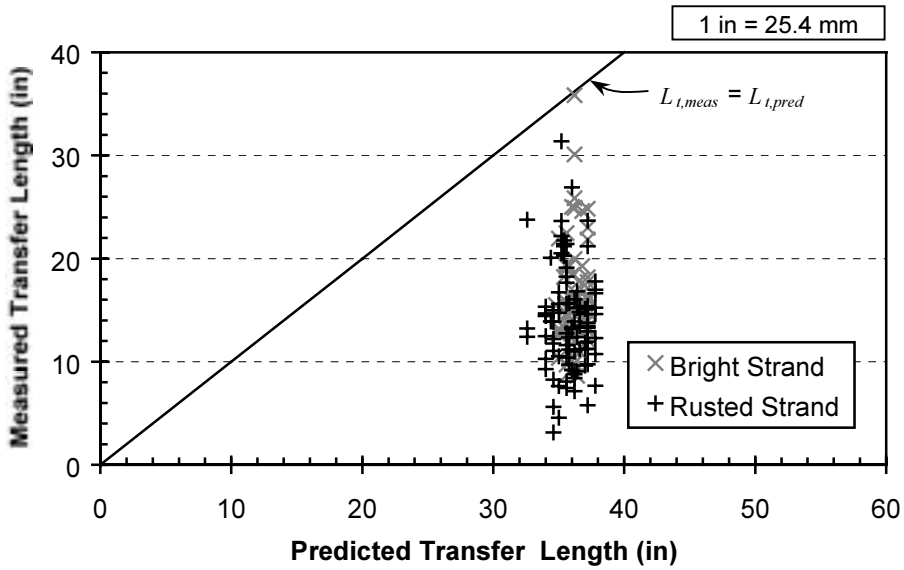


**Figure 5.17: Comparison of Measured Transfer Lengths to ACI 318-R12.9 Values**

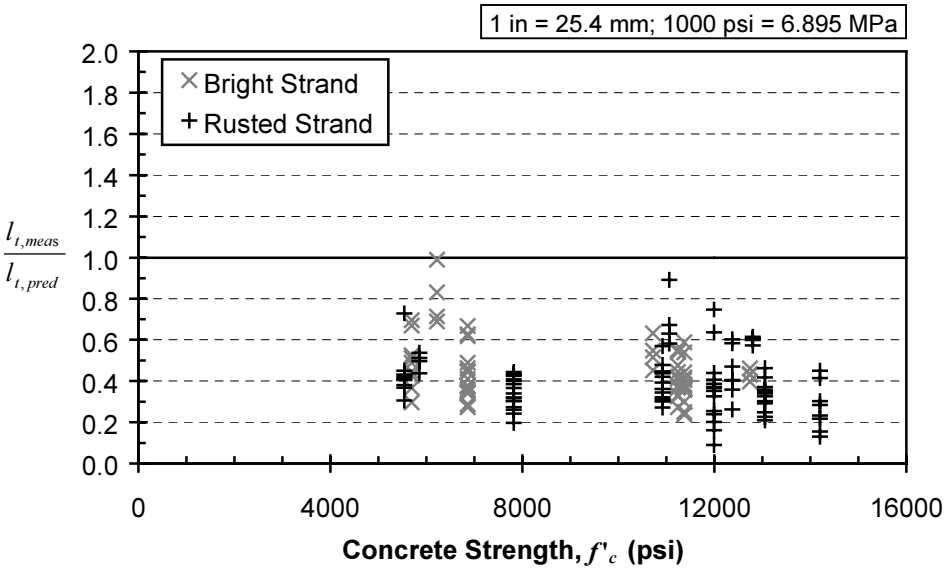


**Figure 5.18: Comparison to ACI 318-R12.9 Values over Concrete Strength Range**

Figure 5.19 and Figure 5.20 illustrate the relationship between the data and the transfer length relationship described in the shear provisions of the ACI Building Code (ACI 318-99, 11.4.3, 11.4.4) and the AASHTO Standard Specifications (AASHTO 1996, 9.20.2.4) in which the transfer length is assumed equal to $50d_b$. This expression has much the same relationship with the data as the one from the ACI 318 Commentary except that it is slightly less conservative because values of effective prestress, $f_{pe}$, are now larger than was generally assumed (150 ksi) at the time the $50d_b$ assumption was codified. The more recently developed AASHTO LRFD Specifications (AASHTO 1998, 5.11.4.1) incorporate an assumed transfer length of $60d_b$ in the shear provisions, more accurately reflecting the levels of prestress common in contemporary practice. This expression ($60d_b$) is compared with the test data in Figure 5.21 and Figure 5.22. These figures exhibit about the same level of conservatism that is evident in Figure 5.17 and Figure 5.18.

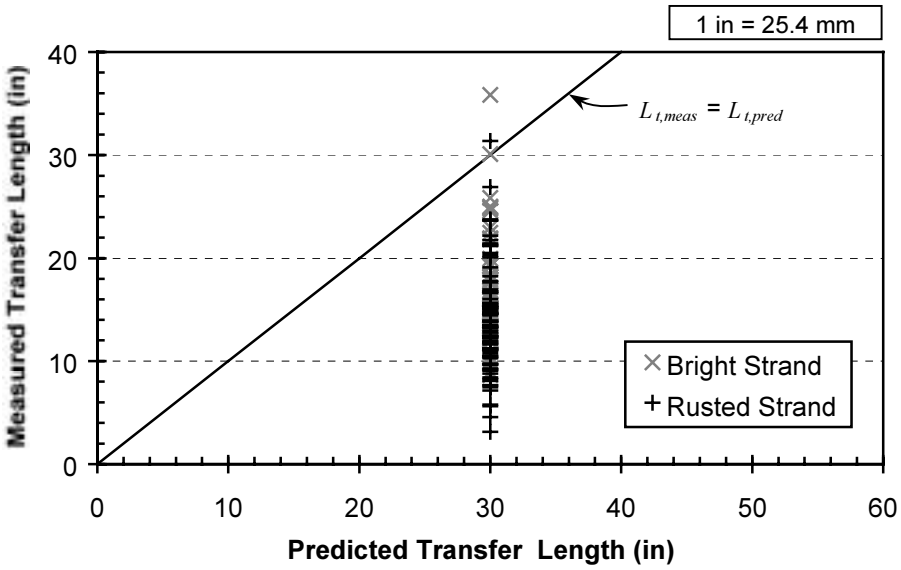


**Figure 5.19: Comparison of Measured Transfer Lengths to Values from ACI 318 and AASHTO Standard Shear Provisions**

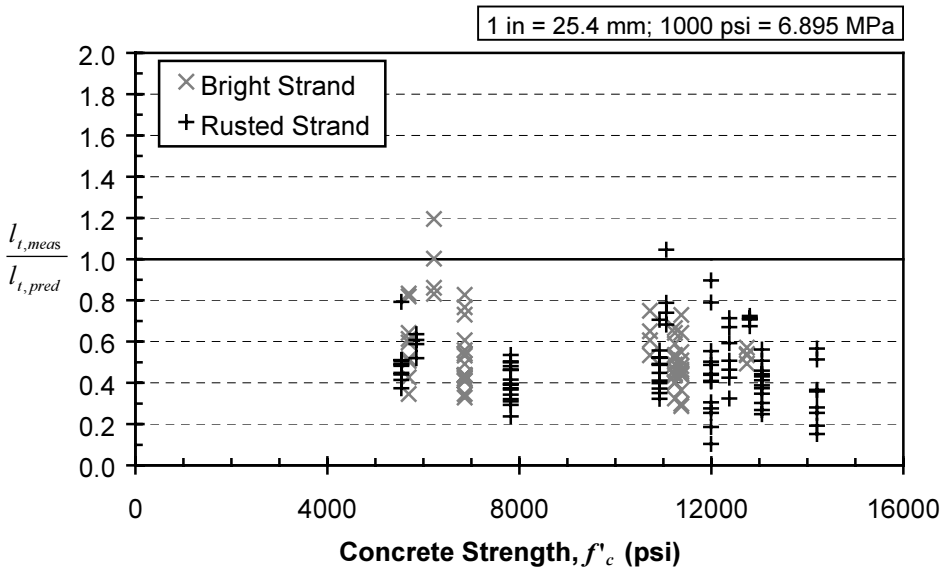


**Figure 5.20: Comparison to Values from ACI 318 and AASHTO Standard Shear Provisions over Concrete Strength Range**

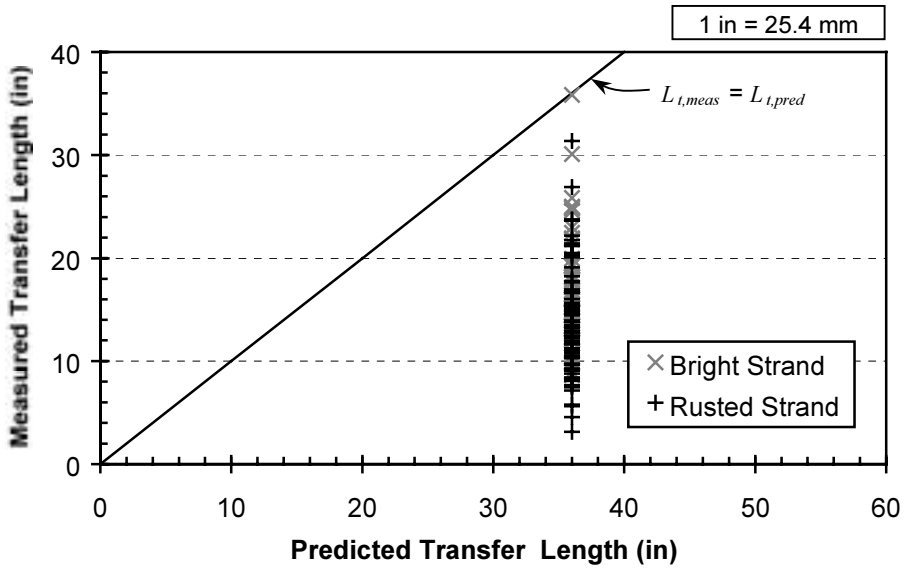


**Figure 5.21: Comparison of Measured Transfer Lengths to Values from AASHTO LRFD Shear Provisions**

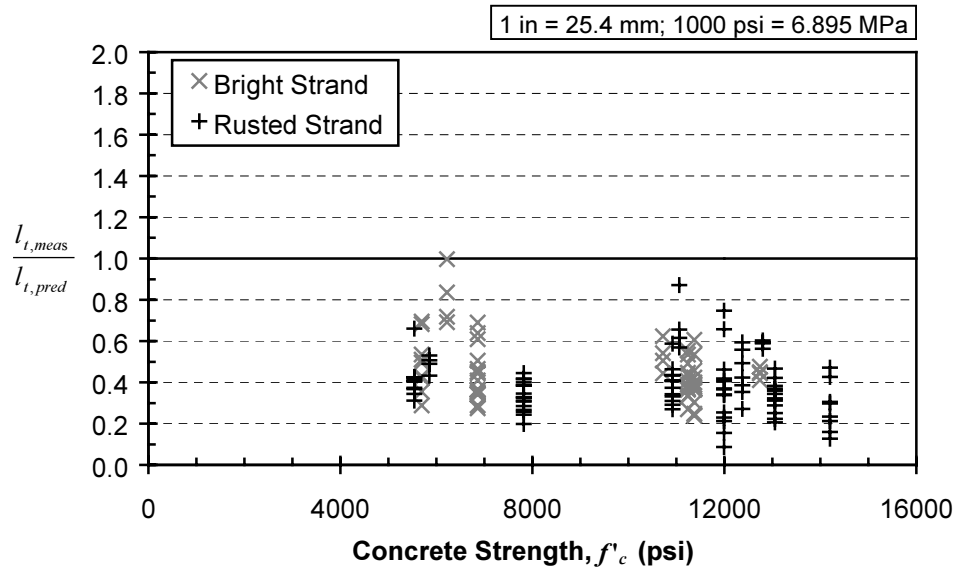


**Figure 5.22: Comparison to Values from AASHTO LRFD Shear Provisions over Concrete Strength Range**

Figure 5.23 and Figure 5.24 compare the test data with the transfer length expression proposed by Buckner (1995), $l_t = \frac{f_{pt}}{3\,\text{ksi}} d_b$. This expression is simply the ACI Commentary expression modified to include the steel stress immediately after transfer, rather than the steel stress after all time-dependent losses. As might be expected, the relationship between this expression and the data is quite similar to that of the other expressions considered in this section. All of these expressions effectively estimate the upper bound of the data for lower concrete strengths. However, they do not reflect the trend of the experimental transfer lengths to decrease with increasing concrete strength.

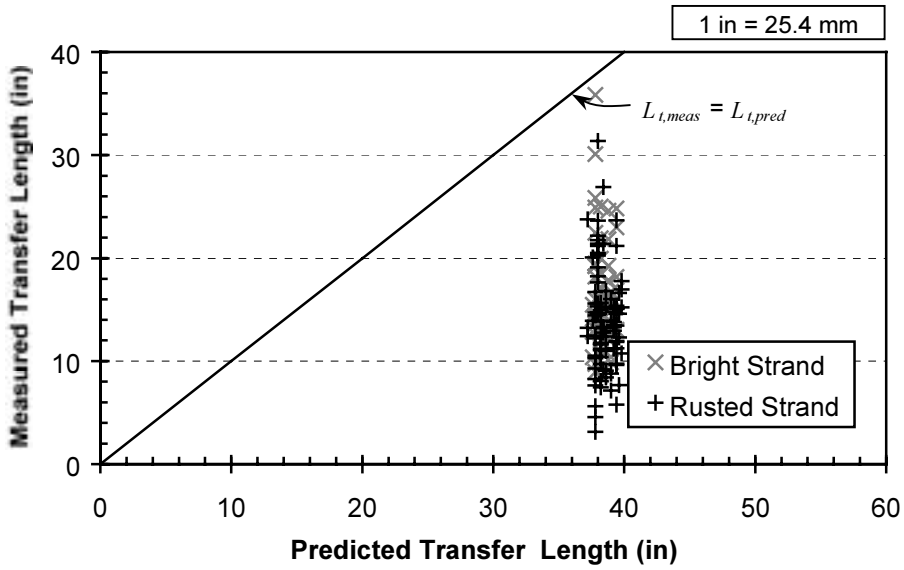


**Figure 5.23: Comparison of Measured Transfer Lengths to Values from Buckner Expression**

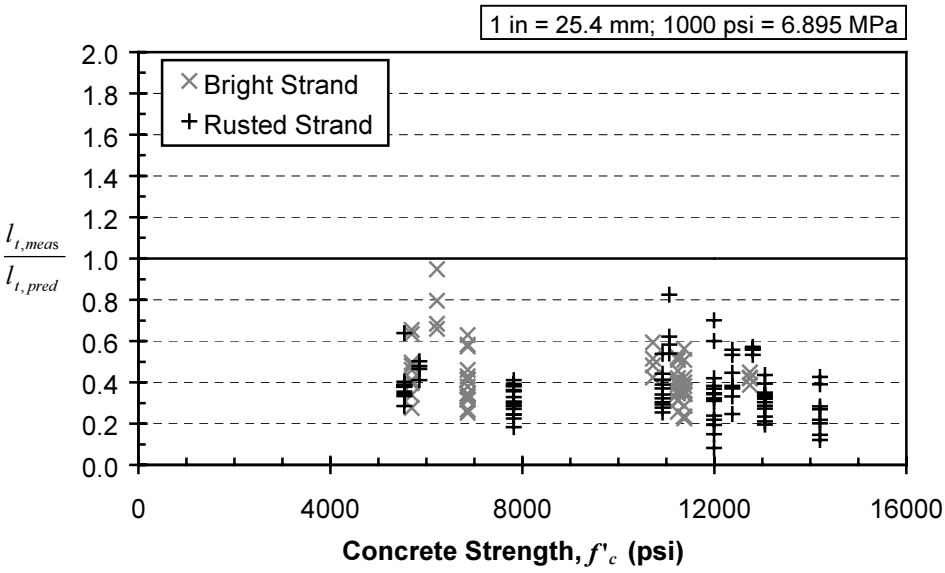


**Figure 5.24: Comparison to Values from Buckner Expression over Concrete Strength Range**

### *5.5.1.2 Expressions That Include Concrete Strength*

The figures in this section compare the test data to proposed expressions that do include the concrete strength as a parameter. Figure 5.25 and Figure 5.26 compare the test data to an expression proposed by Zia and Mostafa (1978), $l_t = 1.5 \frac{f_{pt}}{f'_{ci}} d_b - 4.6 \text{ in}$. This expression was developed on the basis of a review of published test results. However, results from specimens with $f'_c$ < 2000 psi (14 MPa) and $f'_c$ > 8000 psi (55MPa) were intentionally excluded.

Thus, although this expression is purported to relate transfer length to concrete strength, its effective range is quite limited in terms of concrete strengths used in present practice. The presence of a constant term in the expression is not rational. As prestress levels approach zero, transfer lengths should approach zero, not a physically meaningless value such as –4.6 in. The inadequacy of this expression for higher strength specimens is apparent in Figure 5.26. The expression is obviously oversensitive to the concrete strength.

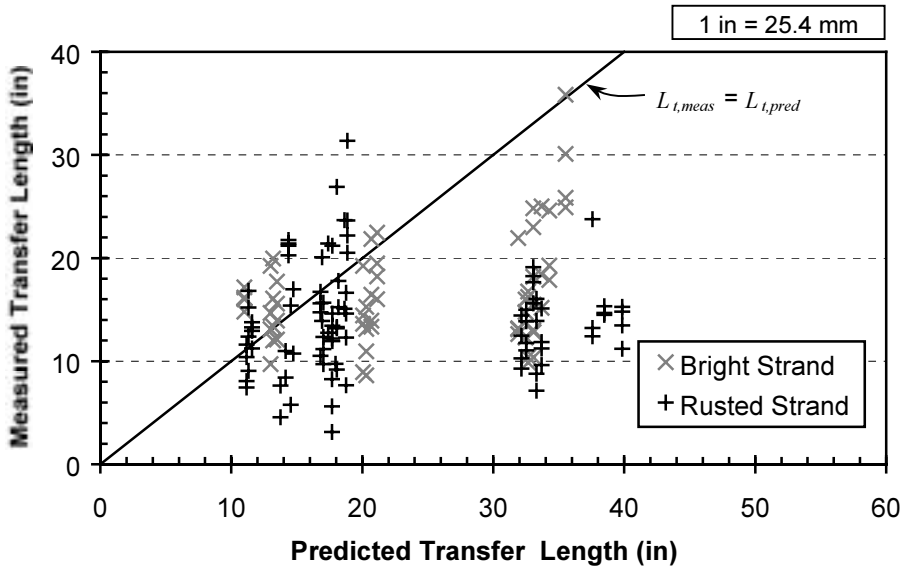


**Figure 5.25: Comparison of Measured Transfer Lengths to Values from Zia and Mostafa Expression**

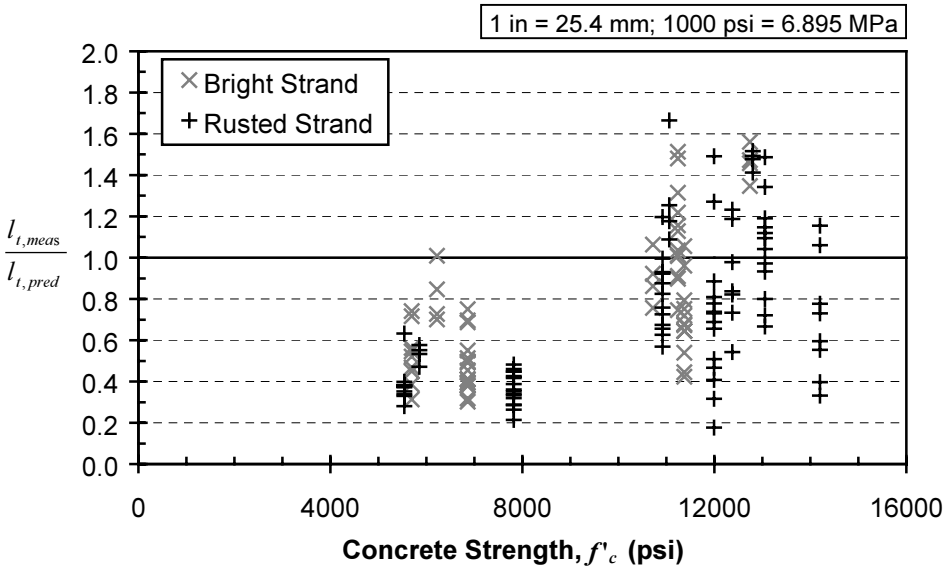


**Figure 5.26: Comparison to Values from Zia and Mostafa Expression over Concrete Strength Range**

Figure 5.26 and Figure 5.27 exhibit a comparison between the test data and the expression developed by Lane (1998), $l_t = 4\frac{f_{pj}}{f'_c} d_b - 5\,\text{in}$. Although considerably more conservative than that of Zia and Mostafa, this expression

suffers from similar faults. It is based on a statistical analysis of data from a variety of studies that primarily featured values of $f_c'$ less than 10,000 psi (69 MPa). Accordingly, in the same manner that the Zia and Mostafa expression was overly sensitive to $f_c'$, the Lane expression becomes less conservative as concrete strength increases. Due to a lack of data incorporation higher concrete strengths, Lane recommends that the value of $f_c'$ in the expression be limited to 10,000 psi. Figure 5.29 displays a comparison between the test data and the Lane expression when modified in this manner.

As with the Zia and Mostafa expression, the Lane expression contains a constant term that cannot be rationalized from a behavioral point of view. This constant term originally resulted from acceptance of a linear regression result that featured the highest statistical correlation coefficient (Lane 1998, 34). A simpler, more rational expression might have been developed at the expense of a slight decrease in statistical correlation with the available test results.

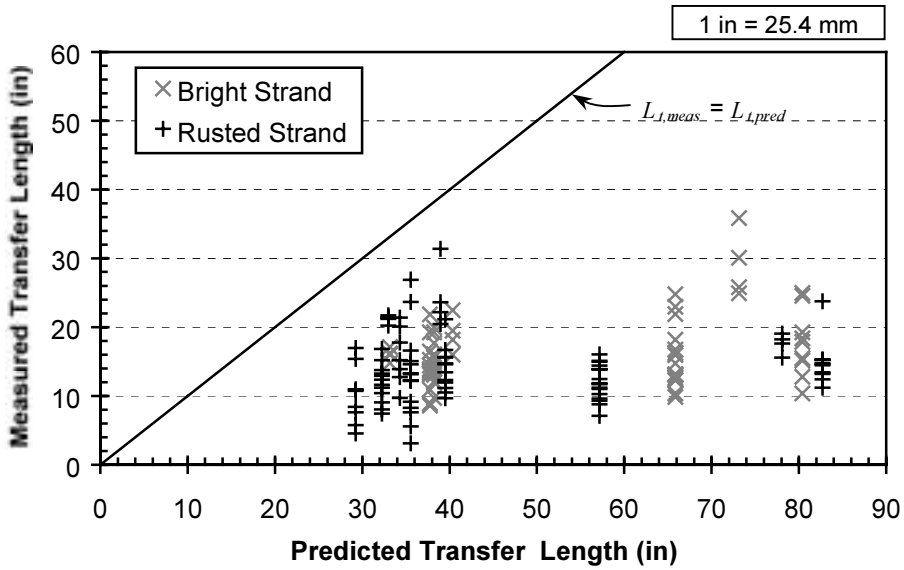


**Figure 5.27: Comparison of Measured Transfer Lengths to Values from Lane Expression**

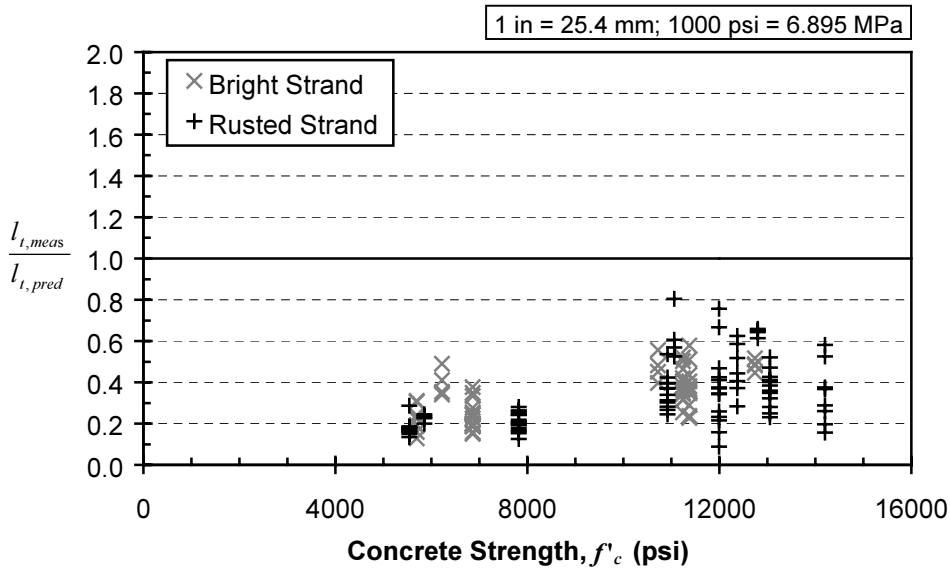


**Figure 5.28: Comparison to Values from Lane Expression over Concrete Strength Range**

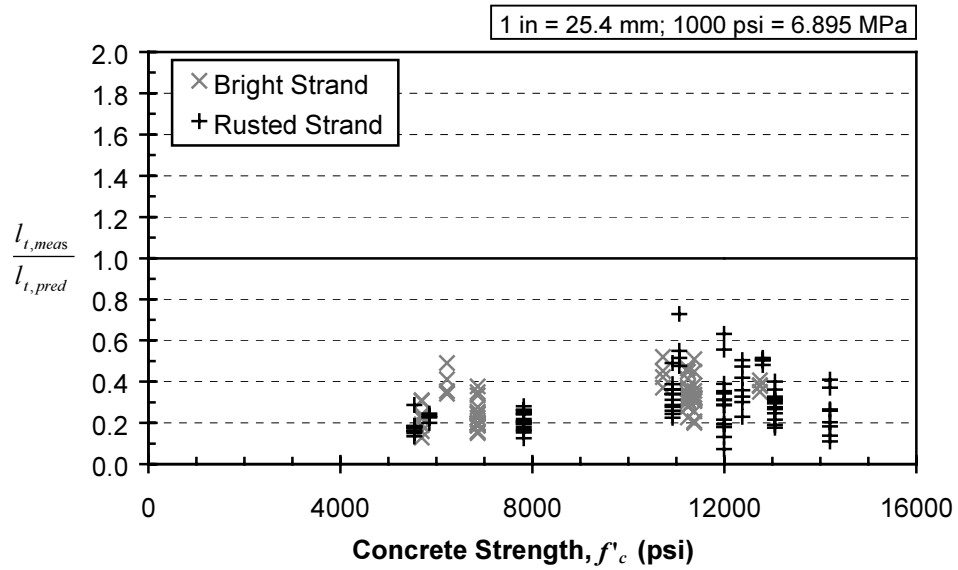


**Figure 5.29: Comparison to Values from Modified Lane Expression over Concrete Strength Range**

The final two expressions considered in this section result from a synthesis of behavioral considerations and experimental results. The first of these is the expression for transfer length included in the CEB-FIP Model Code 90 (CEB-FIP 1990, 6.9.11.4). Formulation of the MC90 expression is explained in depth by den Uijl (1992). In the MC90 expression, transfer length is directly proportional to the jacking stress of the tendons, $f_{pj}$, as well as the tendon diameter, $d_b$, and indirectly proportional to the tensile strength of the concrete at the time of prestress release. Thus, this relationship is quite similar to those expressed in Equation 5.5 and Equation 5.6 above. However, following the standard European practice, MC90 directly relates the tensile strength of the concrete at release to $\left(f'_{ci}\right)^{0.67}$, rather than the $\sqrt{f'_{ci}}$ of North American practice. Nonetheless, Figure 5.30 and Figure 5.31 show that, while quite conservative with respect to the test data, the MC90 expression does follow the trend of the bright strand data fairly well.

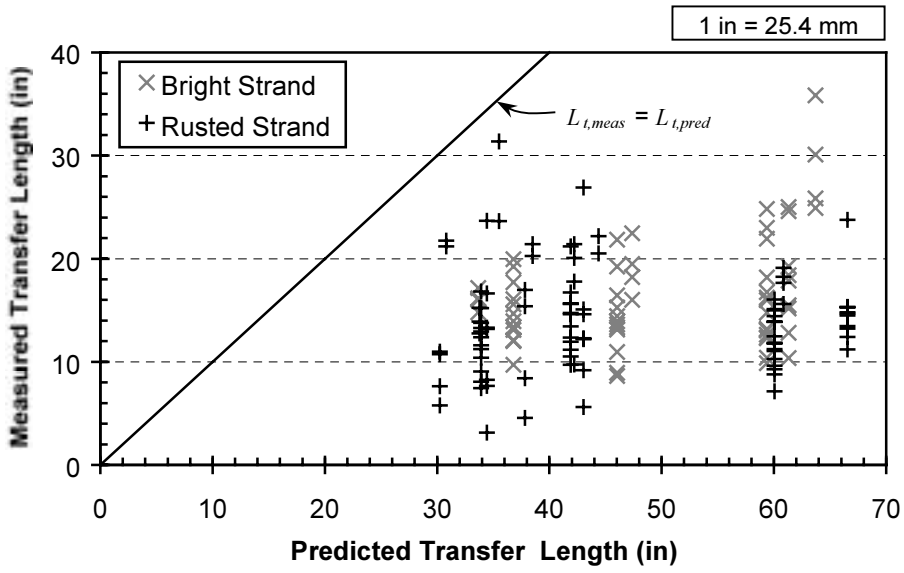


**Figure 5.30: Comparison of Measured Transfer Lengths to Values from MC90 Expression**

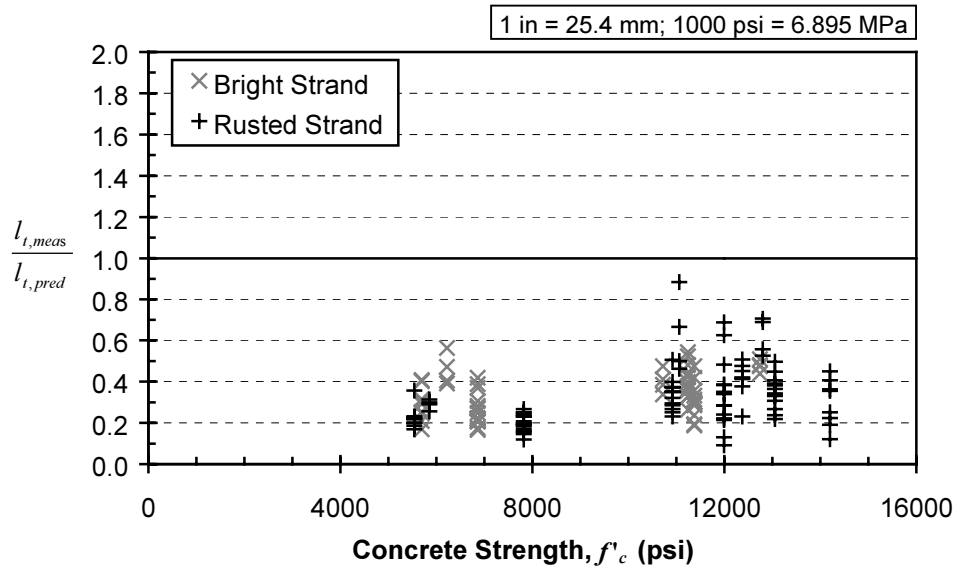


**Figure 5.31: Comparison to Values from MC90 Expression over Concrete Strength Range**

The final expression under consideration in this section is that put forward by Mitchell et al. (1993), $l_t = 0.33\,\text{ksi}^{-1} f_{pt} d_b \sqrt{\frac{3\,\text{ksi}}{f'_{ci}}}$. Because this expression is practically identical to the expression $l_t = 0.57\,\text{ksi}^{-0.5} \frac{f_{pt}}{\sqrt{f'_{ci}}} d_b$, it also serves as an excellent upper bound to the data in this study. The Mitchell et al. expression results from an experimental study involving $^3/_8$, ½, and 0.6 in (9.5, 12.7, and 15.7 mm) strand embedded in concrete with strengths at release ranging from 3050 to 7250 psi (21 to 50 MPa). The prestress force was transferred to the concrete gradually.

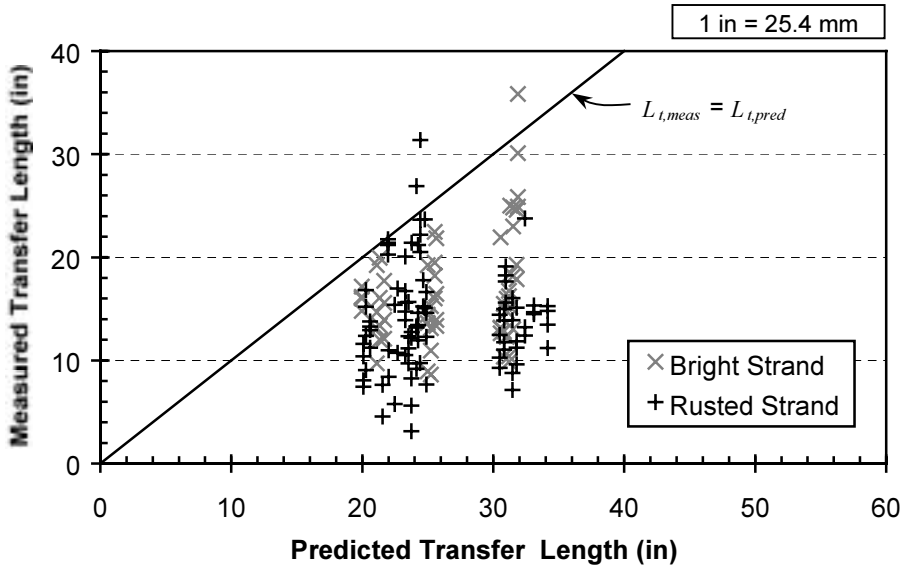


**Figure 5.32: Comparison of Measured Transfer Lengths to Values from Mitchell et al. Expression**

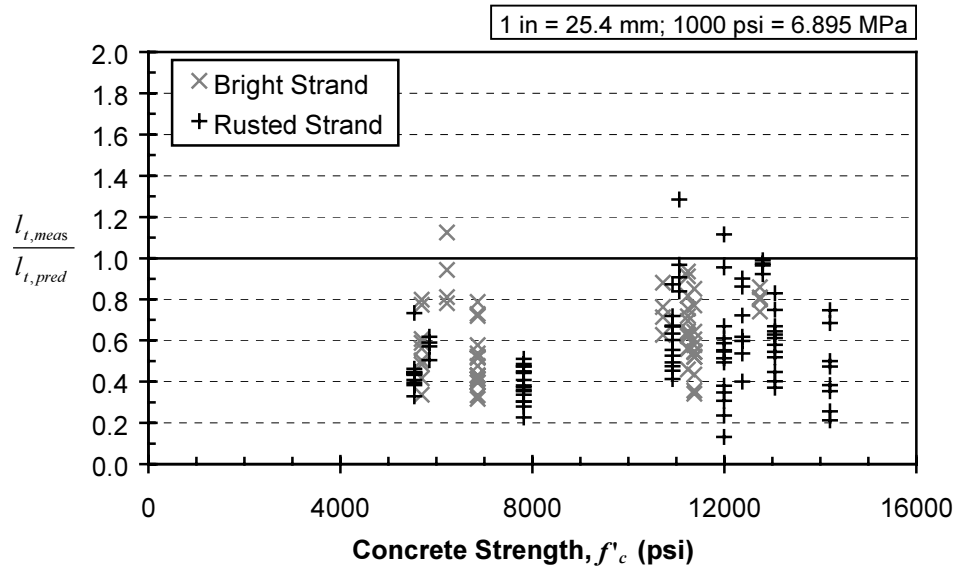


**Figure 5.33: Comparison to Values from Mitchell et al. Expression over Concrete Strength Range**

## 5.6 RECOMMENDED EXPRESSION FOR TRANSFER LENGTH

As discussed in Section 5.4, the expression $l_t = \alpha \frac{f_{pt}}{\sqrt{f'_c}} d_b$ may be used to calculate transfer length, so long as the chosen value of $\alpha$ reflects the effects of variables other than the prestress level, the strand diameter, and the concrete strength. Figure 5.11 illustrates that selecting a value of $\alpha$ equal to 0.57 ksi$^{-0.5}$ results in an expression that serves as a conservative upper bound for the long-term transfer lengths for the bright strand used in this study. In developing a design expression, it is critical to incorporate test results from a variety of sources. For this reason, data were collected from other studies focusing on transfer lengths in large-scale prestressed beams.

The additional data were obtained from the following test programs:

1. FHWA Phase II (Lane 1998)—Transfer lengths measured on AASHTO Type II I-beams at an age of 28 days. Beams were prestressed with 0.5 in (12.7 mm) or 0.6 in (15.2 mm) strand. Thirty transfer lengths are included.
2. Florida DOT (Shahawy, Issa, and deV. Batchelor 1992)—Transfer lengths measured on AASHTO Type II I-beams after release. Beams were prestressed with 0.5 in (12.7 mm) or 0.6 in (15.2 mm) strand. Twenty-six transfer lengths are included.
3. Auburn University (Simmons 1995)—Transfer lengths measured on 22 in (560 mm) deep T-beams after release. Beams were prestressed with 0.5 in (12.7 mm) strand. Twenty-seven transfer lengths are included.
4. University of Colorado (Shing et al. 1997)—Transfer lengths measured on three 21.75 in (550 mm) deep box girders after release. Beams were prestressed with 0.6 in (15.2 mm) strand. Only average value of the six transfer lengths is reported.
5. Tulane/CTL (Bruce et al. 1994)—Transfer lengths measured on three 54 in (1370 mm) bulb-tee girders at an age of 28 days. Beams were prestressed with 0.5 in (12.7 mm) strand. Six transfer lengths are included.
6. University of Virginia (Ozyildrium, Gomez, and Elhanal 1996)—Transfer lengths measured on two AASHTO Type II I-beams after release. Four transfer lengths are included.
7. University of Minnesota (Ahlborn, Shield, and French 1996)—Transfer lengths measured on two MnDOT 45M I-beams. Beams were prestressed with 0.6 in (15.2 mm) strand. Maximum and minimum values of the four transfer lengths were reported.

8. The University of Texas at Austin (Russell and Burns 1993)—Transfer lengths measured on 22 in (560 mm) and 23.5 in (595 mm) I-beams after release. Beams were prestressed with 0.5 in (12.7 mm) or 0.6 in (15.2 mm) strand. Twenty-eight transfer lengths are included.
9. The University of Texas at Austin (Gross and Burns 1995)—Transfer lengths measured on two 42 in (1065 mm) rectangular beams after release. Beams were prestressed with 0.6 in (15.2 mm) strand. Four transfer lengths are included.
10. The University of Texas at Austin (Cordova 1996)—Transfer lengths measured on four AASHTO Type III I-beams at ages ranging from one to six months after release. Beams were prestressed with 0.6 in (15.2 mm) strand. Eight transfer lengths are included. Four of these transfer lengths are as yet unpublished.

Figure 5.34 depicts these data along with the bright strand data from this research study. The experimentally determined transfer lengths are plotted against the quantity $\frac{f_{pt}}{\sqrt{f'_{ci}}} d_b$ corresponding to each specimen. The relationship $l_t = 0.57 \text{ ksi}^{-0.5} \frac{f_{pt}}{\sqrt{f'_{ci}}} d_b$, which serves as an upper bound for the data from this study, is plotted for comparative purposes.

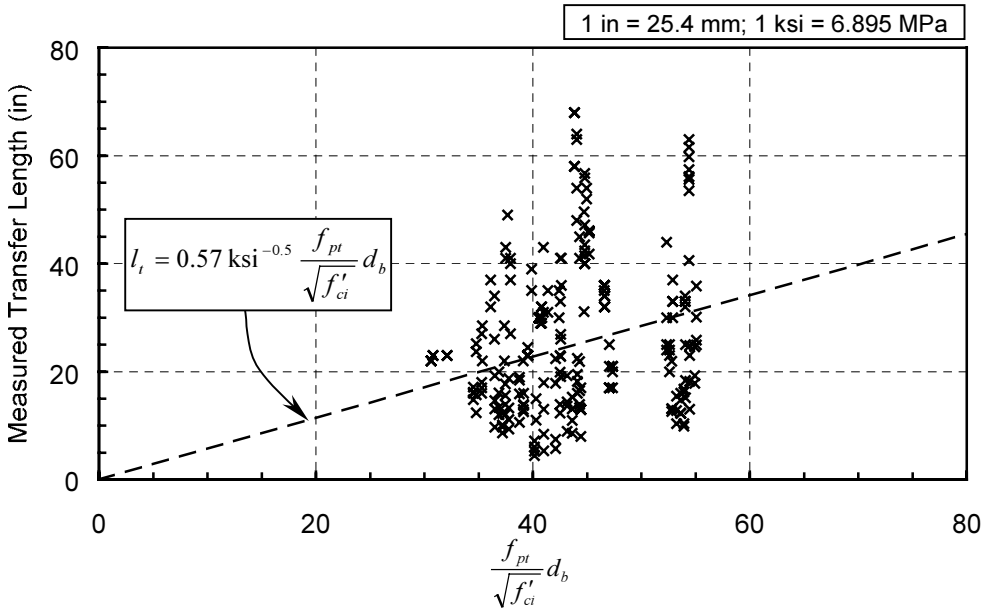


**Figure 5.34: Transfer Lengths from Various Studies**

It is evident from Figure 5.34 that the transfer lengths obtained from other studies are, on average, significantly larger than those obtained in this study. Rather than serving as an upper bound, the expression $l_t = 0.57 \text{ ksi}^{-0.5} \frac{f_{pt}}{\sqrt{f'_{ci}}} d_b$ underestimates roughly half of the transfer lengths.

The same data are plotted again in Figure 5.35, but differentiated according to strand manufacturer. Aside from the specimens for which the strand manufacturer is not known, the two largest groups of specimens are those containing strands from Manufacturer A (including the specimens of this study) and Manufacturer B (including the specimens of the other large UT study). Only a few data represent strands from Manufacturers C and D. On average, the transfer lengths of specimens containing strands from Manufacturer B are more than twice as long as those of specimens containing strands from Manufacturer A. This apparent disparity in performance lends credence to the theory (discussed in Chapter 4) that strands produced by different strand manufacturers may have significantly different bond characteristics.

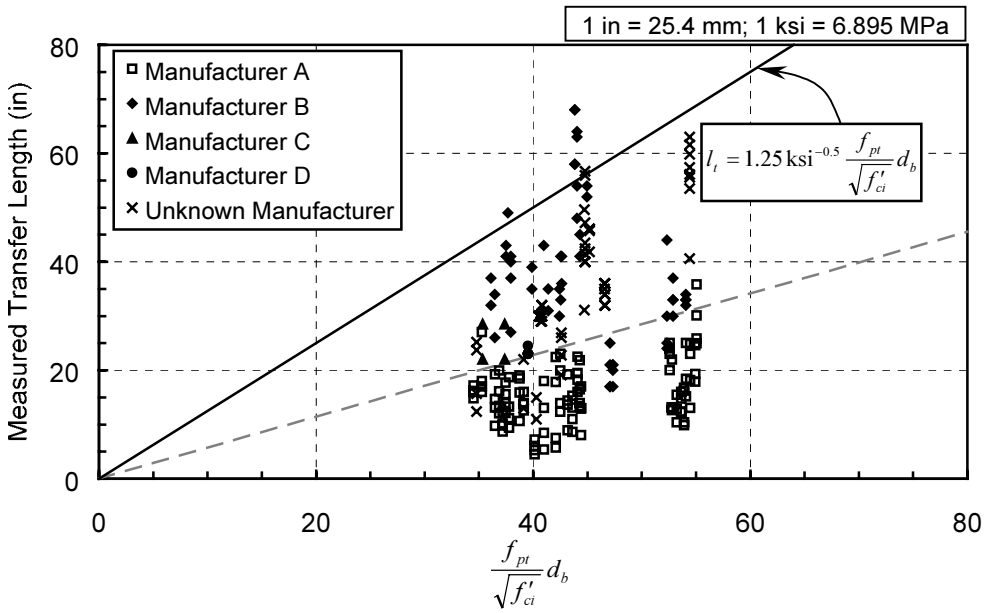


**Figure 5.35: Transfer Lengths of Strands from Various Manufacturers**

While the expression $l_t = 0.57\,\text{ksi}^{-0.5}\frac{f_{pt}}{\sqrt{f'_{ci}}}d_b$ still serves as an effective upper bound expression for long-term transfer lengths of bright strand produced by Manufacturer A, a larger value of $\alpha$ is required to effectively bound the transfer lengths of strands from all producers. Based on the data presented here, the expression $l_t = 1.25\,\text{ksi}^{-0.5}\frac{f_{pt}}{\sqrt{f'_{ci}}}d_b$ is recommended for providing an upper bound estimate of the transfer length for design purposes. This expression, depicted in Figure 5.35, yields a transfer length value nearly twice that of the current ACI Commentary expression when concrete with a release strength, $f'_{ci}$, equal to 4 ksi (28 MPa) is employed. This difference is not out of line considering the significant discrepancies between the original PCA test data and the ACI Commentary expression for transfer length. These discrepancies are discussed in Chapter 2. Figure 2.2 indicates that if the ACI Commentary expression were doubled, it would have bounded approximately 90 percent of the PCA data.

When designing to satisfy allowable concrete stresses, conservative design practice usually requires that a *lower bound* estimate of the transfer length be used to calculate concrete stresses in the anchorage region. A lower bound expression for transfer length could also be developed that incorporates the prestress level, strand diameter, and concrete strength. However, considering the short transfer lengths measured in many of the specimens of this study, it seems quite practical to simply assume a transfer length of 6 in (150 mm) or less for this purpose. Assuming a value of zero would be safe, simple, and probably not result in significant extra cost.

In this study and previous studies, surface weathering of strand has served to shorten average transfer lengths. This effect is far from consistent however. Depending upon a specific degree of surface weathering to improve bond performance is impractical. The upper bound relationship proposed above reflects the fact that sudden prestress release was employed for many of the test specimens in the studies listed. Thus, the expression need not be amplified if sudden prestress release is expected. Until the apparent significant disparity in bond performance among strands produced by different manufacturers is reduced or at least better understood, attempting to refine the transfer length expression to reflect the influence of prestress release method is impractical. The apparent difference in transfer length attributable to differences in manufacturing processes can largely outweigh the difference resulting from varying the release method.

Further research is necessary to verify and/or quantify the "top bar effect" on the transfer length of pretensioned strands. Until such research has been performed and suitable conclusions reached, conservatism suggests that the transfer lengths of tendons satisfying the ACI Code definition of top bars be increased by at least 30 percent.

## 5.7 SUMMARY AND CONCLUSIONS

Transfer lengths were experimentally determined for thirty-six plant-cast AASHTO Type I I-beams. Concrete compressive strains were measured at the surface of each beam. Initial and long-term transfer lengths were determined by analyzing the corresponding compressive strain profiles. The influence of concrete compressive strength, strand surface condition, prestress release method, and time were investigated.

On average, transfer lengths were found to be indirectly proportional to $\sqrt{f'_{ci}}$. Previous research has established that transfer length is proportional to the strand prestress at release, $f_{pt}$, and the diameter of the strand, $d_b$. Transfer lengths were found to increase approximately 10 to 20 percent over time, on average. Increases in a few specimens exceeded 50 percent.

Average transfer lengths of rusted strands were shorter than average transfer lengths of bright strands, particularly for specimens constructed with normal strength concrete. However, the dispersion of rusted strand results was significantly larger than that of bright strands. In some cases, rusted strands exhibited longer transfer lengths than those of bright strands in comparable specimens. In short, surface weathering cannot be relied upon to reduce transfer lengths.

In this test program, the method of prestress release was only varied for specimens with concrete release strengths larger than 7000 psi (48 MPa). For these specimens, the method of prestress release had no significant influence on transfer length of bright strand specimens. For rusted strands, the use of sudden prestress release resulted in transfer lengths 30 to 50 percent larger than those associated with more gradual release.

The experimental results of this study as well as others (Russell and Burns 1993; Shahawy, Issa, and deV. Batchelor 1992) indicate that transfer lengths of debonded strands are no longer than those of similar fully bonded strands.

The measured compressive strain profiles depicted in Figure 5.6 and Appendix C indicate the effectiveness of using staggered debonding of strands to reduce the intensity of concrete stresses in the end regions of beams. These results indicate that partial debonding of strands may be used as a viable alternative to draping for effectively tailoring concrete stresses to satisfy allowable stress limitations immediately after prestress release. A lower bound estimate of the transfer length should be used when checking allowable stresses. For simplicity and safety, the transfer length may be estimated as zero for this purpose.

The data collected from this test program indicate that long-term transfer lengths can be conservatively estimated from the upper bound expression $l_t = 0.57\,\text{ksi}^{-0.5}\,\dfrac{f_{pt}}{\sqrt{f'_{ci}}}\,d_b$. Study of transfer length results from other test programs reveals that this expression underestimates the transfer lengths of specimens reinforced with strand produced by other manufacturers. A more conservative transfer length expression was developed based on data collected from a variety of research studies on strands from various manufacturers. The following expression is proposed for conservatively estimating long-term transfer length:

$$l_t = \frac{5}{4}\,\text{ksi}^{-0.5}\,\frac{f_{pt}}{\sqrt{f'_{ci}}}\,d_b$$

This expression takes into account uncertainties that exist during design such as: strand manufacturing process, method of prestress release, and strand surface condition.

# CHAPTER 6: DRAW-IN TEST PROGRAM

## 6.1 INTRODUCTION

In order to evaluate the effectiveness of using draw-in measurements to predict transfer and flexural bond behavior, a program of draw-in testing was performed in tandem with the transfer length test program described in Chapter 5. Draw-in, often referred to as "free end slip" or "suck-in," is the displacement of the prestressing tendon, resulting from the release of prestress, relative to the end of the member. In this study, the term "draw-in" is used to prevent possible confusion with the term "end slip," which is used to describe movement of the strand resulting from external loads applied during development length testing.

## 6.2 BACKGROUND

Anderson and Anderson (1976) describe the theoretical basis for a direct relationship between strand draw-in and transfer length. Figure 6.1 illustrates the derivation that follows in the next few paragraphs. Guyon (1953, 195) gives a comparable derivation. Because there is no displacement of the steel relative to the concrete at the end of the transfer length, the draw-in length may be calculated as:

$$l_{draw-in} = \Delta_{pt} - \Delta_{ct}$$

where:

$l_{draw-in}$ = draw-in length

$\Delta_{pt}$ = contraction of the tendon along the transfer length, and

$\Delta_{ct}$ = contraction of the concrete along the transfer length.

The values of steel and concrete contraction may be calculated by integrating strains that result from prestress release along the transfer length, $l_t$:

$$\Delta_{pt} = \int_{l_t} \Delta\varepsilon_p dx \text{ and } \Delta_{ct} = \int_{l_t} \Delta\varepsilon_c dx$$

where:

$\Delta\varepsilon_p$ = change in steel strain that results from prestress release, and

$\Delta\varepsilon_c$ = change in concrete strain that results from prestress release.

Thus,

**Equation 6.1**

$$l_{draw-in} = \int_{l_t} \left(\Delta\varepsilon_p - \Delta\varepsilon_c\right) dx$$

At the start of the transfer length (point of initiation of bond), $\Delta\varepsilon_c$ is zero, and the change in steel strain may be calculated as:

$$\Delta\varepsilon_p = \frac{\Delta f_p}{E_p} = \frac{f_{pj}^*}{E_p}$$

where:

$\Delta f_p$ = change in steel stress that results from prestress release,

$f_{pj}^*$ = stress in the steel immediately prior to transfer (the jacking stress, $f_{pj}$, minus losses due to relaxation between stressing and release), and

$E_p$ = modulus of elasticity of the tendon.

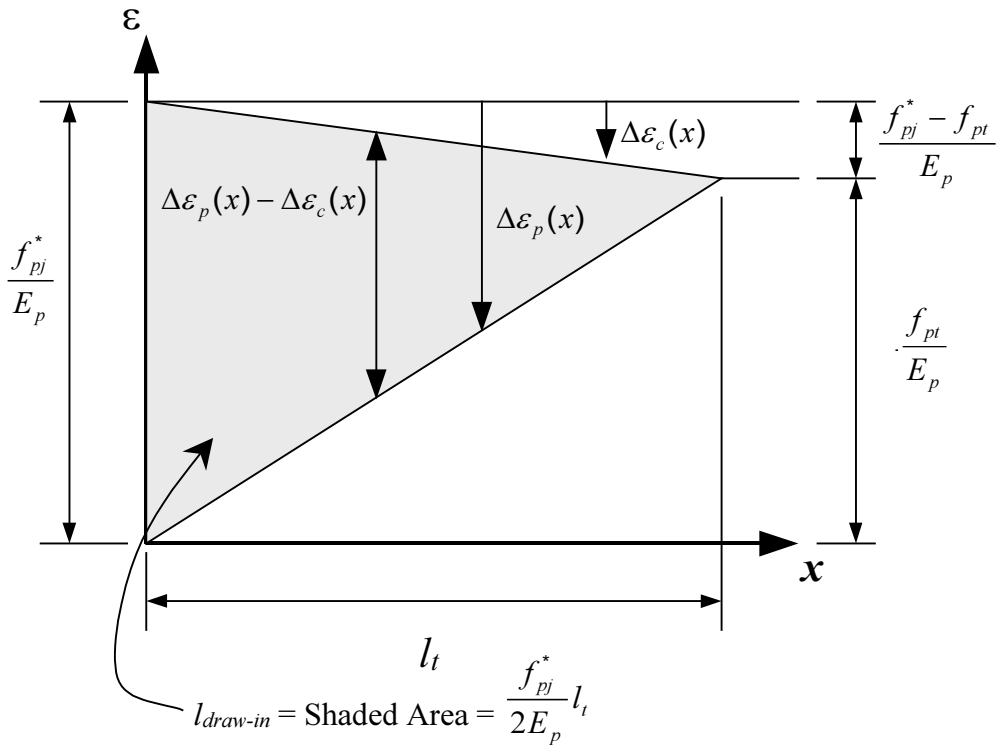


**Figure 6.1: Relationship between Draw-In and Transfer Length**

At the end of the transfer length, the concrete and steel strains are compatible, and the residual steel stress is $f_{pt}$. Thus,

$$\Delta\varepsilon_c = \Delta\varepsilon_p = \frac{\Delta f_p}{E_p} = \frac{f_{pj}^* - f_{pt}}{E_p}$$

where:

$f_{pt}$ = stress in prestressing steel immediately after transfer.

If both the steel and concrete strains are assumed to vary linearly along the transfer length, then the integrand in Equation 6.1 varies linearly from a value of $\frac{f_{pj}^*}{E_p}$ at the start of the transfer length to a value of zero at the end of the transfer length. Therefore, Equation 6.2 results as an expression that directly relates draw-in to transfer length.

**Equation 6.2**

$$l_{draw-in} = \frac{f_{pj}^*}{2E_p} l_t$$

Equation 6.3 results from inverting this expression. Given values of $E_p$ and $f_{pj}^*$, Equation 6.3 may be used to estimate transfer lengths based on measured draw-in values.

**Equation 6.3**

$$l_t = \frac{2E_p}{f_{pj}^*} l_{draw-in}$$

Anderson and Anderson further propose that draw-in, in addition to indicating the actual transfer length, may indicate the flexural bond capacity of a member. They conducted a series of repeated load tests on hollow-core products from five manufacturers. Three different processes were used to manufacturer the hollow-core units. Both center-point and third-point loading configurations were used. The test results indicate a "strong correlation between excessive free end slip and premature bond failure." The results were used to develop an expression for a

limiting value of draw-in. If the measured draw-in is less than this limiting value, the ACI 318 development length is adequate to ensure flexural failure. Otherwise, Anderson and Anderson propose capacity reduction factors to be used based on the measured draw-in.

Brooks, Gerstle, and Logan (1988) report a strand draw-in theory developed by Robert Mast. Mast's theory, a refinement of the ideas of Anderson and Anderson, assumes that the initial draw-in serves as a "direct indication of the bond quality of the concrete." Because low-slump concrete is typically used in the production of hollow-core units, consolidation of the concrete around the strand presents more difficulty than in pretensioned products, such as bridge girders, that are cast with higher-slump concrete. Thus, bond behavior may be poorer than indicated by the ACI 318 expression for development length. Mast's draw-in theory accepts measured draw-in as a direct indicator of the transfer and flexural bond capacity of the strand. Instead of Equation 6.2 above, the theory is based on the similar expression:

$$l_{draw-in} = \frac{f_{pt}}{2E_p} l_t$$

in which the prestress immediately *after* release is used. Substitution of the expression $l_t = \frac{f_{pe}}{3\text{ ksi}} d_b$ from the ACI 318 Commentary results in an allowable draw-in value, $\delta_{all}$, that corresponds to a transfer length equal to that implied in the Commentary:

$$\delta_{all} = \frac{f_{pe} f_{pt}}{(6\text{ ksi})\, E_p} d_b$$

The theory maintains that the actual transfer and flexural bond lengths of a member are in the same proportion to the ACI 318 Commentary expressions as the measured draw-in value is to $\delta_{all}$. If $l_{draw-in} > \delta_{all}$, the resulting magnified transfer and flexural bond lengths are then used to compute the bond capacity of the tendon. The results of an experimental program described by Brooks, Gerstle, and Logan support the validity of this theory when $l_{draw-in} > \delta_{all}$. Bond capacity calculations based on the ACI Code expression for development length, $l_d = \left( f_{ps} - \frac{2}{3} f_{pe} \right) d_b$, overestimate the ultimate capacities of test specimens that displayed excessive draw-in.

Draw-in measurements were taken as part of the Stresscon test program (Logan 1997) described in Section 4.2.3. Mast's theory provided "excellent correlation" with the results of development length tests performed on simply-supported and cantilever beam specimens pretensioned with strands from a variety of manufacturers. Measurements were conducted up to an age of 21 days, and significant draw-in growth occurred with time. Thus, Logan concludes that draw-in values obtained immediately upon release of prestress might not serve as an adequate indicator of bond quality or capacity. Logan also reports that the NCSU test specimens (Cousins, Johnston and Zia 1990) that exhibited extremely poor transfer and flexural bond behavior—and resulted in the FHWA moratorium—featured measured draw-in values significantly longer than draw-in values measured for hollow-core slabs at the Stresscon plant. This observation reinforces the link between draw-in and bond quality.

Rose and Russell (1997) report results of a study aimed at assessing the usefulness of several proposed bond quality test methods. Measured values of draw-in were compared with measured transfer lengths. Considering data from several transfer length studies, Rose and Russell found very good correlation for the relationship expressed in Equation 6.3 above. They conclude that draw-in measurements provide the best correlation with transfer length when compared to all other test methods. More detail about this study is provided in Section 4.2.2. Rose and Russell cite the possible growth of draw-in with time as a potential shortcoming to the use of draw-in measurements as a method of assessing bond quality.

## 6.3 TEST PROCEDURE

Two different techniques were used for measuring the strand draw-in in this study. For the first two specimen pairs fabricated (L0B and M0B), a small C-shaped, aluminum alignment bracket was secured to each strand by means of a hose clamp. These brackets, shown in Figure 6.2, were used to carefully align a digital depth gauge that was used to measure the distance from each bracket to the end face of each beam. The depth gauge featured a precision of 0.00025 in (0.006 mm), and the dual arms of the alignment brackets were utilized to improve the accuracy of repeated readings.

**Figure 6.2: Alignment Brackets for Measuring Strand Draw-In**

One set of measurements was recorded prior to the release of prestress. Immediately after the tendons were cut, another round of measurements was performed in order to provide data for the calculation of initial strand draw-in. Long-term draw-in results were calculated using another set of measurements taken at a later date.

The use of these alignment brackets proved largely ineffective because the strands were flame-cut. The shock from the sudden prestress release jarred most of the brackets loose thereby terminating their effectiveness as benchmarks for subsequent measurements. Of the brackets that appeared to have remained securely fastened, careful visual inspection revealed that some had obviously translated relative to the strand. This cast doubt on the validity of the readings obtained from brackets that appeared snugly attached. Attempts to remedy the situation by attaching extra hose clamps to the strands of the M0B specimen pair were ineffective. Thus, few of the draw-in results are reported for the L0B beam pair, and none are reported for the M0B pair. Use of the alignment brackets was abandoned after these two pairs of beams were cast. Although this system was ineffective with sudden prestress release, it has proven quite successful in other research involving gradual release methods.

A simpler, more robust technique was utilized to obtain draw-in data for the remaining specimens. As shown in Figure 6.3, researchers spray-painted each strand to provide a benchmark for measurements. Masking tape was used to provide a straight line for making accurate measurements. A steel rule, graduated in increments of 0.01 in (0.25 mm) was used for measuring the distance from the strand to the beam end. In order to reduce error, only one researcher performed all draw-in measurements. Measurements were recorded to the nearest 0.005 in (0.13 mm). Switching to this system resulted in measurements that were more reliable but less precise.

**Figure 6.3: Strands Painted to Provide References for Draw-In Measurements**

As is evident in Figure 6.4, the shock resulting from the flame-cutting procedure was intense, particularly for the partially debonded strands. It was common for the various wires composing a single partially debonded strand to exhibit different values of draw-in. Because it was impossible to measure the displacement of all seven wires per strand (the center wire in particular would have presented a unique challenge). The displacements of the three topmost strands were recorded and later averaged during the calculation process. The extreme "unwrapping" deformations experienced by some of the debonded strands (such as Strands A2 and A3 in Figure 6.4) made it difficult to obtain accurate readings after prestress release. This was one of several factors that hindered the estimation of true draw-in for partially debonded strands. Other factors will be discussed in the next section.

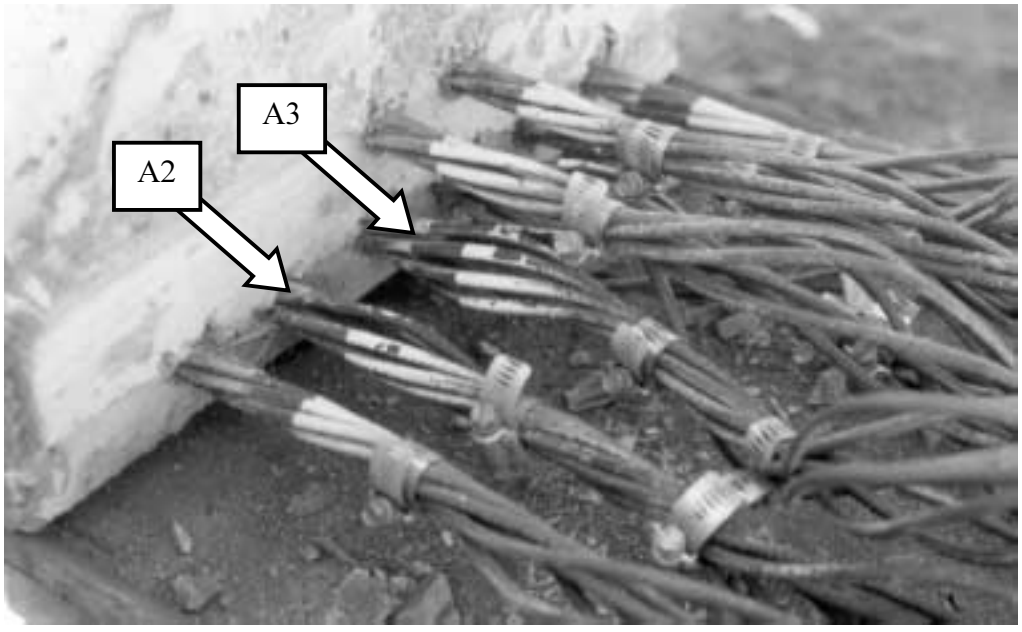


**Figure 6.4: Flame-Cut Strands after Release of Prestress**

## 6.4 DETERMINATION OF DRAW-IN VALUE

Determination of the draw-in of the strand relative to the concrete was relatively simple for the fully bonded strands. The initial draw-in value was calculated as the difference between the distance measured immediately after prestress release and the distance measured prior to prestress release. A final refinement involved the subtraction of the free contraction of the tendon occurring between the measurement benchmark and the end of the beam. The free contraction of the strand along this length was calculated as $\frac{f_{pj}^*}{E_p}\Delta_0$, where $\Delta_0$ is the distance from the benchmark to the end of the beam prior to prestress release. Thus, for fully bonded strands,

**Equation 6.4**

$$l_{draw-in,t} = \Delta_t - \Delta_0 - \frac{f_{pj}^*}{E_p}\Delta_0$$

where:

$l_{draw-in,t}$ = draw-in value at time *t*,

$\Delta_t$ = distance from benchmark to end of beam at time *t*,

$\Delta_0$ = distance from benchmark to end of beam prior to prestress release,

$f_{pj}^*$ = stress in tendon immediately prior to prestress release, and

$E_p$ = modulus of elasticity of tendon.

Calculation of the draw-in along the transfer length of partially debonded strands is more complex. For these strands, the displacement of the tendon relative to the concrete at the end of the beam is only an indication of the relative displacement at the point of initiation of bond. In order to convert the recorded measurements to a useful estimate of actual draw-in along the transfer length, an accurate picture of the relative displacement of the concrete and steel along the debonded length is required. The draw-in along the transfer length may be formulated as follows:

$$l_{draw-in,t} = (\Delta_t - \Delta_0) - (\Delta_{p,db,t} - \Delta_{c,db,t}) - \frac{f_{pj}^*}{E_p}\Delta_0$$

where:

$\Delta_{p,db,t}$ = total contraction of the tendon along the debonded length at time *t*, and

$\Delta_{c,db,t}$ = total contraction of the concrete along the debonded length at time *t*.

The calculation of the first of these terms, $\Delta_{p,db,t}$, is relatively simple if the frictional resistance transferred from the concrete to the tendon along the debonded length, $l_{db}$, is insignificant. If so, $\Delta_{p,db,t}$ may be accurately estimated as $\frac{f_{pj}^*}{E_p}l_{db}$.

On the other hand, the accurate computation of $\Delta_{c,db,t}$ is fraught with difficulty, particularly at any time other than immediately after prestress release. Calculation of this quantity requires integration of the concrete strains along the debonded length. After prestress release, these strains are not uniform. The concrete stresses and strains accumulate along the debonded length due to the influence of other strands that are bonded along either all or a portion of this length. Accurate integration requires knowledge of the stress level induced by the bonded strands, the transfer length of each strand, and the stiffness of the concrete. Integrated over long debonded lengths, small errors in estimating these quantities can result in significant errors in $\Delta_{c,db,t}$. In the case of long-term measurements, creep and shrinkage deformations can eclipse the elastic deformations within a few weeks. This continued contraction of concrete along the debonded length of strands has led some precasters to marvel at the tendency of debonded strands to "push out" of the beam. Compounding these deformation uncertainties with the dubious accuracy associated with

measuring the movement of strands such as A3 and A4 in Figure 6.4 leaves the validity of the calculated draw-in values for debonded strands in doubt. Nonetheless, every attempt was made to accurately estimate the elastic and time-dependent strains along the debonded length so as to calculate a value for draw-in. Time-dependent deformations were calculated using procedures described by Collins and Mitchell (1991).

## 6.5 DISCUSSION OF RESULTS

Values of the initial and long-term draw-in for all specimens were calculated according to the procedure outlined in the previous section. The results are presented graphically in Appendix D. Some of the results for partially debonded strands, such as those shown in Figure 6.5, agree fairly well with those of the fully bonded strands in the same specimen. However, the results shown in Figure 6.6 are characteristic of the poor results more commonly obtained. Often, the draw-in results for one debonded length of strands varied considerably compared to those of other debonded strand lengths and those of the fully bonded strands in the same specimen. The negative draw-in values calculated for some of the debonded strands indicate that some frictional force was transferred through the strand jacketing along the debonded length. However, the various measurement and calculation difficulties associated with debonded strands severely damage any certitude regarding this matter. Significant transfer of prestress along the debonded length of the strands should have been evident from the surface strain profiles, and there is no clear evidence that this occurred. Because of the lack of confidence associated with the results obtained from partially debonded strands, the comparisons and discussions that constitute the remainder of this section consider only those results obtained from fully bonded strands.

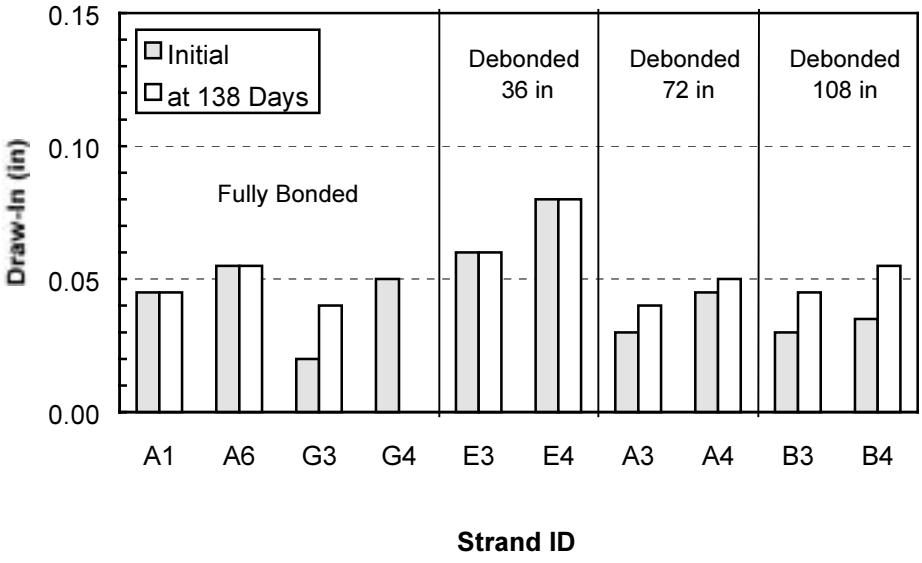


**Figure 6.5: L6B-B Strand Draw-In Results—Bright Strand, Simultaneous Flame Release (1 in = 25.4 mm)**

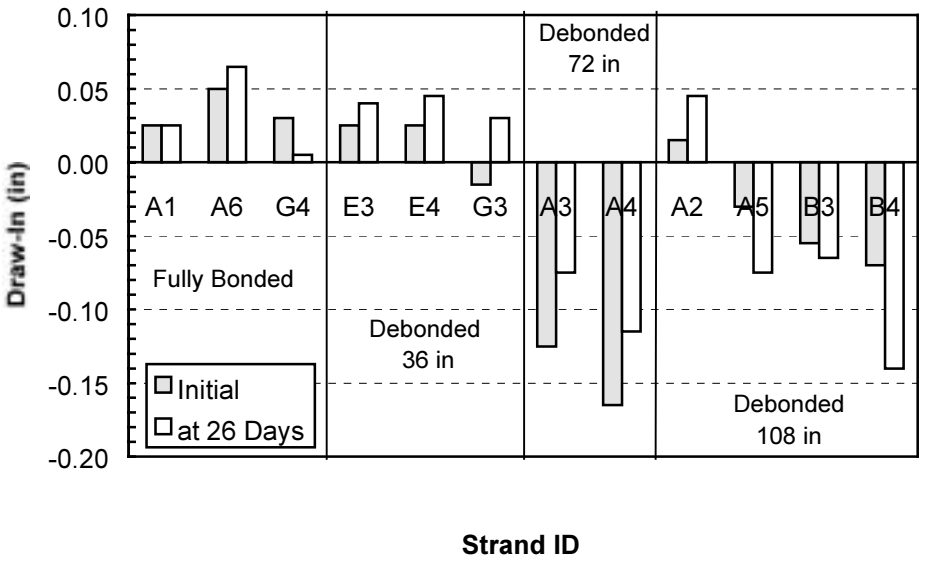


**Figure 6.6: M9B-C Strand Draw-In Results—Bright Strand, Live End of Flame Release (1 in = 25.4 mm)**

The number of draw-in readings associated with each fully bonded strand transfer length at each event (initial or long-term) range from three to eight depending on the number of strands. Thus, it is not immediately clear what value of $l_{draw-in}$ should be used to calculate the transfer length, $l_t'$, predicted from these draw-in data by means of Equation 6.3. In the comparisons that follow, two methods are used. One value, denoted $l_{t,avg}'$, is calculated by substituting the average draw-in value in Equation 6.3. Another value, $l_{t,max}'$, is calculated by substituting the maximum draw-in value. The transfer length predicted on the basis of draw-in is denoted $l_t'$ to distinguish it from $l_t$, the transfer length obtained by the procedure described in Chapter 5.

If a value of 170 ksi (1170 MPa) is assumed for tendon prestress after all losses, $f_{pe}$, the ACI 318 Commentary Section R12.9 indicates a transfer length of $\frac{f_{pe}}{3\,\text{ksi}} d_b$ = 34 in (860 mm) for these specimens. Substitution of this value into Equation 6.2 results in a value of $l_{draw-in}$ = 0.12 in (3.1 mm) that corresponds to the Commentary transfer length. All of the long-term draw-in values obtained from fully bonded strands in this study are less than 0.12 in. Hence, application of Mast's draw-in theory (Brooks, Gerstle, and Logan 1988) suggests that both the transfer and flexural bond lengths of the specimens in this study are less than predicted by the Commentary expressions. Accordingly, Figure 5.17 and Figure 5.18 illustrate that the measured transfer lengths do not exceed the values predicted by the Commentary expression. Flexural bond behavior of the test specimens is discussed in Chapter 7.

The subsequent four figures, Figure 6.7 through Figure 6.10, show relationships between measured transfer lengths and strand draw-in values obtained in this study. The dashed line in each figure represents the relationship expressed in Equation 6.3. Using values characteristic of these specimens, $E_p$ = 28,000 ksi (193 GPa) and $f_{pj}^*$ = 200 ksi (1380 MPa), this relationship reduces to $l_t = 280 l_{draw-in}$. None of these four figures exhibits a correlation between transfer length and draw-in that is nearly as good as that reported by Rose and Russell (1997). This weaker correlation may be partly due to the fact that neither the transfer length nor draw-in measurements were performed under laboratory conditions as in other studies. The Rose and Russell specimens featured a rectangular cross section prestressed with just two strands each. The specimen cross section used in this study was more complex and more than twice as large. In addition, the transfer zones of the fully bonded strands contained up to eight strands in a variety of patterns. These complexities may have contributed to the variability of the results.

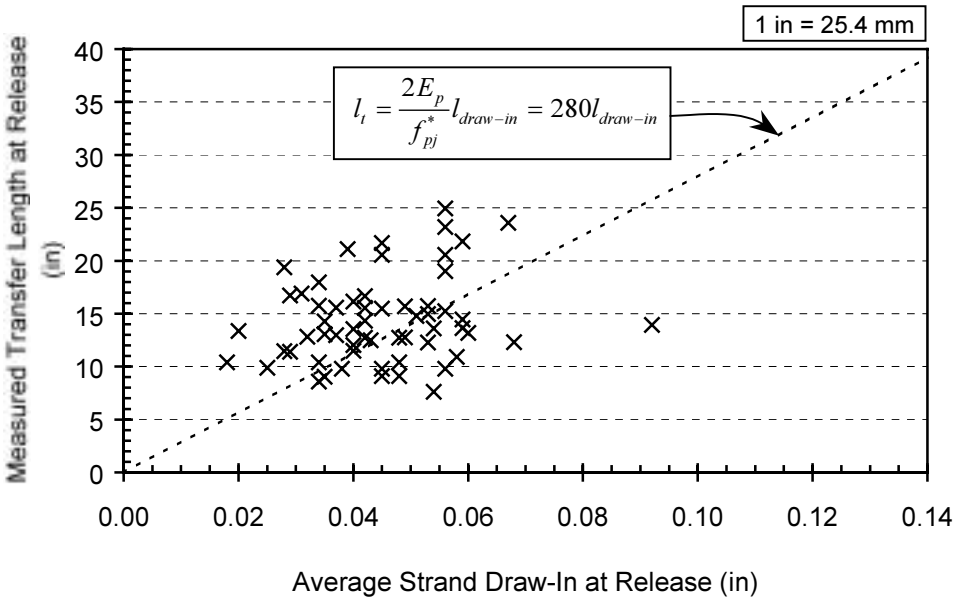


**Figure 6.7: Measured Initial Transfer Length vs. Average Draw-In Value at Release**

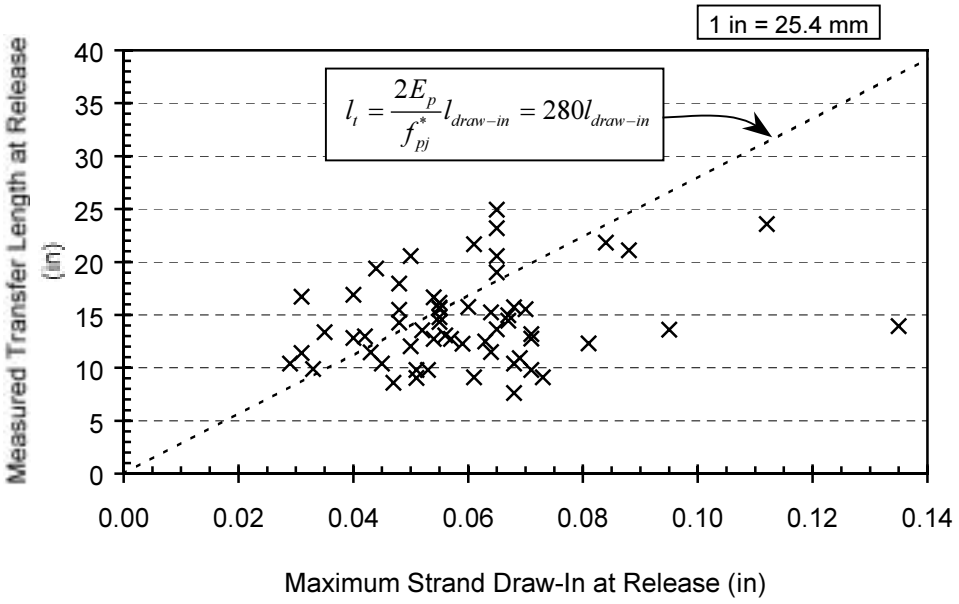


**Figure 6.8: Measured Initial Transfer Length vs. Maximum Draw-In Value at Release**

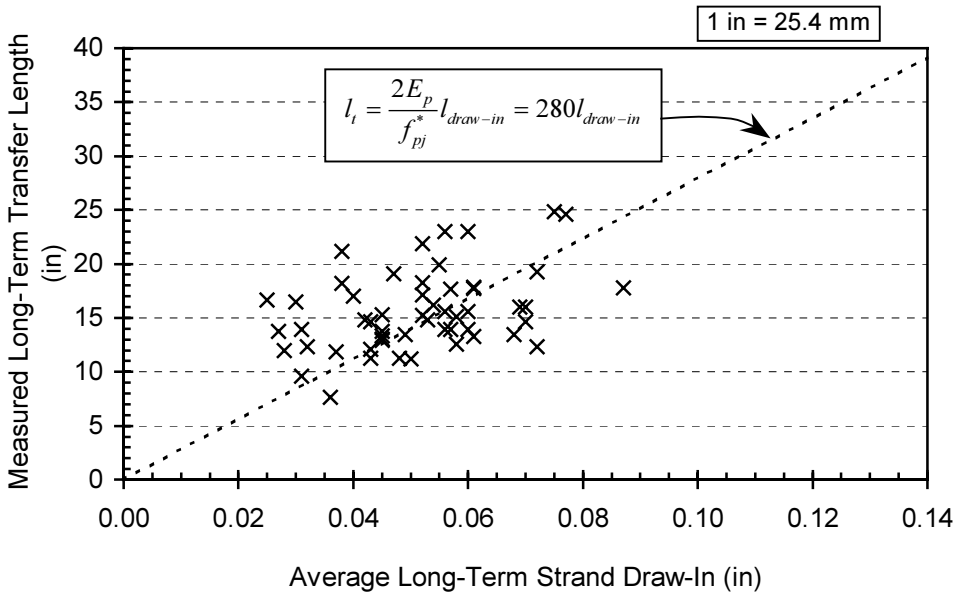


**Figure 6.9: Measured Long-Term Transfer Length vs. Average Long-Term Draw-In Value**

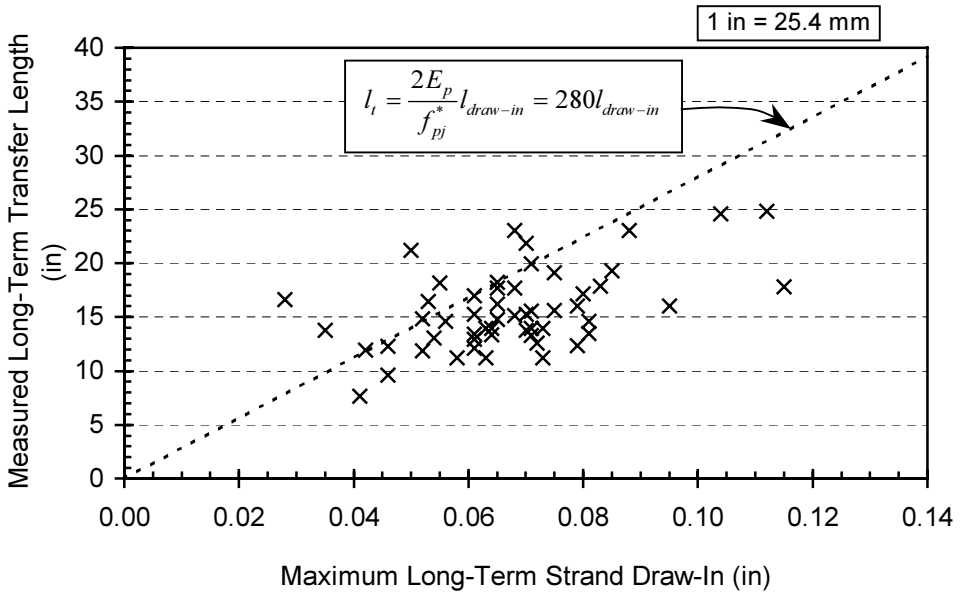


**Figure 6.10: Measured Long-Term Transfer Length vs. Maximum Long-Term Draw-In Value**

Figure 6.7 and Figure 6.9 illustrate that Equation 6.3 results in an underestimation of the majority of initial and long-term transfer lengths when the average value of draw-in at the corresponding time is used. This is likely because the full transfer length depends on the bond performance of all the strands. The total prestress force for the transfer zone cannot be transferred until the worst-performing strand has transferred its prestress. Because it is impossible to determine exactly where the full prestress force is achieved, techniques such as the 95% AMS Method are used to evaluate the transfer length. If some of the strands transfer prestress to the concrete more rapidly than others, 95 percent of the aggregate prestress force will be transferred over a length shorter than 95 percent of the length required by the strands with poorer bond performance. Thus, the transfer length obtained for a group of strands should lie between the average transfer length of the individual strands and the transfer length of the worst-

performing strand. This idea is also supported by Figure 6.8 and Figure 6.10 which indicate that Equation 6.3 overestimates the majority of measured transfer lengths when the maximum draw-in value is used.

Figure 6.11 through Figure 6.14 represent histograms of various ratios of the transfer length predicted from Equation 6.3 to the transfer length calculated from surface strain measurements. Figure 6.11 and Figure 6.12 include the data obtained immediately after prestress release; Figure 6.13 and Figure 6.14 show the relationship between the long-term observations. The first figure of each pair represents the use of the average draw-in value to predict the transfer length, while the second represents use of the maximum draw-in value for each group of strands. The histograms can be thought of as representing the frequency of occurrence of errors of different relative magnitudes when trying to predict the transfer length by means of Equation 6.3.

The average tendency of average draw-in lengths to underestimate the transfer lengths is readily discernible in these figures, as is the average tendency of maximum draw-in values to overestimate the transfer lengths. The relationship of long-term draw-in values to long-term transfer lengths is better behaved than that between the initial values. The values represented in Figure 6.13 and Figure 6.14 are more normally distributed and exhibit a smaller of degree of relative dispersion (as measured by the coefficients of variation noted in the figures) than those shown in Figure 6.11 and Figure 6.12. This may indicate that the steel and concrete strain profiles become more linear—as assumed in the derivation of Equation 6.3—with time. In other words, if the stress/strain gradient does vary initially along the transfer length, the decrease over time of the larger strain gradients—where the bond stress is more intense—may be more pronounced than that of the smaller strain gradients—where the bond stress is less intense. Thus, the linearity of the stress/strain profile may increase with time.

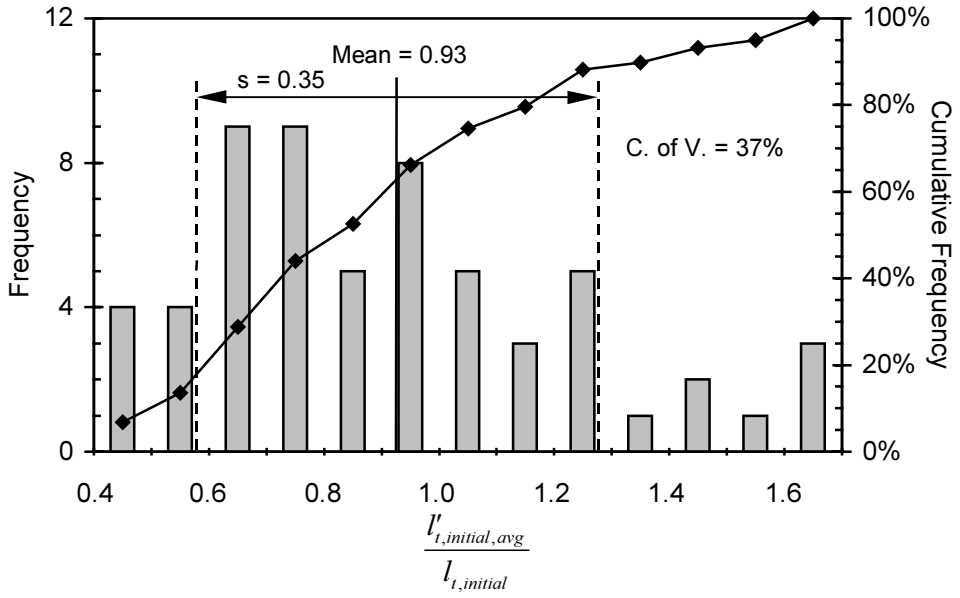


**Figure 6.11: Histogram—Ratio of Transfer Length Calculated from Average Initial Draw-In to Measured Initial Transfer Length**

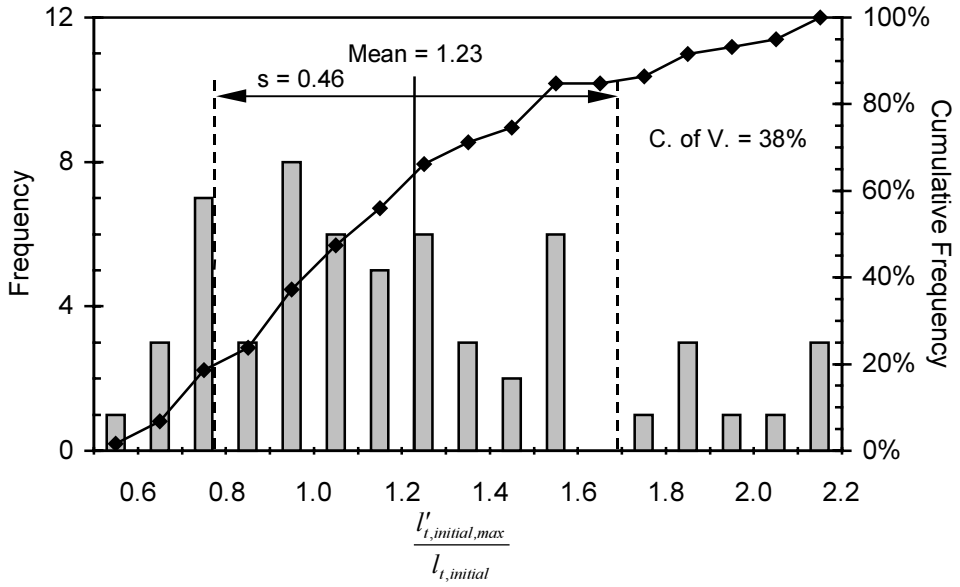


**Figure 6.12: Histogram—Ratio of Transfer Length Calculated from Maximum Initial Draw-In to Measured Initial Transfer Length**

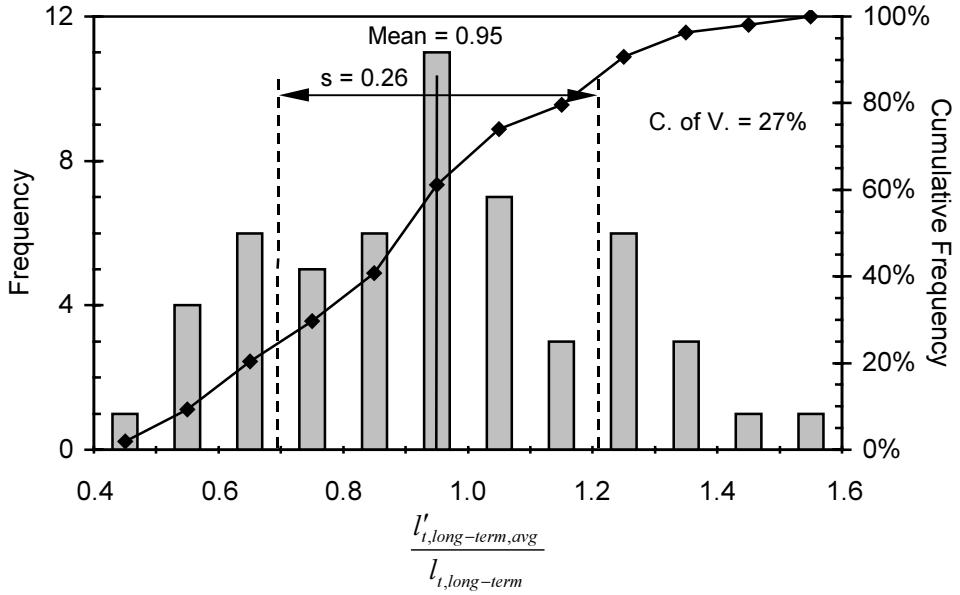


**Figure 6.13: Histogram—Ratio of Transfer Length Calculated from Average Long-Term Draw-In to Measured Long-Term Transfer Length**

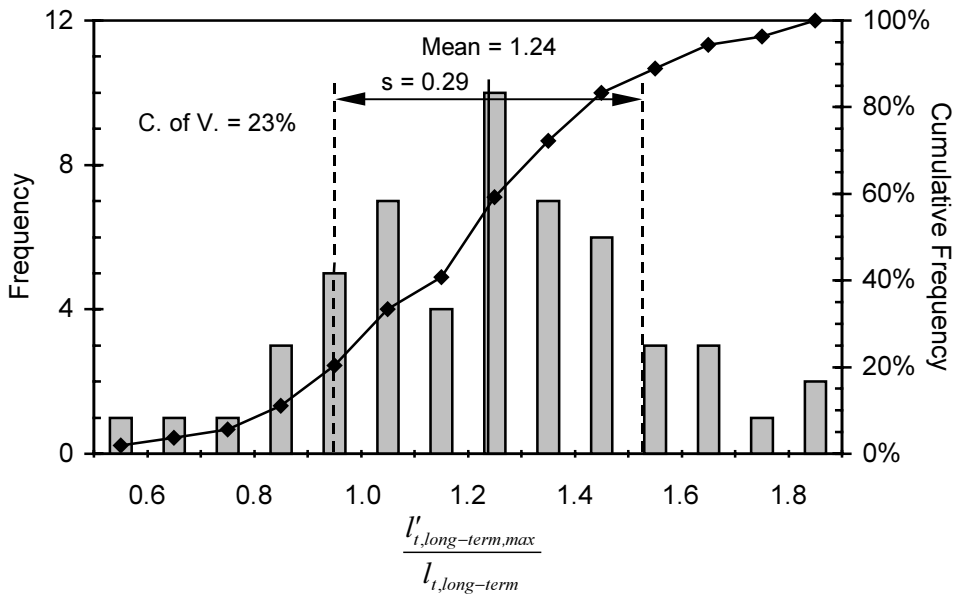


**Figure 6.14: Histogram—Ratio of Transfer Length Calculated from Maximum Long-Term Draw-In to Measured Long-Term Transfer Length**

Based on these histograms, it can be argued that application of Equation 6.3 using the average value of draw-in results in the best estimate of the actual long-term transfer length. Use of the maximum value of draw-in results in the safest (i.e. least probability of underestimation) estimate of the long-term transfer length. However, the relative dispersion evident from these results indicates that implementation of draw-in measurements for quality control purposes must be done prudently. For example, use of the maximum long-term draw-in measurement is attractive from a safety point-of-view because it appears to result in underestimation of the transfer length by more than 20 percent in less than 5 percent of cases. The precast producer, on the other hand, would be less than satisfied with this method because it results in overestimation of the transfer length in 80 percent of cases. In fact, it results in overestimation by more than 25 percent in roughly half of the cases. Use of the average draw-in length brings the average predicted transfer length closer to the actual transfer length, but is not effective in resolving the problem presented by the dispersion of the data.

Thus, for a quality control program based on draw-in measurements to be implemented fairly and effectively, a proper database including a large number of results must be developed and maintained. In the long run, the use of the average draw-in result to estimate a particular transfer length will probably prove to be more dependable than the use of the maximum draw-in result. Dependence on a single measurement, particularly when that measurement is performed under field conditions, is more prone to significant error than dependence on an average value. The dispersion of the data must be properly considered; rejection of a single product should only occur when the average draw-in reading for a transfer zone is significantly larger than that expected to meet an established transfer length limitation. The size of draw-in discrepancy necessary to indicate a high probability of poor bond performance would depend upon the variance of results from a significantly large sample of similar products.

One potential obstacle to the implementation of a quality control program involving draw-in measurements is the issue of time. Draw-in measurements were originally proposed as a relatively simple and immediate method of estimating the bond behavior of particular precast products. Implementation of a quality control program that involves long-term draw-in measurements on actual precast products (as opposed to test specimens) will be difficult. Although most studies have indicated that significant transfer length and draw-in growth only occurs in the first month after release, this may still prove to be an exorbitantly long time period for the precaster to keep products in storage before being able to cut the strand extensions and/or dress the beam ends prior to shipping. In light of this concern, Figure 6.15 and Figure 6.16 indicate the ability of Equation 6.3 to predict the *long-term* transfer length when *initial* values of draw-in are considered.

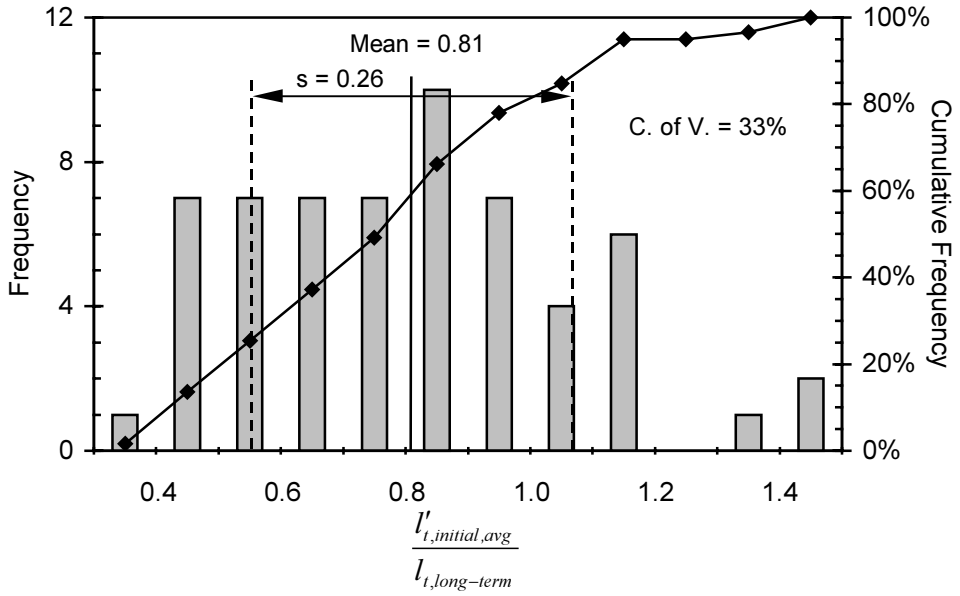


**Figure 6.15: Histogram—Ratio of Transfer Length Calculated from Average Initial Draw-In to Measured Long-Term Transfer Length**

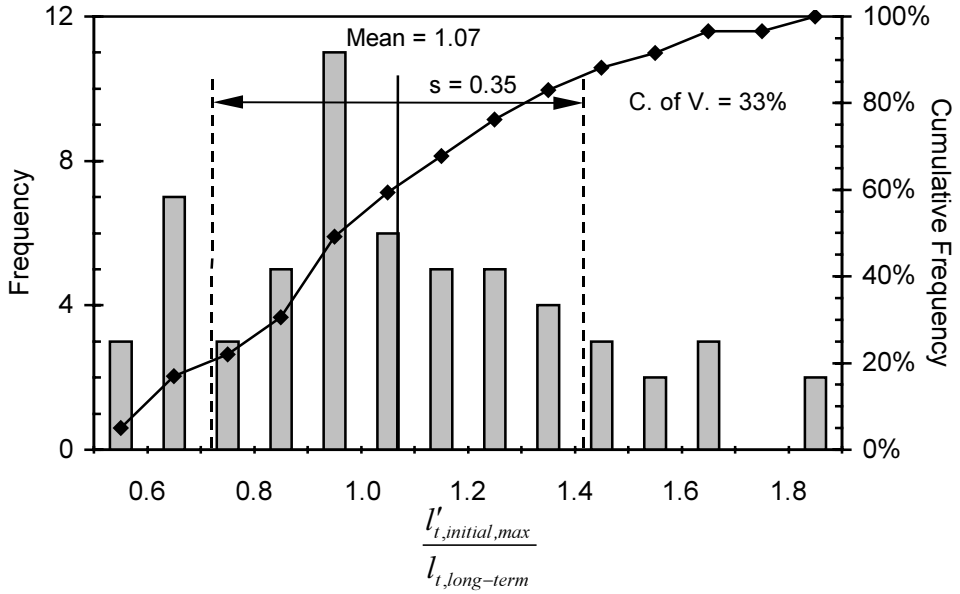


**Figure 6.16: Histogram—Ratio of Transfer Length Calculated from Maximum Initial Draw-In to Measured Long-Term Transfer Length**

It is not surprising that neither of the distributions is as well behaved as those that use the long-term values of draw-in (Figure 6.13 and Figure 6.14). On the other hand, the coefficients of variation are slightly better than those for the initial transfer length distributions shown in Figure 6.11 and Figure 6.12. Although the distributions shown in Figure 6.15 and Figure 6.16 are less than ideal, it appears that the initial draw-in might serve as an adequate quality control parameter with the development of an adequate database and statistically determined correction factors. Of course, companion long-term draw-in measurements would still have to be sampled on a periodic basis to ensure that the relationship between long-term and initial behavior remains statistically unchanged.

In this study, the average growth of the long-term draw-in values relative to the initial draw-in values reflected the average growth of the measured transfer lengths of the corresponding fully bonded strands. The average growth of these measured transfer lengths was 15 percent. The average growth of the maximum transfer draw-in values was 16 percent, while the average growth of the average draw-in values was 19 percent.

## 6.6 SUMMARY AND CONCLUSIONS

In order to evaluate the efficacy of using measured draw-in values to quantify bond behavior in pretensioned members, both initial and long-term draw-in measurements were performed on the test specimens in this research study. The sudden method of prestress release resulted in instrumentation difficulties, and may have resulted in significantly erroneous readings for the partially debonded strands in the study. Conversion of measured values to actual draw-in values along the transfer length of partially debonded strands also introduces a significant level of uncertainty into the values calculated for these strands. Thus, although the relative magnitudes of the measured values of draw-in obtained from the debonded strands indicates that the strands transferred little or no prestress force to the concrete over the debonded length, the use of measured draw-in values to accurately estimate the actual transfer or development length of partially debonded strands was judged impractical.

The more reliable values of draw-in measured for fully bonded strands were compared to the corresponding transfer lengths obtained as described in the previous chapter. According to Mast's draw-in theory, the long-term draw-in values obtained indicate that all of the tendons should exhibit transfer and flexural bond behavior that complies with the current ACI 318-99 development length provisions (Sections 12.9 and R12.9). This agrees with the transfer length results reported in Chapter 5, which do not exceed values predicted by the expression provided in the ACI 318 Commentary.

Equation 6.3 was derived as a means of predicting the transfer length for a strand given its draw-in value. It was found that using the average value of the long-term draw-in for a group of strands most accurately predicted the measured long-term transfer length for that group of strands. However, on average, the value predicted by this method tends to slightly underestimate the transfer length. A more conservative estimate may be obtained by using the maximum draw-in value for the group of strands. The average proportional increase of draw-in values with time did not vary significantly from the average proportional increase of the corresponding measured transfer lengths with time.

Correlation between the measured draw-in values and the measured transfer lengths was significantly poorer than found in previous studies conducted on laboratory specimens. The dispersion of the data from this study was such that it would be difficult to implement a quality control program based on this data alone. A single average draw-in value on the order of two to three times the expected value might indicate a bond deficiency in a precast product. On the other hand, a single average value in the range of one to one-and-a-half times the expected value would hardly justify the product's rejection, but repeated observations in this range might indeed indicate a problem. The scope and size of the collected data is insufficient to serve as a basis for prescribing quality control criteria at this time.

Conclusions regarding the ability of measured draw-in values to indicate flexural bond behavior are reserved until the next chapter.

## 6.7 RECOMMENDATIONS

The use of draw-in measurements to predict the bond behavior of partially debonded strands is impractical and therefore not recommended.

Draw-in measurements may be used to indicate trends in transfer bond behavior. Historical evidence suggests that gross deficiencies in bond quality may be effectively indicated by this test method. However, the use of small sample sizes can be unreliable, and any inferences constructed from draw-in measurements should reflect the considerable degree of dispersion evidenced by this test program.

A detailed, statistical study of the relationship between draw-in and transfer length should be performed prior to instituting a quality control system involving draw-in measurements. Such a study should be performed on a statistically significant number of specimens produced by a variety of precasters using the full range of production methods currently in use (such as the various methods of prestress release). Particular attention should be paid to the growth of transfer length with time and how this growth is reflected in both the initial and long-term draw-in measurements. If the long-term transfer length can be reliably predicted by the average initial draw-in value, this

presents the ideal quality control situation. Any attempt to develop such a quality control program should involve the cooperation of inspectors, building officials and precast producers. Consultation with specialists experienced with anchorage of pretensioned reinforcement and the application of statistical theory for quality control would be prudent.

# CHAPTER 7: DEVELOPMENT LENGTH TEST PROGRAM

## 7.1 INTRODUCTION

After cast-in-place deck slabs were added to each pair of I-beam specimens, preparation for development length testing commenced. The two beams of each pair were designed to be identical with the exception of the horizontal web reinforcement present in one end (End C) of one beam of the pair. Each beam pair featured a unique combination of the three primary variables under investigation: concrete strength, strand surface condition, and debonding pattern. One development length test was performed on each end of each beam. Thus, for each combination of variables, a total of four tests was performed—one of which included the horizontal web reinforcement described in Section 3.3.3. This chapter includes an explanation of the development length testing configuration and instrumentation. General testing procedure is described, and results are presented and discussed.

## 7.2 TEST APPROACH

Development length cannot be determined directly from a single experiment. For this test program, an indirect approach was employed. Each test consisted of loading the beam specimen to failure. The resulting failure type indicated whether the bonded length of strand provided is adequate to develop the steel stress, $f_{ps}$, necessary for nominal flexural strength at the critical section. The critical section is defined as the section closest to the end of the member expected to develop full strength when subjected to the applied loading. The bonded length anchoring the strand at the critical section is referred to as the embedment length, $l_e$. The ultimate moment resisted at the critical section and the behavior of the strands during each test can be used to evaluate whether the embedment length provided is greater than or less than the necessary development length. A series of tests, each featuring a different loading configuration (and therefore embedment length), can be used to establish bounds for the development length characteristic of each combination of primary variables.

For each pair of beams in this test program, three tests (on Beam Ends A, B, and D) were used to evaluate the development length corresponding to the combination of primary variables represented. The fourth test, conducted on End C, was used to evaluate the potential benefit of horizontal web reinforcement on the anchorage behavior of the beam. In order to allow a direct comparison with the anchorage behavior without horizontal web reinforcement, this fourth test usually featured a loading configuration identical to one of the other three tests.

As explained in Chapter 3, the final term in each test designation represents the embedment length tested (in inches). For specimens with partially debonded strands, there are actually multiple embedment lengths for each test. The embedment length for each strand depends upon the debonded length of strand. If the specimen contains debonded strands, the designated embedment length refers to the shortest embedded length of strand at the critical section, i.e. that of the group of strands with the longest debonded length. This group of strands is subjected to the highest average bond stress under the test loading configuration.

## 7.3 TEST CONFIGURATION

During development length testing, the I-beam specimen was supported so that the beam end not under investigation was free from the direct effects of applied load. One support was placed beneath the beam end being tested; the other support was placed in the interior region of the beam to limit damage to the far end of the beam. Therefore, the beam end not being tested was cantilevered and isolated from the shear and moment resulting from the applied load.

The beam was directly supported on heavily reinforced, neoprene bearing pads of 3 in (76 mm) thickness which rested on reinforced concrete pedestals. Each pad was 11 in by 18 in (270 mm by 457 mm) in plan. Under the loads and deformations recorded during the test program, the pads were incapable of developing a horizontal thrust large enough to significantly affect either the applied moment or the moment resistance of the beam.

The use of these bearing pads resulted in a gradual shortening of the effective span length during each development length test. Due to camber, the beam was effectively supported at the exterior of each bearing pad prior to load application. As the beam deformed under the applied load, the sections at each support rotated, and the effective center of support moved inward (in relation to the span). Due to the large rotations experienced after yielding at the

critical section, the beam was supported near the interior edge of each bearing pad at the end of the test. The resulting shortening of the span length was somewhat offset by the outward shearing of the pads, but its magnitude was significant nonetheless. These effects can be seen in Figure 7.1. Accordingly, measurements were recorded during each test and incorporated into moment calculations.

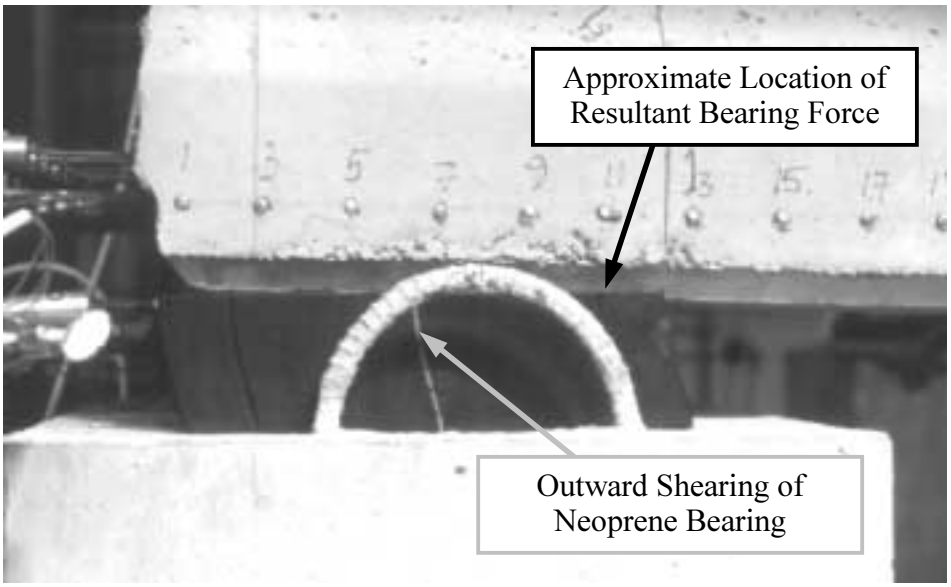


**Figure 7.1: Rotation of Beam Section at Support and Shearing of Neoprene Bearing Pad—Test L0B-A-96 at Final Load**

The test loading resulted from piston displacement of a hydraulic cylinder with a capacity of 2000 kips (8.9 MN). This cylinder was installed in the movable loading frame that can be seen in Figure 7.3. The resulting load was transferred to a steel spreader beam, which in turn distributed the load to two steel cylinders spaced 36 in (305 mm) apart in the direction of the span. These cylinders transferred the load to steel plates mounted on the deck of the composite beam. These components of the load application system may be seen in Figure 7.2. The roller closest to the anchorage zone under investigation was placed at the section corresponding to the test embedment length. The hydraulic ram was positioned so that the region of the beam between the two rollers was subjected to a nearly constant maximum moment. The beam's weight precluded attainment of a perfectly constant moment in this region. A schematic of the test geometry is presented in Figure 7.4. Figure 7.5 shows a test specimen under loading. Table 7.1 and Table 7.2 summarize the test configurations for all sixty development length tests performed at the Phil M. Ferguson Structural Engineering Laboratory.

**Figure 7.2: Load Application Components—Test H0R-D-66**

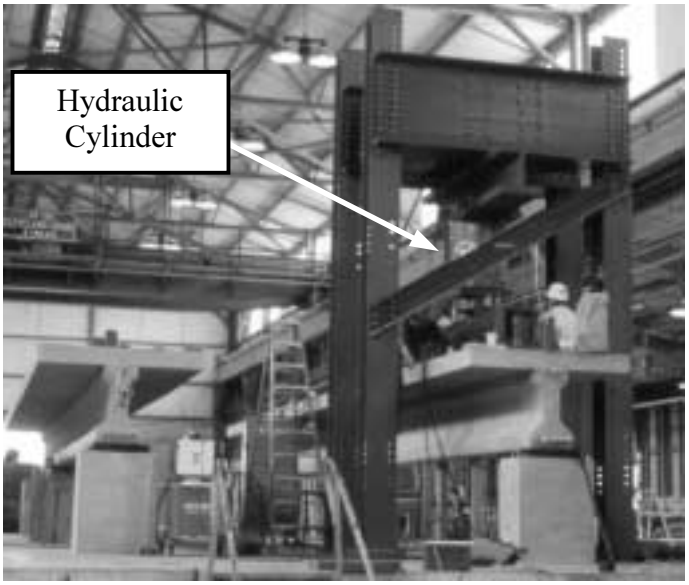


**Figure 7.3: Loading Frame and Hydraulic Cylinder Used to Apply Test Loads**

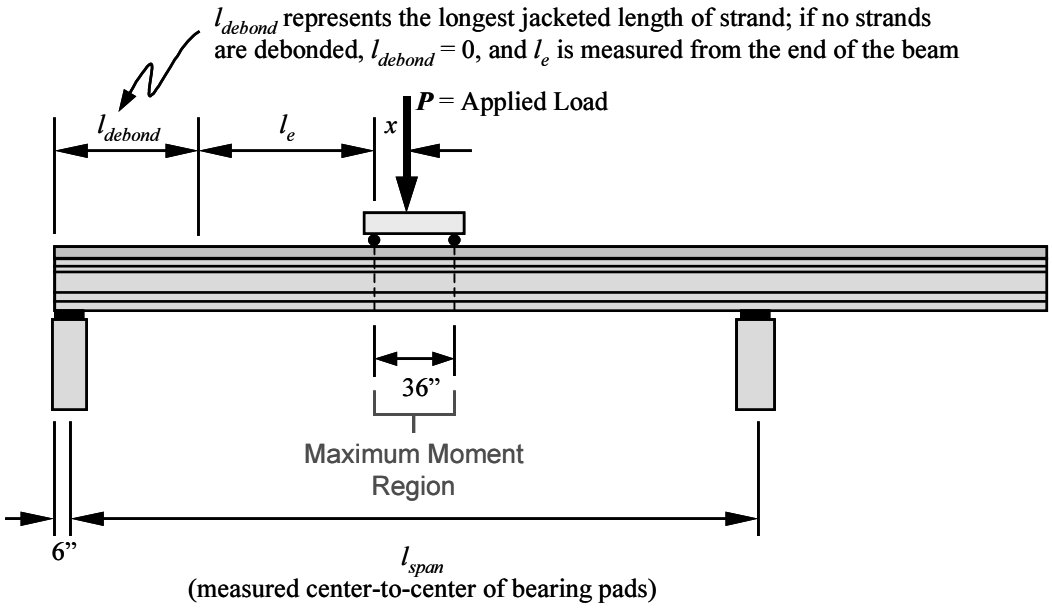


**Figure 7.4: Configuration of Supports and Applied Load for Development Length Tests (1 in = 25.4 mm)**

**Figure 7.5: Test H9R-C-96H under Load**

**Table 7.1: Test Configurations for Specimens Containing Bright Strand (1 in = 25.4 mm)**

| Test I.D. | Beam Length (in) | $l_{span}$ (in) | $l_{debond}$ (in) | $l_e$ (in) | $x$ (in) |
|---|---|---|---|---|---|
| L0B-A-96 | 480 | 240 | 0 | 96 | 16.88 |
| L0B-B-72 | 480 | 240 | 0 | 72 | 12.31 |
| L0B-C-54H | 480 | 240 | 0 | 54 | 8.88 |
| L0B-D-54 | 480 | 240 | 0 | 54 | 8.88 |
| M0B-A-96 | 480 | 240 | 0 | 96 | 16.63 |
| M0B-B-72 | 480 | 240 | 0 | 72 | 12.25 |
| M0B-C-54H | 480 | 240 | 0 | 54 | 8.88 |
| M0B-D-54 | 480 | 240 | 0 | 54 | 8.88 |
| H0B-A-96 | 480 | 240 | 0 | 96 | 16.63 |
| H0B-B-72 | 480 | 240 | 0 | 72 | 11.38 |
| H0B-C-54H | 480 | 240 | 0 | 54 | 9.00 |
| H0B-D-54 | 480 | 240 | 0 | 54 | 9.00 |
| L4B-A-48 | 648 | 348 | 72 (36, 0) | 48 | 13.31 |
| L4B-B-96 | 648 | 360 | 72 (36, 0) | 96 | 19.25 |
| L4B-C-48H | 648 | 348 | 72 (36, 0) | 48 | 13.31 |
| L4B-D-60 | 648 | 360 | 72 (36, 0) | 60 | 14.81 |
| M4B-A-60 | 648 | 360 | 72 (36, 0) | 60 | 14.81 |
| M4B-B-48 | 648 | 360 | 72 (36, 0) | 48 | 13.31 |
| M4B-C-56H | 648 | 360 | 72 (36, 0) | 56 | 14.31 |
| M4B-D-56 | 648 | 360 | 72 (36, 0) | 56 | 14.31 |
| H4B-A-56 | 648 | 360 | 72 (36, 0) | 56 | 14.38 |
| H4B-B-50 | 648 | 360 | 72 (36, 0) | 50 | 13.63 |
| H4B-C-62H | 648 | 360 | 72 (36, 0) | 62 | 14.63 |
| H4B-D-62 | 648 | 360 | 72 (36, 0) | 62 | 14.63 |
| L6B-A-96 | 648 | 432 | 108 (72, 36, 0) | 96 | 18.75 |
| L6B-B-114 | 648 | 468 | 108 (72, 36, 0) | 114 | 18.75 |
| L6B-C-84H | 648 | 408 | 108 (72, 36, 0) | 84 | 18.5 |
| L6B-D-84 | 648 | 408 | 108 (72, 36, 0) | 84 | 18.5 |
| M9B-A-180 | 648 | 480 | 108 (72, 36, 0) | 180 | 23.88 |
| M9B-B-96 | 648 | 432 | 108 (72, 36, 0) | 96 | 18.38 |
| M9B-C-96H | 648 | 432 | 108 (72, 36, 0) | 96 | 18.5 |
| M9B-D-114 | 648 | 468 | 108 (72, 36, 0) | 114 | 18.38 |
| H9B-A-180 | 648 | 480 | 108 (72, 36, 0) | 180 | 23.88 |
| H9B-B-96 | 648 | 432 | 108 (72, 36, 0) | 96 | 18.5 |
| H9B-C-96H | 648 | 432 | 108 (72, 36, 0) | 96 | 18.5 |
| H9B-D-114 | 648 | 468 | 108 (72, 36, 0) | 114 | 18.38 |

**Table 7.2: Test Configurations for Specimens Containing Rusted Strand (1 in = 25.4 mm)**

| Test I.D. | Beam Length (in) | $l_{span}$ (in) | $l_{debond}$ (in) | $l_e$ (in) | $x$ (in) |
|---|---|---|---|---|---|
| M0R-A-96 | 480 | 240 | 12 (0) | 96 | 18.75 |
| M0R-B-54 | 480 | 240 | 12 (0) | 54 | 11.00 |
| M0R-C-46H | 480 | 240 | 12 (0) | 46 | 9.50 |
| M0R-D-46 | 480 | 240 | 12 (0) | 46 | 9.50 |
| H0R-A-96 | 480 | 240 | 12 (0) | 96 | 18.75 |
| H0R-B-46 | 480 | 240 | 12 (0) | 46 | 9.50 |
| H0R-C-46H | 480 | 240 | 12 (0) | 46 | 9.50 |
| H0R-D-66 | 480 | 240 | 12 (0) | 66 | 13.25 |
| M4R-A-96 | 648 | 360 | 72 (36, 0) | 96 | 19.25 |
| M4R-B-56 | 648 | 360 | 72 (36, 0) | 56 | 14.38 |
| M4R-C-78H | 648 | 360 | 72 (36, 0) | 78 | 17.06 |
| M4R-D-90 | 648 | 360 | 72 (36, 0) | 90 | 18.50 |
| H4R-A-82 | 648 | 360 | 72 (36, 0) | 82 | 17.56 |
| H4R-B-72 | 648 | 360 | 72 (36, 0) | 72 | 16.38 |
| H4R-C-72H | 648 | 360 | 72 (36, 0) | 72 | 16.38 |
| H4R-D-78 | 648 | 360 | 72 (36, 0) | 78 | 17.06 |
| M9R-A-180 | 648 | 480 | 108 (72, 36, 0) | 180 | 23.88 |
| M9R-B-96 | 648 | 432 | 108 (72, 36, 0) | 96 | 18.38 |
| M9R-C-96H | 648 | 432 | 108 (72, 36, 0) | 96 | 18.5 |
| M9R-D-114 | 648 | 468 | 108 (72, 36, 0) | 114 | 18.38 |
| H9R-A-180 | 648 | 480 | 108 (72, 36, 0) | 180 | 23.88 |
| H9R-B-96 | 648 | 432 | 108 (72, 36, 0) | 96 | 18.5 |
| H9R-C-96H | 648 | 432 | 108 (72, 36, 0) | 96 | 18.5 |
| H9R-D-114 | 648 | 468 | 108 (72, 36, 0) | 114 | 18.38 |

## 7.4 INSTRUMENTATION

This section consists of a description of the instruments used to measure the response of each beam specimen to the applied deformation. Both primary and backup systems are detailed below.

### 7.4.1 Measurement of Applied Load

The load resulting from the applied deformation was measured between the hydraulic cylinder and the spreader beam by means of a 1000-kip (4.45 MN), shear-type load cell. This load cell was attached to the piston of the hydraulic cylinder. A 5000 psi (34.5 MPa) pressure transducer served as a backup instrument. The pressure transducer monitored the hydraulic pressure supplied to the cylinder by the air-powered pump. The load cell readings were later used in the calculation of sectional moments and the resulting member stresses.

### 7.4.2 Measurement of Displacements

The primary system of measuring specimen displacements consisted of linear potentiometers. Shown in Figure 7.6, these potentiometers were used to measure the displacement of the beam relative to the floor in the maximum moment region. Vertical and horizontal support deflections were also measured with linear potentiometers. The displacement of the beam relative to the supports was calculated based on these collected values. This calculated value was verified by means of the tension-wire system shown in Figure 7.7. This system featured a tensioned piano wire strung between anchor bolts at each support, and a steel rule affixed to the beam midway between the two load points. The displacement of the beam relative to the supports was measured by reading the position of the piano wire relative to the rule with a precision of 0.01 in (0.25 mm). A mirror was employed to improve the consistency of readings. Unless otherwise noted deflections reported in this report represent the deflection, relative to a straight line connecting the supports, at the section midway between the two points of load application.

**Figure 7.6: Linear Potentiometers Used to Measure Beam Deflection**

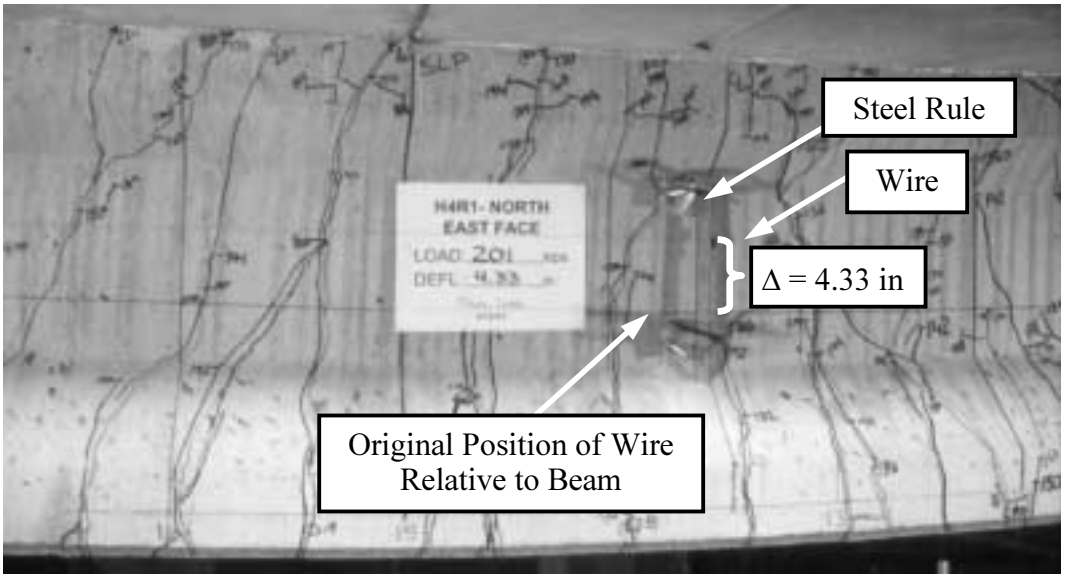


**Figure 7.7: Tension-Wire System for Measuring Beam Deflections—Test H4R-C-72H at Final Load**

### 7.4.3 Measurement of Strand Slip

Strand slip was measured by means of linear potentiometers attached to each strand at the end of the beam. These potentiometers are shown in Figure 7.8 and Figure 7.9 along with potentiometers used to measure support deformations. The slips were measured relative to the end of the beam. For partially debonded strands, the strand slip relative to the beam end is not equivalent to the slip occurring at the end of the bonded length. The widths of cracks opening along the jacketed length of strand are reflected in the potentiometer measurement, as well as the elastic elongation of the concrete along this length. In order to obtain an estimation of the true strand slip along the *bonded* length these quantities must be subtracted from the potentiometer reading. Crack widths in this region were recorded, and concrete strains along the debonded length were calculated and integrated to obtain an estimate of the concrete elongation. These values were subtracted from the potentiometer readings to obtain the values of strand end slip reported in this report.

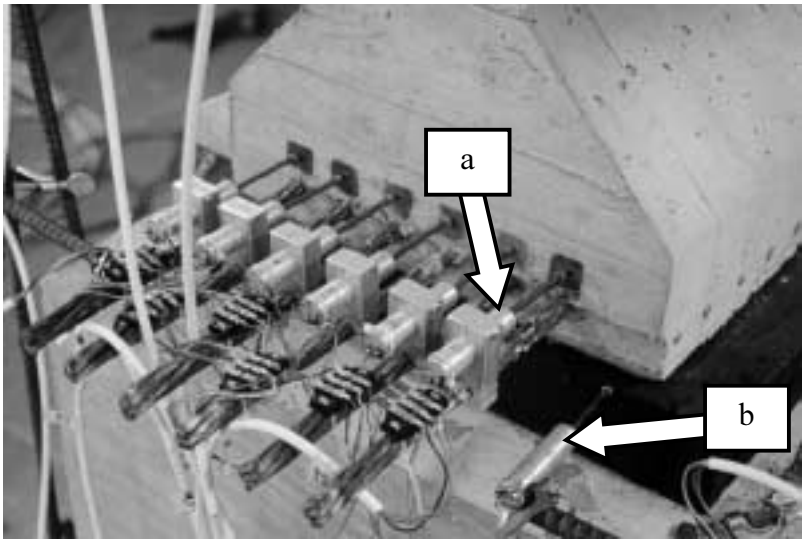


**Figure 7.8: Linear Potentiometers Used to Measure a) Strand Slip and b) Horizontal Bearing Pad Deformation**

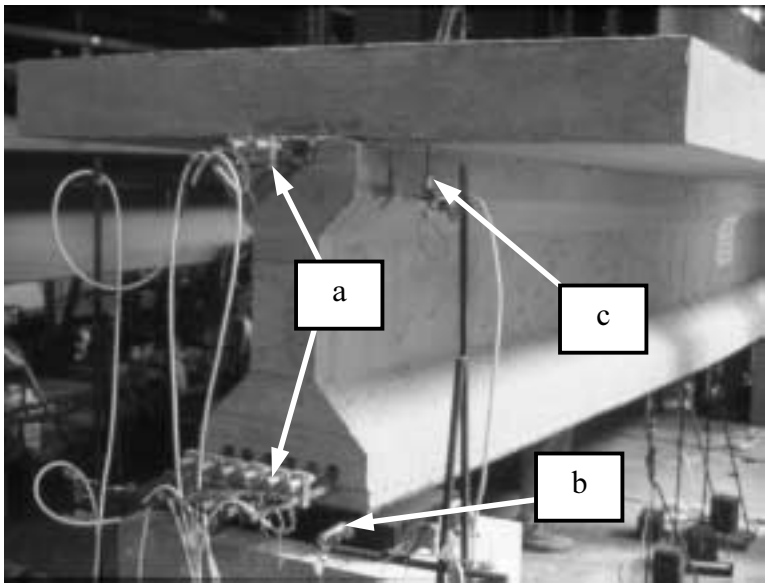


**Figure 7.9: Linear Potentiometers Used to Measure a) Strand Slip, b) Horizontal Bearing Pad Deformation, and c) Vertical Support Displacement**

### 7.4.4 Measurement of Strains at the Extreme Compression Fiber

Compressive strains at the deck surface were monitored throughout each test in an effort to foresee the onset of deck concrete crushing prior to failure. These strains were measured with Electrical Resistance Strain Gauges (ERSG's) with a 2.36 in (60 mm) gauge length. Originally, eight ERSG's were used in the maximum moment region of each test. The gauges were arranged along the length and across the width of the beam. Half of the gauges for one test are shown in Figure 7.10. Once it was verified that the compressive strain was being reasonably well distributed across the full width of the deck slab, only six gauges were used. These six gauges were arranged in three pairs along the length of the specimen between the load points.

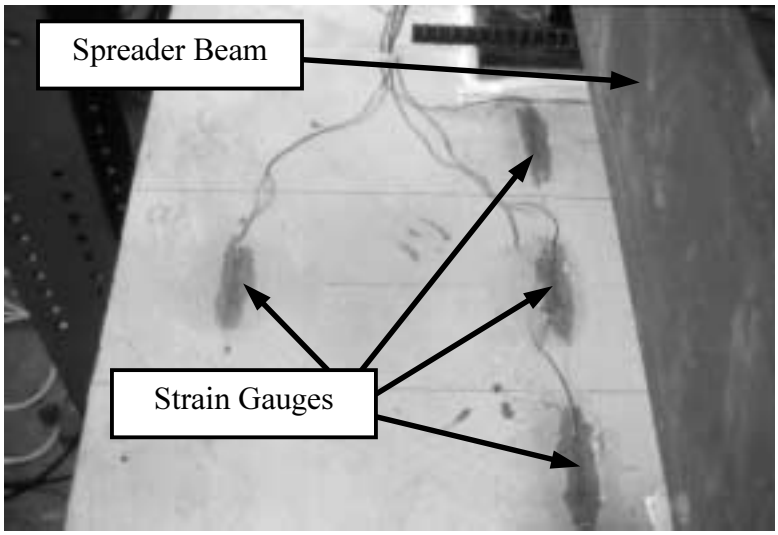


**Figure 7.10: Four Strain Gauges Bonded to Concrete Deck for Measurement of Extreme Compression Fiber Strains**

### 7.4.5 Data Acquisition

Upon operator demand, signal voltages from the electronic instruments were read by a Hewlett Packard HP3852A Data Acquisition/Control Unit. The voltage readings were then transmitted to a microcomputer, where they were recorded and converted to engineering units. A hard copy of the data was printed during the course of the test as a backup. An X-Y plotter was also used to graphically display the relationship between the applied load and the beam deflection during the test.

## 7.5 TEST PROCEDURE

Prior to the start of each test, the specimen was subjected to several cycles of load to verify that the electronic instruments and data acquisition system were functioning properly. The load applied during these cycles was limited to approximately 25 percent of the anticipated flexural cracking load. Once the instruments were checked out and initial readings were recorded, testing commenced with the application of the first load increment. Load was applied in regular increments of 10 to 20 percent of the applied load anticipated to initiate flexural cracking of the beam. At the end of each predetermined load increment, the displacement of the hydraulic cylinder was halted, and measurements were acquired from the various instruments, both manual and electronic. Once the data were acquired, application of load commenced again. As the applied load neared the anticipated flexural cracking load, the load increment was reduced to 5 kips (22 kN) in an effort to accurately pinpoint this load.

Observation of the first flexural crack signaled the end of the load increment in progress. The corresponding load and deflection were recorded, and the crack pattern was photographed. These and all subsequent cracks were marked with felt-tipped markers at the termination of each load increment. The cracks were labeled with the corresponding causative load level. Other observed events for which the ongoing load increment ceased included the initiation of web shear cracking, flexure-shear (or shear-flexure) cracking, or cracking within any strand transfer

zone. These events were also recorded photographically. In some of the specimens featuring short shear spans, web shear cracking preceded flexural cracking as expected.

Beyond the initiation of cracking, regular increments of load (usually on the order of 5 to 10 kips [22 to 44 kN]) were applied until attainment of a load level approximately corresponding to yield of the tensile reinforcement in the maximum moment region. Beyond this load level, regular displacement increments were utilized until the end of testing. Figure 7.11 depicts a test specimen after significant yielding of tension reinforcement.

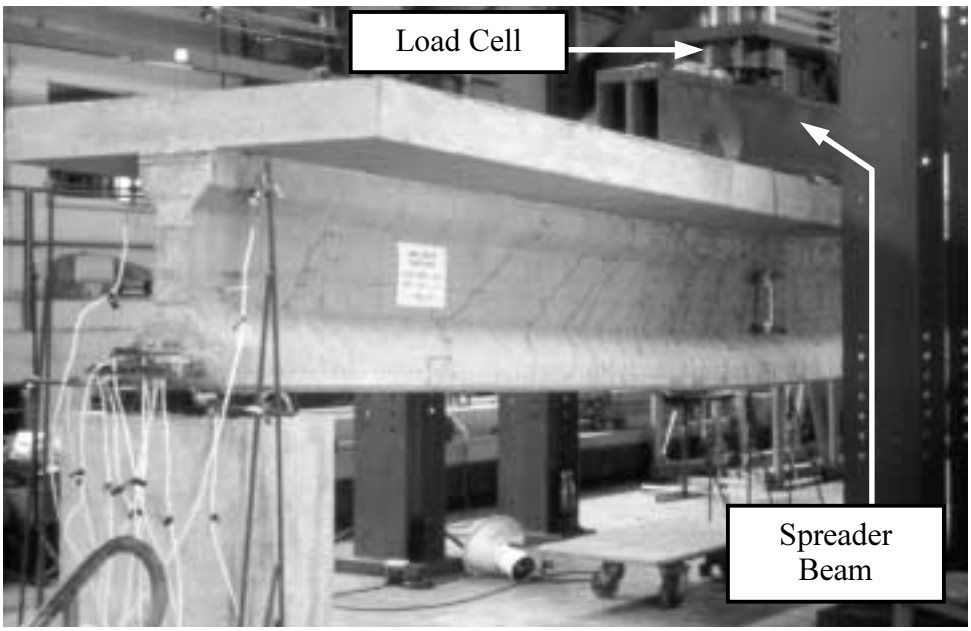


**Figure 7.11: Test H4B-D-62 after Yield of Tension Reinforcement**

In most cases, testing ceased after the deck slab suffered a local compression failure. In a few instances, testing ceased prior to crushing of the slab. This usually occurred because the beam had already exhibited the expected flexural strength and further deflection was constrained by the test setup. In other instances, testing ceased because the researchers judged that the potential safety risk outweighed the value of any information yet to be gleaned from the test.

After the completion of testing of one end of a beam, the beam supports were moved into position to test the strand anchorage at the opposite end of the beam. Every effort was made to position the supports for each test so that the damage from the first test would not extend into the span of the second test. Due to practical limits on the total length of beam specimens and the desire for each test to have a span long enough to ensure flexural behavior, this was often impossible. For the specimens with 60–75 percent of strands debonded, some flexural cracking from the first test extended into the span of the second test. This appeared to have no effect on the results of the second test other than the expected decreased stiffness evidenced by the load-deflection behavior.

## 7.6 ANALYSIS PROCEDURES

Stresses and strains present in the test specimens prior to development length testing were computed from analysis assuming elastic uncracked response. Transformed section properties were used rather than gross section properties. Stress-strain relationships were based on the results of tests conducted on the materials used to fabricate the specimens. Relaxation of the prestressing steel was modeled as described by Collins and Mitchell (1991; 90–92) for low-relaxation strand. Creep and shrinkage were addressed according to the provisions of Articles 5.4.2.3.2 and 5.4.2.3.3 of the AASHTO LRFD specifications. Stresses and strains in the concrete and steel were calculated for each specimen immediately prior to release, immediately after release, prior to casting the deck concrete, after the removal of deck shores, after the movement of supports, and immediately prior to development length testing. Differential shrinkage of the deck and beam concrete was considered in calculating all stresses and strains occurring after casting of the deck concrete.

Stress and moment-curvature analysis of the composite beam during development length testing were performed using the layer-by-layer approach described by Collins and Mitchell (1991; 173–175, 182-187). The composite beam cross section was discretized into thin layers which were analyzed individually as members subjected to axial load. The relative deformations of these layers were constrained by the "plane sections remain plane" hypothesis. The deck was subdivided into thirteen layers each with a thickness of 0.5 in (12.7 mm). The precast beam section was subdivided into twenty-eight layers each with a thickness of 1.0 in (25.4 mm). Each horizontal row of mild steel reinforcement and prestressing strand was represented as an additional layer. Initial stresses and strains in each layer were determined from the elastic uncracked analysis described above.

For each assumed value of strain at the top fiber of the section, the resulting curvature was calculated from equilibrium conditions, i.e. when the sum of the layer forces equaled the applied axial load of zero. Once each curvature was established, the corresponding moment was calculated by summing the individual moments resulting from the layer axial forces. By repeating this process for a series of top fiber strains, the full cracked section moment-curvature response was obtained.

The complete compressive stress-strain response of concrete was modeled according to the generalized Thorenfeldt, Tomaszewicz, and Jensen expression (1987) described by Collins and Mitchell (1991; 61–64). The compressive strength and modulus of elasticity of concrete were obtained from cylinder tests and are recorded in Appendix B. The complete stress-strain response of the prestressing steel was modeled according to an expression developed from tensile tests of representative strand samples. The expression is given and plotted in Section 3.4.3.1.

According to the general procedure given by Collins and Mitchell (1991; 142–147), tension stiffening was considered for predicting the load-deflection response of the composite beam. After cracking, concrete fibers located within $7.5d_b$ of reinforcement were assigned average tensile stresses according to the following relationship:

$$f_c = \frac{\alpha_1 f_{cr}}{1+\sqrt{500\varepsilon_c}}$$

where

$f_c$ = average stress in concrete

$\alpha_1$ = 1.0 for deformed reinforcing bars

$\alpha_1$ = 0.7 for bonded strands

$f_{cr}$ = concrete cracking stress = $7.5\sqrt{f'_c}$

$\varepsilon_c$ = concrete strain

For members with partially debonded strands, moment-curvature analyses were performed for each pattern of bonded reinforcement present in the beam. The deflection response of the beam was then calculated from the curvatures corresponding to each level of applied load. Appendix E contains comparisons of the predicted load-deflection response and the experimentally obtained response for each development length test. The load is plotted in terms of the moment at the critical section normalized with respect to the calculated moment capacity of the member.

## 7.7 PRESENTATION AND DISCUSSION OF TEST RESULTS

This section includes the results of the sixty development length tests performed at the Ferguson Laboratory at the The University of Texas at Austin (UT). For purposes of discussion, the tests are divided into four groups depending upon the amount of debonding characteristic of each specimen:

1. specimens with all strands fully bonded (L0B, M0B, H0B)
2. specimens with four strands partially debonded over the support (M0R, H0R)
3. specimens with 50% of bottom flange strands partially debonded (x4x)
4. specimens with more than 50% of strands partially debonded (x6x, x9x).

Each test is briefly described, and relevant quantitative results are tabulated. The behavioral response of the test specimens are compared with existing code provisions. Each transfer length referred to in the test descriptions

below corresponds to the actual value obtained in the transfer length test program described in Chapter 5. Results of the development length tests performed at Texas Tech University (TTU) are discussed after each set of corresponding UT tests.

### 7.7.1 Specimens with All Strands Fully Bonded

Twelve development length tests were conducted at the Ferguson Laboratory on specimens containing only fully bonded strands. All of these specimens contained bright strand. Four of these tests (those cast with L Series concrete) corresponded directly with four tests conducted at Texas Tech University on specimens with rusted strands. This section includes brief descriptions of each of these tests. Test results are tabulated in Table 7.3. The value of maximum slip reported in Table 7.3 is the largest strand end slip corresponding to the maximum moment resisted at the critical section. The value of $\varepsilon_{max,calc}$ represents the calculated strain in the bottom row of strands at the calculated nominal moment resistance of the beam. This value was calculated using the analysis procedures described in Section 7.6. For all specimens in which no slip occurred, the apparent depth of the neutral axis (estimated from the depth of cracking) and measured extreme fiber concrete strains indicated that the actual bottom row strand elongation was at least as large as the calculated value. For tests in which end slip occurred, it is impossible to accurately calculate the actual strand strain because little is known about the magnitude of the strand slip at the critical section. Thus, each tabulated value serves as an indication of the strand strain required to achieve the full flexural capacity of each specimen.

**Table 7.3: Development Length Test Results for Specimens with All Strands Fully Bonded (1 in = 25.4 mm)**

| Test I.D. | $\frac{l_e}{l_{d,ACI}}$ | $\frac{M_{test}}{M_{calc}}$ | Failure Type | Max. Slip (in) | $\varepsilon_{max,calc}$ |
|---|---|---|---|---|---|
| L0B-A-96 | 1.05 | 1.00 | Flexural | — | 0.045 |
| L0B-B-72 | 0.78 | 1.04 | Flex. w/ Slip | 0.003 | 0.045 |
| L0B-D-54 | 0.58 | 1.02 | Flex. w/ Slip | 0.008 | 0.045 |
| L0B-C-54H | 0.58 | 1.04 | Flex. w/ Slip | 0.005 | 0.045 |
| M0B-A-96 | 1.05 | 1.02 | Flexural | — | 0.037 |
| M0B-B-72 | 0.78 | 1.02 | Flexural | — | 0.038 |
| M0B-D-54 | 0.58 | 1.00 | Flex. w/ Slip | 0.015 | 0.040 |
| M0B-C-54H | 0.58 | 1.03 | Flex. w/ Slip | 0.015 | 0.040 |
| H0B-A-96 | 1.08 | 1.02 | Flexural | — | 0.040 |
| H0B-B-72 | 0.81 | 1.04 | Flexural | — | 0.040 |
| H0B-D-54 | 0.60 | 1.01 | Flex. w/ Slip | 0.015 | 0.041 |
| H0B-C-54H | 0.60 | 1.02 | Flex. w/ Slip | 0.015 | 0.042 |

#### *7.7.1.1 L0B-A-96*

The embedment length, $l_e$, for this test was 1.05 times the development length, $l_{d,ACI}$, calculated with the ACI/AASHTO expression. The specimen failed in a flexural manner. The maximum moment resisted, $M_{test}$, was equivalent to the nominal moment resistance calculated based on strain compatibility analysis, $M_{calc}$. No strand end slip was detected during the test. At maximum load, no cracks crossed the strands closer than 32 in (0.81 m) from the end of the transfer length (as obtained from the transfer length testing described in Chapter 5). First flexural cracking occurred at a moment equal to 94 percent of the calculated cracking moment. The pattern of cracking corresponding to the maximum load is depicted in Figure 7.12. This crack pattern is typical of all the tests in this group that exhibited flexural failure with no bond slip.

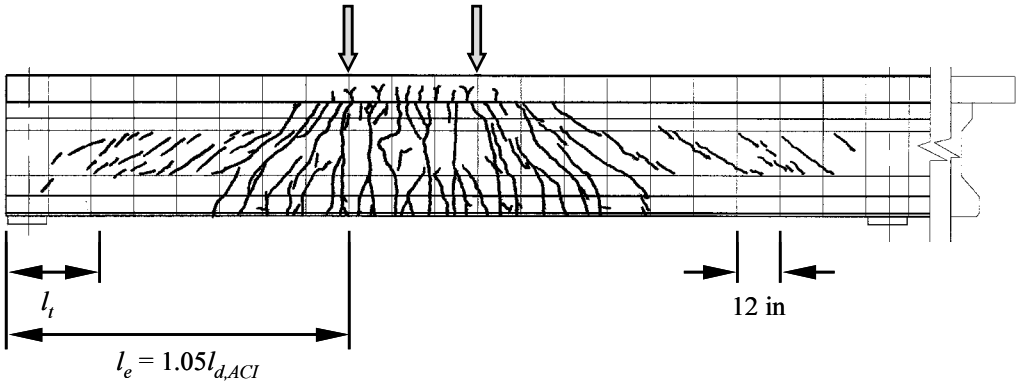


**Figure 7.12: Crack Pattern for Test L0B-A-96 at Flexural Failure**

#### *7.7.1.2 L0B-B-72*

For this test, $l_e = 0.78 l_{d,ACI}$. The beam failed in a flexural manner. A small slip of 0.003 in (0.08 mm) occurred in one strand at an applied load greater than the calculated failure load. This slip initiated with the opening of a flexural crack 12 in (305 mm) from the transfer length. Web shear cracks extended to the level of the strands at the center of the support at peak load. The maximum moment resisted was 4 percent greater than the calculated nominal moment strength. First flexural cracking occurred at a moment equal to 95 percent of the calculated cracking moment.

#### *7.7.1.3 L0B-D-54*

This test exhibited a flexural failure with strand end slip in the exterior two strands only. This slip was initiated as shear cracks extended to the beam soffit in front of the support (within the transfer length). The maximum slip at ultimate strength was 0.008 in (0.20 mm). Figure 7.13 depicts the anchorage region of the beam at the peak load. The maximum moment resisted was 2 percent greater than the calculated nominal moment strength. First flexural cracking occurred at a moment equal to 97 percent of the calculated cracking moment. For both this test and Test L0B-C-54H, $l_e = 0.58 l_{d,ACI}$. Figure 7.14 illustrates the pattern of cracking for this test at final load. This crack pattern is typical of all the tests in this group that exhibited a flexural failure with strand end slip.

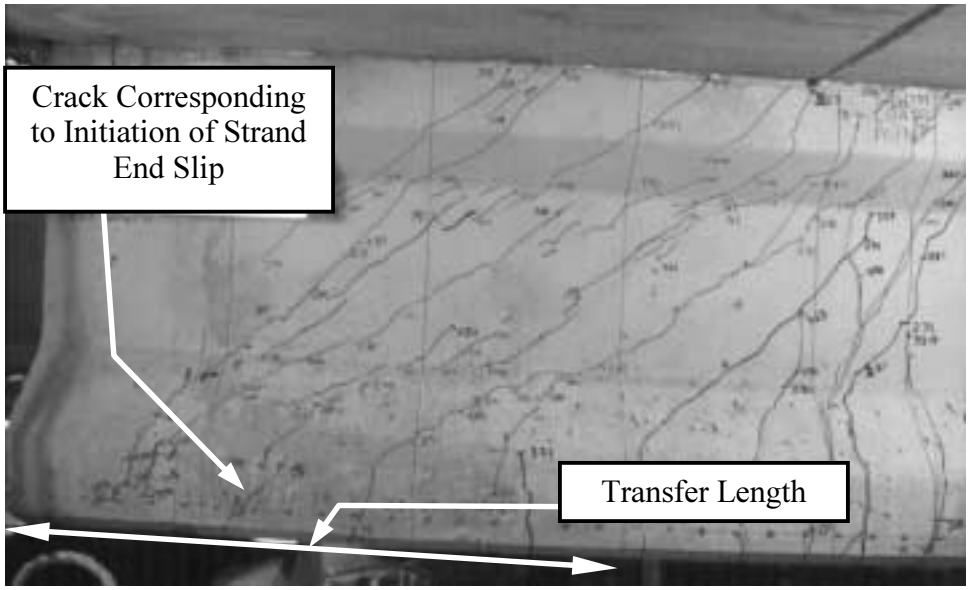


**Figure 7.13: Test L0B-D-54 at Final Load**

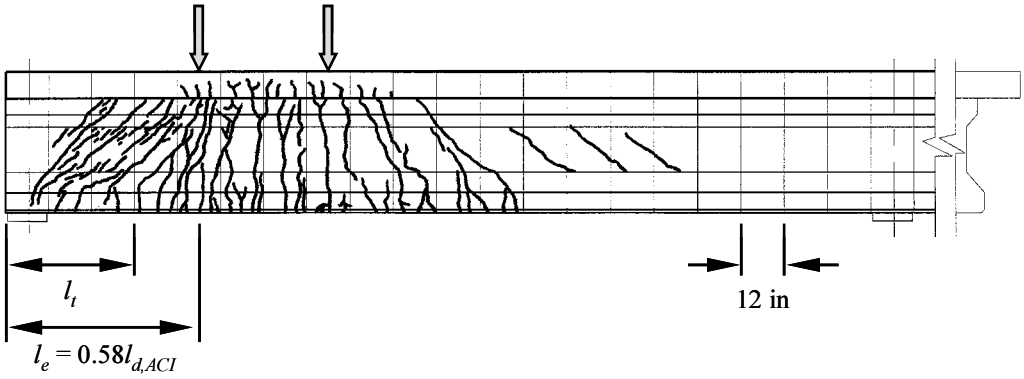


**Figure 7.14: Crack Pattern for Test L0B-D-54 at Flexural Failure with Strand Slip**

#### *7.7.1.4 L0B-C-54H*

This test included horizontal web reinforcement and also exhibited a flexural failure with strand end slip in the exterior two strands only. As in the companion test without horizontal web reinforcement (L0B-D-54), slip was initiated by shear cracks extending through the transfer length of the strands. Maximum slip was 0.005 in (0.13 mm) at flexural failure. The maximum moment resisted was 4 percent greater than the calculated nominal moment strength. First flexural cracking occurred at a moment equal to 97 percent of the calculated cracking moment.

#### *7.7.1.5 Corresponding Texas Tech Tests (L0R Series)*

Four of the development length tests conducted at Texas Tech University (TTU) corresponded to the four L0B Series tests summarized above, except the TTU specimens featured rusted strand rather than bright strand (Burkett and Kose 1999). All four of the TTU tests exhibited flexural failures, and no strand end slip was detected during any of the four tests. The strand end slips were measured manually, and the effective precision of the measurements may have precluded the observation of slips as small as those occurring in the corresponding UT tests. Thus, it appears that the rusted strand specimens appeared to perform at least as well as the bright strand specimens.

#### *7.7.1.6 M0B-A-96*

This specimen, with $l_e = 1.05l_{d,ACI}$, failed in a flexural manner. The maximum moment resisted was 2 percent greater than the calculated nominal moment resistance. No strand end slip was detected during the test. At maximum load, no cracks crossed the strands closer than 43 in (1.09 m) from the end of the transfer length. First flexural cracking occurred at a moment equal to 99 percent of the calculated cracking moment. Web shear cracks extended to just above the strand depth at the support.

#### *7.7.1.7 M0B-B-72*

This specimen, with $l_e = 0.78l_{d,ACI}$, also failed in a flexural manner. The maximum moment resisted was 2 percent greater than the calculated nominal moment resistance. No strand end slip was detected during the test. At maximum load, no cracks crossed the strands closer than 19 in (0.48 m) from the end of the transfer length. First flexural cracking occurred at a moment 1 percent greater than the calculated cracking moment. Web shear cracks extended to the strand depth at the support.

#### *7.7.1.8 M0B-D-54*

M0B-D-54 and M0B-C-54H behaved similarly to L0B-D-54 and L0B-C-54H. This specimen, with $l_e = 0.58l_{d,ACI}$, failed in a flexural manner with a maximum slip of 0.015 in (0.38 mm). Slip occurred only in the two exterior strands of the bottom row and both the strands of the second row. This end slip was initiated by shear cracks at the support and shear cracks extending through strands at a distance of 5 in from the transfer length. The maximum moment resisted was equal to the calculated nominal moment resistance. First flexural cracking occurred at a moment 5 percent greater than the calculated cracking moment.

#### *7.7.1.9 M0B-C-54H*

This specimen, also with $l_e = 0.58l_{d,ACI}$ but containing horizontal web reinforcement, failed in a flexural manner with a maximum slip of 0.015 in (0.38 mm). Slip occurred only in the two strands of the second row. This end slip was initiated by shear cracks extending through the transfer length at the support. The maximum moment resisted was 3 percent greater than the calculated nominal moment resistance. First flexural cracking occurred at a moment 5 percent greater than the calculated cracking moment.

#### *7.7.1.10 H0B-A-96*

This specimen, with $l_e = 1.08l_{d,ACI}$, failed in a flexural manner. The maximum moment resisted was 2 percent greater than the calculated nominal moment resistance. No strand end slip was detected during the test. At maximum load, no cracks crossed the strands closer than 45 in (1.14 m) from the end of the transfer length. First flexural cracking occurred at a moment equal to 93 percent of the calculated cracking moment. Web shear cracks extended to the strand depth at the support.

#### *7.7.1.11 H0B-B-72*

This specimen, which behaved much like M0B-B-72, also failed in a flexural manner. The maximum moment resisted was 4 percent greater than the calculated nominal moment resistance. No strand end slip was detected during the test. At maximum load, no cracks crossed the strands closer than 28 in (0.71 m) from the end of the transfer length. First flexural cracking occurred at a moment equal to 95 percent of the calculated cracking moment. Web shear cracks extended to the strand depth at the support.

#### *7.7.1.12 H0B-D-54*

This specimen, with $l_e = 0.60l_{d,ACI}$, failed in a flexural manner with a maximum slip of 0.015 in (0.38 mm). Slip occurred only in the strands of the second row. Shear cracks passed through the strands at the support prior to strand end slip. End slip initiated with flexural cracking 20 in (0.51 m) from the end of the transfer length. The maximum

moment resisted was 1 percent greater than the calculated nominal moment resistance. First flexural cracking occurred at a moment equal to 96 percent of the calculated cracking moment.

#### *7.7.1.13 H0B-C-54H*

This specimen, although reinforced with horizontal web steel in the anchorage region, failed in a manner similar to H0B-D-54. Failure was flexural with a maximum strand end slip of 0.015 in (0.38 mm). Slip occurred only in the strands of the second row. Shear cracks passed through the strands at the support prior to strand end slip. End slip initiated with flexural cracking 15 in (0.38 m) from the end of the transfer length. The maximum moment resisted was 2 percent greater than the calculated nominal moment resistance. First flexural cracking occurred at a moment equal to 92 percent of the calculated cracking moment.

#### *7.7.1.14 Summary of Tests Performed on Specimens with All Strands Fully Bonded*

All specimens in this group failed in a flexural manner at moments equal to or exceeding the predicted nominal moment. For the L-Series tests, general bond slip occurred for specimens with embedment lengths less than $0.8l_{d,ACI}$. In the higher strength beams, general bond slip did not occur in the tests with embedment lengths approximately equal to $0.8l_{d,ACI}$, but did occur in tests with embedment lengths approximately equal to $0.6l_{d,ACI}$. No intermediate embedment lengths were tested. In the L0B and M0B tests, general bond slip was a direct result of cracking in or near (within $20d_b$) the transfer length. In addition to large flexural bond stresses, shear cracking at the support may have contributed to the general bond slip that occurred in the H0B tests.

From these tests, it is apparent that the necessary development length for these specimens is less than that predicted by the ACI/AASHTO expression for development length of fully bonded 0.6 in (15.2 mm) diameter strands. In order to more accurately assess the flexural bond performance of these specimens, it is helpful to compare the flexural bond lengths tested to the flexural bond length from the ACI Code. This is done in an attempt to isolate the flexural bond behavior from the transfer bond behavior.

In Figure 7.15, data are plotted from the tests in which slip occurred. The ordinate of each point represents $\frac{f_{p,slip} - f_{pe}}{f_{ps} - f_{pe}}$. The numerator in this expression is the difference between the calculated tendon stress at the critical section when slip occurs, $f_{p,slip}$, and the effective prestress prior to application of load, $f_{pe}$. This numerator represents the portion of the tendon stress developed by flexural bond stresses at the occurrence of end slip. For equitable comparison with other specimens, this value is normalized with respect to $f_{ps} - f_{pe}$, which represents the increase in strand stress that would be developed by flexural bond stresses at nominal flexural strength given adequate anchorage. The abscissa of each point represents the flexural bond length provided, $l_e - l_t$, normalized with respect to the flexural bond length implied by the ACI/AASHTO expression for the development length of fully bonded strands, $l_{fb,ACI} = (f_{ps} - f_{pe})d_b$. The solid line represents the flexural bond length expression from Commentary Section R12.9 of ACI 318-99 if general bond slip is the accepted performance criterion. Thus, data above and to the left of the line indicate that the existing expression is a conservative predictor of the flexural bond length required to prevent general bond slip. Accordingly, the data from this group of tests indicate that the ACI 318-99 Commentary expression is conservative with respect to general bond slip.

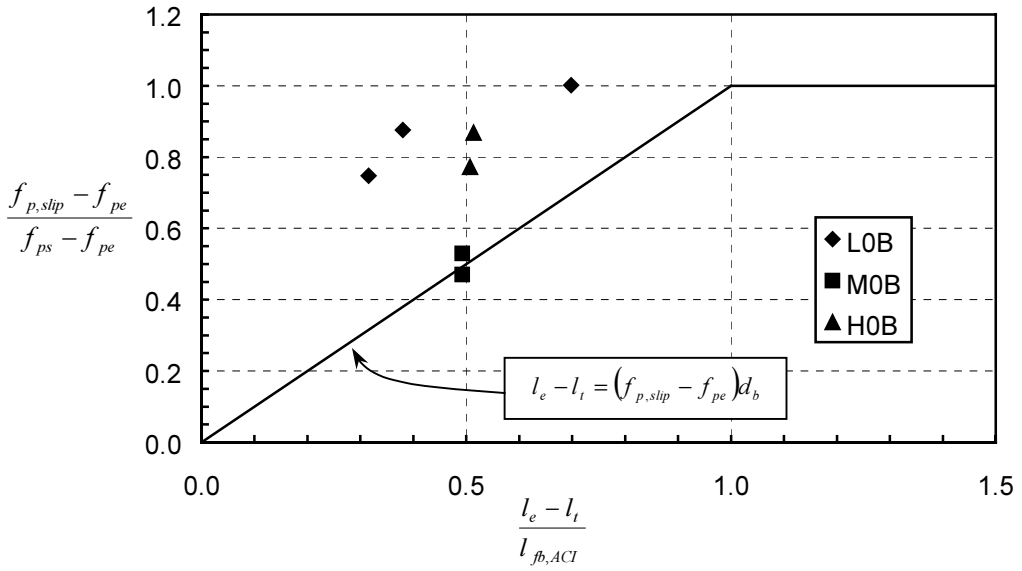


**Figure 7.15: Flexural Bond Performance of Fully Bonded Specimens—Normalized Flexural Tendon Stress at Slip vs. Normalized Flexural Bond Length Provided**

In a manner similar to Figure 7.15, Figure 7.16 illustrates the conservatism of the Commentary expression for flexural bond length if achievement of calculated nominal strength is the performance criterion. In this chart, the ordinate represents the portion of the tendon stress developed by flexural bond stresses at the maximum moment resisted during testing. The solid line represents the flexural bond length expression from Commentary Section R12.9 of ACI 318-99 with achievement of the full nominal strength of the member (assuming adequate bond) as the performance criterion. All the tests of the group are represented in this chart, regardless of whether or not slip occurred. Because the full flexural strength was obtained in all of these tests, the data indicate that the Commentary expression is quite conservative with respect to attainment of the nominal capacity calculated with the assumption of adequate bond.[1]

[1] This method of evaluating the effectiveness of the Commentary expression for flexural bond length is similar to the method applied by Mattock to the PCA data when developing this expression (Tabatabai and Dickson 1993).

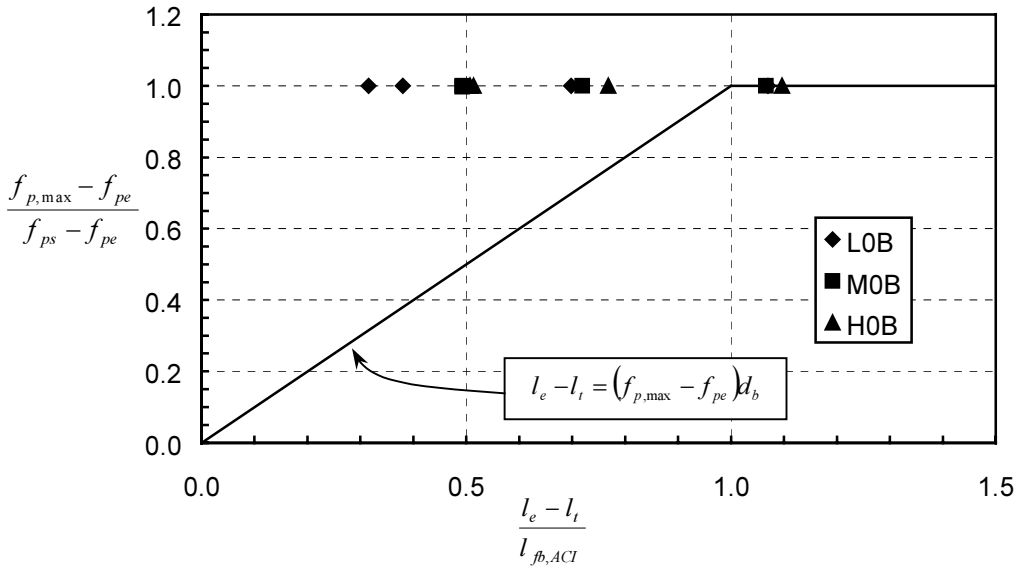


**Figure 7.16: Flexural Bond Performance of Fully Bonded Specimens—Normalized Flexural Tendon Stress at Ultimate Strength vs. Normalized Flexural Bond Length Provided**

It should be noted that shear forces were extremely high in these specimens. In all specimens in which general bond slip occurred, the slip initiated at levels of shear beyond that allowed by ACI 318-99, Section 11.5.6.9 (assuming a shear resistance factor, $\phi_v$, of unity). In other words, the shear demand in the anchorage region exceeded the concrete shear resistance, $V_c$, by more than $8\sqrt{f_c'}b_w d$. Nonetheless, in the most shear-critical of these tests, the calculated shear resistance provided according the ACI/AASHTO Standard method, $V_{n,ACI}$, was approximately 13 percent larger than the maximum shear demand during testing, $V_{max}$ ($\phi_v$ = 1). The shear resistance provided according to the AASHTO LRFD sectional method, $V_{n,LRFD}$, was approximately 6 percent larger than $V_{max}$. Thus, these specimens, particularly those with the shortest embedment lengths, did not have an excess of shear reinforcement.

All strand end slips were limited to approximately 0.015 in. Based on the limited number of tests performed, no definite correlation between concrete strength and *flexural* bond resistance was evident. Based on a comparison with the corresponding Texas Tech tests, specimens with rusted strand behaved similarly to those with bright strand. Aside from reducing crack widths, the horizontal web reinforcement did not appear to significantly enhance resistance to general bond slip.

### 7.7.2 Specimens with Four Strands Partially Debonded over Support

Because no bond failures occurred in the tests conducted on specimens containing only fully bonded strands, it was hypothesized that the large vertical support reaction was preventing significant slip of the strands. Because the moment resistance is approximately constant for each series of tests, the size of this "clamping" force increases with decreasing embedment length. In an effort to partially discount the beneficial effects of this force, the four interior strands (A2, A3, A4, and A5) of the bottom row were debonded over a length of 12 in (305 mm) at the support in the specimens subjected to the eight tests described in this section. This short debonding was not performed to reduce the stresses in the girder, but to reduce the influence of the confining pressure due to the large reaction force at the support. These eight tests were performed on the specimens containing rusted strands and cast with either M or H Series concrete. Table 7.4 includes the results of these tests.

**Table 7.4: Development Length Test Results for Specimens with Four Strands Partially Debonded over the Support (1 in = 25.4 mm)**

| Test I.D. | $\frac{l_e}{l_{d,ACI}}$ | $\frac{M_{test}}{M_{calc}}$ | Failure Type | Max. Slip (in) | $\varepsilon_{max,calc}$ |
|---|---|---|---|---|---|
| M0R-A-96 | 1.04 | 1.04 | Flexural | — | 0.031 |
| M0R-B-54 | 0.58 | 1.05 | Flex. w/ Slip | 0.110 | 0.036 |
| M0R-D-46 | 0.49 | 1.00 | Flex. w/ Slip | 0.215 | 0.035 |
| M0R-C-46H | 0.49 | 0.95 | Bond | 0.165 | 0.038 |
| H0R-A-96 | 1.03 | 1.01 | Flexural | — | 0.032 |
| H0R-D-66 | 0.70 | 1.00 | Flexural | — | 0.040 |
| H0R-B-46 | 0.49 | 0.93 | Bond | 0.500 | 0.036 |
| H0R-C-46H | 0.49 | 1.00 | Flex. w/ Slip | 0.015 | 0.041 |

#### *7.7.2.1 M0R-A-96*

This specimen behaved similarly to the fully bonded specimens with the same embedment length ($l_e$ = 1.04$l_{d,ACI}$). The beam failed in a flexural manner with no strand end slip. The closest crack crossing the tendons was located 40 in (1.02m) from the transfer length. No web shear cracks extended into the bottom flange in the vicinity of the transfer length. The maximum moment resisted was 4 percent greater than the calculated nominal moment resistance. First flexural cracking occurred at a moment 4 percent greater than the calculated cracking moment.

#### *7.7.2.2 M0R-B-54*

This specimen also exhibited a flexural type of failure, although end slip occurred in the four debonded strands (A3 and A4). This slip appeared to initiate with the opening of a flexural crack 11 in (0.28 m) from the transfer length of these strands. The two outer debonded strands (A2 and A5) slipped less than 0.010 in (0.25 mm) prior to achievement of flexural failure. The innermost strands (A3 and A4) gradually slipped up to approximately 0.030 in (0.8 mm) at a load corresponding to a moment at the critical section 1 percent greater than the calculated nominal strength of the beam. At this point, an additional crack formed at the end of the transfer length, and the strands continued to slip with little increase in moment resistance. The maximum moment achieved was 2 percent greater than the calculated nominal moment resistance. Loss of capacity resulted from crushing of the deck concrete. The maximum strand slip at the maximum load was 0.110 in (2.8 mm). No strand slip was recorded in the fully bonded strands, which had an embedment length approximately equal to 0.7$l_{d,ACI}$. First flexural cracking occurred at a moment 5 percent greater than the calculated cracking moment.

#### *7.7.2.3 M0R-D-46*

The embedment length for this test (approximately half of the ACI/AASHTO development length for fully bonded strands) was shorter than any in the group of tests on specimens with only fully bonded strands. Although the failure type has been classified above as a flexural failure with strand end slip, it might also be described as a ductile bond failure that occurred at the nominal flexural strength of the member. All four of the debonded strands slipped during the test. Initiation of slip corresponded to the extension of a shear crack to the soffit of the beam within the transfer length of the debonded strands. At an applied load corresponding to a moment within 0.5 percent of the calculated nominal strength of the beam, one of the innermost strands (A3) began to slip more rapidly than the rest. This strand slipped as much as 0.215 in (5.5 mm) prior to achievement of maximum moment at the critical section with crushing of the deck. The other debonded strands slipped approximately 0.040 in (1.0 mm). No end slip of the fully bonded strands was observed. The maximum moment was equal to the calculated nominal strength of the member. First flexural cracking occurred at a moment 3 percent greater than the calculated cracking moment.

#### *7.7.2.4 M0R-C-46H*

This beam end was identical to that tested in M0R-D-46 except for the addition of horizontal web reinforcement. In this test, however, bond failure caused premature flexural failure. End slip of the four debonded strands initiated with flexural cracking 40 in (1.02 m) from the end of the transfer length. A shear crack had already passed through the transfer length of the strands at a lower load. As in the previous test, the debonded strands slipped up to a maximum of 0.040 in (1.0 mm) except for one strand. This one strand (A4), began to slip more rapidly than the others at a moment approximately 10 percent less than the calculated nominal strength of the member. Once the slip of this strand exceeded 0.100 in (2.5 mm), no significant increase in moment resistance was achieved. The strand slipped a total of 0.165 in (4.2 mm) at which point a sudden slip of approximately 0.050 in (1.3 mm) resulted in a drop in moment capacity. The peak moment (immediately prior to the sudden slip) was equal to 95 percent of the calculated moment capacity. After the sudden slip, the beam resisted a moment equal 92 percent of the calculated moment capacity before deck crushing. No slip of fully bonded strands was detected. First flexural cracking occurred at a moment equal to 99 percent of the calculated cracking moment. Figure 7.17 shows the pattern of cracking in the anchorage region at the end of the test.

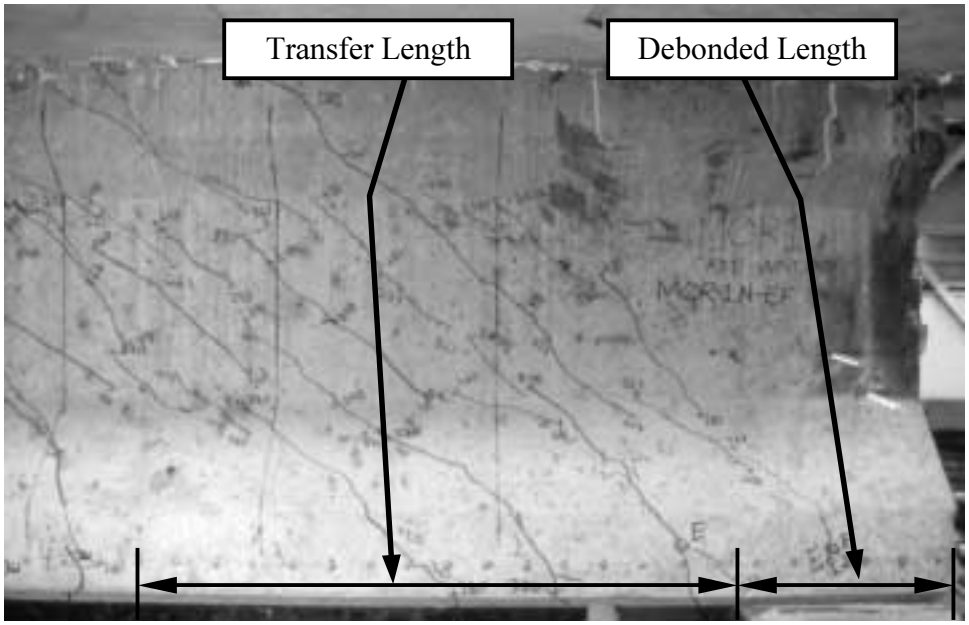


**Figure 7.17: Cracking in the Anchorage Region of M0R-C-46H at Final Load**

#### *7.7.2.5 H0R-A-96*

This test was very similar to M0R-A-96. Flexural failure occurred with no strand slip. The closest crack crossing the strands was located 39 in (0.99 m) from the transfer length. The maximum moment resisted was 1 percent greater than the calculated nominal moment resistance. First flexural cracking occurred at a moment equal to 95 percent of the calculated cracking moment.

#### *7.7.2.6 H0R-D-66*

This test, which featured an embedment length approximately equal to $0.7l_{d,ACI}$, also exhibited a flexural failure with no strand slip. The closest crack crossing the strands was located 14 in (0.36 m) from the transfer length. Two web shear cracks extended to the depth of the strands over support. The maximum moment equaled the calculated moment capacity. Flexural cracking commenced at a moment equal to 97 percent of the calculated cracking moment.

### *7.7.2.7 H0R-B-46*

Much like M0R-C-46H, this test exhibited a premature flexural failure caused by a lack of bond capacity. End slip of all four debonded strands was initiated when a shear crack extended through the transfer length of the strands. Slip in these strands progressed slowly up to a magnitude of approximately 0.035 in (0.9 mm) at a moment equal to $0.92M_{n,calc}$. Slip of strands A3 and A4 then increased rapidly with little increase in resisted moment. The resisted moment remained fairly constant throughout an additional deflection of approximately 0.6 in (15 mm) until crushing of the deck concrete occurred. Slip of strands A3 and A4 at crushing was approximately 0.50 in (13 mm). The maximum moment resisted was equal to 93 percent of the calculated moment capacity. First flexural cracking occurred at a moment corresponding to 99 percent of the calculated cracking moment. No slip of fully bonded strands was detected. Figure 7.18 shows the pattern of cracking in the anchorage region at ultimate strength.

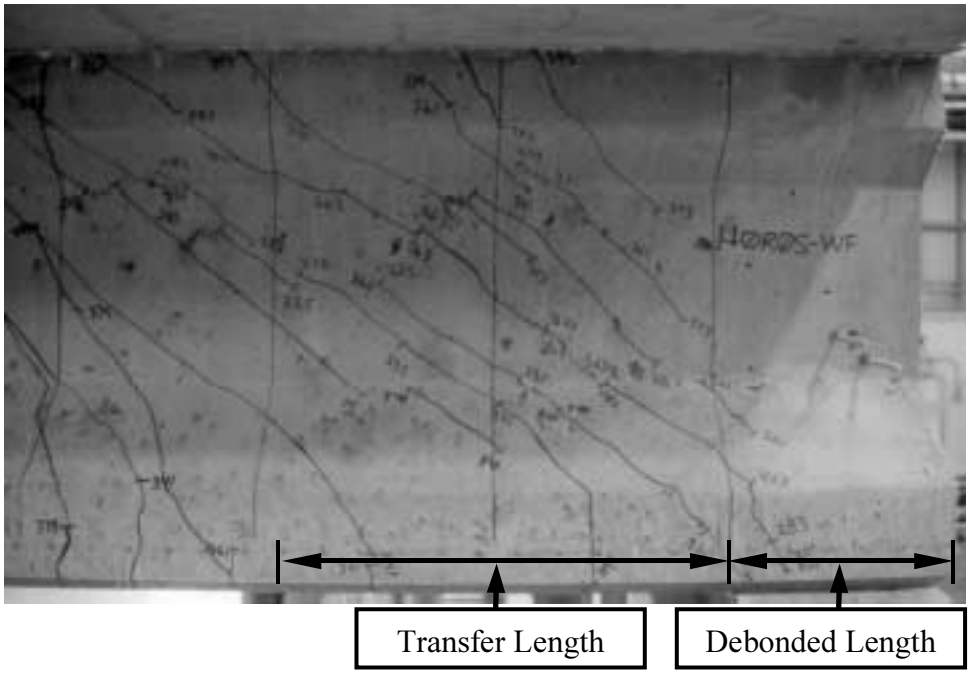


**Figure 7.18: H0R-B-46 Anchorage Region after Final Load**

### *7.7.2.8 H0R-C-46H*

This specimen experienced a flexural failure accompanied by relatively small end slip of the debonded strands. This end slip initiated with a shear crack crossing the transfer length of the strands. The slip gradually increased to a maximum of 0.015 in (0.4 mm) at flexural failure. The maximum moment was equivalent to the calculated moment capacity of the beam. First flexural cracking occurred at a moment corresponding to 97 percent of the calculated cracking moment. No slip of fully bonded strands was detected. Figure 7.19 shows the pattern of cracking in the anchorage region of the beam at ultimate load.

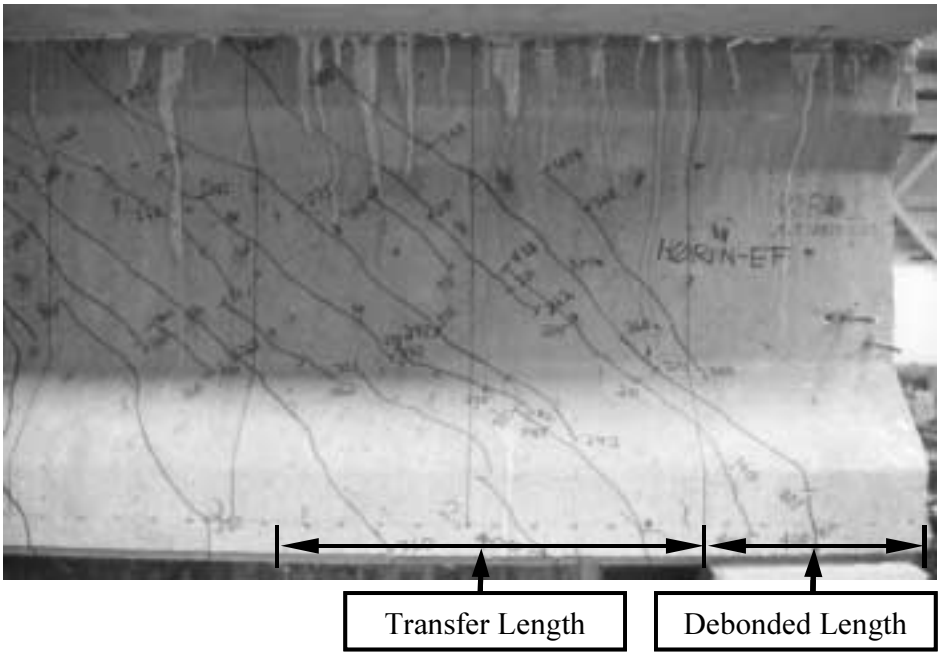


**Figure 7.19: H0R-C-46H Anchorage Region after Final Load**

Note that the crack pattern is quite similar to that of the previous test (Figure 7.18) despite the fact that H0R-B-46 failed due to inadequate bond strength. A comparison of these two tests seems to indicate that the horizontal web reinforcement was effective in preventing premature failure of H0R-C-46H, despite the influence of cracking within the transfer length. The behavior of M0R-C-46H (depicted in Figure 7.17) precludes this conclusion however. That test, which exhibited cracking very similar to that of both H0R-B-46 and H0R-D-46H, suffered a premature failure due to insufficient bond capacity despite the presence of horizontal web reinforcement. Its companion specimen without horizontal web reinforcement, M0R-D-46, did not suffer a loss of capacity due to inadequate bond. Thus, the amount of horizontal web reinforcement provided did not consistently improve the anchorage behavior in these tests.

#### *7.7.2.9 Summary of Tests Performed on Specimens with Four Strands Partially Debonded over Support*

For the strands debonded for 12 in (305 mm) over the support, general bond slip occurred in the tests where the provided embedment length was less than 70 percent of the ACI/AASHTO development length for debonded strands. No slip was detected in any of fully bonded strands, which had embedment lengths as short as $0.58l_{d,ACI}$. This appears to indicate that the performance of the fully bonded rusted strands was better with respect to prevention of general bond slip than that of the fully bonded bright strands.

The strand slip response of M0R-B-54 indicates that the rusted strands debonded over the support slipped significantly more than their bright, fully bonded counterparts in Tests M0B-D-54 and M0B-C-54H. This is likely due to the large "clamping" force present above the support that increased the bond resistance of the strands bonded along this additional 12 in (305 mm) length. All strands appeared to be able to slip up to 0.03–0.04 in (0.8–1.0 mm) and still support increases in strand stress. Beyond this level, strands tended to slip without increase in load. Even if strands did slip, moment resistance only dropped slightly after slip (less than 3 percent of the nominal moment capacity) until the slab crushed.

Figure 7.20 and Figure 7.21 depict the flexural bond behavior of these eight specimens with respect to ACI Commentary expression for development length. Figure 7.20 represents the addition of the data from this group of tests to the chart originally presented in Figure 7.15. This chart indicates the conservatism of the Commentary expression if prevention of general bond slip is the performance criterion. Here again, these tests indicate that the expression conservatively predicts the flexural bond length required to prevent general bond slip, even though the four strands were debonded for 12 in (305 mm) over the support.

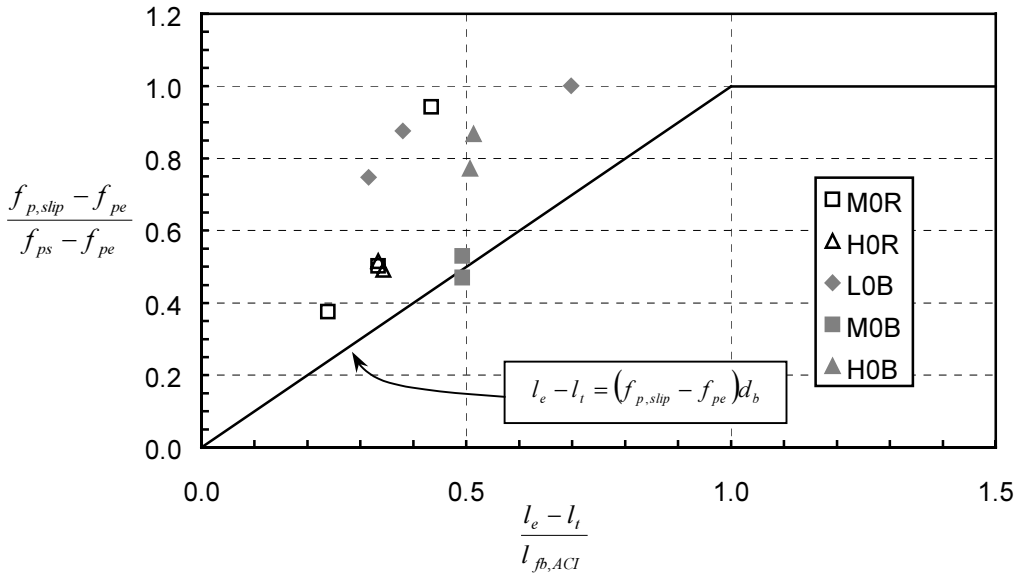


**Figure 7.20: Flexural Bond Performance of Specimens with Four Strands Partially Debonded over Support—Normalized Flexural Tendon Stress at Slip vs. Normalized Flexural Bond Length Provided**

Figure 7.21 is analogous to Figure 7.16 included in the discussion of the fully bonded test specimens. The results of this group of tests also indicate that the Commentary expression is very conservative if strength reduction due to inadequate bond is the failure criterion. Although half of the primary tension reinforcement was partially debonded, premature failures only occurred for specimens with less than half the flexural bond length for fully bonded strands according to the ACI Commentary expression.

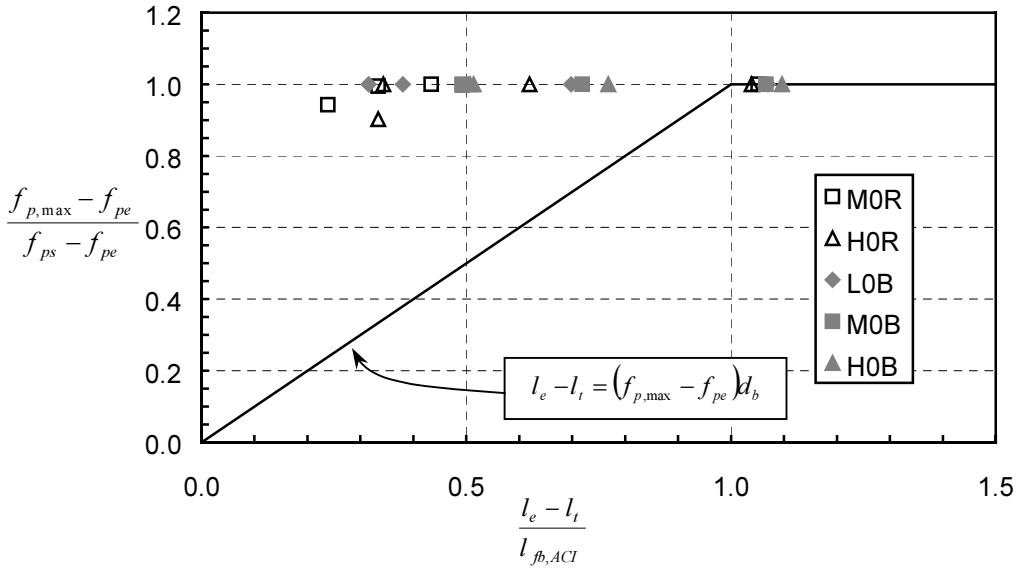


**Figure 7.21: Flexural Bond Performance of Specimens with Four Strands Partially Debonded over Support—Normalized Flexural Tendon Stress at Ultimate Strength vs. Normalized Flexural Bond Length Provided**

Except for larger strand end slips in some specimens, the specimens with four strands debonded over the support exhibited flexural bond behavior quite similar to the specimens with all strands fully bonded. All of these specimens performed at least as well as the bond performance indicated by the ACI/AASHTO expression for development

length of fully bonded strands. Based on these results, it can be concluded that the anchorage performance of specimens reinforced with both fully bonded and partially debonded strands does not simply depend upon the percentage of strands debonded.

Examining Figure 7.20 and Figure 7.21, it appears that concrete strength does not play a significant role in the flexural bond resistance of pretensioned strand. The influence of concrete strength on the overall development length seems effectively limited to the portion of the development length represented by the transfer length. Any influence of strand surface condition on the flexural bond behavior is also unclear. Strand end slips may have been slightly smaller for rusted strands than for the corresponding bright strands, but the surface condition did not seem to significantly affect the overall behavior of the member. As discussed above, the presence of horizontal web reinforcement did not consistently improve anchorage performance. In one case, a specimen containing H-bars suffered a bond failure while the corresponding specimen without H-bars did not.

### 7.7.3 Specimens with 50 Percent of Bottom Flange Strands Partially Debonded

This group of tests featured specimens with four partially debonded strands out of the eight strands in the bottom flange. Two fully bonded strands were required at the top of some of the beams in order to satisfy allowable stress requirements. The partially debonded strands lay in the bottom row. Two were debonded for 36 in (914 mm); two were debonded for 72 in (1829 mm). The two exterior strands of the bottom row and the two strands of the second row were fully bonded. Further details regarding these specimens are recorded in Chapter 3. As discussed in Section 3.3.1, these girders violated the provisions of the AASHTO LRFD Specification (1998) Article 5.11.4.3 because 1) more than 25 percent of the strands were partially debonded, and 2) more than 40 percent of the strands in the bottom row were debonded.

Test results for specimens with bright strands are tabulated in Table 7.5. Test results for specimens with rusted strands are tabulated in Table 7.6. In each of these tables, there are two rows of data corresponding to each test. The first row of the pair contains data pertaining to the pair of strands debonded for 72 in (1829 mm); the second contains data pertaining to the pair of strands debonded for 36 in (914 mm).

The fully bonded strands in these specimens did not exhibit end slip. The shortest embedment length of fully bonded strands in this group of tests occurred in Tests L4B-A-48 and L4B-C-48H. The 120 in (3.05 m) embedment length of fully bonded strands in these tests was approximately equal to $1.25l_{d,ACI}$. The fact that no slip occurred in these strands agrees with the results obtained from tests on specimens containing only fully bonded strands, in which slip only occurred in strands with an embedment length considerably less than $l_{d,ACI}$.

**Table 7.5: Development Length Test Results for Specimens with 50% of Bottom Flange Strands Partially Debonded—Bright Strands (1 in = 25.4 mm)**

| Test I.D. | Debonded Length (in) | $l_e$ (in) | $\frac{l_e}{l_{d,ACI}}$ | $\frac{M_{test}}{M_{calc}}$ | Failure Type | Max. Slip (in) | $\varepsilon_{max,calc}$ |
|---|---|---|---|---|---|---|---|
| L4B-B-96 | 72 | 96 | 1.02 | 0.97 | Flexural | — | 0.040 |
| | 36 | 132 | 1.44 | | | — | |
| L4B-D-60 | 72 | 60 | 0.64 | 1.01 | Flex. w/ Slip | 0.400 | 0.038 |
| | 36 | 96 | 1.05 | | | 0.015 | |
| L4B-A-48 | 72 | 48 | 0.50 | 0.94 | Bond | 0.950 | 0.046 |
| | 36 | 84 | 0.90 | | | 0.060 | |
| L4B-C-48H | 72 | 48 | 0.50 | 0.98 | Bond | 0.980 | 0.044 |
| | 36 | 84 | 0.90 | | | 0.045 | |
| M4B-A-60 | 72 | 60 | 0.66 | 1.04 | Flex. w/ Slip | 0.470 | 0.037 |
| | 36 | 96 | 1.07 | | | — | |
| M4B-D-56 | 72 | 56 | 0.60 | 0.97 | Bond | 0.390 | 0.041 |
| | 36 | 92 | 1.01 | | | 0.010 | |
| M4B-C-56H | 72 | 56 | 0.60 | 1.01 | Flex. w/ Slip | 0.750 | 0.042 |
| | 36 | 92 | 1.01 | | | 0.030 | |
| M4B-B-48 | 72 | 48 | 0.52 | 0.96 | Bond | 0.730 | 0.039 |
| | 36 | 84 | 0.93 | | | 0.015 | |
| H4B-D-62 | 72 | 62 | 0.66 | 1.02 | Flex. w/ Slip | 0.700 | 0.051 |
| | 36 | 98 | 1.05 | | | 0.010 | |
| H4B-C-62H | 72 | 62 | 0.65 | 1.06 | Flex. w/ Slip | 0.650 | 0.053 |
| | 36 | 98 | 1.05 | | | 0.010 | |
| H4B-A-56 | 72 | 56 | 0.60 | 1.01 | Flex. w/ Slip | 0.460 | 0.043 |
| | 36 | 92 | 1.00 | | | — | |
| H4B-B-50 | 72 | 50 | 0.54 | 0.99 | Bond | 0.850 | 0.044 |
| | 36 | 86 | 0.94 | | | 0.005 | |

**Table 7.6: Development Length Test Results for Specimens with 50% of Bottom Flange Strands Partially Debonded—Rusted Strands (1 in = 25.4 mm)**

| Test I.D. | Debonded Length (in) | $l_e$ (in) | $\frac{l_e}{l_{d,ACI}}$ | $\frac{M_{test}}{M_{calc}}$ | Failure Type | Max. Slip (in) | $\varepsilon_{max,calc}$ |
|---|---|---|---|---|---|---|---|
| M4R-A-96 | 72 | 96 | 1.05 | 1.03 | Flexural | — | 0.031 |
| | 36 | 132 | 1.47 | | | — | |
| M4R-D-90 | 72 | 90 | 0.97 | 1.01 | Flexural | — | 0.036 |
| | 36 | 126 | 1.39 | | | — | |
| M4R-C-78H | 72 | 78 | 0.84 | 1.03 | Flex. w/ Slip | 0.085 | 0.037 |
| | 36 | 114 | 1.25 | | | — | |
| M4R-B-56 | 72 | 56 | 0.61 | 0.98 | Bond | 0.910 | 0.031 |
| | 36 | 92 | 1.03 | | | — | |
| H4R-A-82 | 72 | 82 | 0.88 | 0.99 | Flexural | — | 0.045 |
| | 36 | 118 | 1.28 | | | — | |
| H4R-D-78 | 72 | 78 | 0.83 | 1.00 | Flexural | — | 0.044 |
| | 36 | 114 | 1.24 | | | — | |
| H4R-B-72 | 72 | 72 | 0.77 | 0.99 | Flex. w/ Slip | 0.055 | 0.047 |
| | 36 | 108 | 1.17 | | | — | |
| H4R-C-72H | 72 | 72 | 0.77 | 1.02 | Flex. w/ Slip | 0.025 | 0.045 |
| | 36 | 108 | 1.17 | | | — | |

#### *7.7.3.1 L4B-B-96*

The shortest embedment length, $l_e$, for this test was 1.02 times the development length, $l_{d,ACI}$, calculated with the ACI/AASHTO expression. Although the maximum moment resisted, $M_{test}$, was slightly less than the calculated moment resistance, the specimen failed in a flexural manner, and no strand end slip was detected. At maximum load, no cracks crossed the strands closer than 22 in (0.56 m) from the end of the transfer length of the strands debonded for 72 in (1.83 m). Web shear cracks opened above the transfer length of these strands, but these cracks did not extend into the bottom flange of the beam. First flexural cracking occurred at a moment equal to 98 percent of the calculated cracking moment.

#### *7.7.3.2 L4B-D-60*

The shortest embedment length, $l_e$, for this test was 0.64 times the development length, $l_{d,ACI}$, calculated with the ACI/AASHTO expression. The embedment length of the strands debonded 36 in (0.91 m) was $1.05l_{d,ACI}$. The beam failed in a flexural manner, but both pairs of debonded strands slipped prior to achieving the maximum moment resistance. The maximum moment resisted was 1 percent greater than the calculated moment resistance of the beam. First flexural cracking occurred at a moment equal to 98 percent of the calculated cracking moment.

The first strands to slip were those with the shortest embedment length. The slip of these strands initiated with the opening of a shear-flexure crack within their transfer length when the moment at the critical section was 77 percent of the calculated failure moment. At the crack location, the calculated tensile stress in the bottom fiber was equal to $1.0\sqrt{f'_c}$ ; the principal tensile stress at the junction of the web and bottom flange was equal to $5.3\sqrt{f'_c}$ . Shear at the section was equal to 1.04 times the web shear resistance of the concrete, $V_{cw}$, according to ACI 318-99. As more cracks opened within the transfer length, the end slip of these strands increased gradually to a magnitude of approximately 0.40 in (10 mm) under the maximum load. The transfer length cracking is shown in Figure 7.22.

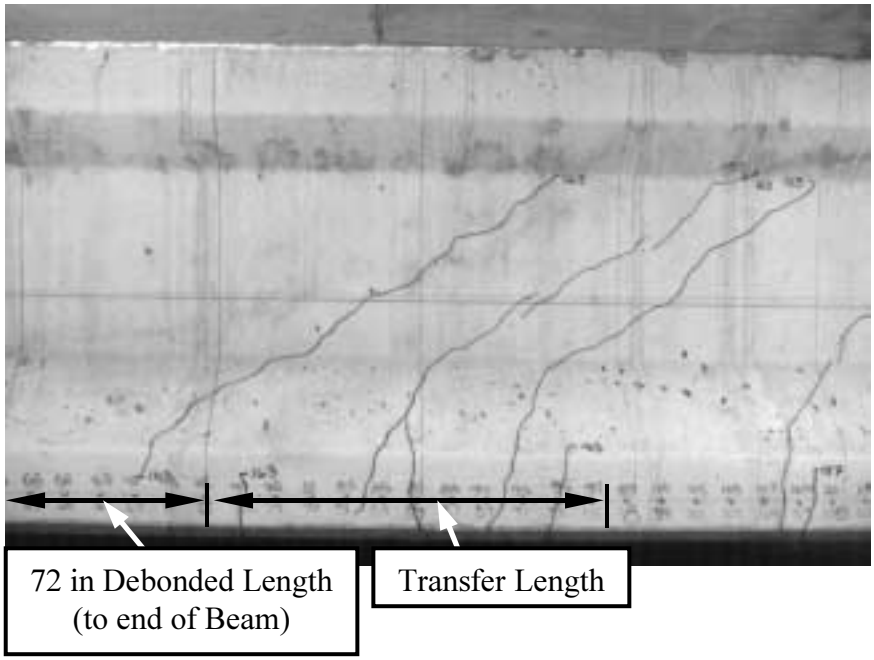


**Figure 7.22: Test L4B-D-60—Shear-Flexure Cracks within Transfer Length of Strands Debonded for 72 in (1.83 m)**

The strands with a debonded length of 36 in (0.91 m) began to slip when two shear-flexure cracks opened within their transfer length. These cracks occurred when the moment at the critical section was equal to the calculated moment strength of the beam. At the crack location, the calculated tensile stress in the bottom fiber was equal to $0.6\sqrt{f_c'}$ ; the principal tensile stress at the junction of the web and bottom flange was equal to $7.2\sqrt{f_c'}$ . Shear at the section was equal to $1.44V_{cw,ACI}$. These strands slipped less than 0.015 in (0.4 mm) prior to flexural failure of the beam.

#### *7.7.3.3 L4B-A-48*

The shortest embedment length, $l_e$, for this test was 0.50 times the development length, $l_{d,ACI}$, calculated with the ACI/AASHTO expression. The embedment length of the strands debonded 36 in (0.91 m) was $0.90l_{d,ACI}$. The beam failed prematurely due to insufficient bond capacity, with end slip occurring in both pairs of debonded strands. The maximum moment resisted was equal to 94 percent of the calculated moment resistance of the beam. First flexural cracking occurred at a moment equal to 94 percent of the calculated cracking moment.

The first strands to slip were those with the shortest embedment length. The slip of these strands initiated with the opening of a shear-flexure crack within their transfer length when the moment at the critical section was 72 percent of the calculated failure moment. At the crack location, the calculated stress in the bottom fiber was equal to 49 psi (0.34 MPa) of *compression*; the principal tensile stress at the junction of the web and bottom flange was equal to $5.1\sqrt{f_c'}$ . Shear at the section was equal to $1.02V_{cw,ACI}$. The end slip of these strands increased gradually to a magnitude of approximately 0.50 in (13 mm) prior to achievement of the maximum load. The beam held this load through an additional deflection of approximately 1 in (25 mm) prior to cessation of testing. At the end of this additional deflection, the total slip of these strands was approximately 0.95 in (24 mm).

The strands with a debonded length of 36 in (0.91 m) began to slip when a shear-flexure crack opened 12 in (305 mm) from their transfer length. This crack occurred when the moment at the critical section was equal to 82 percent of the calculated moment strength of the beam. At the crack location, the calculated tensile stress in the bottom fiber was equal to $5.3\sqrt{f_c'}$ ; the principal tensile stress at the junction of the web and bottom flange was equal to $7.6\sqrt{f_c'}$ . Shear at the section was equal to $1.23V_{cw,ACI}$. These strands slipped gradually up to 0.040 in

(1.0 mm) prior to achievement of the maximum load. At the end of the test, these strands had slipped a total of 0.060 in (1.5 mm).

#### *7.7.3.4 L4B-C-48H*

This specimen was identical to L4B-A-48 except for the presence of horizontal web reinforcement. The shortest embedment length, $l_e$, for this test was 0.50 times the development length, $l_{d,ACI}$, calculated with the ACI/AASHTO expression. The embedment length of the strands debonded 36 in (0.91 m) was $0.90l_{d,ACI}$. This specimen also failed prematurely due to insufficient bond capacity, with end slip occurring in both pairs of debonded strands. The maximum moment resisted was equal to 98 percent of the calculated moment resistance of the beam. First flexural cracking occurred at a moment equal to 96 percent of the calculated cracking moment.

The first strands to slip were those with the shortest embedment length. Just as in Test L4B-A-48, the slip of these strands initiated with the opening of a shear-flexure crack within their transfer length when the moment at the critical section was 72 percent of the calculated failure moment. At the crack location, the calculated tensile stress in the bottom fiber was equal to $2.2\sqrt{f_c'}$ ; the principal tensile stress at the junction of the web and bottom flange was equal to $5.6\sqrt{f_c'}$ . Shear at the section was equal to $1.07V_{cw,ACI}$. The end slip of these strands increased gradually to a magnitude of approximately 0.15 in (3.8 mm) corresponding to a deflection of approximately 2 in (50 mm) and a critical section moment equal to 96 percent of the calculated strength. The strands then slipped an additional 0.15 in (3.8 mm) while the beam deflected approximately 0.4 in (10 mm) without a significant increase in moment resistance. The load then began to increase again with increasing strand slip and beam deflection until the maximum moment was reached at a deflection of 3.8 in (97 mm) and a corresponding strand slip of 0.87 in (22 mm). A very slight decrease in the resisted load occurred over the next 0.2 in (5 mm) of deflection at which point the test was ended. The final strand slip was approximately 0.98 in (25 mm).

The strands with a debonded length of 36 in (0.91 m) began to slip when a shear-flexure crack opened within their transfer length. This crack occurred when the moment at the critical section was equal to 85 percent of the calculated moment strength of the beam. At the crack location, the calculated tensile stress in the bottom fiber was equal to $2.3\sqrt{f_c'}$ ; the principal tensile stress at the junction of the web and bottom flange was equal to $7.1\sqrt{f_c'}$ . Shear at the section was equal to $1.33V_{cw,ACI}$. These strands slipped gradually up to 0.045 in (1.1 mm) prior to achievement of the maximum load and the end of testing. Figure 7.23 depicts the extent of cracking in the anchorage region at the end of the test.

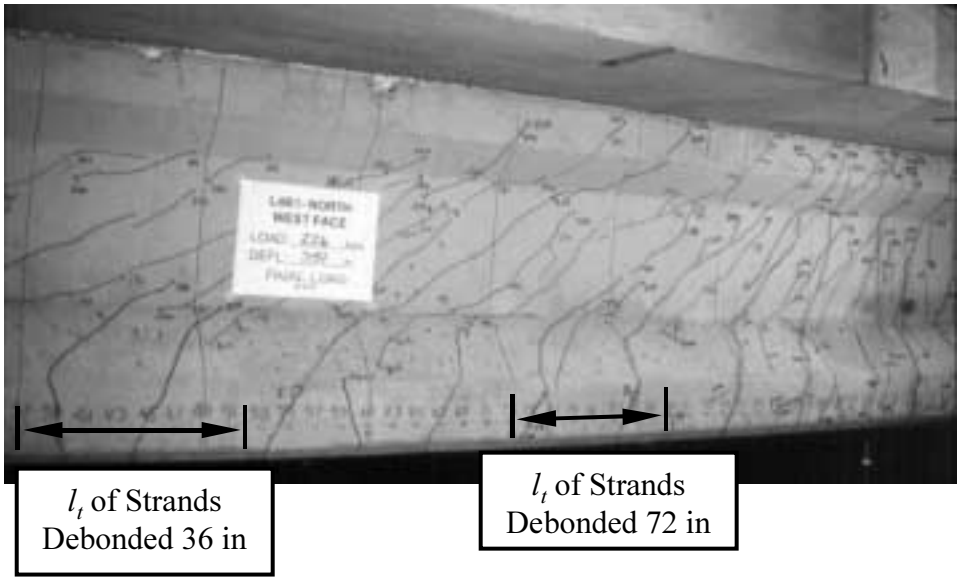


**Figure 7.23: Test L4B-C-48H—Cracking within Strand Transfer Lengths at Final Load**

### *7.7.3.5 Corresponding Texas Tech Tests (L4R Series)*

The L4R pair of beams was tested at Texas Tech (Burkett and Kose 1999). These specimens were designed to be identical to the L4B pair except that they were prestressed with rusted strand. The results of these four development length tests are summarized in Table 7.7.

**Table 7.7: Summary of Texas Tech Development Length Test Results for Specimens with 50% of Bottom Flange Strands Partially Debonded—Rusted Strands (1 in = 25.4 mm)**

| Test I.D. | Debonded Length (in) | $l_e$ (in) | $\frac{l_e}{l_{d,ACI}}$ | Failure Type | Max. Slip (in) |
|---|---|---|---|---|---|
| L4R-114 | 72 | 114 | 1.2 | Flexural | — |
| | 36 | 150 | 1.55 | | — |
| L4R-96 | 72 | 96 | 1.0 | Flexural | — |
| | 36 | 132 | 1.4 | | — |
| L4R-96H | 72 | 96 | 1.0 | Flexural | — |
| | 36 | 132 | 1.4 | | — |
| L4R-60 | 72 | 60 | 0.65 | Bond | >1.0 |
| | 36 | 96 | 1.0 | | — |

The results largely agree with those obtained from the L4B tests conducted at the Ferguson Laboratory. All tests featuring a shortest embedment length, $l_e$, of 96 in (2.44 m) or more failed in a flexural manner with no strand end slip. The only difference between the two groups of tests is that the L4R-60 test failed prematurely due to a lack of bond capacity while the corresponding bright strand test (L4B-D-60) exhibited less strand slip and achieved the calculated moment capacity. In this case, rusted strand performed slightly *worse* than bright strand in terms of anchorage capacity. It is impossible to draw any conclusions regarding the effectiveness of the horizontal web reinforcement from these tests because both L4R-96 and L4R-96H were flexural failures with no strand slip.

### *7.7.3.6 M4B-A-60*

The shortest embedment length, $l_e$, for this test was 0.66 times the development length, $l_{d,ACI}$, calculated with the ACI/AASHTO expression. The embedment length of the strands debonded 36 in (0.91 m) was $1.07 l_{d,ACI}$. The beam failed in a flexural manner, but the pair of strands debonded for 72 in (1.83 m) slipped prior to achieving the maximum moment resistance. The maximum moment resisted was 4 percent greater than the calculated moment resistance of the beam. First flexural cracking occurred at a moment equal to 90 percent of the calculated cracking moment.

Strand end slip initiated with the opening of a shear-flexure crack within the transfer length when the moment at the critical section was 83 percent of the calculated failure moment. Figure 7.24 depicts the extent of the crack immediately after it opened. At the crack location, the calculated *compressive* stress in the bottom fiber was equal to 120 psi = $1.1\sqrt{f_c'}$ ; the principal tensile stress at the junction of the web and bottom flange was equal to 475 psi = $4.6\sqrt{f_c'}$ . Shear at the section was equal to $1.26 V_{cw,ACI}$[2]. The end slip of these strands increased gradually to a magnitude of approximately 0.47 in (12 mm) when the deck concrete crushed at the critical section under the maximum load.

---

[2] According to the provisions of ACI 318-99, the value of $\sqrt{f_c'}$ used in this calculation is limited to 100 psi for values of $f_c'$ greater than 10,000 psi.

The strands with a debonded length of 36 in (0.91 m) did not slip. No cracks crossed these strands closer than 16 in (0.41 m) from the end of the transfer length. Web shear cracking did not extend into the bottom flange in this region. According to uncracked section analysis, the bottom fiber of the beam was not yet in tension within this transfer length at maximum load.

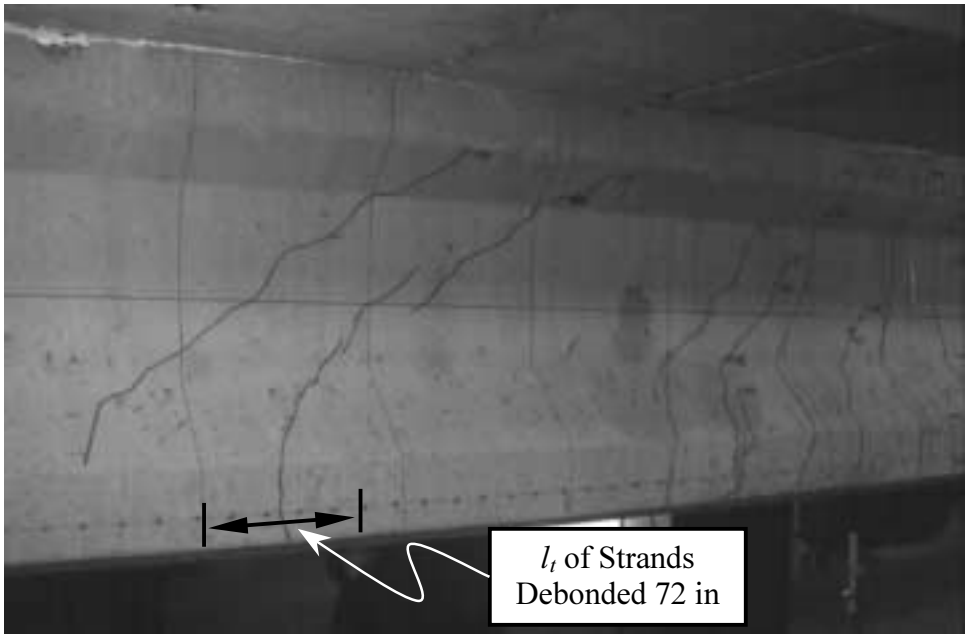


**Figure 7.24: Test M4B-A-60—Shear-Flexure Crack within Transfer Length of Strands Debonded 72 in (1.83 m)**

#### *7.7.3.7 M4B-D-56*

The shortest embedment length, $l_e$, for this test was 0.60 times the development length, $l_{d,ACI}$, calculated with the ACI/AASHTO expression. The embedment length of the strands debonded 36 in (0.91 m) was $1.01 l_{d,ACI}$. The beam failed prematurely due to insufficient bond capacity, with end slip occurring in both pairs of debonded strands. The maximum moment resisted was equal to 97 percent of the calculated moment resistance of the beam. First flexural cracking occurred at a moment equal to 87 percent of the calculated cracking moment.

The first strands to slip were those with the shortest embedment length. The slip of these strands initiated with the opening of two shear-flexure cracks within their transfer length when the moment at the critical section was 77 percent of the calculated failure moment. At the crack location, the calculated stress in the bottom fiber was approximately equal to 110 psi (0.76 MPa) of *compression*; the principal tensile stress at the junction of the web and bottom flange was equal to 455 psi = $4.4\sqrt{f'_c}$ . Shear at the section was equal to $1.22 V_{cw,ACI}$. The end slip of these strands increased gradually to a magnitude of approximately 0.39 in (10 mm) prior to achievement of the maximum load. The beam held this approximate load through an additional deflection of slightly more than 1 in (25 mm) prior to cessation of testing. At the end of this additional deflection, the total slip of these strands was approximately 0.95 in (24 mm).

The strands with a debonded length of 36 in (0.91 m) began to slip when a shear-flexure crack opened within their transfer length. This crack occurred when the moment at the critical section was equal to 91 percent of the calculated moment strength of the beam. At the crack location, the calculated tensile stress in the bottom fiber was equal to 240 psi (1.65 MPa) of *compression*; the principal tensile stress at the junction of the web and bottom flange was equal to 530 psi = $5.1\sqrt{f'_c}$ . Shear at the section was equal to $1.54 V_{cw,ACI}$. These strands slipped gradually up to 0.010 in (2.5 mm) prior to achievement of the maximum load and the slip then remained virtually constant until the end of the test.

#### *7.7.3.8 M4B-C-56H*

This specimen was identical to M4B-D-56 except for the presence of horizontal web reinforcement. The shortest embedment length, $l_e$, for this test was 0.60 times the development length, $l_{d,ACI}$, calculated with the ACI/AASHTO expression. The embedment length of the strands debonded 36 in (0.91 m) was $1.01 l_{d,ACI}$. The beam failed in a flexural manner, with end slip occurring in both pairs of debonded strands. The maximum moment resisted was 1 percent greater than the calculated moment resistance of the beam. First flexural cracking occurred at a moment equal to 87 percent of the calculated cracking moment.

The first strands to slip were those with the shortest embedment length. The slip of these strands initiated with the opening of a shear-flexure crack within their transfer length when the moment at the critical section was 74 percent of the calculated failure moment. At the crack location, the calculated stress in the bottom fiber was approximately equal to 15 psi (0.09 MPa) of *compression*; the principal tensile stress at the junction of the web and bottom flange was equal to 475 psi = $4.6\sqrt{f_c'}$. Shear at the section was equal to $1.21 V_{cw,ACI}$. The end slip of these strands increased gradually to a magnitude of approximately 0.75 in (19 mm) prior to achievement of the maximum load at the end of testing.

The strands with a debonded length of 36 in (0.91 m) began to slip when a shear-flexure crack opened within their transfer length. This crack occurred when the moment at the critical section was equal to 86 percent of the calculated moment strength of the beam. At the crack location, the calculated tensile stress in the bottom fiber was equal to 440 psi (3.03 MPa) of *compression*; the principal tensile stress at the junction of the web and bottom flange was equal to 450 psi = $4.4\sqrt{f_c'}$. Shear at the section was equal to $1.44 V_{cw,ACI}$. These strands slipped gradually up to 0.030 in (0.8 mm) prior to the end of testing.

#### *7.7.3.9 M4B-B-48*

The shortest embedment length, $l_e$, for this test was 0.52 times the development length, $l_{d,ACI}$, calculated with the ACI/AASHTO expression. The embedment length of the strands debonded 36 in (0.91 m) was $0.93 l_{d,ACI}$. The beam failed prematurely due to insufficient bond capacity, with end slip occurring in both pairs of debonded strands. The maximum moment resisted was equal to 96 percent of the calculated moment resistance of the beam. First flexural cracking occurred at a moment equal to 86 percent of the calculated cracking moment.

The first strands to slip were those with the shortest embedment length. The slip of these strands initiated with the opening of a shear-flexure crack within their transfer length when the moment at the critical section was 73 percent of the calculated failure moment. At the crack location, the calculated tensile stress in the bottom fiber was equal to 20 psi (0.14 MPa); the principal tensile stress at the junction of the web and bottom flange was equal to 490 psi = $4.7\sqrt{f_c'}$. Shear at the section was equal to $1.24 V_{cw,ACI}$. The end slip of these strands increased gradually to a magnitude of approximately 0.38 in (10 mm) at a beam deflection of 2.2 in (55 mm) corresponding to a critical section moment equal to 95 percent of the calculated moment capacity. The beam deflected an additional 2.0 in (50 mm) prior to crushing of the concrete deck. During this additional deflection, the moment resisted remained relatively constant as the strands slipped an additional 0.63 in (16 mm). The peak moment corresponded to a cumulative strand slip of 0.73 in (18.5 mm).

The strands with a debonded length of 36 in (0.91 m) began to slip when a shear-flexure crack opened within their transfer length. This crack occurred when the moment at the critical section was equal to 90 percent of the calculated moment strength of the beam. At the crack location, the calculated stress in the bottom fiber was equal to 140 psi (1.0 MPa) of *compression*; the principal tensile stress at the junction of the web and bottom flange was equal to 580 psi = $5.6\sqrt{f_c'}$. Shear at the section was equal to $1.63 V_{cw,ACI}$. These strands slipped gradually up to 0.015 in (1.0 mm) prior to achievement of the maximum load. The slip then remained constant until the end of testing.

#### *7.7.3.10 H4B-D-62*

The shortest embedment length, $l_e$, for this test was $0.66 l_{d,ACI}$. The embedment length of the strands debonded 36 in (0.91 m) was $1.05 l_{d,ACI}$. The beam failed in a flexural manner, with end slip occurring in both pairs of debonded strands. The maximum moment resisted was 2 percent greater than the calculated moment resistance of the beam. First flexural cracking occurred at a moment equal to 95 percent of the calculated cracking moment.

The first strands to slip were those with the shortest embedment length. The slip of these strands initiated with the opening of two shear-flexure cracks within their transfer length when the moment at the critical section was 88 percent of the calculated failure moment. These cracks are shown in Figure 7.25. At the crack location, the calculated tensile stress in the bottom fiber was approximately equal to 160 psi = $1.5\sqrt{f'_c}$ ; the principal tensile stress at the junction of the web and bottom flange was equal to 560 psi = $5.3\sqrt{f'_c}$ . Shear at the section was equal to $1.43V_{cw,ACI}$. The end slip of these strands increased gradually to a magnitude of approximately 0.25 in (6.4 mm) prior to achievement of the maximum load at a deflection of 4.0 in (100 mm). The beam deflected an additional 1.2 in (30 mm) without a significant loss in capacity prior to the end of the test. At the end of the test, the cumulative strand slip was 0.70 in (17.8 mm).

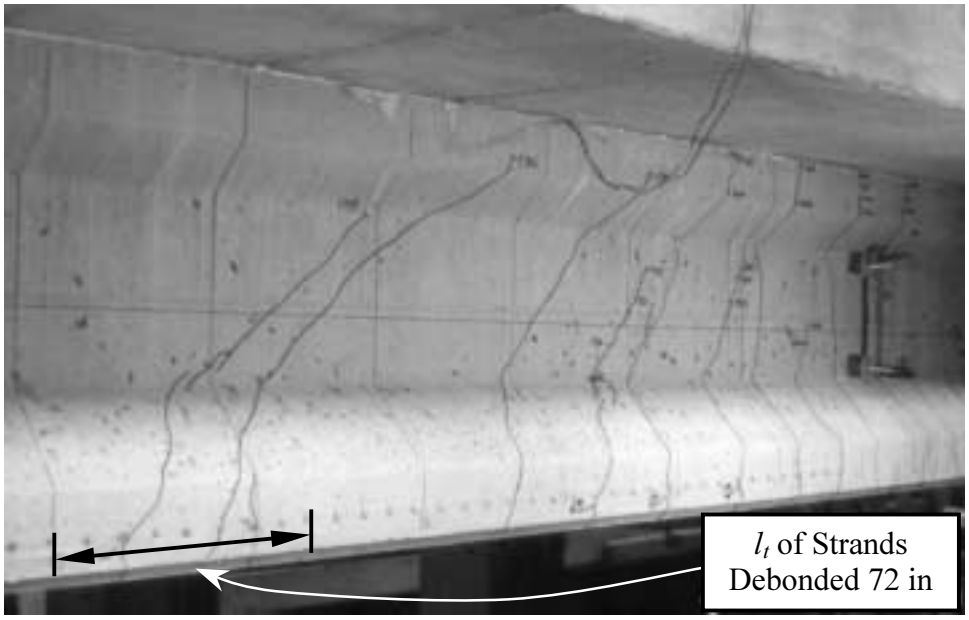


**Figure 7.25: Test H4B-D-62—Shear-Flexure Cracking within Transfer Length of Strands Debonded for 72 in (1.83 m)**

The strands with a debonded length of 36 in (0.91 m) began to slip when a shear-flexure crack opened within their transfer length. This crack occurred when the moment at the critical section was equal to 96 percent of the calculated moment strength of the beam. At the crack location, the calculated tensile stress in the bottom fiber was equal to 245 psi (1.69 MPa) of *compression*; the principal tensile stress at the junction of the web and bottom flange was equal to 525 psi = $5.0\sqrt{f'_c}$ . Shear at the section was equal to $1.65V_{cw,ACI}$. These strands slipped gradually up to 0.010 in (0.3 mm) prior to the end of testing. This shear-flexure crack can be seen at the far right of Figure 7.26, which depicts the extent of cracking at the end of the test (for the beam face opposite that shown in Figure 7.25).

**Figure 7.26: Test H4B-D-62—Extent of Cracking at End of Test**

### *7.7.3.11 H4B-C-62H*

The shortest embedment length, $l_e$, for this test was $0.65l_{d,ACI}$. The embedment length of the strands debonded 36 in (0.91 m) was $1.05l_{d,ACI}$. The beam failed in a flexural manner, with end slip occurring in both pairs of debonded strands. The maximum moment resisted was 6 percent greater than the calculated moment resistance of the beam. First flexural cracking occurred at a moment equal to 96 percent of the calculated cracking moment.

The first strands to slip were those with the shortest embedment length. The slip of these strands initiated with the opening of two shear-flexure cracks within their transfer length when the moment at the critical section was 88 percent of the calculated failure moment. At the crack location, the calculated tensile stress in the bottom fiber was approximately equal to zero; the principal tensile stress at the junction of the web and bottom flange was equal to 525 psi = $4.9\sqrt{f'_c}$. Shear at the section was equal to $1.32V_{cw,ACI}$. The end slip of these strands increased gradually to a magnitude of approximately 0.33 in (8.4 mm) prior to achievement of the maximum load at a deflection of 4.5 in (113 mm). The beam deflected an additional 1.3 in (33 mm) without a significant loss in capacity prior to the end of the test. At the end of the test, the cumulative stand slip was 0.65 in (16.5 mm).

The strands with a debonded length of 36 in (0.91 m) began to slip when a shear-flexure crack opened within their transfer length. This crack occurred when the moment at the critical section was equal to 95 percent of the calculated moment strength of the beam. At the crack location, the calculated tensile stress in the bottom fiber was equal to 175 psi (1.21 MPa) of *compression*; the principal tensile stress at the junction of the web and bottom flange was equal to 535 psi = $5.0\sqrt{f'_c}$. Shear at the section was equal to $1.52V_{cw,ACI}$. These strands slipped gradually up to 0.010 in (0.3 mm) prior to the end of testing.

Despite the additional horizontal web reinforcement present in this specimen, its behavior was very similar to that of H4B-D-62 described above.

### *7.7.3.12 H4B-A-56*

The shortest embedment length, $l_e$, for this test was equal to $0.60l_{d,ACI}$. The embedment length of the strands debonded 36 in (0.91 m) was equal to $1.00l_{d,ACI}$. The beam failed in a flexural manner, with end slip occurring only in the pair of strands debonded for 72 in (1.83 m). The maximum moment resisted was 1 percent greater than the calculated moment resistance of the beam. First flexural cracking occurred at a moment equal to 91 percent of the calculated cracking moment.

Strand end slip initiated with the opening of a shear-flexure crack within the transfer length when the moment at the critical section was 83 percent of the calculated failure moment. At the crack location, the calculated tensile stress

in the bottom fiber was approximately equal to 50 psi = $0.5\sqrt{f'_c}$ ; the principal tensile stress at the junction of the web and bottom flange was equal to 540 psi = $5.1\sqrt{f'_c}$ . Shear at the section was equal to $1.38V_{cw,ACI}$. The end slip of these strands increased gradually to a magnitude of approximately 0.46 in (12 mm) prior to achievement of the load at the end of the test.

The strands with a debonded length of 36 in (0.91 m) did not slip. At the final load, the nearest crack crossing the strands was located 16 in (0.41 m) from the transfer length. According to uncracked section analysis, the bottom fiber of the beam was not yet in tension within this transfer length at maximum load.

#### *7.7.3.13 H4B-B-50*

The shortest embedment length, $l_e$, for this test was equal to $0.54l_{d,ACI}$. The embedment length of the strands debonded 36 in (0.91 m) was equal to $0.94l_{d,ACI}$. The beam failed prematurely due to insufficient bond capacity, with end slip occurring in both pairs of debonded strands. The maximum moment resisted was equal to 99 percent of the calculated moment resistance of the beam. First flexural cracking occurred at a moment equal to 95 percent of the calculated cracking moment.

The first strands to slip were those with the shortest embedment length. The slip of these strands initiated with the opening of two shear-flexure cracks within the transfer length when the moment at the critical section was 82 percent of the calculated failure moment. At the crack location, the calculated tensile stress in the bottom fiber was equal to 70 psi = $0.7\sqrt{f'_c}$ ; the principal tensile stress at the junction of the web and bottom flange was equal to 560 psi = $5.3\sqrt{f'_c}$ . Shear at the section was equal to $1.41V_{cw,ACI}$. The end slip of these strands increased gradually to a magnitude of approximately 0.20 in (5 mm) at a beam deflection of 2.0 in (50 mm) corresponding to a critical section moment equal to 98 percent of the calculated moment capacity. The beam deflected an additional 1.5 in (38 mm) until the test was stopped. During this additional deflection, the moment resisted remained relatively constant as the strands slipped an additional 0.65 in (17 mm). The peak moment corresponded to a cumulative strand slip of 0.40 in (10 mm).

The strands with a debonded length of 36 in (0.91 m) began to slip when a shear-flexure crack opened within their transfer length. This crack occurred when the moment at the critical section was equal to 90 percent of the calculated moment strength of the beam. At the crack location, the calculated stress in the bottom fiber was equal to 300 psi (2.07 MPa) of compression; the principal tensile stress at the junction of the web and bottom flange was equal to 540 psi = $5.1\sqrt{f'_c}$ . Shear at the section was equal to $1.64V_{cw,ACI}$. These strands slipped gradually up to 0.005 in (1.0 mm) prior to achievement of the maximum load plateau. The slip then remained constant until the end of testing.

#### *7.7.3.14 M4R-A-96*

The shortest embedment length, $l_e$, for this test was equal to $1.05l_{d,ACI}$. The maximum moment resisted was 3 percent greater than the calculated moment resistance. The specimen failed in a flexural manner, and no strand end slip was detected. At maximum load, no cracks crossed the strands closer than 29 in (0.74 m) from the end of the transfer length of the strands debonded for 72 in (1.83 m). Although the shear demand at maximum load was as high as $1.28V_{cw,ACI}$, there were no web shear cracks in the anchorage region. First flexural cracking occurred at a moment equal to 97 percent of the calculated cracking moment.

#### *7.7.3.15 M4R-D-90*

The shortest embedment length, $l_e$, for this test was equal to $0.97l_{d,ACI}$. The maximum moment resisted was 1 percent greater than the calculated moment resistance. The specimen failed in a flexural manner, and no strand end slip was detected. At maximum load, no cracks crossed the strands closer than 27 in (0.69 m) from the end of the transfer length of the strands debonded for 72 in (1.83 m). Although the shear demand at maximum load was as high as $1.33V_{cw,ACI}$, there were no web shear cracks in the anchorage region. First flexural cracking occurred at a moment equal to 94 percent of the calculated cracking moment.

#### *7.7.3.16 M4R-C-78H*

The shortest embedment length, $l_e$, for this test was equal to $0.84l_{d,ACI}$. The embedment length of the strands debonded 36 in (0.91 m) was equal to $1.25l_{d,ACI}$. The beam failed in a flexural manner, with end slip occurring only in the pair of strands debonded for 72 in (1.83 m). The maximum moment resisted was 3 percent greater than the calculated moment resistance of the beam. First flexural cracking occurred at a moment equal to 91 percent of the calculated cracking moment.

Strand end slip initiated with the opening of a shear-flexure crack within the transfer length when the moment at the critical section was 99 percent of the calculated failure moment. At the crack location, the calculated tensile stress in the bottom fiber was approximately equal to 335 psi = $3.2\sqrt{f'_c}$ ; the principal tensile stress at the junction of the web and bottom flange was equal to 610 psi = $5.8\sqrt{f'_c}$ . Shear at the section was equal to $1.31V_{cw,ACI}$. The end slip of these strands increased gradually to a magnitude of approximately 0.085 in (2.2 mm) at the maximum load corresponding to crushing of the deck concrete.

The strands with a debonded length of 36 in (0.91 m) did not slip. At the final load, the nearest crack crossing the strands was located 27 in (0.69 m) from the transfer length. According to uncracked section analysis, the bottom fiber of the beam was not yet in tension within this transfer length at maximum load.

#### *7.7.3.17 M4R-B-56*

The shortest embedment length, $l_e$, for this test was equal to $0.61l_{d,ACI}$. The embedment length of the strands debonded 36 in (0.91 m) was equal to $1.03l_{d,ACI}$. The beam failed prematurely due to insufficient bond capacity, with end slip occurring only in the pair of strands debonded for 72 in (1.83 m). The maximum moment resisted was equal to 98 percent of the calculated moment resistance of the beam. First flexural cracking occurred at a moment equal to 96 percent of the calculated cracking moment.

Strand end slip initiated with the opening of two shear-flexure cracks within the transfer length when the moment at the critical section was equal to 84 percent of the calculated failure moment. At the crack location, the calculated tensile stress in the bottom fiber was approximately equal to 205 psi = $2.0\sqrt{f'_c}$ ; the principal tensile stress at the junction of the web and bottom flange was equal to 525 psi = $5.0\sqrt{f'_c}$ . Shear at the section was equal to $1.24V_{cw,ACI}$. The end slip of these strands increased gradually to a magnitude of approximately 0.250 in (6.4 mm) at a beam deflection of 2.45 in (62 mm) corresponding to a critical section moment equal to 98 percent of the calculated moment capacity. The beam deflected an additional 1.55 in (39 mm) until the test was stopped when the deck concrete began to crush. During this additional deflection, the moment resistance remained almost constant as the strands slipped an additional 0.66 in (17 mm).

The pair of strands with a debonded length of 36 in (0.91 m) did not slip. At the final load, the nearest crack crossing the strands was located 8 in (0.20 m) from the transfer length. According to uncracked section analysis, the bottom fiber of the beam was not yet in tension within this transfer length at maximum load.

#### *7.7.3.18 H4R-A-82*

The shortest embedment length, $l_e$, for this test was equal to $0.88l_{d,ACI}$. Although the maximum moment resisted was slightly less than the calculated moment resistance, the specimen failed in a flexural manner, and no strand end slip was detected. At maximum load, no cracks crossed the strands that were debonded for 72 in (1.83 m) closer than 24 in (0.61 m) from the end of the transfer length. Although the shear demand at maximum load was as high as $1.47V_{cw,ACI}$, there were no web shear cracks in the anchorage region. First flexural cracking occurred at a moment equal to 89 percent of the calculated cracking moment.

#### *7.7.3.19 H4R-D-78*

The shortest embedment length, $l_e$, for this test was equal to $0.83l_{d,ACI}$. The maximum moment resisted was equal to the calculated moment resistance, and the specimen failed in a flexural manner. No strand end slip was detected. At maximum load, no cracks crossed the strands that were debonded for 72 in (1.83 m) closer than 22 in (0.56 m) from the end of the transfer length. Although the shear demand at maximum load was as high as $1.51V_{cw,ACI}$, there were

no web shear cracks in the anchorage region. First flexural cracking occurred at a moment equal to 93 percent of the calculated cracking moment.

#### *7.7.3.20 H4R-B-72*

The shortest embedment length, $l_e$, for this test was equal to $0.77l_{d,ACI}$. The embedment length of the strands debonded 36 in (0.91 m) was equal to $1.17l_{d,ACI}$. The beam failed in a flexural manner, with end slip occurring only in the pair of strands debonded for 72 in (1.83 m). The maximum moment resisted was 1 percent less than the calculated moment resistance of the beam. First flexural cracking occurred at a moment equal to 89 percent of the calculated cracking moment.

Strand end slip initiated with the opening of a shear-flexure crack within the transfer length when the moment at the critical section was 95 percent of the calculated failure moment. At the crack location, the calculated tensile stress in the bottom fiber was approximately equal to 175 psi = $1.6\sqrt{f_c'}$ ; the principal tensile stress at the junction of the web and bottom flange was equal to 555 psi = $4.8\sqrt{f_c'}$ . Shear at the section was equal to $1.37V_{cw,ACI}$. The end slip of these strands increased gradually to a magnitude of approximately 0.055 in (1.4 mm) at the maximum load corresponding to crushing of the deck concrete.

The strands with a debonded length of 36 in (0.91 m) did not slip. At the final load, the nearest crack crossing these strands was located 18 in (0.69 m) from the transfer length. According to uncracked section analysis, the bottom fiber of the beam was not yet in tension within this transfer length at maximum load.

#### *7.7.3.21 H4R-C-72H*

The shortest embedment length, $l_e$, for this test was equal to $0.77l_{d,ACI}$. The embedment length of the strands debonded 36 in (0.91 m) was equal to $1.17l_{d,ACI}$. The beam failed in a flexural manner, with end slip occurring only in the pair of strands debonded for 72 in (1.83 m). The maximum moment resisted was 2 percent greater than the calculated moment resistance of the beam. First flexural cracking occurred at a moment equal to 88 percent of the calculated cracking moment.

Strand end slip initiated with the opening of a shear-flexure crack within the transfer length when the moment at the critical section was equal to the calculated failure moment. At the crack location, the calculated tensile stress in the bottom fiber was approximately equal to 225 psi = $2.0\sqrt{f_c'}$ ; the principal tensile stress at the junction of the web and bottom flange was equal to 590 psi = $5.1\sqrt{f_c'}$ . Shear at the section was equal to $1.39V_{cw,ACI}$. The end slip of these strands increased gradually to a magnitude of approximately 0.025 in (1.4 mm) at the maximum load corresponding to crushing of the deck concrete.

The strands with a debonded length of 36 in (0.91 m) did not slip. At the final load, the nearest crack crossing these strands was located 28 in (0.71 m) from the transfer length. According to uncracked section analysis, the bottom fiber of the beam was not yet in tension within this transfer length at maximum load.

#### *7.7.3.22 Summary of Tests Performed on Specimens with 50 Percent of Bottom Flange Strands Partially Debonded*

Specimens in this group exhibited all three types of failures: flexural, flexural with strand slip, and bond. Loss of adequate anchorage strength resulting from inadequate bond only occurred in strands with a bonded embedment length of approximately 0.6 times the ACI development length for fully bonded strands. All strands with embedment lengths greater than $0.61l_{d,ACI}$ exhibited the required anchorage strength to develop the full flexural strength of the beam. For strand with a debonded length of 72 in (1.83 m), general bond slip only occurred when the bonded embedment length was less than $0.85l_{d,ACI}$. For strand with a debonded length of 36 in (0.91 m), general bond slip only occurred when the bonded embedment length was less than or equal to $1.05l_{d,ACI}$. Among strands with bonded embedment lengths between $0.85l_{d,ACI}$ and $1.0l_{d,ACI}$, strands debonded 36 in (0.91 m) exhibited general bond slip, while strands debonded 72 in (1.83 m) did not.

Regardless of performance criterion (prevention of slip or adequate strength), these results indicate that the necessary development length for these specimens is less than or approximately equal to $l_{d,ACI}$ for *fully bonded*

strands. In order to remove the influence of the transfer length portion of the development length, the flexural bond performance of these specimens is illustrated in the next four figures. These graphs are formulated in the same manner described in Section 7.7.1.14 above for Figure 7.20 and Figure 7.21. Figure 7.27 depicts the flexural bond performance of the strands debonded for 72 in (1.83 m) in these specimens relative to the ACI Commentary expression when prevention of general bond slip is the assumed performance criterion. The Commentary expression appears to be a good indicator of the embedment length required to prevent general bond slip of these strands. The graph also indicates that neither strand surface condition nor concrete strength seems to significantly alter the flexural bond length required to prevent general bond slip.

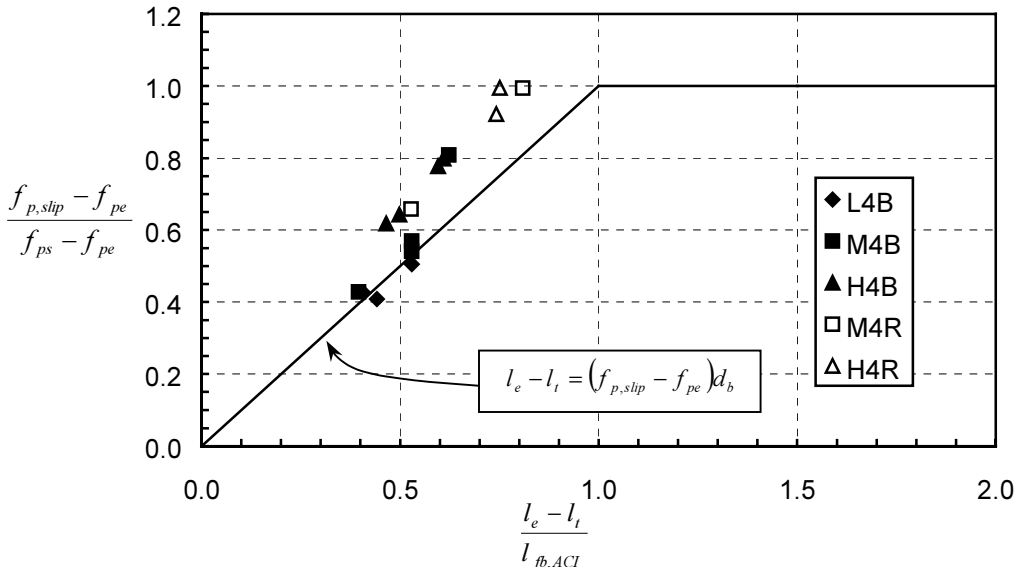


**Figure 7.27: Flexural Bond Performance of Specimens with 50 Percent of Strands Partially Debonded—Normalized Flexural Tendon Stress at Slip vs. Normalized Flexural Bond Length Provided—Strands Debonded 72 in (1.83 m)**

Figure 7.28 shows the flexural bond performance of the strands debonded for 72 in (1.83 m) in these specimens relative to the ACI Commentary expression when adequate anchorage strength is the assumed performance criterion. For these strands, a flexural bond length equal to 75 percent of that calculated from the Commentary expression appears adequate to provide the anchorage strength that will result in a flexural failure mode. It is difficult to draw any conclusions from these data regarding the influence of strand surface condition or concrete strength on the post-slip behavior.

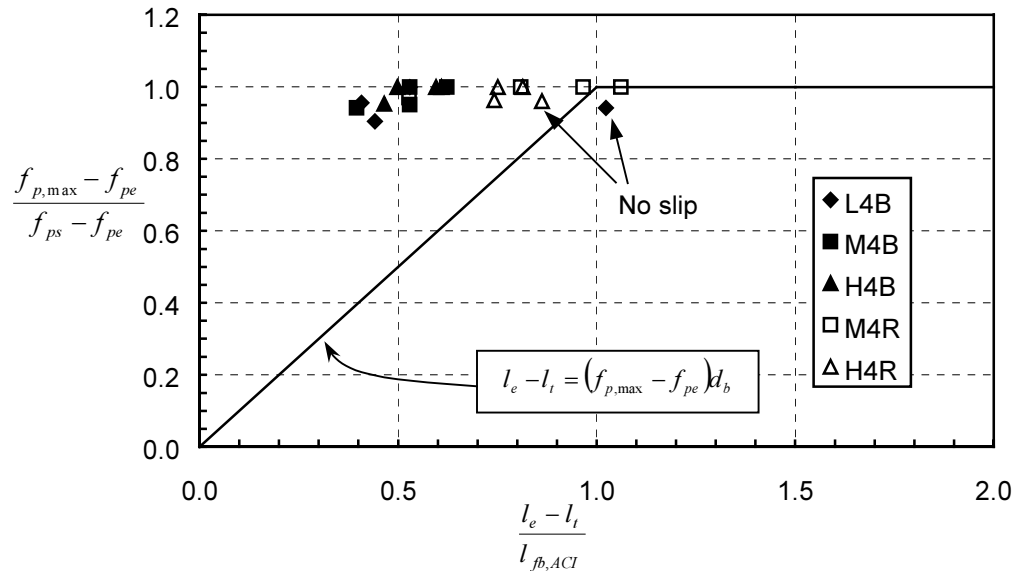


**Figure 7.28: Flexural Bond Performance of Specimens with 50 Percent of Strands Partially Debonded—Normalized Flexural Tendon Stress at Ultimate Strength vs. Normalized Flexural Bond Length Provided—Strands Debonded 72 in (1.83 m)**

Figure 7.29 shows the flexural bond performance of the strands debonded for 36 in (0.91 m) relative to the ACI Commentary expression when prevention of general bond slip is the assumed performance criterion. Once again, the strand surface condition and the concrete strength appear to have little influence on the flexural bond length required to prevent general bond slip. Unlike the 72 in (1.83 m) debonded strands, these strands appear to require a flexural bond length to prevent bond slip greater than that resulting from the ACI Commentary expression. Figure 7.30 indicates that the Commentary expression provides a flexural bond length adequate for development of the full flexural strength for the strands debonded 36 in (0.91 m).

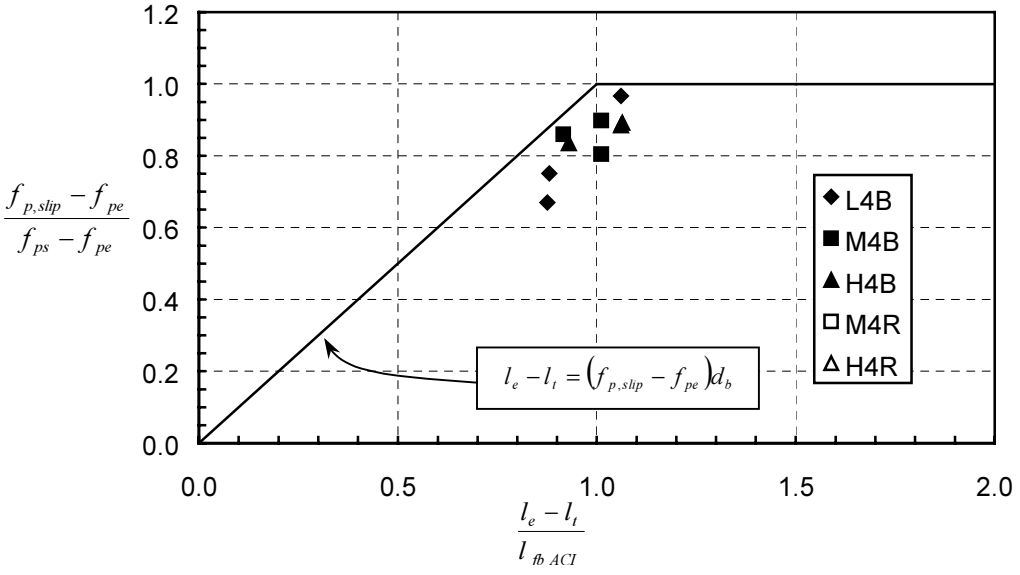


**Figure 7.29: Flexural Bond Performance of Specimens with 50 Percent of Strands Partially Debonded—Normalized Flexural Tendon Stress at Slip vs. Normalized Flexural Bond Length Provided—Strands Debonded 36 in (0.91 m)**

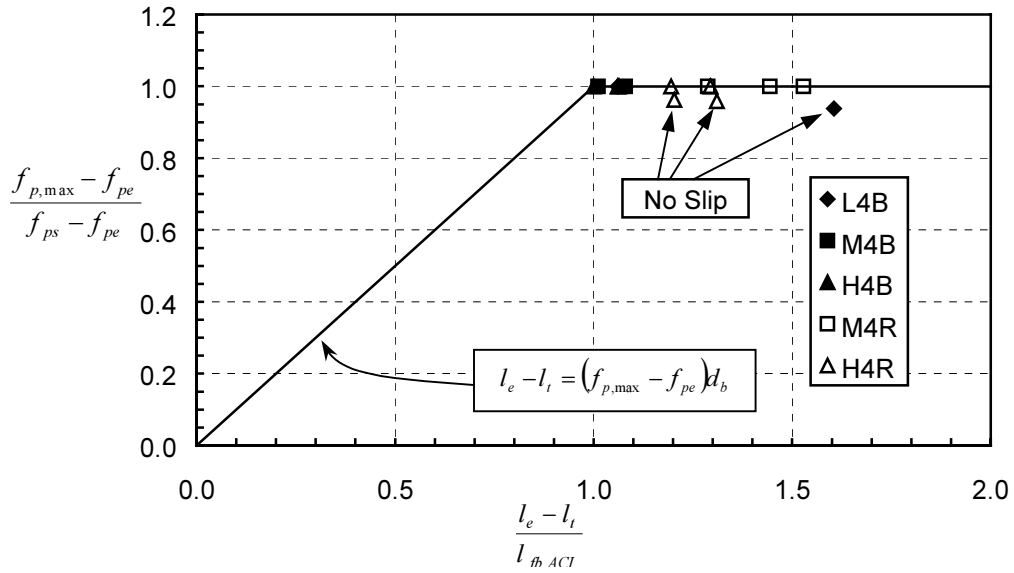


**Figure 7.30: Flexural Bond Performance of Specimens with 50 Percent of Strands Partially Debonded—Normalized Flexural Tendon Stress at Ultimate Strength vs. Normalized Flexural Bond Length Provided—Strands Debonded 36 in (0.91 m)**

In this group of specimens, only a slight improvement in anchorage behavior resulted from the addition of horizontal web reinforcement. Considering the pair of L4B specimens with $l_e$ = 48 in (1.22 m), both exhibited bond failures, but the specimen with horizontal web reinforcement achieved 98 percent of the calculated flexural strength compared to 94 percent for the specimen without the H-bar. Test M4B-D-56 resulted in a bond failure at 97 percent of the flexural capacity while the companion test, M4B-C-56H, resulted in a achievement of the flexural capacity with strand end slip. However, horizontal web reinforcement was ineffective as a means of increasing the resistance to general bond slip in this group of tests.

Because of the larger shear spans that were characteristic of this group of tests, the shear demand was less than that in the tests on fully bonded specimens. In the most shear-critical of these tests, $V_{n,ACI}$ was approximately equal to $1.8V_{max}$ throughout the anchorage region. $V_{n,LRFD}$ was approximately equal to $1.8V_{max}$ near the support, and decreased to $1.4V_{max}$ at the end of the 72 in (1.83 m) debonded length, where the critical strand slip occurred.

### 7.7.4 Specimens with More than 50 Percent of Strands Partially Debonded

The specimens in this group had either 60 percent (L6x specimens) or 75 percent (M9x and H9x specimens) of the total strands debonded. The L6x specimens had only four fully bonded strands out of a total of ten. The M9x and H9x specimens had only three fully bonded strands out of a total of twelve. Three different debonding lengths, 36, 72, and 108 in (0.91, 1.83, and 2.74 m), were used in each specimen. Further details regarding these specimens are recorded in Chapter 3. These girders violated the provisions of the AASHTO LRFD Specification (1998) Article 5.11.4.3 in the following ways:

1. More than 25 percent of the total number of strands were partially debonded.
2. More than 40 percent of the strands in several horizontal rows were partially debonded.
3. The debonding pattern was not symmetric in the M9x and H9x specimens.
4. Exterior strands in several of the rows were partially debonded.

Test results for specimens with bright strands are tabulated in Table 7.8. Test results for specimens with rusted strands are tabulated in Table 7.9. In each of these tables, there are two rows of data corresponding to each test. The first row of the pair contains data pertaining to the pair of strands debonded for 108 in (2.74 m); the second contains data pertaining to the pair of strands debonded for 72 in (1.83 m).

Neither the fully bonded strands or those with a debonded length of 36 in (0.91 m) exhibited significant end slip in these tests. The embedment length of these strands was not less than $1.6l_{d,ACI}$ in any of these tests. Based on the results of the previous groups of tests, no end slip was expected for these strands, nor was it noted in the tests.

**Table 7.8: Development Length Test Results for Specimens with More than 50% of Bottom Flange Strands Partially Debonded—Bright Strands (1 in = 25.4 mm)**

| Test I.D. | Debonded Length (in) | $l_e$ (in) | $\frac{l_e}{l_{d,ACI}}$ | $\frac{M_{test}}{M_{calc}}$ | Failure Type | Max. Slip (in) | $\varepsilon_{max,calc}$ |
|---|---|---|---|---|---|---|---|
| L6B-B-114 | 108 | 114 | 1.21 | 1.00 | Flexural | — | 0.038 |
| | 72 | 150 | 1.61 | | | — | |
| L6B-A-96 | 108 | 96 | 1.03 | 1.06 | Flex. w/ Slip | 0.030 | 0.033 |
| | 72 | 132 | 1.43 | | | 0.030 | |
| L6B-D-84 | 108 | 84 | 0.88 | 0.99 | Flex. w/ Slip | 0.060 | 0.042 |
| | 72 | 120 | 1.27 | | | 0.080 | |
| L6B-C-84H | 108 | 84 | 0.88 | 1.01 | Flex. w/ Slip | 0.075 | 0.042 |
| | 72 | 120 | 1.28 | | | 0.040 | |
| M9B-A-180 | 108 | 180 | 1.99 | 1.01 | Flexural | — | 0.031 |
| | 72 | 216 | 2.47 | | | — | |
| M9B-D-114 | 108 | 114 | 1.25 | 1.01 | Flexural | — | 0.041 |
| | 72 | 150 | 1.66 | | | — | |
| M9B-B-96 | 108 | 96 | 1.05 | 1.00 | Flex. w/ Slip | 0.185 | 0.034 |
| | 72 | 132 | 1.49 | | | 0.075 | |
| M9B-C-96H | 108 | 96 | 1.04 | 1.03 | Flex. w/ Slip | 0.050 | 0.042 |
| | 72 | 132 | 1.46 | | | 0.080 | |
| H9B-A-180 | 108 | 180 | 1.95 | 0.99 | Flexural | — | 0.034 |
| | 72 | 216 | 2.42 | | | — | |
| H9B-D-114 | 108 | 114 | 1.23 | 1.02 | Flexural | — | 0.035 |
| | 72 | 150 | 1.67 | | | — | |
| H9B-B-96 | 108 | 96 | 1.04 | 0.97 | Bond | 0.040 | 0.034 |
| | 72 | 132 | 1.48 | | | 0.150 | |
| H9B-C-96H | 108 | 96 | 1.03 | 1.02 | Flex. w/ Slip | 0.050 | 0.035 |
| | 72 | 132 | 1.47 | | | 0.060 | |

**Table 7.9: Development Length Test Results for Specimens with More than 50% of Bottom Flange Strands Partially Debonded—Rusted Strands (1 in = 25.4 mm)**

| Test I.D. | Debonded Length (in) | $l_e$ (in) | $\frac{l_e}{l_{d,ACI}}$ | $\frac{M_{test}}{M_{calc}}$ | Failure Type | Max. Slip (in) | $\varepsilon_{max,calc}$ |
|---|---|---|---|---|---|---|---|
| M9R-A-180 | 108 | 180 | 1.95 | 0.99 | Flexural | — | 0.030 |
| | 72 | 216 | 2.42 | | | — | |
| M9R-D-114 | 108 | 114 | 1.23 | 1.01 | Flexural | — | 0.032 |
| | 72 | 150 | 1.67 | | | — | |
| M9R-B-96 | 108 | 96 | 1.04 | 1.01 | Flex. w/ Slip | 0.055 | 0.032 |
| | 72 | 132 | 1.48 | | | 0.050 | |
| M9R-C-96H | 108 | 96 | 1.03 | 1.02 | Flex. w/ Slip | 0.045 | 0.033 |
| | 72 | 132 | 1.47 | | | 0.070 | |
| H9R-A-180 | 108 | 180 | 1.92 | 1.00 | Flexural | — | 0.032 |
| | 72 | 216 | 2.39 | | | — | |
| H9R-D-114 | 108 | 114 | 1.23 | 1.01 | Flexural | — | 0.033 |
| | 72 | 150 | 1.67 | | | — | |
| H9R-B-96 | 108 | 96 | 1.02 | 1.01 | Flex. w/ Slip | 0.015 | 0.032 |
| | 72 | 132 | 1.46 | | | 0.160 | |
| H9R-C-96H | 108 | 96 | 1.03 | 1.00 | Flex. w/ Slip | 0.035 | 0.036 |
| | 72 | 132 | 1.46 | | | 0.060 | |

#### *7.7.4.1 L6B-B-114*

The shortest embedment length, $l_e$, for this test was equal to $1.21l_{d,ACI}$ (for the strands with a debonded length of 108 in [2.74 m]). The maximum moment resisted was equal to the calculated moment resistance. The specimen failed in a flexural manner, and no strand end slip was detected. First flexural cracking occurred at a moment 2 percent greater than the calculated cracking moment.

No cracking occurred in the anchorage region of the beam until the moment at the critical section was equal to 93 percent of the calculated moment capacity of the member. At this point, the shear-flexure crack shown in Figure 7.31 opened. This crack crossed through the bottom flange at the point where jacketing ended for the strands debonded 108 in (2.74 m). Therefore, this crack did not exert any anchorage demand on these strands. This crack crossed the strands at a distance of 24 in (0.61 m) from the transfer length of the strands that were jacketed for 72 in (1.83 in). Accordingly, this crack did not result in end slip of either group of debonded strands.

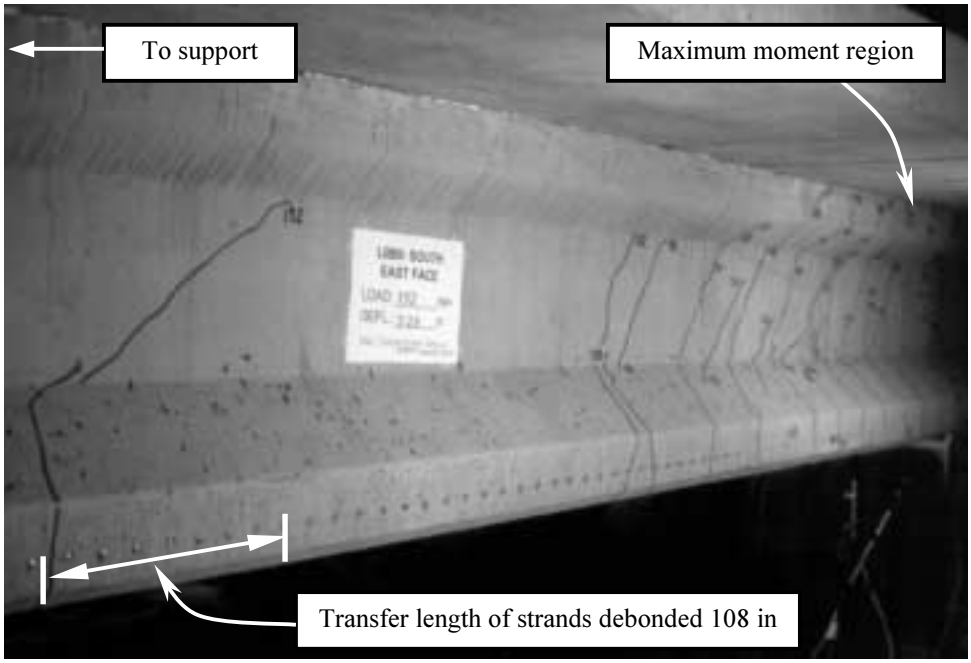


**Figure 7.31: Test L6B-B-114—Crack Passing Across Strands at End of 108 in (2.74 m) Debonded Length**

This crack is particularly noteworthy because of its position relative to the other cracks present at the time it opened. As can be seen in Figure 7.31, the crack opened at a considerable distance from the flexural cracks that were progressing out from the region of maximum moment. The crack opened where it did because of the reduced level of prestress force present at that section. Accordingly, the concrete resistance to flexural and shear cracking was significantly less at this section than at sections closer to the maximum moment region. Just prior to cracking, the tensile stress in the bottom fiber was approximately equal to 415 psi = $5.0\sqrt{f'_c}$. The shear at the section was only equal to $0.78V_{cw,ACI}$. However, the principal tensile stress due to combined flexure and shear at the junction of the web and the bottom flange was equal to 330 psi = $4.0\sqrt{f'_c}$. This level of stress is capable of causing cracking of concrete subjected to a biaxial state of stress.

This type of cracking, which begins at the junction of the web and the bottom flange due to the interaction of flexure and shear, occurred repeatedly in the test specimens of this group. However, resistance to this type of cracking is not explicitly addressed in ACI or AASHTO code provisions. In the formulation of the expression for concrete resistance to web shear cracking, $V_{cw}$, cracking is assumed to initiate due to shear when the principal tensile stress exceeds $4\sqrt{f'_c}$ at the centroid of the composite section (or at the junction of the web and the top flange if the centroid lies within the top flange). In the formulation of the expression for concrete resistance to flexure-shear cracking, $V_{ci}$, cracking is assumed to initiate at the extreme tensile fiber when the tensile stress exceeds $6\sqrt{f'_c}$. Neither of these expressions would have indicated the opening of the shear-flexure crack in this specimen because the critical location in terms of principal tensile stress occurred at the bottom of the web due to shear-moment interaction. Figure 7.32 shows the beam under the final test load.

**Figure 7.32: Test L6B-B-114—Cracks at Final Load**

### *7.7.4.2 L6B-A-96*

The shortest embedment length, $l_e$, for this test was equal to $1.03l_{d,ACI}$. The embedment length of the strands debonded 72 in (1.83 m) was $1.43l_{d,ACI}$. The beam failed in a flexural manner, but both pairs of debonded strands slipped prior to achieving the maximum moment resistance. The maximum moment resisted was 6 percent greater than the calculated moment resistance of the beam. First flexural cracking occurred at a moment equal to 99 percent of the calculated cracking moment.

The first strands to slip were *not* those with the shortest embedment length. The strands that were debonded for 72 in (1.83 m) started to slip with the opening of a shear-flexure crack within their transfer length when the moment at the critical section was equal to 90 percent of the calculated failure moment. At the crack location, the calculated tensile stress in the bottom fiber was equal to 145 psi = $1.7\sqrt{f'_c}$ ; the principal tensile stress at the junction of the web and bottom flange was equal to 295 psi = $3.6\sqrt{f'_c}$ . Shear at the section was equal to $0.84V_{cw,ACI}$,. The end slip of these strands increased gradually to a magnitude of approximately 0.030 in (0.8 mm) under the maximum load.

The strands with a debonded length of 108 in (2.74 m) began to slip when several shear-flexure cracks opened within and near their transfer length. These cracks occurred when the moment at the critical section was equal to 95 percent of the calculated moment strength. At the crack location, the calculated tensile stress in the bottom fiber was equal to 555 psi = $6.7\sqrt{f'_c}$ ; the calculated principal tensile stress at the junction of the web and bottom flange was equal to 410 psi = $4.9\sqrt{f'_c}$ . Shear at the section was equal to $0.85V_{cw,ACI}$. These strands slipped approximately 0.030 in (0.8 mm) prior to flexural failure of the beam.

### *7.7.4.3 L6B-D-84*

The shortest embedment length, $l_e$, for this test was equal to $0.88l_{d,ACI}$. The embedment length of the strands debonded 72 in (1.83 m) was $1.27l_{d,ACI}$. The beam failed in a flexural manner, but both pairs of debonded strands slipped prior to achieving the maximum moment resistance. The maximum moment resisted was 1 percent less than the calculated moment resistance of the beam. First flexural cracking occurred at a moment equal to 96 percent of the calculated cracking moment.

The first strands to slip were those with the shortest embedment length. The strands with a debonded length of 108 in (2.74 m) began to slip when a shear-flexure crack opened within their transfer length. These cracks occurred when the moment at the critical section was equal to 80 percent of the calculated moment strength. At the crack location, the calculated tensile stress in the bottom fiber was equal to 380 psi = $4.6\sqrt{f'_c}$ ; the calculated principal

tensile stress at the junction of the web and bottom flange was equal to 335 psi = 4.1 $\sqrt{f'_c}$ . Shear at the section was equal to 0.77$V_{cw,ACI}$. These strands slipped approximately 0.060 in (1.5 mm) prior to flexural failure of the beam.

The strands that were debonded for 72 in (1.83 m) started to slip with the opening of a shear-flexure crack within their transfer length when the moment at the critical section was equal to 89 percent of the calculated failure moment. At the crack location, the calculated tensile stress in the bottom fiber was equal to 355 psi = 4.3 $\sqrt{f'_c}$ ; the principal tensile stress at the junction of the web and bottom flange was equal to 375 psi = 4.5 $\sqrt{f'_c}$ . Shear at the section was equal to 0.89$V_{cw,ACI}$,. The end slip of these strands increased gradually to a magnitude of approximately 0.080 in (2.0 mm) under the maximum load.

The shear-flexure cracks that initiated the strand slip of the two groups of debonded strands discussed above are shown in Figure 7.33. The cracking pattern of the beam at flexural failure is depicted in Figure 7.34.

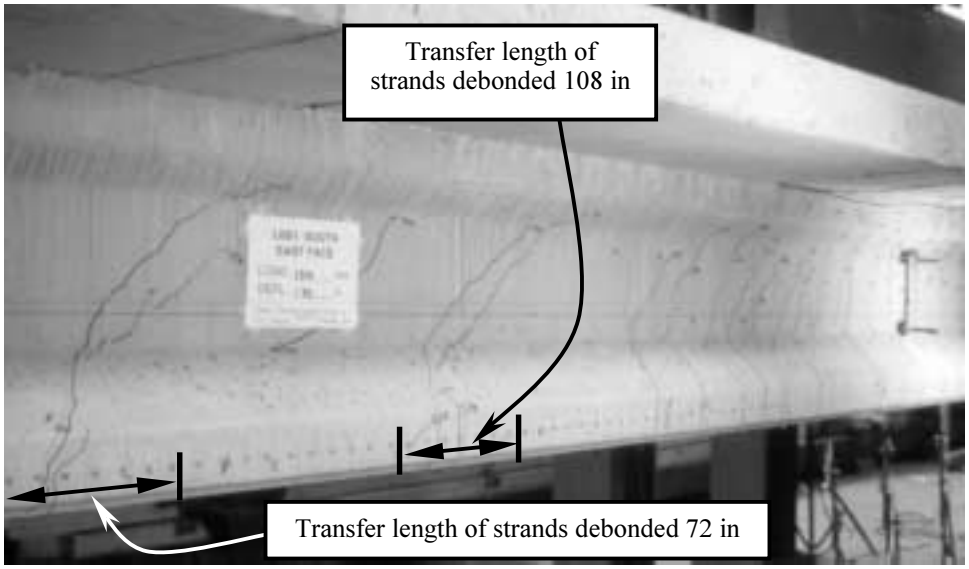


**Figure 7.33: Test L6B-D-84—Shear-Flexure Cracks within Transfer Lengths of Debonded Strands**

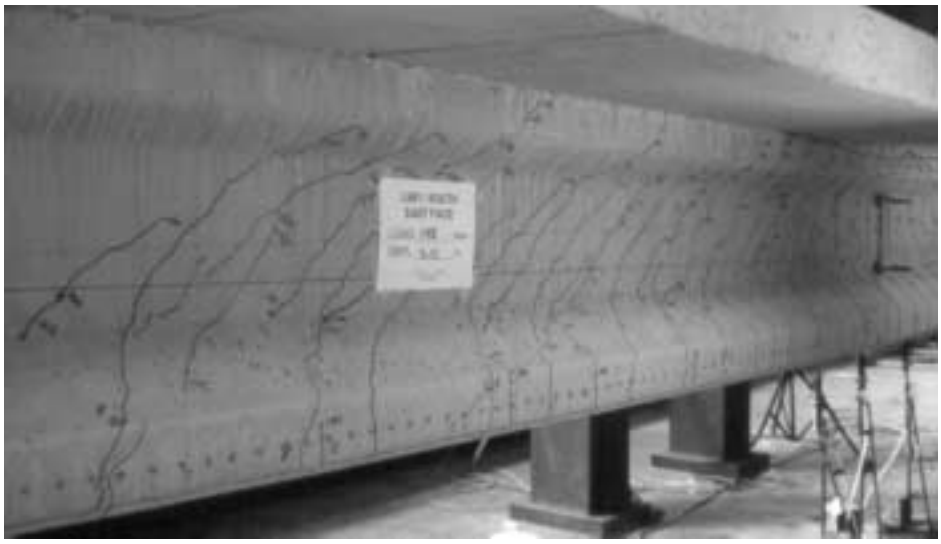

**Figure 7.34: Test L6B-D-84—Cracks at Final Load**

#### *7.7.4.4 L6B-C-84H*

The shortest embedment length, $l_e$, for this test was equal to $0.88l_{d,ACI}$. The embedment length of the strands debonded for 72 in (1.83 m) was $1.28l_{d,ACI}$. The beam failed in a flexural manner, but both pairs of debonded strands slipped prior to achieving the maximum moment resistance. The maximum moment resisted was 1 percent greater than the calculated moment resistance of the beam. First flexural cracking occurred at a moment equal to 97 percent of the calculated cracking moment.

The strands with a debonded length of 108 in (2.74 m) began to slip when a shear-flexure crack opened within their transfer length. These cracks occurred when the moment at the critical section was equal to 81 percent of the calculated moment strength. At the crack location, the calculated tensile stress in the bottom fiber was equal to 300 psi = $3.6\sqrt{f_c'}$; the calculated principal tensile stress at the junction of the web and bottom flange was equal to 310 psi = $3.8\sqrt{f_c'}$. Shear at the section was equal to $0.73V_{cw,ACI}$. These strands slipped approximately 0.075 in (1.9 mm) prior to flexural failure of the beam.

The strands that were debonded for 72 in (1.83 m) also started to slip with the opening of a shear-flexure crack within their transfer length when the moment at the critical section was equal to 81 percent of the calculated failure moment. At the crack location, the calculated tensile stress in the bottom fiber was equal to 265 psi = $3.2\sqrt{f_c'}$; the principal tensile stress at the junction of the web and bottom flange was equal to 315 psi = $3.8\sqrt{f_c'}$. Shear at the section was equal to $0.81V_{cw,ACI}$,. The end slip of these strands increased gradually to a magnitude of approximately 0.040 in (1.0 mm) under the maximum load.

#### *7.7.4.5 Corresponding Texas Tech Tests (L6R Series)*

The L6R pair of beams was tested at Texas Tech (Burkett and Kose 1999). These specimens were designed to be identical to the L6B pair except that they were prestressed with rusted strand. The four development length tests conducted on these specimens corresponded exactly with the four L6B tests described above. The results of the TTU tests matched those of the companion bright strand specimens very closely. The same failure mode was observed for each corresponding test, and strand end slip values were approximately the same. These results indicate no significant difference in the anchorage performance of bright and rusted strands.

#### *7.7.4.6 M9B-A-180*

The shortest embedment length, $l_e$, for this test was equal to $1.99l_{d,ACI}$ (for the strands with a debonded length of 108 in [2.74 m]). The maximum moment resisted was 1 percent greater than the calculated moment resistance. The specimen failed in a flexural manner, and no strand end slip was detected. No crack crossed any strands within 79 in (2.01 m) of the transfer length. First flexural cracking occurred at a moment equal to 99 percent of the calculated cracking moment. In the transfer regions of debonded strands, tensile stresses at the bottom fiber were limited to approximately $3\sqrt{f_c'}$, and principal tensile stresses at the junction of the web and the bottom flange were limited to less than $3\sqrt{f_c'}$ at the maximum load. Figure 7.35 depicts the cracking pattern at the end of the test.

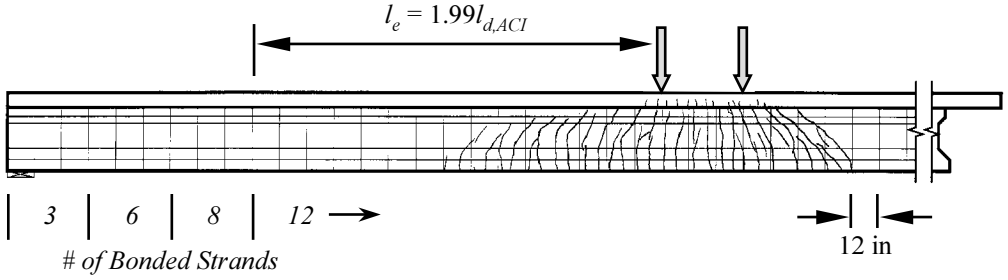


**Figure 7.35: Crack Pattern for Test M9B-A-180 at Flexural Failure**

### *7.7.4.7 M9B-D-114*

This test, along with the other tests in this group featuring a shortest embedment length of 114 in (2.90 m), was fairly similar to Test L6B-B-114. The shortest embedment length was equal to $1.25l_{d,ACI}$ (for the strands with a debonded length of 108 in [2.74 m]). The embedment length of the strands that were debonded for 72 in (1.83 m) was equal to $1.66l_{d,ACI}$. The maximum moment resisted was 1 percent greater than the calculated moment resistance. The specimen failed in a flexural manner, and no strand end slip was detected. First flexural cracking occurred at a moment equal to 99 percent of the calculated cracking moment.

At a load corresponding to a critical section moment equal to 84 percent of the calculated moment capacity, a shear-flexure crack opened at the end of the 108 in (2.74 m) debonded length. This crack was very similar to the crack shown in Figure 7.31 above for Test L6B-B-114. As in that test, the crack did not cross the transfer length of any strands, and there was no accompanying strand slip. When this crack occurred, the calculated tensile stress in the bottom fiber at that location was equal to 615 psi = $5.5\sqrt{f'_c}$ ; the principal tensile stress at the junction of the web and the bottom flange was equal to 415 psi = $3.7\sqrt{f'_c}$ . The shear force was equal to $0.77V_{cw,ACI}$.

Unlike Test L6B-B-114, a similar crack also opened at the end of the 72 in (1.83 m) debonded length at a load corresponding to a critical section moment equal to 91 percent of the calculated moment capacity. This crack also did not cross the transfer length of any strands, and there was no accompanying strand slip. The calculated tensile stress in the bottom fiber at that location was equal to 580 psi = $5.2\sqrt{f'_c}$ ; the principal tensile stress at the junction of the web and the bottom flange was equal to 445 psi = $4.0\sqrt{f'_c}$ . The shear force was equal to $0.86V_{cw,ACI}$.

### *7.7.4.8 M9B-B-96*

The shortest embedment length was equal to $1.05l_{d,ACI}$ (for the strands with a debonded length of 108 in [2.74 m]). The embedment length of the strands that were debonded for 72 in (1.83 m) was equal to $1.49l_{d,ACI}$. The maximum moment resisted was equal to the calculated moment resistance. The specimen failed in a flexural manner, and some strand end slip occurred in the debonded strands. First flexural cracking occurred at a moment 2 percent greater than the calculated cracking moment.

At a load corresponding to a critical section moment equal to 82 percent of the calculated moment capacity, a shear-flexure crack opened at the end of the 108 in (2.74 m) debonded length. The crack did not cross the transfer length of any strands, and there was no accompanying strand slip. When this crack occurred, the calculated tensile stress in the bottom fiber at that location was equal to 735 psi = $6.6\sqrt{f'_c}$ ; the principal tensile stress at the junction of the web and the bottom flange was equal to 460 psi = $4.2\sqrt{f'_c}$ . The shear force was equal to $0.79V_{cw,ACI}$.

A similar crack also opened at the end of the 72 in (1.83 m) debonded length at a load corresponding to a critical section moment equal to 91 percent of the calculated moment capacity. This crack also did not cross the transfer length of any strands, and there was no accompanying strand slip. The calculated tensile stress in the bottom fiber at the initial crack location was equal to 720 psi = $6.5\sqrt{f'_c}$ ; the principal tensile stress at the junction of the web and the bottom flange was equal to 520 psi = $4.7\sqrt{f'_c}$ . The shear force was equal to $0.92V_{cw,ACI}$.

At a load corresponding to a critical section moment equal to 93 percent of the calculated moment capacity, a shear-flexure crack opened within the transfer length of the strands that were debonded for 108 in (2.74 m). These strands then proceeded to slip as much as 0.185 in (4.7 mm) prior to achievement of the peak load. At the initiation of these transfer length cracks, the calculated tensile stress in the bottom fiber at the initial crack location was equal to 430 psi = $3.9\sqrt{f'_c}$ ; the principal tensile stress at the junction of the web and the bottom flange was equal to 435 psi = $3.9\sqrt{f'_c}$ . The shear force was equal to $0.85V_{cw,ACI}$.

At a load corresponding to a critical section moment equal to 96 percent of the calculated moment capacity, a shear-flexure crack opened within the transfer length of the strands that were debonded for 72 in (1.83 m). These strands then proceeded to slip as much as 0.075 in (1.9 mm) prior to achievement of the peak load corresponding to crushing of the deck concrete. At the initiation of these transfer length cracks, the calculated tensile stress in the

bottom fiber at the initial crack location was equal to 525 psi = 4.7 $\sqrt{f_c'}$ ; the principal tensile stress at the junction of the web and the bottom flange was equal to 485 psi = 4.4 $\sqrt{f_c'}$ . The shear force was equal to $0.95V_{cw,ACI}$.

Figure 7.36 depicts the cracking pattern at the end of this test. This pattern of cracking was typical of the other tests in this group with $l_e$ = 96 in (2.44 m).

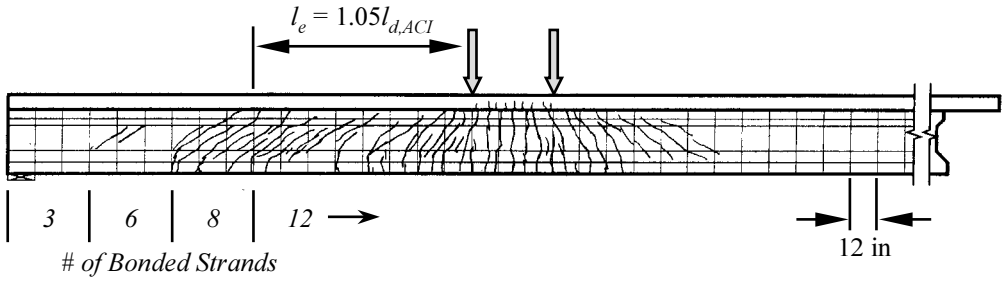


**Figure 7.36: Crack Pattern for Test M9B-B-96 at Flexural Failure with Strand Slip**

### *7.7.4.9 M9B-C-96H*

The shortest embedment length was equal to $1.04l_{d,ACI}$ (for the strands with a debonded length of 108 in [2.74 m]). The embedment length of the strands that were debonded for 72 in (1.83 m) was equal to $1.46l_{d,ACI}$. The maximum moment resisted was 3 percent greater than the calculated moment resistance. The specimen failed in a flexural manner, and some strand end slip occurred in the debonded strands. First flexural cracking occurred at a moment 1 percent less than the calculated cracking moment.

At a load corresponding to a critical section moment equal to 80 percent of the calculated moment capacity, a shear-flexure crack opened at the end of the 108 in (2.74 m) debonded length. The crack did not cross the transfer length of any strands, and there was no accompanying strand slip. When this crack occurred, the calculated tensile stress in the bottom fiber at that location was equal to 700 psi = 6.3 $\sqrt{f_c'}$ ; the principal tensile stress at the junction of the web and the bottom flange was equal to 450 psi = 4.1 $\sqrt{f_c'}$ . The shear force was equal to $0.77V_{cw,ACI}$.

A similar crack also opened at the end of the 72 in (1.83 m) debonded length at a load corresponding to a critical section moment equal to 87 percent of the calculated moment capacity. This crack also did not cross the transfer length of any strands, and there was no accompanying strand slip. The calculated tensile stress in the bottom fiber at the initial crack location was equal to 670 psi = 6.1 $\sqrt{f_c'}$ ; the principal tensile stress at the junction of the web and the bottom flange was equal to 490 psi = 4.4 $\sqrt{f_c'}$ . The shear force was equal to $0.88V_{cw,ACI}$.

At a load corresponding to a critical section moment equal to 94 percent of the calculated moment capacity, a shear-flexure crack opened within 8 in (0.20 m) of the transfer length of the strands that were debonded for 72 in (1.83 m). These strands then proceeded to slip as much as 0.080 in (2.0 mm) prior to achievement of the peak load corresponding to crushing of the deck concrete. At the initiation of these transfer length cracks, the calculated tensile stress in the bottom fiber at the initial crack location was equal to 530 psi = 4.8 $\sqrt{f_c'}$ ; the principal tensile stress at the junction of the web and the bottom flange was equal to 460 psi = 4.1 $\sqrt{f_c'}$ . The shear force was equal to $0.92V_{cw,ACI}$.

At a load corresponding to a critical section moment equal to 96 percent of the calculated moment capacity, a shear-flexure crack opened within the transfer length of the strands that were debonded for 108 in (2.74 m). These strands then proceeded to slip as much as 0.050 in (1.3 mm) prior to achievement of the peak load. At the initiation of these transfer length cracks, the calculated tensile stress in the bottom fiber at the initial crack location was equal to

755 psi = $6.8\sqrt{f_c'}$ ; the principal tensile stress at the junction of the web and the bottom flange was equal to 545 psi = $4.9\sqrt{f_c'}$ . The shear force was equal to $0.90V_{cw,ACI}$.

#### *7.7.4.10 H9B-A-180*

The shortest embedment length, $l_e$, for this test was equal to $1.95l_{d,ACI}$ (for the strands with a debonded length of 108 in [2.74 m]). Although the maximum moment resisted was 1 percent less than the calculated moment resistance, the specimen failed in a flexural manner, and no strand end slip was detected. No crack crossed any strands within 74 in (1.88 m) of the transfer length. First flexural cracking occurred at a moment equal to 94 percent of the calculated cracking moment. In the transfer regions of debonded strands, tensile stresses at the bottom fiber were limited to less than $3\sqrt{f_c'}$ , and principal tensile stresses at the junction of the web and the bottom flange were limited to less than $3\sqrt{f_c'}$ at the maximum load.

#### *7.7.4.11 H9B-D-114*

This specimen behaved very much like M9B-D-114. The shortest embedment length was equal to $1.23l_{d,ACI}$ (for the strands with a debonded length of 108 in [2.74 m]). The embedment length of the strands that were debonded for 72 in (1.83 m) was equal to $1.67l_{d,ACI}$. The maximum moment resisted was 2 percent greater than the calculated moment resistance. The specimen failed in a flexural manner, and no strand end slip was detected. First flexural cracking occurred at a moment equal to 97 percent of the calculated cracking moment.

At a load corresponding to a critical section moment equal to 82 percent of the calculated moment capacity, a shear-flexure crack opened at the end of the 108 in (2.74 m) debonded length. As in previous tests with this embedment length, the crack did not cross the transfer length of any strands, and there was no accompanying strand slip. When this crack occurred, the calculated tensile stress in the bottom fiber at that location was equal to 630 psi = $5.3\sqrt{f_c'}$ ; the principal tensile stress at the junction of the web and the bottom flange was equal to 390 psi = $3.3\sqrt{f_c'}$ . The shear force was equal to $0.71V_{cw,ACI}$.

A similar crack also opened at the end of the 72 in (1.83 m) debonded length at a load corresponding to a critical section moment equal to 92 percent of the calculated moment capacity. This crack also did not cross the transfer length of any strands, and there was no accompanying strand slip. The calculated tensile stress in the bottom fiber at that location was equal to 675 psi = $5.7\sqrt{f_c'}$ ; the principal tensile stress at the junction of the web and the bottom flange was equal to 465 psi = $3.9\sqrt{f_c'}$ . The shear force was equal to $0.83V_{cw,ACI}$. Figure 7.37 depicts these cracks, which are typical of all the M9x and H9x tests with an embedment length of 114 in (2.90 m), at the final test load.

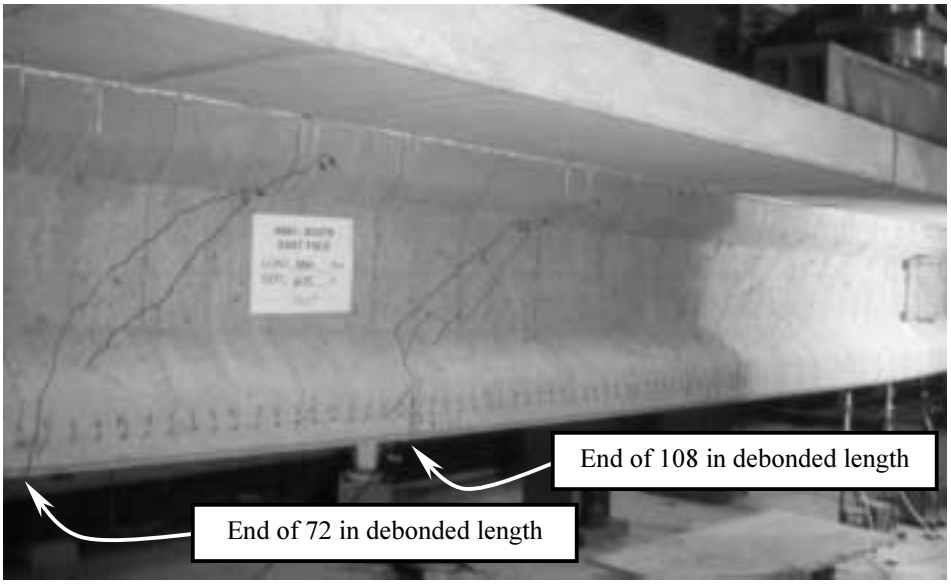


**Figure 7.37: Test H9B-D-114—Cracks at End of Strand Debonded Lengths (at Final Load)**

### *7.7.4.12 H9B-B-96*

The shortest embedment length was equal to $1.04l_{d,ACI}$ (for the strands with a debonded length of 108 in [2.74 m]). The embedment length of the strands that were debonded for 72 in (1.83 m) was equal to $1.48l_{d,ACI}$. The maximum moment resisted was equal to 97 percent of the calculated moment resistance. The specimen failed due to a loss of bond capacity. First flexural cracking occurred at a moment approximately equal to the calculated cracking moment.

At a load corresponding to a moment at the critical section equal to 75 percent of the calculated moment capacity, a shear-flexure crack opened at the end of the 108 in (2.74 m) debonded length. The crack did not cross the transfer length of any strands, and there was no accompanying strand slip. When this crack occurred, the calculated tensile stress in the bottom fiber at that location was equal to 610 psi = $5.2\sqrt{f_c'}$ ; the principal tensile stress at the junction of the web and the bottom flange was equal to 390 psi = $3.3\sqrt{f_c'}$ . The shear force was equal to $0.69V_{cw,ACI}$.

At a load corresponding to a moment at the critical section equal to 81 percent of the calculated moment capacity, a shear-flexure crack opened within the transfer length of the strands that were debonded for 72 in (1.83 m). Slip of these strands initiated with this crack. When this crack occurred, the calculated tensile stress in the bottom fiber at that location was equal to 610 psi = $5.2\sqrt{f_c'}$ ; the principal tensile stress at the junction of the web and the bottom flange was equal to 410 psi = $3.5\sqrt{f_c'}$ . The shear force was equal to $0.79V_{cw,ACI}$. The resulting slip increased gradually with increasing load resistance up to a magnitude of 0.150 in (3.8 mm) when the maximum load was reached (97 percent of the calculated beam capacity). At this point, two more cracks opened within the transfer length, and this pair of strands began to slip very rapidly. The load resisted by the beam decreased immediately, and further application of deflection to the beam resulted in a larger reduction in resistance as the slip continued to increase. The maximum strain at the extreme compression fiber was less than two-thirds of the typical value at which crushing of the deck occurred in tests that failed in a flexural manner. Thus, the maximum resistance of the beam was controlled by the bond capacity of the strands rather than the deformation capacity of the deck concrete as it would have been in a flexural failure.

The strands debonded for 108 in (2.74 m) began to slip when a shear-flexure crack opened within their transfer length at a load corresponding to a moment at the critical section equal to 92 percent of the calculated moment capacity. When this crack occurred, the calculated tensile stress in the bottom fiber at that location was equal to 600 psi = $5.1\sqrt{f_c'}$ ; the principal tensile stress at the junction of the web and the bottom flange was equal to 445 psi

= 3.8$\sqrt{f_c'}$ . The shear force was equal to 0.83$V_{cw,ACI}$. These strands slipped up to 0.040in (1.0 mm) prior to the maximum load, which corresponded to the sudden slip of the strands debonded for 72 in (1.83m).

#### *7.7.4.13 H9B-C-96H*

The shortest embedment length was equal to 1.03$l_{d,ACI}$ (for the strands with a debonded length of 108 in [2.74 m]). The embedment length of the strands that were debonded for 72 in (1.83 m) was equal to 1.47$l_{d,ACI}$. The maximum moment resisted was 2 percent higher than the calculated moment resistance. The specimen failed in a flexural manner, and some strand end slip occurred in the debonded strands. First flexural cracking occurred at a moment approximately equal to the calculated cracking moment.

At a load corresponding to a critical section moment equal to 77 percent of the calculated moment capacity, a shear-flexure crack opened at the end of the 108 in (2.74 m) debonded length. The crack did not cross the transfer length of any strands, and there was no accompanying strand slip. When this crack occurred, the calculated tensile stress in the bottom fiber at that location was equal to 710 psi = 6.1$\sqrt{f_c'}$ ; the principal tensile stress at the junction of the web and the bottom flange was equal to 425 psi = 3.6$\sqrt{f_c'}$ . The shear force was equal to 0.71$V_{cw,ACI}$.

A similar crack also opened at the end of the 72 in (1.83 m) debonded length at a load corresponding to a critical section moment equal to 80 percent of the calculated moment capacity. This crack also did not cross the transfer length of any strands, and there was no accompanying strand slip. The calculated tensile stress in the bottom fiber at the initial crack location was equal to 620 psi = 5.3$\sqrt{f_c'}$ ; the principal tensile stress at the junction of the web and the bottom flange was equal to 420 psi = 3.6$\sqrt{f_c'}$ . The shear force was equal to 0.77$V_{cw,ACI}$.

At a load corresponding to a critical section moment equal to 92 percent of the calculated moment capacity, a shear-flexure crack opened within 2 in (50 mm) of the end of the transfer length of the strands that were debonded for 72 in (1.83 m). These strands then proceeded to slip as much as 0.060 in (1.5 mm) prior to achievement of the peak load corresponding to crushing of the deck concrete. At the initiation of these transfer length cracks, the calculated tensile stress in the bottom fiber at the initial crack location was equal to 520 psi = 4.4$\sqrt{f_c'}$ ; the principal tensile stress at the junction of the web and the bottom flange was equal to 435 psi = 3.7$\sqrt{f_c'}$ . The shear force was equal to 0.86$V_{cw,ACI}$.

At a load corresponding to a critical section moment equal to 96 percent of the calculated moment capacity, a shear-flexure crack opened within the transfer length of the strands that were debonded for 108 in (2.74 m). These strands then proceeded to slip as much as 0.050 in (1.3 mm) prior to achievement of the peak load. At the initiation of these transfer length cracks, the calculated tensile stress in the bottom fiber at the initial crack location was equal to 590 psi = 5.0$\sqrt{f_c'}$ ; the principal tensile stress at the junction of the web and the bottom flange was equal to 450 psi = 3.8$\sqrt{f_c'}$ . The shear force was equal to 0.83$V_{cw,ACI}$.

#### *7.7.4.14 M9R-A-180*

The shortest embedment length for this test was equal to 1.95$l_{d,ACI}$ (for the strands with a debonded length of 108 in [2.74 m]). Although the maximum moment resisted was 1 percent less than the calculated moment resistance, the specimen failed in a flexural manner, and no strand end slip was detected. No crack crossed any strands within 92 in (2.01 m) of the transfer length. First flexural cracking occurred at a moment equal to 99 percent of the calculated cracking moment. In the transfer regions of debonded strands, tensile stresses at the bottom fiber were limited to approximately 3.5$\sqrt{f_c'}$ , and principal tensile stresses at the junction of the web and the bottom flange were limited to less than 3$\sqrt{f_c'}$ at the maximum load.

#### *7.7.4.15 M9R-D-114*

This specimen behaved very much like M9B-D-114 and H9B-D-114. The shortest embedment length was equal to $1.23l_{d,ACI}$ (for the strands with a debonded length of 108 in [2.74 m]). The embedment length of the strands that were debonded for 72 in (1.83 m) was equal to $1.67l_{d,ACI}$. The maximum moment resisted was 1 percent greater than the calculated moment resistance. The specimen failed in a flexural manner, and no strand end slip was detected. First flexural cracking occurred at a moment equal to the calculated cracking moment.

At a load corresponding to a critical section moment equal to 81 percent of the calculated moment capacity, a shear-flexure crack opened at the end of the 108 in (2.74 m) debonded length. As in previous tests with this embedment length, the crack did not cross the transfer length of any strands, and there was no accompanying strand slip. When this crack occurred, the calculated tensile stress in the bottom fiber at that location was equal to 530 psi = $4.6\sqrt{f'_c}$; the principal tensile stress at the junction of the web and the bottom flange was equal to 365 psi = $3.2\sqrt{f'_c}$. The shear force was equal to $0.71V_{cw,ACI}$.

A similar crack also opened at the end of the 72 in (1.83 m) debonded length at a load corresponding to a critical section moment equal to 97 percent of the calculated moment capacity. This crack also did not cross the transfer length of any strands, and there was no accompanying strand slip. The calculated tensile stress in the bottom fiber at that location was equal to 715 psi = $6.3\sqrt{f'_c}$; the principal tensile stress at the junction of the web and the bottom flange was equal to 500 psi = $4.4\sqrt{f'_c}$. The shear force was equal to $0.80V_{cw,ACI}$.

#### *7.7.4.16 M9R-B-96*

The shortest embedment length was equal to $1.04l_{d,ACI}$ (for the strands with a debonded length of 108 in [2.74 m]). The embedment length of the strands that were debonded for 72 in (1.83 m) was equal to $1.48l_{d,ACI}$. The maximum moment resisted was 1 percent greater than the calculated moment resistance. The specimen failed in a flexural manner, and some strand end slip occurred in the debonded strands. First flexural cracking occurred at a moment 3 percent larger than the calculated cracking moment.

At a load corresponding to a critical section moment equal to 75 percent of the calculated moment capacity, a shear-flexure crack opened within transfer length of the strands that were debonded for 72 in (1.83 m). A small slip of these strands began with the opening of this crack. This strand slip gradually increased to a magnitude of 0.050 in (1.3 mm) at the final load. When this crack occurred, the calculated tensile stress in the bottom fiber at that location was equal to 780 psi = $6.8\sqrt{f'_c}$; the principal tensile stress at the junction of the web and the bottom flange was equal to 615 psi = $5.4\sqrt{f'_c}$. The shear force was equal to $0.88V_{cw,ACI}$.

At a load corresponding to a critical section moment equal to 83 percent of the calculated moment capacity, a shear-flexure crack opened at the end of the 108 in (2.74 m) debonded length. The crack did not cross the transfer length of any strands, and there was no accompanying strand slip. When this crack occurred, the calculated tensile stress in the bottom fiber at that location was equal to 785 psi = $6.9\sqrt{f'_c}$; the principal tensile stress at the junction of the web and the bottom flange was equal to 480 psi = $4.2\sqrt{f'_c}$. The shear force was equal to $0.79V_{cw,ACI}$.

A similar crack also opened at the end of the 72 in (1.83 m) debonded length at a load corresponding to a critical section moment equal to 99 percent of the calculated moment capacity. This crack also did not cross the transfer length of any strands, and there was no accompanying strand slip. The calculated tensile stress in the bottom fiber at the initial crack location was equal to 875 psi = $7.7\sqrt{f'_c}$; the principal tensile stress at the junction of the web and the bottom flange was equal to 610 psi = $5.3\sqrt{f'_c}$. The shear force was equal to $0.99V_{cw,ACI}$.

At a load corresponding to a critical section moment equal to 98 percent of the calculated moment capacity, a shear-flexure crack opened within the transfer length of the strands that were debonded for 108 in (2.74 m). These strands then proceeded to slip as much as 0.055 in (1.4 mm) prior to achievement of the peak load. At the initiation of these transfer length cracks, the calculated tensile stress in the bottom fiber at the initial crack location was equal to

465 psi = 4.1 $\sqrt{f_c'}$ ; the principal tensile stress at the junction of the web and the bottom flange was equal to 460 psi = 4.0 $\sqrt{f_c'}$ . The shear force was equal to 0.93$V_{cw,ACI}$.

### *7.7.4.17 M9R-C-96H*

The shortest embedment length was equal to 1.04$l_{d,ACI}$ (for the strands with a debonded length of 108 in [2.74 m]). The embedment length of the strands that were debonded for 72 in (1.83 m) was equal to 1.48$l_{d,ACI}$. The maximum moment resisted was 2 percent greater than the calculated moment resistance. The specimen failed in a flexural manner, and some strand end slip occurred in the debonded strands. First flexural cracking occurred at a moment approximately equal to the calculated cracking moment.

At a load corresponding to a critical section moment equal to 78 percent of the calculated moment capacity, a shear-flexure crack opened at the end of the 108 in (2.74 m) debonded length. The crack did not cross the transfer length of any strands, and there was no accompanying strand slip. When this crack occurred, the calculated tensile stress in the bottom fiber at that location was equal to 720 psi = 6.3 $\sqrt{f_c'}$ ; the principal tensile stress at the junction of the web and the bottom flange was equal to 440 psi = 3.8 $\sqrt{f_c'}$ . The shear force was equal to 0.76$V_{cw,ACI}$.

A similar crack also opened at the end of the 72 in (1.83 m) debonded length at a load corresponding to a critical section moment equal to 83 percent of the calculated moment capacity. This crack also did not cross the transfer length of any strands, and there was no accompanying strand slip. The calculated tensile stress in the bottom fiber at the initial crack location was equal to 620 psi = 5.4 $\sqrt{f_c'}$ ; the principal tensile stress at the junction of the web and the bottom flange was equal to 440 psi = 3.8 $\sqrt{f_c'}$ . The shear force was equal to 0.83$V_{cw,ACI}$.

At a load corresponding to a critical section moment equal to 97 percent of the calculated moment capacity, a shear-flexure crack opened within the transfer length of the strands that were debonded for 108 in (2.74 m). These strands then proceeded to slip as much as 0.045 in (1.1 mm) prior to achievement of the peak load. At the initiation of these transfer length cracks, the calculated tensile stress in the bottom fiber at the initial crack location was equal to 810 psi = 7.0 $\sqrt{f_c'}$ ; the principal tensile stress at the junction of the web and the bottom flange was equal to 550 psi = 4.8 $\sqrt{f_c'}$ . The shear force was equal to 0.89$V_{cw,ACI}$.

At a load corresponding to a critical section moment equal to 101 percent of the calculated moment capacity, a shear-flexure crack opened within the transfer length of the strands that were debonded for 72 in (1.83 m). These strands then proceeded to slip as much as 0.070 in (1.8 mm) prior to achievement of the peak load corresponding to crushing of the deck concrete. At the initiation of these transfer length cracks, the calculated tensile stress in the bottom fiber at the initial crack location was equal to 530 psi = 4.7 $\sqrt{f_c'}$ ; the principal tensile stress at the junction of the web and the bottom flange was equal to 510 psi = 4.5 $\sqrt{f_c'}$ . The shear force was equal to 1.00$V_{cw,ACI}$.

### *7.7.4.18 H9R-A-180*

The shortest embedment length, $l_e$, for this test was equal to 1.92$l_{d,ACI}$ (for the strands with a debonded length of 108 in [2.74 m]). The maximum moment resisted was equal to the calculated moment resistance. The specimen failed in a flexural manner, and no strand end slip was detected. No crack crossed any strands within 82 in (2.08 m) of the transfer length. First flexural cracking occurred at a moment equal to 99 percent of the calculated cracking moment. In the transfer regions of debonded strands, tensile stresses at the bottom fiber were limited to approximately $4.5\sqrt{f_c'}$ , and principal tensile stresses at the junction of the web and the bottom flange were limited to less than $3.2\sqrt{f_c'}$ at the maximum load.

#### *7.7.4.19 H9R-D-114*

This specimen behaved very much like M9B-D-114, H9B-D-114, and M9R-D-114. The shortest embedment length was equal to $1.23l_{d,ACI}$ (for the strands with a debonded length of 108 in [2.74 m]). The embedment length of the strands that were debonded for 72 in (1.83 m) was equal to $1.67l_{d,ACI}$. The maximum moment resisted was 1 percent greater than the calculated moment resistance. The specimen failed in a flexural manner, and no strand end slip was detected. First flexural cracking occurred at a moment equal to the calculated cracking moment.

At a load corresponding to a critical section moment equal to 79 percent of the calculated moment capacity, a shear-flexure crack opened at the end of the 108 in (2.74 m) debonded length. As in previous tests with this embedment length, the crack did not cross the transfer length of any strands, and there was no accompanying strand slip. When this crack occurred, the calculated tensile stress in the bottom fiber at that location was equal to 530 psi = $4.4\sqrt{f'_c}$; the principal tensile stress at the junction of the web and the bottom flange was equal to 360 psi = $3.0\sqrt{f'_c}$. The shear force was equal to $0.72V_{cw,ACI}$.

A similar crack also opened at the end of the 72 in (1.83 m) debonded length at a load corresponding to a critical section moment equal to 85 percent of the calculated moment capacity. This crack also did not cross the transfer length of any strands, and there was no accompanying strand slip. The calculated tensile stress in the bottom fiber at that location was equal to 505 psi = $4.2\sqrt{f'_c}$; the principal tensile stress at the junction of the web and the bottom flange was equal to 415 psi = $3.4\sqrt{f'_c}$. The shear force was equal to $0.81V_{cw,ACI}$.

#### *7.7.4.20 H9R-B-96*

The shortest embedment length was equal to $1.02l_{d,ACI}$ (for the strands with a debonded length of 108 in [2.74 m]). The embedment length of the strands that were debonded for 72 in (1.83 m) was equal to $1.46l_{d,ACI}$. The maximum moment resisted was 1 percent greater than the calculated moment resistance. The specimen failed in a flexural manner, and some strand end slip occurred in the debonded strands. First flexural cracking occurred at a moment equal to the calculated cracking moment.

At a load corresponding to a critical section moment equal to 83 percent of the calculated moment capacity, a shear-flexure crack opened at the end of the 108 in (2.74 m) debonded length. The crack did not cross the transfer length of any strands, and there was no accompanying strand slip. When this crack occurred, the calculated tensile stress in the bottom fiber at that location was equal to 815 psi = $7.3\sqrt{f'_c}$; the principal tensile stress at the junction of the web and the bottom flange was equal to 500 psi = $4.5\sqrt{f'_c}$. The shear force was equal to $0.79V_{cw,ACI}$.

A similar crack also opened at the end of the 72 in (1.83 m) debonded length at a load corresponding to a critical section moment equal to 101 percent of the calculated moment capacity. This crack also did not cross the transfer length of any strands, but three more cracks immediately followed which crossed the transfer length of the strands that were debonded for 72 in (18.3 m). The calculated tensile stress in the bottom fiber at the initial crack location was equal to 935 psi = $8.4\sqrt{f'_c}$; the principal tensile stress at the junction of the web and the bottom flange was equal to 635 psi = $5.7\sqrt{f'_c}$. The shear force was equal to $1.00V_{cw,ACI}$. Strand slip of these strands accompanied the opening of these cracks. The strand slip increased with the transfer length cracking up to a magnitude of 0.160 in (4.1 mm) prior to achievement of the maximum load when crushing of the deck concrete occurred.

The strands that were debonded 108 in (2.74 m) may have slipped a small amount (less than 0.015 in [0.4 mm]). Because of the number of cracks that crossed the jacketed portion of these strands, more precise calculation of the true slip values based on values measured at the end of the beam is difficult.

#### *7.7.4.21 H9R-C-96H*

The shortest embedment length was equal to $1.03l_{d,ACI}$ (for the strands with a debonded length of 108 in [2.74 m]). The embedment length of the strands that were debonded for 72 in (1.83 m) was equal to $1.46l_{d,ACI}$. The maximum moment resisted was equal to the calculated moment resistance. The specimen failed in a flexural manner, and

some strand end slip occurred in the debonded strands. First flexural cracking occurred at a moment approximately equal to the calculated cracking moment.

At a load corresponding to a critical section moment equal to 75 percent of the calculated moment capacity, a shear-flexure crack opened at the end of the 108 in (2.74 m) debonded length. The crack, which is shown in Figure 7.38, did not cross the transfer length of any strands, and there was no accompanying strand slip. When this crack occurred, the calculated tensile stress in the bottom fiber at that location was equal to 630 psi = $5.2\sqrt{f_c'}$ ; the principal tensile stress at the junction of the web and the bottom flange was equal to 400 psi = $3.3\sqrt{f_c'}$ . The shear force was equal to $0.72V_{cw,ACI}$.

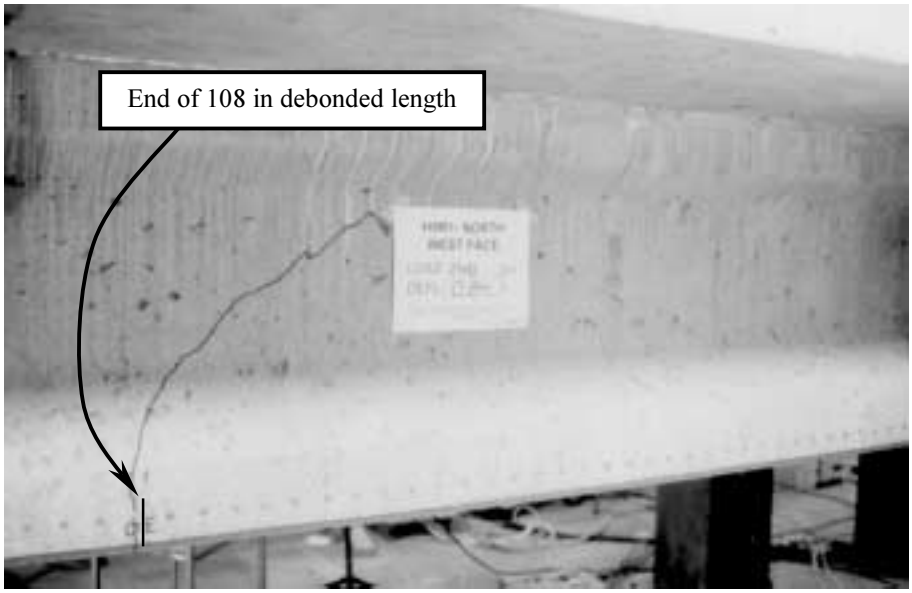


**Figure 7.38: Test H9R-C-96H—Crack at End of 108 in (2.74 m) Debonded Length**

A similar crack also opened at the end of the 72 in (1.83 m) debonded length at a load corresponding to a critical section moment equal to 84 percent of the calculated moment capacity. This crack also did not cross the transfer length of any strands, and there was no accompanying strand slip. The calculated tensile stress in the bottom fiber at the initial crack location was equal to 660 psi = $5.4\sqrt{f_c'}$ ; the principal tensile stress at the junction of the web and the bottom flange was equal to 470 psi = $3.9\sqrt{f_c'}$ . The shear force was equal to $0.84V_{cw,ACI}$. Both this crack and the crack at the end of the 108 in (2.74 m) debonded length are shown in Figure 7.39. Note how isolated they are from the region of flexural cracking in the constant moment portion of the beam. This illustration indicates how the reduction in effective prestress force that results from strand debonding can significantly reduce cracking resistance.

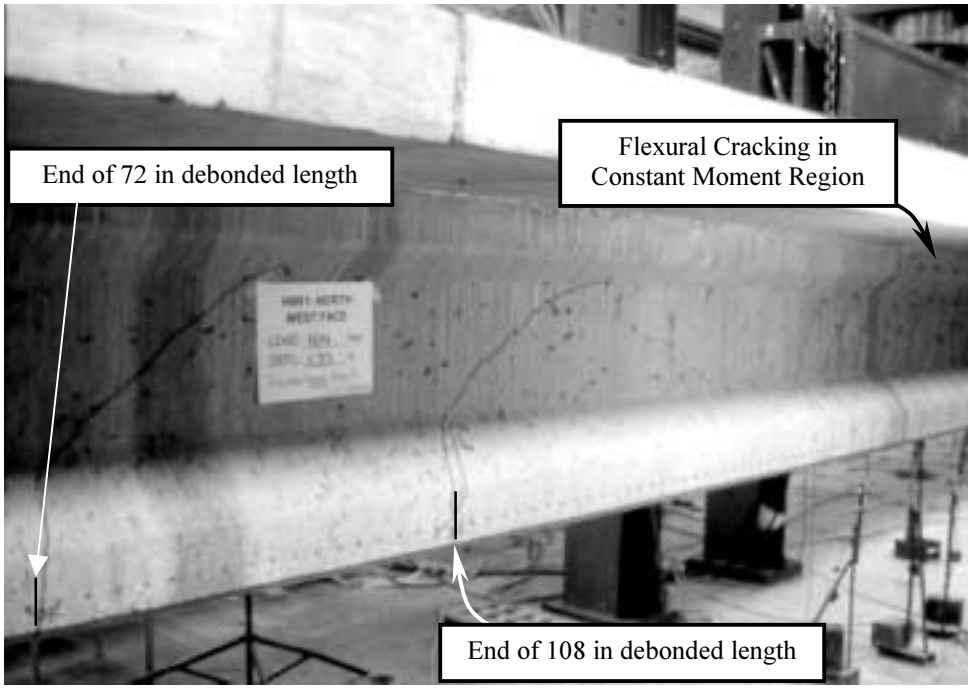


**Figure 7.39: Test H9R-C-96H—Cracks at Ends of 72 (1.83 m) and 108 in (2.74 m) Debonded Lengths**

At a load corresponding to a critical section moment equal to 99 percent of the calculated moment capacity, shear-flexure cracking began within the transfer length of the strands that were debonded for 72 in (1.83 m). These strands began to slip and three cracks rapidly formed in this transfer region. These strands slipped as much as 0.060 in (1.5 mm) prior to achievement of the peak load corresponding to crushing of the deck concrete. At the initiation of these transfer length cracks, the calculated tensile stress in the bottom fiber at the initial crack location was equal to 600 psi = $4.9\sqrt{f_c'}$ ; the principal tensile stress at the junction of the web and the bottom flange was equal to 515 psi = $4.2\sqrt{f_c'}$ . The shear force was equal to $0.96V_{cw,ACI}$.

Immediately after the opening of these cracks and the accompanying strand slip, a crack opened within the transfer length of the strands that were debonded for 108 in (2.74 m). These strands also began to slip. The total slip in these strands was approximately 0.035 in (0.9 mm) at the achievement of the maximum load.

The cracking pattern at the end of the test is depicted in Figure 7.40. The general progression of cracking and strand slip described here was typical of all the specimens in this group featuring embedment lengths of 96 in (2.44 m) or less.

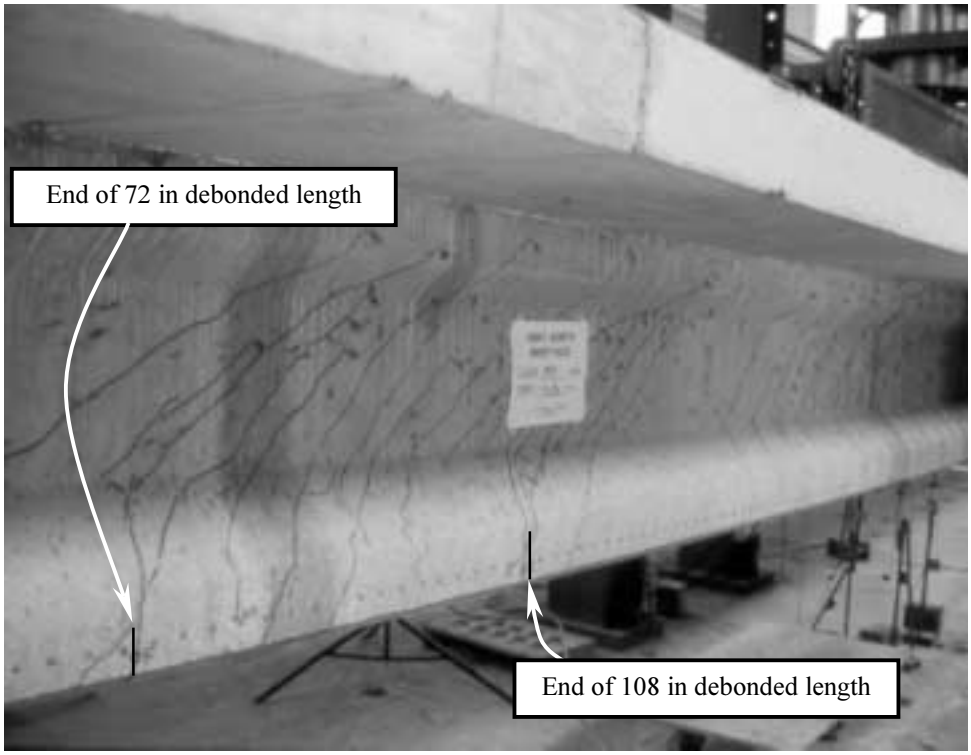


**Figure 7.40: Test H9R-C-96H—Cracks at Final Load (Flexural Failure with Strand Slip)**

#### *7.7.4.22 Summary of Tests Performed on Specimens with More than 50 Percent of Strands Partially Debonded*

As for the previous group of tests, the anchorage behavior of the strands varied according to the debonded length. For strand with a debonded length of 108 in (2.74 m), anchorage strength was adequate in all of the tests. For strand with a debonded length of 72 in (1.83 m), anchorage strength was adequate in all tests except one, which featured an embedment length equal to approximately $1.5l_{d,ACI}$. Other specimens with embedment lengths as short as $1.3l_{d,ACI}$ resulted in flexural failures however.

For strand with a debonded length of 108 in (2.74 m), general bond slip only occurred for strand with bonded embedment lengths less than or equal to $1.05l_{d,ACI}$. For strand with a debonded length of 72 in (1.83 m), general bond slip occurred for embedment lengths up to $1.5l_{d,ACI}$. Among strands with bonded embedment lengths between $1.05l_{d,ACI}$ and $1.5l_{d,ACI}$, strands debonded 72 in (0.91 m) exhibited general bond slip, while strands debonded 108 in (2.74 m) did not.

Figure 7.41 depicts the flexural bond performance of the strands debonded for 96 in (2.74 m) relative to the ACI Commentary expression for fully bonded strands when prevention of general bond slip is the performance criterion. The Commentary expression appears to be slightly unconservative when used to predict the flexural bond length required to prevent general bond slip of these strands. Strand surface condition and concrete strength appear to have no significant influence on the required flexural bond length.

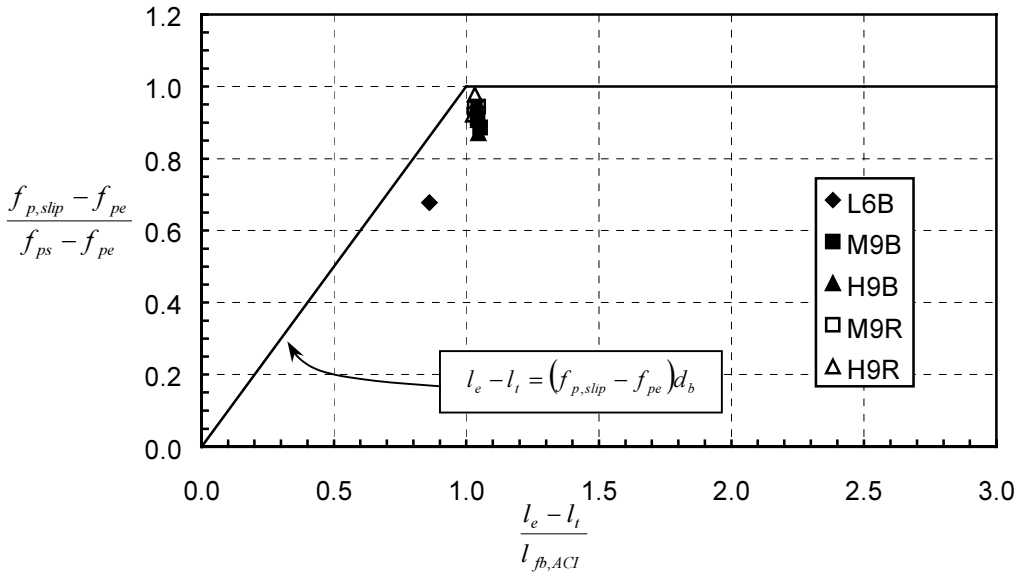


**Figure 7.41: Flexural Bond Performance of Specimens with More than 50 Percent of Strands Partially Debonded—Normalized Flexural Tendon Stress at Slip vs. Normalized Flexural Bond Length Provided—Strands Debonded 108 in (2.74 m)**

Figure 7.42 depicts the flexural bond performance of the strands debonded for 108 in (2.74 m) relative to the ACI Commentary expression when adequate anchorage strength is the performance criterion. Because no bond failure of these strands occurred in this group of tests, the flexural bond length calculated from the Commentary expression appears adequate to provide the necessary anchorage strength for a flexural failure mode. No conclusions can be drawn from these data regarding the influence of either strand surface condition or concrete strength on the post-slip behavior.

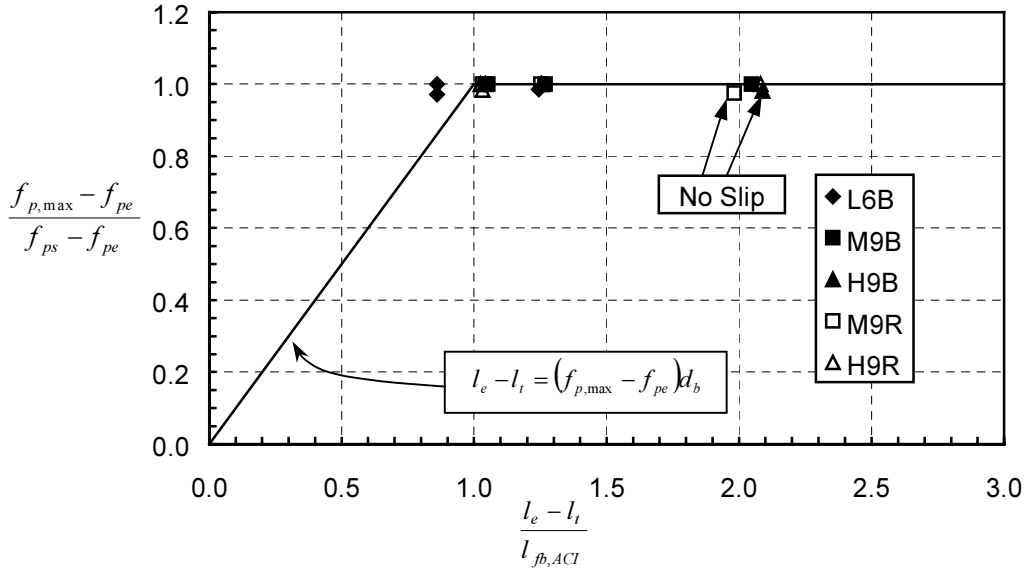


**Figure 7.42: Flexural Bond Performance of Specimens with More than 50 Percent of Strands Partially Debonded—Normalized Flexural Tendon Stress at Ultimate Strength vs. Normalized Flexural Bond Length Provided—Strands Debonded 108 in (2.74 m)**

Figure 7.43 depicts the flexural bond performance of the strands debonded for 72 in (1.83 m) relative to the Commentary expression with prevention of general bond slip as the performance criterion. Again, the strand surface condition and concrete strength appear to have little influence on the flexural bond length required to prevent general bond slip. A flexural bond length on the order of 1.5 to 2 times the Commentary expression would be required to prevent flexural bond slip. Note that the performance of these strands differs significantly from that of the 96 in (2.74 m) debonded strands in this group of tests (Figure 7.41) and the 72 in (1.83 m) debonded strands in the previous group of tests (Figure 7.27). The flexural bond length required to prevent general bond slip increases as a larger percentage of strands are debonded. However, within a group of specimens featuring the same percentage of debonded strands, the required flexural bond length appears to increase with decreasing debonded length. These trends indicate that the general bond slip capacity of debonded strand cannot be simply predicted using a uniform or average bond stress approach.

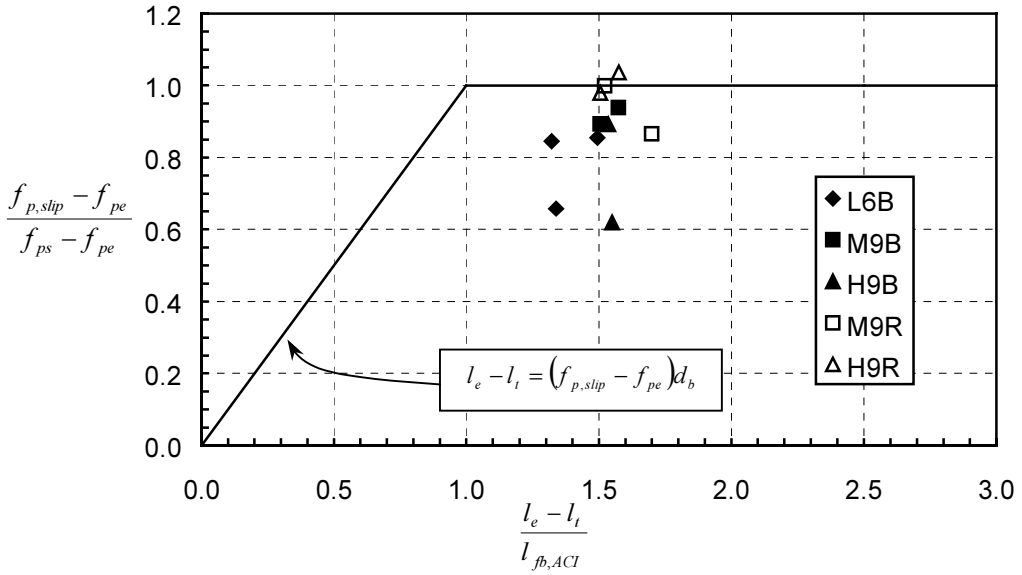


**Figure 7.43: Flexural Bond Performance of Specimens with More than 50 Percent of Strands Partially Debonded—Normalized Flexural Tendon Stress at Slip vs. Normalized Flexural Bond Length Provided—Strands Debonded 72 in (1.83 m)**

Figure 7.44 illustrates the flexural bond performance of these strands relative to the Commentary expression when evaluated with respect to anchorage strength. Although these strands experienced slip in eleven of the twenty tests, they were only unable to develop the required flexural stress in one test (H9B-B-96). Although tests with shorter embedment lengths resulted in flexural failures, this single test indicates that a flexural bond length approximately equal to 1.7 times the ACI Commentary value is necessary to provide adequate anchorage strength for this strand configuration.

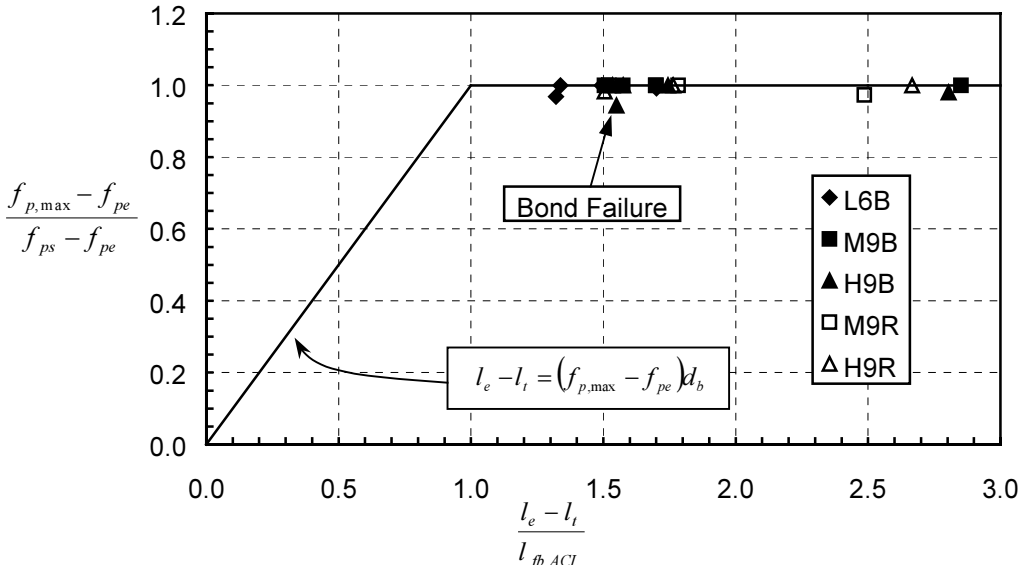


**Figure 7.44: Flexural Bond Performance of Specimens with More than 50 Percent of Strands Partially Debonded—Normalized Flexural Tendon Stress at Ultimate Strength vs. Normalized Flexural Bond Length Provided—Strands Debonded 72 in (1.83 m)**

Although Test H9B-B-96 exhibited a premature bond failure, the companion test with horizontal web reinforcement (H9B-C-96H) exhibited a flexural failure with slip. However, it is difficult to argue that this improvement was solely due to the presence of the H-bar. All the other tests in this group that featured the same embedment length without horizontal web reinforcement (L6B-A-96, M9B-B-96, M9R-B-96, and H9R-B-96) exhibited flexural failures with slip. None of the other specimens with horizontal web reinforcement behaved markedly better than their companion specimens.

In the most shear-critical of these tests, the ACI/AASHTO Standard shear capacity of the beam was approximately 2.5 times the maximum shear demand. The shear capacity according to the AASHTO LRFD sectional method was approximately 2.0 times the maximum shear demand. This was the case in the anchorage zone of the strands that failed due to inadequate bond in Test H9B-B-96.

## 7.8 EFFECTS OF CRACKING ON THE DEVELOPMENT LENGTH OF DEBONDED STRANDS

The results of this test program indicate clearly that the development length required to prevent general bond slip tends to increase as a larger proportion of the strands are debonded. In addition, it also appears to vary according to the debonded length of the strand. These observations support the theory that general bond slip not only results from excess flexural bond stresses along the development length (Mode 1 discussed in Section 2.5), but also from the opening of cracks across the strands within or near the transfer length (Mode 2). The debonded length of the strand dictates where the transfer length lies in relation to the load effects. The amount and configuration of debonding determine the cracking resistance of each transfer region. Except in a few specimens with minimal debonding and embedment lengths significantly shorter than suggested by the current expression, initiation of general bond slip in every group of strands in the debonded specimens of this test program coincided with the opening of a crack within or adjacent to the transfer length of these strands.

The theory that transfer length cracking initiates strand slip and leads to bond failure is not new (Russell and Burns 1993). However, some researchers have fostered a "chicken or the egg" type of debate by asserting that excess flexural bond stresses cause the strand slip, which in turn causes a crack due to the resulting reduction in effective prestress (Buckner 1995). In an attempt to illuminate the correct causative sequence, concrete principal stresses at the initiation of slip/cracking were calculated for each of the tests in which this phenomenon occurred. These stresses were calculated according to the load and location at which the crack opened. The standard assumptions of engineering beam theory were applied. Transformed section properties were calculated, and the section was

assumed to be uncracked and to behave elastically prior to crack initiation. The effective prestress force was assumed to vary linearly from the beginning to the end of the measured transfer length for each specimen.

Principal stresses were calculated at three depths on the section: the bottom fiber (soffit), the junction of the web and bottom flange, and the junction of the web and top flange. Because of the interaction between flexural and shear stresses in the regions where slip occurred, the principal stress at the bottom of the web was always more critical than at the top of the web, where the flexural stress component was usually small. The results of these analyses are listed in the individual test descriptions above and plotted in the figures that follow.

Figure 7.45 illustrates the principal tensile stresses immediately prior to the cracking associated with the first general bond slip of each partially debonded strand. The abscissa represents the principal tensile stress, $f_1$, at the soffit divided by $\sqrt{f'_c}$. The ordinate corresponds to the principal tensile stress at the junction of the web and the bottom flange. This value is also divided by $\sqrt{f'_c}$. The heavy, dashed line represents the boundary of the principal stress values for which a crack through the bottom flange might be expected to open. This line is based on the assumption that cracking occurs for tensile stresses greater than $6\sqrt{f'_c}$ at the bottom of the beam, or for principal tensile stresses greater than $4\sqrt{f'_c}$ in the web, where a biaxial state of stress exists. From Figure 7.45, it is obvious that all of these cracks opened at applied stress levels greater than or very close to those that should have been expected. If these cracks had been caused by a loss of effective prestress resulting from strand slip, the corresponding values of calculated principal tensile stresses would have been smaller than those seen here.

The location of the data relative to the boundaries indicating imminent cracking indicates that the cracking initiated at or near the junction of the web and bottom flange for most, if not all, of these tests. This agrees with the experimental observations. Upon opening, the extent of each crack was usually from the soffit to the top of the web, but it appeared to have opened in the upper portion of the bottom flange and extended outward from there. The initial crack widths were largest in the upper portion of the bottom flange.

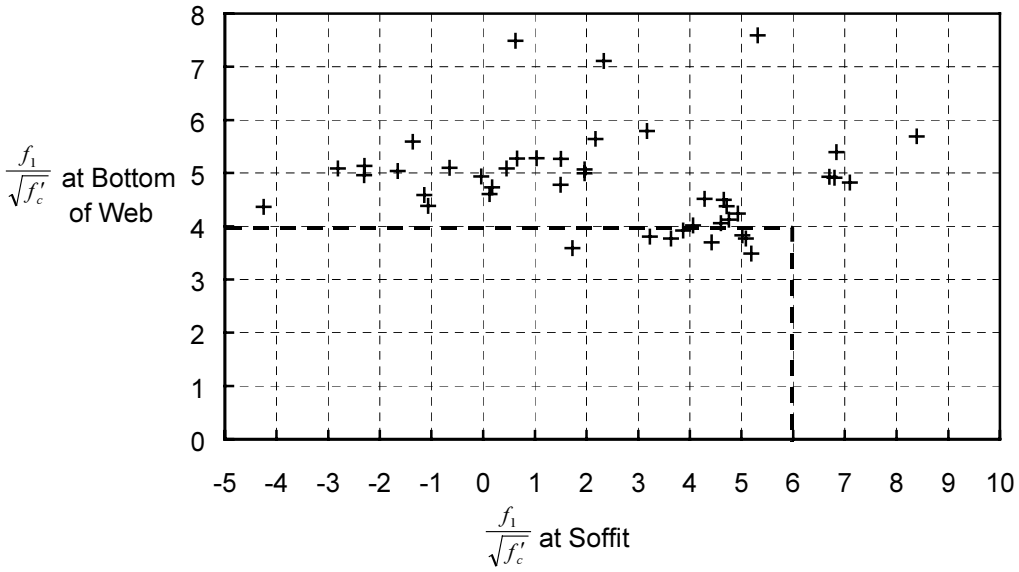


**Figure 7.45: Principal Tensile Stresses at Cracking Associated with Strand Slip**

Because most of the specimens were constructed of concrete with a compressive strength in excess of 10,000 psi (69 MPa), the data is plotted again in Figure 7.46. In this figure, the value of $\sqrt{f'_c}$ is limited to 100 psi, as presently required by the ACI Code. When plotted in this fashion, the results are slightly more uniform with respect to the principal tensile stress at the bottom of the web at crack initiation. However, considering the scatter in the data, which is typical of results involving the shear or tensile properties of concrete, the difference is not very significant.

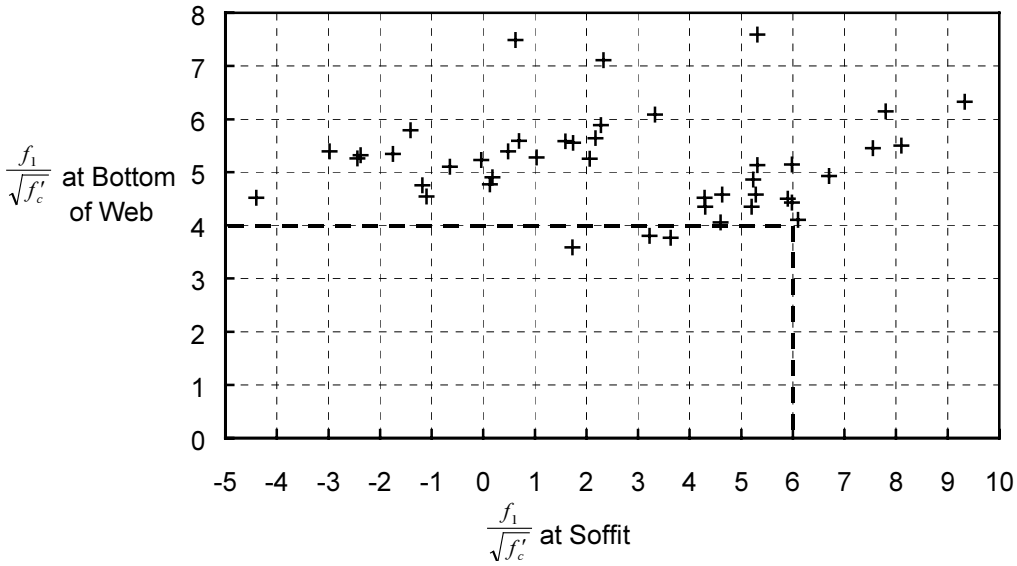


**Figure 7.46: Principal Tensile Stresses at Cracking Associated with Strand Slip—$\sqrt{f_c'}$ Limited to 100 psi**

As noted in the discussion of Test L6B-B-114, this type of shear-flexure cracking is not addressed in the ACI or AASHTO specifications. Shear cracking is assumed to initiate near the centroid of the member when the principal tensile stress at that location exceeds a value of approximately $4\sqrt{f_c'}$. Within the transfer lengths of debonded strands in these tests, the principal tensile stress at the *bottom* of the web exceeded this value before it was exceeded near the centroid or the top of the web. This fact explains why the calculated value of $V_{cw,ACI}$ served as a poor indicator of the shear force required to initiate cracking, particularly in the specimens with more than 50 percent of the strands debonded. In the ACI shear provisions, flexure-shear cracking is assumed to begin with flexure cracking at the extreme tensile fiber when the tensile stress exceeds $6\sqrt{f_c'}$. The figures above demonstrate that cracking occurred in most specimens before the stress at the beam soffit had reached this level. Thus, the calculated value of $V_{ci,ACI}$ would have overestimated the shear force that initiated cracking in most these specimens.

In all debonded specimens in which cracking occurred within the transfer length, general bond slip resulted. In a few specimens, general bond slip resulted from cracks that crossed the strands near the end of the measured transfer length. The furthest crack from the transfer length that appeared to cause general bond slip crossed the strand at a distance of 8 in (200 mm), approximately $14d_b$, from the end of the transfer length. The closest crack that crossed the strand but did *not* cause general bond failure was located 16 in (400 mm), or approximately $27d_b$, from the end of the transfer length. These results are in agreement with the estimate of $20d_b$ for the length of the crack influence length that was theorized in Section 2.5.

From the theory and test results discussed herein, it appears that two conditions must be met to prevent general bond slip in pretensioned strands. First, the bonded embedment length of strand must be long enough to assure that adequate bond capacity exists to prevent strand slip. This is the philosophy embodied in the current expression for the development length of fully bonded strands. Second, cracks must not cross the strand within $20d_b$ of the transfer length. This second mode of failure is not addressed in current code provisions.

Of the specimens in this test program, it appears that only those with all strands fully bonded and those with strands partially debonded only over the support were potentially influenced by the first mode of failure. These tests indicate that the portion of the code expression devoted to flexural bond length is conservative with respect to this type of failure.

Prevention of the second mode of failure involves a larger computational burden. Principal tensile stresses in the concrete must be checked at the beginning and at a distance of $20d_b$ from the end of each debonded strand transfer length. Enough checks must be performed to ensure that cracking does not occur. For members such as these test specimens, in which the debonded strands are contained within a flange, the extreme fiber tensile stress should be

limited to $6\sqrt{f_c'}$, and the principal tensile stress at the boundary of the flange and the web should be limited to $4\sqrt{f_c'}$. For members in which the strands are not contained within a flange, enough checks should be performed to ensure that the principal tensile stress does not exceed $4\sqrt{f_c'}$ anywhere over the depth of the beam between the centroid and the extreme tensile fiber. If these conditions are not met, a bilinear development length expression, described in Method A in Section 2.9.4, cannot be relied upon. Cracking results in the loss of the transfer bond capacity as observed in the specimens in this test program which experienced bond failure.

## 7.9 RECOMMENDED EXPRESSION FOR DEVELOPMENT LENGTH

As long as cracking did not occur near the transfer length, the ACI/AASHTO expressions for the flexural bond length and development length of fully bonded strands proved to be conservative in all of the tests performed in this study. This has not been the case in other studies however. As with the transfer bond performance, the observed flexural bond performance seems to vary greatly according to strand manufacturer. Simmons (1995) reviewed previously published development length test results obtained from specimens prestressed with 0.5 in (12.7 mm) strands. Reported development lengths from the five studies under review ranged up to 90 percent greater than those calculated from the ACI/AASHTO expression. Only one of the five studies featured results that were approximately equal to the ACI/AASHTO value.

The results of development length tests conducted at Auburn University and reported by Simmons offer an indication of the difference in the bond characteristics of strands from different manufacturing sources. These development length tests were performed on T-beams with depths of 22 in (560 mm) and reinforced with 0.5 in (12.7 mm) diameter strand obtained from the manufacturer labeled as Manufacturer B in Chapter 5. The development length indicated by the test results was approximately 120 in (3.0 m), or $240d_b$ for specimens with concrete strengths ranging from 6300 to 8000 psi (43 to 55 MPa). The ACI/AASHTO development length for these specimens was $142d_b$. In the development length tests reported herein, which were performed on specimens reinforced with strand from Manufacturer A, adequate anchorage was achieved with embedment lengths as short as 60 percent of the ACI/AASHTO development length tests.

Further evidence of the disparity between the bond performance of the two types of strand can be found in the cracking behavior of the specimens. Typical flexural crack spacing in the specimens of this study was 6 in (150 mm) or less. In the Auburn study, typical crack spacing was on the order of 2 to 4 times as large, despite the fact that stirrup spacing was only 33 percent greater. This indicates that the strands from Manufacturer A were able to develop significantly larger bond stresses than those from Manufacturer B.

As in the transfer length case, formulating an expression for flexural bond behavior solely on the basis of test results from specimens reinforced with strand from Manufacturer A would be unsafe. Lane (1998) has developed an expression for flexural bond length of fully bonded strands based on experimental results from thirteen different sources. The recommended flexural bond length expression is:

$$l_{fb} = 6.4\frac{f_{ps} - f_{pe}}{f_c'}d_b + 15\,\text{in}$$

Because very few data were included for concrete strengths in excess of 10 ksi (69 MPa), $f_c'$ in the expression is limited to this value.

Lane's expression is based on a purely statistical analysis of the available test data. No attempt is made to explain the use of the concrete compressive strength or the constant term from a behavioral standpoint. The sixty development length tests performed in this study indicate no dependence of the flexural bond length on concrete strength. In order to investigate the possibility of using a simpler and more rational expression that does not include the concrete compressive strength as a parameter, a review of the development length data used to formulate the Lane expression was performed. Used in conjunction with the transfer length expression proposed in Chapter 5, the following expression serves as a conservative upper bound relationship for flexural bond length:

$$l_{fb} = 1.25\,\text{ksi}^{-1}\left(f_{ps} - f_{pe}\right)d_b$$

When this expression is combined with the recommended transfer length expression, the following development length expression for fully bonded strand results (ksi and inch units):

$$l_d = \frac{5}{4}\left[\frac{f_{pt}}{\sqrt{f'_{ci}}} + \left(f_{ps} - f_{pe}\right)\right] d_b$$

For strand embedded in concrete with a compressive strength at release of 4000 psi (28 MPa), the development length resulting from this expression is approximately 50 percent larger than that resulting from the current ACI/AASHTO expression. If the compressive strength at release is 9000 psi (62 MPa), the result is 30 percent larger than that resulting from the current expression.

In Section 2.3.4.1, an example was used to compare the development length recommended by Hanson and Kaar (1959) to that of the ACI/AASHTO expression. Applying the proposed expression to that same example yields a development length of 108 in (2.74 m) for 0.5 in (12.7 mm) strand. A release strength of 4000 psi (28 MPa) is assumed to correspond to the 28-day strength of 5500 psi (38 MPa) given in the example. The development length recommended by Hanson and Kaar is 104 in (2.64 m). When one considers that the proportion of cross-sectional area to strand perimeter has increased by approximately 5 percent since 1959, these two values for development length are in excellent agreement.

## 7.10 SUMMARY AND CONCLUSIONS

An experimental program was conducted to assess the development length necessary for I-beams reinforced with 0.6 in (15.2 mm) pretensioned strands. The test specimens consisted of plant-cast AASHTO Type I I-beams with composite, cast-in-place concrete decks. Sixty development length tests were performed at The University of Texas at Austin, and twelve were performed at Texas Tech University. All of the specimens were designed such that a total strain of at least 0.035 was expected in the extreme row of tensile reinforcement at flexural failure.

The primary variables under investigation were concrete strength, strand surface condition, and debonding configuration. In addition, the influence of horizontal web reinforcement on anchorage capacity was explored to a very limited extent.

For fully bonded strands, the results of this test program indicate that the current ACI/AASHTO expression for development length is adequate. Whether judged against the criterion of preventing strand slip or the criterion of providing adequate anchorage capacity to develop the full flexural strength of the member, the current expression for the flexural bond length portion of the development length was conservative. This was the case for fully bonded strands as well as those debonded only in the support region. Thus, the Moustafa Pull-Out Test results discussed in Chapter 4 accurately indicated the excellent bond performance of the strands used in this study with respect to the existing ACI/AASHTO expression for development length. In accordance with Mast's draw-in theory, the measured strand draw-in values reported in Chapter 6 accurately predicted that the development length of strands in these test specimens would be shorter than the development length resulting from the ACI/AASHTO expression.

In the case of partially debonded strands, it is clear that prevention of general bond slip requires that no cracking cross the bonded portion of the strands within the transfer length or closer to the transfer length than approximately $20d_b$. If this condition is met, and the strands are embedded for a length greater than or equal to the development length of fully bonded strands, no general bond slip should occur. This held true for specimens with up to 75 percent of the strands partially debonded.

For the I-shaped specimens in this test program, cracking within or near the transfer lengths of debonded strands could be prevented by limiting the calculated principal tensile stresses in these regions to $6\sqrt{f'_c}$ at the extreme tensile fiber and approximately $4\sqrt{f'_c}$ at the junction of the web and the bottom flange. When performing principal stress calculations, the designer should carefully consider the amount of effective prestress force that may be developed at the section in question.

The test results did not indicate that concrete strength had a significant influence of the flexural bond length portion of the development length. Strand surface condition had a slight influence on the flexural bond behavior of fully bonded strands, in which cracking through the transfer length was not critical. Because opening of cracks within the transfer length controlled the anchorage behavior of debonded strands, the strand surface condition had no influence on the flexural bond length required to prevent slip in these strands.

The results of comparison tests to determine the effect of horizontal web reinforcement were mixed. Overall, the horizontal web reinforcement yielded only slightly improved performance. The use of this type of reinforcement

had been suggested by experimental tests in which premature shear failures were caused by a lack of bond capacity (Russell and Burns 1993). In this test program, however, loss of bond capacity resulted in premature failures of the flexural type. This may be attributed to the excess vertical shear reinforcement that was provided in the anchorage regions of the debonded strands. Had shear failures occurred in this test program, it is likely that the companion tests with horizontal web reinforcement would have yielded more significant improvements in strength.

Although the strands incorporated in this test program exhibited anchorage behavior at least as good as that indicated by the current code expression for development length, results of other research studies indicate that this expression does not adequately reflect the behavior of strands from a variety of manufacturers. Until a performance standard is established for the bond performance (or "bond quality") of prestressing strand, a safe design expression for development length should bound the behavior of all strands available for use in pretensioned products. To that end, the following development length equation is recommended for design purposes:

$$l_d = \frac{5}{4}\left[\frac{f_{pt}}{\sqrt{f'_{ci}}} + \left(f_{ps} - f_{pe}\right)\right] d_b$$

For partially debonded strands, the above equation is also applicable as long as cracking is prevented within or near the transfer length as discussed above.

# CHAPTER 8: RECOMMENDATIONS

## 8.1 DESIGN RECOMMENDATIONS

This section includes design recommendations specific to the transfer and development length of seven-wire strands. In addition, the general process for designing a member with partially debonded strands is outlined.

### 8.1.1 Transfer Length

For seven-wire prestressing strand, the transfer length, $l_t$, should be calculated as:

$$l_t = \frac{5}{4}\frac{f_{pt}}{\sqrt{f'_{ci}}}d_b$$

where the stresses are in ksi and the lengths are in inches. The resulting value defines the maximum extent of the transfer length. For purposes of calculating member strength, the effective prestress force transferred to the concrete from a bonded prestressing strand should be assumed to vary linearly from zero at the initiation of bond to a maximum over a distance equal to this transfer length.

For purposes of design in which conservatism dictates the selection of a lower-bound value for transfer length, such as when comparing concrete stresses to permissible values, a transfer length no longer than $10d_b$ should be assumed.

### 8.1.2 Development Length

For seven-wire prestressing strand, the development length, $l_d$, should be calculated as:

$$l_d = \frac{5}{4}\left[\frac{f_{pt}}{\sqrt{f'_{ci}}} + f_{ps} - f_{pe}\right]d_b$$

where the stresses are in ksi and the lengths are in inches.

Section 12.9.2 of ACI 318-99 (and corresponding Section 9.28.2 of the AASHTO Standard Specification) should be deleted. This provision, which limits investigations to cross sections nearest the ends of the member that are required to develop full design strength, was placed in the Code at a time when partial debonding of prestressing tendons was hardly used, if at all. Likewise, little was known or codified about the effects of terminating tension reinforcement in reinforced concrete members. In the past four decades, much has been learned regarding the interaction between shear and bond and its effect in regions where tension steel is terminated. Numerous rules for the termination of tension reinforcement have been codified. When subjected to ultimate loads, partially debonded strands in prestressed concrete members assume a role identical to that played by cutoff bars in reinforced concrete members. Accordingly, establishment of the debonded lengths of prestressing tendons should be subject to code provisions that regulate the termination points of cutoff bars.

Through the deletion of Section 12.9.2, or the clarification that the included language only applies to fully bonded strands, the provisions of Sections 12.10, 12.11, 12.12 become applicable to partially debonded strands. For typical simply supported, pretensioned members the specific provisions discussed below are most pertinent. Suggested changes to reflect application to partially debonded strands are shown in brackets.

> **12.10.2** — Critical sections for development of reinforcement in flexural members are at points of maximum stress and at points within the span where adjacent [bonded] reinforcement terminates, or is bent. Provisions of 12.11.3 must be satisfied. (AASHTO Standard 8.24.1.2; LRFD 5.11.1.2.1)

Note that Section 12.11.3 deals with the anchorage of reinforcement at supports and at points of inflection. This would not directly apply to partially debonded strands in simply supported members. Whether or not it should apply to the fully bonded strands at the support is open to debate. On the one hand, because simply supported, pretensioned members typically have considerably more flexural strength than required at the support, the type of

anchorage failure addressed by Section 12.11.3 has not been an issue. On the other hand, if a significant portion of strands are debonded in the support region, excess strength may be more limited, leaving the member susceptible to this type of failure. For this provision to apply to prestressing strands, it would require modification to reflect the bilinear nature of the development length expression.

> **12.10.3** — [Bonded] reinforcement shall extend beyond the point at which it is no longer required to resist flexure for a distance equal to the effective depth of the member or $12d_b$, whichever is greater, except at the supports of simple spans and at free ends of cantilevers. (AASHTO Standard 8.24.1.2.1; LRFD 5.11.1.2.1)

It should be noted that all the specimens whose substandard performance resulted in the existing code development length modifications for debonded strands (Kaar and Magura 1965; Rabbat et al. 1979) violated the above provision. Those of the Kaar and Magura study also failed to satisfy the following provision:

> **12.10.4** — Continuing reinforcement shall have an embedment length not less than the development length $l_d$ beyond the point where bent[, debonded,] or terminated tension reinforcement is no longer required to resist flexure. (AASHTO Standard 8.24.1.2.2; LRFD 5.11.1.2.1)

> **12.10.5** — [Bonded] flexural reinforcement shall not be terminated in a tension zone unless one of the following conditions is satisfied (AASHTO Standard 8.24.1.4):
>
> **12.10.5.1** — Shear at the cutoff [or debonding] point does not exceed two-thirds that permitted, including shear strength of shear reinforcement provided.
>
> **12.10.5.2** — Stirrup area in excess of that required for shear and torsion is provided along each terminated [or debonded] bar[, strand,] or wire over a distance from the termination [or debonding] point equal to three-fourths the effective depth of the member. Excess stirrup area $A_v$ shall be not less than $60b_w s/f_y$. Spacing $s$ shall not exceed $d/8\beta_b$ where $\beta_b$ is the ratio of area of reinforcement cut off [or debonded] to total area of tension reinforcement at the section.
>
> **12.10.5.3** — For No. 11 bar and smaller, [and prestressing strand,] continuing reinforcement provides double the area required for flexure at the cutoff [or debonding] point and shear does not exceed three-fourths that permitted.

Until further research can establish a reliable indication of the post-slip anchorage capacity of prestressing tendons, adequate anchorage of debonded strands can only be guaranteed by preventing cracking across the bonded length of strand inside or within $20d_b$ of the transfer length. This is best accomplished by calculating the principal tensile stresses at the beginning and end of this region. For members, such as I-beams, U-beams, or box beams, in which the debonded strands are contained within the flange, the tensile stress at the extreme fiber should be limited to a value equal to $6\sqrt{f'_c}$, and the principal tensile stress at the junction of the web and the flange containing the strands should be limited to $4\sqrt{f'_c}$. These expressions are in psi units; the corresponding limits are $\frac{\sqrt{f'_c}}{2}$ and $\frac{\sqrt{f'_c}}{3}$, respectively, in MPa units. For other members, the principal tensile stresses in this region should be limited to $4\sqrt{f'_c}$ (in psi units) between the centroid and the extreme tensile fiber; the corresponding limit is $\frac{\sqrt{f'_c}}{3}$ in MPa units. Gross section properties may be used in the calculation of the principal stresses.

Bond fatigue should be prevented by preventing tensile stress within the same length ($l_t$ plus $20d_b$) under service level loadings. As long as the conditions in the previous paragraph are met for the ultimate loads, however, this consideration should not control design. It may only become critical if transfer length cracking and the resulting general bond slip are allowed under ultimate loads.

If the above conditions are met for the anchorage of debonded strands, Section 12.9.3 of ACI 318-99 (and the corresponding language in AASHTO Standard Section 9.28.3 and LRFD Article 5.11.4.3), which requires the doubling of the development length for debonded strands in members designed for tension under service loads, is

unnecessary. Likewise, the rules in Article 5.11.4.3 that limit the percentage of debonded strands in the member and in each horizontal row are unnecessary if the above conditions are satisfied.

### 8.1.3 Design Process

The following general steps should be taken when designing the reinforcement pattern for pretensioned concrete members. These steps are applicable to the design of simply supported beams in particular, but the process may be extended to other types of members.

#### *8.1.3.1 Design of Midspan Section for Flexural Resistance*

For the typical bridge member, the total amount of prestressed reinforcement will depend upon the flexural demand at the midspan section. Design of this section will usually determine the number and pattern of prestressing strands in the member. The quantity of reinforcement will be controlled by either the allowable concrete tensile stress at the bottom fiber under Service Limit State loading, or the ultimate moment strength required to resist Strength Limit State loading.

#### *8.1.3.2 Determination of Strand Debonding Lengths and Configuration*

Once the number, size and pattern of prestressing strands has been determined, the allowable concrete stresses immediately after prestress release dictate the possible strand debonding configurations. Because the amount of reinforcement has already been determined, optimal design is that which results in the *minimum* amount of strand debonding that satisfies allowable stress limits. For calculation of concrete stresses immediately after release, the transfer length may be conservatively estimated as zero. Strands should not be debonded over lengths longer than necessary to satisfy allowable stress limits. If multiple strands require long debonded lengths, staggered debonding should be employed if possible (Russell and Burns 1993).

#### *8.1.3.3 Strength Limit State Performance Checks*

Once a debonding pattern has been established, the anchorage capacity of the member must be verified with respect to Strength Limit State loadings. For simply supported members, this can be achieved by satisfying the provisions of ACI 318-99 Section 12.10 listed above.

The condition that general bond slip be prevented from occurring has been used as the performance criterion for anchorage design of prestressing strands in the past (Tabatabai and Dickson 1993). At present, there are insufficient research results regarding the post-slip behavior of seven-wire strands to justify a change in this philosophy. Thus, general bond slip of partially debonded strands must be prevented. This can only be accomplished if cracking is precluded across the length of bonded strand that lies between the debond point and a point at a distance of $20d_b$ beyond the transfer length. This condition may be satisfied by performing the stress checks described in Section 8.1.2 above. Gross section properties may be used to simplify the calculations involved.

#### *8.1.3.4 Service Limit State Checks*

If cracking is prevented within or near the transfer length under Strength Limit State loading, then no further checks are required for anchorage capacity in the Service Limit State. If future research results in development provisions that allow cracking in this region under Strength Limit State loads, the bond fatigue may control anchorage design. In order to prevent bond fatigue, tensile stresses should be prevented within the strand transfer length under Service Level loads.

#### *8.1.3.5 Calculation of Prestress Forces at Sections Where Strands Are Not Fully Developed*

When nominal resistances (such as $M_n$, $V_n$, or $T_n$) are calculated at sections that lie within the tendon development length, careful consideration must be given to the amount of prestress force that may be relied upon. If the anchorage requirements discussed above are satisfied, the available prestress for nominal strength, $f_{ps}$, may be calculated according to the following bilinear relationship.

For $l_e \le l_t$, $f_{ps} = \frac{4}{5}\frac{f_{pe}}{f_{pt}}\sqrt{f'_{ci}}\,\frac{l_e}{d_b}$

For $l_e > l_t$, $f_{ps} = f_{pe} + \frac{4}{5}\frac{l_e}{d_b} - \frac{f_{pt}}{\sqrt{f'_{ci}}}$

where $l_e$ is the bonded length of strand beyond the section being considered. These relationships were obtained by inverting the recommended expression for development length. As in that expression, stresses are in ksi and lengths are in inches.

## 8.2 RECOMMENDATIONS FOR FURTHER RESEARCH

### 8.2.1 Strand Bond Quality

The results of various test programs have revealed tremendous variability in the bond behavior of prestressing strands. There is significant evidence to suggest that strand produced by one manufacturer may perform quite differently than that produced by another. Researchers should continue to investigate this problem by attempting to identify the source of the discrepancy and/or establishing a performance test for measuring strand bond quality. If a reliable performance standard can be adopted, the variability of bond behavior can be reduced. With more predictable bond behavior, expressions for transfer and development length can more accurately model the behavior of all strands.

### 8.2.2 Post-Slip Anchorage Strength

If a safe, reliable estimate of the post-slip strength of prestressing strand can be established, anchorage design of pretensioned members with debonded strands can be greatly simplified. Such an estimate might be used to formulate an expression for development length that allows for the presence of cracking in the transfer length. Partially debonded strands could then be designed by simply using rules identical or comparable to the rules presently used for the design of cutoff bars. Tedious stress computations would no longer be necessary.

### 8.2.3 Bond-Shear Interaction

The effects of shear on bond resistance of pretensioned strand are not addressed in present code expressions. Likewise, the existing provisions do not reflect the extra embedment length that is required to prevent premature shear failures where bonded tension reinforcement terminates in a flexural member. The principles and rules developed for reinforced concrete construction need to be extended or adapted for use in pretensioned members.

### 8.2.4 "Top Bar" Effect

It has been hypothesized that strands near the top of member casting position will exhibit reduced bond capacity relative to those cast near the bottom, as is known to be the case with reinforcing bars. This effect has yet to be quantified for prestressing strands however.

# CHAPTER 9: SUMMARY AND CONCLUSIONS

## 9.1 SUMMARY

The use of 0.6 in (15.2 mm) prestressing strand at a center-to-center spacing of 2 in (51 mm) allows for the optimal implementation of High Strength Concrete (HSC) in precast, prestressed concrete bridge superstructures. Because of the relatively large prestress forces developed with this strand configuration, partial debonding of strands is an attractive alternative to the more traditional method of draping strands for alleviating extreme concrete stresses in the end regions of pretensioned members.

Recent experimental evidence suggests that the existing ACI and AASHTO code provisions that address the anchorage of pretensioned strands do not adequately describe the behavior of these strands. In addition, the anchorage behavior of partially debonded strands is not fully understood. At the time the research reported herein was initiated, the Federal Highway Administration (FHWA) had imposed a moratorium on the use of 0.6 in (15.2 mm) strand in pretensioned applications, thereby hindering the optimal implementation of HSC in pretensioned construction.

In order to further investigate the anchorage behavior of large-diameter prestressing strands, the Center for Transportation Research of The University of Texas at Austin along with Texas Tech University initiated a joint research study in 1995 entitled *Development Length of 15-mm (0.6-inch) Diameter Prestressing Strand at 50-mm (2-inch) Grid Spacing in Standard I-shaped Pretensioned Concrete Beams*. The details of this study, funded by the Texas Department of Transportation (TxDOT) as Research Project No. 0-1388 and by FHWA as Program No. SPR 0511, are described in this report.

The stated objective of the research was to measure the transfer and development lengths for 0.6 in (15.2 mm) diameter prestressing strand at 2 in (50 mm) grid spacing in tests of several standard AASHTO Type I pretensioned beams. The more general objective of the study was a better understanding of the anchorage behavior of pretensioned concrete flexural members. In order to achieve this general objective, several specific objectives were identified:

1. Assess the effect of concrete strength on anchorage behavior,
2. Examine the anchorage behavior of strands exhibiting the range of surface conditions found in practice, and
3. Develop rational means of predicting the anchorage behavior of debonded strands.

In addition, research effort was focused on assessing the usefulness of pull-out tests and strand draw-in measurements as indicators of anchorage behavior.

The research study encompassed the transfer and development length testing of thirty-six plant-cast, AASHTO Type I (Texas Type A), pretensioned concrete I-beams. Transfer length testing was performed at the plant; both immediate and long-term transfer lengths were measured. Corresponding values of strand draw-in were also measured. Pull-out tests were performed in an effort to quantify strand bond quality. Development length tests were performed on thirty of the beams at the Phil M. Ferguson Structural Engineering Laboratory at The University of Texas at Austin. Development length testing of the remaining six beams was carried out at Texas Tech University. In an effort to achieve ultimate tendon elongation values exceeding 3.5 percent, a cast-in-place, composite deck was added to each beam prior to development length testing.

Three different levels of beam concrete strength were investigated. Compressive strengths at prestress release varied from 4000 to 11,000 psi (27 to 76 MPa). Strengths at time of development length testing ranged from 5700 to 14,700 psi (39 to 102 MPa). Specimens were reinforced with strands having either a “bright” or a “rusted” surface condition. A variety of strand debonding schemes were tested. Some specimens contained strands that were all fully bonded, while other specimens featured percentages of debonded strands ranging up to 75 percent. The study included a limited investigation of the effect of horizontal web reinforcement on anchorage behavior.

A review of the anchorage behavior of pretensioning strands is presented in Chapter 2. This chapter also includes a discussion of the evolutions and apparent shortcomings of the existing code provisions that address this topic. The effect of cracking within the transfer length on development length is addressed. Ruminations on general methods for anchorage design of pretensioned members are included.

The experimental portion of the study is presented in Chapters 3 through 7. Chapter 3 includes the test specimen details. The specimen identification system is explained, and the design details of each specimen are recorded. Material properties are given. The chapter concludes with a description of the fabrication of the precast I-beams and the casting of the composite decks.

The strand pull-out test program is the subject of Chapter 4. A brief history of the use of strand pull-out testing to evaluate strand bond quality is presented. The test program is described, and the experimental results are presented and discussed.

Chapter 5 is devoted to the program of transfer length testing performed on all thirty-six beams. The test procedure is detailed, as well as the method used to determine the transfer lengths from the measured data. Modifications to the standard 95% AMS Method for determining transfer length are discussed. These modifications are used to equitably extend the applicability of the method to partially debonded strands and long-term transfer length testing. The results of the transfer length tests are presented and discussed. The influence of concrete strength, strand surface condition, prestress release method, and time are examined. The results are compared to existing code provisions for transfer length, as well as several expressions that have been proposed by researchers. The results are also compared to results obtained in other relevant studies. Based on the results of this and other studies, a conservative design expression for transfer length is proposed that includes the influence of concrete strength.

In conjunction with transfer length testing, a program of strand draw-in testing was conducted. The test procedure and results are presented in Chapter 6. The chapter includes a discussion of the practicality of using draw-in testing as a means of quality control for the bond of pretensioned strands.

The development length test program conducted at the Phil M. Ferguson Structural Engineering Laboratory is the focus of Chapter 7. The test method, instrumentation, and procedure are described. Quantitative results are tabulated, and a brief description of each of the sixty tests is included. The behavior of the test specimens is compared to that implied by existing code provisions, and the results from the twelve tests conducted at Texas Tech University are compared to those from the corresponding UT specimens. The influence of cracking on the development length is discussed, as is the susceptibility of debonded regions to cracking that results from the interaction of shear and moment. A conservative expression for development length is presented which takes into account the results of a variety of relevant research studies.

Chapter 8 is a collection of recommendations resulting from this study. These include recommendations for the anchorage design of pretensioned strands as well as recommendations for further research relevant to the topic.

## 9.2 CONCLUSIONS

The conclusions that follow have been drawn from the background research and experimental results of this study. Further discussion of the conclusions drawn from the experimental results can be found at the end of the relevant chapter.

### 9.2.1 General Conclusions

1. The results of this study confirm that 0.6 in (15.2 mm) prestressing strands may be safely used at a center-to-center spacing of 2 in (51 mm).
2. Staggered debonding of strands is an effective method for selectively reducing concrete stresses in the end regions of pretensioned concrete members and may be effectively implemented as an alternative to draping strands.
3. The bond behavior exhibited by seven-wire strands has varied greatly in different research studies. The bond quality of prestressing strand appears to vary from manufacturer to manufacturer. Because of this significant lack of uniformity and the lack of an established performance standard, very conservative relationships must be used to model anchorage behavior for design.
4. Existing ACI and AASHTO specifications concerning the anchorage behavior of fully bonded prestressing strands are unconservative. They also do not adequately address the adverse effects resulting from the reduced effective prestress at debonded sections and the interaction of shear and moment near the debond points.

5. Increased concrete strength enhances the anchorage capacity of prestressing strand, and this relationship should be reflected in Code expressions for transfer and development length. Larger bond stresses may be developed due to the increased concrete stiffness and tensile strength along the transfer length. Also, the cracking resistance of anchorage zones increases slightly with increasing tensile strength.
6. Extending and/or modifying the existing design rules for terminating mild steel tension reinforcement to the design of partially debonded prestressing tendons offers the potential simplification of the design of these tendons while more accurately reflecting their behavior. However, the conservatism of applying such a method has yet to be experimentally determined.

## 9.2.2 Detailed Conclusions

### *9.2.2.1 Strand Pull-out Testing*

1. The Moustafa Pull-out Test, in conjunction with the Logan's performance benchmark, accurately indicated the excellent bond behavior of the strands used in this study with respect to the existing ACI/AASHTO transfer and development length relationships.
2. Properly consolidated concrete is vital to adequate bond performance. Particular care should be taken to ensure the workability and proper consolidation of HSC when casting pretensioned products.

### *9.2.2.2 Transfer Length Testing*

1. On average, transfer lengths are indirectly proportional to the square root of the concrete strength at release, $\sqrt{f'_{ci}}$ .
2. Transfer length can increase significantly in the first few weeks after release. Average increases in this study ranged from 10 to 20 percent. Increases in a few specimens exceeded 50 percent. All significant increase appears to occur in the first 28 days after release.
3. Surface weathering of prestressing strand can reduce transfer length, but this effect is not reliable enough to incorporate into design.
4. Although sudden prestress release has been shown to adversely affect transfer length in previous studies, which featured specimens constructed with normal strength concrete, varying the method of prestress release had minimal influence on the transfer length of bright strand specimens constructed of concrete with release strengths exceeding 7000 psi (48 MPa) in this study. This indicates that HSC is less susceptible to the influence of prestress release method.
5. Transfer lengths of partially debonded strands are no longer than those of fully bonded strands.
6. Very short transfer lengths are possible. When performing design checks of allowable stresses for the Service Limit State, a transfer length of less than $10d_b$ should be assumed. Assuming a length of zero enhances conservatism and simplifies calculations without unduly sacrificing economy.
7. The following relationship can be used to conservatively estimate the transfer length of seven-wire pretensioned strand regardless of manufacturer (stresses in ksi and lengths in inches):

$$l_t = \frac{5}{4}\frac{f_{pt}}{\sqrt{f'_{ci}}}d_b$$

### *9.2.2.3 Draw-In Testing*

1. Mast's draw-in theory correctly indicated the excellent bond behavior of the strands used in this study with respect to the existing ACI/AASHTO transfer and development length relationships.
2. Draw-in measurements may be used to indicate trends in bond behavior, and to indicate gross deficiencies in bond quality.

3. The correlation of obtained transfer lengths and draw-in values indicates that a detailed, statistical study must be performed and a large database of results must be developed before instituting any quality control system that relies on draw-in to establish the adequacy of bond in pretensioned members.
4. The use of draw-in measurements to calculate the transfer length of partially debonded strands is difficult and not recommended.

#### *9.2.2.4 Development Length Testing*

1. The following relationship can be used to conservatively estimate the development length of seven-wire pretensioned strand regardless of manufacturer (stresses in ksi and lengths in inches):

$$l_d = \frac{5}{4}\left[\frac{f_{pt}}{\sqrt{f'_{ci}}} + f_{ps} - f_{pe}\right]d_b$$

2. Concrete strength and strand surface condition exhibited little influence on the flexural bond length portion of the development length.
3. The presence of horizontal web reinforcement yielded only slightly improved performance compared to that of companion specimens lacking this reinforcement. However, none of the specimens exhibited a premature shear failure due to loss of bond, therefore little demand was exerted on the horizontal web reinforcement in this test program. Where present, horizontal web reinforcement reduced crack widths.
4. For partially debonded strands, prevention of general bond slip requires that no cracking cross the bonded portion of the strands within the transfer length or closer to the transfer length than $20d_b$. If this condition is satisfied, debonded strands will exhibit bond capacity comparable to that of fully bonded strands.
5. Up to 75 percent of strands may be debonded so long as the following conditions are satisfied:
   - cracking is prevented in or near the transfer length
   - the ACI/AASHTO rules for terminating tensile reinforcement are applied to the bonded length of prestressing strand
6. The susceptibility to cracking of regions with debonded strands may be assessed by calculating principal stresses under ultimate loads and satisfying the limits recommended in Section 8.1.2.

# APPENDIX A: CONCRETE MIX DESIGNS

**Table A.1: Series "L" Concrete Mix Design**

| Design Strength | |
|---|---|
| $f'_{ci}$ = 4000 psi (28 MPa) at 1 day | |
| $f'_c$ = 5000–7000 psi (34–48 MPa) at 28 days | |
| Material | Quantity per $yd^3$ (per $m^3$) |
| Cement (Type III) | 528 lb (313 kg) |
| Fly Ash (Class C) | 205 lb (121 kg) |
| ¾-in (19-mm) River Gravel | 1800 lb (1065 kg) |
| Concrete Sand | 1120 lb (664 kg) |
| High-Range, Water-Reducing Admixture | 106 fl oz (4090 $cm^3$) |
| Air-Entraining Admixture | 5.3 fl oz (205 $cm^3$) |
| Retarding Admixture | 16 fl oz (613 $cm^3$) |
| Water | 29.0 gal (0.144 $m^3$) |

**Table A.2: Series "M" Concrete Mix Design**

| Design Strength | |
|---|---|
| $f'_{ci}$ = 7000 psi (48 MPa) at 1 day | |
| $f'_c$ = 9500–11500 psi (66–79 MPa) at 28 days | |
| Material | Quantity per $yd^3$ (per $m^3$) |
| Cement (Type III) | 564 lb (334 kg) |
| Fly Ash (Class C) | 162 lb (96 kg) |
| ¾-in (19-mm) River Gravel | 2000 lb (1185 kg) |
| Concrete Sand | 1155 lb (683 kg) |
| High-Range, Water-Reducing Admixture | 160 fl oz (6190 $cm^3$) |
| Retarding Admixture | 17 fl oz (658 $cm^3$) |
| Water | 24.2 gal (0.120 $m^3$) |

**Table A.3: Series "H" Concrete Mix Design**

| Design Strength | |
|---|---|
| $f'_{ci}$ = 9000 psi (62 MPa) at 1 day | |
| $f'_c$ = 13000–15000 psi (90–103 MPa) at 56 days | |
| Material | Quantity per $yd^3$ (per $m^3$) |
| Cement (Type III) | 671 lb (398 kg) |
| Fly Ash (Class C) | 319 lb (189 kg) |
| ½-in (10-mm) Crushed Limestone | 1880 lb (1115 kg) |
| Concrete Sand | 1050 lb (623 kg) |
| High-Range, Water-Reducing Admixture | 198 fl oz (7660 $cm^3$) |
| Retarding Admixture | 27 fl oz (1045 $cm^3$) |
| Water | 29.4 gal (0.146 $m^3$) |

**Table A.4: Cast-in-Place Deck Concrete Mix Design**

| Design Strength | |
|---|---|
| $f'_c$ = 6000 psi (41 MPa) at 28 days | |
| Material | Quantity per $yd^3$ (per $m^3$) |
| Cement (Type I) | 517 lb (306 kg) |
| ¾-in (19-mm) River Gravel | 1870 lb (1105 kg) |
| Concrete Sand | 1355 lb (803 kg) |
| Retarding Admixture | 20.4 fl oz (789 $cm^3$) |
| Water | 30.0 gal (0.148 $m^3$) |

# APPENDIX B: MATERIAL PROPERTIES

**Table B.1: Mechanical Properties of Beam Specimen Concrete at Time of Release and at Pull-Out Testing**

| Beam Specimens | Release of Prestress | | | Pull-Out Tests | |
|---|---|---|---|---|---|
| | Age days | $f'_{ci}$ psi (MPa) | $E_{ci}$ ksi (GPa) | Age days | $f'_c$ psi (MPa) |
| L0B | 1 | 4240 (29.2) | 4700 (32.4) | 4 | 5250 (36.2) |
| L4B | 1 | 4490 (31.0) | 5050 (34.8) | 4 | 4970 (34.3) |
| L6B | 1 | 4710 (32.5) | 5750 (39.6) | 3 | 5500 (37.9) |
| M0B | 1 | 6610 (45.6) | 6350 (43.8) | 3 | 7800 (53.8) |
| M4B | 1 | 6900 (47.6) | 6100 (42.1) | 6 | 9370 (64.6) |
| M9B | 1 | 7890 (54.4) | 6500 (44.8) | 2 | 8440 (58.2) |
| H0B | 1 | 11030 (76.1) | 7500 (51.7) | 3 | 11070 (76.3) |
| H4B | 1 | 9660 (66.6) | 6750 (46.5) | 3 | 10060 (69.4) |
| H9B | 1 | 9300 (64.1) | 6750 (46.5) | 2 | 10420 (71.8) |
| L0R | 1 | 4540 (31.3) | 5400 (37.2) | 3 | 5100 (35.2) |
| L4R | 1 | 3970 (27.4) | 4400 (30.3) | 3 | 4400 (30.3) |
| L6R | 1 | 4630 (31.9) | 5400 (37.2) | 3 | 5450 (44.5) |
| M0R | 1 | 7290 (50.3) | 6950 (47.9) | 2 | 8290 (57.2) |
| M4R | 1 | 7950 (54.8) | 6050 (41.7) | 4 | 8960 (61.8) |
| M9R | 1 | 7630 (52.6) | 6650 (45.9) | 3 | 9420 (65.0) |
| H0R | 1 | 9020 (62.2) | 6600 (45.5) | 4 | 10480 (72.3) |
| H4R | 1 | 10910 (75.2) | 7350 (50.7) | 4 | 11710 (80.7) |
| H9R-A/B | 1 | 7860 (54.2) | 6150 (42.4) | — | — |
| H9R-C/D | 1 | 9270 (63.9) | 7100 (49.0) | 2 | 10690 (73.7) |

**Table B.2: Mechanical Properties of Concrete upon Removal of Deck Shoring**

| Beam Specimens | | Beam Concrete | | | Cast-in-Place Deck Concrete | | |
|---|---|---|---|---|---|---|---|
| | | Age days | $f'_c$ psi (MPa) | $E_c$ ksi (GPa) | Age days | $f'_c$ psi (MPa) | $E_c$ ksi (GPa) |
| L0B | A/B | 17 | 6000 (41.4) | 5000 (34.5) | 3 | 4070 (28.1) | 4600 (31.7) |
| | C/D | 25 | | | 7 | 4790 (33.0) | 4650 (32.1) |
| L4B | A/B | 53 | 5690 (39.2) | 4450 (30.7) | 5 | 4770 (32.9) | 5000 (34.5) |
| | C/D | 61 | | | 5 | 4470 (30.8) | 5000 (34.5) |
| L6B | A/B | 159 | 6860 (47.3) | 5200 (35.9) | 4 | 4020 (27.7) | 4800 (33.1) |
| | C/D | 162 | | | 2 | 4240 (29.2) | 4900 (33.8) |
| M0B | A/B | 60 | 10720 (73.9) | 6700 (46.2) | 5 | 4630 (31.9) | 4800 (33.1) |
| | C/D | 67 | | | 5 | 4560 (31.4) | 4550 (31.4) |
| M4B | A/B | 50 | 10730 (74.0) | 5800 (40.0) | 3 | 4160 (28.7) | 4700 (32.4) |
| | C/D | 53 | | | 3 | 4340 (29.9) | 4800 (33.1) |
| M9B | A/B | 36 | 12880 (88.8) | 7300 (50.3) | 2 | 3260 (22.5) | 4550 (31.4) |
| | C/D | 42 | | | 2 | 3610 (24.9) | 4550 (31.4) |
| H0B | A/B | 15 | 12600 (86.9) | 7200 (49.6) | 2 | 4350 (30.0) | 5000 (34.5) |
| | C/D | 19 | 12690 (87.5) | 7150 (49.3) | 3 | 4700 (32.4) | 4130 (28.5) |
| H4B | A/B | 80 | 11240 (77.5) | 6000 (41.4) | 3 | 4030 (27.8) | 4500 (31.0) |
| | C/D | 83 | | | 3 | 4260 (29.4) | 4650 (32.1) |
| H9B | A/B | 93 | 13830 (95.4) | 6850 (47.2) | 1 | 2990 (20.6) | 4500 (31.0) |
| | C/D | 98 | | | 1 | 3050 (21.0) | 4350 (30.0) |
| M0R | A/B | 175 | 11750 (81.0) | 6250 (43.1) | 2 | 3480 (24.0) | 4450 (30.7) |
| | C/D | 180 | | | 3 | 4210 (29.0) | 4950 (34.1) |
| M4R | A/B | 88 | 11050 (76.2) | 6400 (44.1) | 5 | 2660 (18.3) | 4300 (29.6) |
| | C/D | 95 | | | 3 | 3930 (27.1) | 4650 (32.1) |
| M9R | A/B | 105 | 12420 (85.6) | 6900 (47.6) | 3 | 4160 (28.7) | 4900 (33.8) |
| | C/D | 109 | | | 2 | 3700 (25.5) | 4550 (31.4) |
| H0R | A/B | 213 | 14170 (97.7) | 6650 (45.9) | 2 | 4080 (28.1) | 4500 (31.0) |
| | C/D | 218 | | | 3 | 4580 (31.6) | 4950 (34.1) |
| H4R | A/B | 123 | 13500 (93.1) | 7050 (48.6) | 4 | 3990 (27.5) | 4550 (31.4) |
| | C/D | 127 | | | 3 | 3950 (27.2) | 4550 (31.4) |
| H9R | A/B | 140 | 12370 (85.3) | 6400 (44.1) | 2 | 3290 (22.7) | 4500 (31.0) |
| | C/D | 151 | 14720 (102) | 7000 (48.3) | 3 | 4880 (33.6) | 5250 (36.2) |

**Table B.3: Mechanical Properties of Concrete at Time of Development Length Testing, Specimens with Bright Strand**

| Beam Specimens | | Beam Concrete | | | Cast-in-Place Deck Concrete | | |
|---|---|---|---|---|---|---|---|
| | | Age days | $f'_c$ psi (MPa) | $E_c$ ksi (GPa) | Age days | $f'_c$ psi (MPa) | $E_c$ ksi (GPa) |
| L0B | A | 30 | 6220 (42.9) | 5000 (34.5) | 16 | 5310 (36.6) | 4700 (32.4) |
| | B | 36 | | | 22 | 5420 (37.4) | |
| | C | 45 | | | 31 | 5470 (37.7) | 4800 (33.1) |
| | D | 42 | | | 28 | | |
| L4B | A | 112 | 5700 (39.3) | 4450 (30.7) | 64 | 6550 (45.2) | 5050 (34.8) |
| | B | 61 | | | 13 | 5750 (39.6) | |
| | C | 119 | | | 63 | 6580 (45.4) | 5150 (35.5) |
| | D | 69 | | | 13 | 5620 (38.7) | |
| L6B | A | 168 | 6860 (47.3) | 5200 (35.9) | 13 | 4970 (34.3) | 4800 (33.1) |
| | B | 175 | | | 20 | 5380 (37.1) | |
| | C | 188 | | | 28 | 6520 (45.0) | 5400 (37.2) |
| | D | 183 | | | 23 | | |
| M0B | A | 69 | 10720 (73.9) | 6700 (46.2) | 14 | 5620 (38.7) | 5300 (36.5) |
| | B | 75 | | | 20 | 5870 (40.5) | |
| | C | 84 | | | 22 | 5830 (40.2) | 5000 (34.5) |
| | D | 81 | | | 19 | | |
| M4B | A | 60 | 10730 (74.0) | 5800 (40.0) | 13 | 5500 (37.9) | 5000 (34.5) |
| | B | 63 | | | 16 | 5700 (39.3) | |
| | C | 76 | | | 26 | 6550 (45.2) | 5150 (35.5) |
| | D | 71 | | | 21 | 6270 (43.2) | |
| M9B | A | 49 | 12880 (88.8) | 6600 (45.5) | 15 | 5300 (36.5) | 5000 (34.5) |
| | B | 71 | 12330 (85.0) | | 37 | 5740 (39.6) | |
| | C | 82 | | | 42 | 7200 (49.6) | 5450 (37.6) |
| | D | 77 | | | 37 | | |
| H0B | A | 22 | 12690 (87.5) | 7150 (49.3) | 9 | 5970 (41.2) | 5200 (35.9) |
| | B | 28 | | | 15 | 6130 (42.3) | 5350 (36.9) |
| | C | 36 | | | 20 | 6230 (43.0) | 5250 (36.2) |
| | D | 33 | | | 17 | 6120 (42.2) | |
| H4B | A | 91 | 11240 (77.5) | 6000 (41.4) | 14 | 5390 (37.2) | 5000 (34.5) |
| | B | 94 | | | 17 | 5560 (38.3) | |
| | C | 107 | | | 27 | 6390 (44.1) | 4950 (34.1) |
| | D | 100 | | | 20 | 6260 (43.2) | |
| H9B | A | 118 | 13830 (95.4) | 6850 (47.2) | 26 | 5820 (40.1) | 5050 (34.8) |
| | B | 125 | | | 33 | 5990 (41.3) | |
| | C | 138 | | | 41 | 6360 (43.9) | 5250 (36.2) |
| | D | 132 | | | 35 | | |

**Table B.4: Mechanical Properties of Concrete at Time of Development Length Testing, Specimens with Rusted Strand**

| Beam Specimens | | Beam Concrete | | | Cast-in-Place Deck Concrete | | |
|---|---|---|---|---|---|---|---|
| | | Age days | $f'_c$ psi (MPa) | $E_c$ ksi (GPa) | Age days | $f'_c$ psi (MPa) | $E_c$ ksi (GPa) |
| M0R | A | 182 | 11750 (81.0) | 6250 (43.1) | 9 | 5280 (36.4) | 5250 (36.2) |
| | B | 184 | | | 12 | 5570 (38.4) | |
| | C | 194 | | | 17 | 5800 (40.0) | 5200 (35.9) |
| | D | 188 | | | 11 | 5480 (37.8) | |
| M4R | A | 97 | 11050 (76.2) | 6400 (44.1) | 14 | 4250 (29.3) | 4500 (31.0) |
| | B | 102 | | | 19 | 4360 (30.1) | |
| | C | 112 | | | 20 | 5690 (39.2) | 5250 (36.2) |
| | D | 109 | | | 17 | 5460 (37.6) | |
| M9R | A | 113 | 12420 (85.6) | 6900 (47.6) | 11 | 5670 (39.1) | 5650 (39.0) |
| | B | 119 | 13010 (89.7) | | 17 | 6100 (42.1) | |
| | C | 129 | | | 22 | 6370 (43.9) | 5600 (38.6) |
| | D | 126 | | | 19 | 6080 (41.9) | |
| H0R | A | 221 | 14170 (97.7) | 6650 (45.9) | 10 | 5210 (35.9) | 5000 (34.5) |
| | B | 226 | | | 15 | 5450 (37.6) | |
| | C | 239 | | | 24 | 6450 (44.5) | 5400 (37.2) |
| | D | 233 | | | 18 | 6370 (43.9) | |
| H4R | A | 131 | 13500 (93.1) | 7050 (48.6) | 12 | 4850 (33.4) | 4450 (30.7) |
| | B | 134 | | | 15 | 5080 (35.0) | |
| | C | 144 | | | 20 | 5250 (36.2) | 4700 (32.4) |
| | D | 139 | | | 15 | 5120 (35.3) | |
| H9R | A | 153 | 12370 (85.3) | 6400 (44.1) | 15 | 5600 (38.6) | 5200 (35.9) |
| | B | 158 | | | 20 | 5620 (38.7) | |
| | C | 167 | 14720 (102) | 7000 (48.3) | 19 | 6740 (46.5) | 5700 (39.3) |
| | D | 162 | | | 14 | 6570 (45.3) | |

**Table B.5: Average Concrete Compressive Strengths Obtained from Member-Cured and Match-Cured Test Cylinders at Various Ages**

| Beam Specimens | Release of Prestress | | Pull-Out Tests | | 28 Days (56 for Hxx) | |
|---|---|---|---|---|---|---|
| | Member-Cured psi (MPa) | Match-Cured psi (MPa) | Member-Cured psi (MPa) | Match-Cured psi (MPa) | Member-Cured psi (MPa) | Match-Cured psi (MPa) |
| L0B | 4240 (29.2) | 5170 (35.6) | 5250 (36.2) | 6230 (43.0) | 6220 (42.9) | 6550 (45.2) |
| L4B | 4490 (31.0) | 5120 (35.3) | 4970 (34.3) | 5720 (39.4) | 5690 (39.2) | 6490 (44.7) |
| L6B | 4710 (32.5) | 5760 (39.7) | 5500 (37.9) | 6710 (46.3) | 6860 (47.3) | 8380 (57.8) |
| M0B | 6610 (45.6) | 7000 (48.3) | 7800 (53.8) | 8540 (58.9) | 10720 (73.9) | 10770 (74.3) |
| M4B | 6900 (47.6) | 8680 (59.8) | 9370 (64.6) | 9930 (68.5) | 11370 (78.4) | 10810 (74.5) |
| M9B | 7890 (54.4) | — | 8440 (58.2) | — | 11760 (81.1) | — |
| H0B | 11030 (76.1) | 11740 (80.9) | 11070 (76.3) | 11900 (82.1) | 12740 (87.8) | 13660 (94.2) |
| H4B | 9660 (66.6) | 10730 (74.0) | 10060 (69.4) | 11120 (76.7) | 11240 (77.5) | 11520 (79.4) |
| H9B | 9300 (64.1) | — | 10420 (71.8) | — | 13790 (95.1) | — |
| L0R | 4540 (31.3) | 5440 (37.5) | 5100 (35.2) | 6120 (42.2) | 5850 (40.3) | 6610 (45.6) |
| L4R | 3970 (27.4) | 4340 (29.9) | 4400 (30.3) | 4910 (33.9) | 5540 (38.2) | 5970 (41.1) |
| L6R | 4630 (31.9) | 5720 (39.4) | 5450 (44.5) | 6260 (43.2) | 7820 (53.9) | 7880 (54.3) |
| M0R | 7290 (50.3) | 7800 (53.8) | 8290 (57.2) | 8750 (60.3) | 11060 (76.3) | 10570 (72.9) |
| M4R | 7950 (54.8) | 8200 (56.5) | 8960 (61.8) | 9110 (62.8) | 10920 (75.3) | 11010 (75.9) |
| M9R | 7630 (52.6) | 8420 (58.1) | 9420 (65.0) | 9550 (65.8) | 11990 (82.7) | 11600 (80.0) |
| H0R | 9020 (62.2) | 11380 (78.5) | 10480 (72.3) | 11570 (79.8) | 12800 (88.3) | 12800 (88.3) |
| H4R | 10910 (75.2) | 12260 (84.5) | 11710 (80.7) | 12380 (85.4) | 13050 (90.0) | 13680 (94.3) |
| H9R-A/B | 7860 (54.2) | 10190 (70.3) | — | 10480 (72.3) | 12370 (85.3) | 11750 (81.0) |
| H9R-C/D | 9270 (63.9) | 11820 (81.5) | 10690 (73.7) | 12180 (84.0) | 14200 (97.9) | 14050 (96.9) |

# APPENDIX C: CONCRETE STRAIN PROFILES

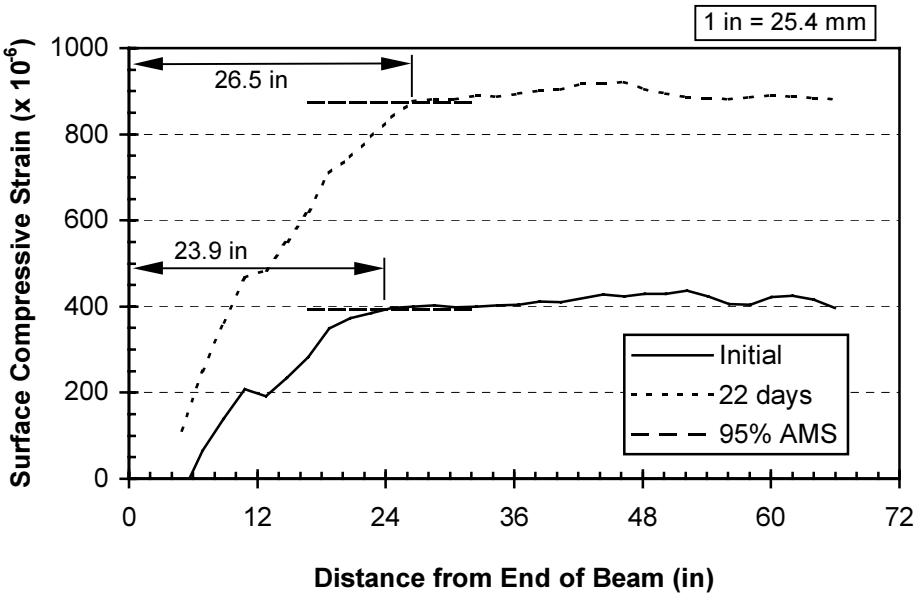


**Figure C.1: Specimen L0B-A Measured Initial and Long Term Strain Profiles**

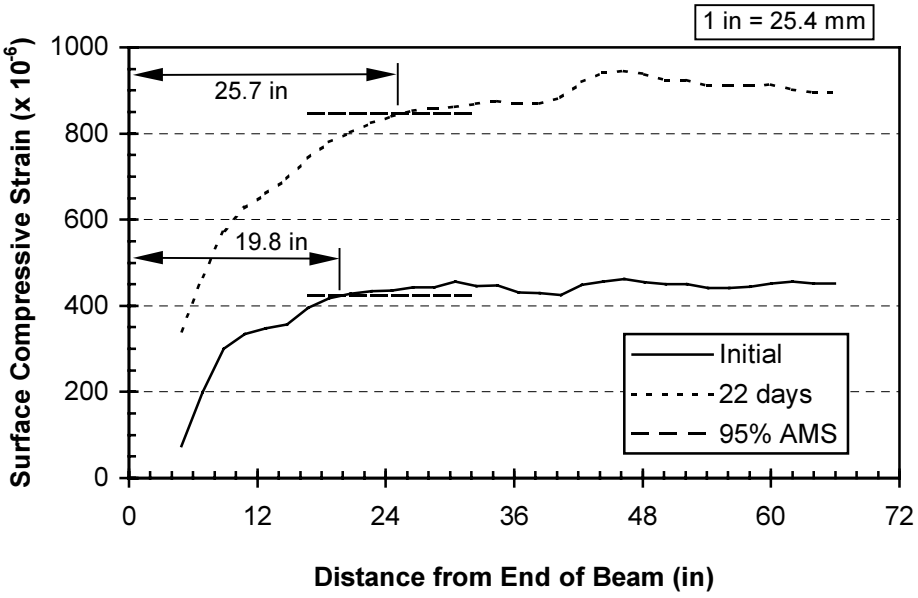


**Figure C.2: Specimen L0B-B Measured Initial and Long Term Strain Profiles**

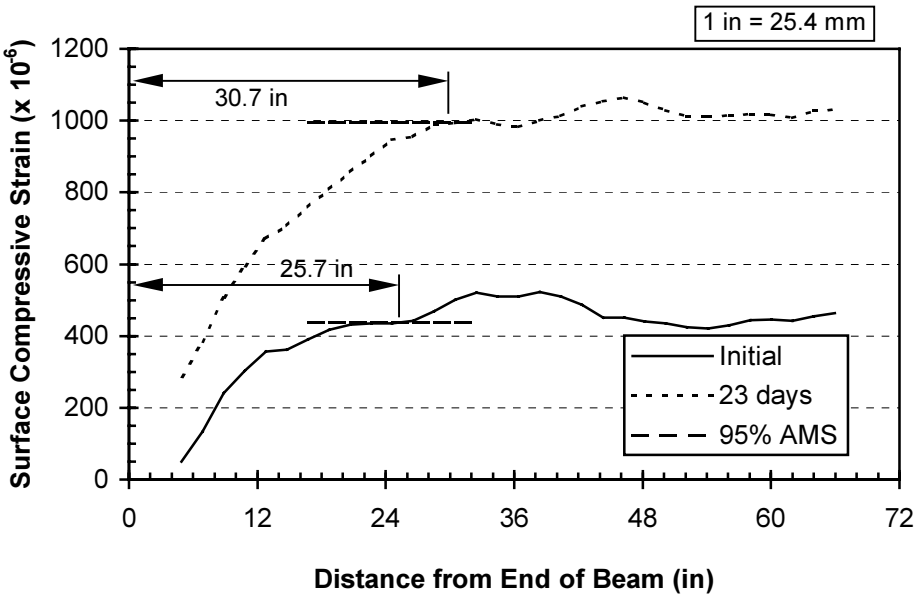


**Figure C.3: Specimen L0B-C Measured Initial and Long Term Strain Profiles**

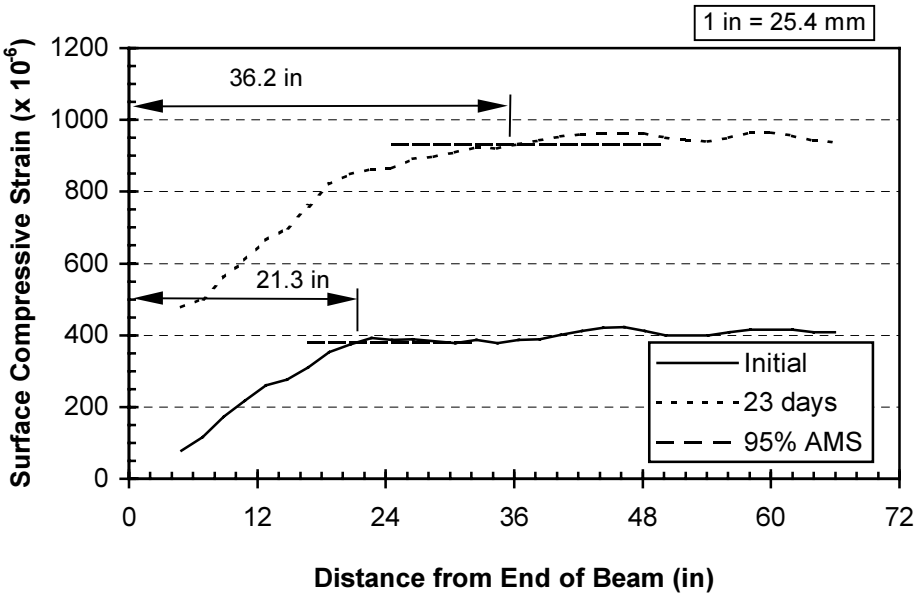


**Figure C.4: Specimen L0B-D Measured Initial and Long Term Strain Profiles**

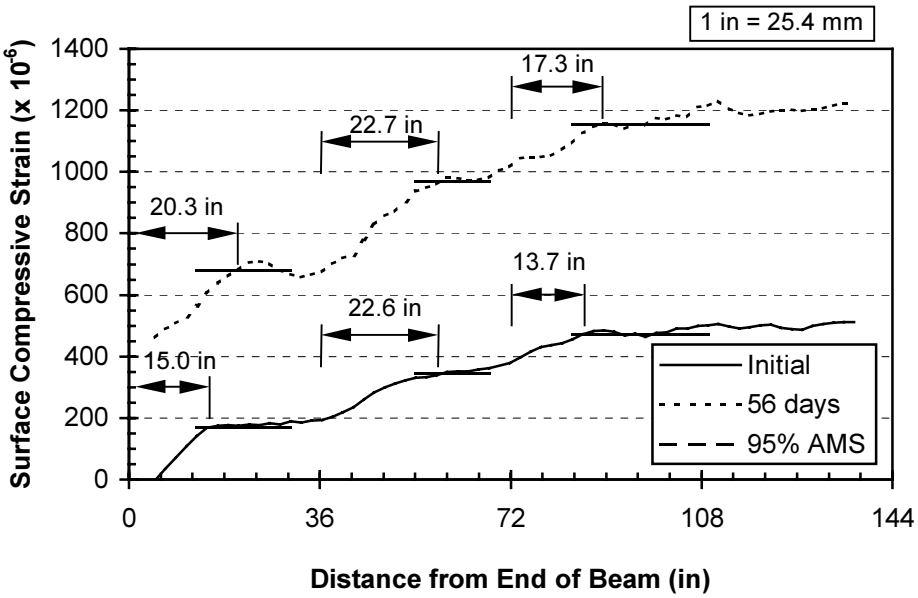


**Figure C.5: Specimen L4B-A Measured Initial and Long Term Strain Profiles**

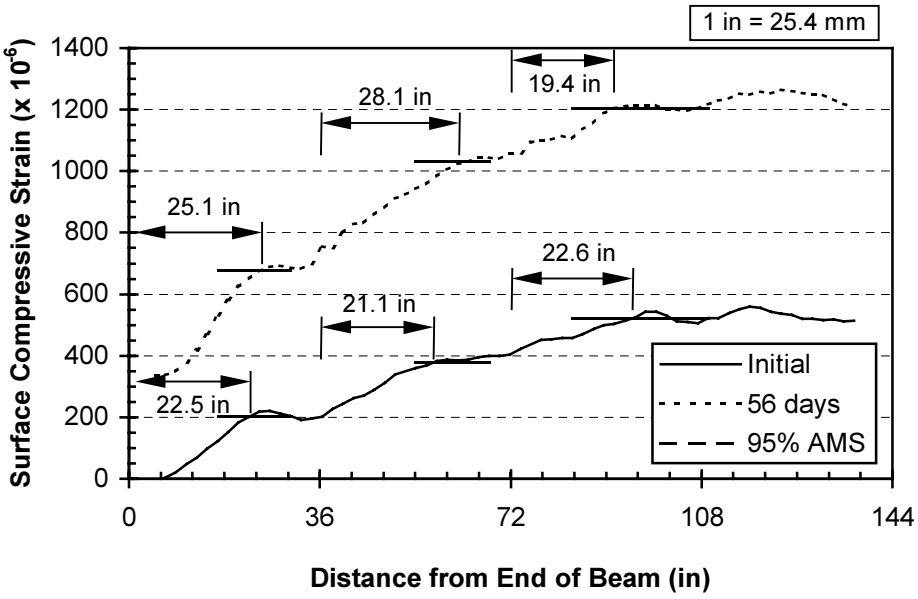


**Figure C.6: Specimen L4B-B Measured Initial and Long Term Strain Profiles**

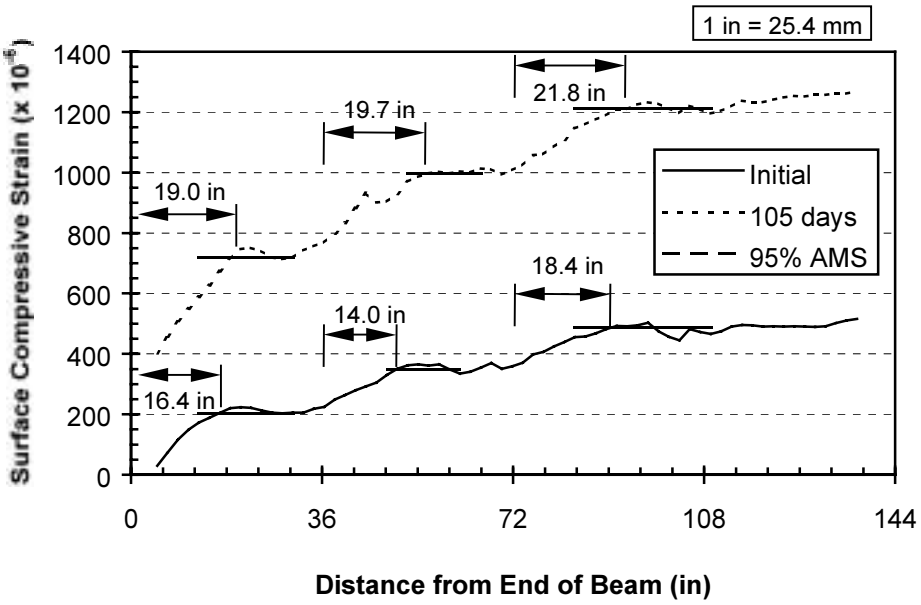


**Figure C.7: Specimen L4B-C Measured Initial and Long Term Strain Profiles**

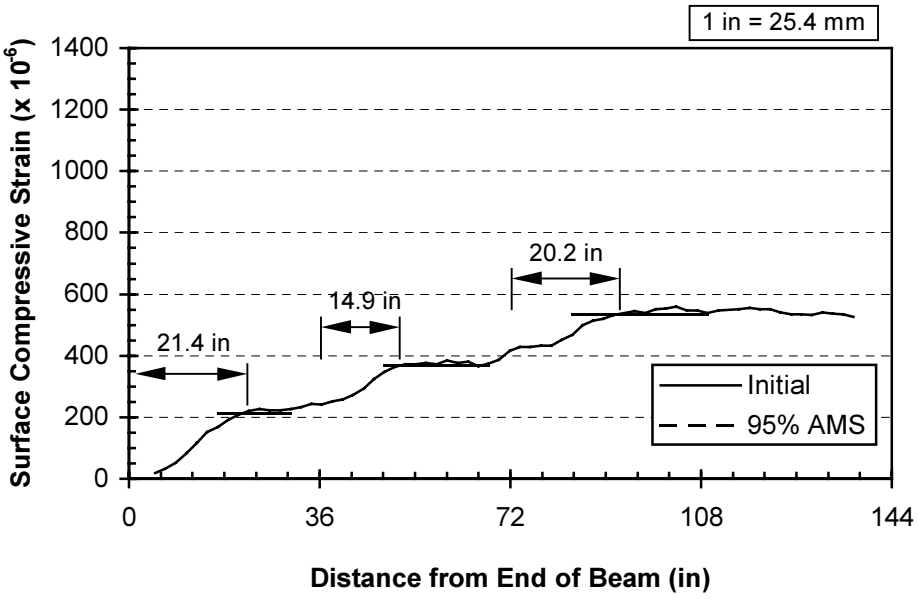


**Figure C.8: Specimen L4B-D Measured Initial Strain Profile (Long Term Strains Not Measured)**

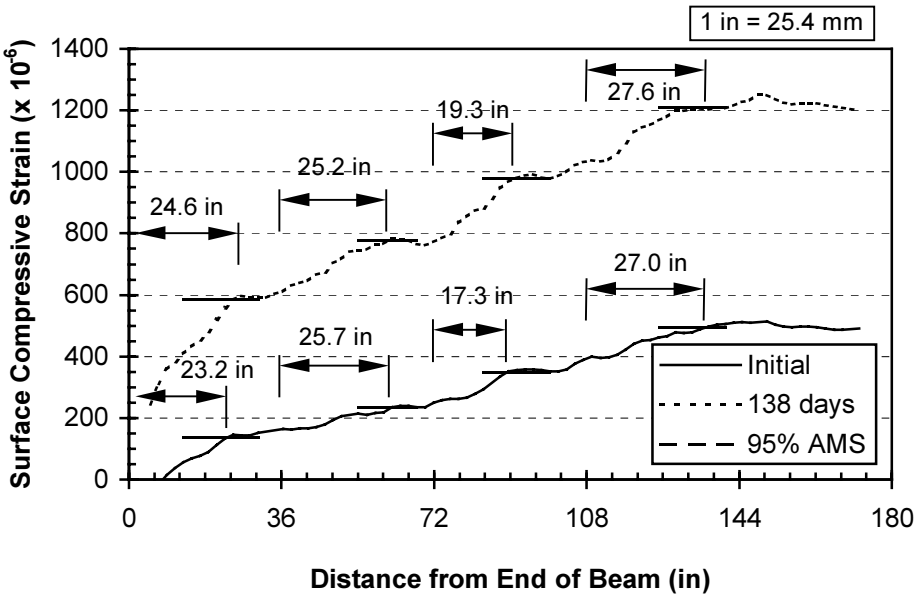


**Figure C.9: Specimen L6B-A Measured Initial and Long Term Strain Profiles**

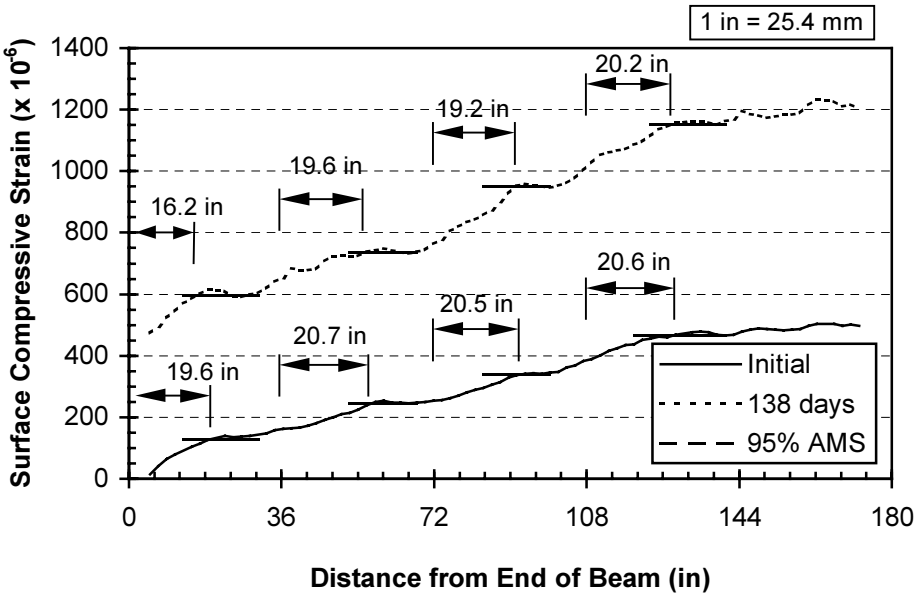


**Figure C.10: Specimen L6B-B Measured Initial and Long Term Strain Profiles**

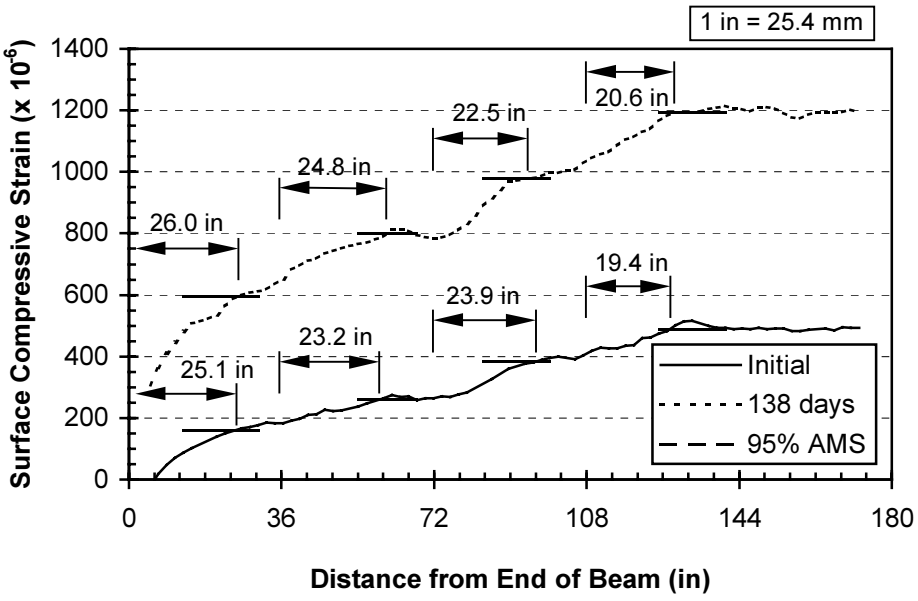


**Figure C.11: Specimen L6B-C Measured Initial and Long Term Strain Profiles**

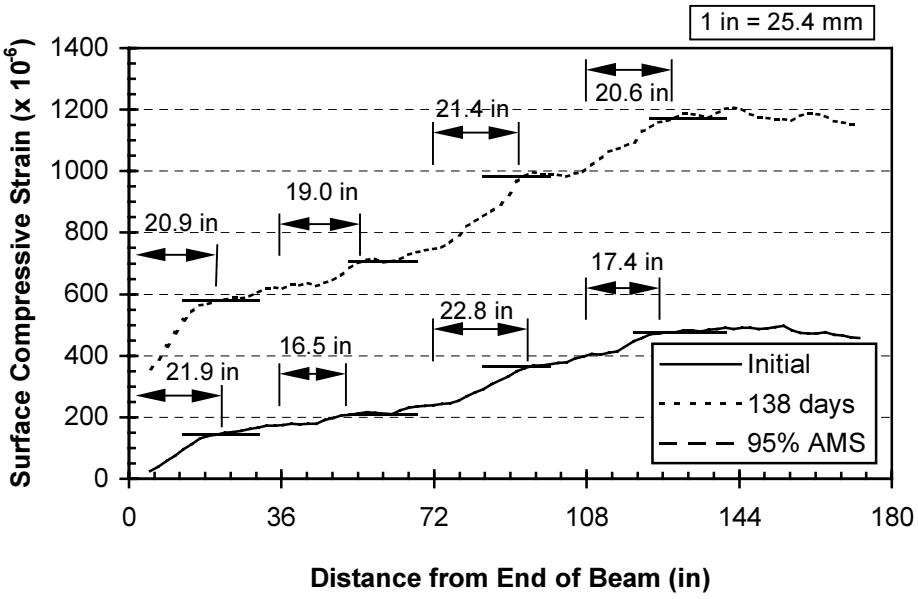


**Figure C.12: Specimen L6B-D Measured Initial and Long Term Strain Profiles**

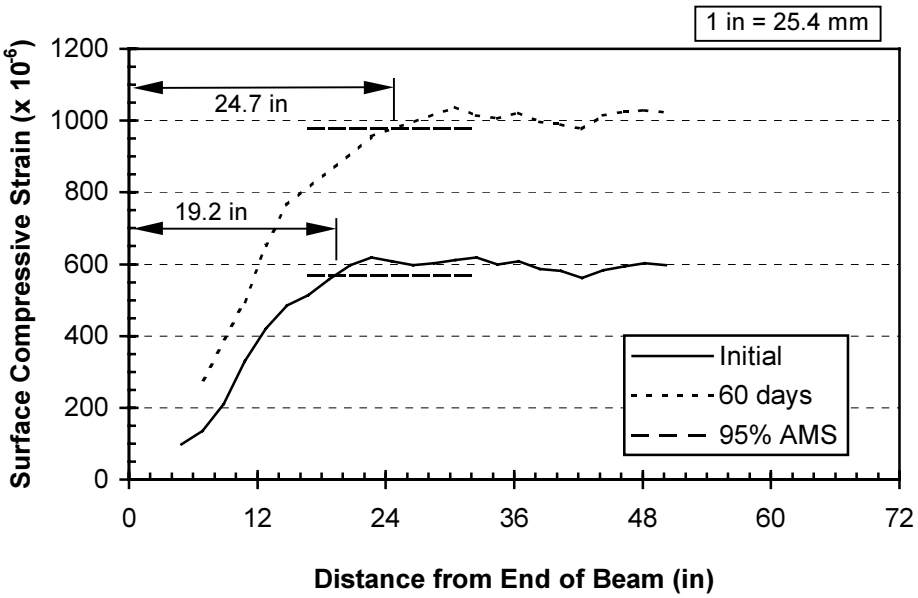


**Figure C.13: Specimen M0B-A Measured Initial and Long Term Strain Profiles**

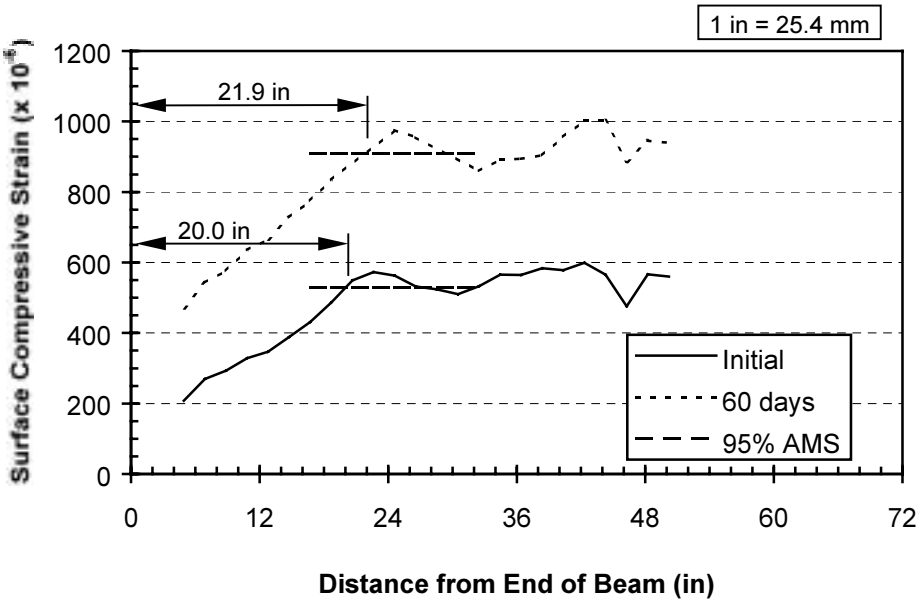


**Figure C.14: Specimen M0B-B Measured Initial and Long Term Strain Profiles**

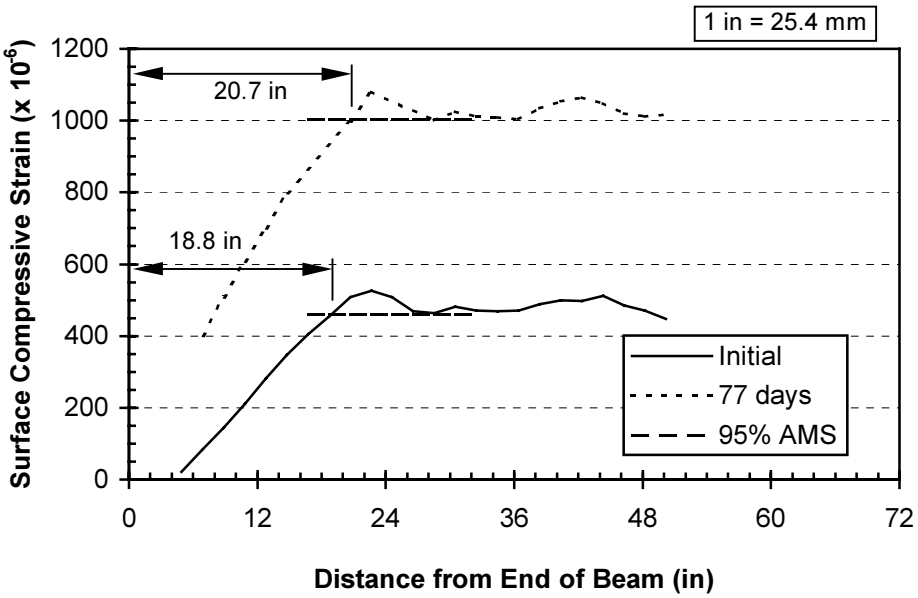


**Figure C.15: Specimen M0B-C Measured Initial and Long Term Strain Profiles**

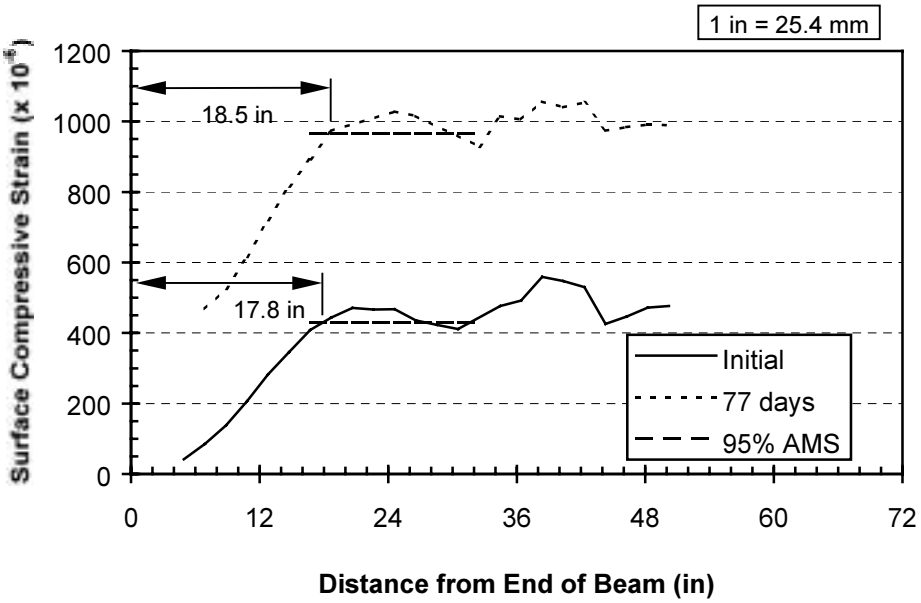


**Figure C.16: Specimen M0B-D Measured Initial and Long Term Strain Profiles**

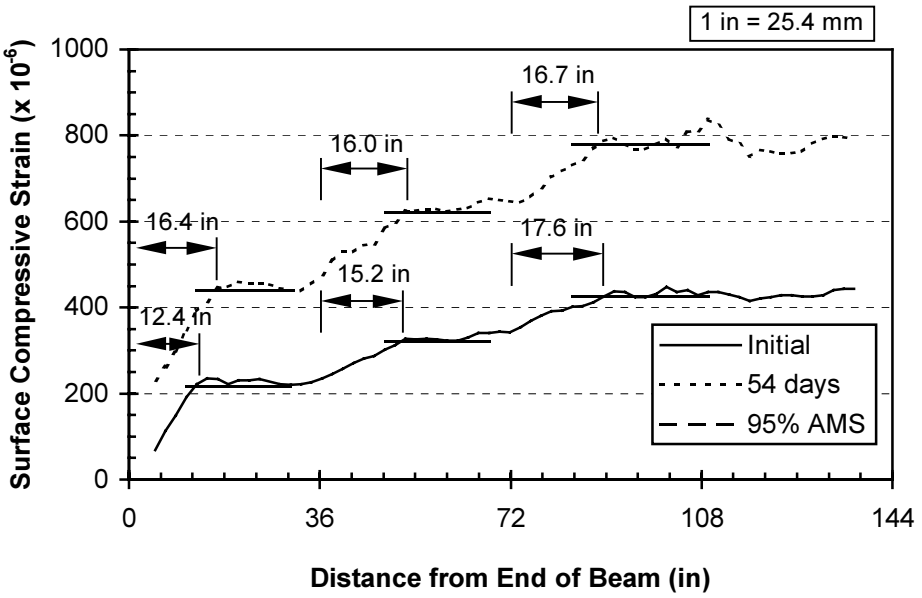


**Figure C.17: Specimen M4B-A Measured Initial and Long Term Strain Profiles**

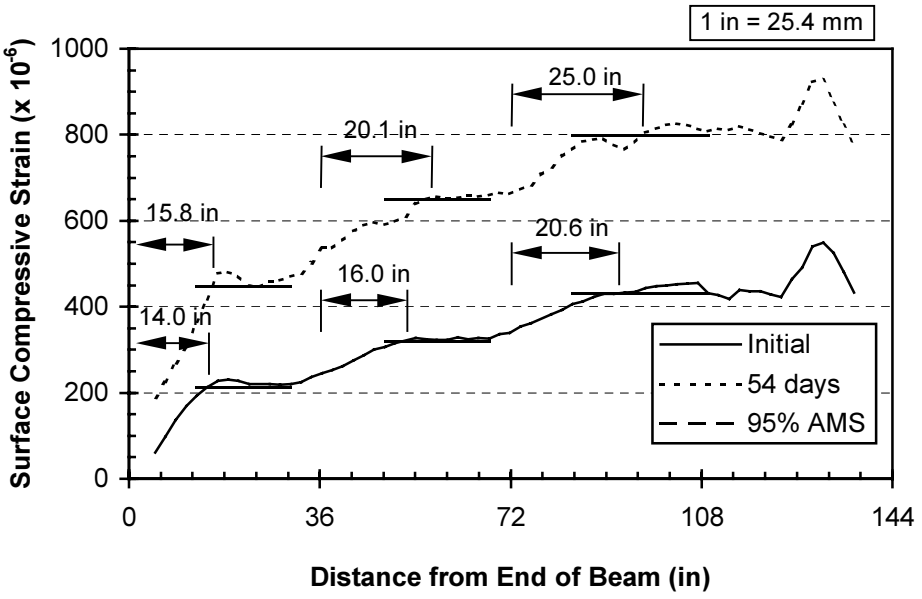


**Figure C.18: Specimen M4B-B Measured Initial and Long Term Strain Profiles**

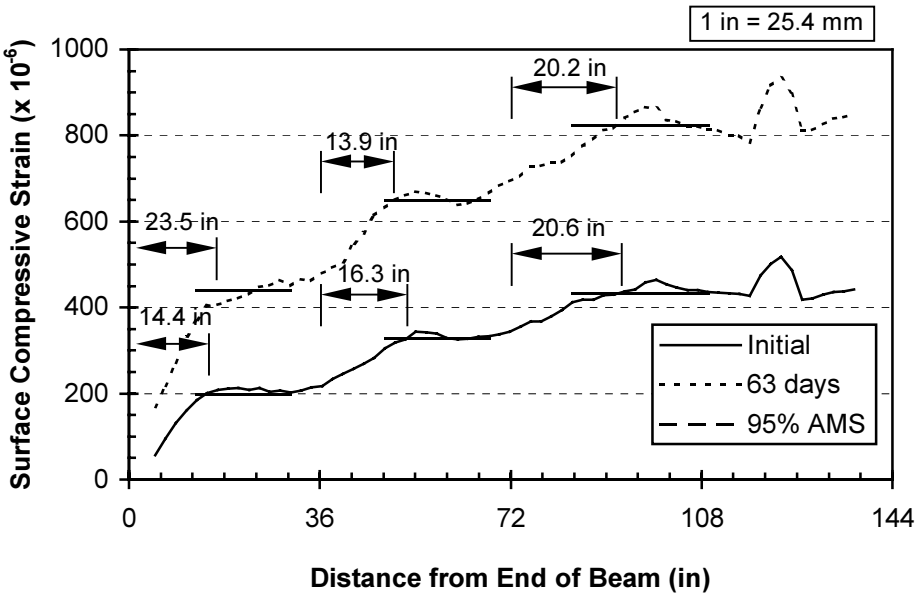


**Figure C.19: Specimen M4B-C Measured Initial and Long Term Strain Profiles**

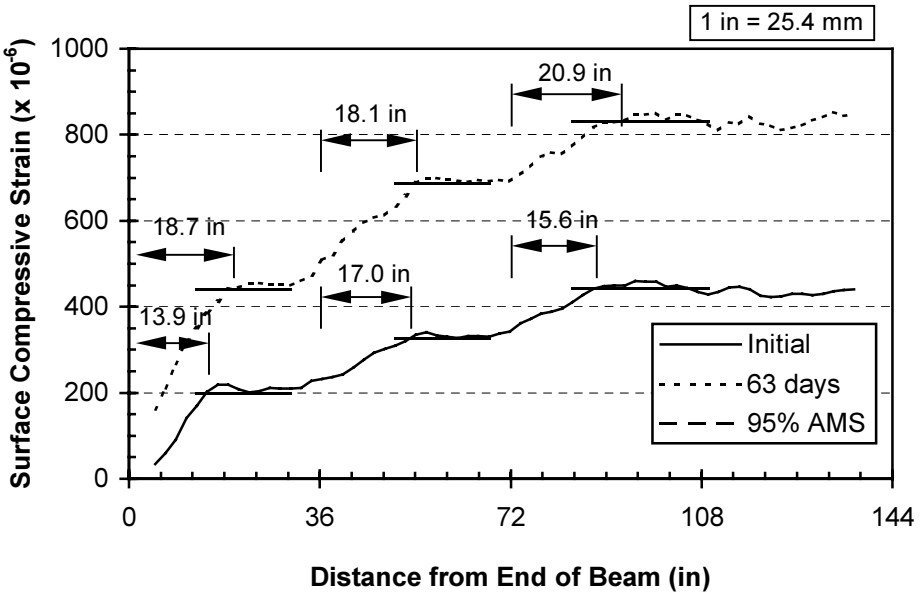


**Figure C.20: Specimen M4B-D Measured Initial and Long Term Strain Profiles**

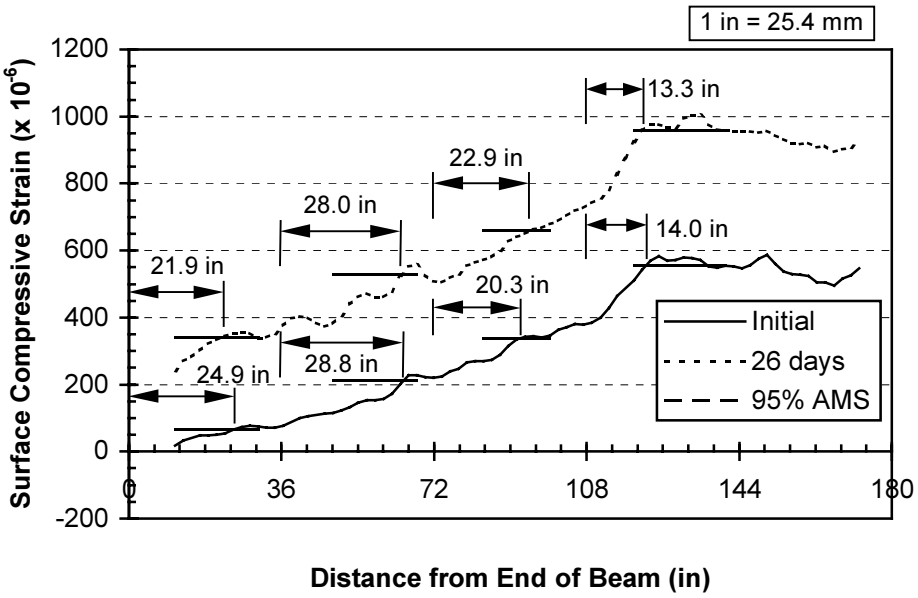


**Figure C.21: Specimen M9B-A Measured Initial and Long Term Strain Profiles**

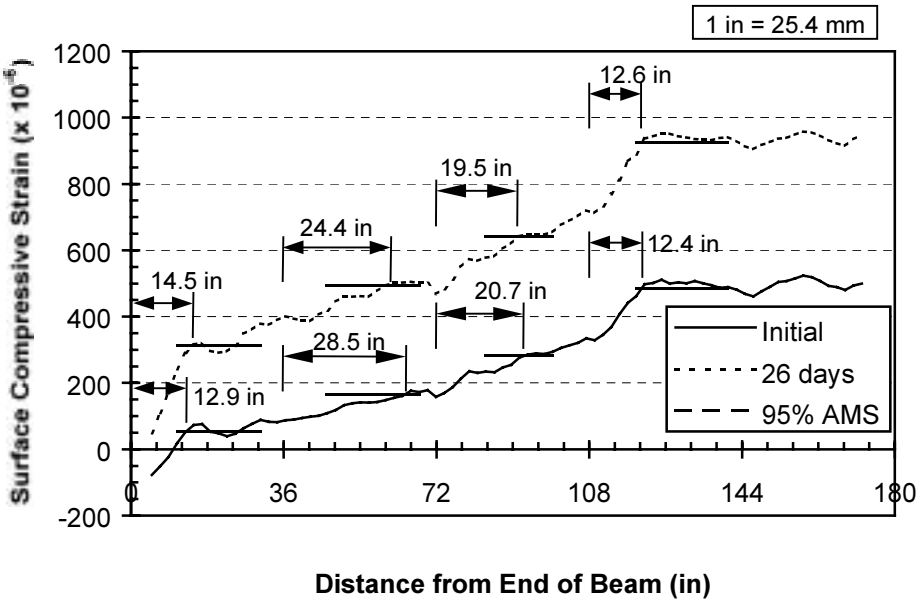


**Figure C.22: Specimen M9B-B Measured Initial and Long Term Strain Profiles**

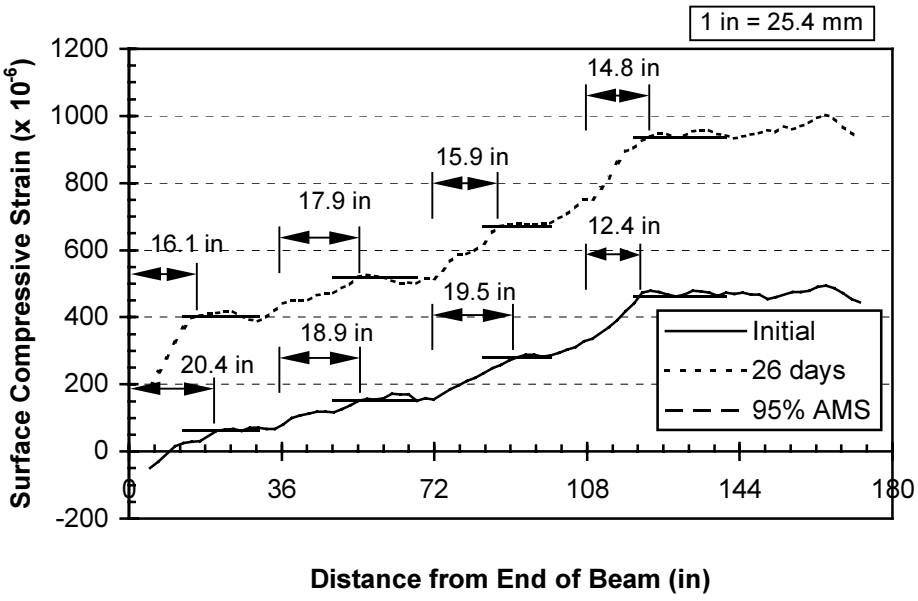


**Figure C.23: Specimen M9B-C Measured Initial and Long Term Strain Profiles**

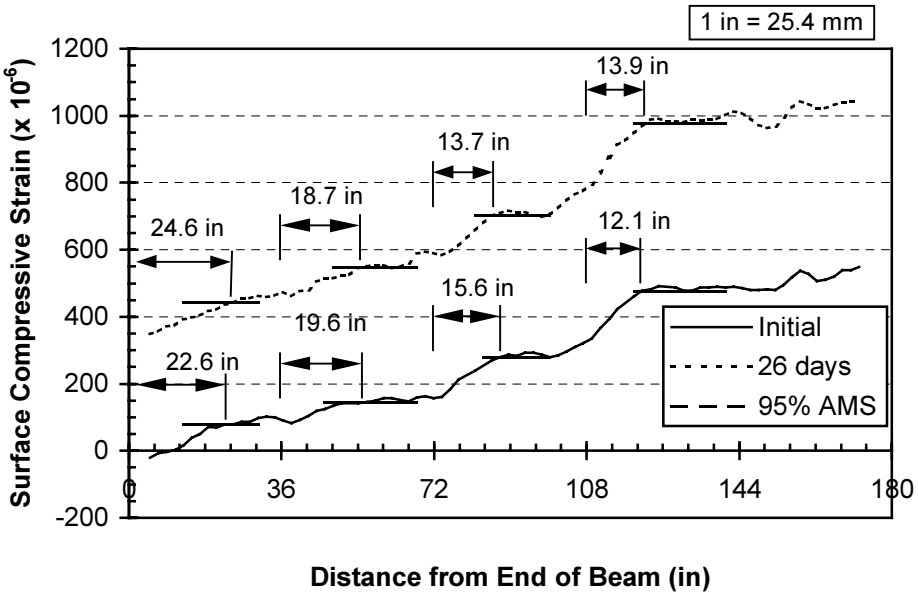


**Figure C.24: Specimen M9B-D Measured Initial and Long Term Strain Profiles**

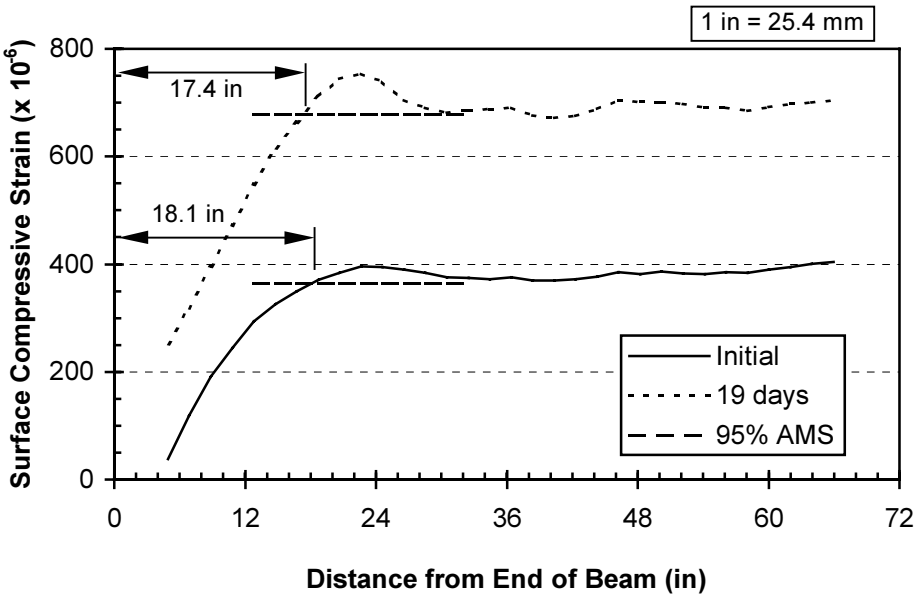


**Figure C.25: Specimen H0B-A Measured Initial and Long Term Strain Profiles**

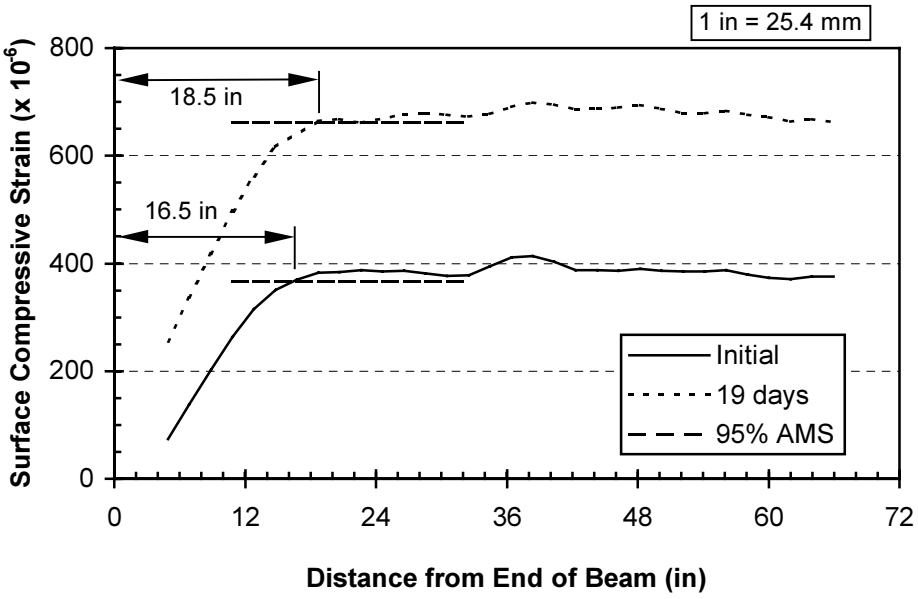


**Figure C.26: Specimen H0B-B Measured Initial and Long Term Strain Profiles**

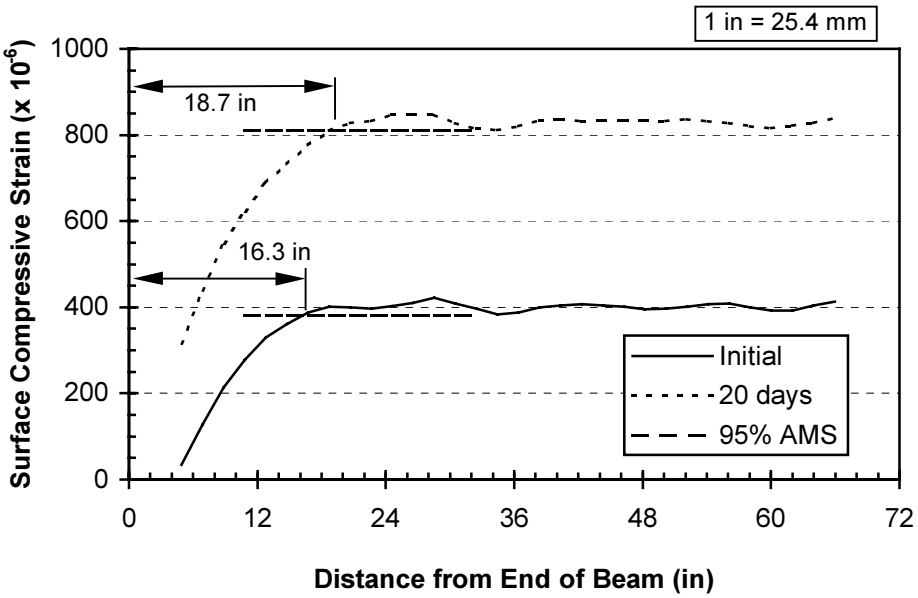


**Figure C.27: Specimen H0B-C Measured Initial and Long Term Strain Profiles**

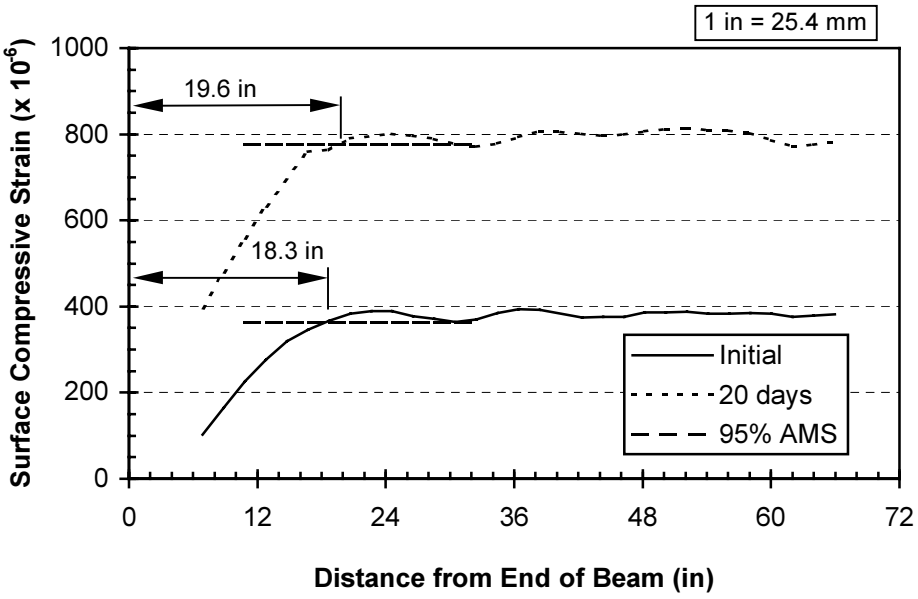


**Figure C.28: Specimen H0B-D Measured Initial and Long Term Strain Profiles**

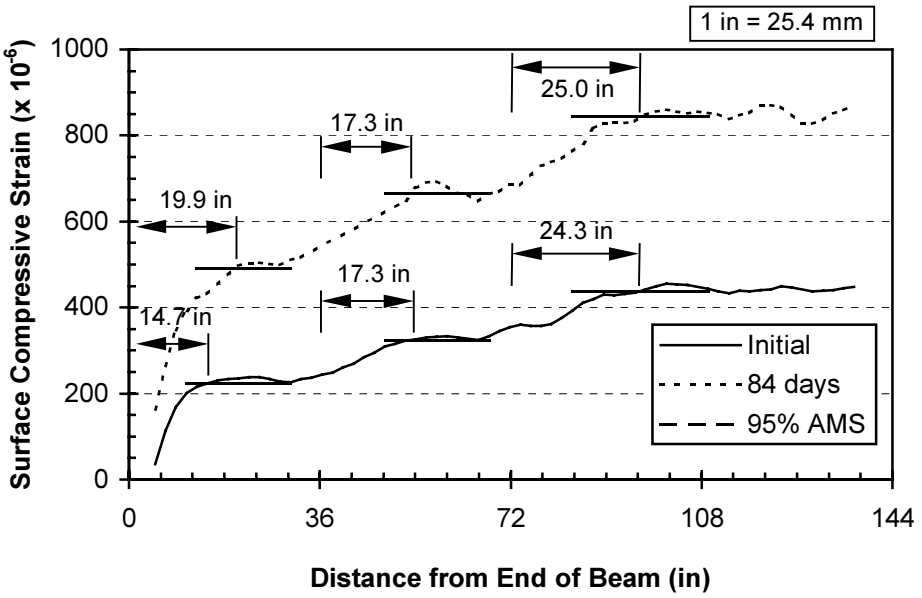


**Figure C.29: Specimen H4B-A Measured Initial and Long Term Strain Profiles**

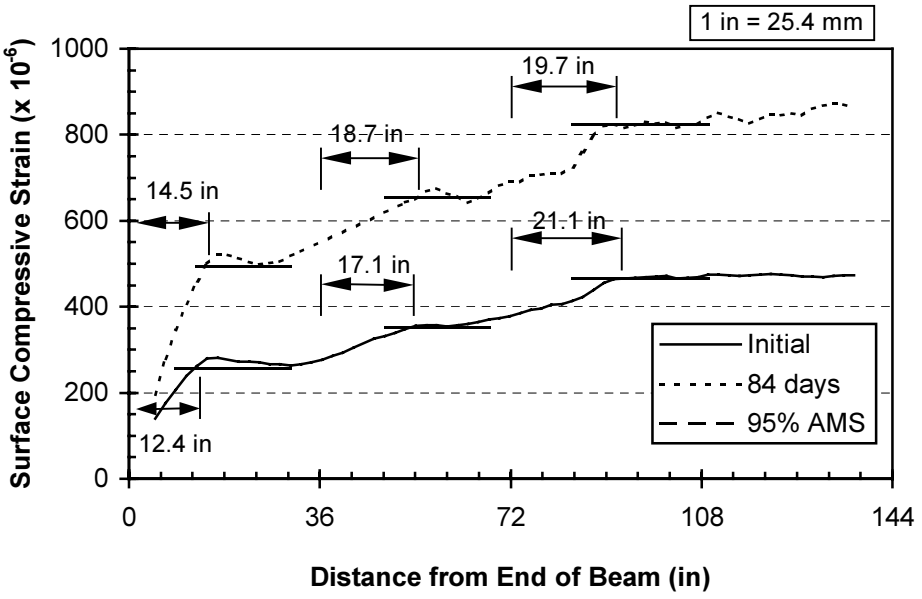


**Figure C.30: Specimen H4B-B Measured Initial and Long Term Strain Profiles**

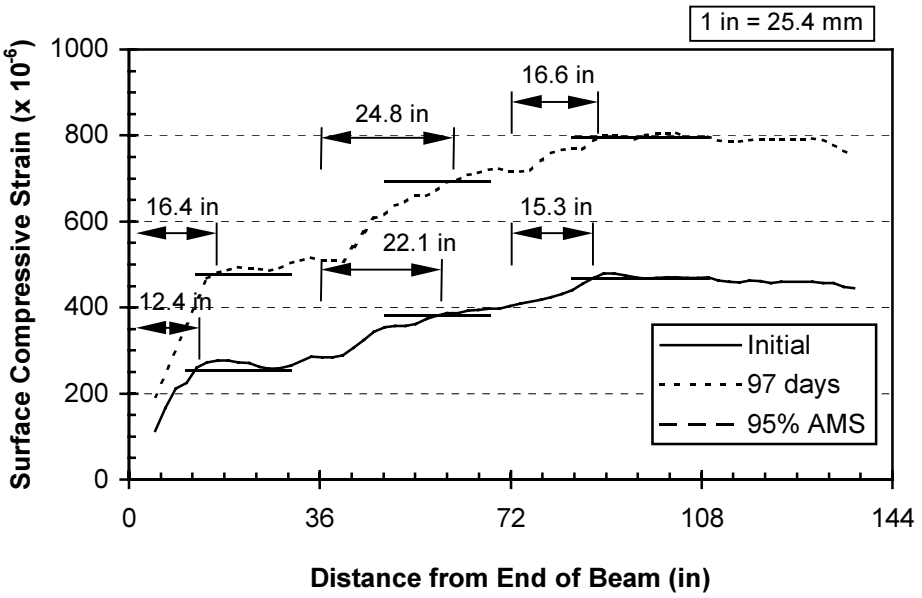


**Figure C.31: Specimen H4B-C Measured Initial and Long Term Strain Profiles**

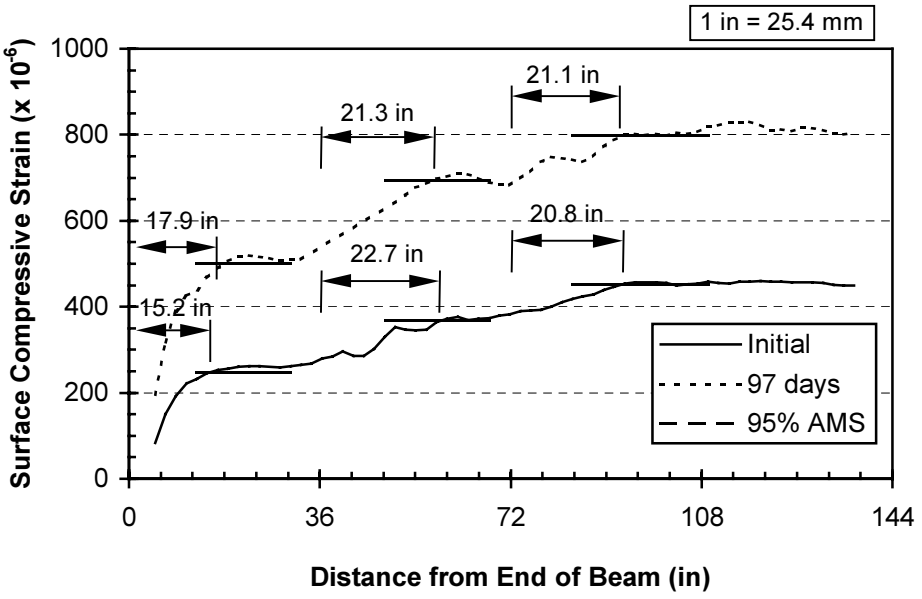


**Figure C.32: Specimen H4B-D Measured Initial and Long Term Strain Profiles**

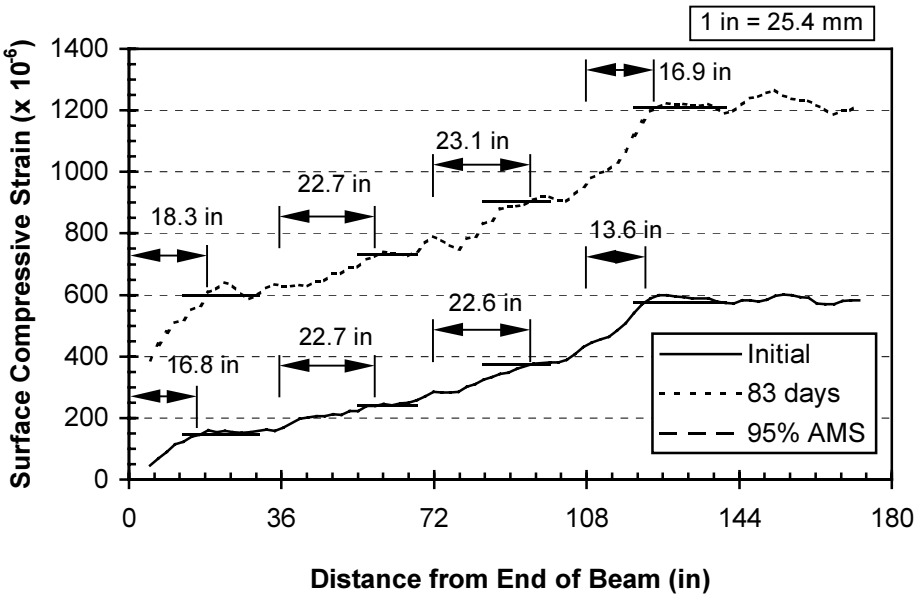


**Figure C.33: Specimen H9B-A Measured Initial and Long Term Strain Profiles**

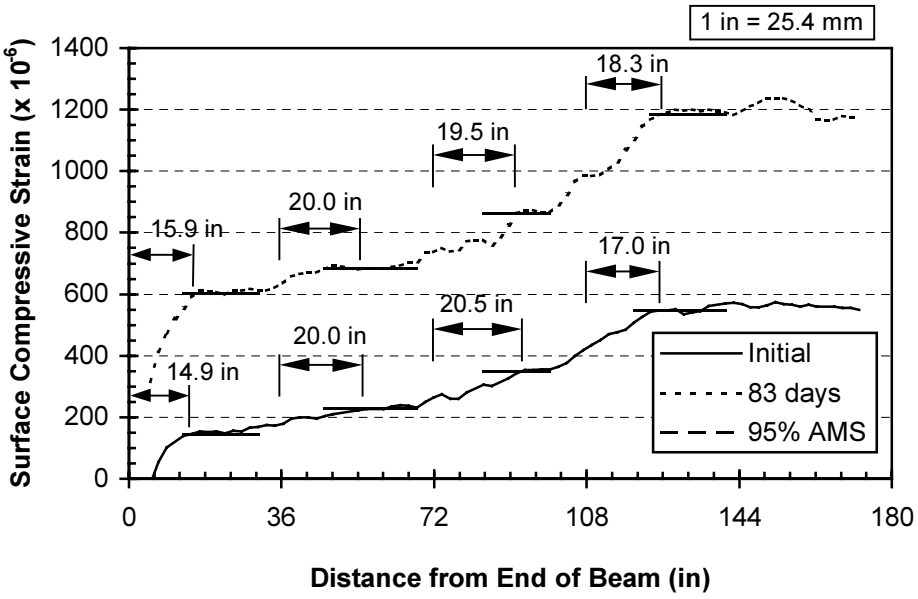


**Figure C.34: Specimen H9B-B Measured Initial and Long Term Strain Profiles**

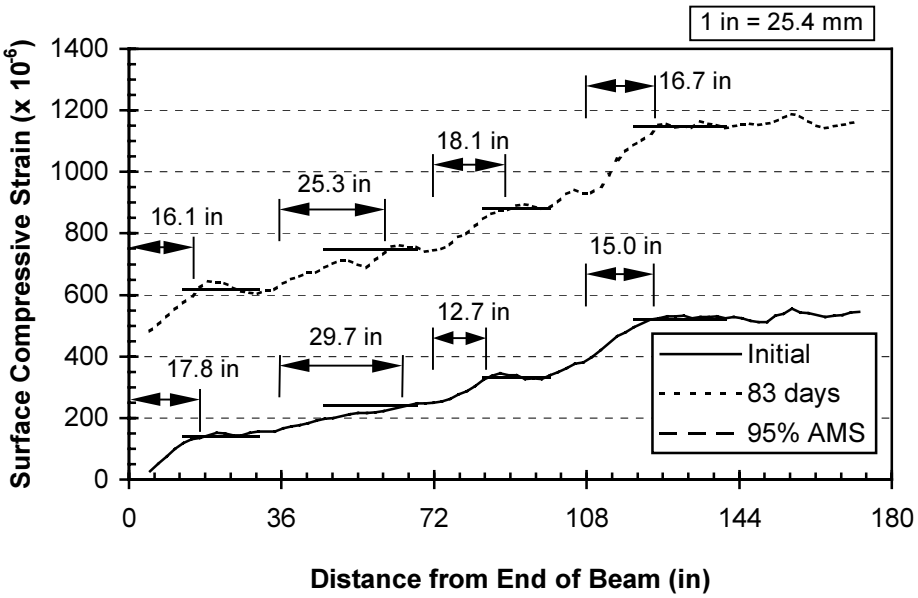


**Figure C.35: Specimen H9B-C Measured Initial and Long Term Strain Profiles**

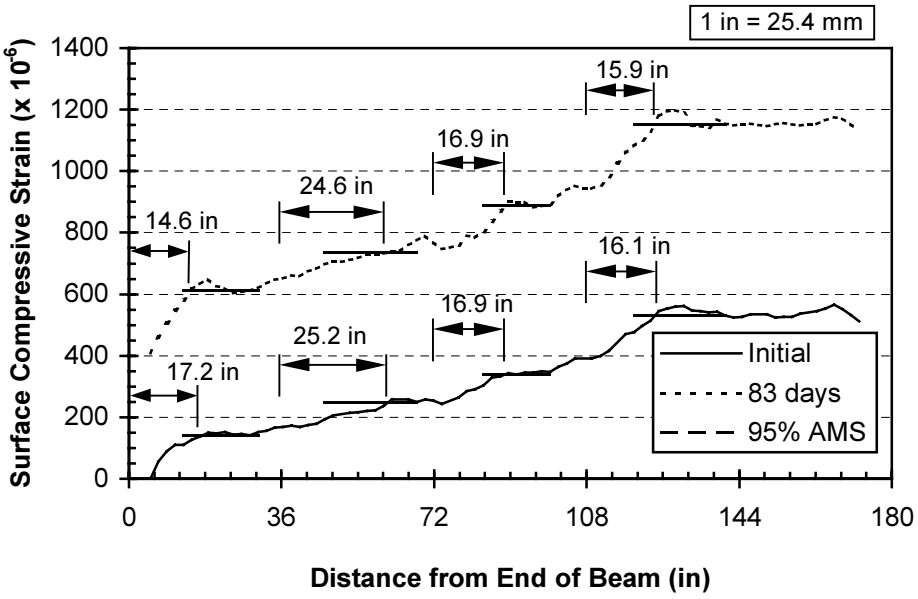


**Figure C.36: Specimen H9B-D Measured Initial and Long Term Strain Profiles**

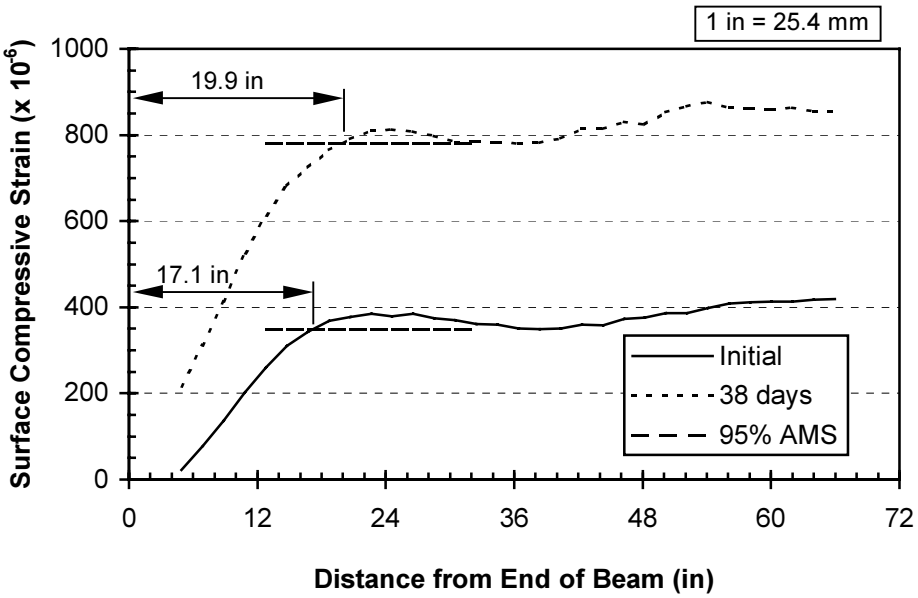


**Figure C.37: Specimen L0R-A Measured Initial and Long Term Strain Profiles**

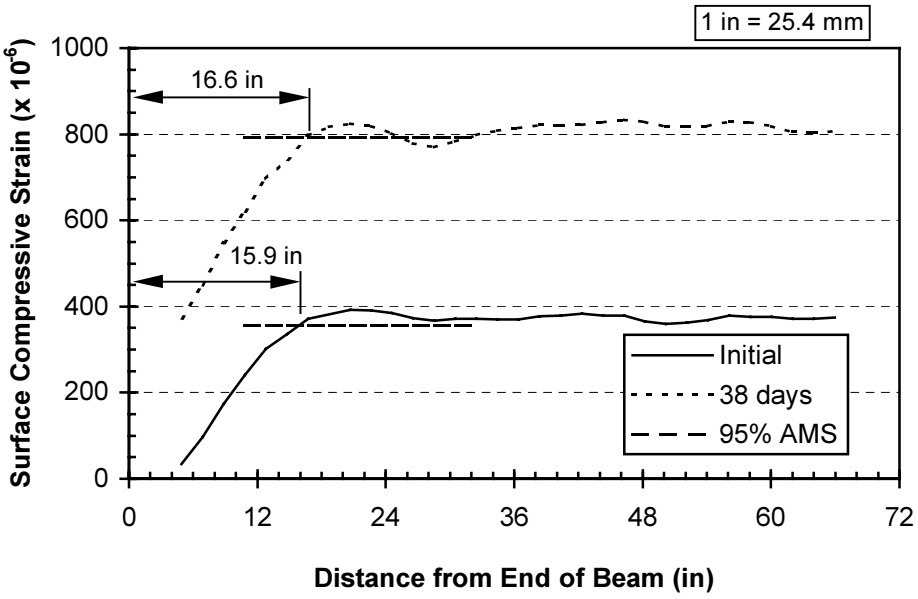


**Figure C.38: Specimen L0R-B Measured Initial and Long Term Strain Profiles**

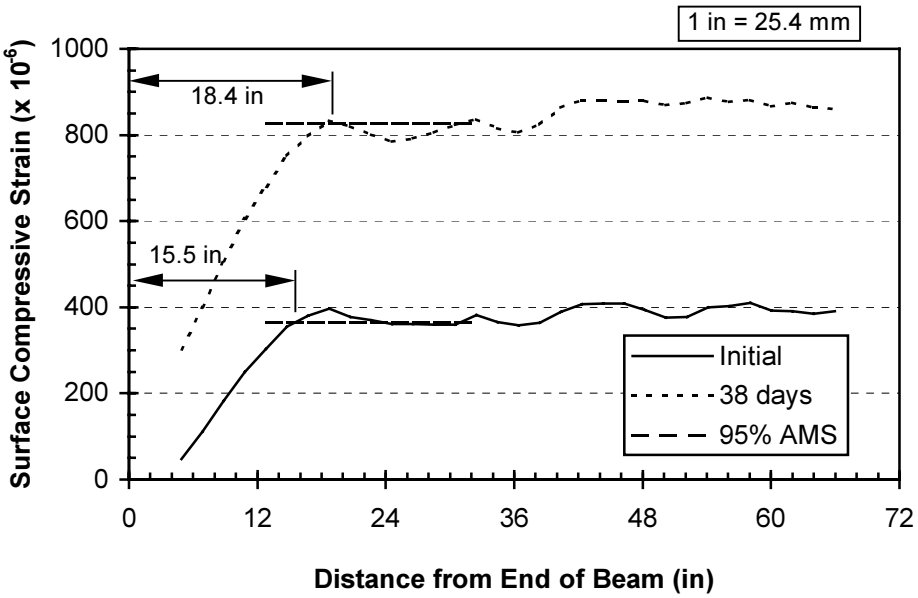


**Figure C.39: Specimen L0R-C Measured Initial and Long Term Strain Profiles**

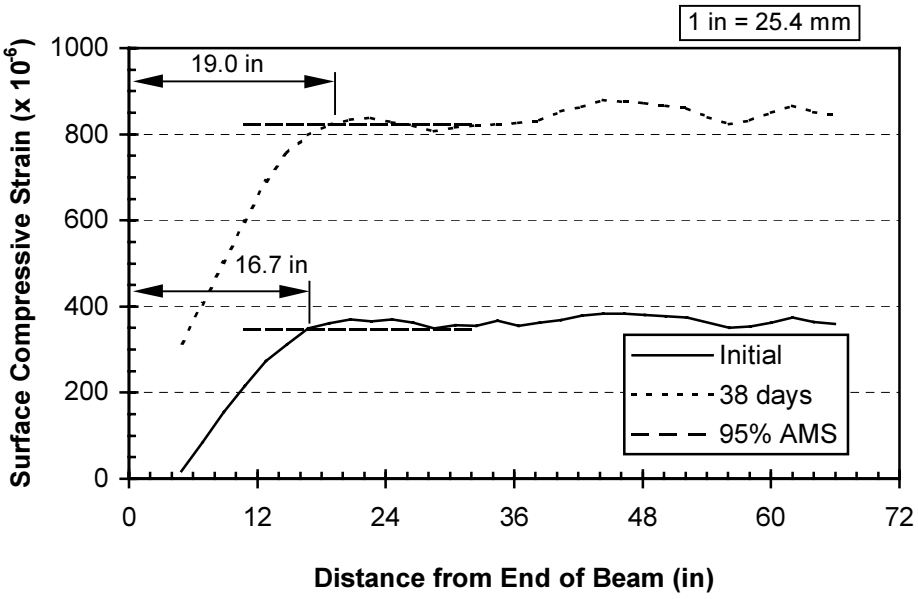


**Figure C.40: Specimen L0R-D Measured Initial and Long Term Strain Profiles**

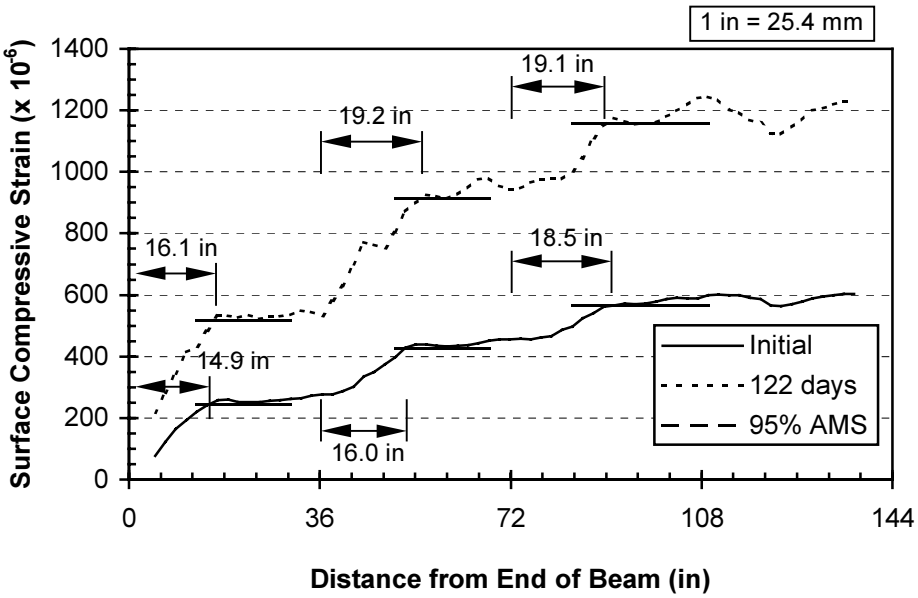


**Figure C.41: Specimen L4R-A Measured Initial and Long Term Strain Profiles**

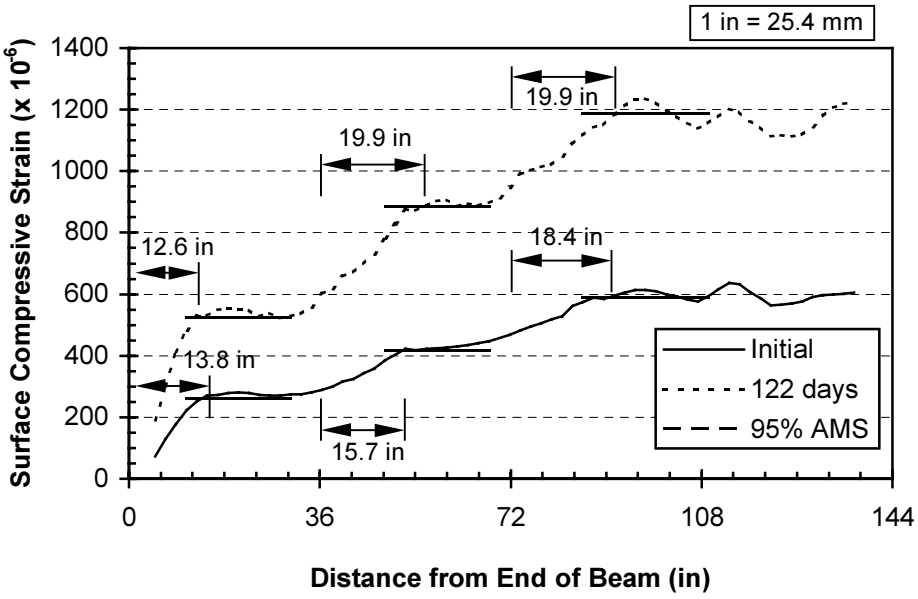


**Figure C.42: Specimen L4R-B Measured Initial and Long Term Strain Profiles**

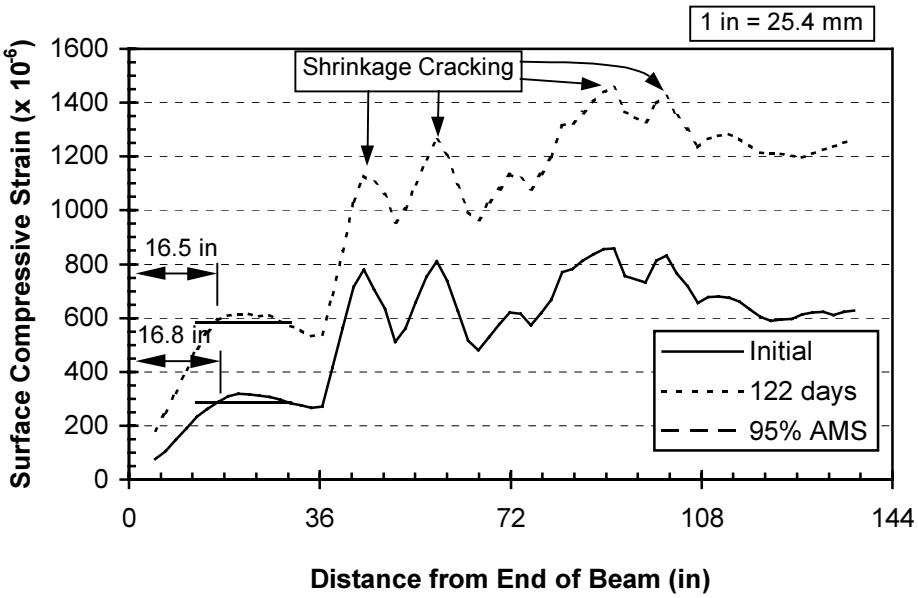


**Figure C.43: Specimen L4R-B Measured Initial and Long Term Strain Profiles**

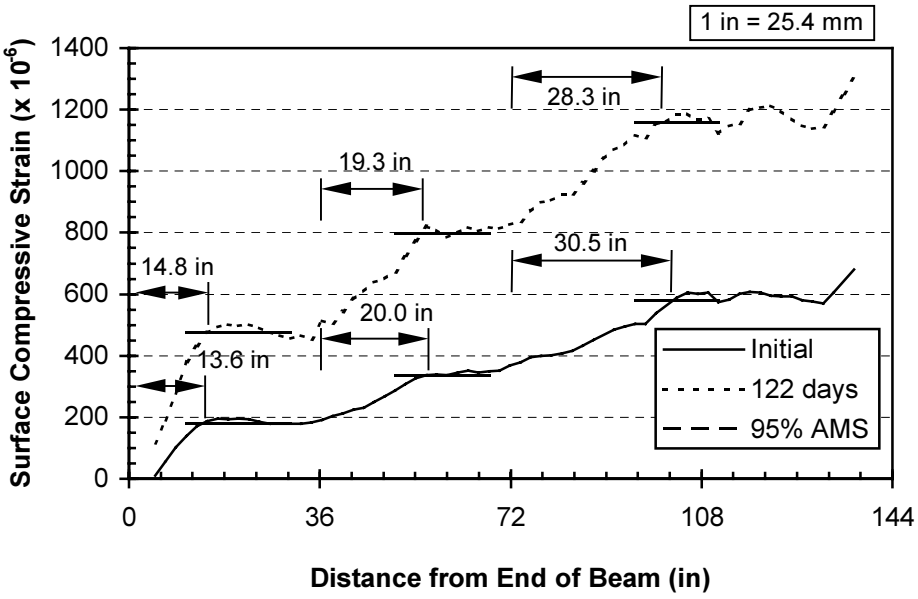


**Figure C.44: Specimen L4R-D Measured Initial and Long Term Strain Profiles**

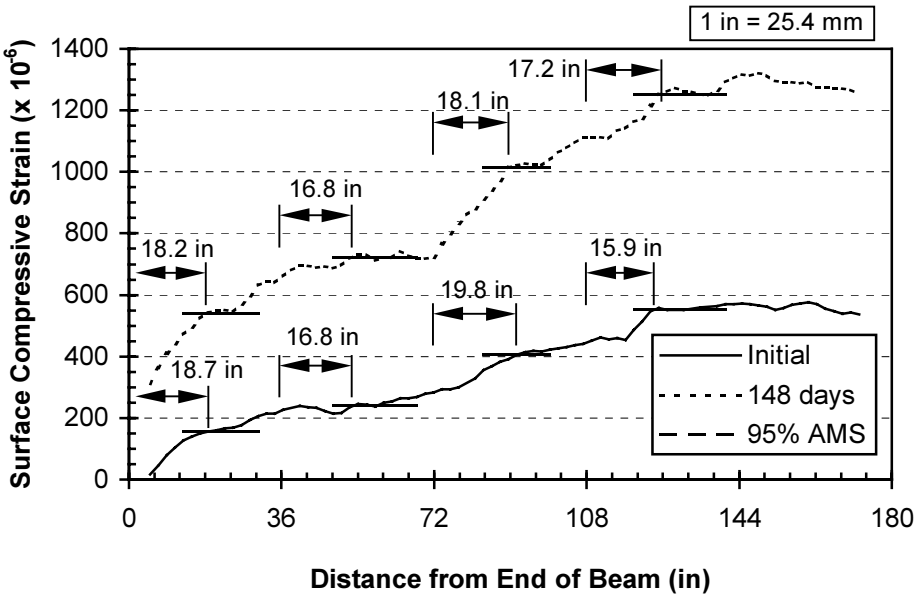


**Figure C.45: Specimen L6R-A Measured Initial and Long Term Strain Profiles**

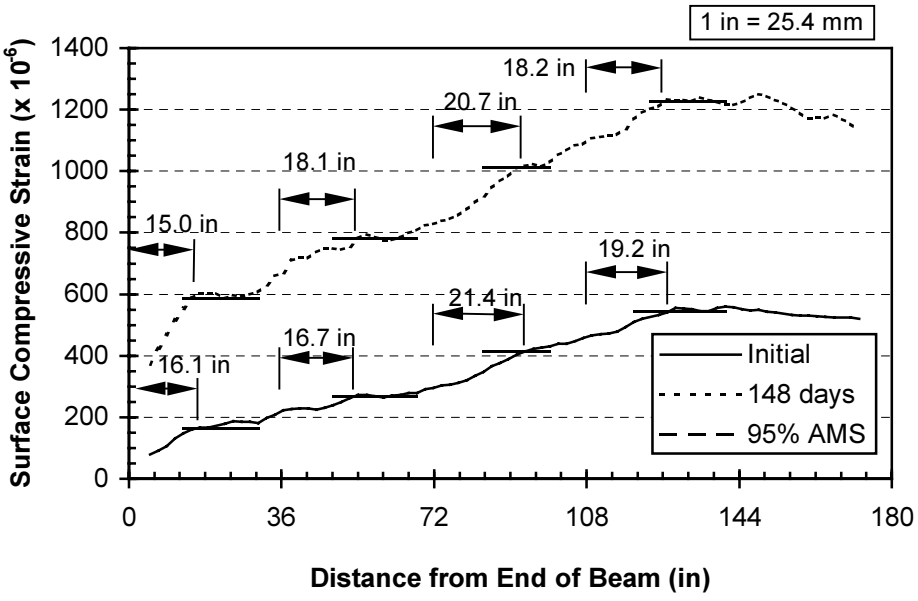


**Figure C.46: Specimen L6R-B Measured Initial and Long Term Strain Profiles**

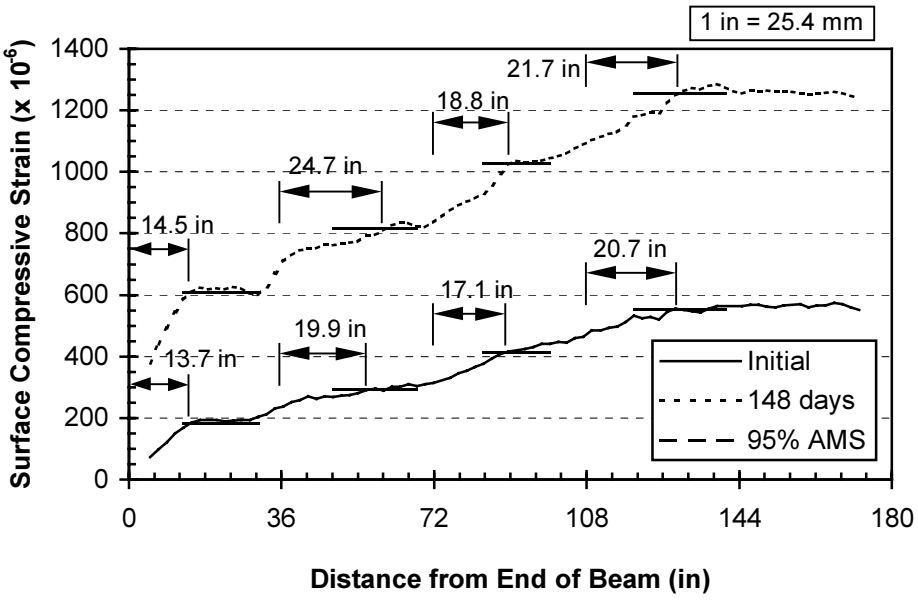


**Figure C.47: Specimen L6R-C Measured Initial and Long Term Strain Profiles**

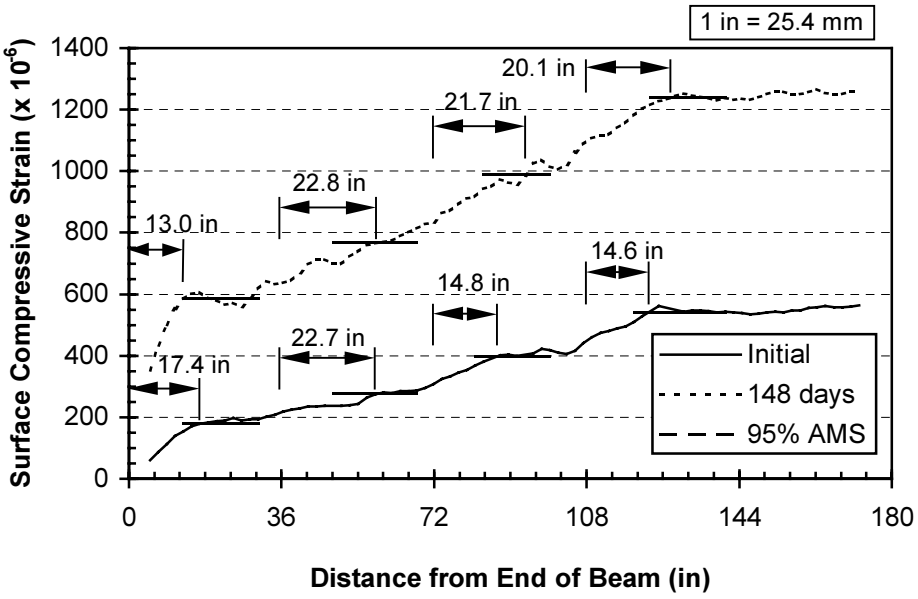


**Figure C.48: Specimen L6R-D Measured Initial and Long Term Strain Profiles**

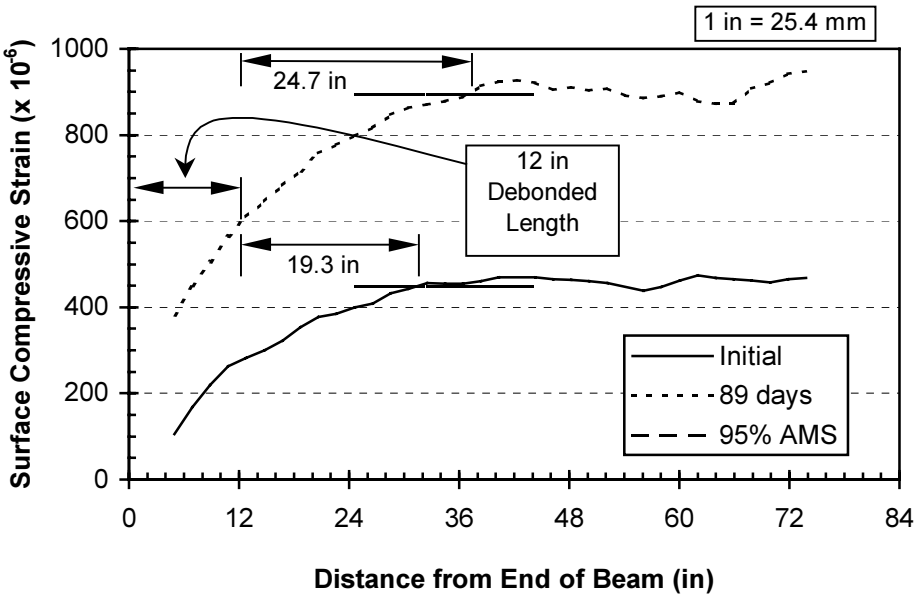


**Figure C.49: Specimen M0R-A Measured Initial and Long Term Strain Profiles**

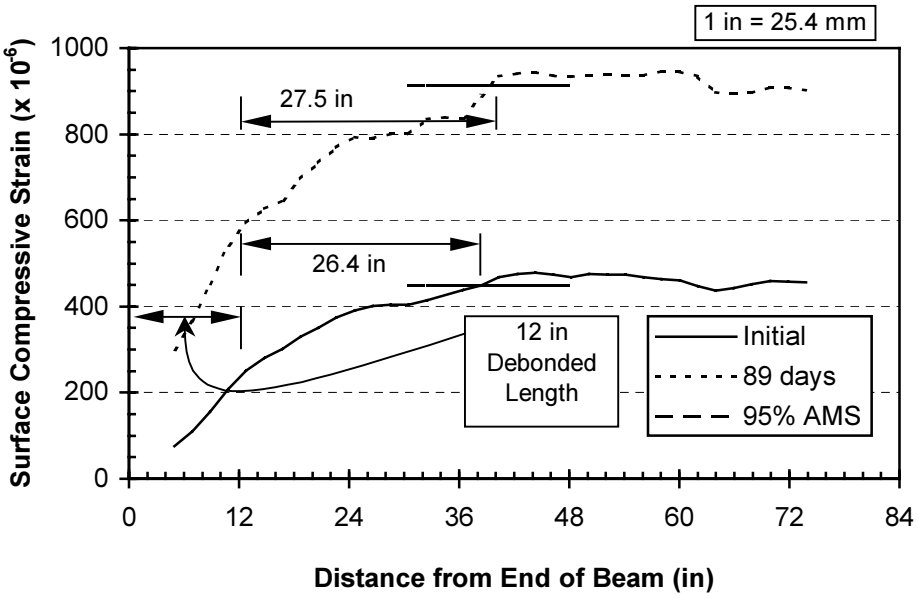


**Figure C.50: Specimen M0R-B Measured Initial and Long Term Strain Profiles**

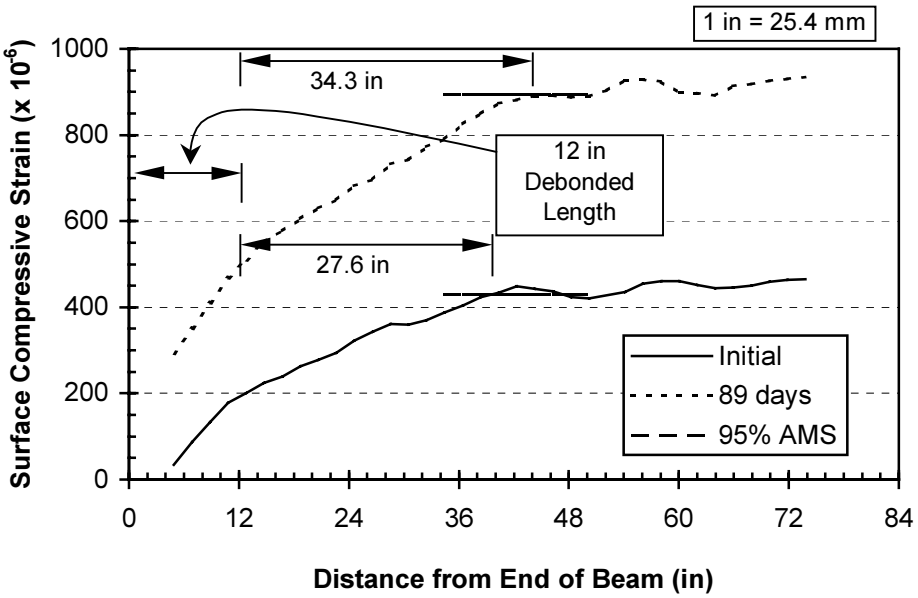


**Figure C.51: Specimen M0R-C Measured Initial and Long Term Strain Profiles**

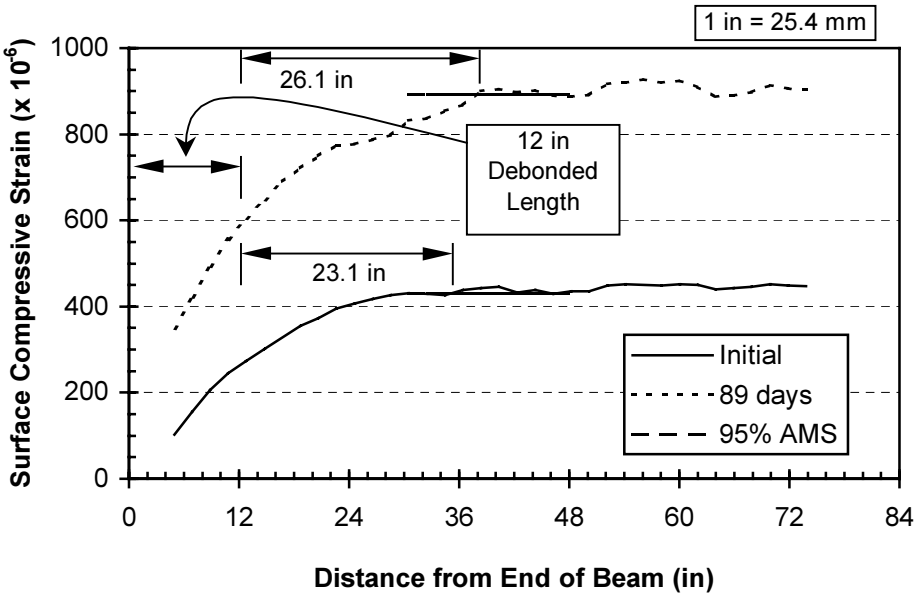


**Figure C.52: Specimen M0R-D Measured Initial and Long Term Strain Profiles**

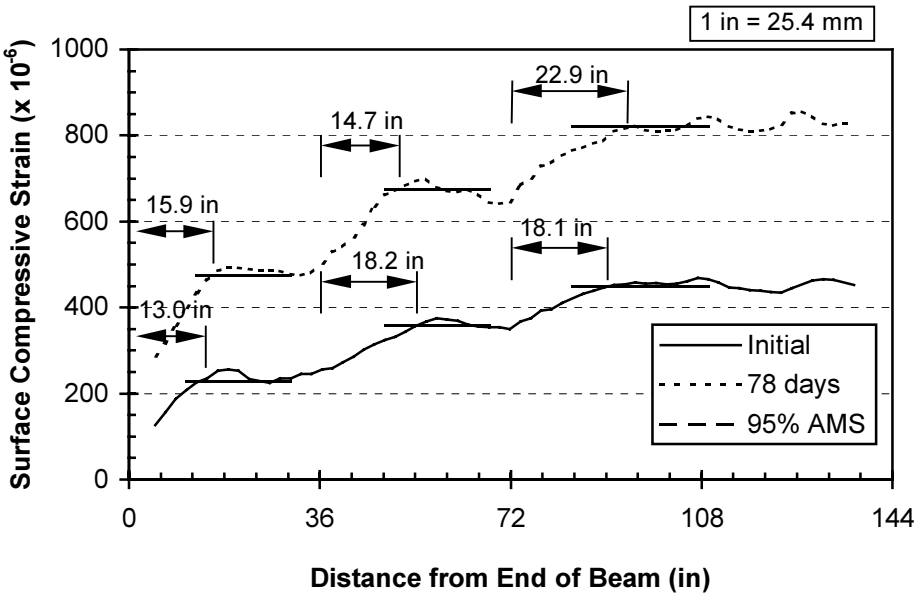


**Figure C.53: Specimen M4R-A Measured Initial and Long Term Strain Profiles**

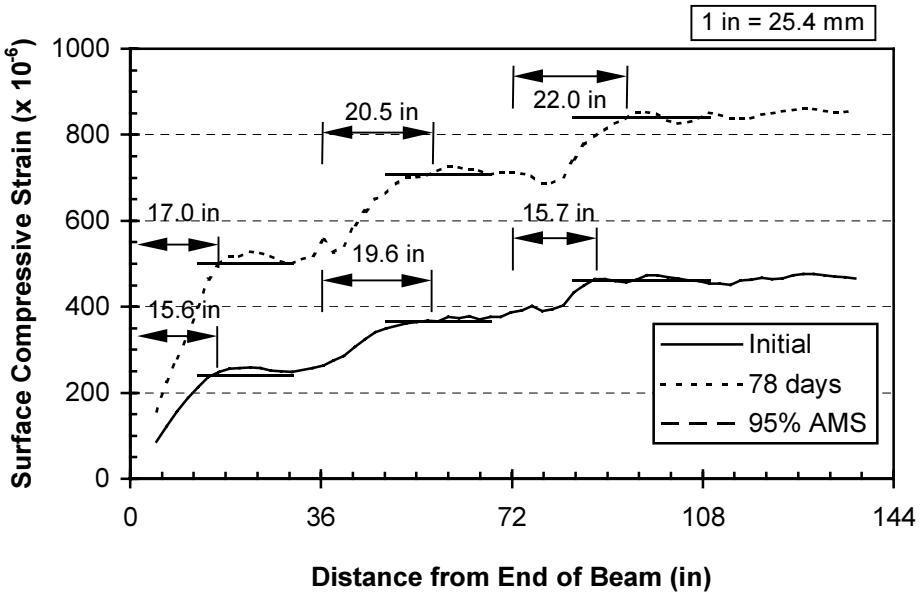


**Figure C.54: Specimen M4R-B Measured Initial and Long Term Strain Profiles**

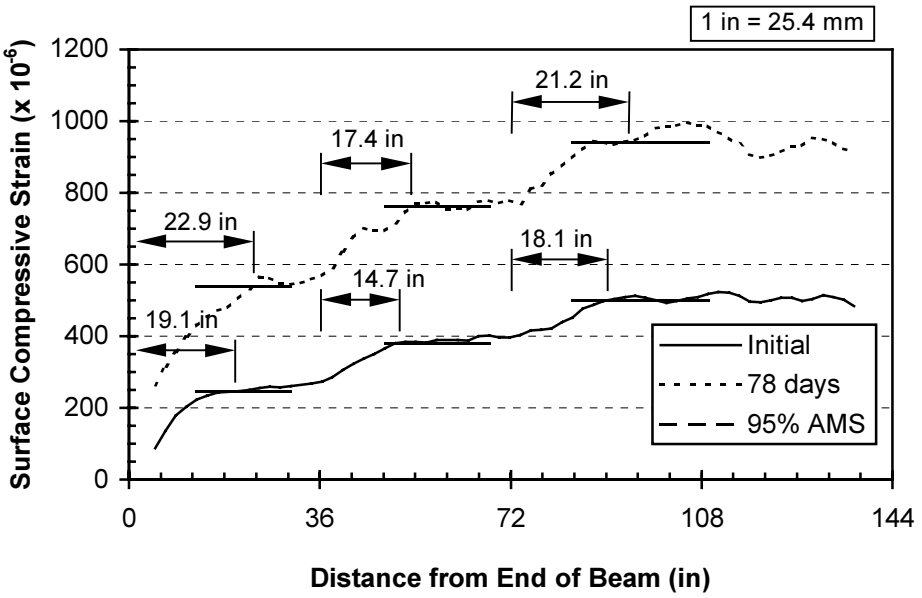


**Figure C.55: Specimen M4R-C Measured Initial and Long Term Strain Profiles**

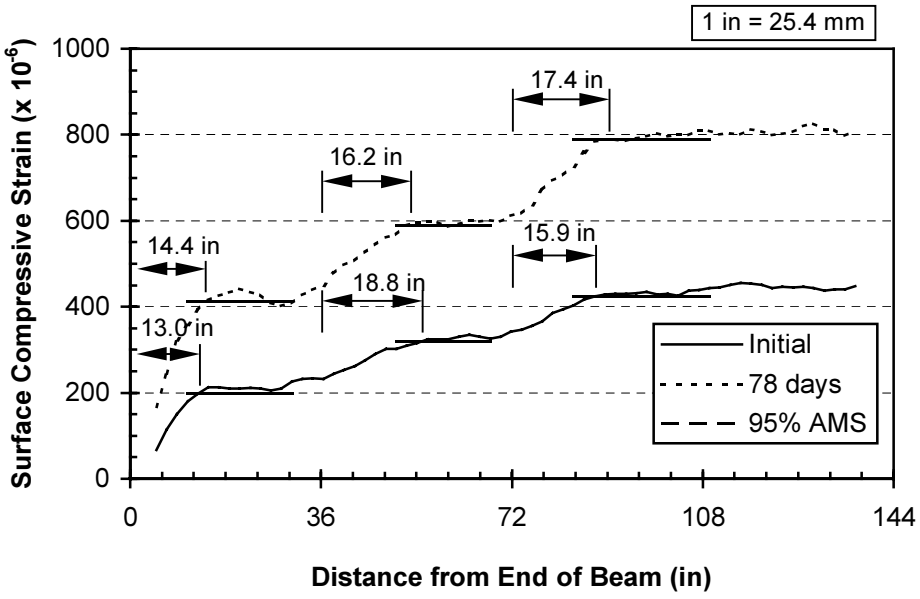


**Figure C.56: Specimen M4R-D Measured Initial and Long Term Strain Profiles**

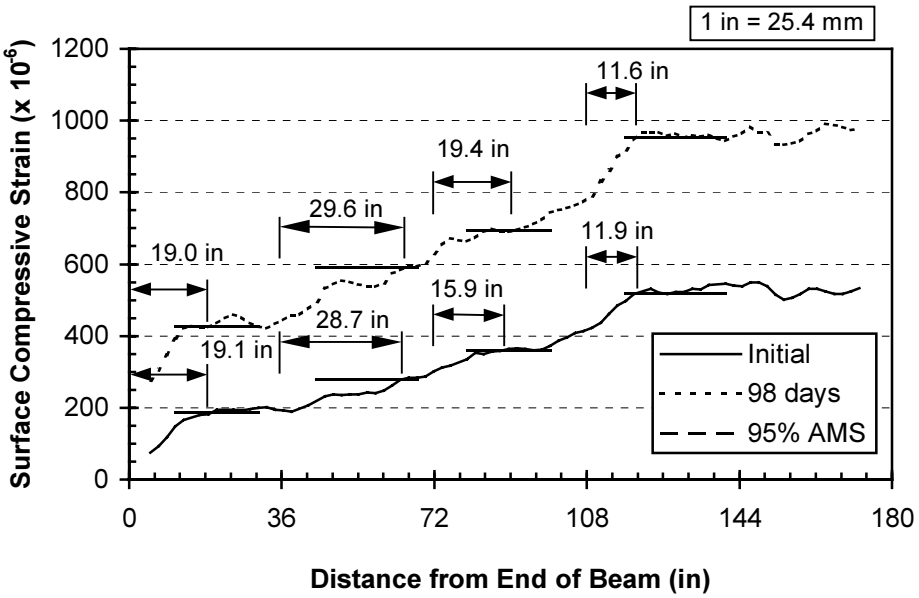


**Figure C.57: Specimen M9R-A Measured Initial and Long Term Strain Profiles**

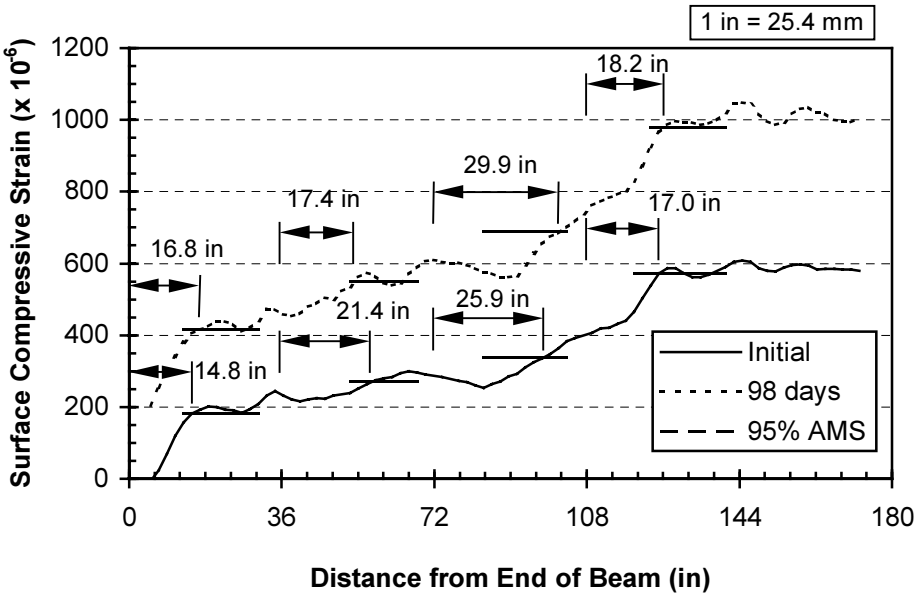


**Figure C.58: Specimen M9R-B Measured Initial and Long Term Strain Profiles**

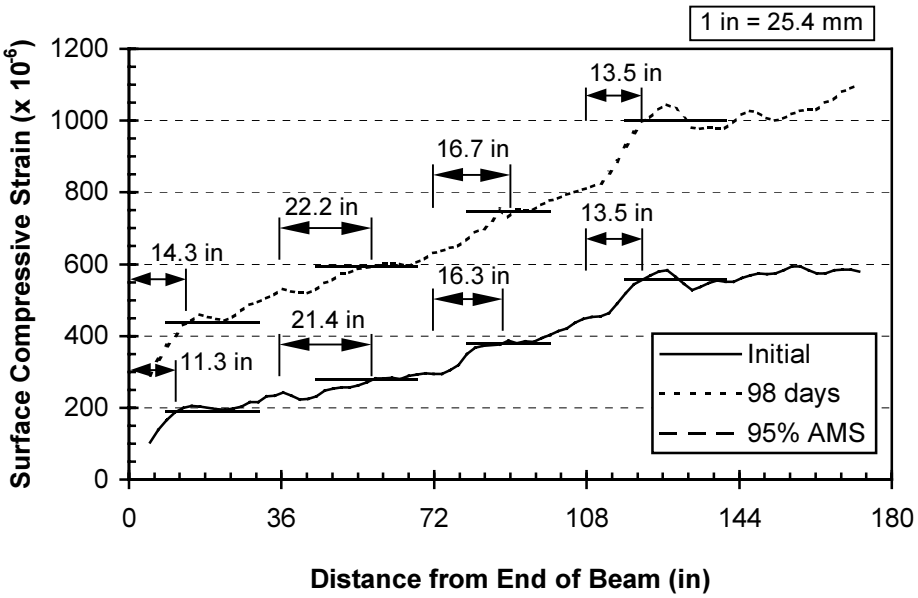


**Figure C.59: Specimen M9R-C Measured Initial and Long Term Strain Profiles**

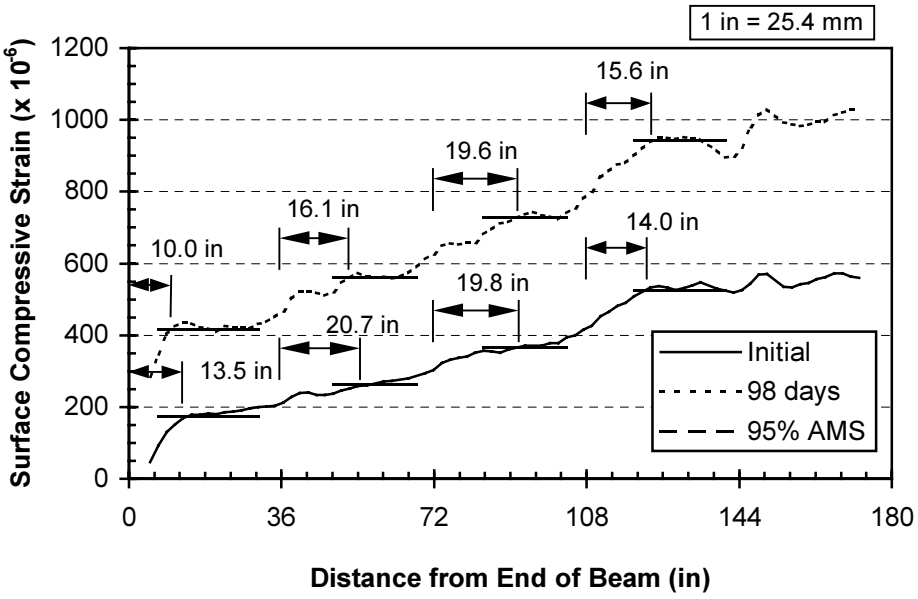


**Figure C.60: Specimen M9R-D Measured Initial and Long Term Strain Profiles**

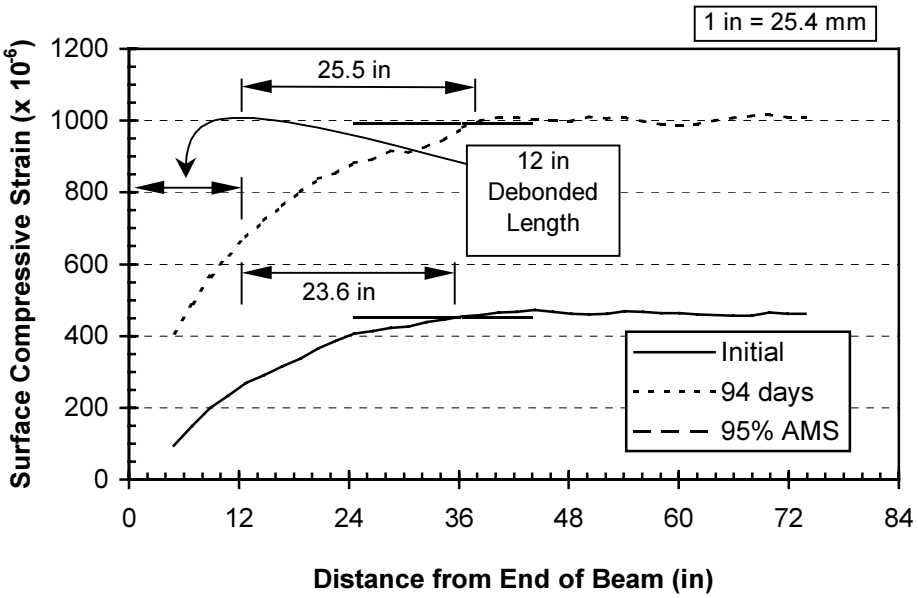


**Figure C.61: Specimen H0R-A Measured Initial and Long Term Strain Profiles**

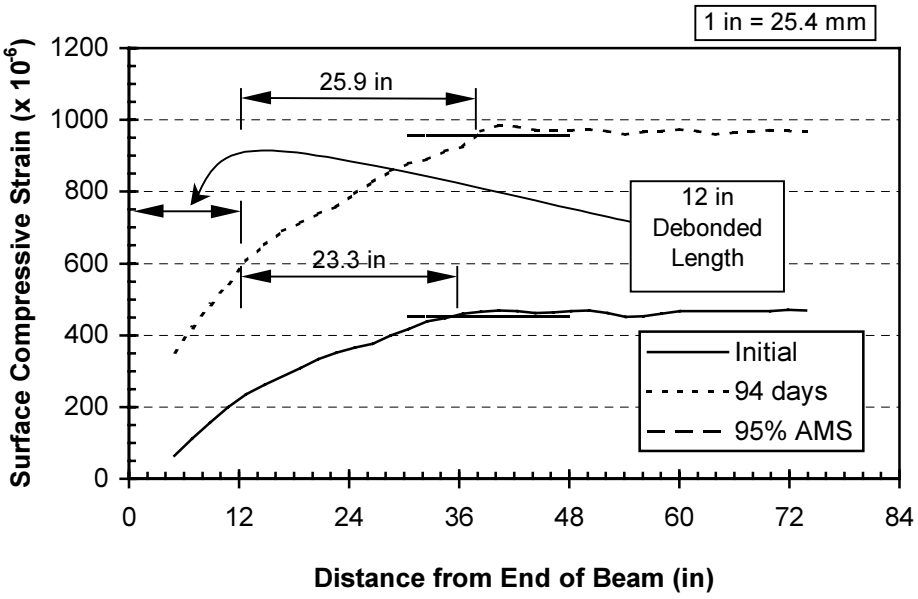


**Figure C.62: Specimen H0R-B Measured Initial and Long Term Strain Profiles**

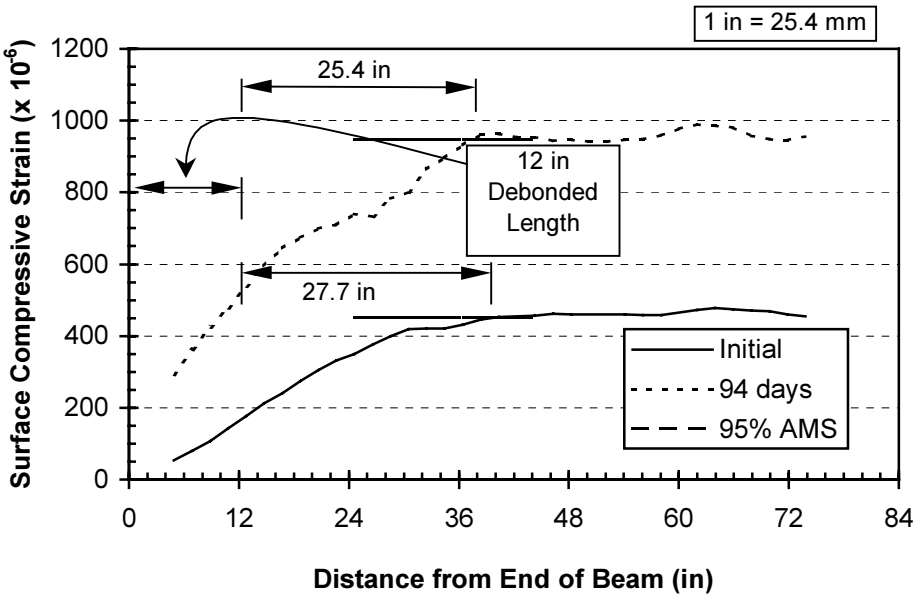


**Figure C.63: Specimen H0R-C Measured Initial and Long Term Strain Profiles**

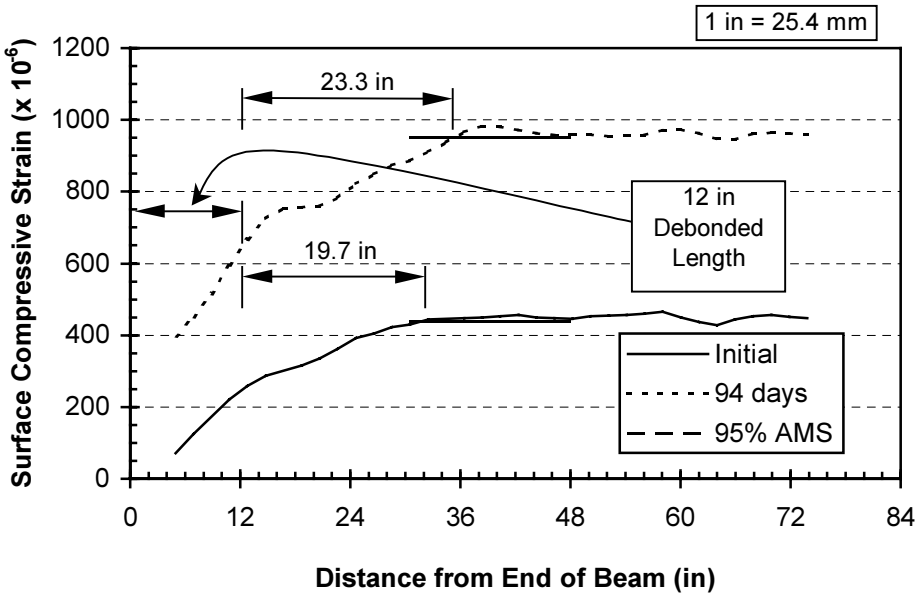


**Figure C.64: Specimen H0R-D Measured Initial and Long Term Strain Profiles**

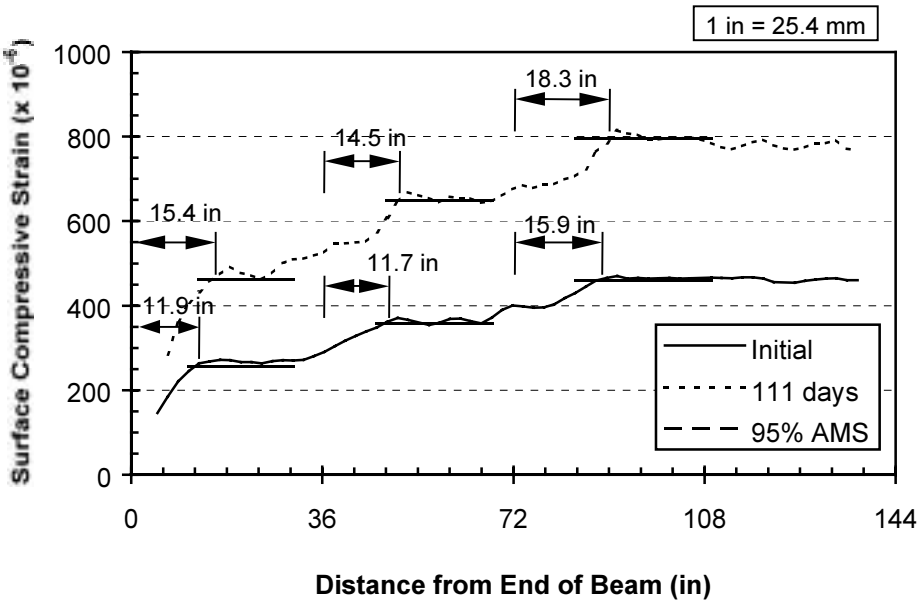


**Figure C.65: Specimen H4R-A Measured Initial and Long Term Strain Profiles**

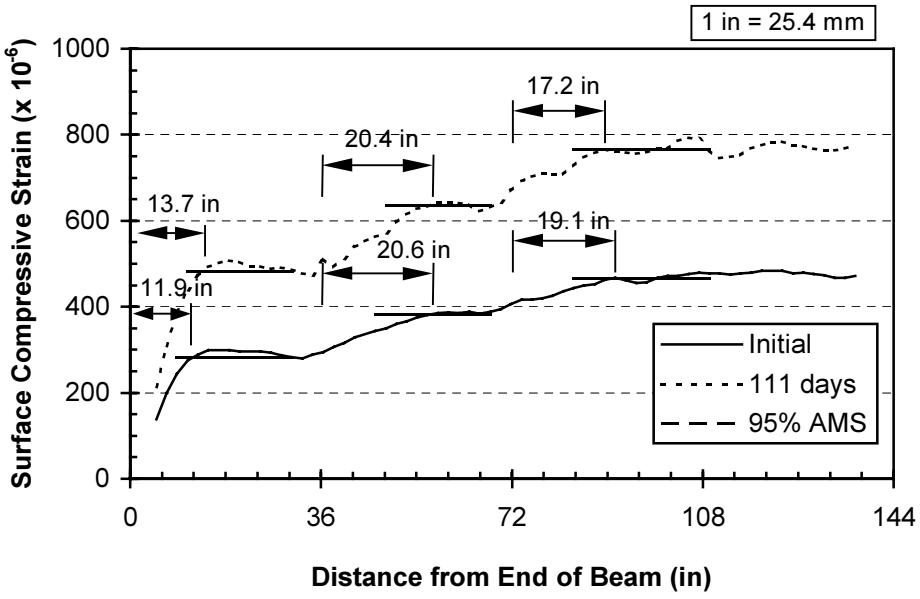


**Figure C.66: Specimen H4R-B Measured Initial and Long Term Strain Profiles**

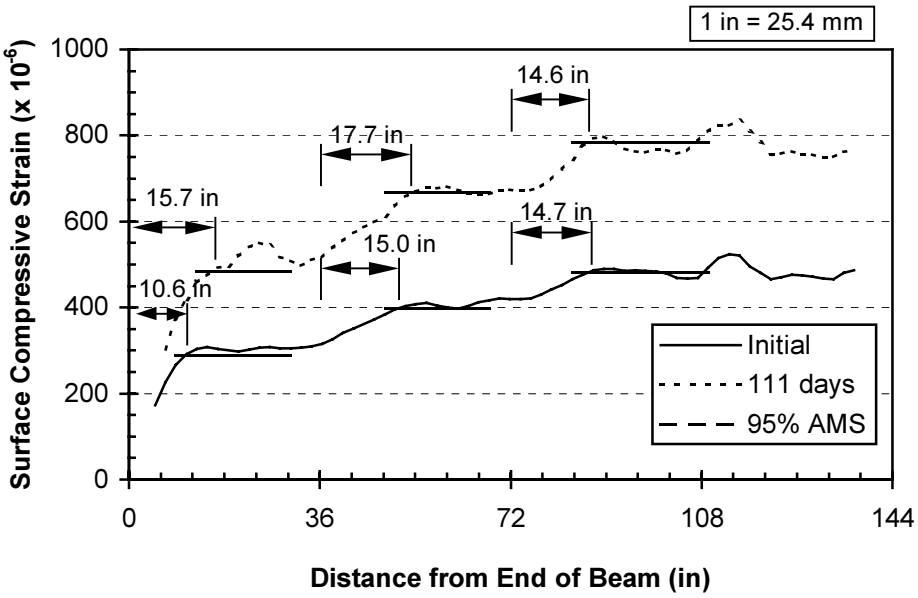


**Figure C.67: Specimen H4R-C Measured Initial and Long Term Strain Profiles**

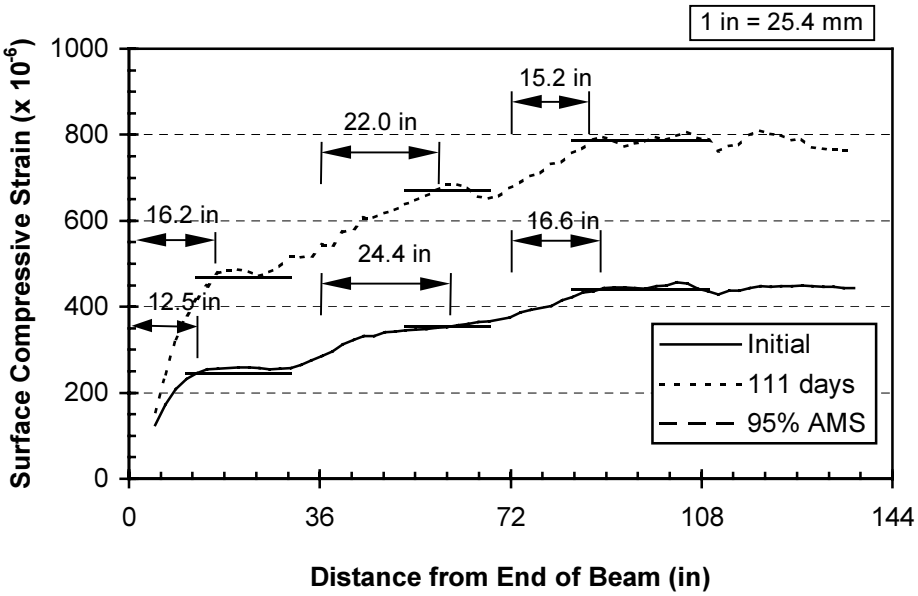


**Figure C.68: Specimen H4R-D Measured Initial and Long Term Strain Profiles**

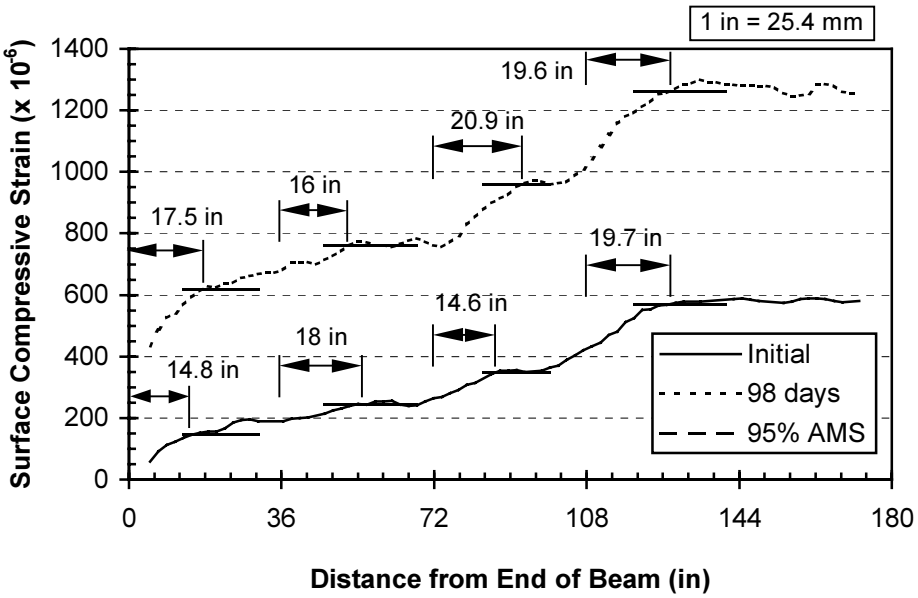


**Figure C.69: Specimen H9R-A Measured Initial and Long Term Strain Profiles**

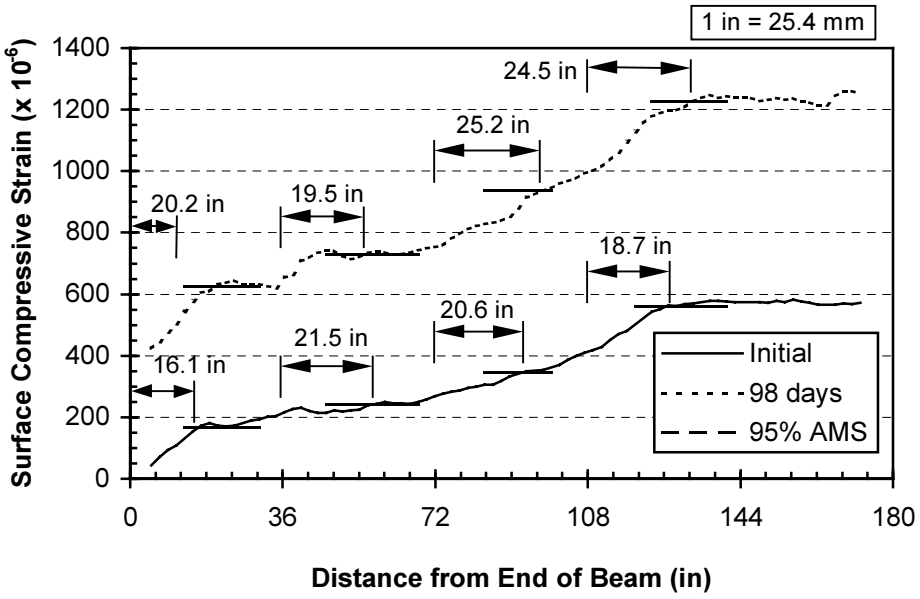


**Figure C.70: Specimen H9R-B Measured Initial and Long Term Strain Profiles**

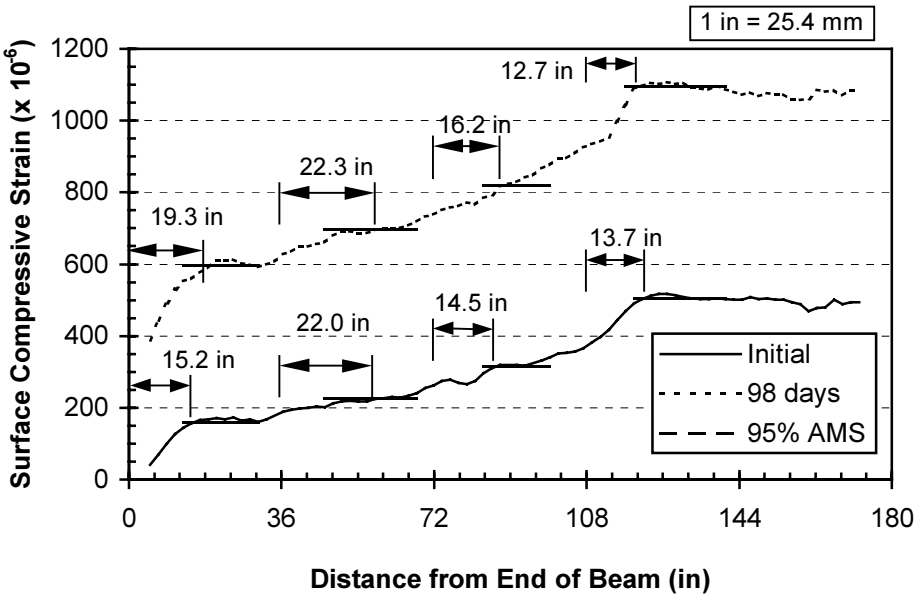


**Figure C.71: Specimen H9R-C Measured Initial and Long Term Strain Profiles**

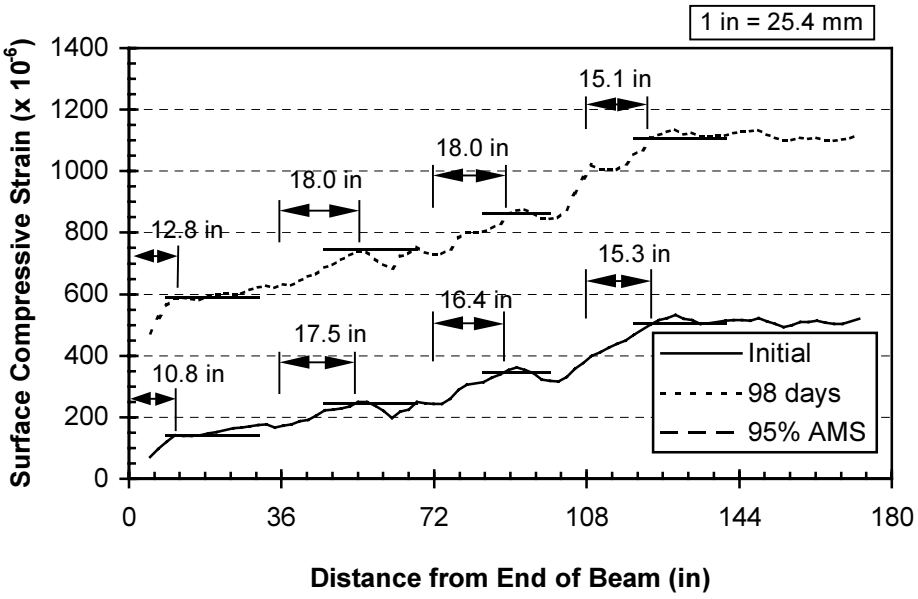


**Figure C.72: Specimen H9R-D Measured Initial and Long Term Strain Profiles**

# APPENDIX D: STRAND DRAW-IN RESULTS

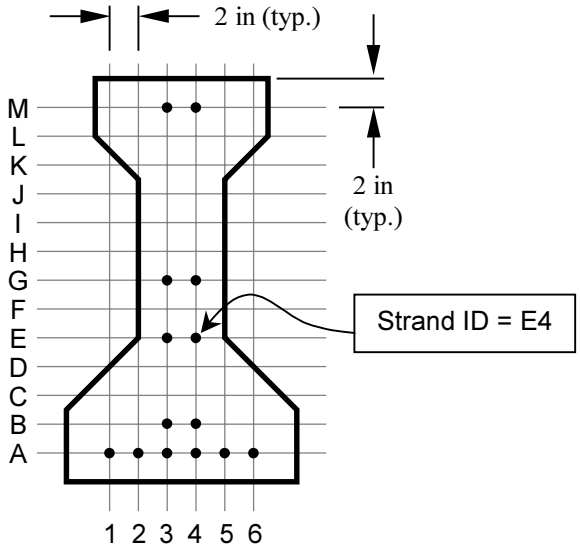


**Figure D.1: Strand Identification Scheme**

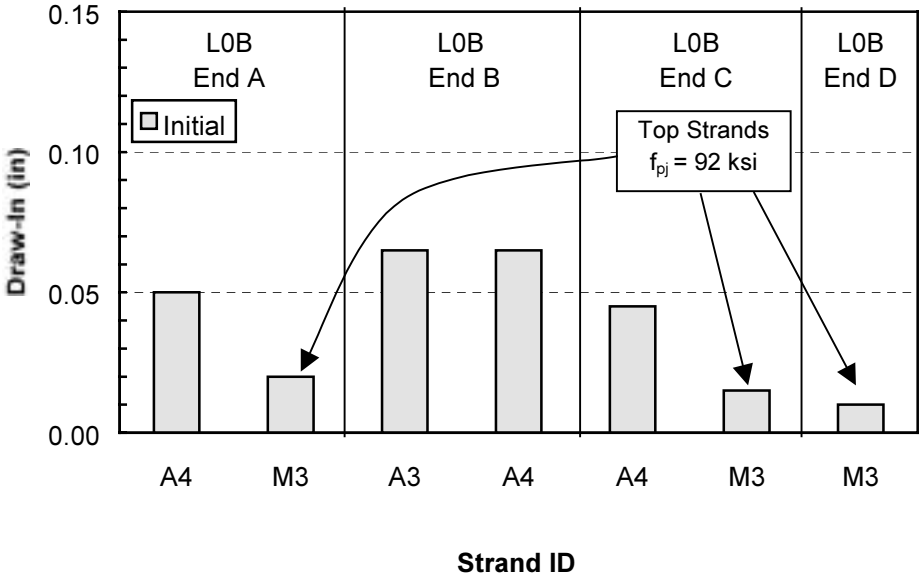


**Figure D.2: Strand Draw-In Results for L0B Beam Specimen Pair (Bright Strand, Simultaneous Flame Release)**

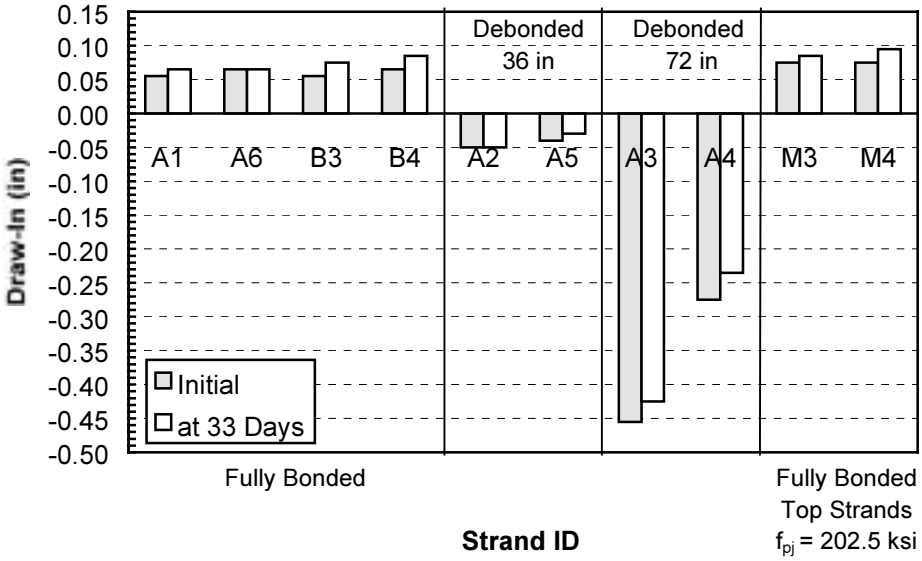


**Figure D.3: L4B-A Strand Draw-In Results (Bright Strand, Simultaneous Flame Release)**

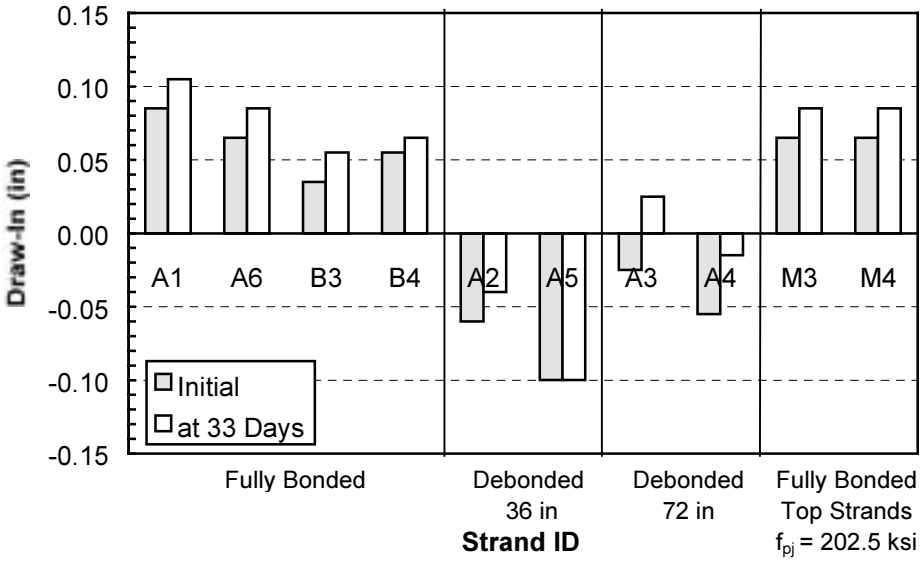


**Figure D.4: L4B-B Strand Draw-In Results (Bright Strand, Simultaneous Flame Release)**

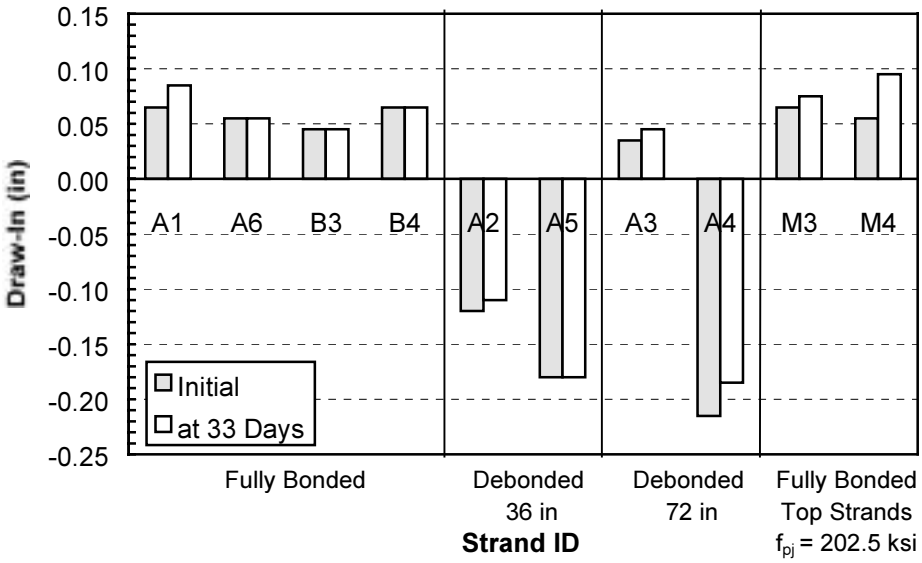


**Figure D.5: L4B-C Strand Draw-In Results (Bright Strand, Simultaneous Flame Release)**

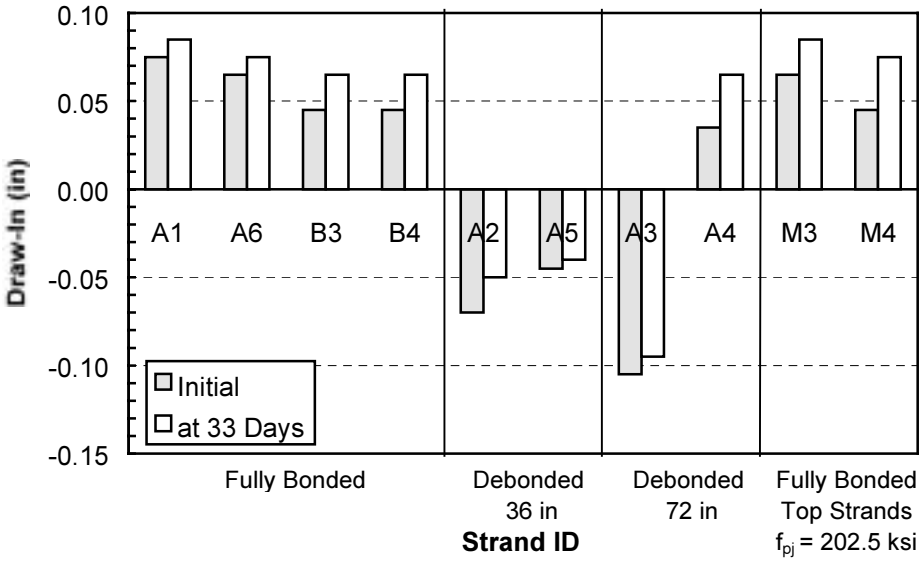


**Figure D.6: L4B-D Strand Draw-In Results (Bright Strand, Simultaneous Flame Release)**

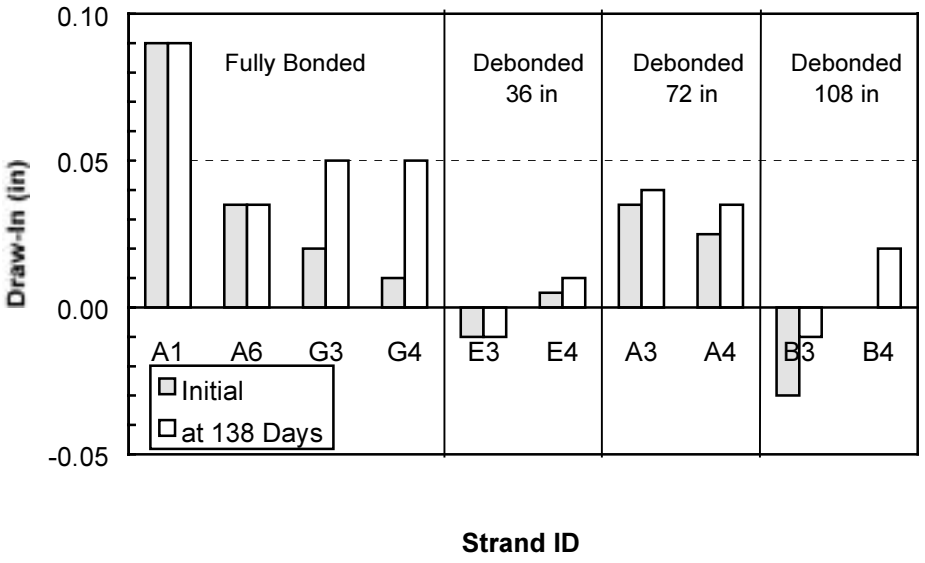


**Figure D.7: L6B-A Strand Draw-In Results (Bright Strand, Simultaneous Flame Release)**

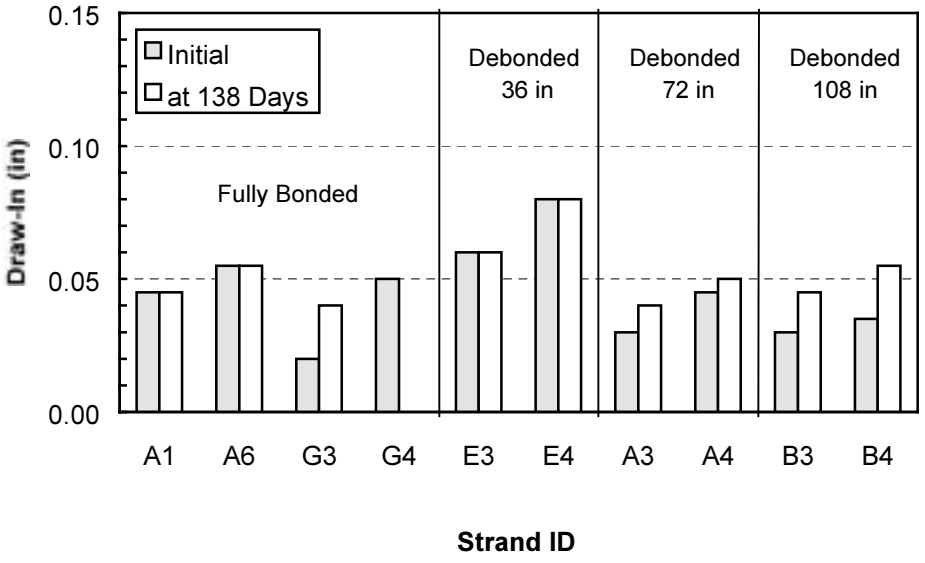


**Figure D.8: L6B-B Strand Draw-In Results (Bright Strand, Simultaneous Flame Release)**

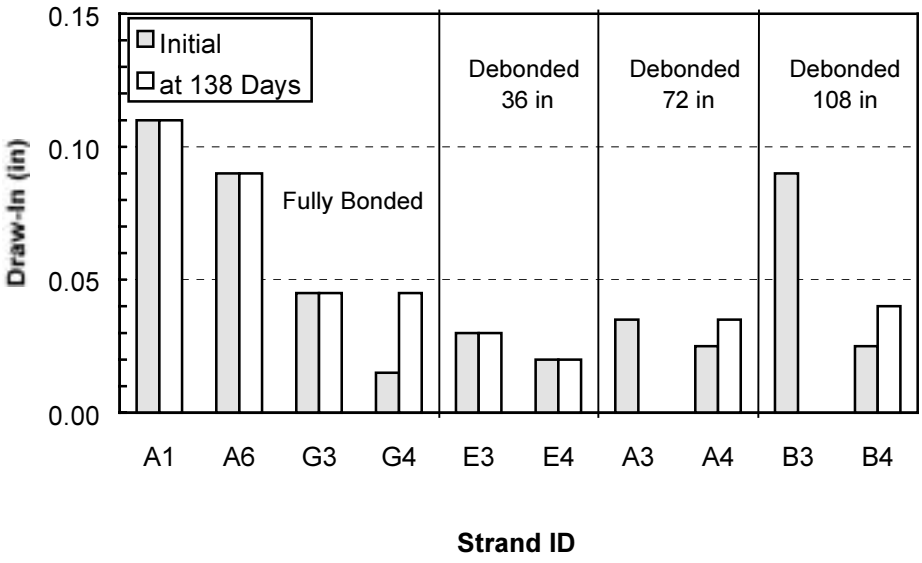


**Figure D.9: L6B-C Strand Draw-In Results (Bright Strand, Simultaneous Flame Release)**

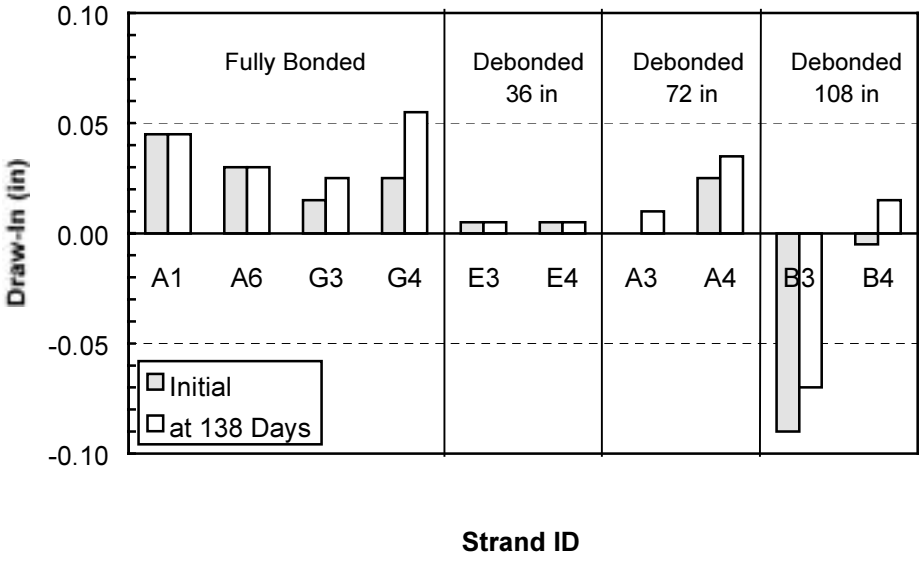


**Figure D.10: L6B-D Strand Draw-In Results (Bright Strand, Simultaneous Flame Release)**

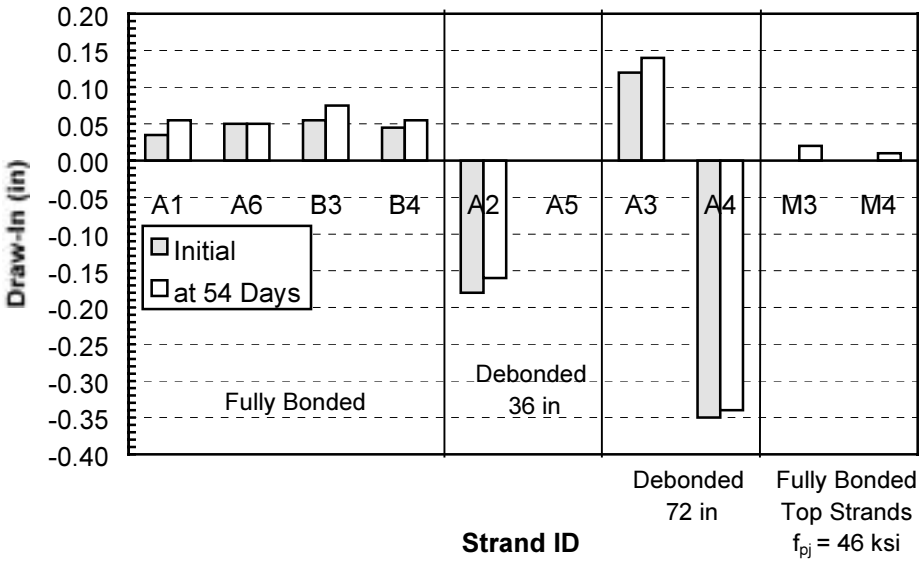


**Figure D.11: M4B-A Strand Draw-In Results (Bright Strand, Simultaneous Flame Release)**

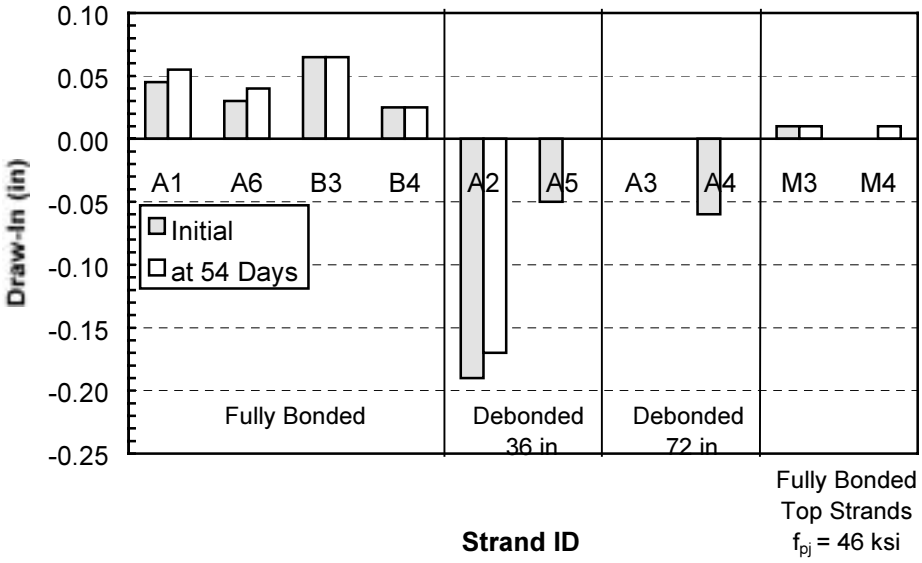


**Figure D.12: M4B-B Strand Draw-In Results (Bright Strand, Simultaneous Flame Release)**

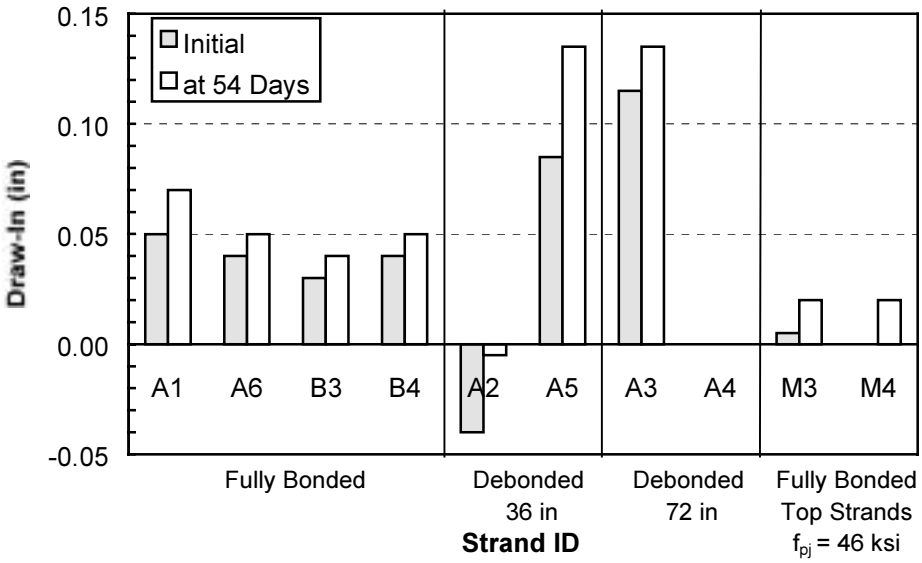


**Figure D.13: M4B-C Strand Draw-In Results (Bright Strand, Simultaneous Flame Release)**

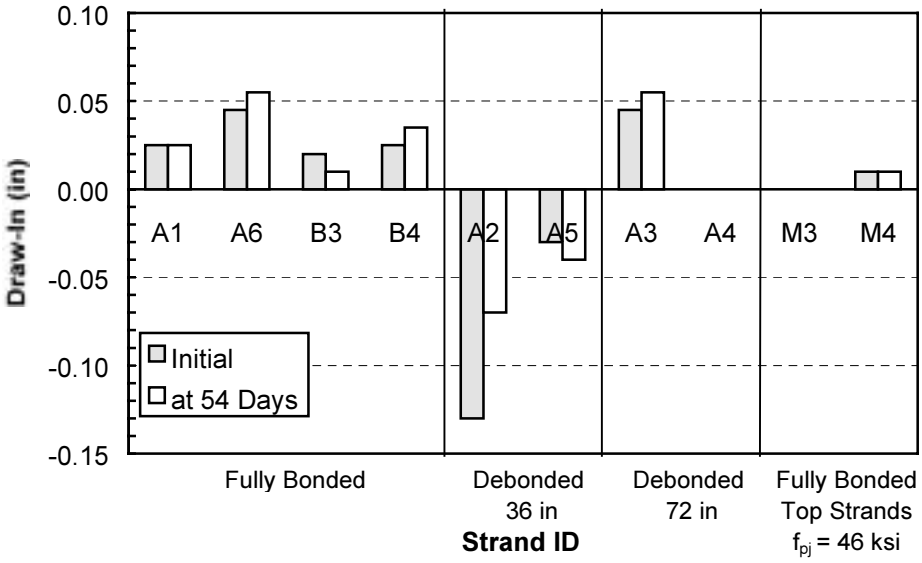


**Figure D.14: M4B-D Strand Draw-In Results (Bright Strand, Simultaneous Flame Release)**

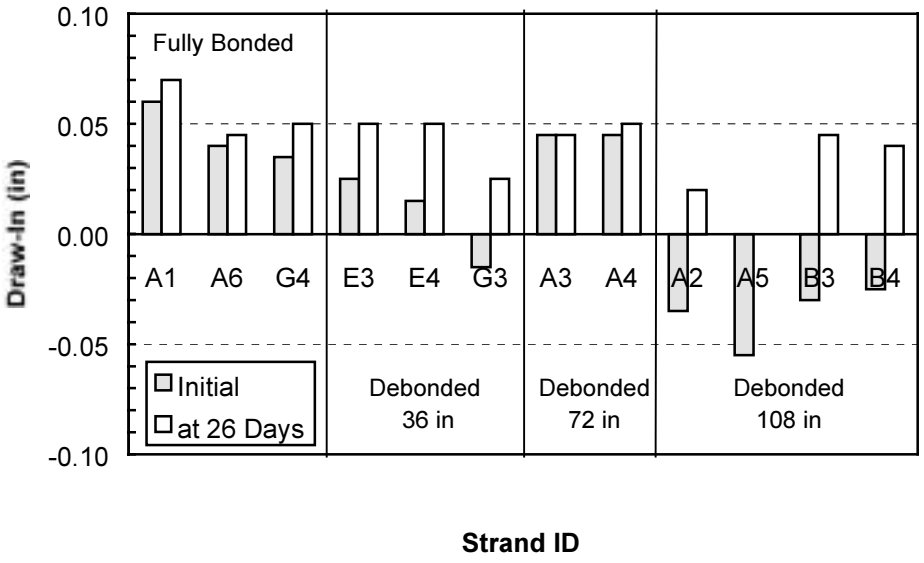


**Figure D.15: M9B-A Strand Draw-In Results (Bright Strand, Dead End of Flame Release)**

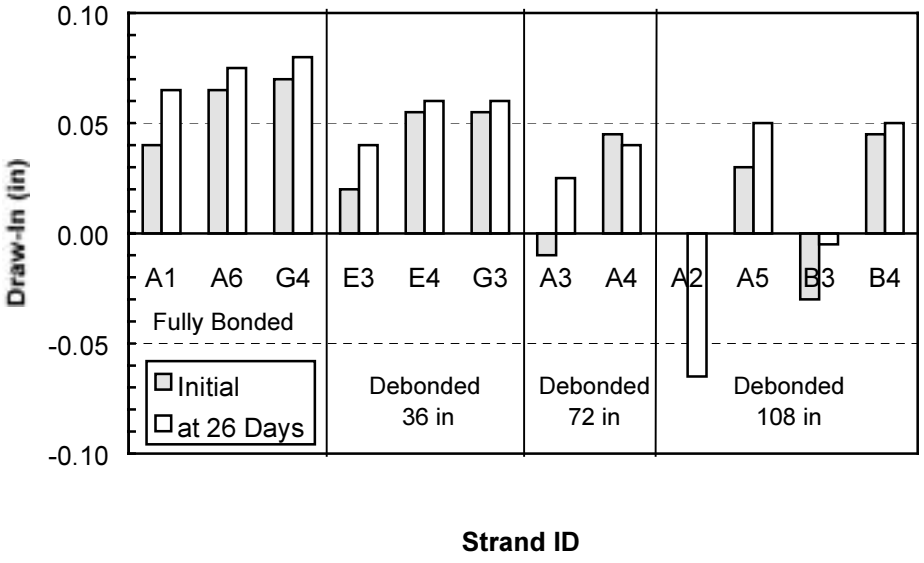


**Figure D.16: M9B-B Strand Draw-In Results (Bright Strand, Live End of Flame Release)**

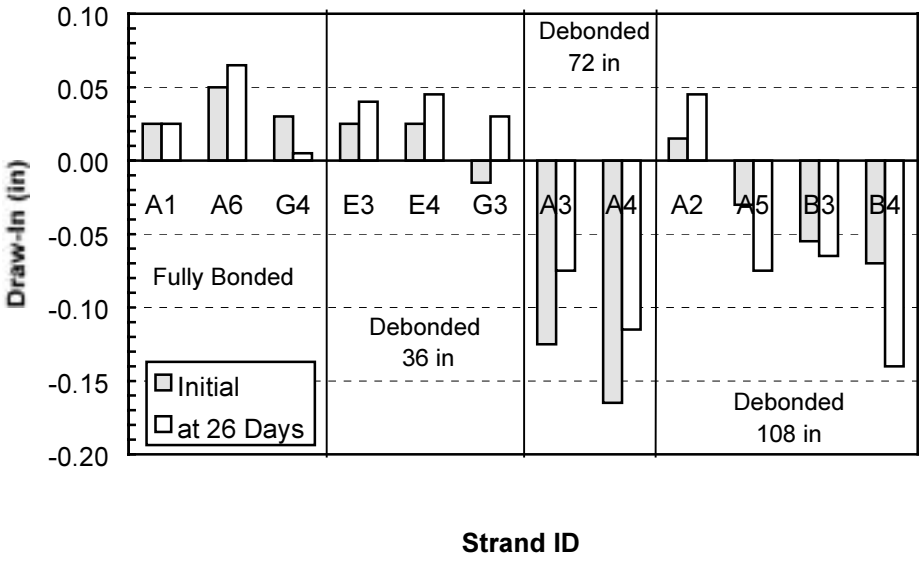


**Figure D.17: M9B-C Strand Draw-In Results (Bright Strand, Live End of Flame Release)**

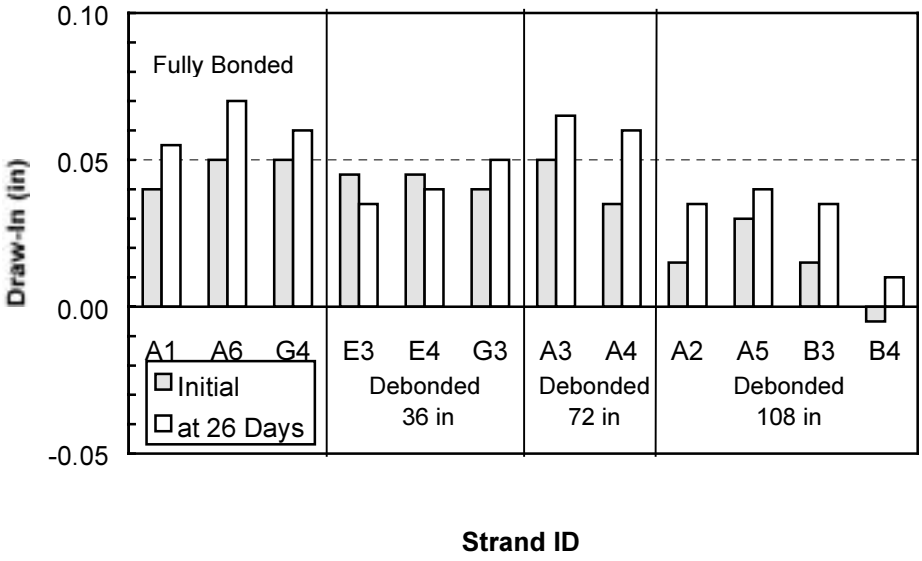


**Figure D.18: M9B-D Strand Draw-In Results (Bright Strand, Dead End of Flame Release)**

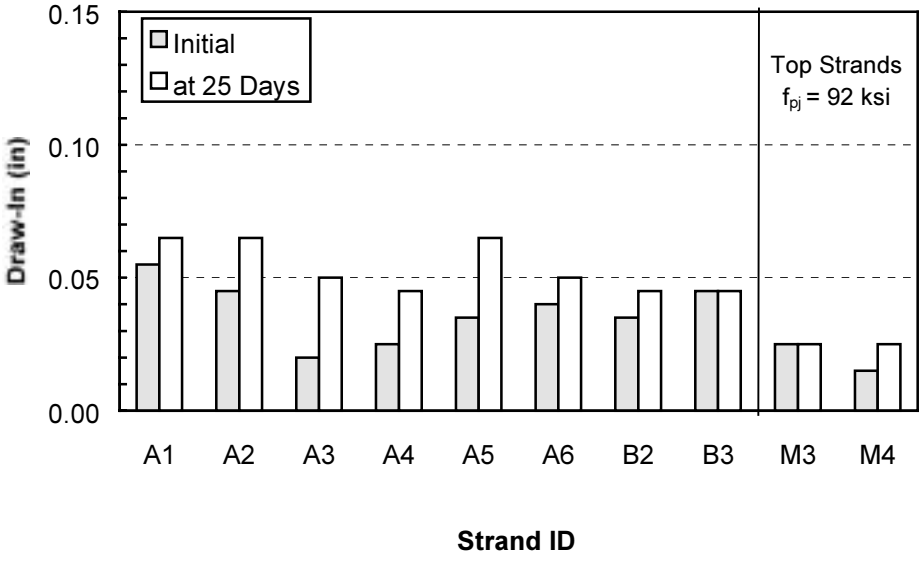


**Figure D.19: H0B-A Strand Draw-In Results (Bright Strand, Simultaneous Flame Release)**

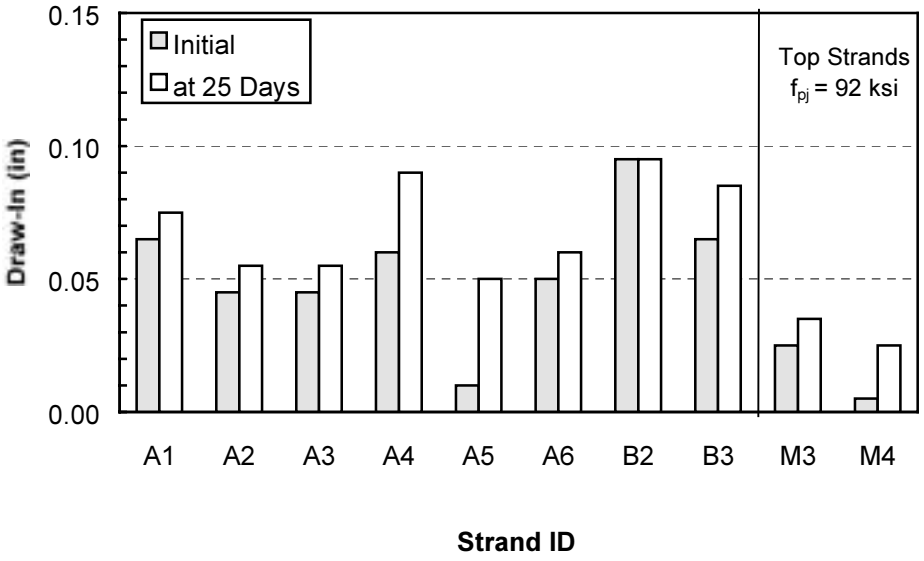


**Figure D.20: H0B-B Strand Draw-In Results (Bright Strand, Simultaneous Flame Release)**

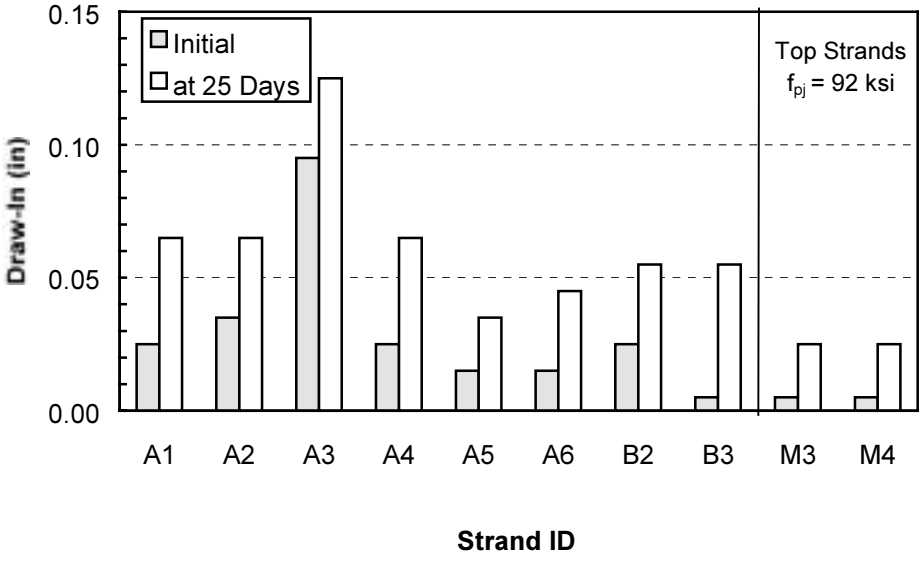


**Figure D.21: H0B-C Strand Draw-In Results (Bright Strand, Simultaneous Flame Release)**

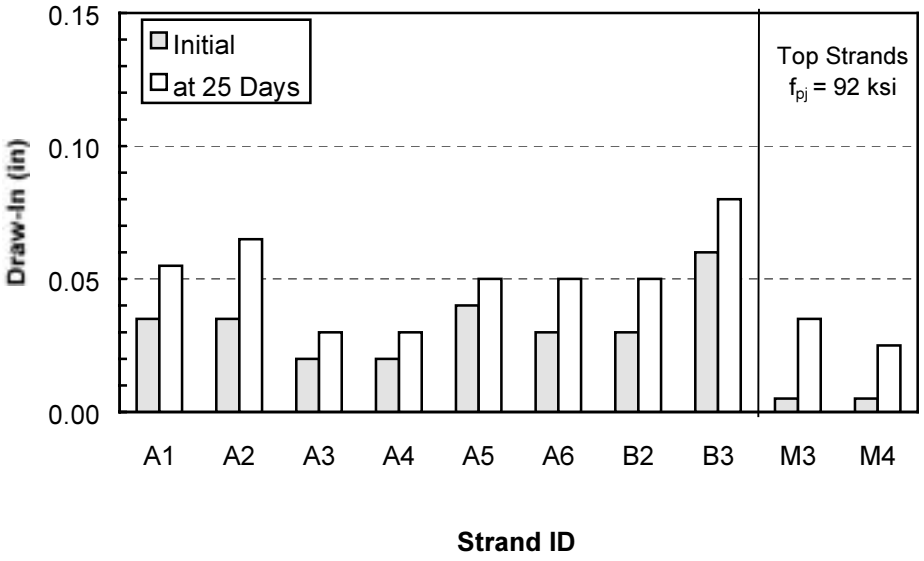


**Figure D.22: H0B-D Strand Draw-In Results (Bright Strand, Simultaneous Flame Release)**

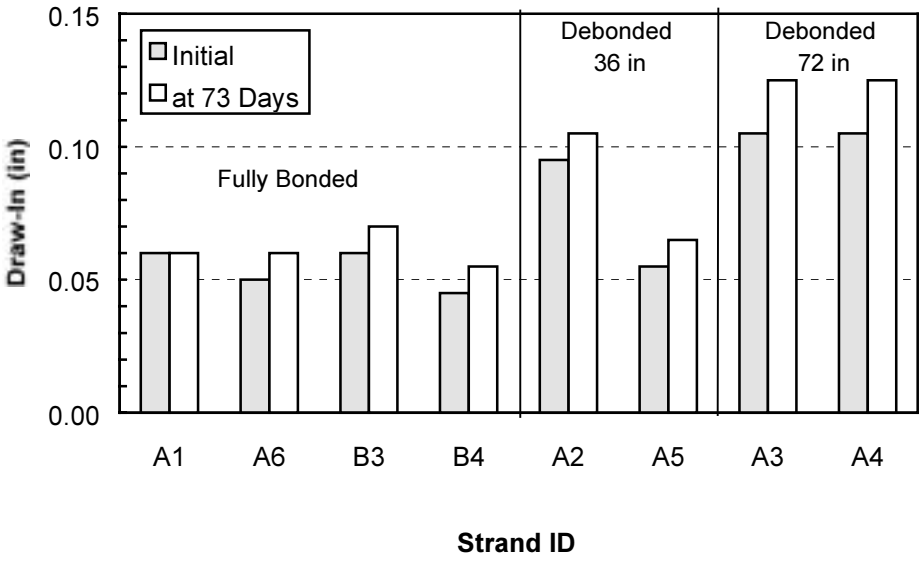


**Figure D.23: H4B-A Strand Draw-In Results (Bright Strand, Simultaneous Flame Release)**

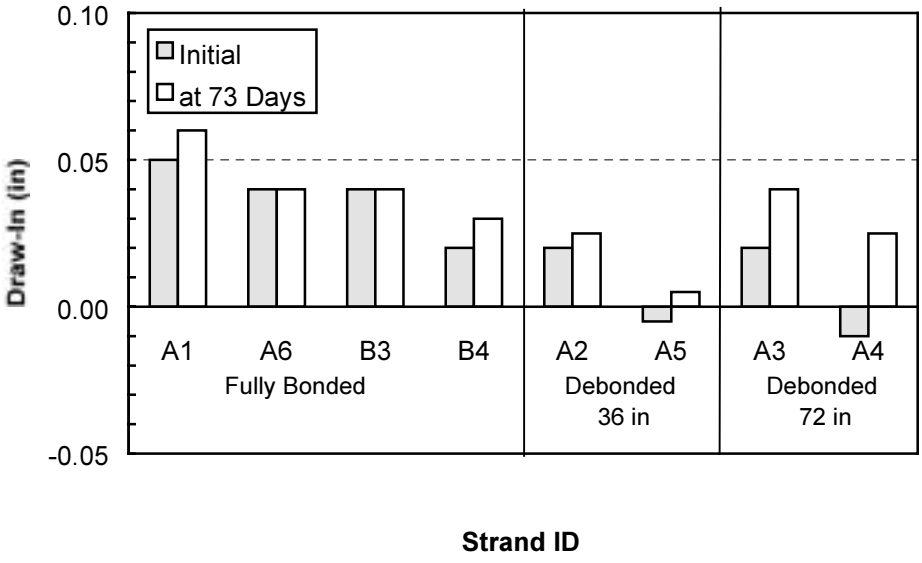


**Figure D.24: H4B-B Strand Draw-In Results (Bright Strand, Simultaneous Flame Release)**

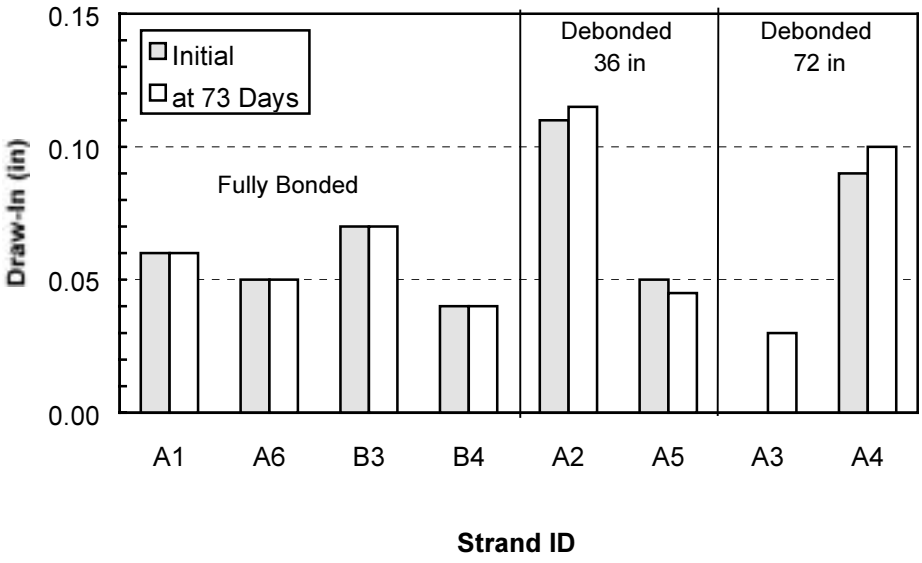


**Figure D.25: H4B-C Strand Draw-In Results (Bright Strand, Simultaneous Flame Release)**

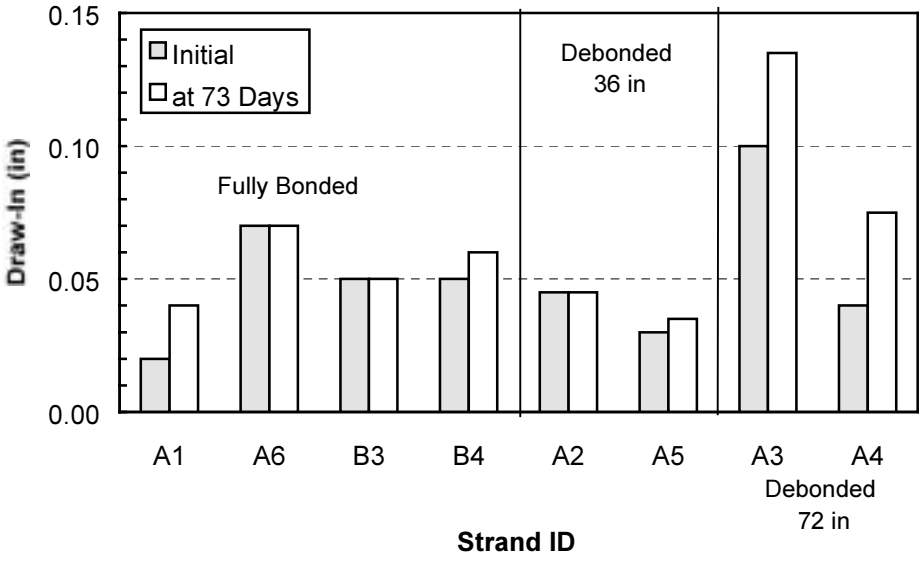


**Figure D.26: H4B-D Strand Draw-In Results (Bright Strand, Simultaneous Flame Release)**

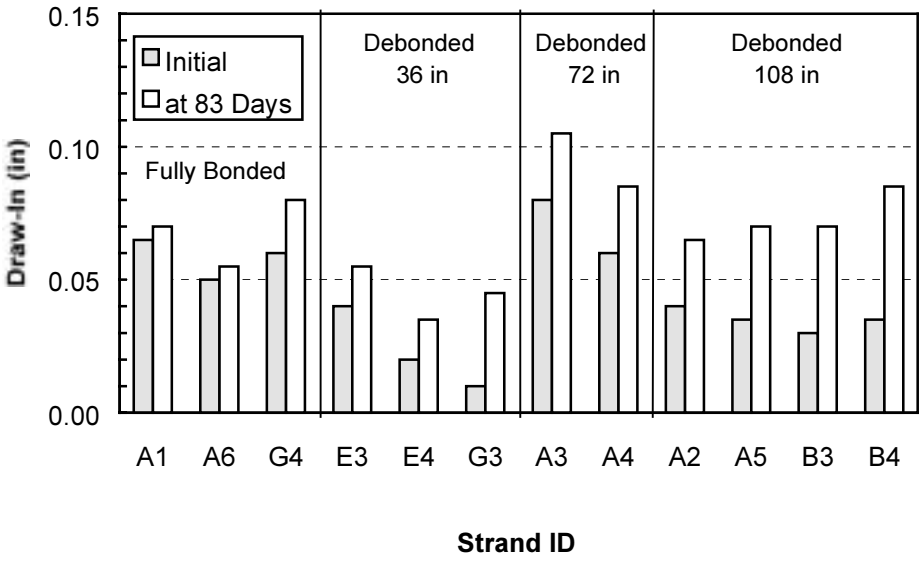


**Figure D.27: H9B-A Strand Draw-In Results (Bright Strand, Dead End of Flame Release)**

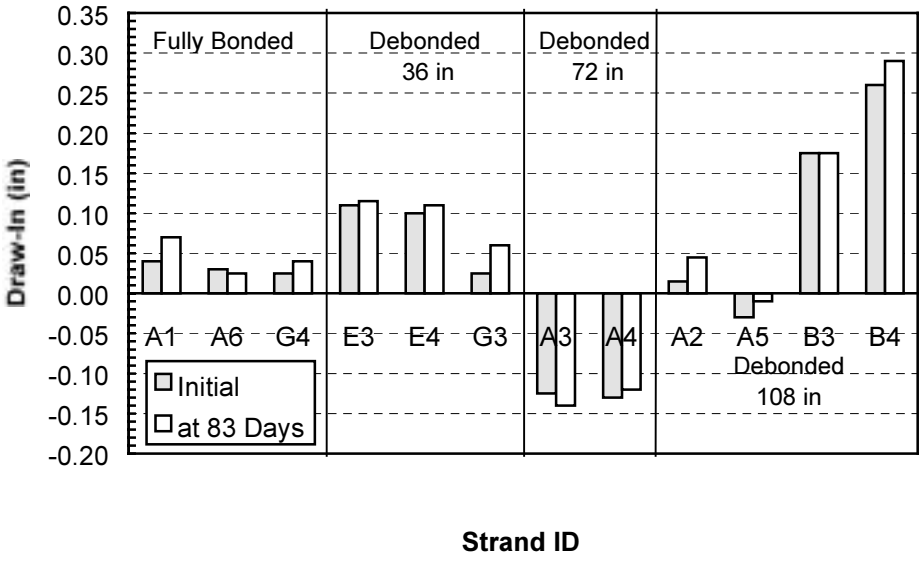


**Figure D.28: H9B-B Strand Draw-In Results (Bright Strand, Live End of Flame Release)**

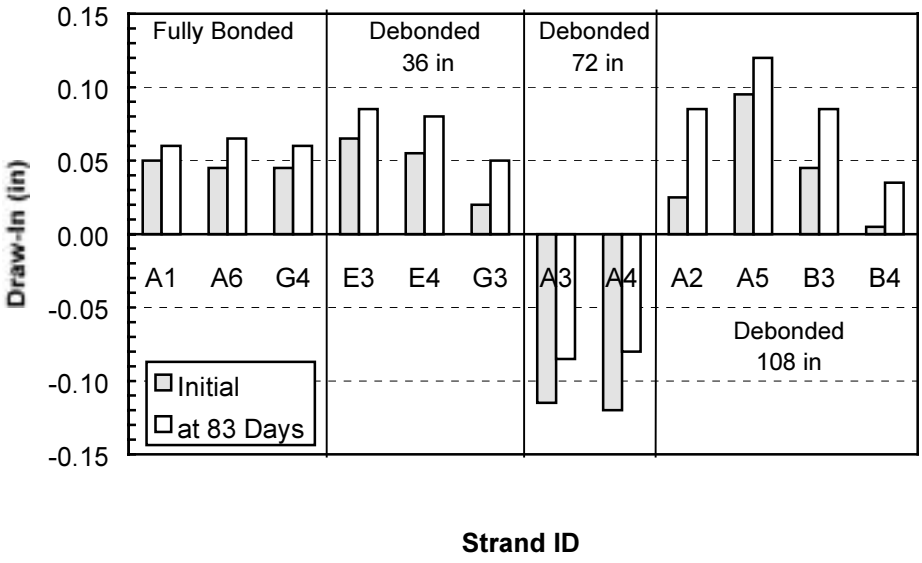


**Figure D.29: H9B-C Strand Draw-In Results (Bright Strand, Live End of Flame Release)**

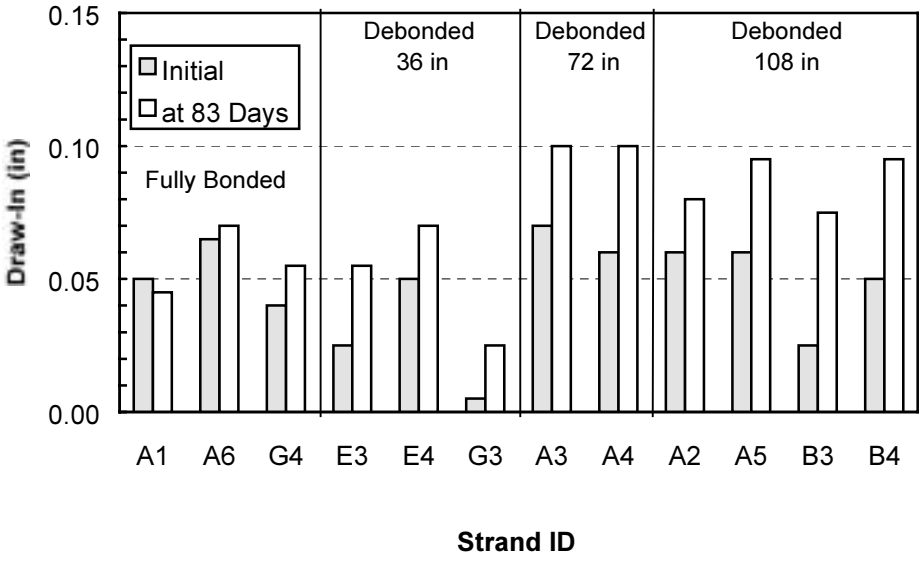


**Figure D.30: H9B-D Strand Draw-In Results (Bright Strand, Dead End of Flame Release)**

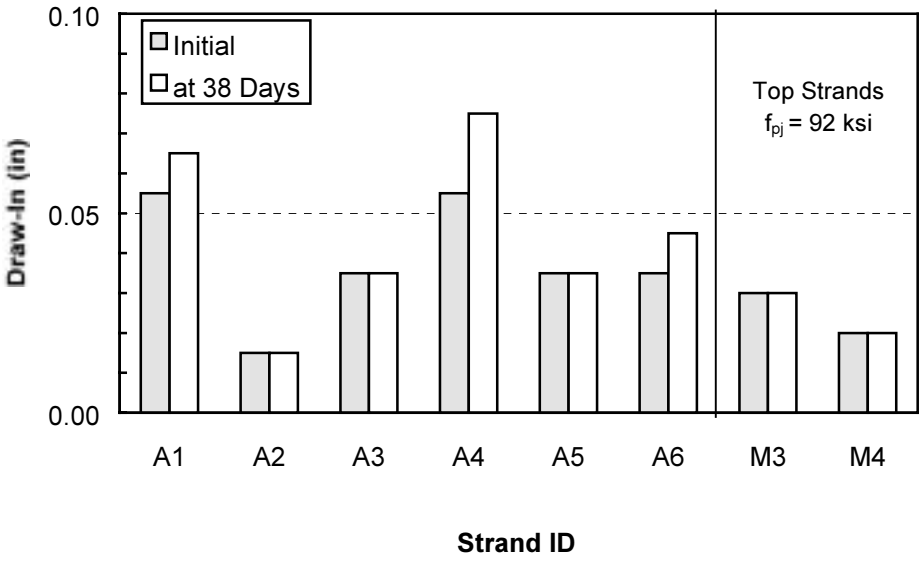


**Figure D.31: L0R-A Strand Draw-In Results (Rusted Strand, Simultaneous Flame Release)**

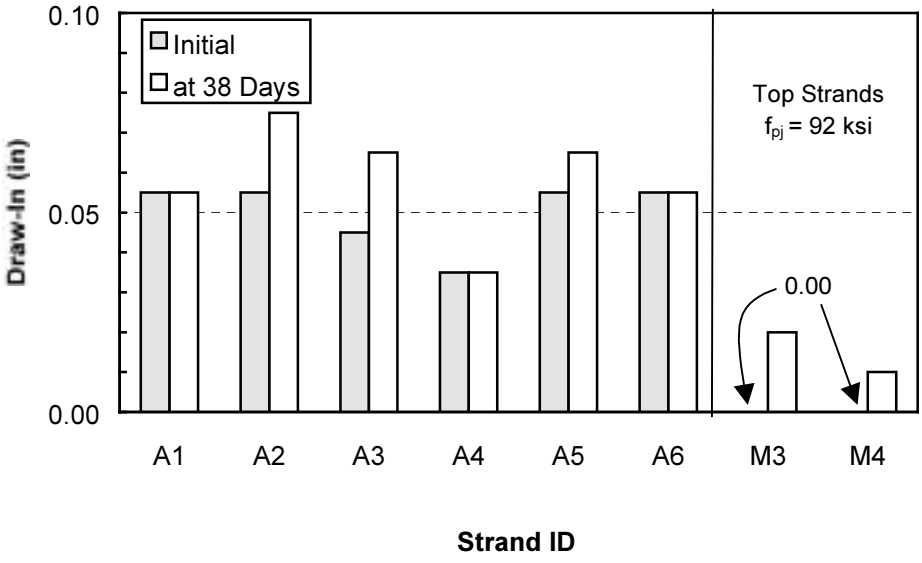


**Figure D.32: L0R-B Strand Draw-In Results (Rusted Strand, Simultaneous Flame Release)**

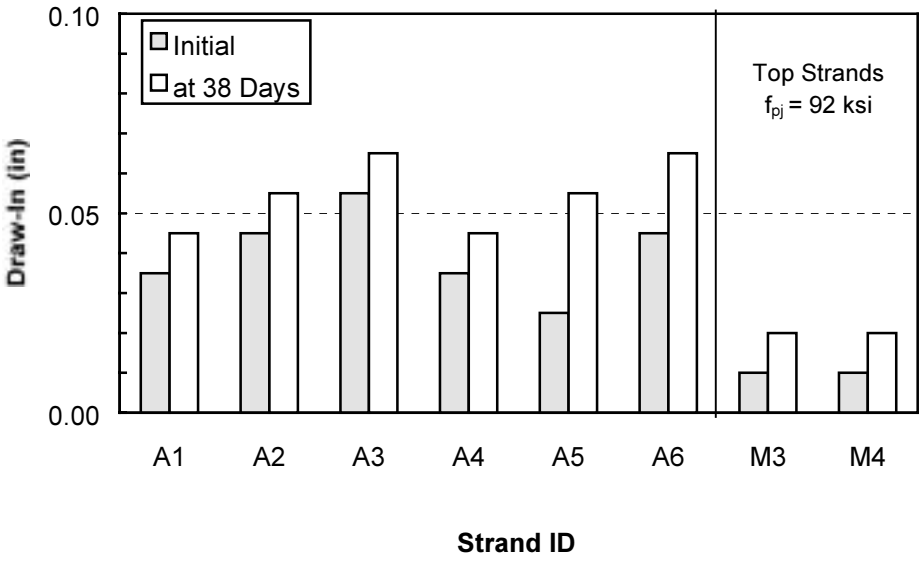


**Figure D.33: L0R-C Strand Draw-In Results (Rusted Strand, Simultaneous Flame Release)**

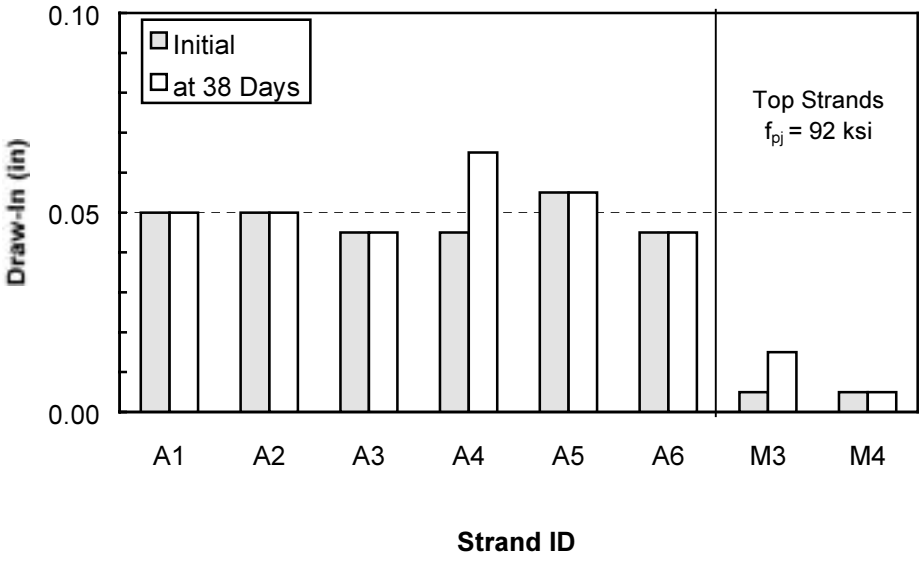


**Figure D.34: L0R-D Strand Draw-In Results (Rusted Strand, Simultaneous Flame Release)**

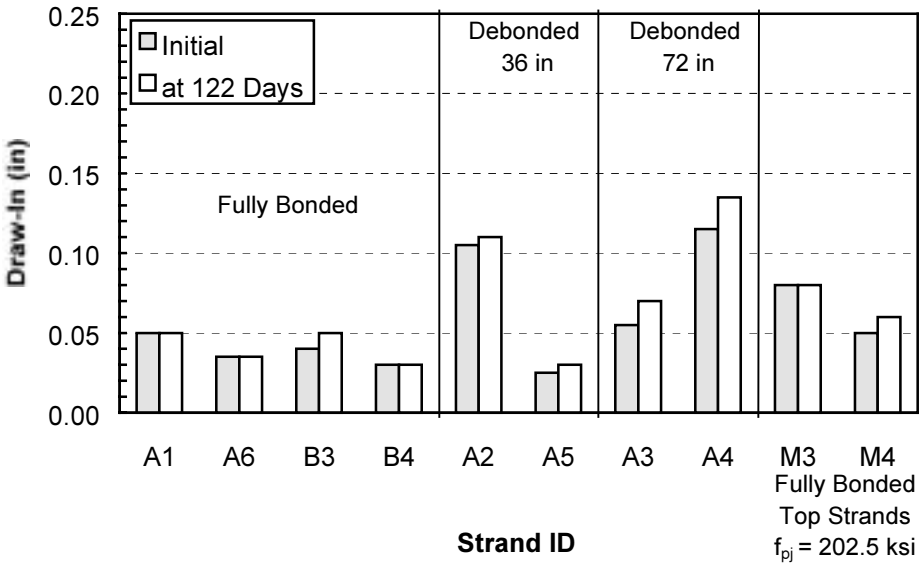


**Figure D.35: L4R-A Strand Draw-In Results (Rusted Strand, Simultaneous Flame Release)**

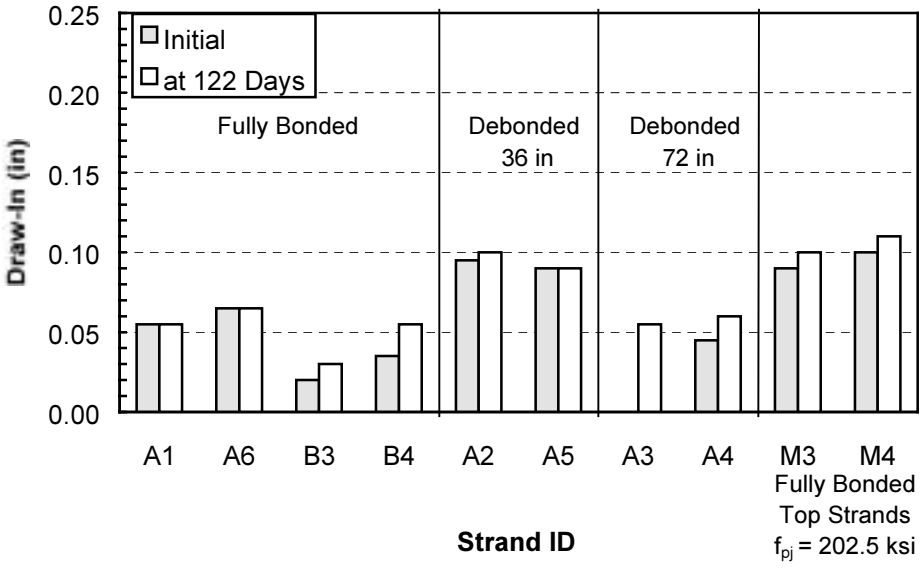


**Figure D.36: L4R-B Strand Draw-In Results (Rusted Strand, Simultaneous Flame Release)**

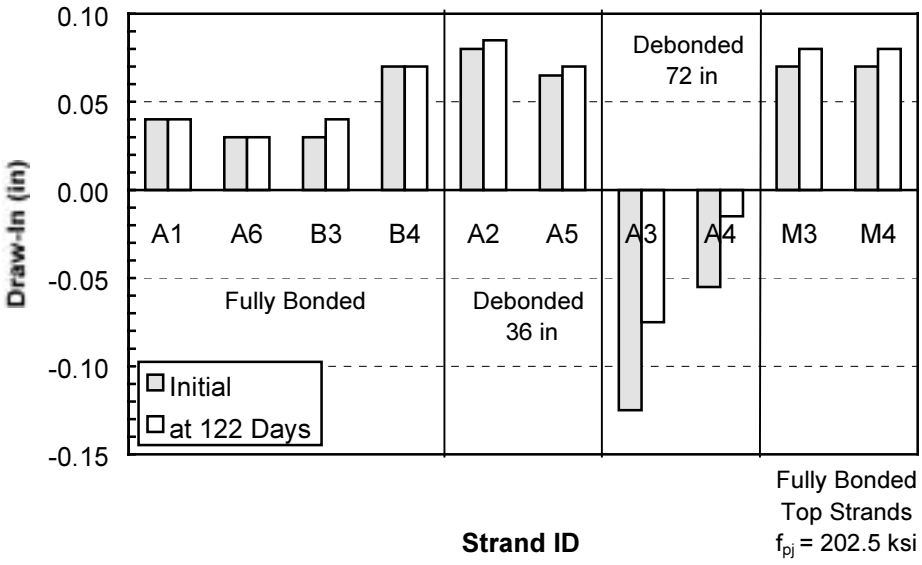


**Figure D.37: L4R-C Strand Draw-In Results (Rusted Strand, Simultaneous Flame Release)**

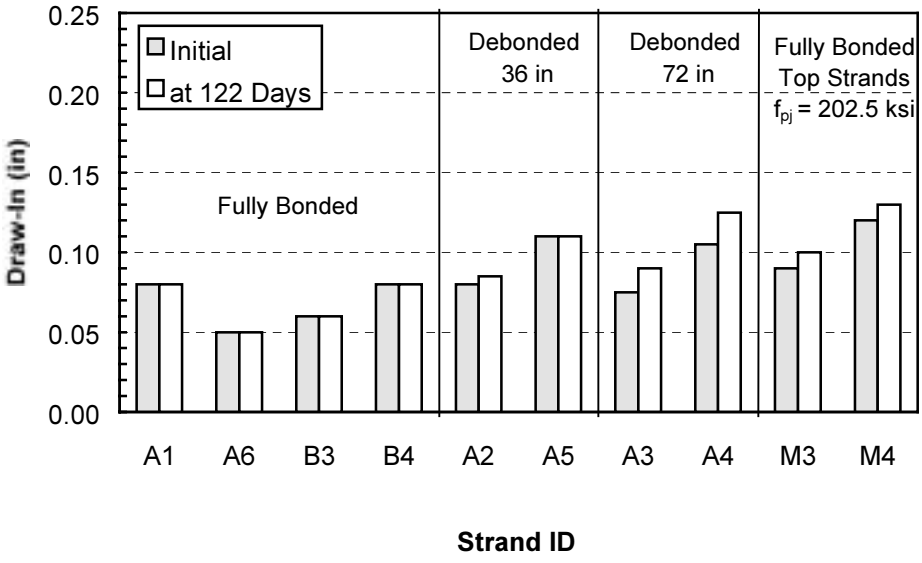


**Figure D.38: L4R-D Strand Draw-In Results (Rusted Strand, Simultaneous Flame Release)**

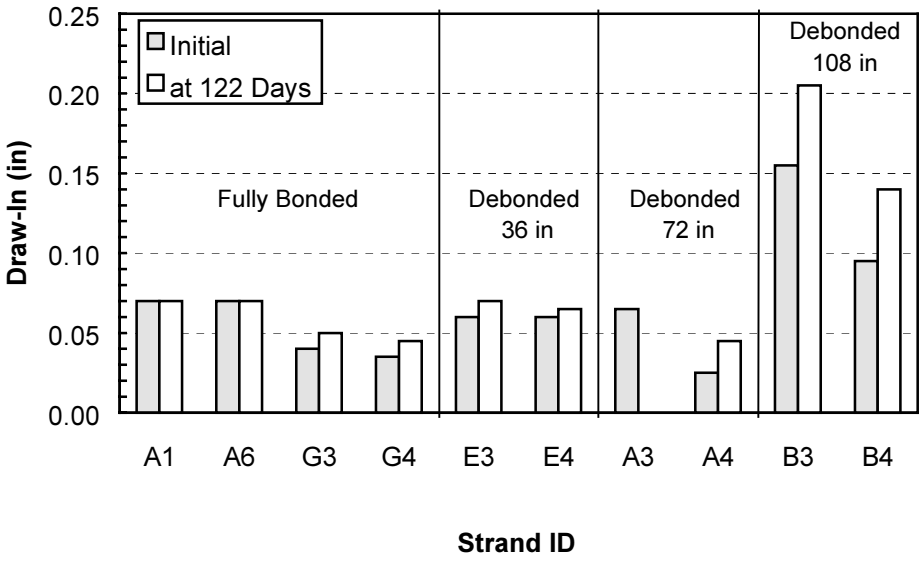


**Figure D.39: L6R-A Strand Draw-In Results (Rusted Strand, Simultaneous Flame Release)**

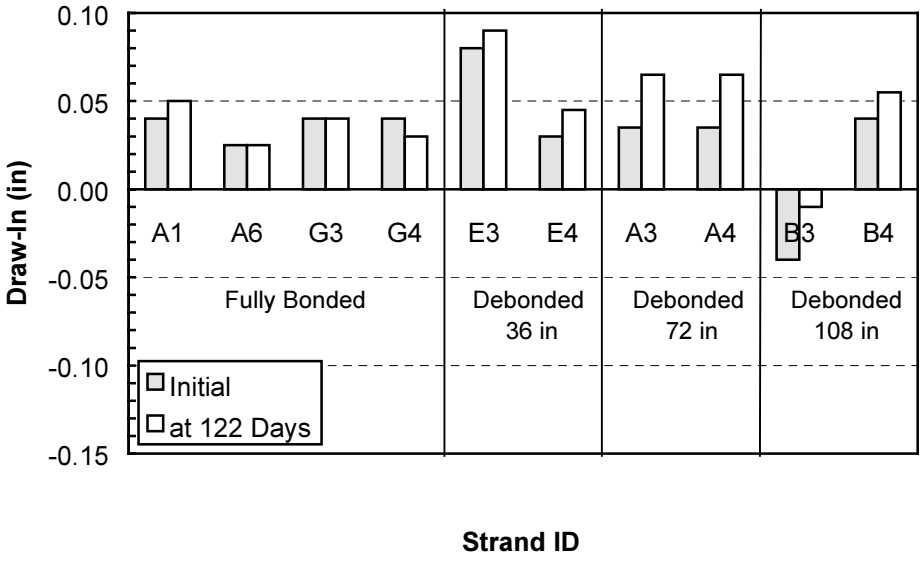


**Figure D.40: L6R-B Strand Draw-In Results (Rusted Strand, Simultaneous Flame Release)**

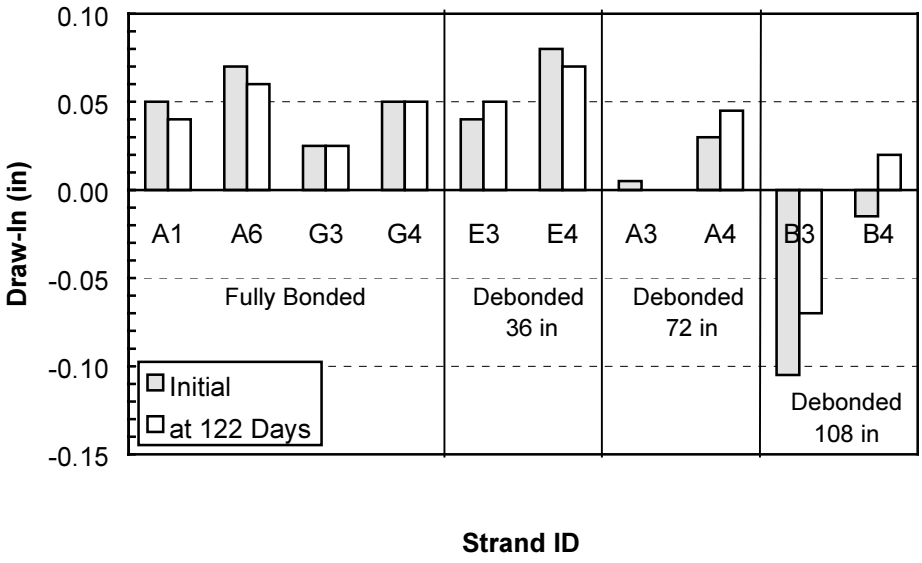


**Figure D.41: L6R-C Strand Draw-In Results (Rusted Strand, Simultaneous Flame Release)**

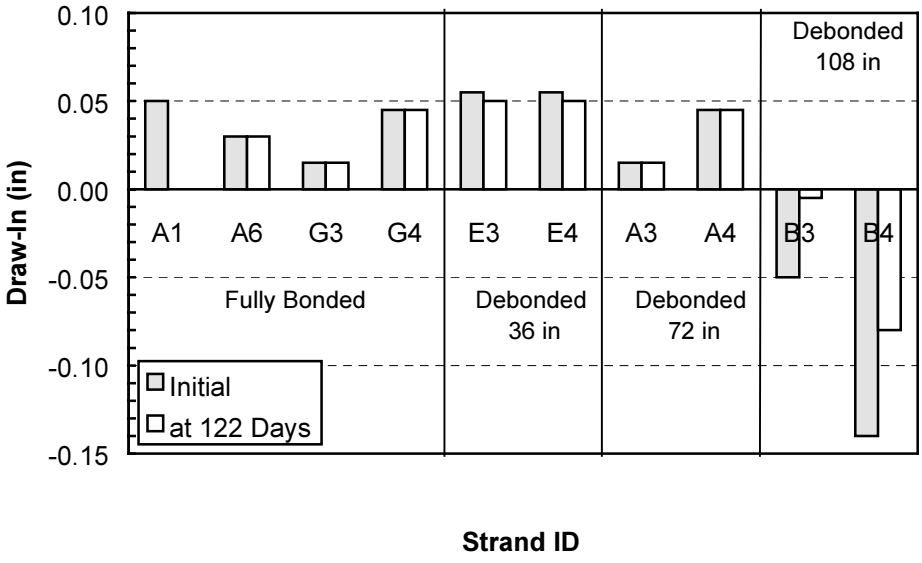


**Figure D.42: L6R-D Strand Draw-In Results (Rusted Strand, Simultaneous Flame Release)**

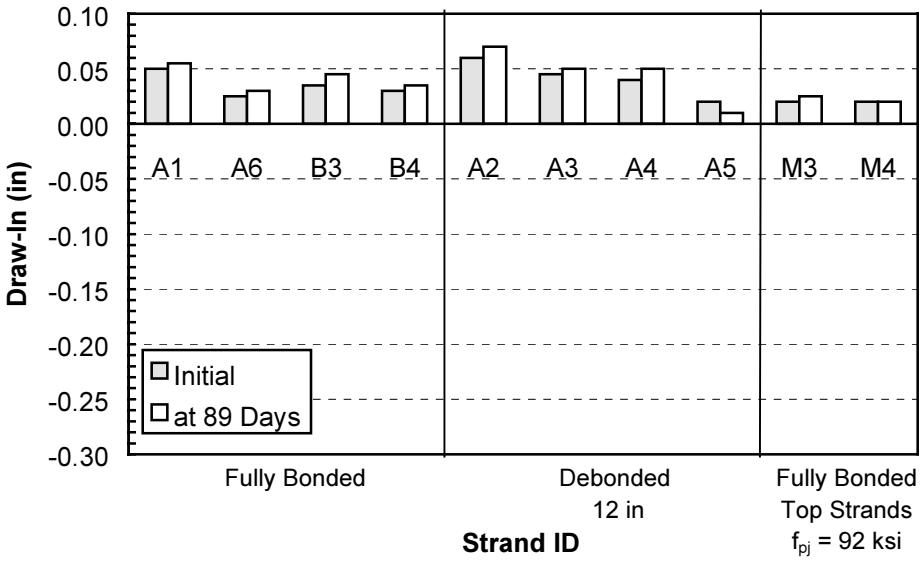


**Figure D.43: M0R-A Strand Draw-In Results (Rusted Strand, Dead End of Flame Release)**

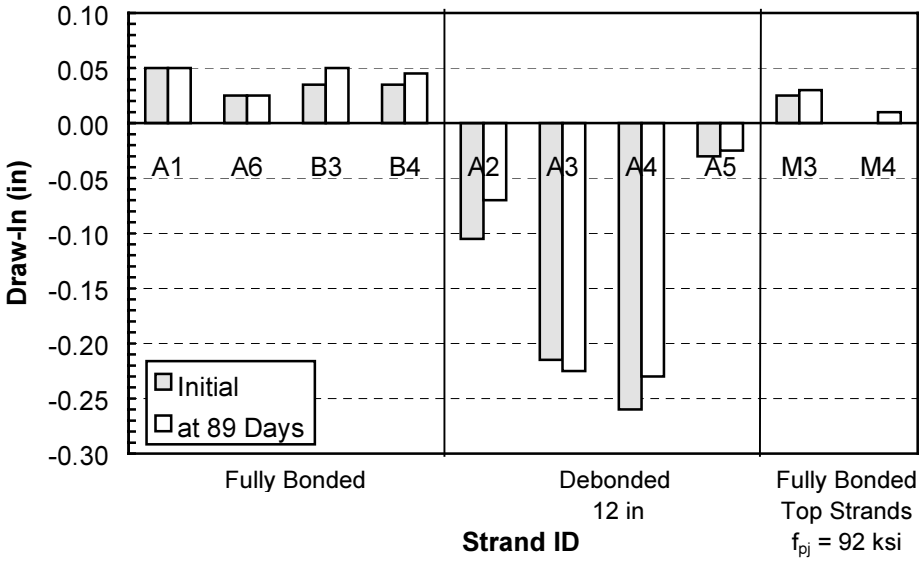


**Figure D.44: M0R-B Strand Draw-In Results (Rusted Strand, Live End of Flame Release)**

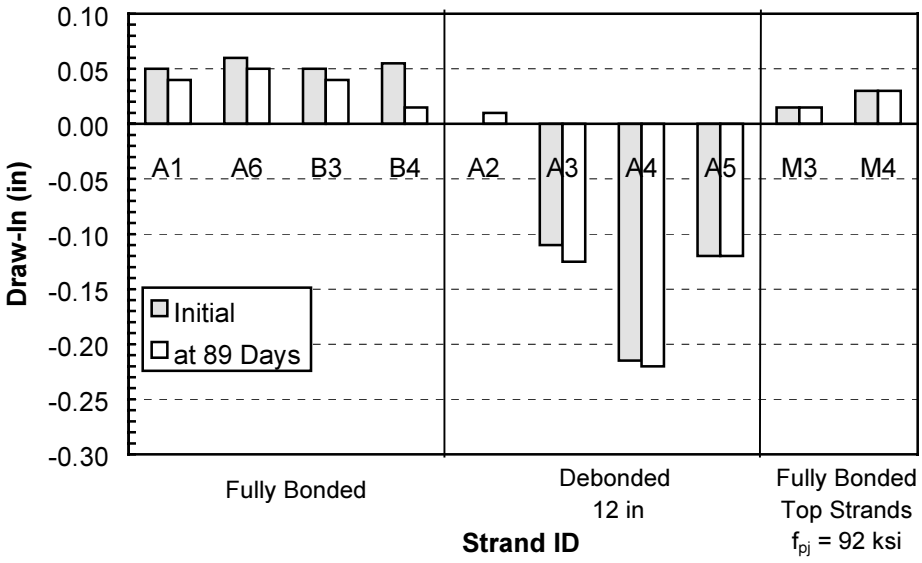


**Figure D.45: M0R-C Strand Draw-In Results (Rusted Strand, Live End of Flame Release)**

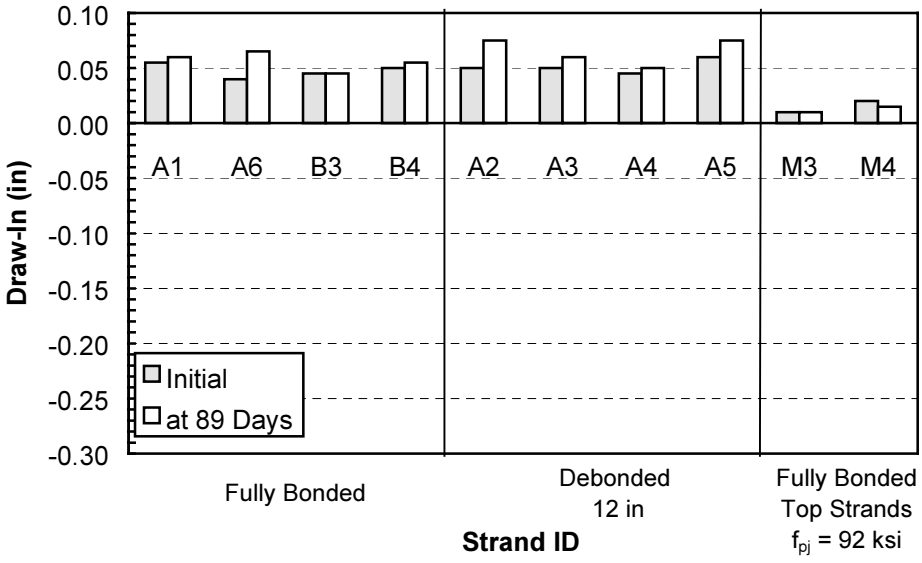


**Figure D.46: M0R-D Strand Draw-In Results (Rusted Strand, Dead End of Flame Release)**

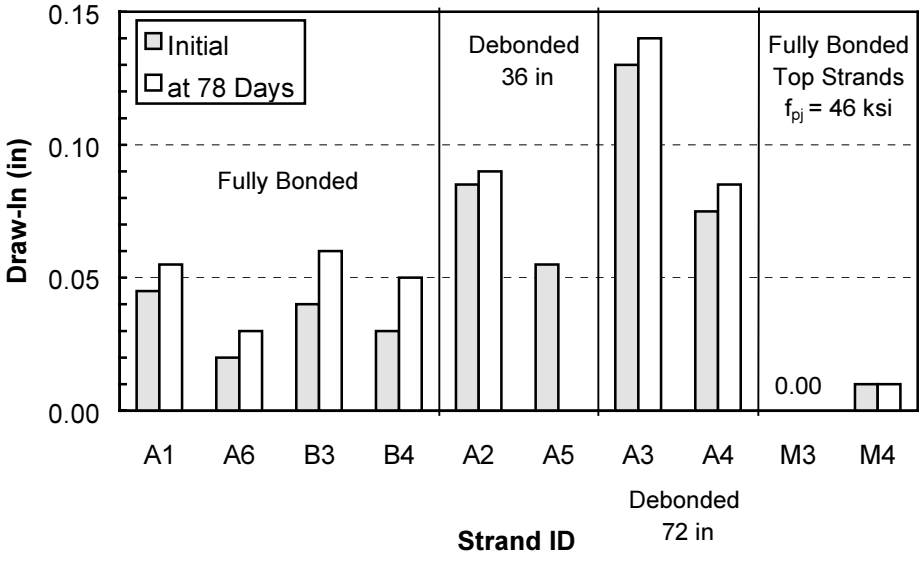


**Figure D.47: M4R-A Strand Draw-In Results (Rusted Strand, Simultaneous Flame Release)**

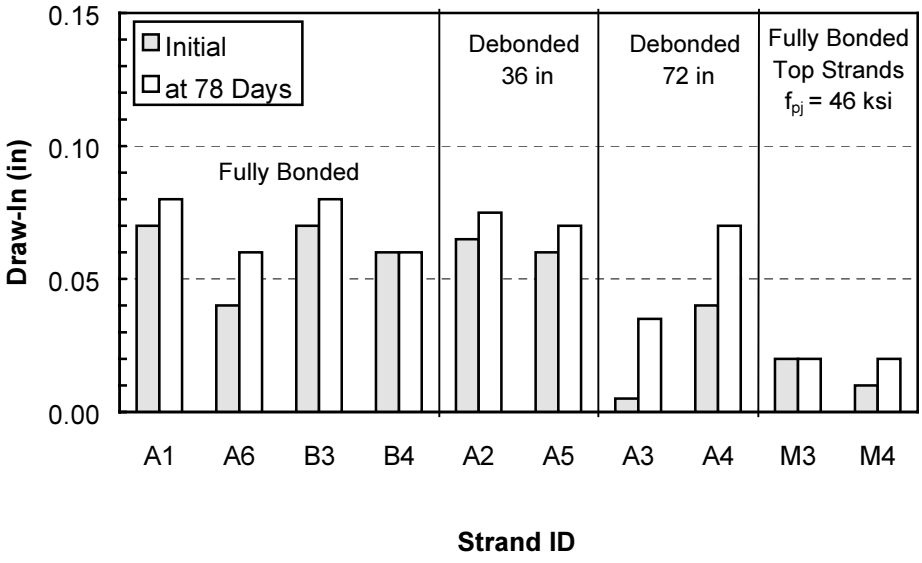


**Figure D.48: M4R-B Strand Draw-In Results (Rusted Strand, Simultaneous Flame Release)**

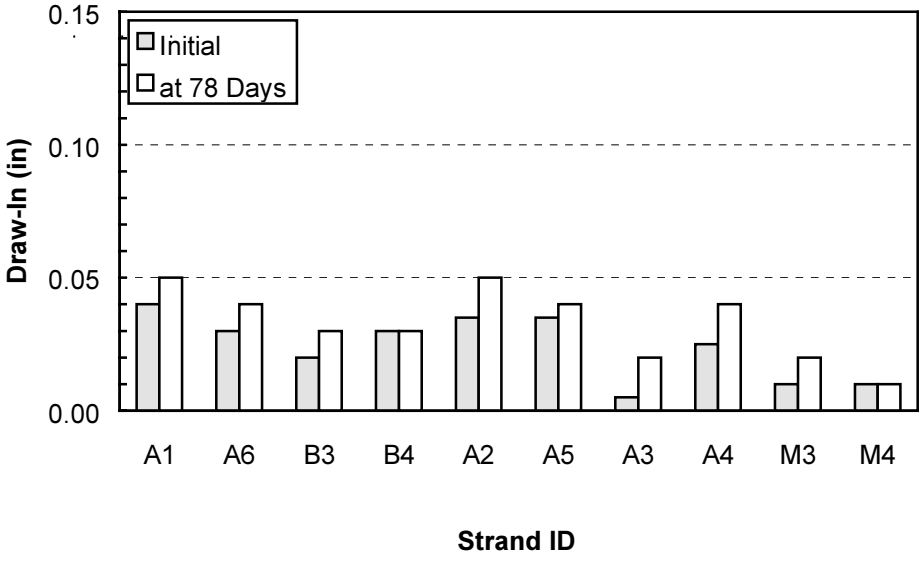


**Figure D.49: M4R-C Strand Draw-In Results (Rusted Strand, Simultaneous Flame Release)**

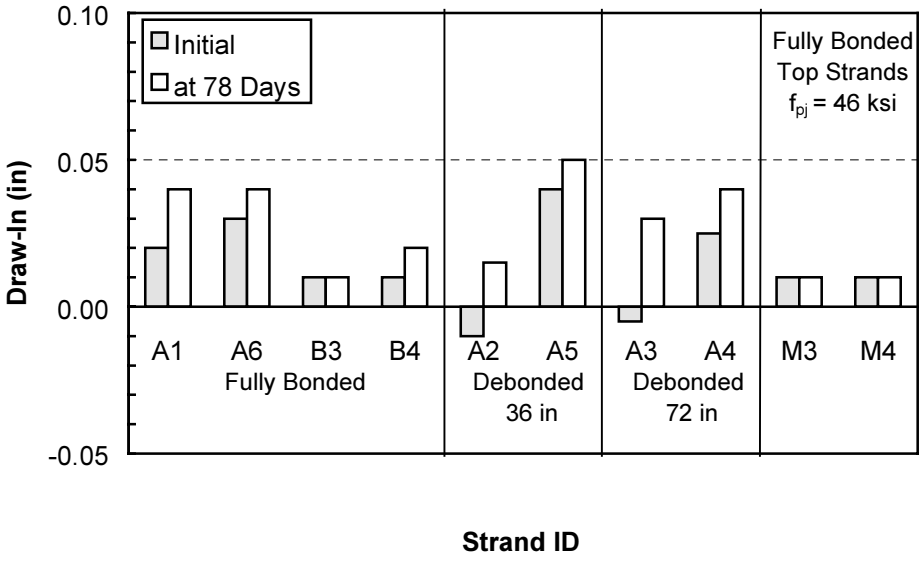


**Figure D.50: M4R-D Strand Draw-In Results (Rusted Strand, Simultaneous Flame Release)**

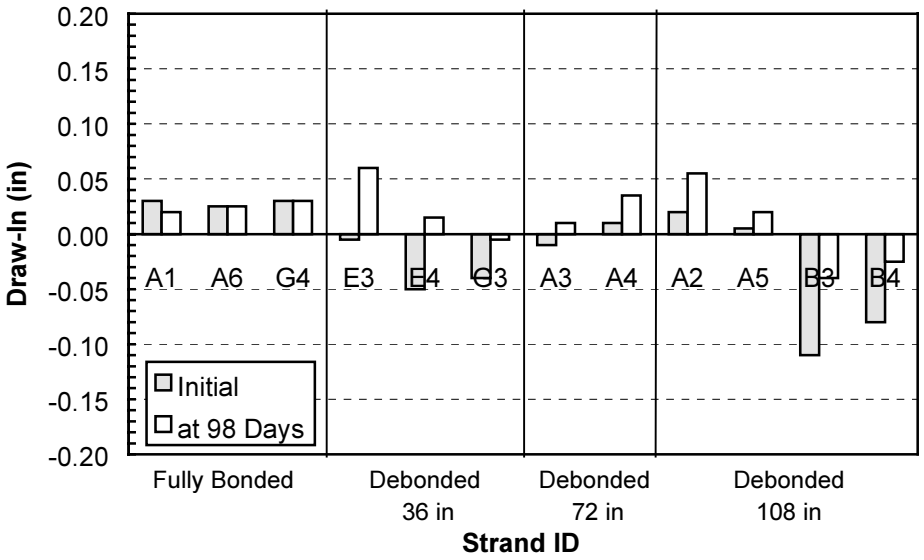


**Figure D.51: M9R-A Strand Draw-In Results (Rusted Strand, Dead End of Flame Release)**

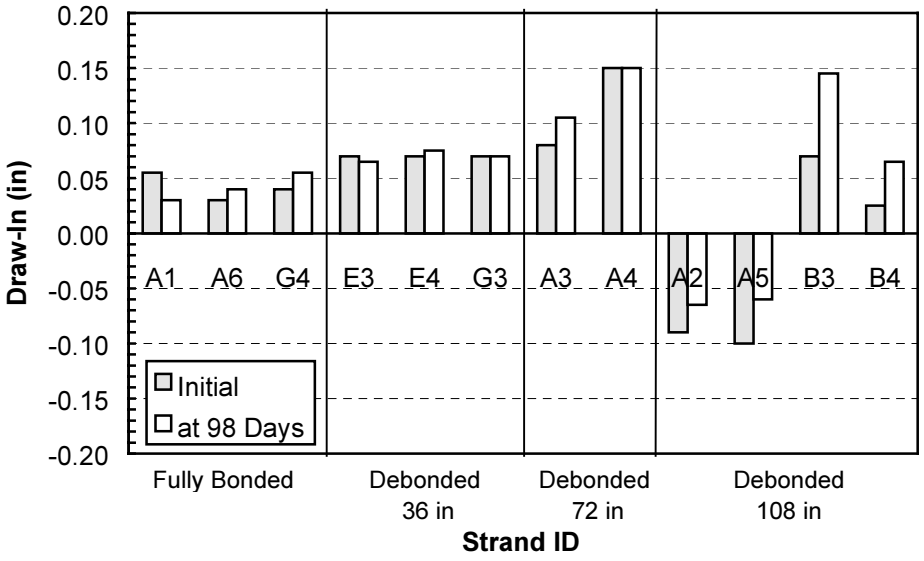


**Figure D.52: M9R-B Strand Draw-In Results (Rusted Strand, Live End of Flame Release)**

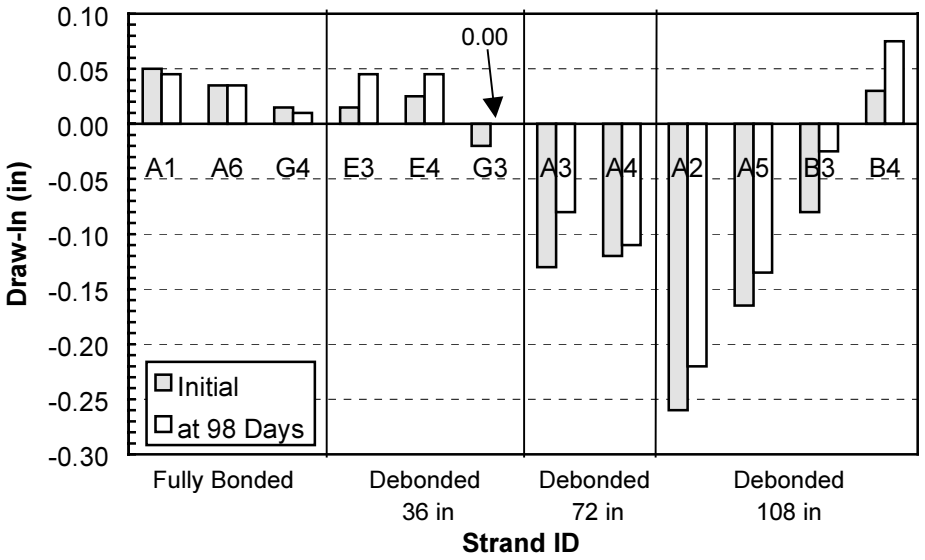


**Figure D.53: M9R-C Strand Draw-In Results (Rusted Strand, Live End of Flame Release)**

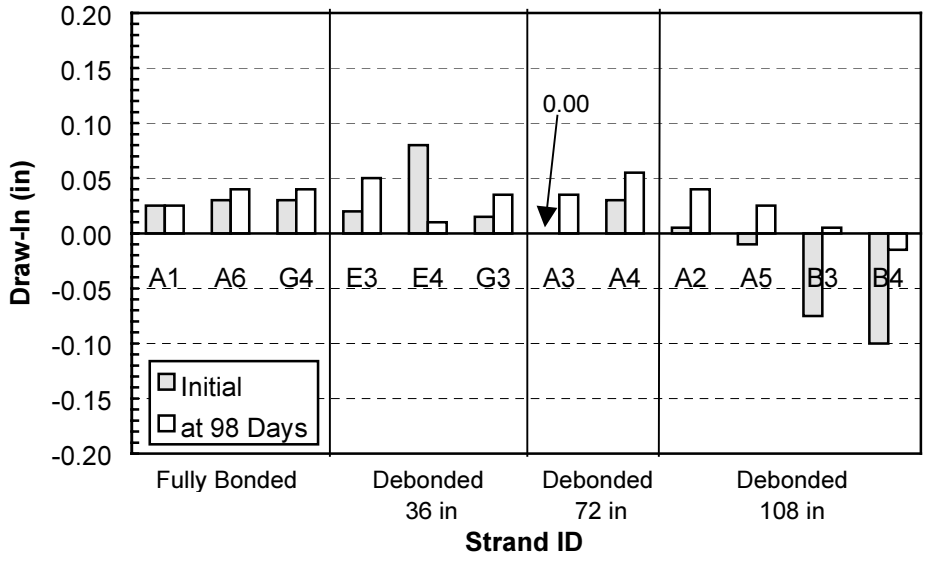


**Figure D.54: M9R-D Strand Draw-In Results (Rusted Strand, Dead End of Flame Release)**

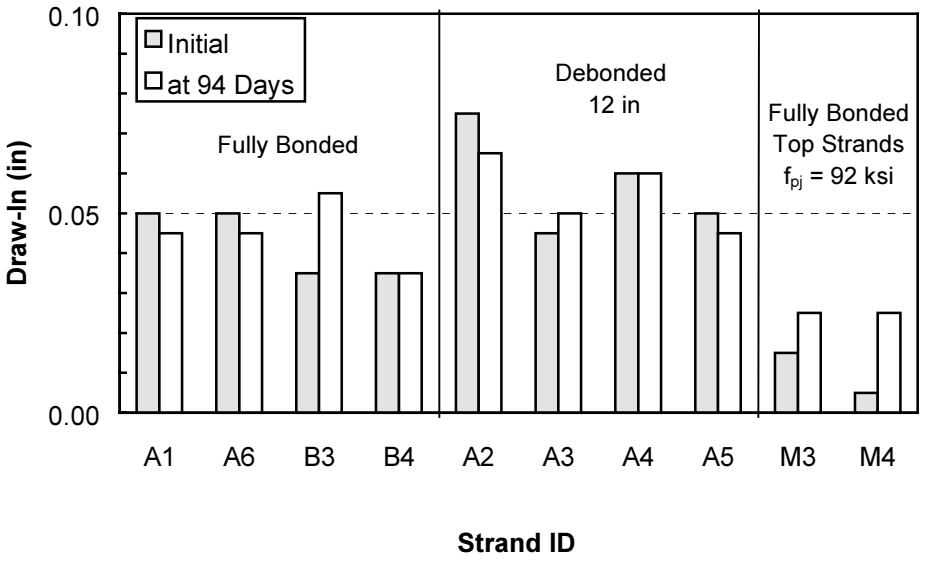


**Figure D.55: H0R-A Strand Draw-In Results (Rusted Strand, Dead End of Flame Release)**

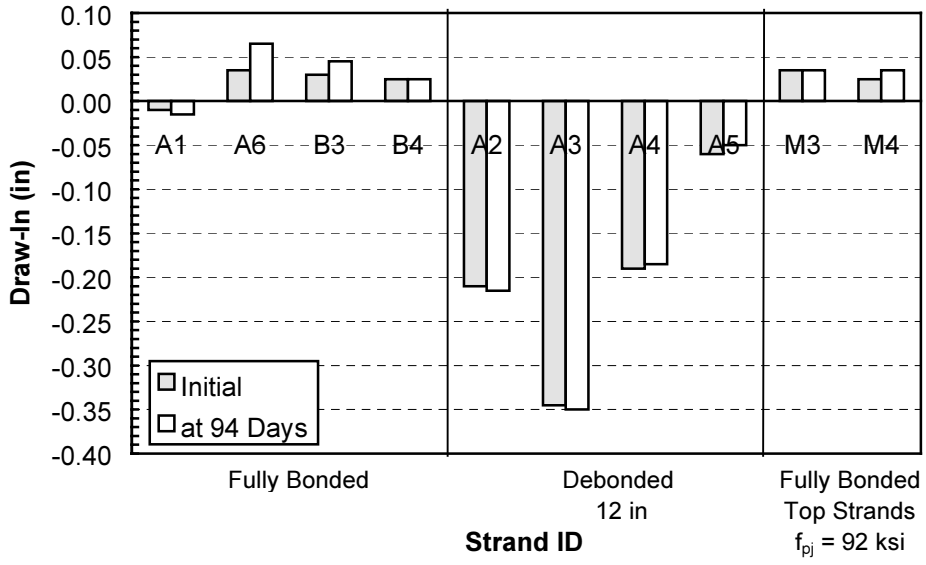


**Figure D.56: H0R-B Strand Draw-In Results (Rusted Strand, Live End of Flame Release)**

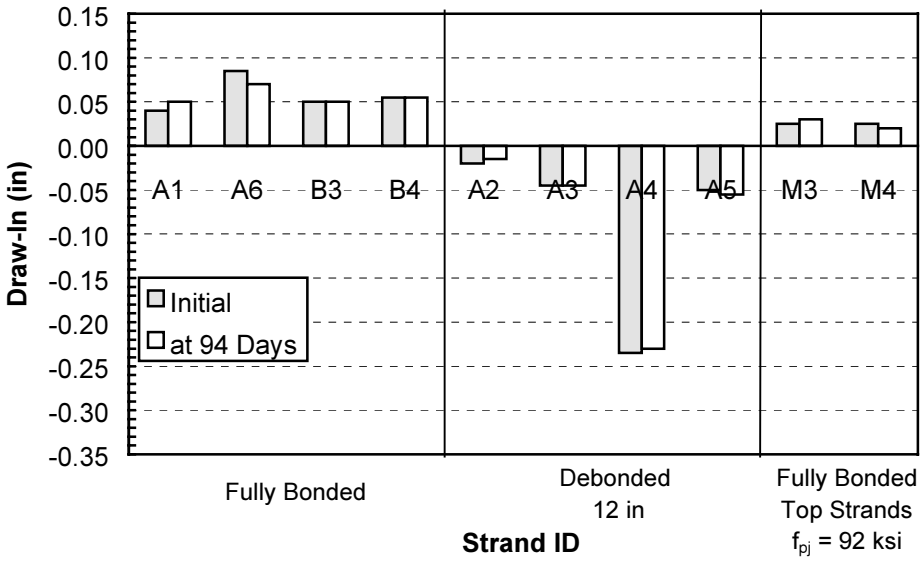


**Figure D.57: H0R-C Strand Draw-In Results (Rusted Strand, Live End of Flame Release)**

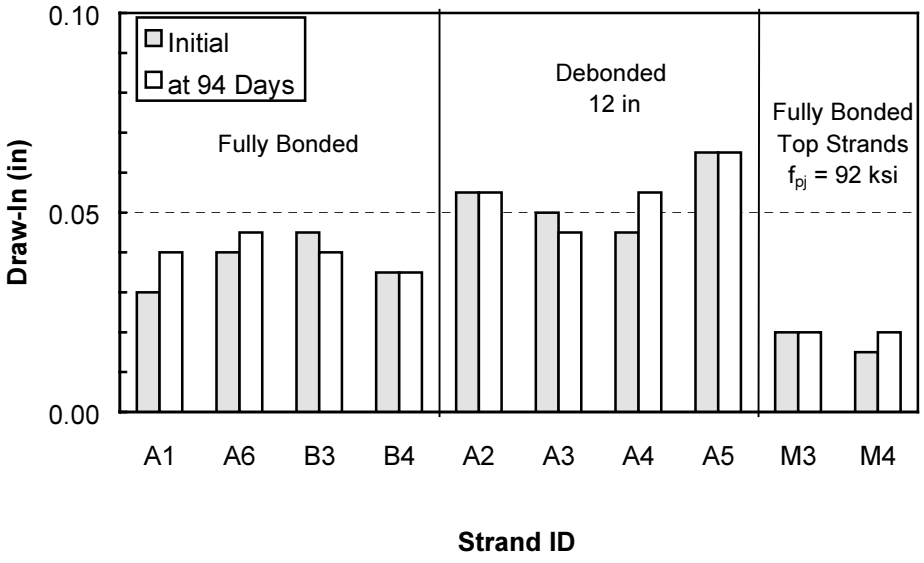


**Figure D.58: H0R-D Strand Draw-In Results (Rusted Strand, Dead End of Flame Release)**

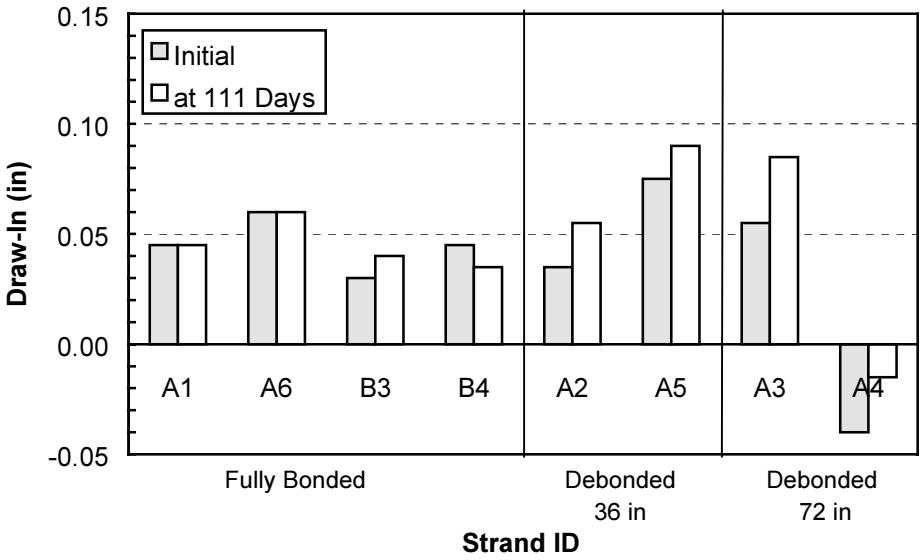


**Figure D.59: H4R-A Strand Draw-In Results (Rusted Strand, Simultaneous Flame Release)**

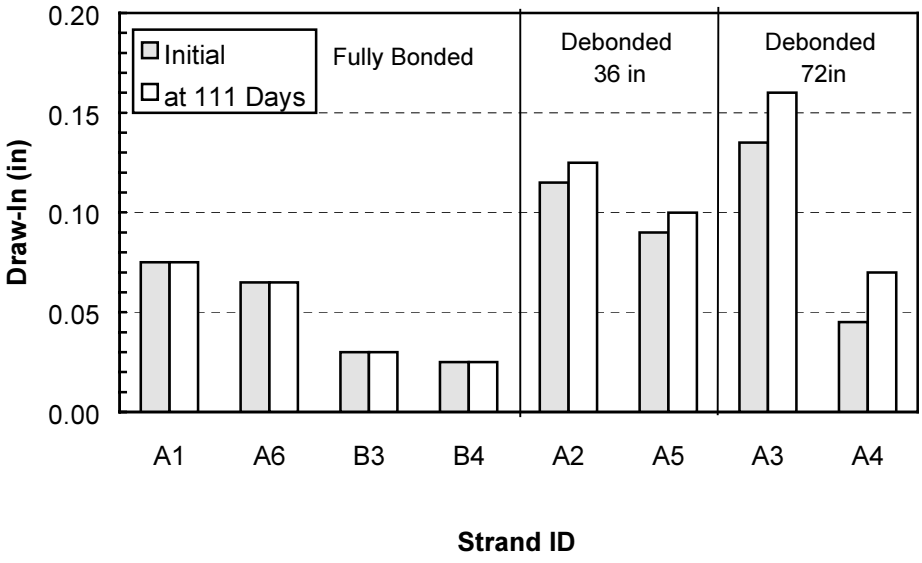


**Figure D.60: H4R-B Strand Draw-In Results (Rusted Strand, Simultaneous Flame Release)**

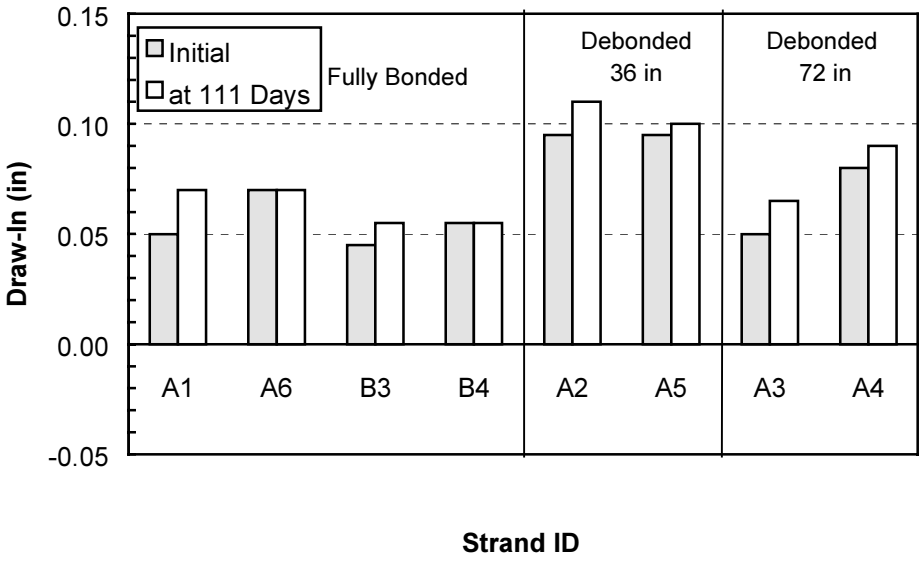


**Figure D.61: H4R-C Strand Draw-In Results (Rusted Strand, Simultaneous Flame Release)**

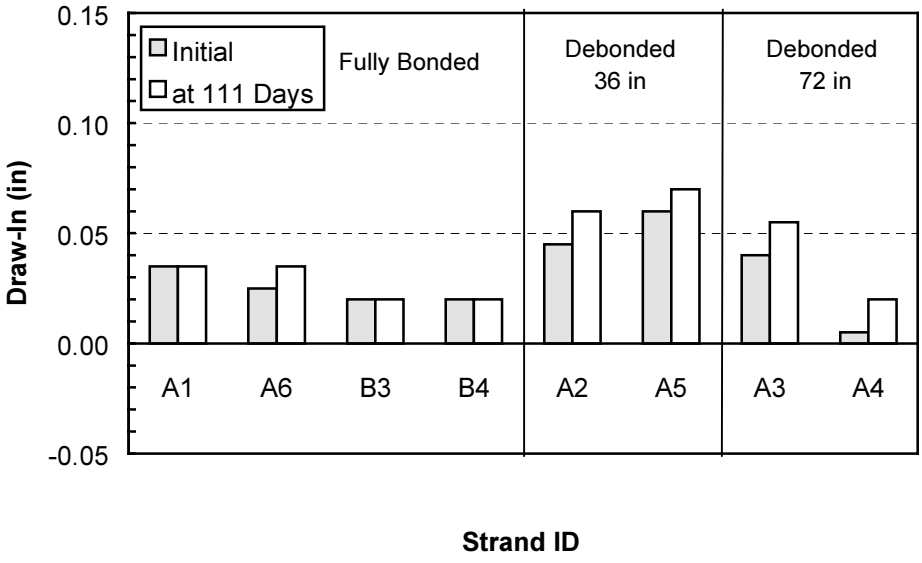


**Figure D.62: H4R-D Strand Draw-In Results (Rusted Strand, Simultaneous Flame Release)**

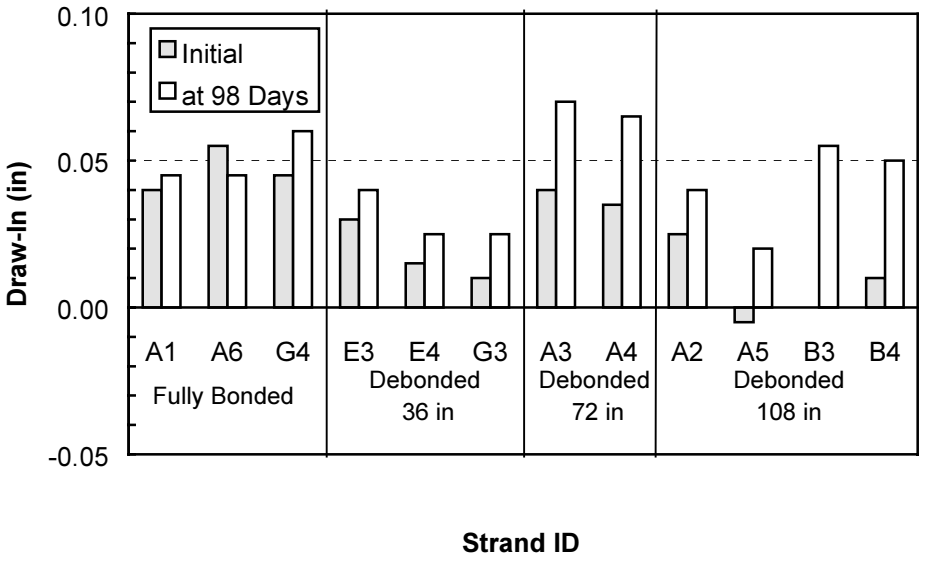


**Figure D.63: H9R-A Strand Draw-In Results (Rusted Strand, Dead End of Flame Release)**

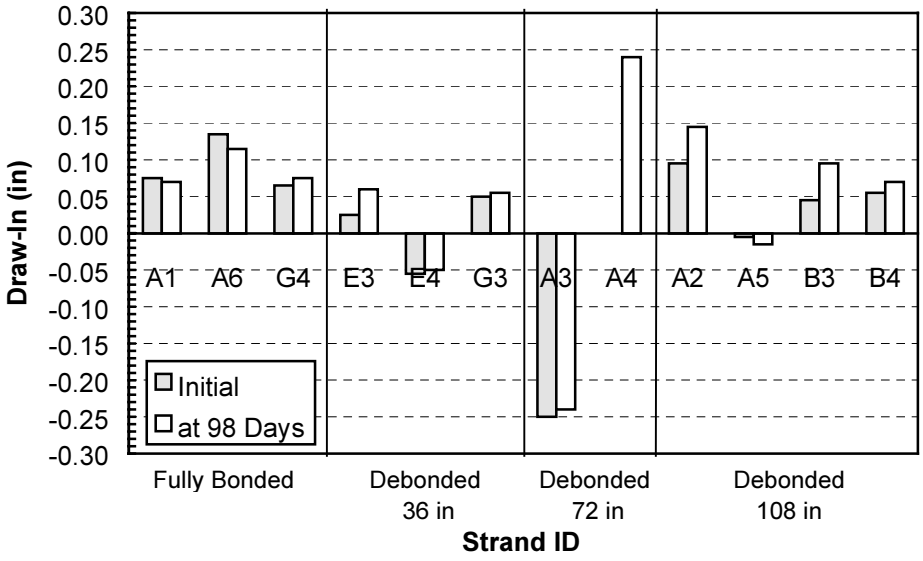


**Figure D.64: H9R-B Strand Draw-In Results (Rusted Strand, Live End of Flame Release)**

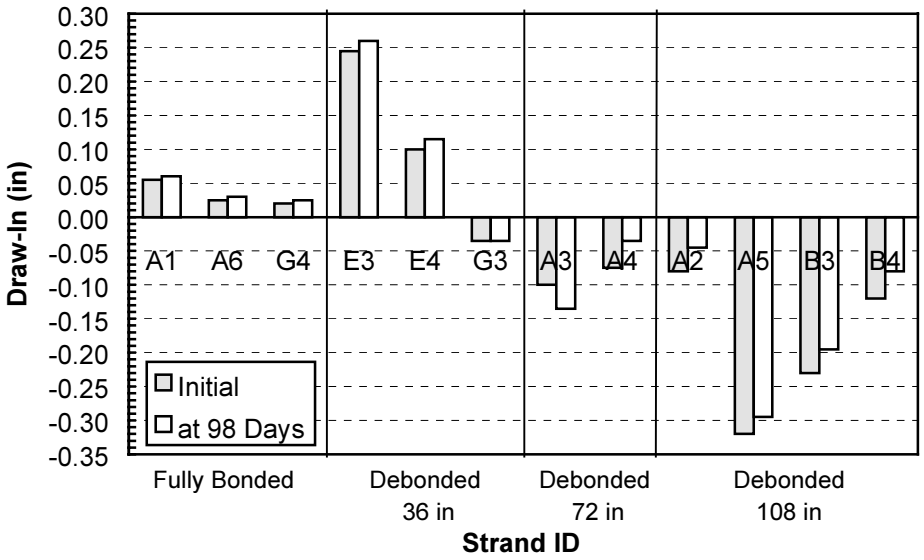


**Figure D.65: H9R-C Strand Draw-In Results (Rusted Strand, Live End of Flame Release)**

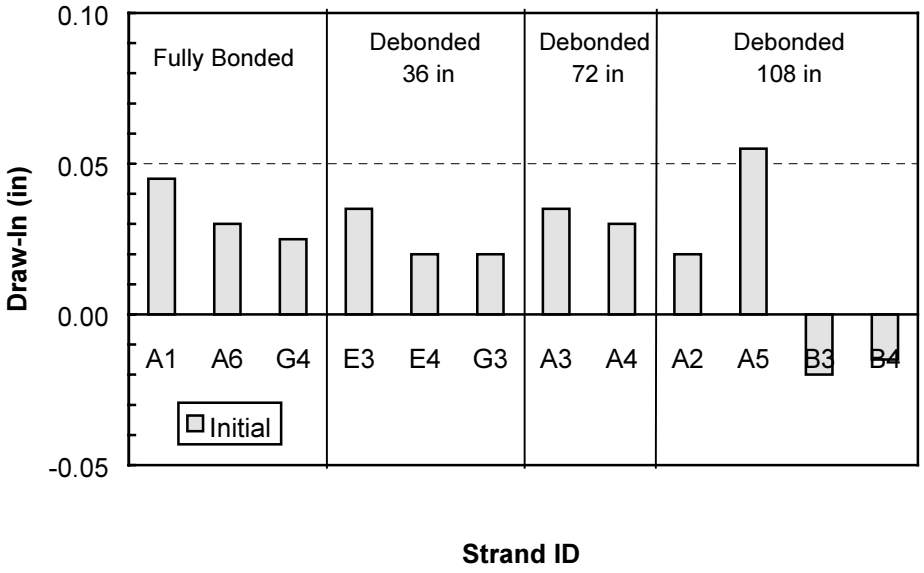


**Figure D.66: H9R-D Strand Draw-In Results (Rusted Strand, Dead End of Flame Release)**

# APPENDIX E: MOMENT VS. DEFLECTION CHARTS

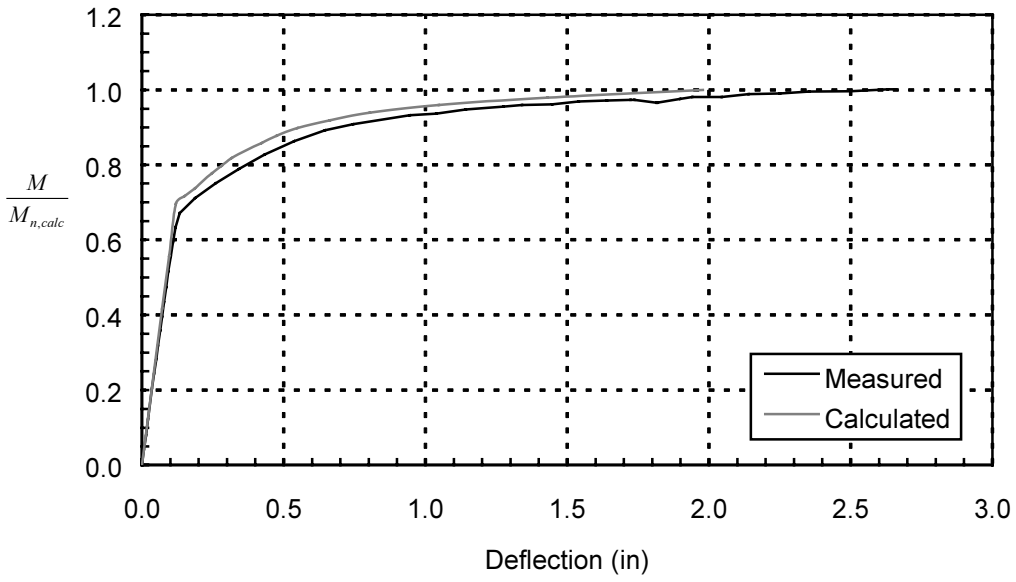


**Figure E.1: Test L0B-A-96—Normalized Moment at Critical Section vs. Deflection (1 in = 25.4 mm)**

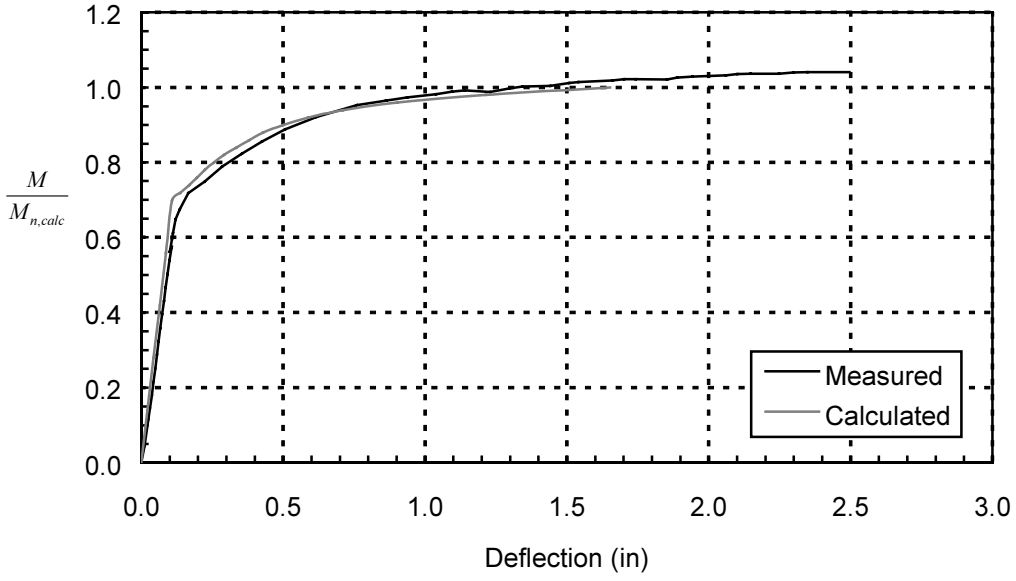


**Figure E.2: Test L0B-B-72—Normalized Moment at Critical Section vs. Deflection (1 in = 25.4 mm)**

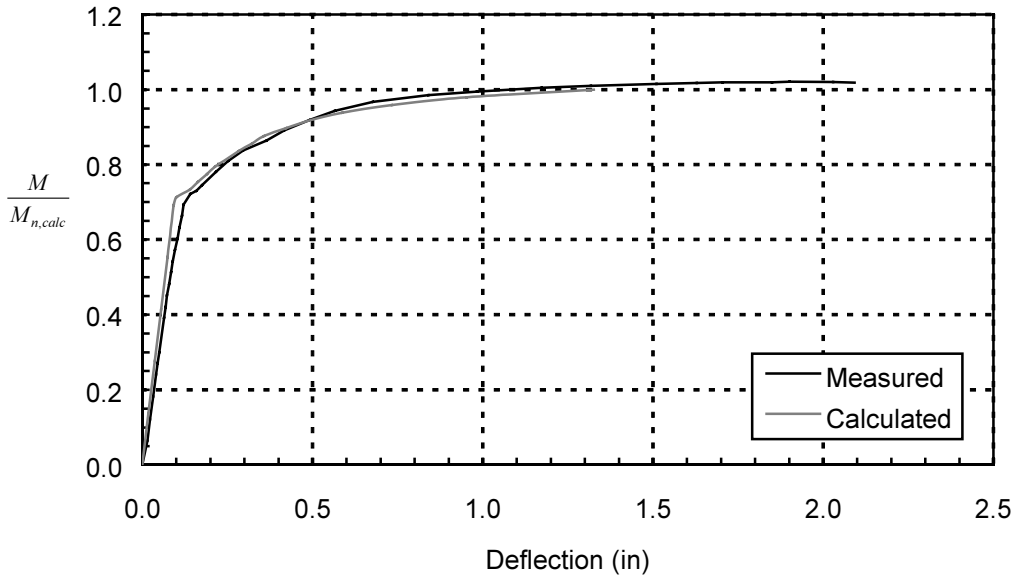


**Figure E.3: Test L0B-D-54—Normalized Moment at Critical Section vs. Deflection (1 in = 25.4 mm)**

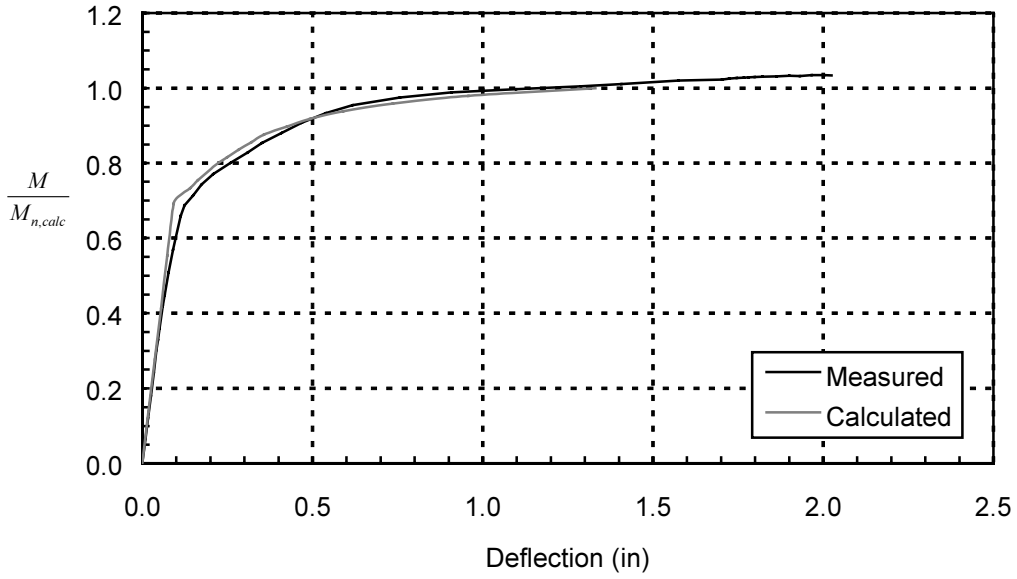


**Figure E.4: Test L0B-C-54H—Normalized Moment at Critical Section vs. Deflection (1 in = 25.4 mm)**

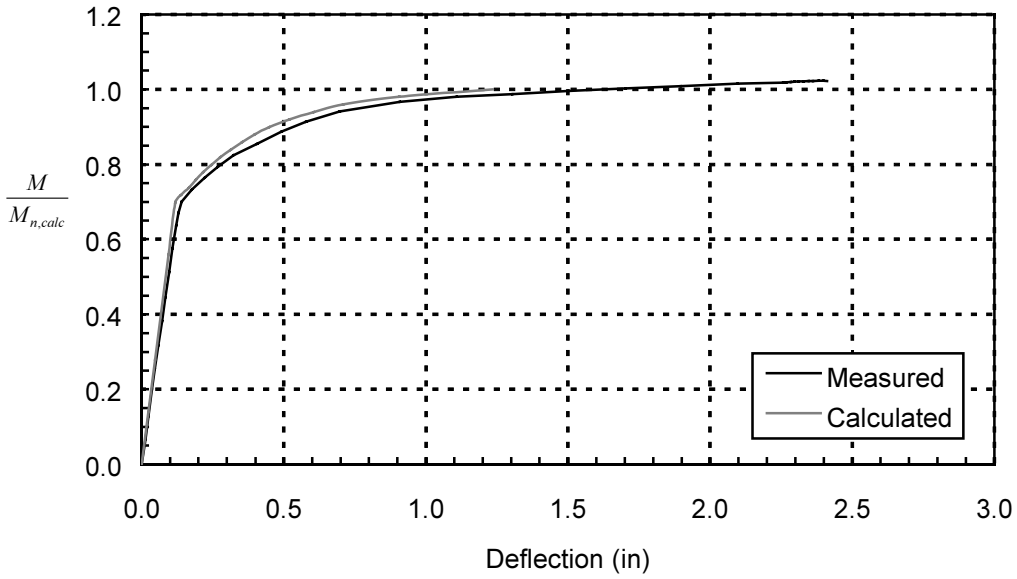


**Figure E.5: Test M0B-A-96—Normalized Moment at Critical Section vs. Deflection (1 in = 25.4 mm)**

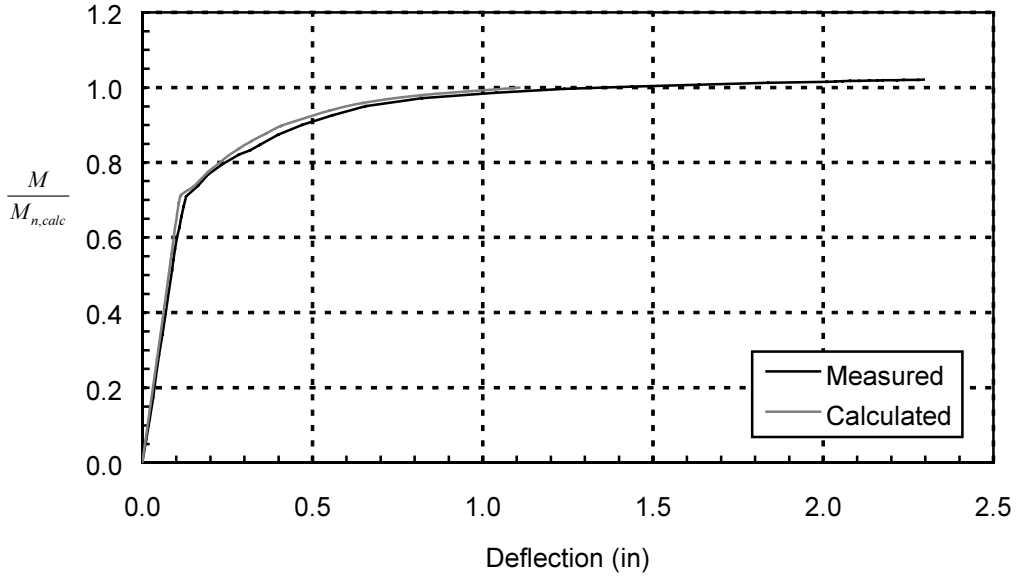


**Figure E.6: Test M0B-B-72—Normalized Moment at Critical Section vs. Deflection (1 in = 25.4 mm)**

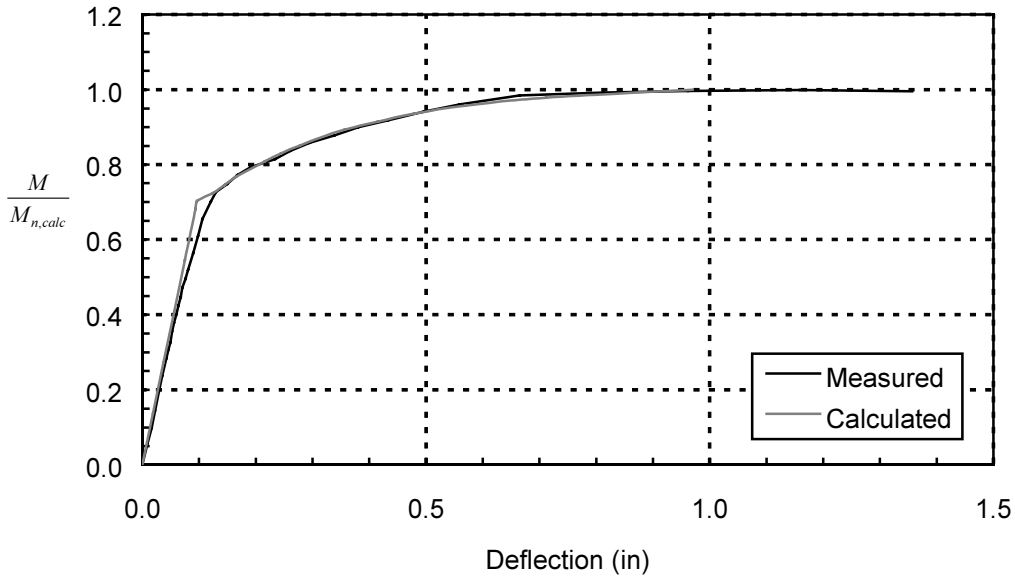


**Figure E.7: Test M0B-D-54—Normalized Moment at Critical Section vs. Deflection (1 in = 25.4 mm)**

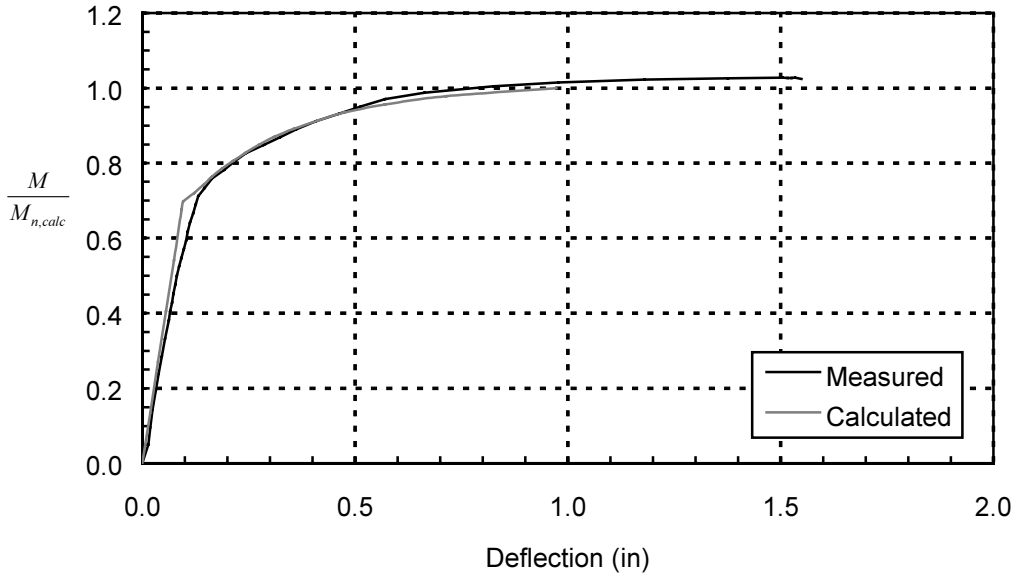


**Figure E.8: Test M0B-C-54H—Normalized Moment at Critical Section vs. Deflection (1 in = 25.4 mm)**

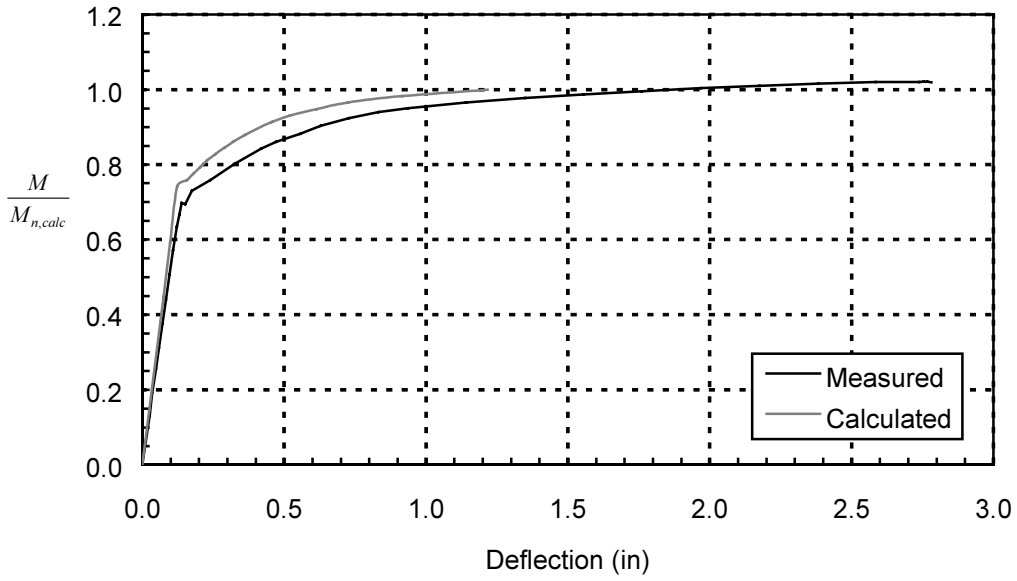


**Figure E.9: Test H0B-A-96—Normalized Moment at Critical Section vs. Deflection (1 in = 25.4 mm)**

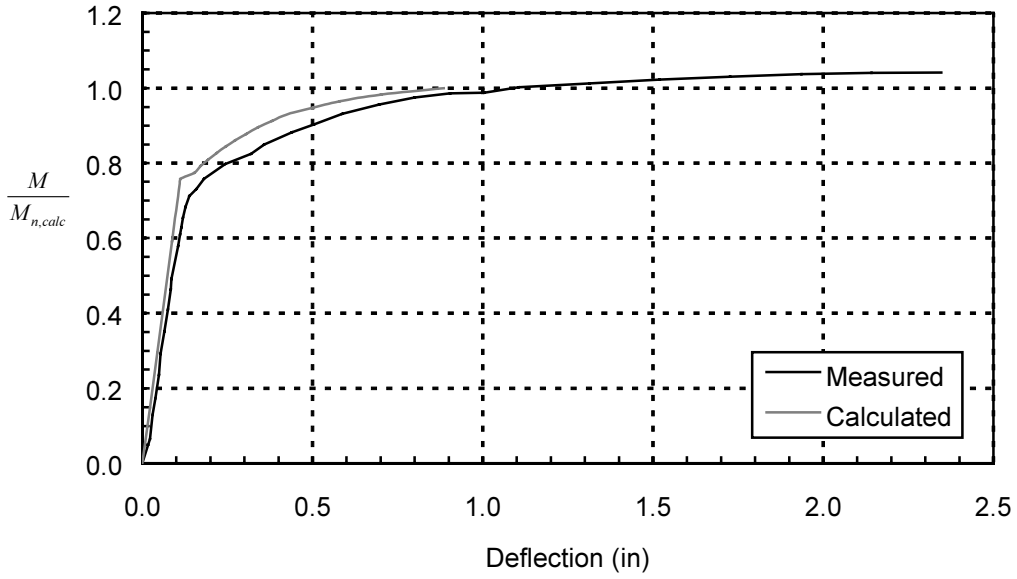


**Figure E.10: Test H0B-B-72—Normalized Moment at Critical Section vs. Deflection (1 in = 25.4 mm)**

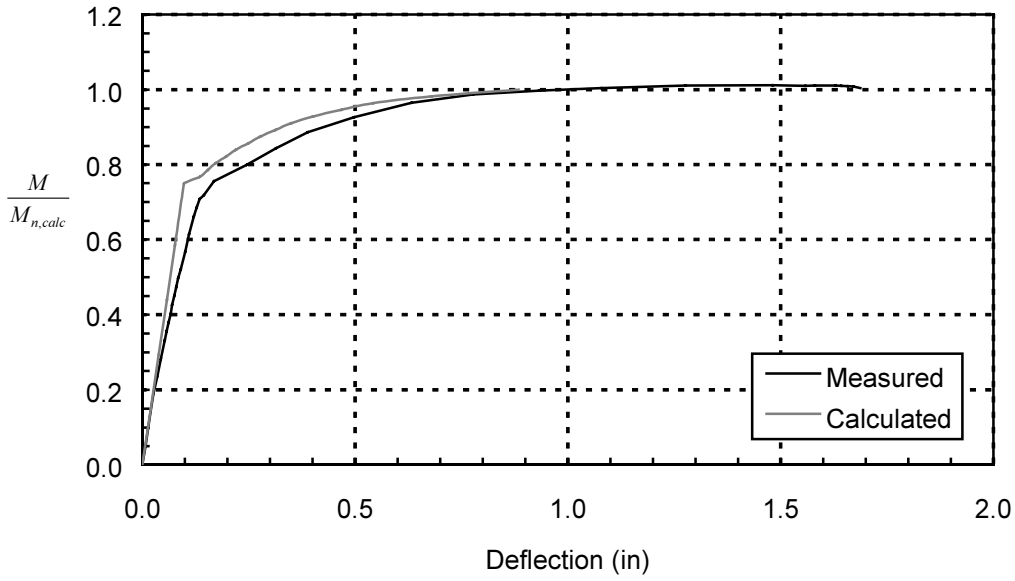


**Figure E.11: Test H0B-D-54—Normalized Moment at Critical Section vs. Deflection (1 in = 25.4 mm)**

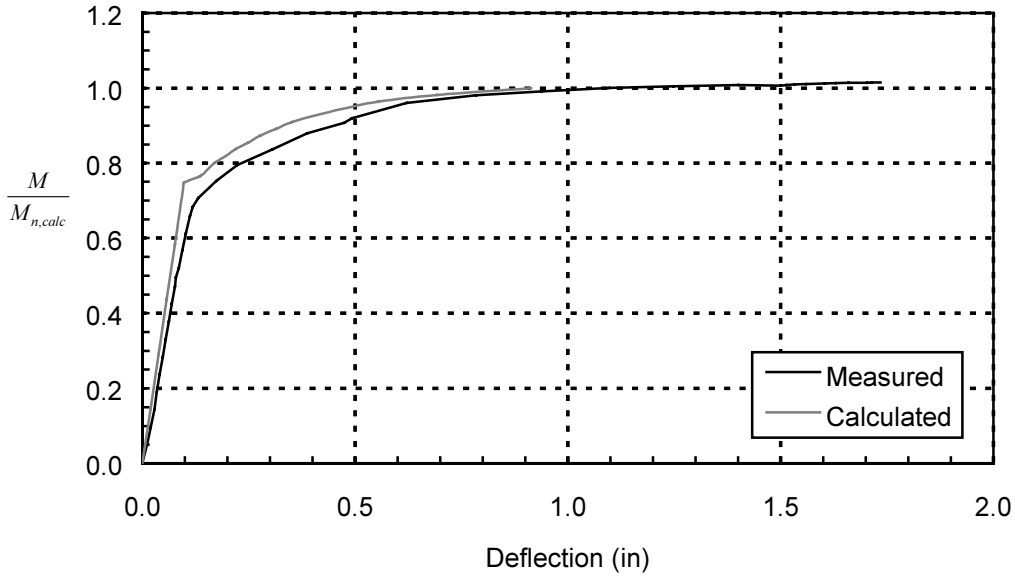


**Figure E.12: Test H0B-C-54H—Normalized Moment at Critical Section vs. Deflection (1 in = 25.4 mm)**

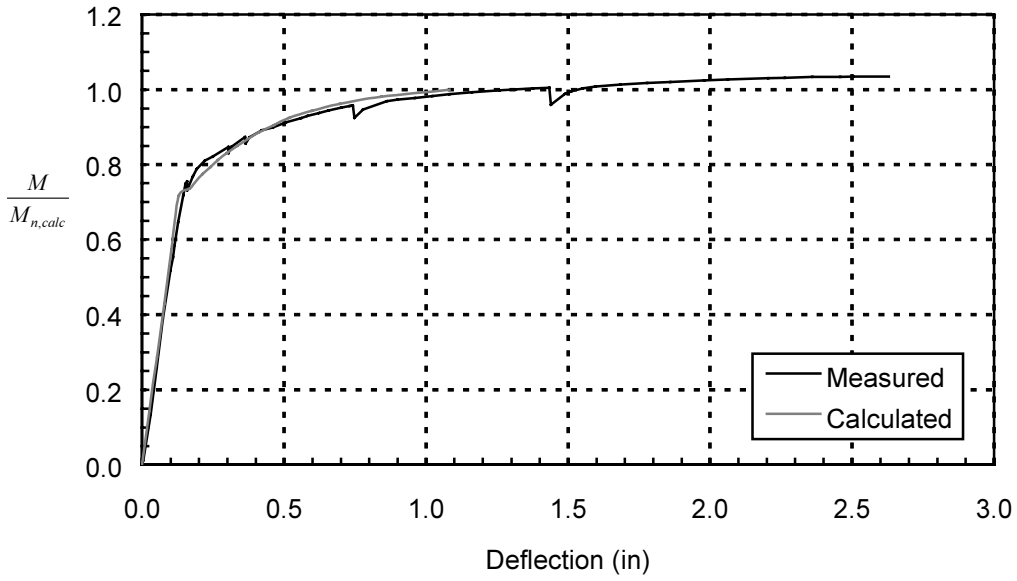


**Figure E.13: Test M0R-A-96—Normalized Moment at Critical Section vs. Deflection (1 in = 25.4 mm)**

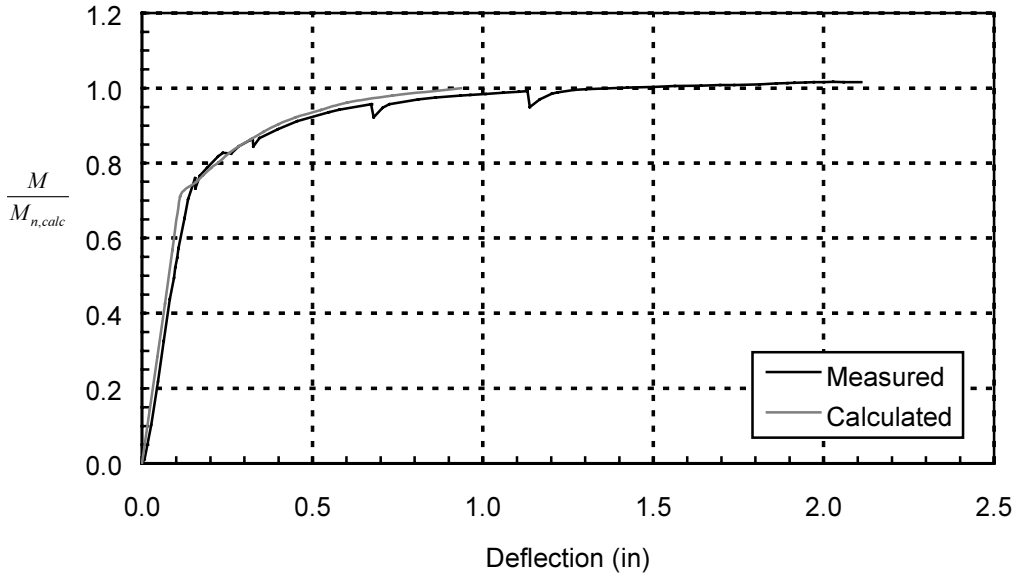


**Figure E.14: Test M0R-B-54—Normalized Moment at Critical Section vs. Deflection (1 in = 25.4 mm)**

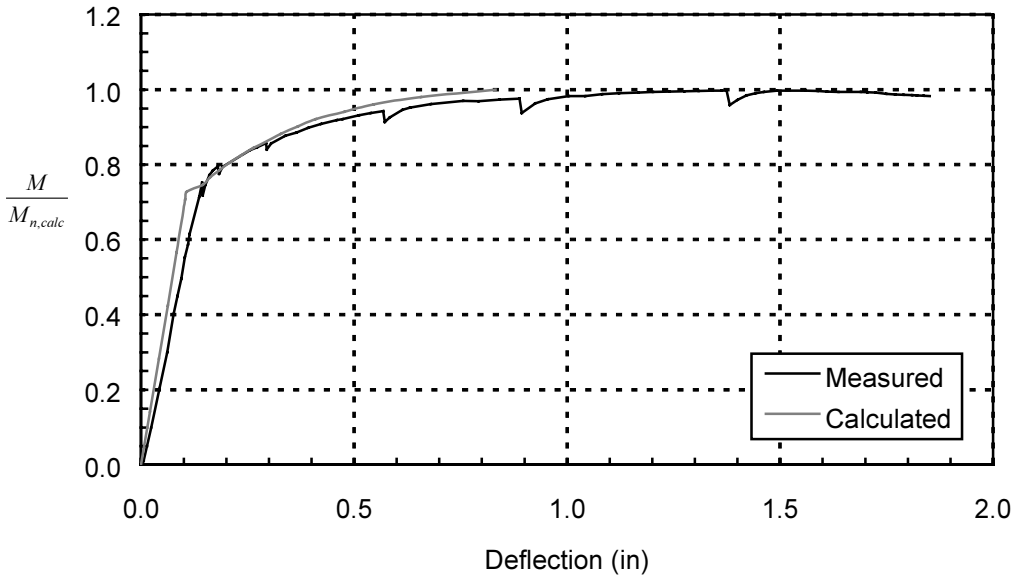


**Figure E.15: Test M0R-D-46—Normalized Moment at Critical Section vs. Deflection (1 in = 25.4 mm)**

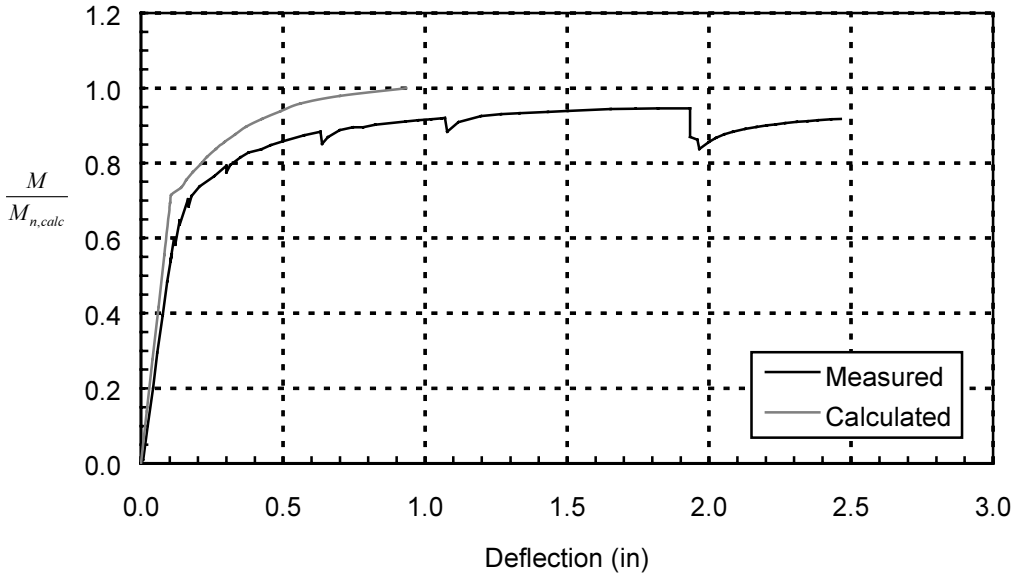


**Figure E.16: Test M0R-C-46H—Normalized Moment at Critical Section vs. Deflection (1 in = 25.4 mm)**

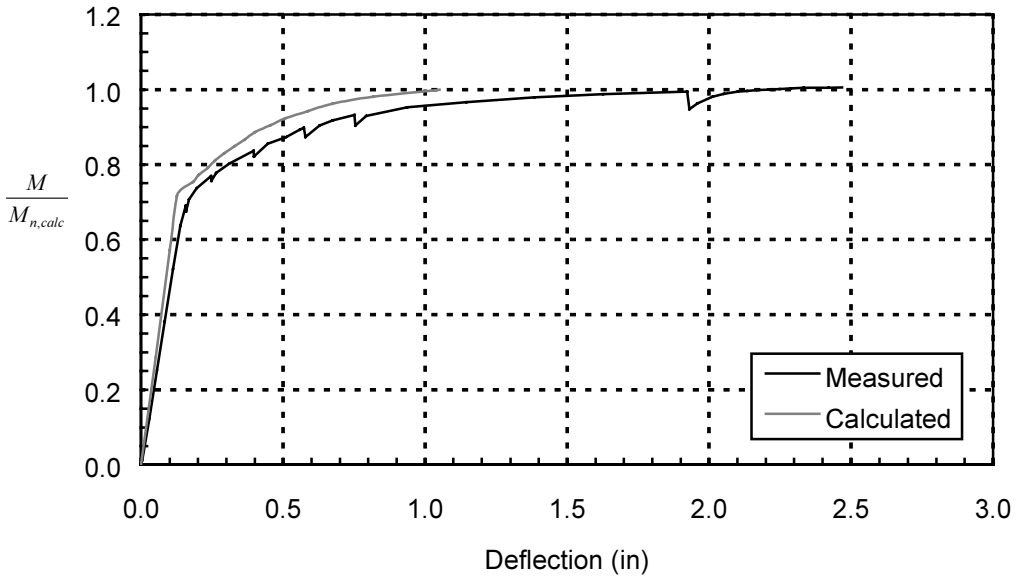


**Figure E.17: Test H0R-A-96—Normalized Moment at Critical Section vs. Deflection (1 in = 25.4 mm)**

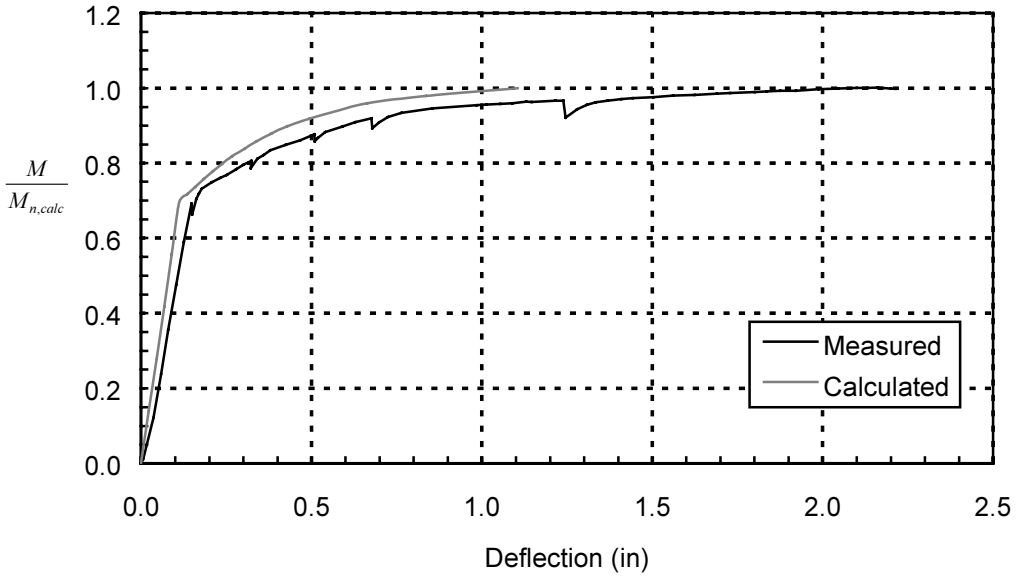


**Figure E.18: Test H0R-D-66—Normalized Moment at Critical Section vs. Deflection (1 in = 25.4 mm)**

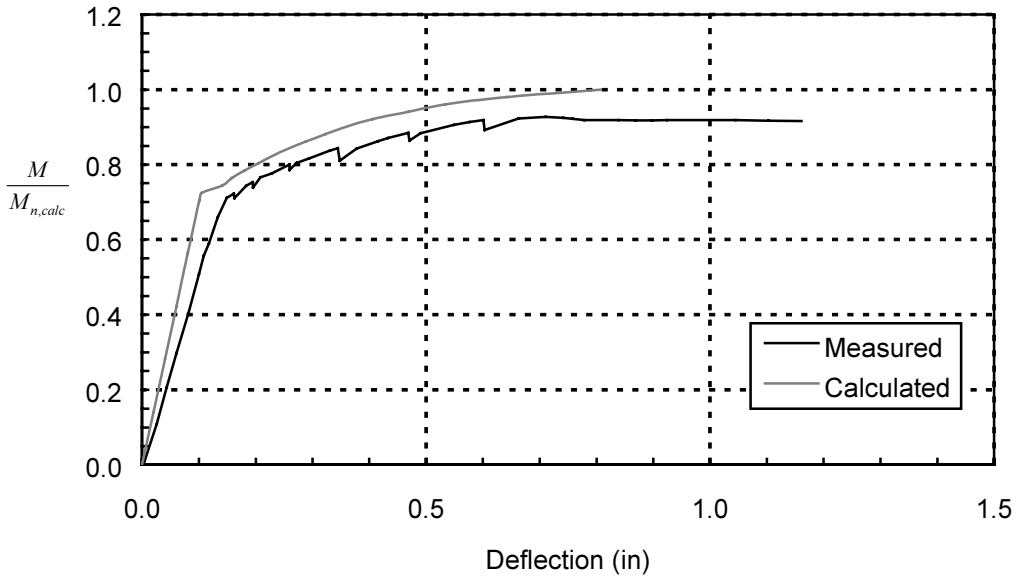


**Figure E.19: Test H0R-B-46—Normalized Moment at Critical Section vs. Deflection (1 in = 25.4 mm)**

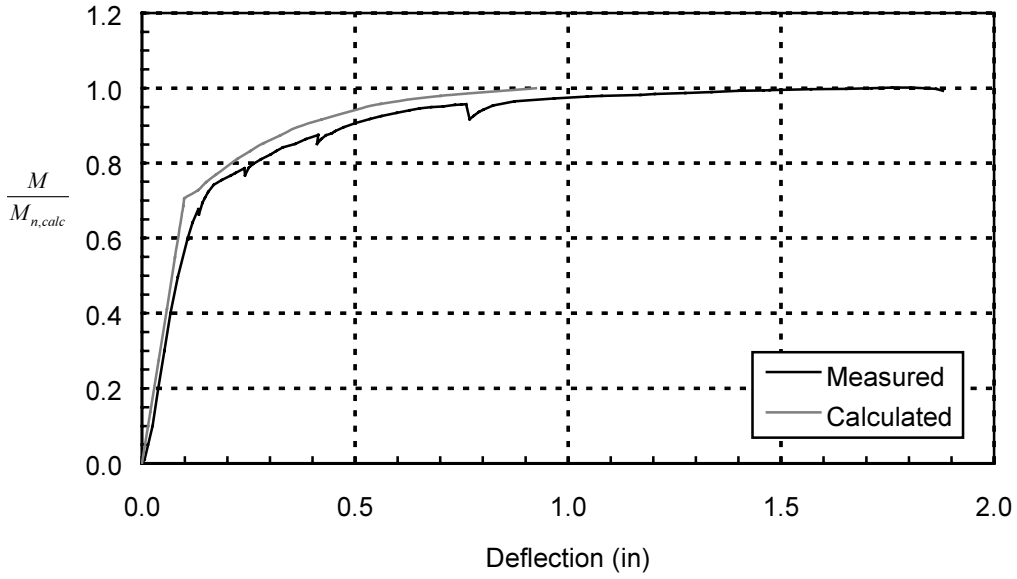


**Figure E.20: Test H0R-C-46H—Normalized Moment at Critical Section vs. Deflection (1 in = 25.4 mm)**

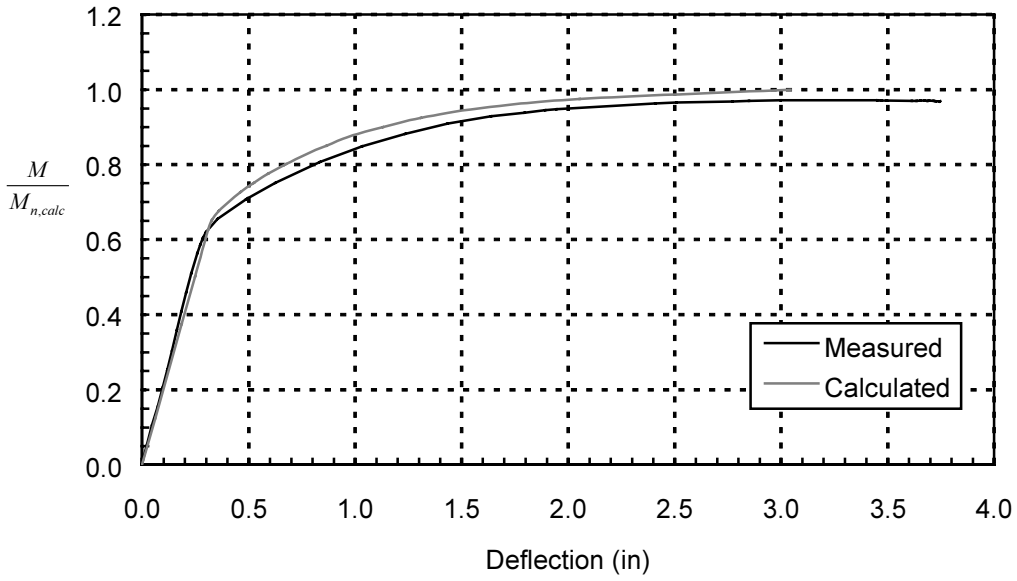


**Figure E.21: Test L4B-B-96—Normalized Moment at Critical Section vs. Deflection (1 in = 25.4 mm)**

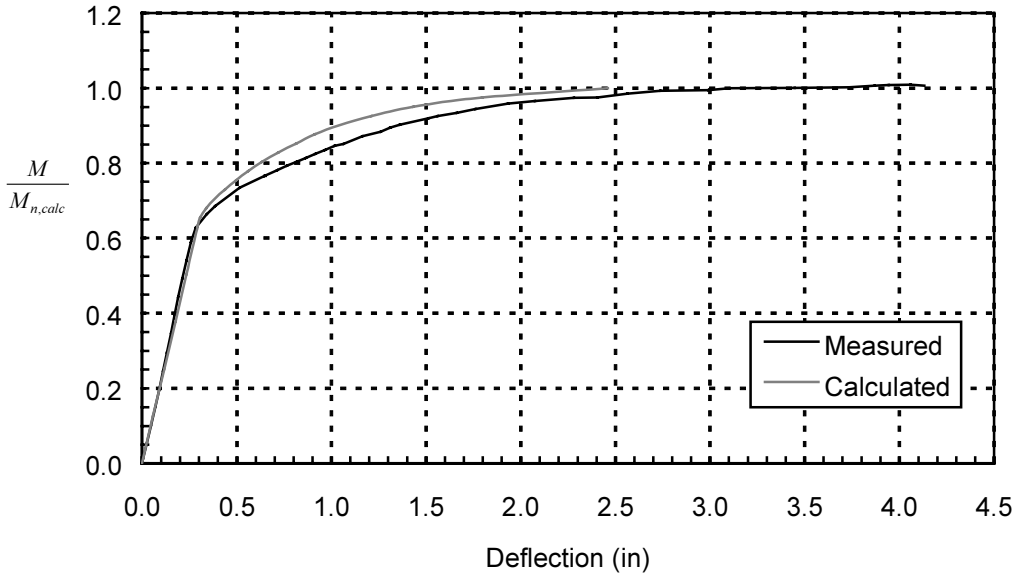


**Figure E.22: Test L4B-D-60—Normalized Moment at Critical Section vs. Deflection (1 in = 25.4 mm)**

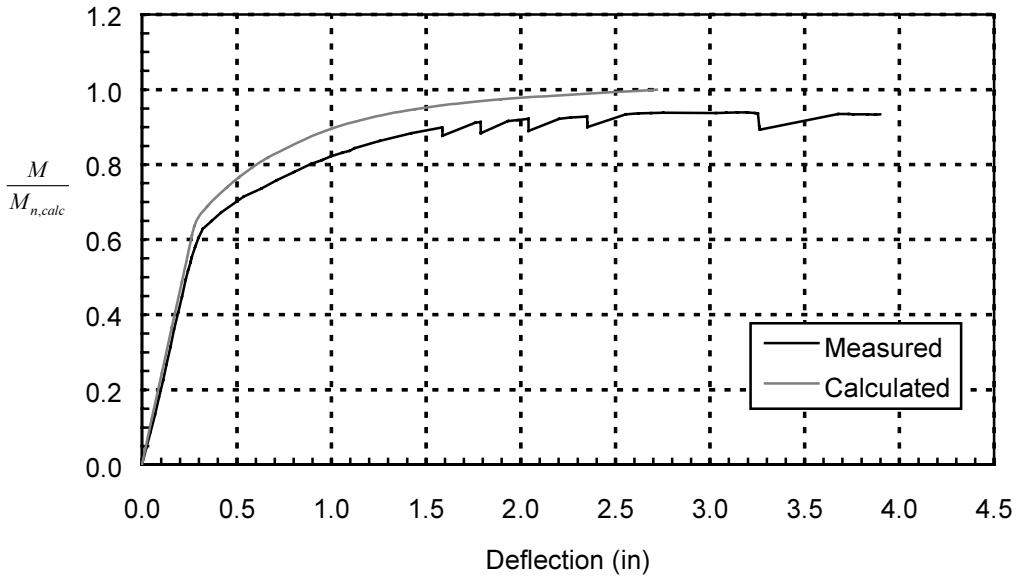


**Figure E.23: Test L4B-A-48—Normalized Moment at Critical Section vs. Deflection (1 in = 25.4 mm)**

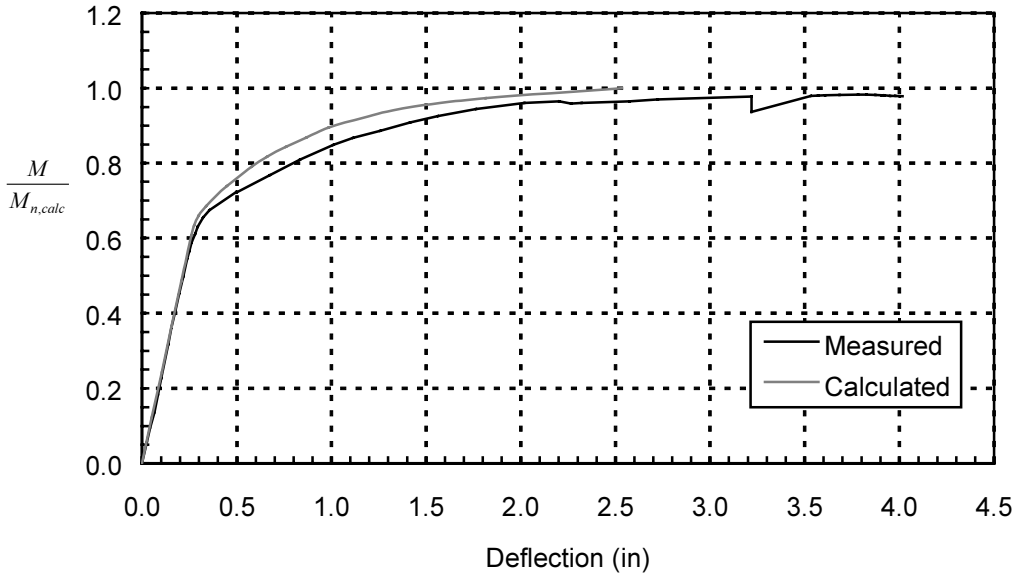


**Figure E.24: Test L4B-C-48H—Normalized Moment at Critical Section vs. Deflection (1 in = 25.4 mm)**

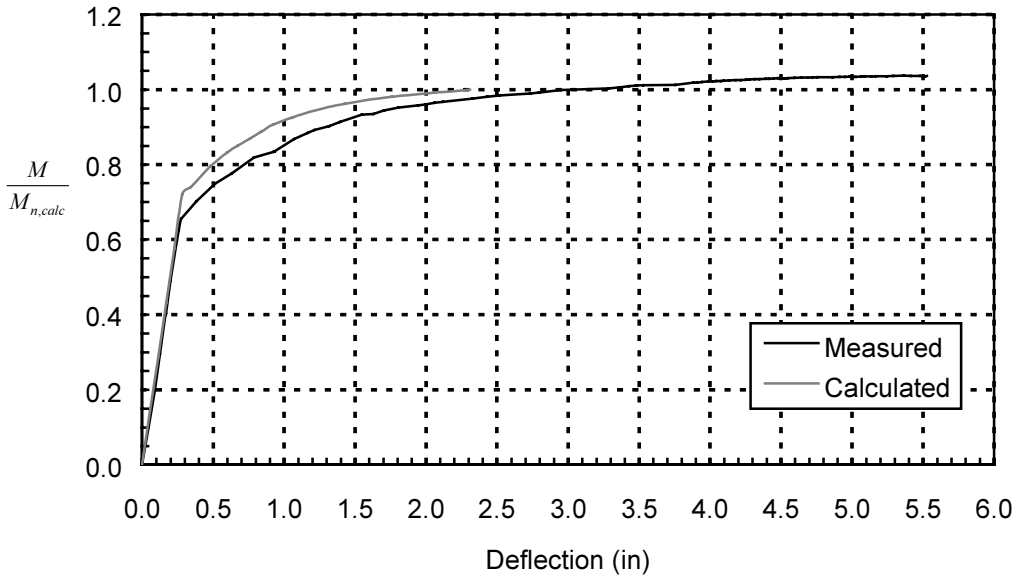


**Figure E.25: Test M4B-A-60—Normalized Moment at Critical Section vs. Deflection (1 in = 25.4 mm)**

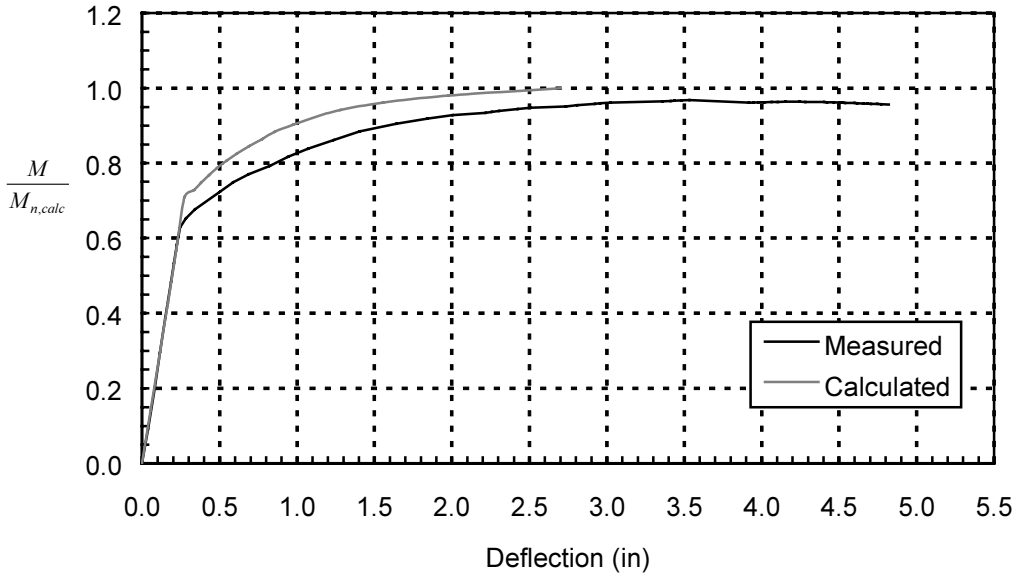


**Figure E.26: Test M4B-D-56—Normalized Moment at Critical Section vs. Deflection (1 in = 25.4 mm)**

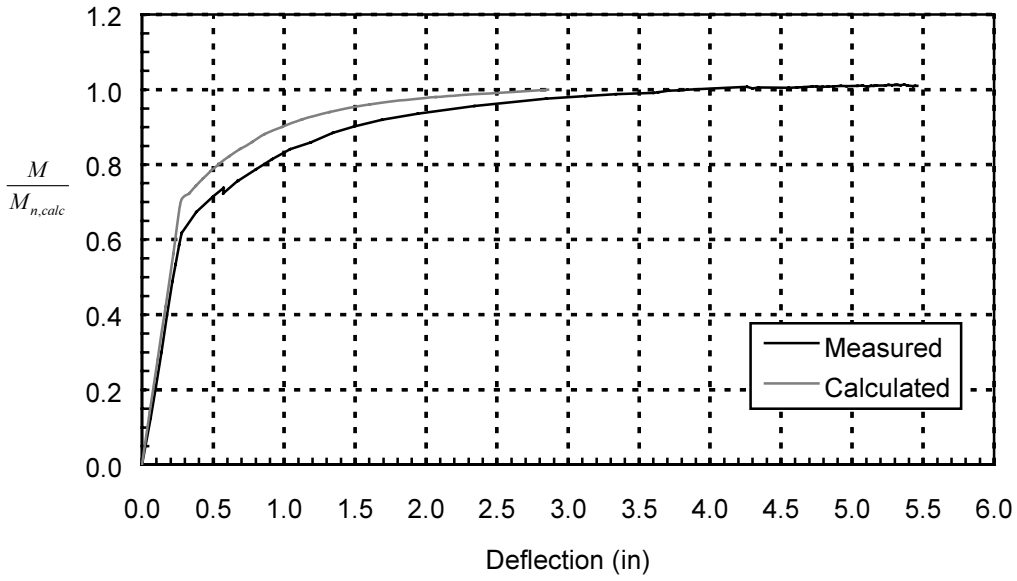


**Figure E.27: Test M4B-C-56H—Normalized Moment at Critical Section vs. Deflection (1 in = 25.4 mm)**

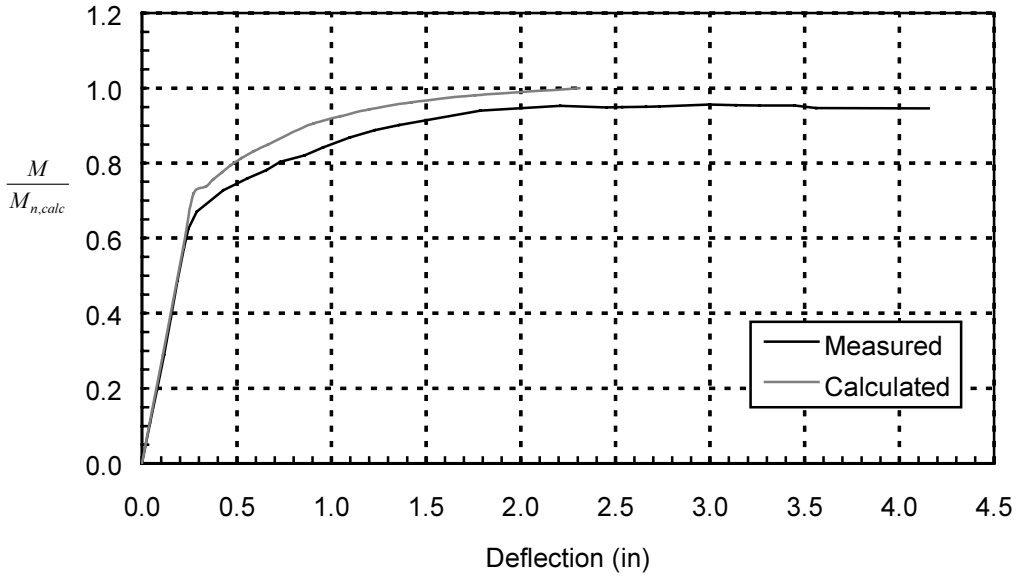


**Figure E.28: Test M4B-B-48—Normalized Moment at Critical Section vs. Deflection (1 in = 25.4 mm)**

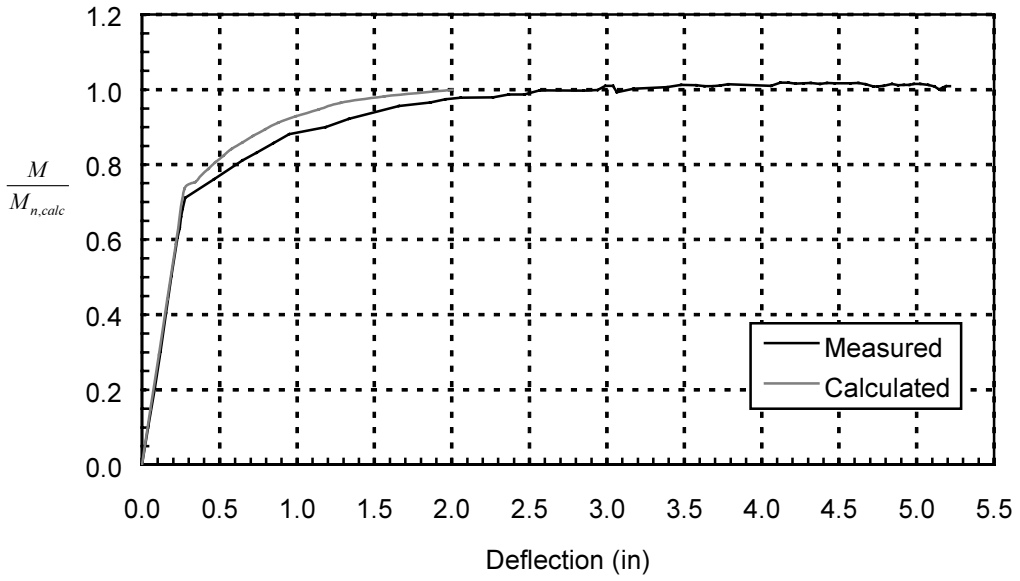


**Figure E.29: Test H4B-D-62—Normalized Moment at Critical Section vs. Deflection (1 in = 25.4 mm)**

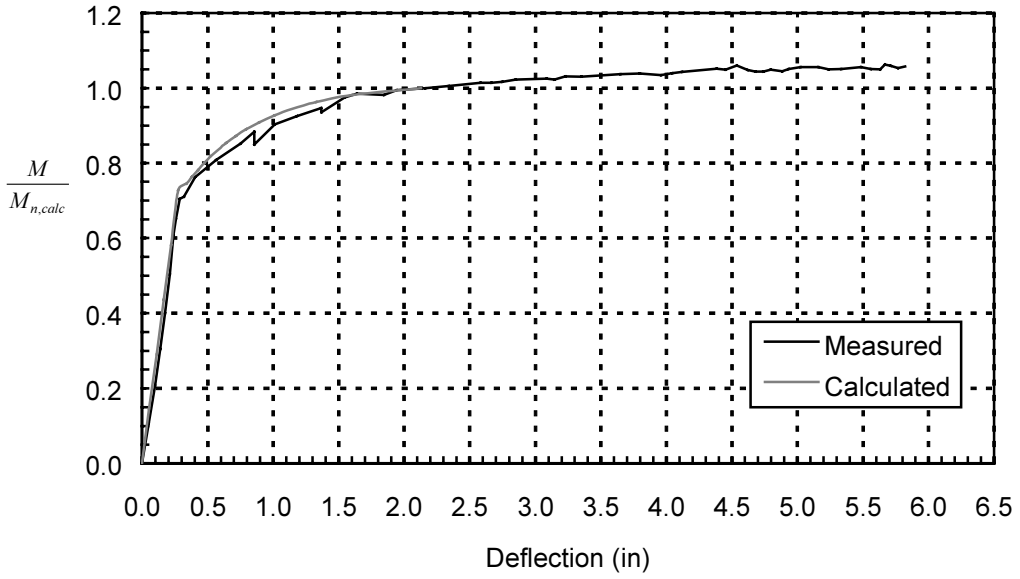


**Figure E.30: Test H4B-C-62H—Normalized Moment at Critical Section vs. Deflection (1 in = 25.4 mm)**

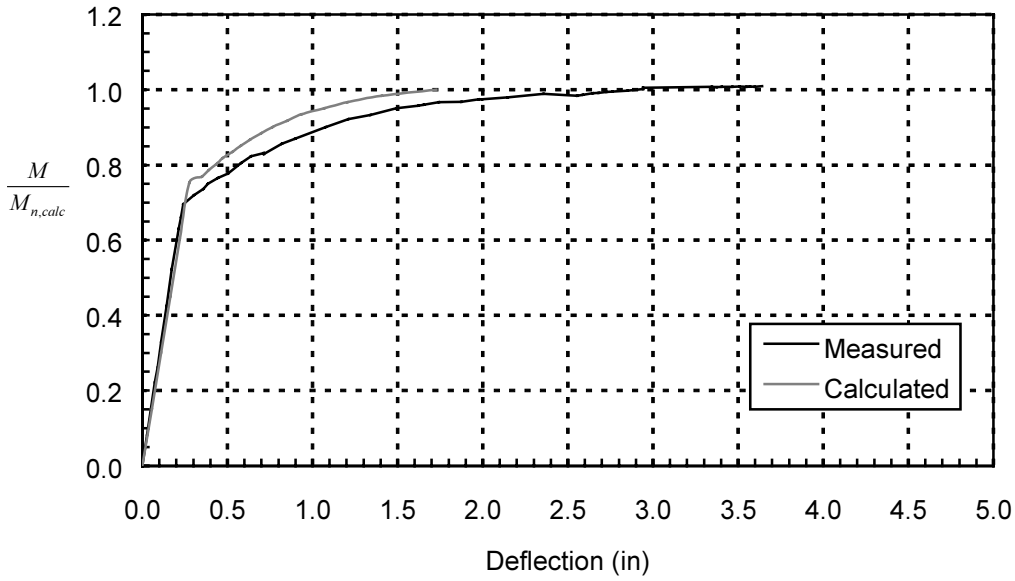


**Figure E.31: Test H4B-A-56—Normalized Moment at Critical Section vs. Deflection (1 in = 25.4 mm)**

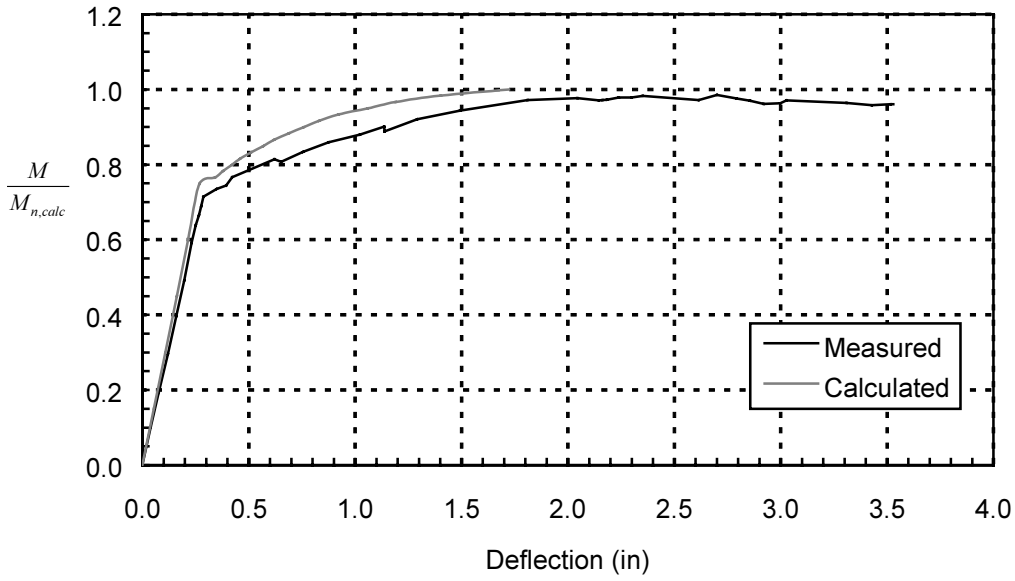


**Figure E.32: Test H4B-B-50—Normalized Moment at Critical Section vs. Deflection (1 in = 25.4 mm)**

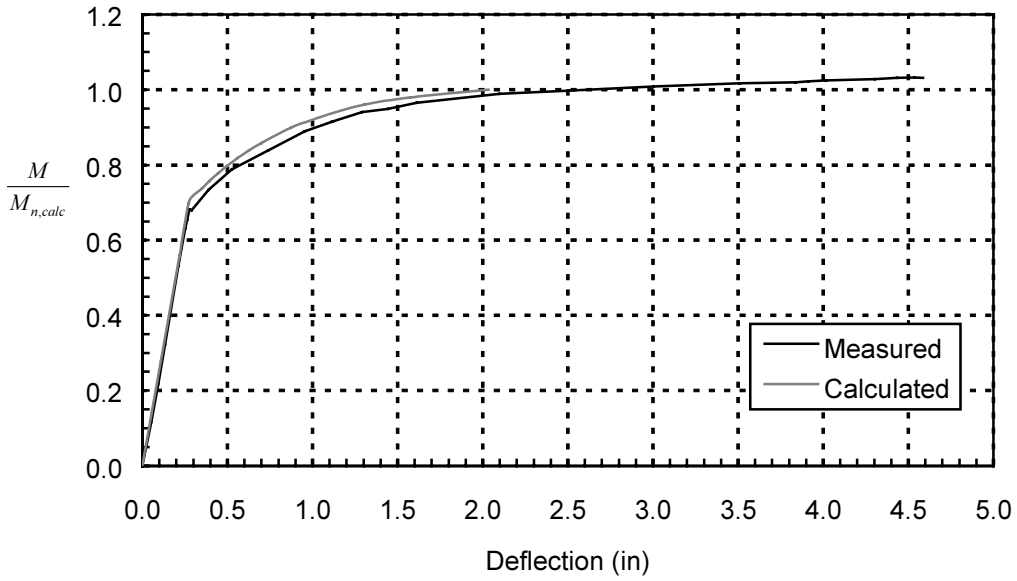


**Figure E.33: Test M4R-A-96—Normalized Moment at Critical Section vs. Deflection (1 in = 25.4 mm)**

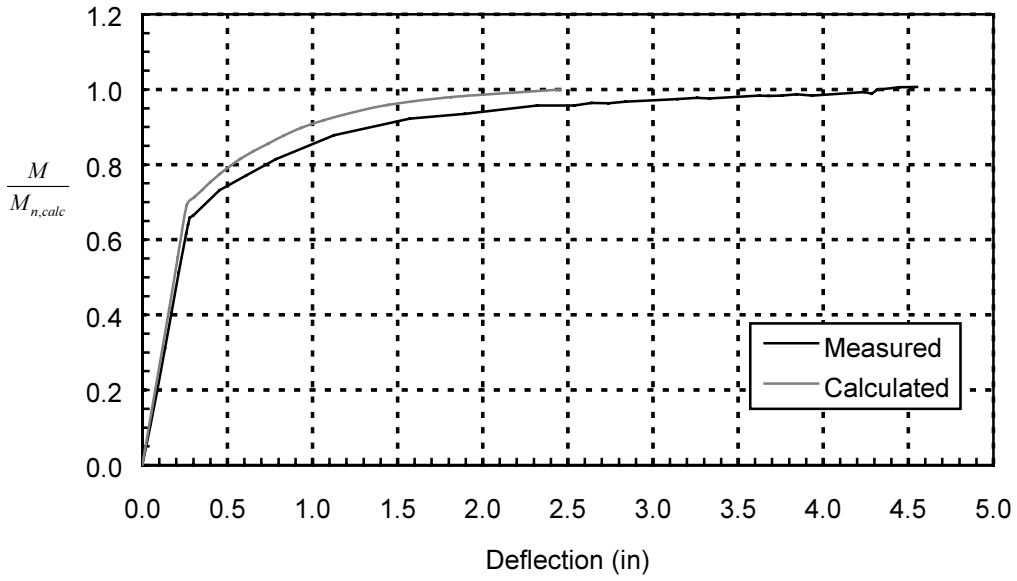


**Figure E.34: Test M4R-D-90—Normalized Moment at Critical Section vs. Deflection (1 in = 25.4 mm)**

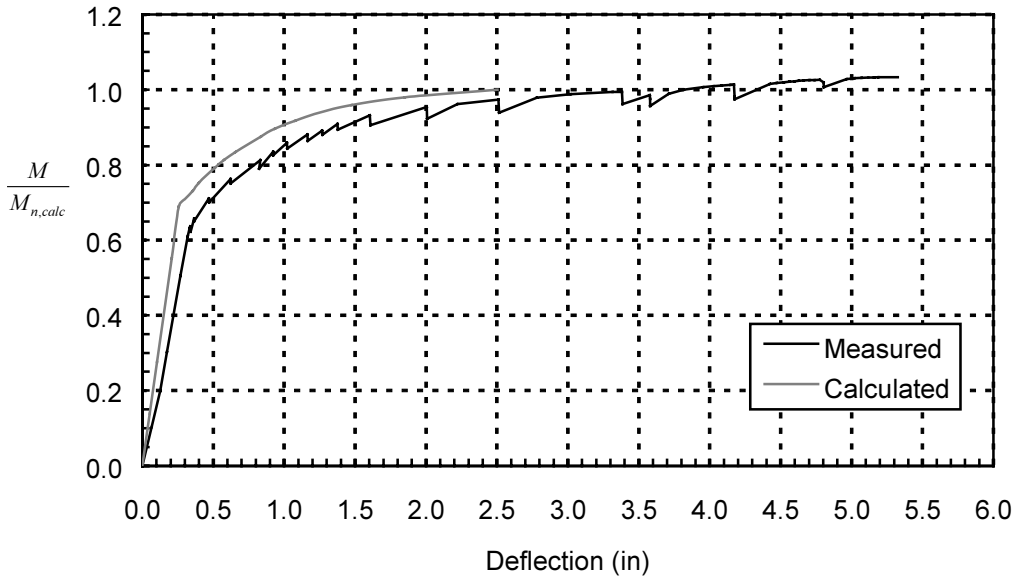


**Figure E.35: Test M4R-C-78H—Normalized Moment at Critical Section vs. Deflection (1 in = 25.4 mm)**

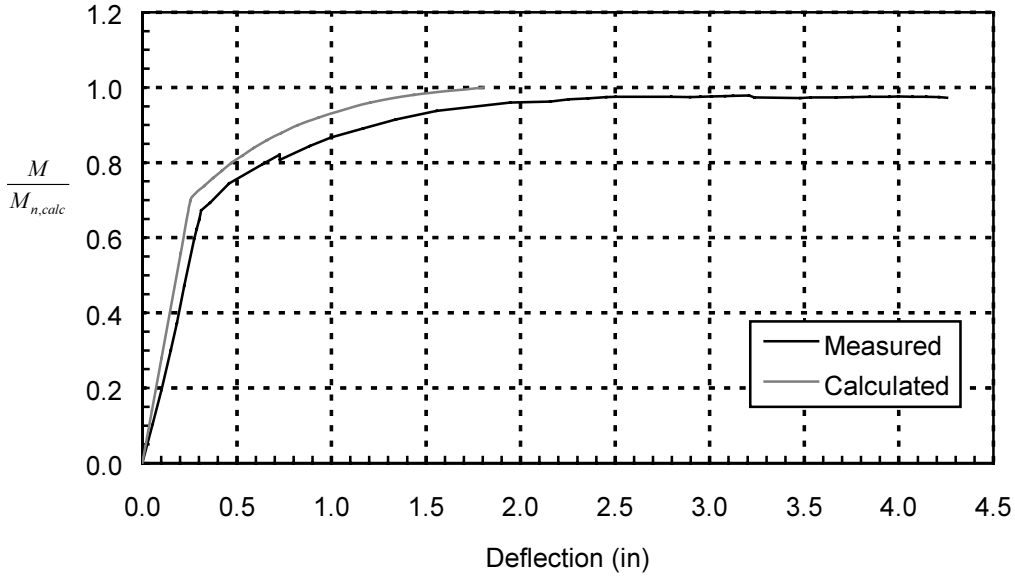


**Figure E.36: Test M4R-B-56—Normalized Moment at Critical Section vs. Deflection (1 in = 25.4 mm)**

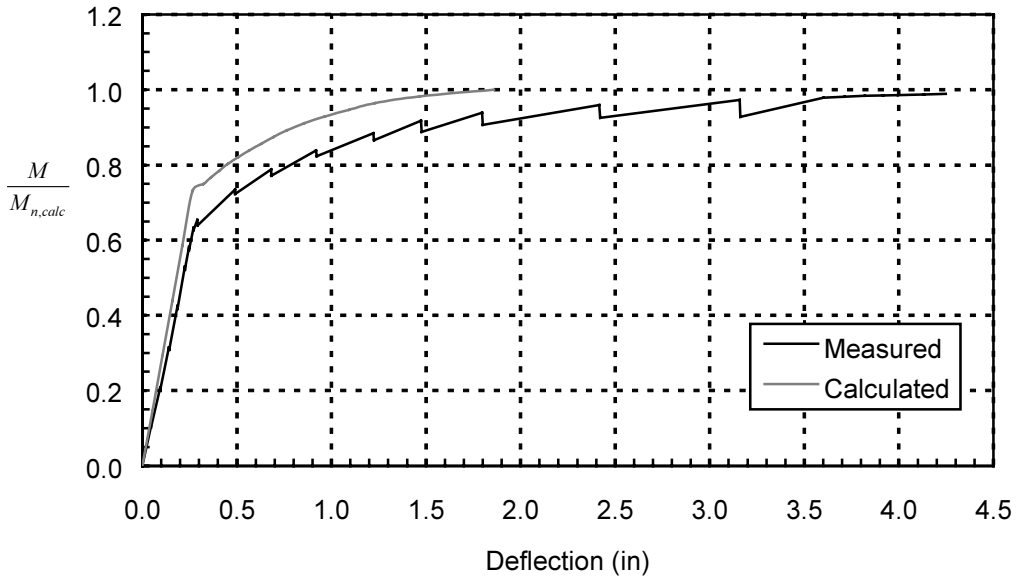


**Figure E.37: Test H4R-A-82—Normalized Moment at Critical Section vs. Deflection (1 in = 25.4 mm)**

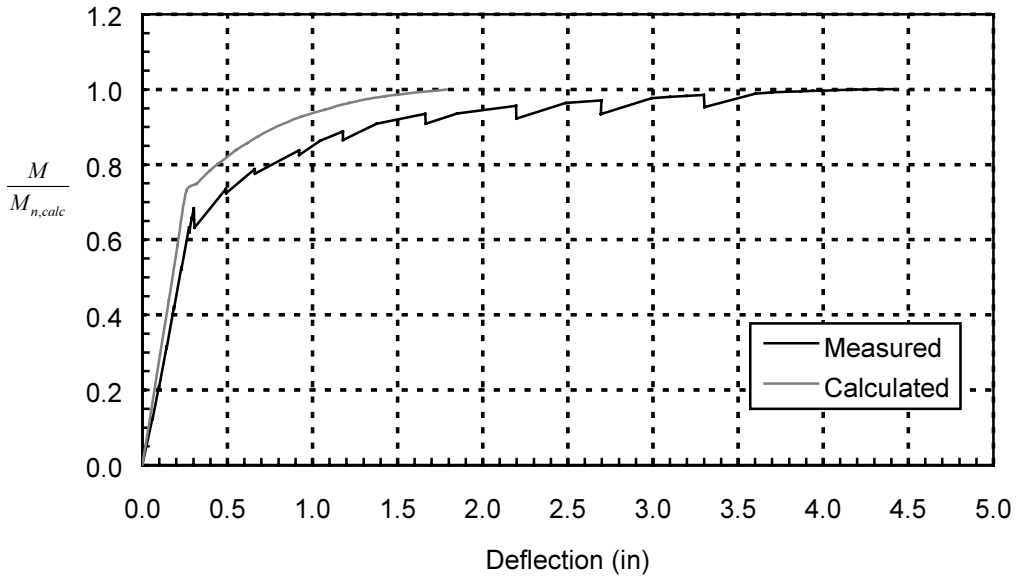


**Figure E.38: Test H4R-D-78—Normalized Moment at Critical Section vs. Deflection (1 in = 25.4 mm)**

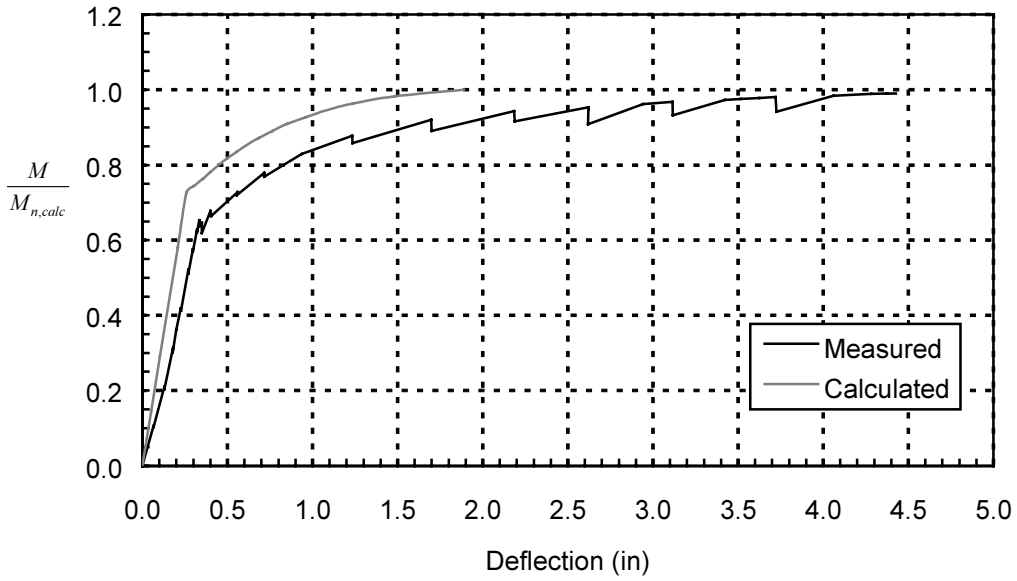


**Figure E.39: Test H4R-B-72—Normalized Moment at Critical Section vs. Deflection (1 in = 25.4 mm)**

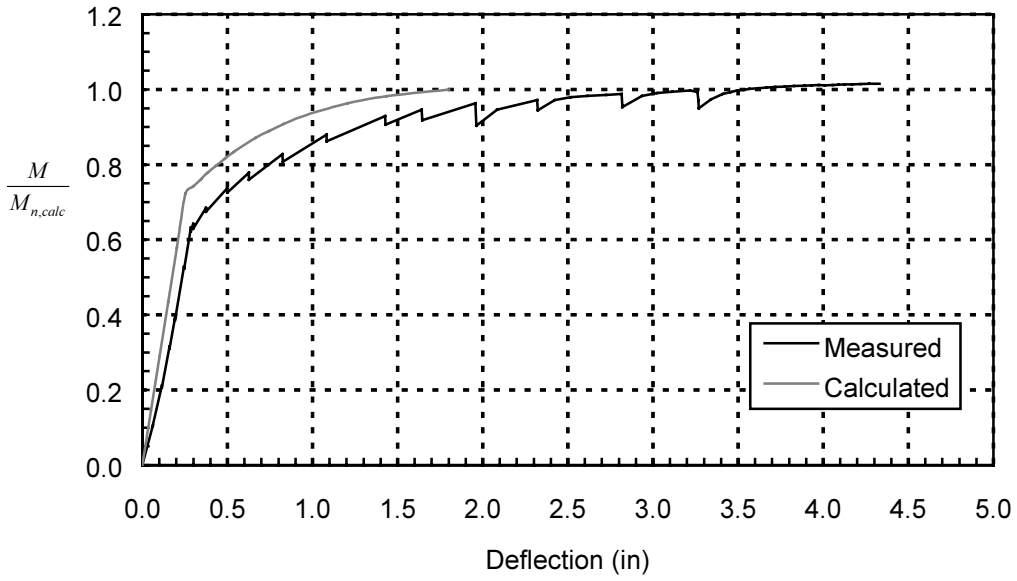


**Figure E.40: Test H4R-C-72H—Normalized Moment at Critical Section vs. Deflection (1 in = 25.4 mm)**

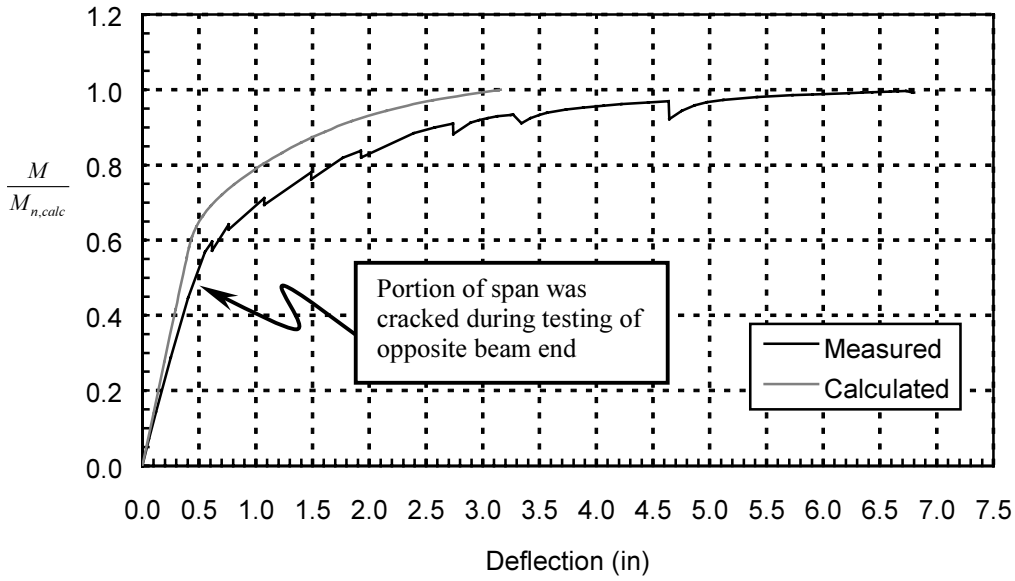


**Figure E.41: Test L6B-B-114—Normalized Moment at Critical Section vs. Deflection (1 in = 25.4 mm)**

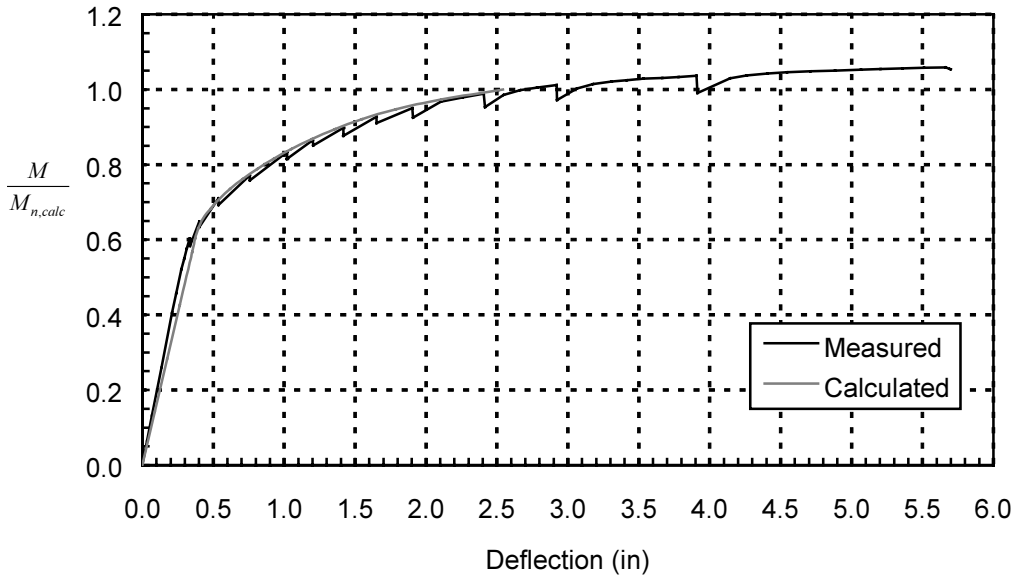


**Figure E.42: Test L6B-A-96—Normalized Moment at Critical Section vs. Deflection (1 in = 25.4 mm)**

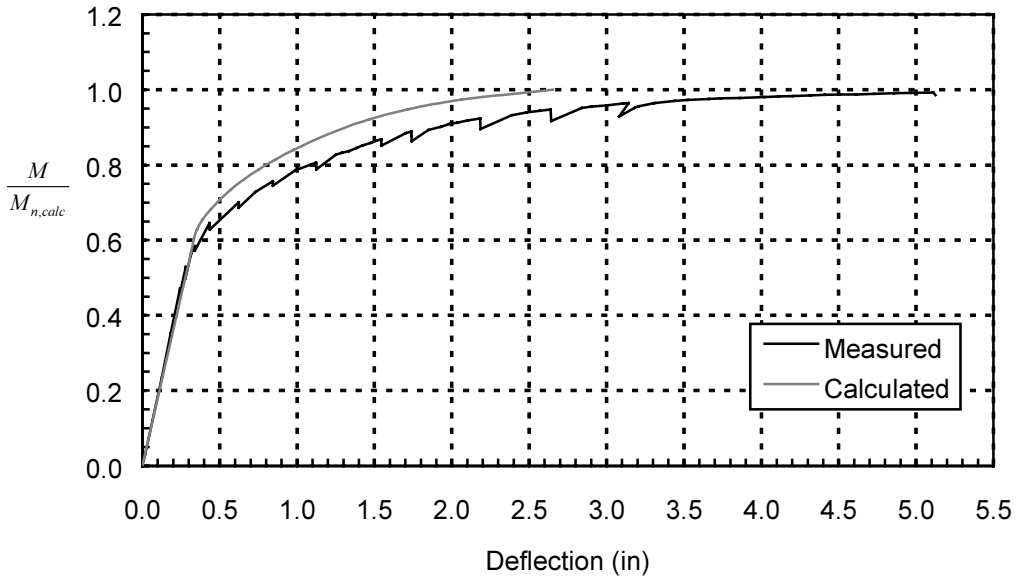


**Figure E.43: Test L6B-D-84—Normalized Moment at Critical Section vs. Deflection (1 in = 25.4 mm)**

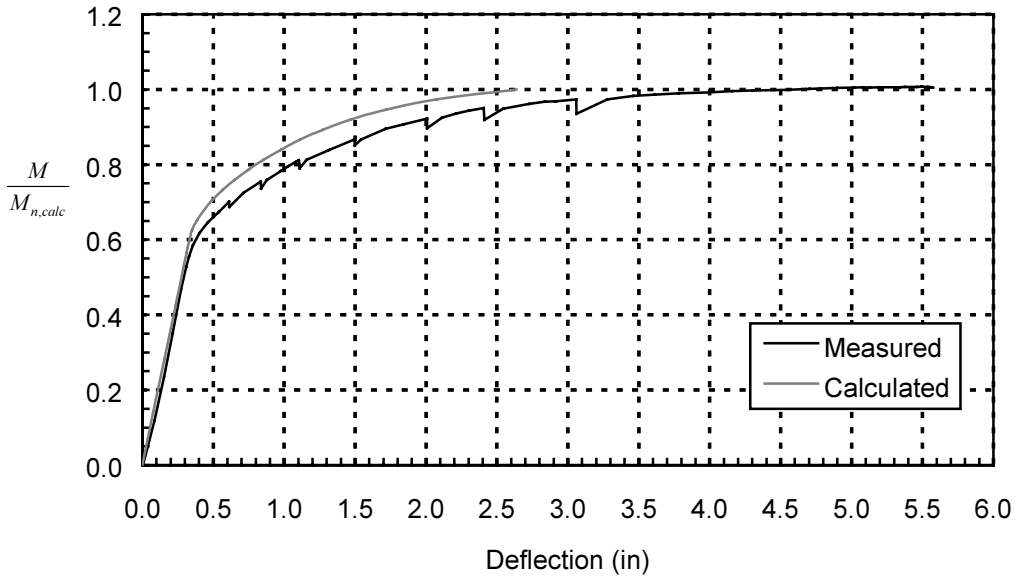


**Figure E.44: Test L6B-C-84H—Normalized Moment at Critical Section vs. Deflection (1 in = 25.4 mm)**

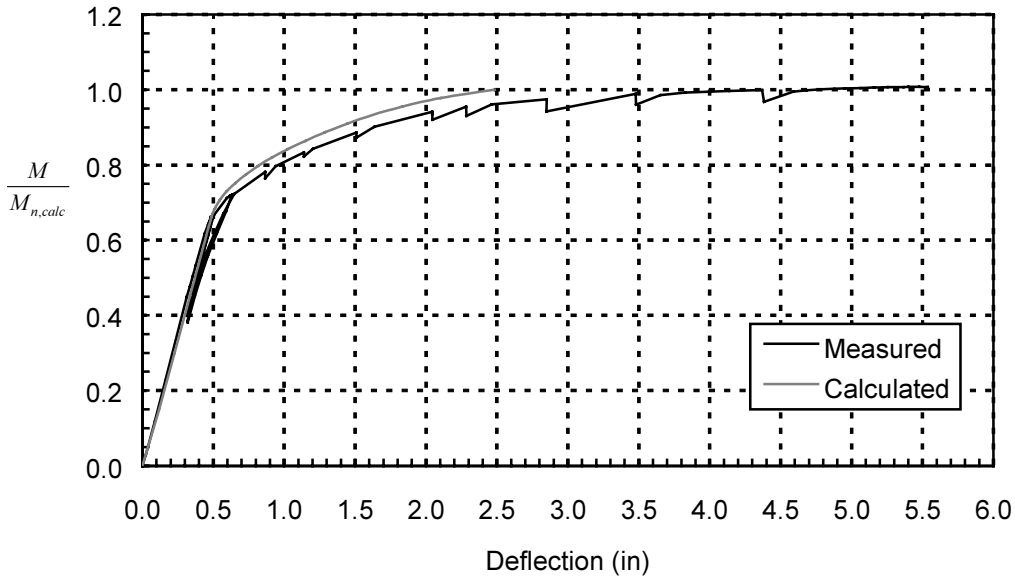


**Figure E.45: Test M9B-A-180—Normalized Moment at Critical Section vs. Deflection (1 in = 25.4 mm)**

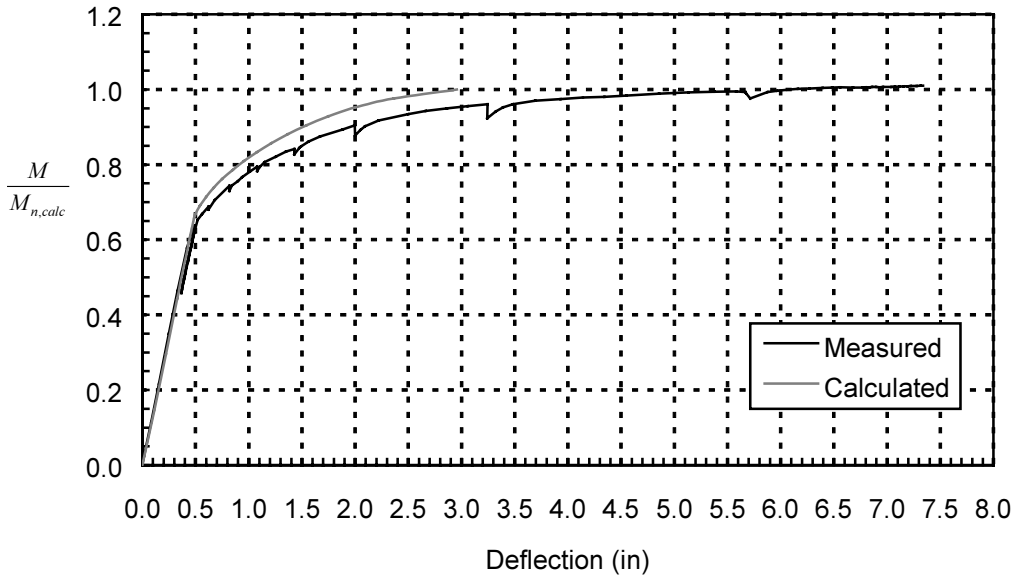


**Figure E.46: Test M9B-D-114—Normalized Moment at Critical Section vs. Deflection (1 in = 25.4 mm)**

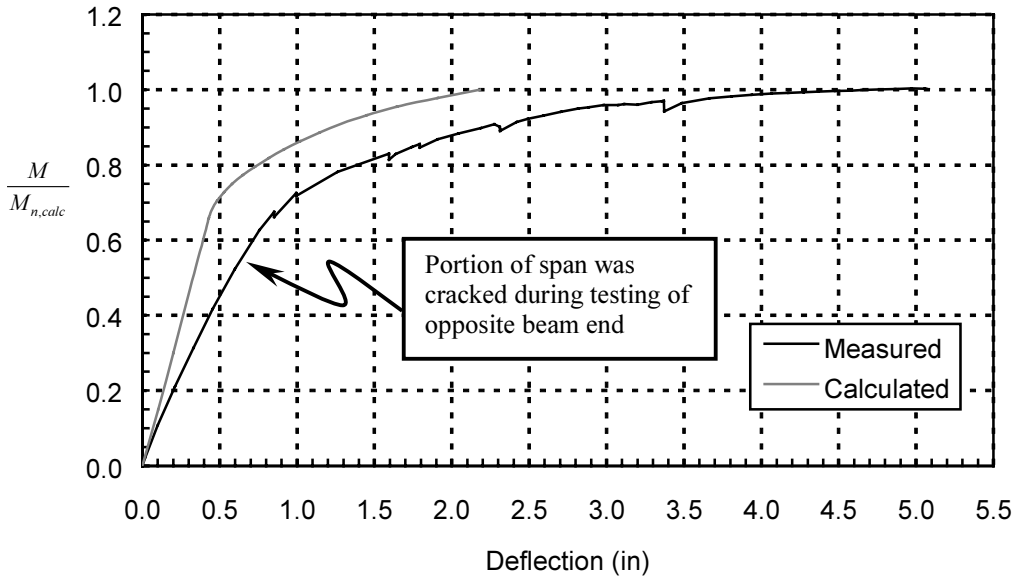


**Figure E.47: Test M9B-B-96—Normalized Moment at Critical Section vs. Deflection (1 in = 25.4 mm)**

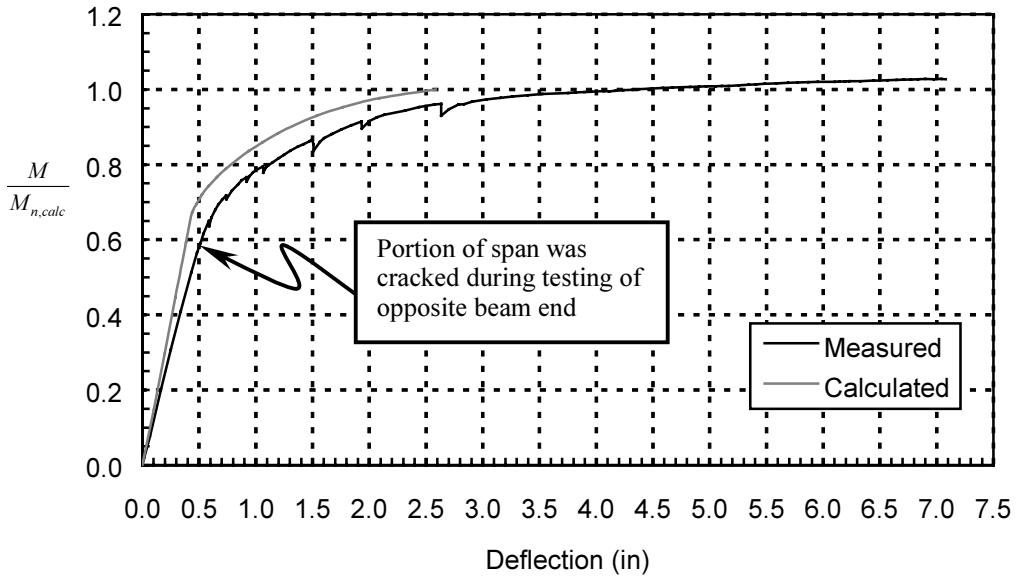


**Figure E.48: Test M9B-C-96H—Normalized Moment at Critical Section vs. Deflection (1 in = 25.4 mm)**

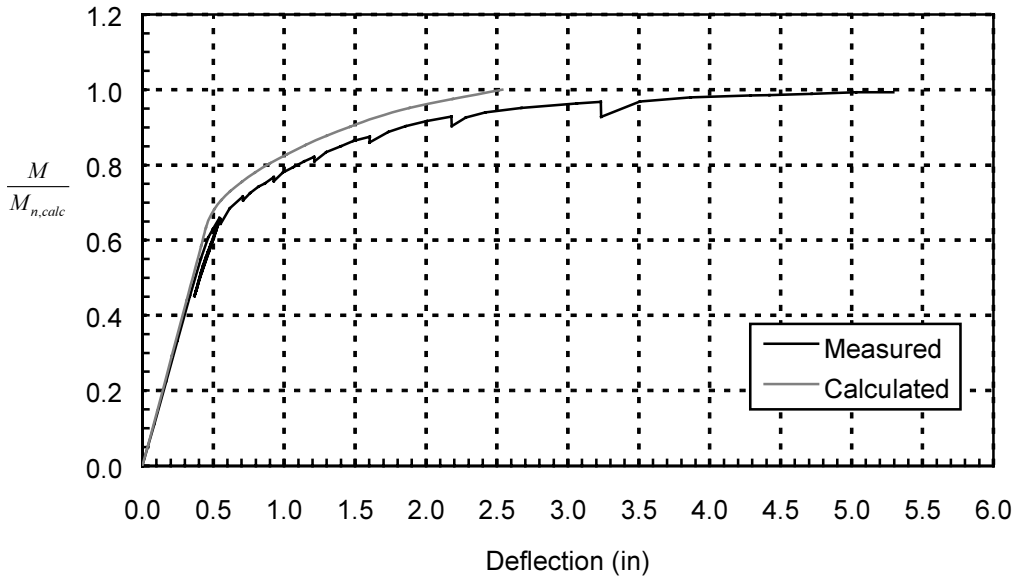


**Figure E.49: Test H9B-A-180—Normalized Moment at Critical Section vs. Deflection (1 in = 25.4 mm)**

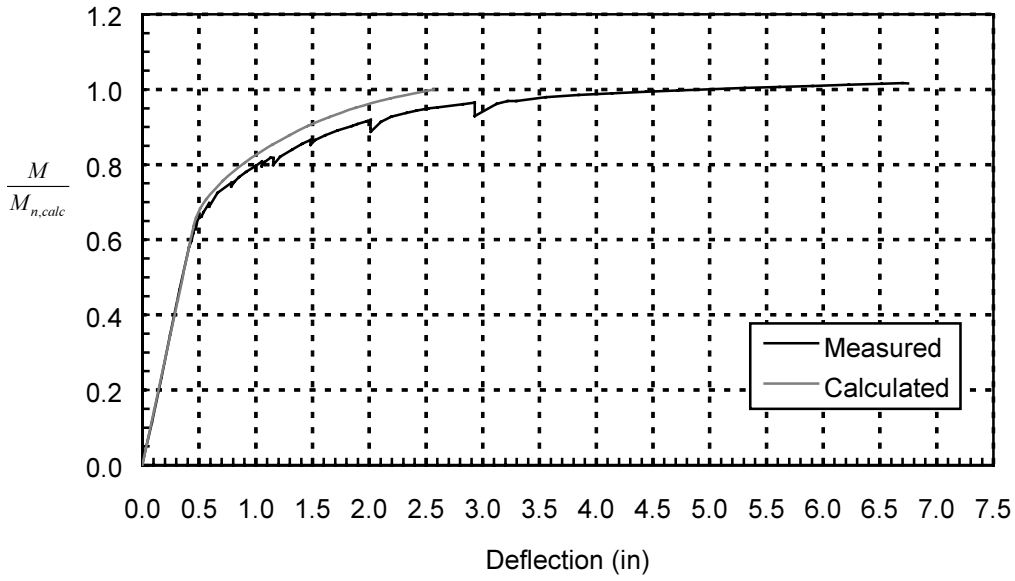


**Figure E.50: Test H9B-D-114—Normalized Moment at Critical Section vs. Deflection (1 in = 25.4 mm)**

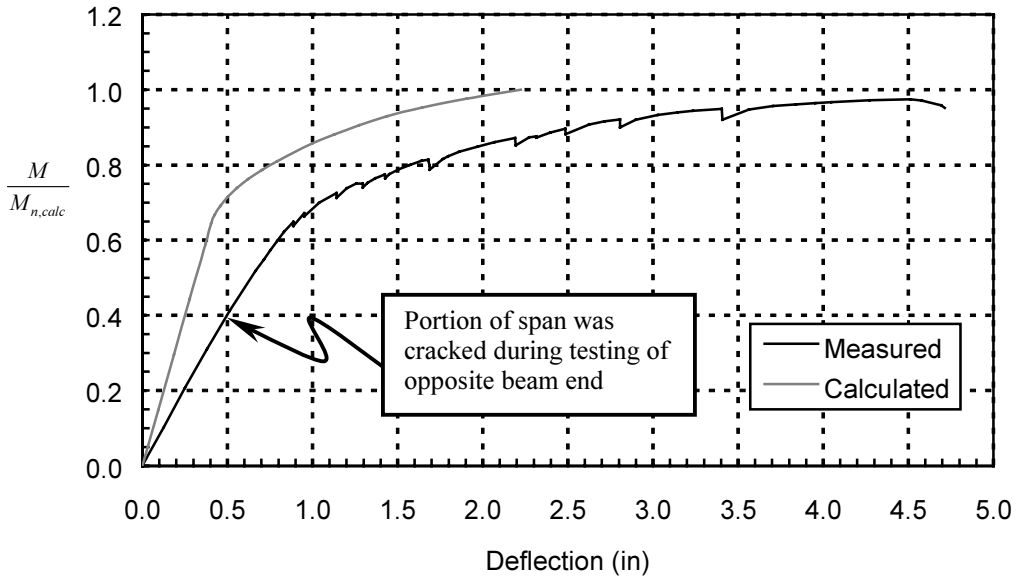


**Figure E.51: Test H9B-B-96—Normalized Moment at Critical Section vs. Deflection (1 in = 25.4 mm)**

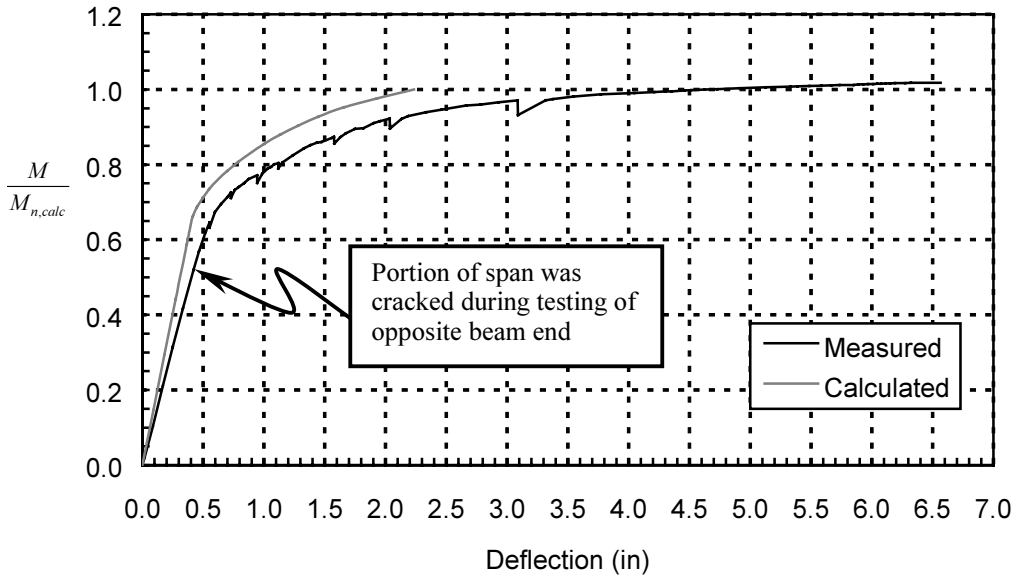


**Figure E.52: Test H9B-C-96H—Normalized Moment at Critical Section vs. Deflection (1 in = 25.4 mm)**

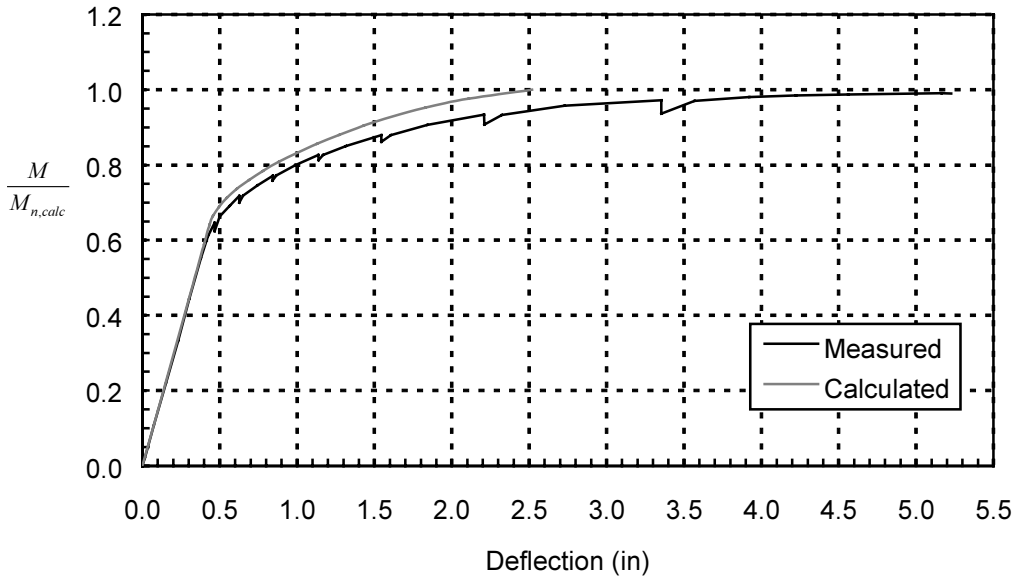


**Figure E.53: Test M9R-A-180—Normalized Moment at Critical Section vs. Deflection (1 in = 25.4 mm)**

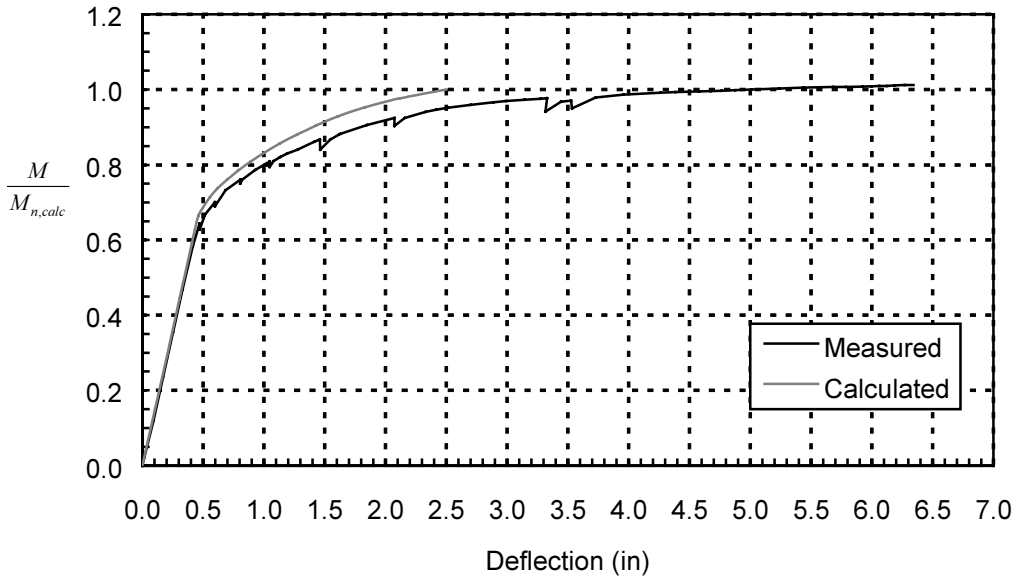


**Figure E.54: Test M9R-D-114—Normalized Moment at Critical Section vs. Deflection (1 in = 25.4 mm)**

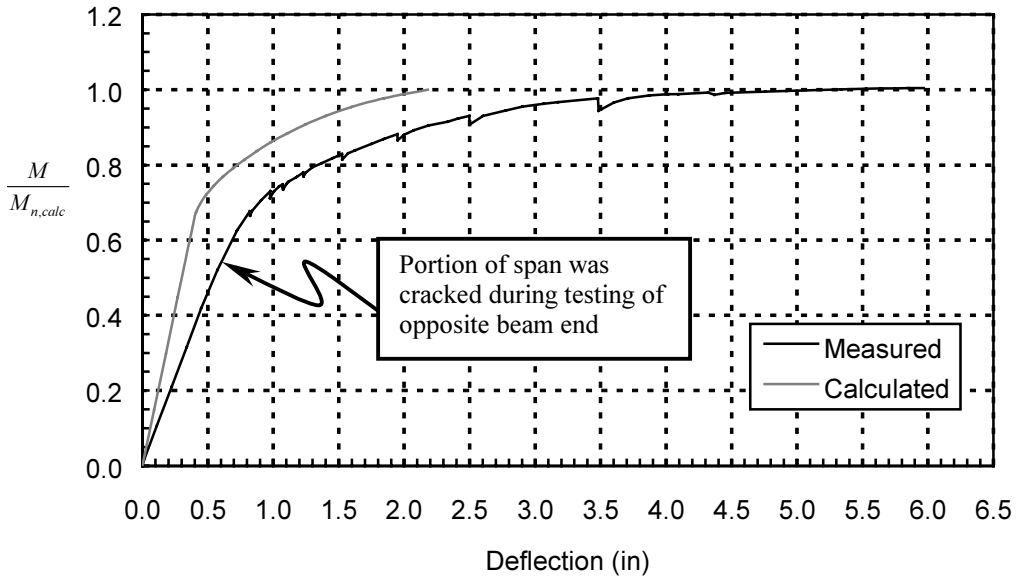


**Figure E.55: Test M9R-B-96—Normalized Moment at Critical Section vs. Deflection (1 in = 25.4 mm)**

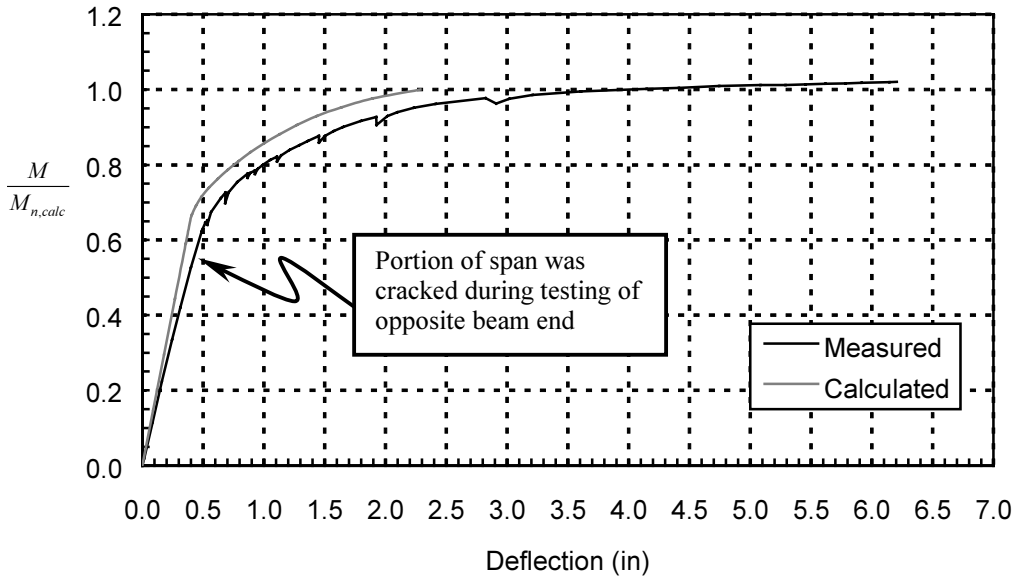


**Figure E.56: Test M9R-C-96H—Normalized Moment at Critical Section vs. Deflection (1 in = 25.4 mm)**

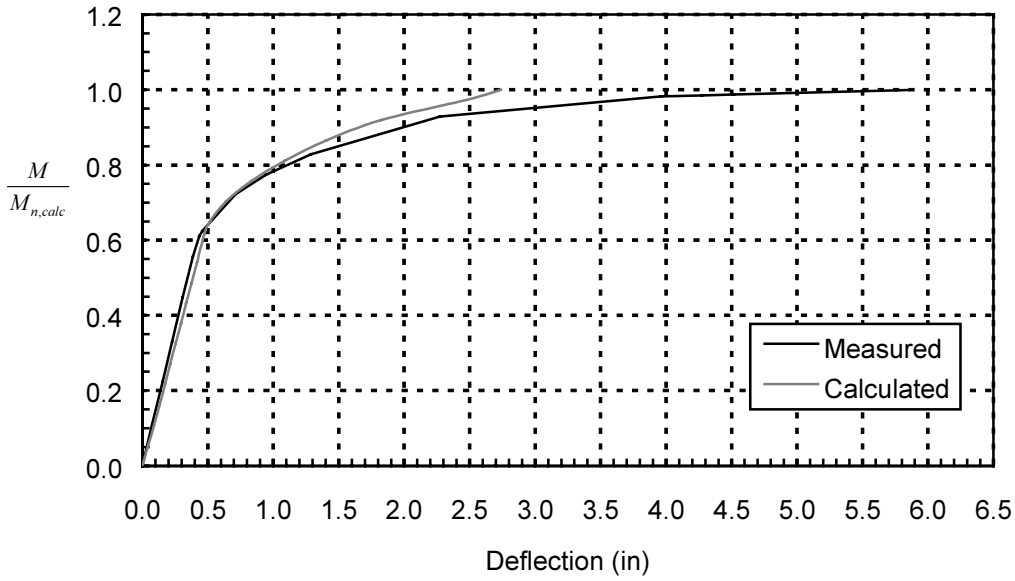


**Figure E.57: Test H9R-A-180—Normalized Moment at Critical Section vs. Deflection (1 in = 25.4 mm)**

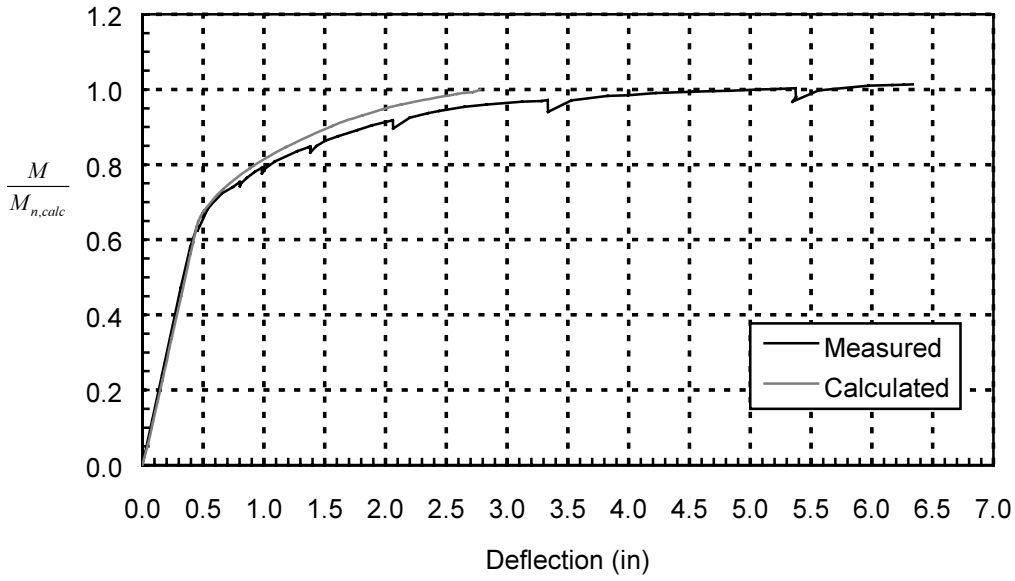


**Figure E.58: Test H9R-D-114—Normalized Moment at Critical Section vs. Deflection (1 in = 25.4 mm)**

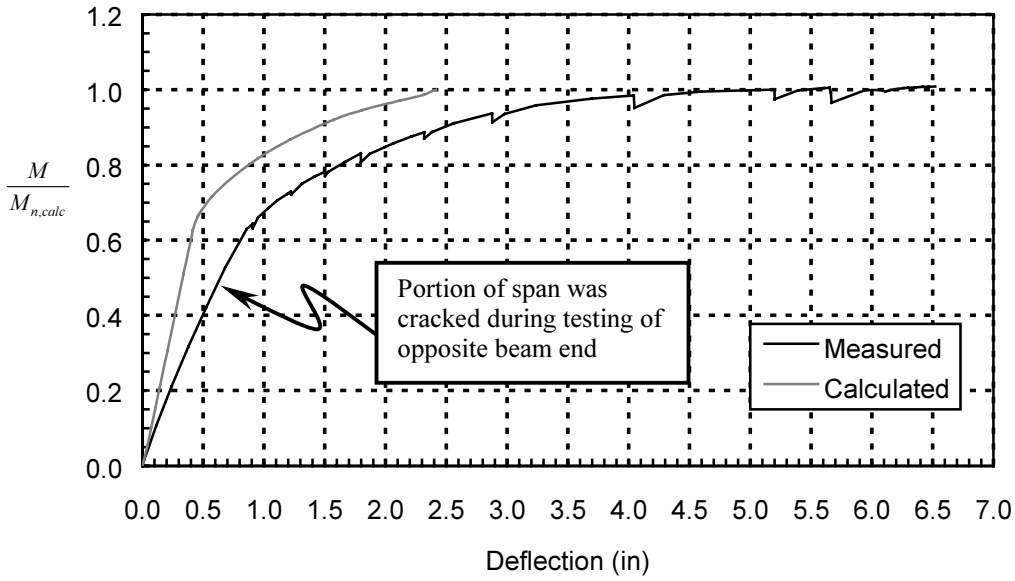


**Figure E.59: Test H9R-B-96—Normalized Moment at Critical Section vs. Deflection (1 in = 25.4 mm)**

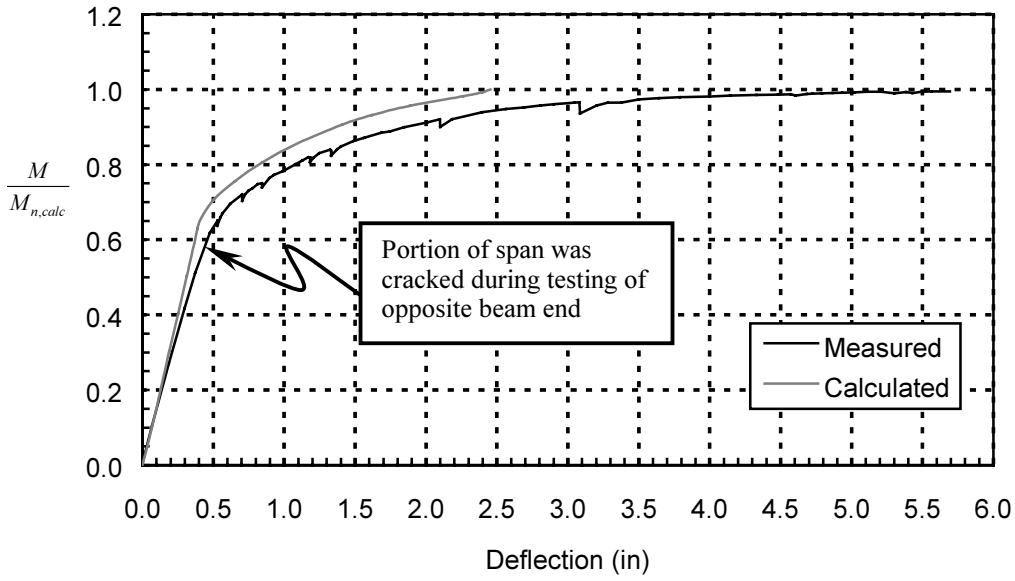


**Figure E.60: Test H9R-C-96H—Normalized Moment at Critical Section vs. Deflection (1 in = 25.4 mm)**

# NOTATION

| Report (AASHTO LRFD) | AASHTO Standard | ACI 318-99 | Description |
|---|---|---|---|
| $A_{ps}$ | $A_s^*$ | $A_{ps}$ | area of prestressing steel |
| $d_b$ | $D$ | $d_b$ | nominal diameter of reinforcement |
| $E_p$ | — | — | modulus of elasticity of prestressing reinforcement |
| $f'_c$ | $f'_c$ | $f'_c$ | specified compressive strength of concrete |
| $f'_{ci}$ | $f'_{ci}$ | $f'_{ci}$ | specified compressive strength of concrete at time of application of prestress force |
| $f_{ct}$ | $f_{ct}$ | $f_{ct}$ | splitting tensile strength of concrete |
| $f_y$ | $f_{sy}$ | $f_y$ | specified minimum yield strength of nonprestressed reinforcement |
| $f_p$ | — | — | stress in prestressing reinforcement (not in AASHTO LRFD) |
| $f_{p,cr}$ | — | — | stress in prestressing reinforcement according to cracked section analysis (not in AASHTO LRFD) |
| $f_{p,slip}$ | — | — | stress in prestressing reinforcement at critical section at general bond slip according to cracked section analysis (not in AASHTO LRFD) |
| $f_{p,un}$ | — | — | stress in prestressing reinforcement according to uncracked section analysis (not in AASHTO LRFD) |
| $f_{pc}$ | $f_{pc}$ | $f_{pc}$ | compressive stress in concrete after all losses have occurred either at the centroid of the cross section resisting live load or at the junction of the web and flange when the centroid lies in the flange; in a composite section, $f_{pc}$ is the resultant compressive stress at the centroid of the composite section, or at the junction of the web and flange when the centroid lies within the flange, that results from both prestress and the bending moments resisted by the precast member acting alone |
| $f_{pe}$ | $f_{se}$ | $f_{se}$ | effective stress in the prestressed reinforcement after losses |
| $f_{pj}$ | — | — | stress in prestressing reinforcement at jacking |
| $f_{pj}^*$ | — | — | stress in prestressing reinforcement immediately prior to transfer (not in AASHTO LRFD) |
| $f_{ps}$ | $f_{su}^*$ | $f_{ps}$ | stress in prestressed reinforcement at nominal strength |
| $f_{pt}$ | — | — | stress in prestressed reinforcement immediately after transfer |
| $f_{pu}$ | $f'_s$ | $f_{pu}$ | specified tensile strength of prestressing reinforcement |

| Report (AASHTO LRFD) | AASHTO Standard | ACI 318-99 | Description |
|---|---|---|---|
| $l_d$ | $l_d$ | $l_d$ | development length (only refers to *nonprestressed* reinforcement in AASHTO Standard and ACI 318) |
| $l_{fb}$ | — | — | flexural bond length (not in AASHTO LRFD) |
| $l_t$ | — | — | transfer length (not in AASHTO LRFD) |
| $n$ | — | $n$ | modular ratio ($\frac{E_p}{E_c}$ or $\frac{E_s}{E_c}$) |
| $\overline{u}$ | — | — | average bond stress (not in AASHTO LRFD) |
| $u_{fb}$ | — | — | flexural bond stress (not in AASHTO LRFD) |
| $\overline{u}_{fb}$ | — | — | flexural bond stress averaged over the transfer length (not in AASHTO LRFD) |
| $u_t$ | — | — | transfer bond stress (not in AASHTO LRFD) |
| $\overline{u}_t$ | — | — | transfer bond stress averaged over the transfer length (not in AASHTO LRFD) |
| $V_c$ | $V_c$ | $V_c$ | nominal shear resistance provided by tensile stresses in the concrete |
| — | $V_{ci}$ | $V_{ci}$ | nominal shear resistance provided by concrete when diagonal cracking results from combined shear and moment |
| — | $V_{cw}$ | $V_{cw}$ | nominal shear strength provided by concrete when diagonal cracking results from excessive principal tensile stress in the web |
| $V_p$ | $V_p$ | $V_p$ | component of the effective prestressing force that acts in the direction opposite to the applied shear |
| $\varepsilon_p$ | — | — | strain in prestressing reinforcement (not in AASHTO LRFD) |
| $\Sigma o$ | — | — | strand perimeter (not in AASHTO LRFD) |

# REFERENCES


Abdalla, O.A., J.A. Ramirez, and R.H. Lee. 1993. *Strand debonding in pretensioned beams—precast, prestressed concrete bridges with debonded strands—simply supported tests*. Part 2, Final Report FHWA/INDOT/JHRP-92. West Lafayette: School of Civil Engineering, Purdue University.

AASHTO. 1998. *AASHTO LRFD bridge design specifications: customary U.S. units*. 2nd ed. Washington, D.C.: American Association of State Highway and Transportation Officials (AASHTO).

AASHTO. 1996. *Standard specifications for highway bridges*. 16th ed. Washington, D.C.: American Association of State Highway and Transportation Officials (AASHTO).

ACI Committee 318. 1963. *Building code requirements for reinforced concrete (318-63)*. Detroit: American Concrete Institute (ACI).

ACI Committee 318. 1999. *Building code requirements for structural concrete (318-99) and commentary (318R-99)*. Farmington Hills, Michigan: American Concrete Institute (ACI).

Ahlborn, Theresa M., Carol K. Shield, and Catherine W. French. 1996. Behavior of two long-span high strength concrete prestressed bridge girders. In *Worldwide advances in structural concrete and masonry: proceedings of the CCMS symposium held in conjunction with Structures Congress XIV*. New York: American Society of Civil Engineers (ASCE).

Anderson, Arthur R., and Richard G. Anderson. 1976. An assurance criterion for flexural bond in pretensioned hollow core units. *ACI Journal, Proceedings* 73(8): 457–464.

ASTM. 1993. Standard test method for compressive strength of cylindrical concrete specimens. *ASTM C39-93*. West Conshohocken, Pennsylvania: American Society for Testing and Materials.

ASTM. 1994. Standard test method for static modulus of elasticity and Poisson's ratio of concrete in compression. *ASTM C469-94*. West Conshohocken, Pennsylvania: American Society for Testing and Materials.

Ban, S., H. Muguruma, and S. Morita. 1960. *Study on bond characteristics of 7-wire strand at prestress transfer*. Technical Report No. 67. Kyoto, Japan: Engineering Research Institute, Kyoto University.

Base, G.D. 1957. Some tests on the effect of time on transmission length in pretensioned concrete. *Magazine of Concrete Research* 9(26): 73–82.

Base, G.D. 1958a. An investigation of transmission length in pre-tensioned concrete. Session III, Paper No. 9 in *Proceedings of the Third Congress of FIP* 1:603–623. Available from the British Cement Association (BCA) or the fédération internationale du béton (fib).

Base, G.D. 1958b. *An investigation of transmission length in pre-tensioned concrete*. Research Report No. 5, London: Cement and Concrete Association.

Breen, John E., Olivier Burdet, Carin Roberts, David Sanders, and Gregor Wollman. 1994. *Anchorage zone reinforcement for post-tensioned concrete girders*. National Cooperative Highway Research Program (NCHRP) Report 356. Washington: National Academy Press.

Brooks, Mark D., Kurt H. Gerstle, and Donald R. Logan. 1988. Effect of initial strand slip on the strength of hollow-core slabs. *PCI Journal* 33(1): 90-111.

Bruce, R.N., H.G. Russell, J.J. Roller, and B.T. Martin. 1994. *Feasibility evaluation of utilizing high-strength concrete in design and construction of highway bridge structures*. Report No. FHWA/LA-94-282. Baton Rouge: Louisiana Transportation Research Center.

Buckner, C. Dale. 1994. *An analysis of transfer and development lengths for pretensioned concrete structures*. Report No. FHWA-RD-94-049. McLean, Virginia: Federal Highway Administration.

Buckner, C. Dale. 1995. A review of strand development length for pretensioned concrete members. *PCI Journal* 40(2): 84–105.

Burkett, William R., and M. Metin Kose. 1999. *Development length of 0.6-inch (15-mm) diameter prestressing strand at 2-inch (50-mm) grid spacing in standard I-shaped pretensioned concrete beams*. Report No. TX/98/1388-2. Lubbock: Department of Engineering Technology, Texas Tech University.

Castrodale, Reid W., Michael E. Kreger, and Ned H. Burns. 1988a. *A study of pretensioned high strength concrete girders in composite highway bridges—laboratory tests*. Research Report 381-3. Austin: Center for Transportation Research, The University of Texas at Austin.

Castrodale, Reid W., Michael E. Kreger, and Ned H. Burns. 1988b. *A study of pretensioned high strength concrete girders in composite highway bridges—design considerations*. Research Report 381-4F. Austin: Center for Transportation Research, The University of Texas at Austin.

*CEB-FIP model code 1990*. Comité Euro-Internationale du Béton (CEB) Bulletin d'Information 213/214. London: Thomas Telford.

Collins, Michael P., and Denis Mitchell. 1991. *Prestressed concrete structures*. Englewood Cliffs, New Jersey: Prentice-Hall.

Cordova, Carlos R., 1996. Transfer and development length of 0.6-inch diameter prestressing strand at two inch spacing in fully bonded normal strength concrete composite Texas Type C beams. M.S.E. thesis, The University of Texas at Austin.

Cousins, Thomas E., David W. Johnston, and Paul Zia. 1990. Transfer and development length of epoxy coated and uncoated prestressing strand. *PCI Journal* 35(4): 92–103.

Devalapura, Ravi K., and Maher K. Tadros. 1992. Critical assessment of ACI 318 Eq. (18-3) for prestressing steel stress at ultimate flexure. *ACI Structural Journal* 89(5): 538–546.

Evans, Rhydwyn Harding. 1951. Research and developments in pre-stressing. *Journal of the Institution of Civil Engineers* (London) 35(4): 231–261.

Federal Highway Administration (FHWA). 1988. *Prestressing strand for pretension applications—development length revisited*. Memorandum from Stanley Gordon, Chief, Bridge Division, Office of Engineering to Regional Federal Highway Administrators and Direct Federal Program Administrator, Washington, D.C. (October 26).

Federal Highway Administration (FHWA). 1996. *Prestressing strand for pretension applications revisited.* Memorandum from Stanley Gordon, Chief, Bridge Division, Office of Engineering to Regional Administrators and Federal Lands Highway Program Administrator, Washington, D.C. (May 8).

Gross, Shawn P., and Ned H. Burns. 1995. *Transfer and development length of 15.2 mm (0.6 in.) diameter prestressing strand in high performance concrete: results of the Hoblitzell-Buckner beam tests*. Research Report 580–2. Austin: Center for Transportation Research, The University of Texas at Austin.

Guyon, Y. 1953. *Prestressed concrete*. New York: John Wiley and Sons.

Hanson, Norman W. 1969. Influence of surface roughness of prestressing strand on bond performance. *PCI Journal* 14(1): 32–45.

Hanson, Norman W., and Paul H. Kaar. 1959. Flexural bond tests of pretensioned prestressed beams. *ACI Journal*. *Proceedings* 55(7): 783–802.

Holmberg, Åke, and Sten Lindgren. 1970. *Anchorage and prestress transmission*. Document D1. Stockholm: National Swedish Institute for Building Research.

Hoyer, E., and E. Friedrich. 1939. Beitrag zur frage der haftspannung in eisenbetonbauteilen (Contribution to the question of bond stress in reinforced concrete elements). *Beton und Eisen* 38(March 20).

Janney, Jack R. 1954. Nature of bond in pre-tensioned prestressed concrete. *ACI Journal*. *Proceedings* 50(9): 717–736.

Janney, Jack R. 1963. Report of stress transfer length studies on 270 k prestressing strand. *PCI Journal* 8(1): 41–45.

Kaar, Paul H., Robert W. LaFraugh, and Mark A. Mass. 1963. Influence of concrete strength on strand transfer length. *PCI Journal* 8(5): 47–67.

Kaar, Paul H., and D.D. Magura. 1965. Effect of strand blanketing on performance of pretensioned girders. *PCI Journal* 10(6): 20–34.

Lane, Susan N. 1992. Transfer lengths in rectangular prestressed concrete concentric specimens. *Public Roads* 56(2): 67–71.

Lane, Susan N. 1998. *A new development length equation for pretensioned strands in bridge beams and piles*. Report No. FHWA-RD-98-116. McLean, Virginia: Federal Highway Administration.

Logan, Donald R. 1997. Acceptance criteria for bond quality of strand for pretensioned prestressed concrete applications. *PCI Journal* 42(2): 52–90.

MacGregor, James G. 1996. *Reinforced concrete: mechanics and design*. 3d ed. Englewood Cliffs, New Jersey: Prentice Hall.

Martin, Leslie D., and Norman L. Scott. 1976. Development of prestressing strand in pretensioned members. *ACI Journal*, *Proceedings* 73(8): 453–456.

Mitchell, Denis, William D. Cook, Arshad A. Kahn, and Thomas Tham. 1993. Influence of high-strength concrete on transfer and development length of pretensioning strand. *PCI Journal* 38(3): 52–66.

Moustafa, Saad. 1974. *Pull-out strength of strand lifting loops*. Technical Bulletin 74-B5, Tacoma, Washington: Concrete Technology Associates.

Myers, John J., and Ramon L. Carrasquillo. 1998. *Production and quality control of high performance concrete in Texas bridge structures*. Research Report 580/589-1. Austin: Center for Transportation Research, The University of Texas at Austin.

Orangun, C.O., J.O. Jirsa, and J.E. Breen. 1977. A reevaluation of test data on development length and splices. *ACI Journal, Proceedings* 74(3): 114–122.

Ozyildrium, Celik, Jose Gomez, and M. Elnahal. 1996. High performance concrete applications in bridge structures in Virginia. In *Worldwide advances in structural concrete and masonry: proceedings of the CCMS symposium held in conjunction with Structures Congress XIV*. New York: American Society of Civil Engineers (ASCE).

PCI. 1999. *PCI design handbook: precast and prestressed concrete*. 5th ed. Chicago: Precast/Prestressed Concrete Institute.

Persson, Bertil S.M., Anders G. Johansson, and Peter S. Johansson. 1999. Prefabrication with HSC. *Concrete International* 21(9): 58–62.

Ratz, E.H., M.M. Holmjanski, and V.M. Kolner. 1958. The transmission of prestress to concrete by bond. Session III, Paper No. 10 in *Proceedings of the Third Congress of FIP* 1:624–640. Available from the British Cement Association (BCA) or the fédération internationale du béton (fib).

Rose, Dallas R., and Bruce W. Russell. 1997. Investigation of standardized tests to measure the bond performance of prestressing strand. *PCI Journal* 42(4): 56–80.

Rüsch, H. and G. Rehm. 1963. Versuchezur bestimmung der über tragungslänge von spannstählen (Tests for determining the transmission length of prestressing wires). Deutscher Ausschuss für Stahlbeton 147: 1-38. Translation by C.V. Amerongen, Cement and Concrete Association, CJ 120 (7/65), London, 1965.

Russell, Bruce W., and Ned H. Burns. 1993. *Design guidelines for transfer, development and debonding of large diameter seven wire strands in pretensioned concrete girders*. Research Report 1210-5F. Austin: Center for Transportation Research, The University of Texas at Austin.

Russell, Bruce W., and Ned H. Burns. 1996. Measured transfer lengths of 0.5 and 0.6 in. strands in pretensioned concrete. *PCI Journal* 41(5): 44–65.

Shahawy, M. and B. DeV. Batchelor. 1991. *Bond and shear behavior of prestressed AASHTO Type II beams*. Progress Report No. 1. Tallahassee: Structural Research Center, Florida Department of Transportation.

Shahawy, Mohsen A., Moussa Issa, and Barrington deV. Batchelor. 1992. Strand transfer lengths in full scale AASHTO prestressed concrete girders. *PCI Journal* 37(3): 84–96.

Shing, P.B., D. Cooke, D.M. Frangopol, M.A. Leonard, M.L. McMullen, and W. Hunter. 1997. Colorado showcase on HPC box-girder bridge: development and transfer length tests. In *PCI/FHWA international symposium on high performance concrete: advanced concrete solutions for bridges and transportation structures*. Chicago: Precast/Prestressed Concrete Institute (PCI).

Simmons, Michael Britt. 1995. Transfer and development in pretensioned, prestressed concrete girders using ½ inch diameter strands. Ph.D. diss., Auburn University.

Stocker, M.F., and Sozen, M.A. 1970. *Investigation of prestressed concrete for highway bridges, part v: bond characteristics of prestressing strand.* Bulletin 503. Urbana: University of Illinois Engineering Experiment Station.

Tabatabai, Habib, and Timothy J. Dickson. 1993. The history of the prestressing strand development length equation. *PCI Journal* 38(6): 64–75.

Thorenfeldt, E., A. Tomaszewicz, and J.J. Jensen. 1987. Mechanical properties of high-strength concrete and applications in design. In *Proceedings of the symposium "Utilization of High Strength Concrete," Stavangar, Norway*. Trondheim: Tapir.

den Uijl, Joop A. 1992. Background CEB-FIP MC90 clauses on anchorage and transverse tensile actions in the anchorage zone of prestressed concrete members. *CEB Bulletin* 212: 71–94.

den Uijl, Joop A. 1997. Bond modelling of prestressing strand. Presented at the 1997 ACI Spring Convention, Seattle. Proceedings published in 1998 as *SP-150: Bond and development of reinforcement—a tribute to Dr. Peter Gergely*. Farmington Hills, Michigan: American Concrete Institute (ACI).

Zia, Paul and Talat Mostafa. 1978. Development length of prestressing strands. *PCI Journal* 22(5): 54–65.